LA-UR-07-6205
Approved for public release; distribution is limited.

NMCRIS # 107505

THE LAND CONVEYANCE AND TRANSFER DATA RECOVERY PROJECT: 7000 YEARS OF LAND USE ON THE PAJARITO PLATEAU

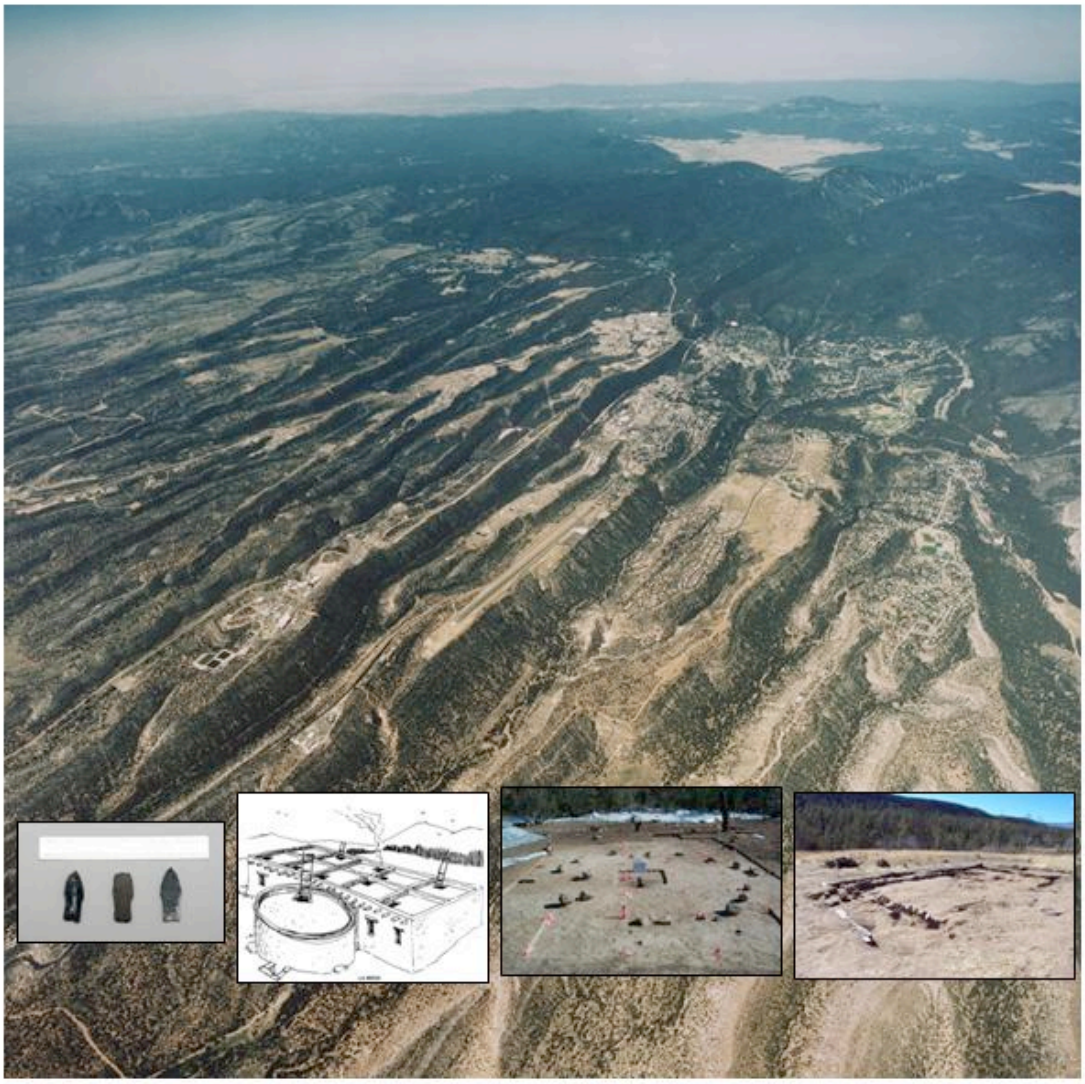

VOLUME 1: BASELINE STUDIES

Edited by Bradley J. Vierra and Kari M. Schmidt

Ecology and Air Quality Group, Los Alamos National Laboratory

June 2008

Edited by Hector Hinojosa, Group IRM-CAS

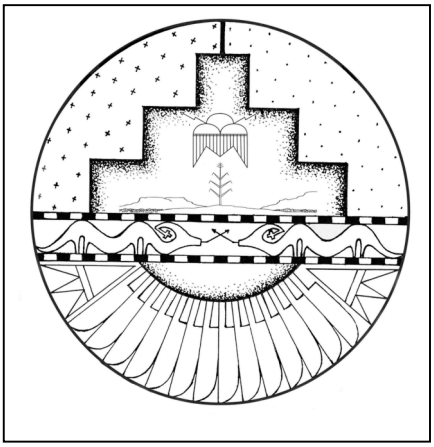

Artistic representation of the Pajarito Plateau; drawn by Aaron Gonzales.

*An Affirmative Action/Equal Opportunity Employe*r

LA-UR-07-6205 NMCRIS # 107505

Title

THE LAND CONVEYANCE AND TRANSFER DATA RECOVERY PROJECT: 7000 YEARS OF LAND USE ON THE PAJARITO PLATEAU

Volume 1: Baseline Studies

Cultural Resources Report No. 273

Prepared for

U.S. Department of Energy
National Nuclear Security Administration
Los Alamos Site Office

Prepared by

Bradley J. Vierra, Ecology and Air Quality Group
Kari M. Schmidt, Ecology and Air Quality Group

Los Alamos, New Mexico 87545

June 2008

This report is dedicated to the memory of Charlie Steen.
Photo courtesy of Los Alamos National Laboratory, IR-74-07-338.

Contents

List of Figures

List of Tables

CHAPTER 1
THE LAND CONVEYANCE AND TRANSFER DATA RECOVERY PROJECT: 7000 YEARS OF LAND USE ON THE PAJARITO PLATEAU

Bradley J. Vierra and Steven R. Hoagland

The Department of Energy (DOE), National Nuclear Security Administration, Los Alamos Site Office and Los Alamos National Laboratory (LANL) are located in north-central New Mexico approximately 100 km north-northeast of Albuquerque and 40 km northwest of Santa Fe (Figure 1.1). The DOE is scheduled to convey properties at or in the vicinity of LANL to the County of Los Alamos, New Mexico, or its designee and to transfer properties to the Secretary of the Interior in trust for the Pueblo of San Ildefonso. The Land Conveyance and Transfer (C&T) Project is directed by Section 632 of PL 105-119, the *Departments of Commerce, Justice, and State, the Judiciary, and Related Agencies Appropriations Act, 1998*, which was passed by Congress on November 26, 1997.

The *Final Environmental Impact Statement (EIS) for the Conveyance and Transfer of Certain Land Parcels Administered by the U.S. Department of Energy and Located at Los Alamos National Laboratory, Los Alamos and Santa Fe, Counties, New Mexico*, 1998, describes the contemplated land use by the County of Los Alamos for the White Rock (A-19), Airport East (A-3), Airport Central (A-7), Airport South (A-5-1), and Rendija Canyon (A-14) tracts as economic development. The mitigation measures involved minimizing impacts to cultural resources by preparing tract-specific Historic Properties Treatment Plans that include provisions for a data recovery program for National Register of Historic Places (NRHP)-eligible archaeological resources that cannot be avoided.

The DOE examined 10 tracts of land (1942 ha; 4796 ac) proposed for the C&T Project (Figure 1.2). As a result of this examination, a July 2002 report entitled *Cultural Resource Assessment for the Department of Energy Conveyance and Transfer Project* (Hoagland et al. 2000a) was produced and submitted by DOE to the New Mexico State Historic Preservation Officer (SHPO) for comments. SHPO concurrence with the recommended NRHP eligibility for the 213 documented archaeological sites was issued on October 6, 2000. One hundred eighty of the sites are eligible or have an undetermined eligibility (i.e., potentially eligible).

The White Rock Tract (A-19) is located directly north of the community of White Rock and State Road 4. The western boundary runs northward from the State Road 4 and Pajarito Road intersection. The tract includes the southern tip of Mesita del Buey and portions of the Cañada del Buey floodplain.

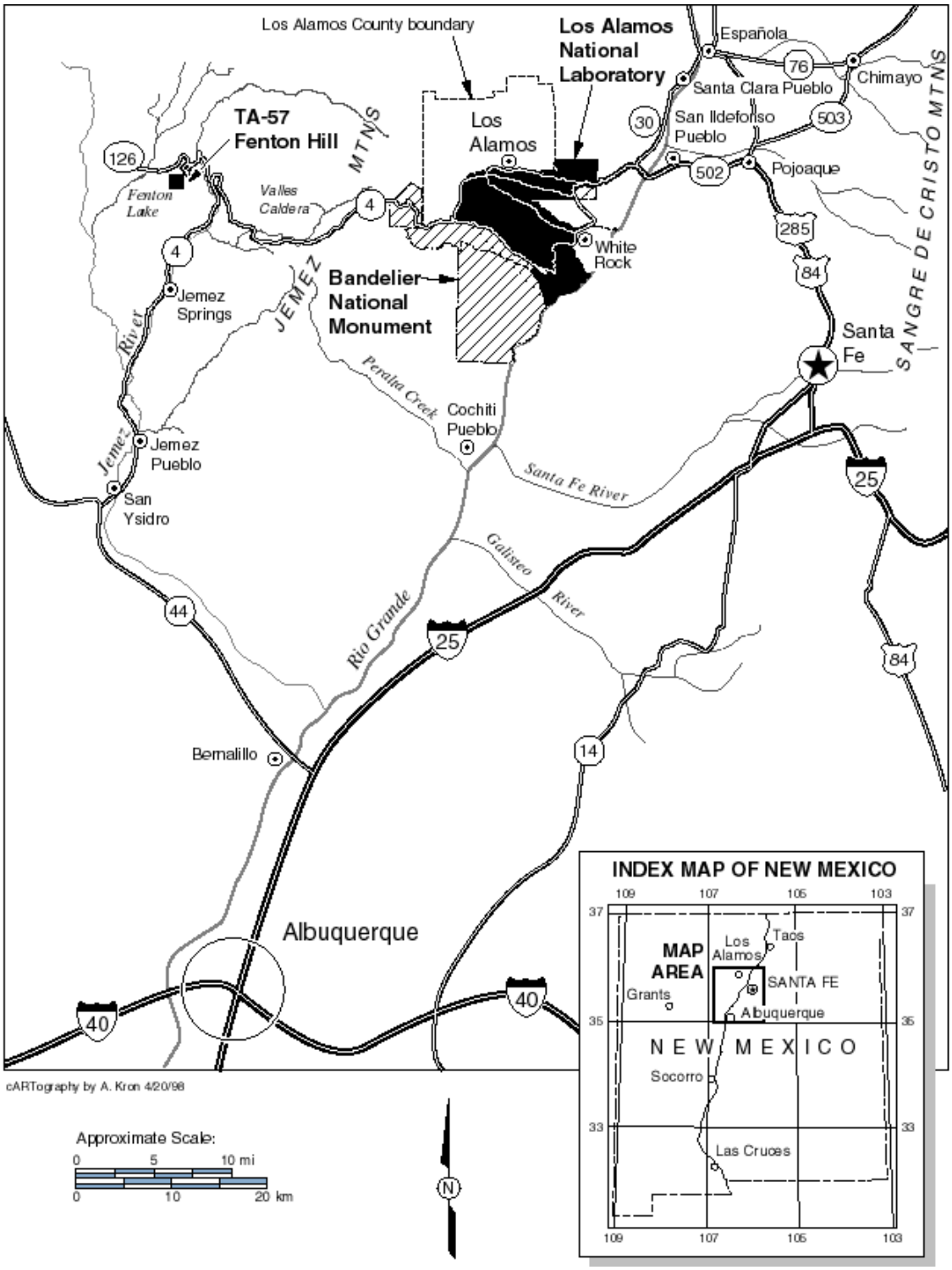

Figure 1.1. Location of Los Alamos National Laboratory (LANL).

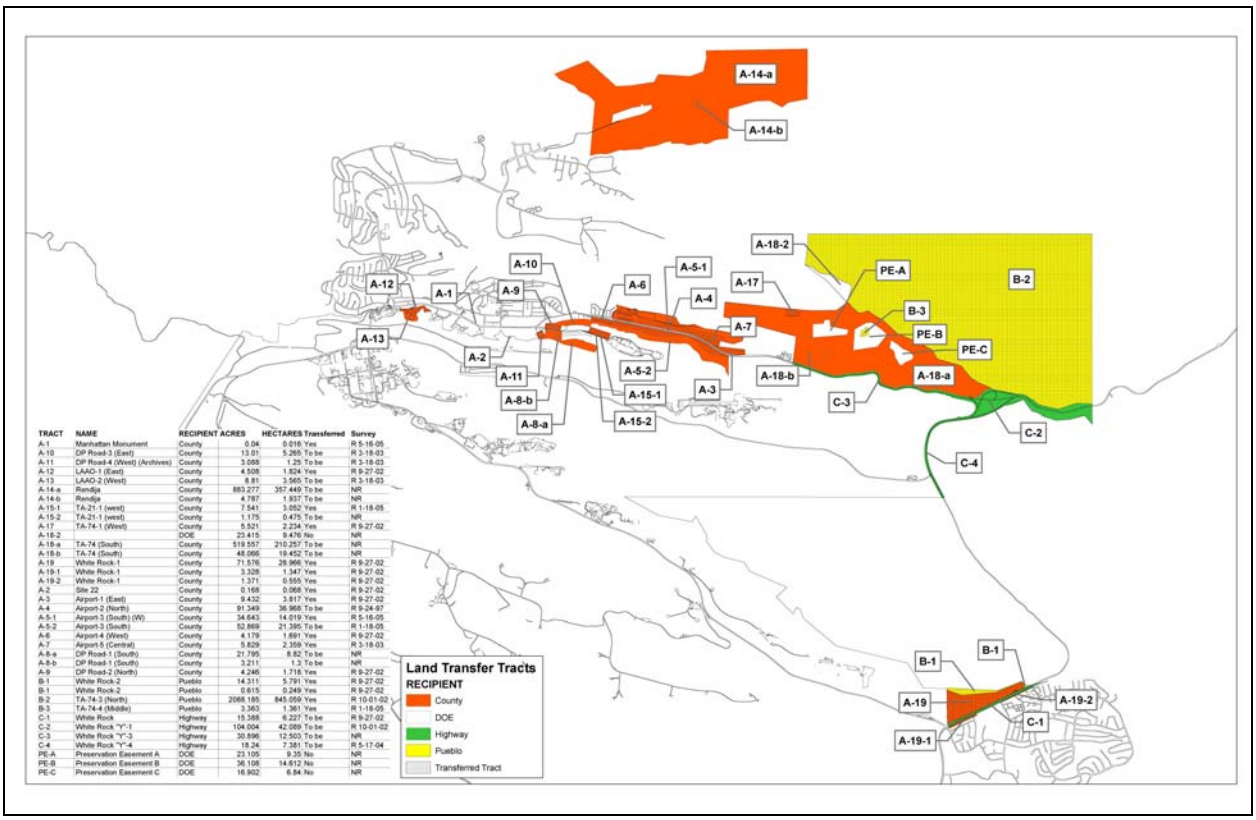

TRACT	NAME	RECIPIENT	ACRES	HECTARES	Transferred	Survey
A-1	Manhattan Monument	County	0.04	0.016	Yes	R 5-16-05
A-10	DP Road-3 (East)	County	13.01	5.265	To be	R 3-18-03
A-11	DP Road-4 (West) (Archives)	County	3.088	1.25	To be	R 3-18-03
A-12	LAAO-1 (East)	County	4.508	1.824	Yes	R 9-27-02
A-13	LAAO-2 (West)	County	8.81	3.565	To be	R 3-18-03
A-14-a	Rendija	County	883.277	357.449	To be	NR
A-14-b	Rendija	County	4.787	1.937	To be	NR
A-15-1	TA-21-1 (west)	County	7.541	3.052	Yes	R 1-18-05
A-15-2	TA-21-1 (west)	County	1.175	0.475	To be	NR
A-17	TA-74-1 (West)	County	5.521	2.234	Yes	R 9-27-02
A-18-2		DOE	23.415	9.476	No	NR
A-18-a	TA-74 (South)	County	519.557	210.257	To be	NR
A-18-b	TA-74 (South)	County	48.066	19.452	To be	NR
A-19	White Rock-1	County	71.576	28.966	Yes	R 9-27-02
A-19-1	White Rock-1	County	3.328	1.347	Yes	R 9-27-02
A-19-2	White Rock-1	County	1.371	0.555	Yes	R 9-27-02
A-2	Site 22	County	0.168	0.068	Yes	R 9-27-02
A-3	Airport-1 (East)	County	9.432	3.817	Yes	R 9-27-02
A-4	Airport-2 (North)	County	91.349	36.968	To be	R 9-24-97
A-5-1	Airport-3 (South) (W)	County	34.643	14.019	Yes	R 5-16-05
A-5-2	Airport-3 (South)	County	52.869	21.395	To be	R 1-18-05
A-6	Airport-4 (West)	County	4.179	1.691	Yes	R 9-27-02
A-7	Airport-5 (Central)	County	5.829	2.359	Yes	R 3-18-03
A-8-a	DP Road-1 (South)	County	21.795	8.82	To be	NR
A-8-b	DP Road-1 (South)	County	3.211	1.3	To be	NR
A-9	DP Road-2 (North)	County	4.246	1.718	Yes	R 9-27-02
B-1	White Rock-2	Pueblo	14.311	5.791	Yes	R 9-27-02
B-1	White Rock-2	Pueblo	0.615	0.249	Yes	R 9-27-02
B-2	TA-74-3 (North)	Pueblo	2088.185	845.059	Yes	R 10-01-02
B-3	TA-74-4 (Middle)	Pueblo	3.363	1.361	Yes	R 1-18-05
C-1	White Rock	Highway	15.388	6.227	To be	R 9-27-02
C-2	White Rock "Y"-1	Highway	104.004	42.089	To be	R 10-01-02
C-3	White Rock "Y"-3	Highway	30.896	12.503	To be	NR
C-4	White Rock "Y"-4	Highway	18.24	7.381	To be	R 5-17-04
PE-A	Preservation Easement A	DOE	23.105	9.35	No	NR
PE-B	Preservation Easement B	DOE	36.108	14.612	No	NR
PE-C	Preservation Easement C	DOE	16.902	6.84	No	NR

Figure 1.2. The location of the Land Conveyance and Transfer (C&T) Project tracts.

The Airport Tracts are located east of the Los Alamos town site. The Airport East (A-3) and Airport Central (A-7) tracts are situated along the north side of State Road 502 (East Road) and the Airport South Tract (A-5-1) on the south side of the road a short distance west of the East Gate Business Park. These tracts are located on the mesa between Pueblo and DP canyons (see Figure 1.2).

The Rendija Tract (A-14) is located north of the Los Alamos town site's Barranca Mesa residential subdivision. The tract is situated within Rendija Canyon and Cabra Canyon. Barranca Mesa forms the southern boundary of the tract and Guaje Mountain forms most of the northern boundary. The Rendija Tract is bounded by U.S. Forest Service property to the north, east, and west and by Los Alamos County lands to the south.

The White Rock Tract (A-19) contains 10 archaeological sites, nine of which are NHRP eligible. Two eligible sites, approximately 80 percent of a third eligible site, and the single non-eligible site are situated on a small portion of land to be transferred to San Ildefonso Pueblo. The remaining six sites and approximately 20 percent of another are within the section to be conveyed to Los Alamos County. The Airport Tract parcels (A-3, A-7, and A-5-1) contain five archaeological sites that are all NRHP eligible. The Rendija Tract (A-14) contains 61 archaeological sites, 49 of which are eligible to the NRHP or have an undetermined eligibility. Nine of these sites have been identified as Traditional Cultural Properties (TCPs) by San

Ildefonso and Santa Clara pueblos and are therefore considered eligible to the NRHP. All of the remaining sites have been deemed eligible or potentially eligible under Criterion D of the NRHP, meaning that they are likely to yield information important to prehistory and/or history of New Mexico.

Land transferred to the Department of the Interior to hold in trust for San Ildefonso Pueblo is not an "undertaking" under the National Historic Preservation Act. Therefore, no further compliance is required for the properties that will be transferred to San Ildefonso Pueblo. This includes their ancestral home of Otowi, which is located within Technical Area (TA) 74. However, under 36 CFR 800.5(vii), the conveyance of lands to Los Alamos County is considered an adverse effect to historic properties, if adequate and legally enforceable restrictions or conditions to ensure the long-term preservation of these properties' historic significance are not established. For example, TA-74 is located east of the Los Alamos town site and below the mesa upon which the town site was built. The southern portion of TA-74 is dominated by Pueblo Canyon, the central portion of Bayo Canyon, and the northern portion of Barrancas Canyon. A total of 98 archaeological sites are situated within this technical area. Portions of the land were transferred to San Ildefonso Pueblo. Limited testing was conducted at nine archaeological sites within TA-74 (A-18a) and two sites within the nearby White Rock Y (C-2) tracts to determine potential eligibility.

A Programmatic Agreement (PA) was entered into by the DOE, Advisory Council for Historic Preservation, New Mexico SHPO, and the County of Los Alamos in order to implement the mitigation measures as specified in the EIS (Appendix A). As previously noted, PL 105-119 provides lands to Los Alamos County for economic development. As a result, the County intends to develop portions, if not all, of the Airport Tract parcels (A-3, A-7, and A-5-1), the Rendija Tract (A-14), and their section of the White Rock Tract (A-19), constituting an adverse effect to the historic properties within. Section IV of the PA (see Appendix A) details the actions to be taken in respect to these parcels. In addition, Attachment B of Appendix A describes the required data recovery standards. In order to resolve this adverse effect, DOE has developed a data recovery strategy for those properties that will be unavoidably destroyed or impacted through development. A data recovery plan entitled *Department of Energy Land Conveyance Data Recovery Plan and Research Design for the Excavation of Archaeological Sites Located within Selected Parcels to be Conveyed to the Incorporated County of Los Alamos, New Mexico* (Vierra et al. 2002a) was submitted by DOE to the SHPO and concurred with on May 5, 2002.

The data recovery plan provides a research design to guide the excavation and analysis of data obtained from the sites to be excavated within the tracts being conveyed to Los Alamos County. A series of research contexts consisting of chronometrics, geoarchaeology, paleoenvironment, settlement patterns, subsistence and seasonality, and technology and interaction are proposed. A total of 68 detailed research questions are presented within these contexts by time period and site type. In addition, the field excavation and laboratory procedures used to collect the data necessary to answering these questions are provided.

This data recovery program was implemented for seven archaeological sites within the White Rock Tract (A-19), five archaeological sites within the Airport Tract parcels (A-3, A-7, and A-5-1), and 27 archaeological sites within the Rendija Tract (A-14) (see Table 1.1). The reduced

number of sites within the latter tract relates to the identification of nine TCPs and the selection of a sample of 10 fieldhouses that were excluded from excavation. In addition, two sites could not be relocated (LA 86553 and LA 70026). The results of the four-year excavation project are presented within this four-volume set. Excavations were conducted from 2002 to 2005. A total of 39 sites were excavated and approximately 150,000 artifacts were collected. Volume 1 (Baseline Studies) provides background information on geology, geomorphology, environment, and dating techniques. Volume 2 (Site Excavations) presents the excavation reports for the sites excavated in the White Rock, Airport, and Rendija tracts, as well as the results of site testing for the TA-74 and White Rock Y tracts. Volume 3 (Artifact and Sample Analyses) provides the detailed results of artifact and sample analyses, and Volume 4 (Research Design) presents various specialized studies and results of the project research questions.

Table 1.1. List of excavated and tested sites.

Tract	LA Number	Year of Excavation	Site Type	Period of Occupation
White Rock (A-19)	LA 12587	2002	Roomblock and fieldhouse	Late Coalition; Classic
	LA 12587 (Area 8)	2002	Lithic scatter	Late Archaic
	LA 86637	2002	Lithic/ceramic scatter	Late Archaic; Middle Classic; Historic
	LA 127625	2002	Lithic/ceramic scatter	Coalition
	LA 127631	2002	Fieldhouse	Coalition/Classic
	LA 128803	2002	Grid garden	Classic
	LA 128804	2002	Check dam and lithic/ceramic scatter	Historic; Late Classic
	LA 128805	2002	Fieldhouse	Late Classic
Airport (A-3, A-7, and A-5-1)	LA 86533	2003	Lithic/ceramic scatter	Ancestral Pueblo
	LA 86534	2002	Roomblock	Middle Coalition
	LA 135290	2003	Roomblock	Middle Coalition
	LA 139418	2003	Grid garden	Classic
	LA 141505	2003	Fieldhouse	Coalition/Classic
Rendija (A-14)	LA 15116	2004	Fieldhouse	Late Classic
	LA 70025	2004	Fieldhouse	Late Classic
	LA 85403	2004	Fieldhouse	Und. (Classic?)
	LA 85404	2004	Fieldhouse	Coalition/Classic
	LA 85407	2005	Homestead	Early 20th century
	LA 85408	2005	Fieldhouse	Late Classic
	LA 85411	2005	Fieldhouse	Early-Late Classic
	LA 85413	2005	Fieldhouse	Early Classic
	LA 85414	2005	Fieldhouse	Classic
	LA 85417	2005	Fieldhouse	Classic
	LA 85859	2003	Lithic scatter	Early Archaic
	LA 85861	2005	Fieldhouse	Coalition/Classic

Tract	LA Number	Year of Excavation	Site Type	Period of Occupation
	LA 85864	2003	Tipi ring- Jicarilla	Late 19th/early 20th century
	LA 85867	2005	Fieldhouse	Classic
	LA 85869	2003	Tipi ring- Jicarilla	Late 19th/early 20th century
	LA 86605	2004	Fieldhouse	Late Classic
	LA 86606	2005	Fieldhouse	Coalition/Classic
	LA 86607	2005	Fieldhouse	Coalition
	LA 87430	2004	Fieldhouse	Late Classic
	LA 99396	2003	Lithic scatter; one-room structure	Archaic; Coalition
	LA 99397	2003	Lithic scatter	Archaic
	LA 127627	2004	Fieldhouse	Classic
	LA 127633	2004	Storage Feature	Und. (Classic?)
	LA 127634	2004	Fieldhouse	Late Classic
	LA 127635	2004	Fieldhouse	Coalition/Classic
	LA 135291	2004	Fieldhouse	Early Classic
	LA 135292	2004	Fieldhouse	Late Classic
TA-74 (A-18a)	LA 21596B	2002	Grid garden	Coalition/Classic
	LA 21596C	2002	Grid garden	Coalition/Classic
	LA 86528	2002	Rockshelter	Und. (Classic/Historic?)
	LA 86531	2002	Lithic/ceramic scatter	Coalition/Historic
	LA 110121	2002	Lithic/ceramic scatter	Und. (Coalition/Historic?)
	LA 110126	2002	Fieldhouse	Late Classic
	LA 110130	2002	Fieldhouse	Und. (Classic?)
	LA 110133	2002	Lithic/ceramic scatter	Ancestral Pueblo
	LA 117883	2002	Lithic scatter	Archaic
White Rock Y (C-2)	LA 61034	2002	Lithic/ceramic scatter	Und. (Classic/Historic?)
	LA 61035	2002	Lithic/ceramic scatter	Classic

CHAPTER 2
THE GEOLOGY OF LOS ALAMOS NATIONAL LABORATORY AS A BACKDROP FOR ARCHAEOLOGICAL STUDIES ON THE PAJARITO PLATEAU

David E. Broxton, Fraser Goff, and Kenneth Wohletz

INTRODUCTION

The geology of the Pajarito Plateau exerted a significant influence on the cultural development of prehistoric inhabitants. The local landscape provided the raw materials for buildings, pottery, tools, and other artifacts. This chapter provides a geologic overview of the Pajarito Plateau with emphasis on bedrock geologic units that were important sources of raw materials for the early inhabitants of the area.

GENERAL GEOLOGIC SETTING

The Los Alamos National Laboratory (LANL) is situated on the Pajarito Plateau, an east-sloping, dissected tableland bounded on the west by the eastern Jemez Mountains (Sierra de los Valles) and on the east by White Rock Canyon of the Rio Grande (Figure 2.1). The geology of the Pajarito Plateau reflects the interplay of volcanism in the Jemez Mountains and surrounding areas with the development of the Rio Grande rift, a series of north-south-trending fault troughs extending from southern Colorado to southern New Mexico (Figure 2.1).

Volcanism over the last 13 million years built up the highlands area of the Jemez Mountains, while contemporaneous tectonic rifting resulted in subsidence of the area extending from the eastern margin of the Jemez Mountains to the western margin of the Sangre de Cristo Mountains. This area of subsidence, locally termed the Española basin of the Rio Grande rift, is a graben between two larger basins—the Albuquerque basin to the south and San Luis basin to the north (Kelley 1978). During this interplay of volcanism and rifting, erosion removed materials from the highlands areas to the west and deposited them downslope to the east into the rifted lowlands, which were contemporaneously receiving sediments from other sources. The Pajarito Plateau developed in and now occupies the western part of the Española basin (Figure 2.2).

The gently east-sloping Bandelier Tuff covers the Pajarito Plateau. Deep canyons are incised into the Bandelier Tuff and expose it to depths of up to several hundred feet below the general level of the Pajarito Plateau. From west to east, these canyons cut progressively deeper into the Bandelier Tuff and, near the Rio Grande, some of the deeper canyons expose older lavas and sedimentary rocks. Figure 2.3 is a geologic cross-section that shows the distribution of rock units beneath the plateau. Volcanic rocks of the Tschicoma Formation and their derivative sediments (fanglomerate facies of the Puye Formation) extend eastward under the plateau where they interfinger with Santa Fe Group rocks and basaltic rocks of the Cerros del Rio volcanic field (also called “basaltic rocks of Chino Mesa”).

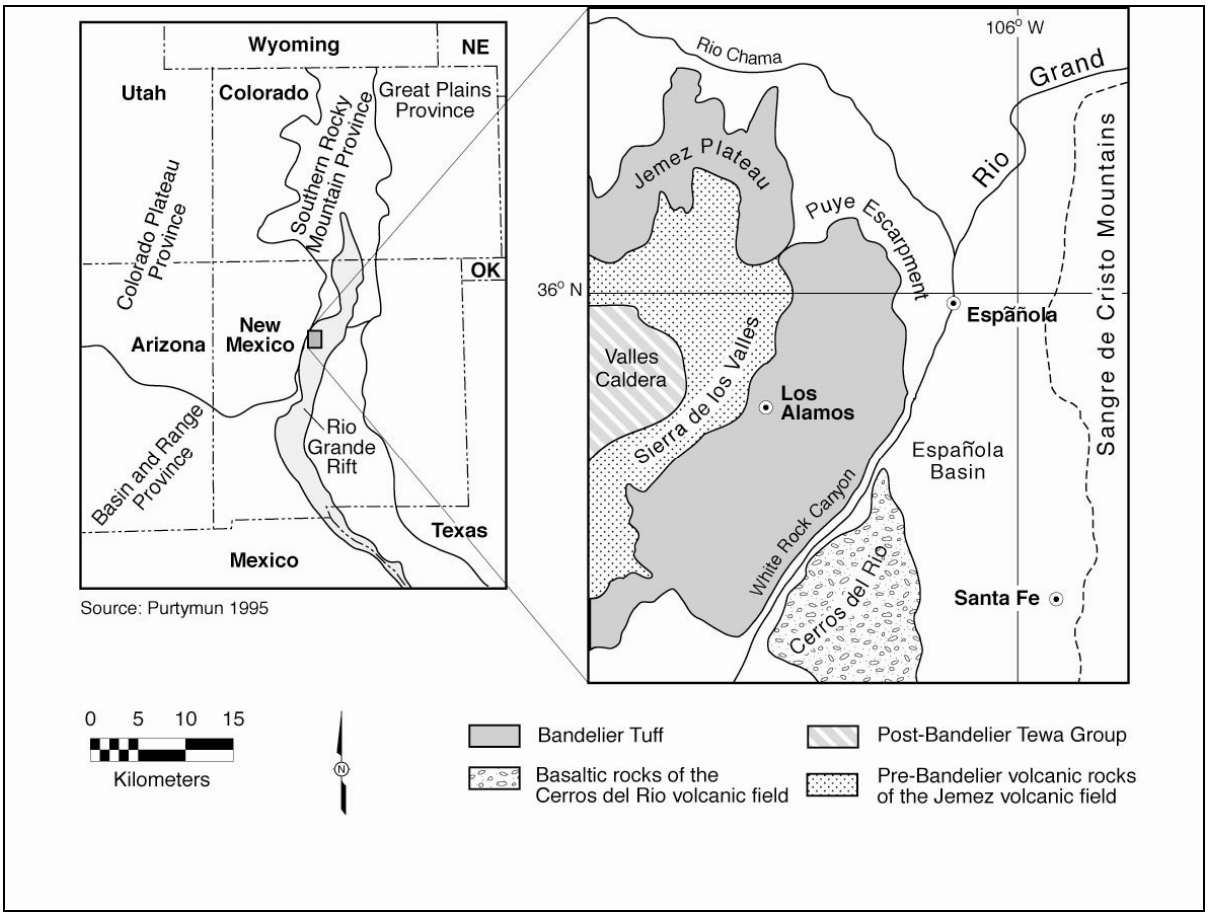

Figure 2.1. Regional setting of the Pajarito Plateau.

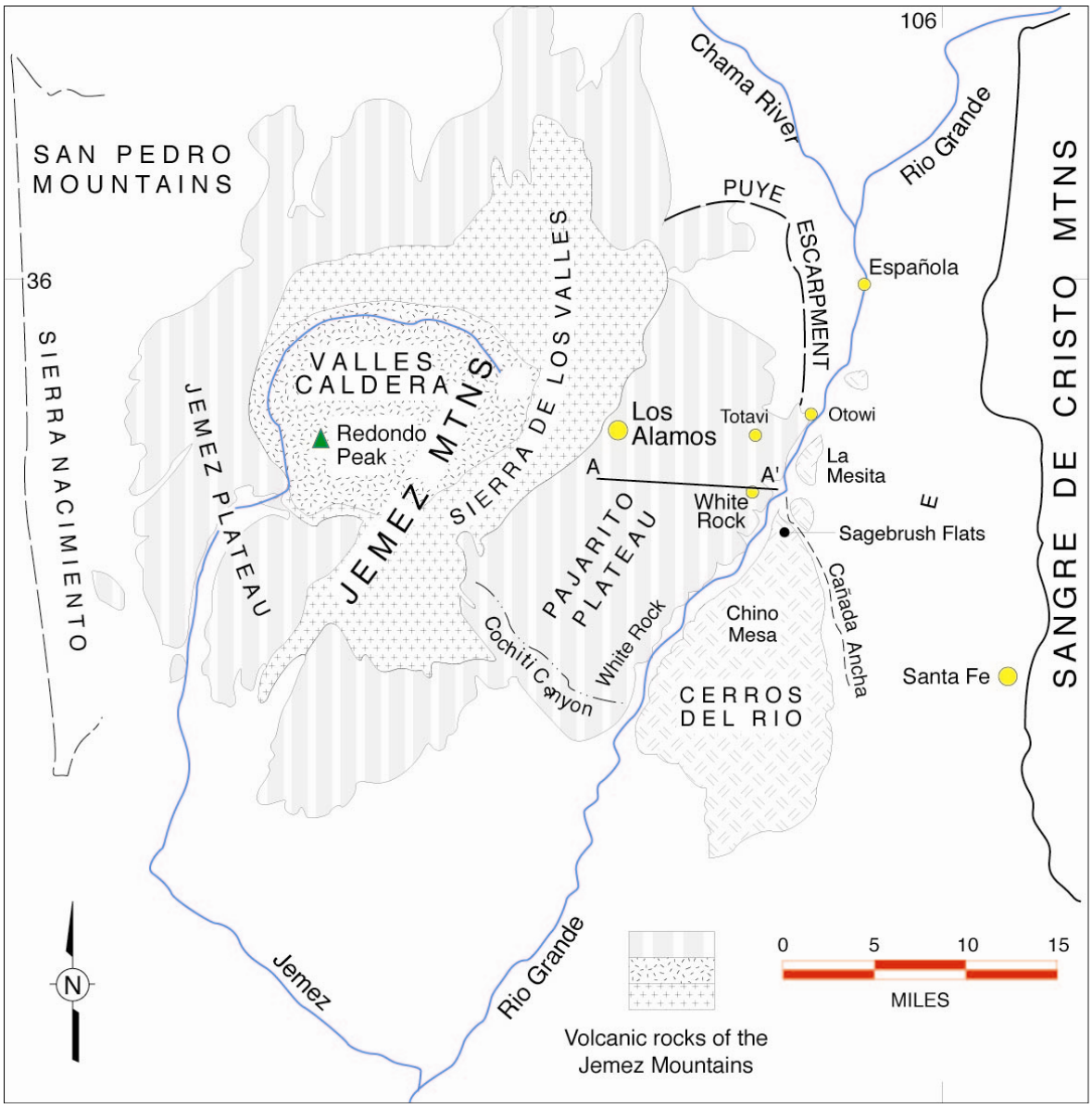

Figure 2.2. Geologic and geographic features of the Pajarito Plateau and surrounding areas. A-A1 is the location of the geologic cross-section in Figure 2.3.

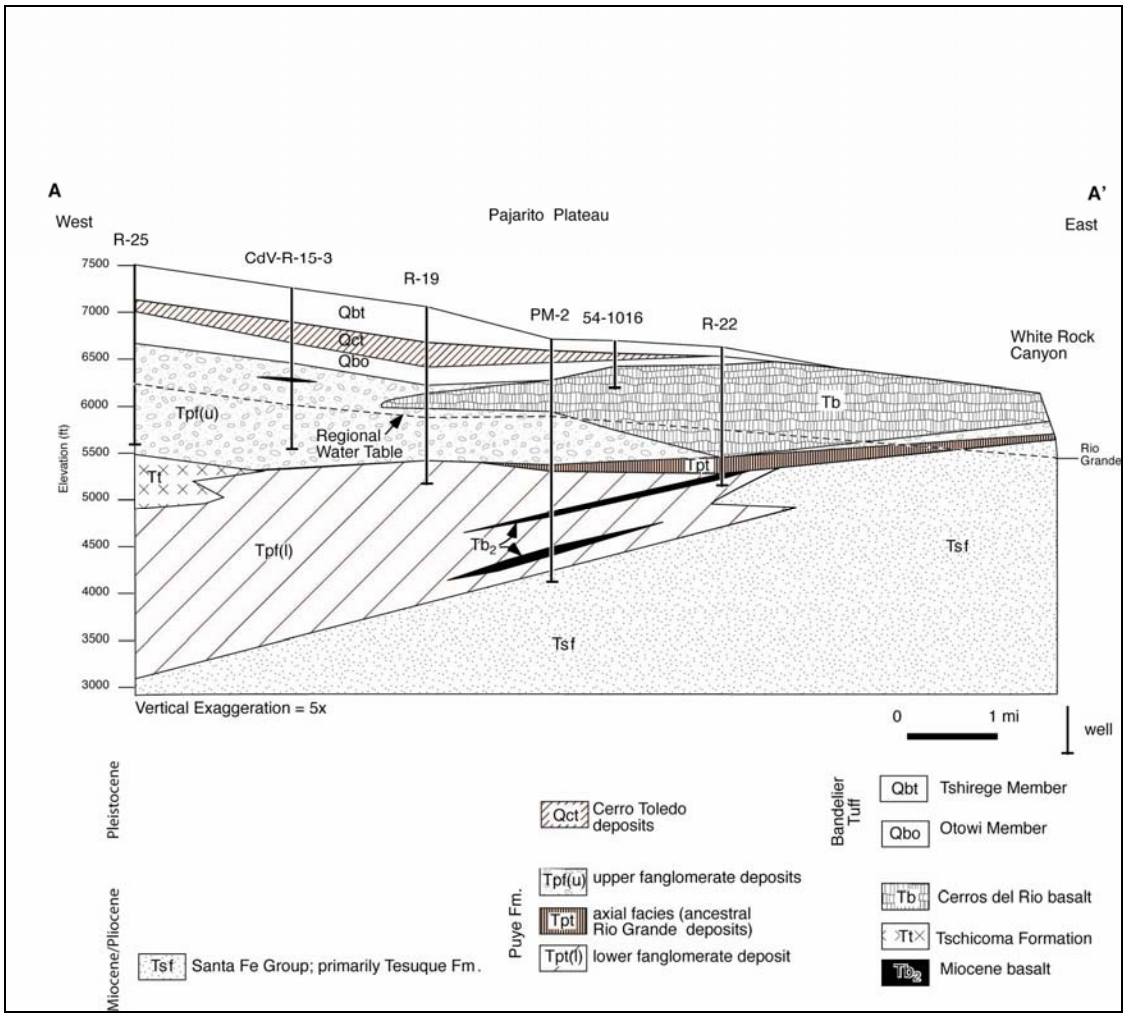

Figure 2.3. East-west cross-section showing stratigraphic relations for geologic units of the Pajarito Plateau; see Figure 2.2 for location of cross-section.

STRATIGRAPHY

A generalized stratigraphic chart for the Jemez volcanic field is shown in Figure 2.4. The following descriptions focus on those rock units that are exposed on or near LANL, starting with the oldest (deepest) and proceeding to the youngest (topmost). Fossil evidence, stratigraphic correlations, and radiometric measurements provide the approximate ages of most of the bedrock units. The bedrock units and their ranges of approximate radiometric ages are listed below in ascending order.

1. Santa Fe Group: 4 to 21 Ma (Manley 1979)
2. Tschicoma Formation: 2.0 to <7.4 Ma (Gardner and Goff 1984; Loeffler et al. 1988; WoldeGabriel 2001, personal communication)
3. Puye Formation: 1.7 to 4 Ma (Spell et al. 1990; Turbeville et al. 1989), which includes a fanglomerate facies, an axial facies (Manley 1979; Turbeville et al. 1989), and a lacustrine facies

4. Basaltic rocks of the Cerros del Rio volcanic field (also known as "basaltic rocks of Chino Mesa") (2 to 3 Ma) (WoldeGabriel 2001, personal communication; WoldeGabriel et al. 1996)
5. Otowi Member of the Bandelier Tuff: 1.61 Ma (Izett and Obradovich 1994; Spell et al. 1996)
6. Volcaniclastic sediments and tephra of the Cerro Toledo interval: the age of this unit is bracketed by the ages of the underlying Otowi Member (1.61 Ma) and the overlying Tshirege Member (1.22 Ma) of the Bandelier Tuff
7. Tshirege Member of the Bandelier Tuff: 1.22 Ma (Izett and Obradovich 1994; Spell et al. 1990, 1996)
8. Valles Rhyolite: <1.133 Ma (Spell and Harrison 1993) to 50 to 60 Ka (thousand years) (Reneau et al. 1996a; Toyoda et al. 1995)

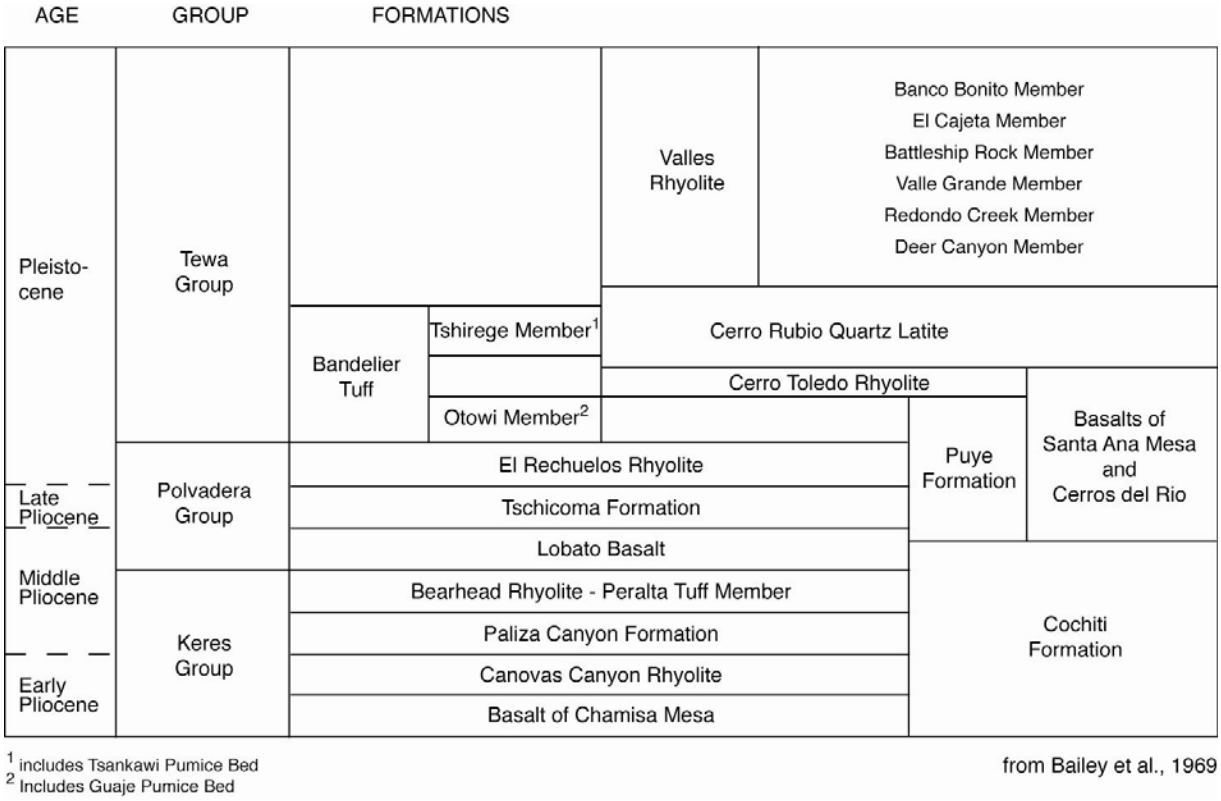

Figure 2.4. Stratigraphic nomenclature for major rock units of the Jemez volcanic field.

A geological map published by R. Smith et al. (1970) shows the distribution of these bedrock units across the Pajarito Plateau. Other general geological maps covering this area are those by Griggs (1964), Kelley (1978), and Goff et al. (1990). More detailed geological maps covering portions of LANL include those by Baltz et al. (1963), Rogers (1995), Vaniman and Wohletz (1990), Reneau et al. (1995), Goff (1995), Goff et al. (2002), Lewis et al. (2002), and Lavine et al. (2003). Figure 2.5 schematically portrays the complex interfingering of volcanic rocks and sediments that occurs below the Pajarito Plateau.

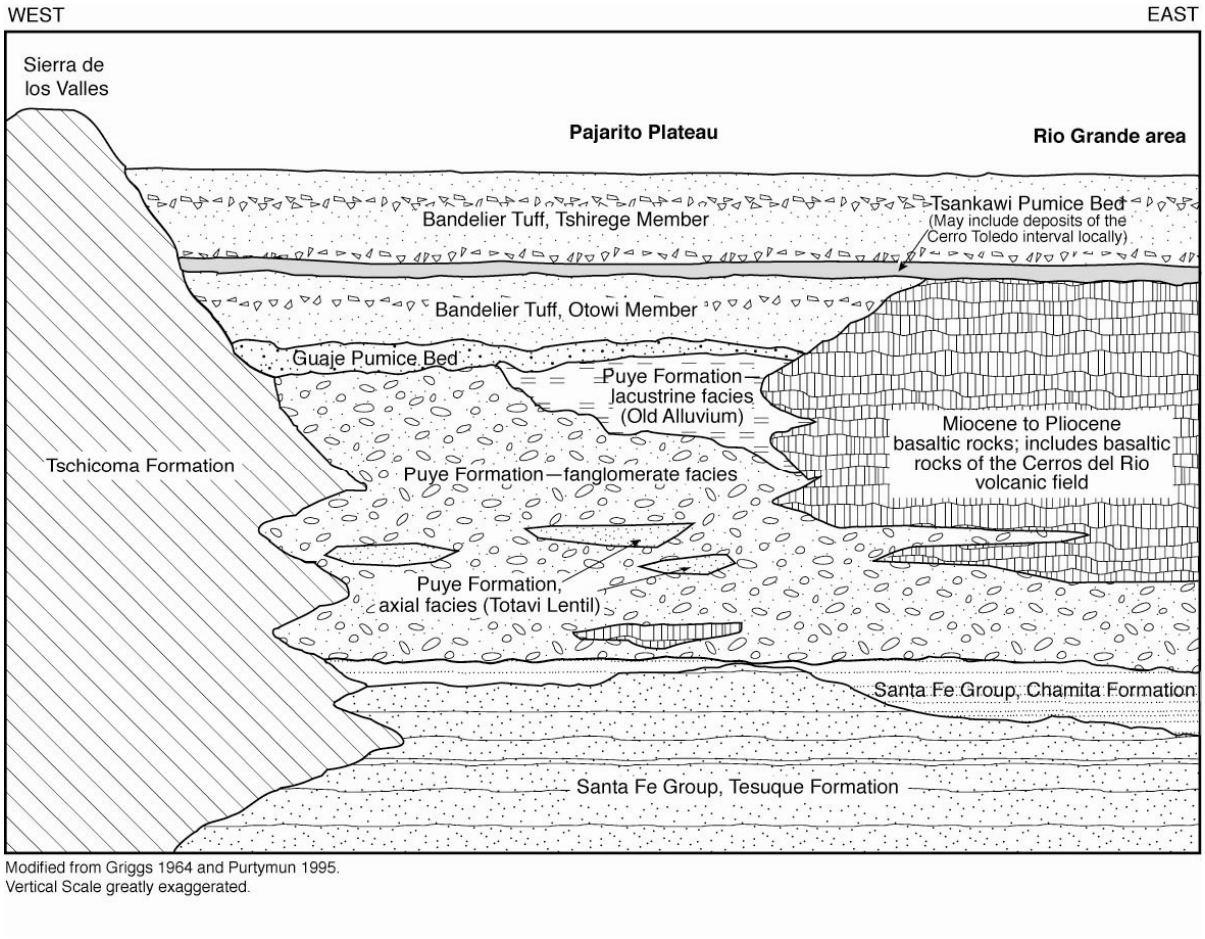

Figure 2.5. Schematic cross-section showing interfingering stratigraphic relationship across the Pajarito Plateau; thicknesses are approximate.

Santa Fe Group

Rocks of the Santa Fe Group crop out in lower Los Alamos Canyon, near the mouth of Guaje Canyon, and along the margins of the Rio Grande from Otowi Bridge south to White Rock. Galusha and Blick (1971) subdivided the Santa Fe Group into formations and members based on geologic mapping and fossil assemblages of late Tertiary mammals. Manley (1979) refined the stratigraphy with additional mapping and dates of interbedded volcanic ash layers, lava flows, and dikes. In the vicinity of the Pajarito Plateau, the stratigraphy and geochronology of the Santa Fe Group is poorly understood because of the near continuous blanket of Bandelier Tuff. Based on exposures near the Rio Grande, the Santa Fe Group beneath the Pajarito Plateau is believed to include, in ascending order, the Tesuque Formation and the Chamita Formation.

Tesuque Formation

The Tesuque Formation is a massive, thick sedimentary deposit consisting of arkosic sediments, derived primarily from Precambrian basement and Tertiary volcanic sources to the east and northeast of the Española basin. This unit is a light pink-to-buff siltstone and silty sandstone with

a few lenses of pebbly conglomerate and clay (Figure 2.6). It is poorly to moderately consolidated and has an age range of about 7 to 21 Ma (Cavazza 1989; Manley 1979). Spiegel and Baldwin (1963) describe the Tesuque Formation at the southern end of the Española basin, including the exposures in the vicinity of Otowi Bridge and along White Rock Canyon. This formation exists in deep well boreholes under the Pajarito Plateau and is the primary aquifer for municipal and industrial water supply in Los Alamos County.

Figure 2.6. The Santa Fe Group was shed into the subsiding Española basin from highlands located to the east and northeast. This figure shows the Tesuque formation, which is typically made up of light pink-to-buff siltstone and silty sandstone with lenses of pebbly conglomerate and clay.

Chamita Formation

The Chamita Formation overlies and interfingers with the Tesuque Formation. It consists of arkosic siltstones, sandstones, and pebbly conglomerate and includes two prominent beds of white ash. This formation is thickest in the northern part of the Española basin and thins to less than 9.1 m (30 ft) or is absent under most of LANL property. Aldrich and Dethier (1990) suggest that the Chamita Formation north of the Pajarito Plateau may be as old as 12 Ma. However, paleomagnetic data in the area indicate an age range of 4.5 to 6 Ma (MacFadden 1977), and tephra dates by Manley (1979) support a younger age of about 5 Ma for at least part of the formation.

Tschicoma Formation

The Tschicoma Formation of the Polvadera Group makes up the rugged Sierra de los Valles highlands west of Los Alamos, and it crops out in the headwaters of the larger canyons that cut the Pajarito Plateau. Deep boreholes along the western perimeter of the Laboratory intersect this unit at depths of several hundred feet or more, but the Tschicoma Formation is generally absent in boreholes penetrating the central and eastern parts of LANL.

The Tschicoma Formation consists of numerous thick lava flows that erupted from large overlapping dome complexes. Fragmental deposits of ash and lava debris occur in the distal parts of the formation. It has a variable thickness due to the lenticular shape of its lava flows, and is at least 762 m (2,500 ft) thick in the Sierra de los Valles. The Tschicoma Formation thins eastward under the Pajarito Plateau where it interfingers with the Puye Formation. The lower parts of the Tschicoma Formation may interfinger with rocks of the upper Santa Fe Group.

The Tschicoma Formation ranges in composition from dacite to rhyolite, but dacites are the predominant rock type. The rocks are mainly gray to purplish gray, but in places they are reddish brown. These flows display pronounced jointing and have tops and bottoms commonly marked by blocky breccia. Flow interiors are commonly devitrified to microcrystalline groundmass minerals giving the rocks a stony appearance. Chilled volcanic glass is some times preserved in flow tops and bottoms.

Dated volcanic domes making up the Sierra de los Valles range in age between 2.91 and 5.03 Ma (WoldeGabriel 2001, personal communication). Turbeville et al. (1989) report an age of 2.53 Ma for a Tschicoma ignimbrite within the Puye Formation. In the northern part of the Jemez volcanic field, the Tschicoma Formation is bracketed in age by the underlying Lobato Basalt (7.4 Ma) and the overlying El Rechuelos Rhyolite (2.0 Ma) (Loeffler et al. 1988).

Puye Formation

The Puye Formation is a large apron of overlapping alluvial fans that were shed eastward from the Jemez volcanic field into the Española basin, covering the Santa Fe Group rocks west of and along the Rio Grande. The Puye Formation is intersected by most deep wells on the Pajarito

Plateau (Purtymun 1995), and it crops out in lower Los Alamos Canyon and in canyons to the north. Turbeville et al. (1989) estimated its areal distribution at 200 km^2 (518 mi^2) and its volume at approximately 15 km^3 (3.6 mi^3). Because its primary sources were Tschicoma domes in the Sierra de los Valles, the Puye Formation overlaps and post-dates the Tschicoma Formation in age.

The lithology of the Puye Formation is dominated by conglomerates and gravels consisting of subangular to subrounded dacitic and andesitic lava clasts in a sandy matrix (Figure 2.7).

Figure 2.7. The Puye formation consists of deposits formed by coalescing alluvial fans shed eastward from Tschicoma volcanic centers in the Sierra de los Valles. These deposits of cobbles, gravels, and sand are exposed in canyons in the northern part of the Pajarito Plateau and along the Rio Grande.

At least 25 ash beds of dacitic to rhyolitic composition are interbedded with the conglomerates and gravels (Turbeville et al. 1989), and basaltic ash and lacustrine layers are present along the eastern margins of this formation. Because of its deposition as alluvial fans, the Puye Formation shows considerable vertical and lateral lithological variability. The formation reaches a maximum thickness of approximately 333 m (>1093 ft) in well R-25 on the western side of LANL but thins to 15 m (50 ft) in areas north of the Pajarito Plateau (Dethier and Manley 1985). In the central and eastern portions of LANL, it is approximately 183 m (600 ft) thick and is interbedded with basaltic lavas of the Cerros del Rio volcanic field.

The Puye Formation as defined by Griggs (1964) originally included three units, in ascending order: an axial facies (called the "Totavi Lentil" by Griggs), a fanglomerate facies, and a lacustrine facies (called "older alluvium" by Griggs).

Axial Facies of the Puye Formation

The axial facies of the Puye Formation (also called "Totavi Lentil" or "Totavi Formation") overlies the Santa Fe Group and crops out at Totavi in Los Alamos Canyon and along the east side of the Pajarito Plateau (Griggs 1964). It is generally approximately 15 m (50 ft) thick near the Rio Grande but thickens in a northwest direction. It consists of coarse, poorly consolidated conglomerate containing cobbles and boulders of silicic to intermediate volcanic rocks and Precambrian quartzite, granite, and pegmatite (Figure 2.8). These rocks probably represent axial-channel deposits of the ancestral Rio Grande. The axial facies forms the oldest deposits in the Puye Formation in many areas, but it also interfingers with the lower part of the fanglomerate facies. The age of the axial facies is poorly constrained.

Fanglomerate Facies of the Puye Formation

The fanglomerate facies is the dominant unit of the Puye Formation beneath most of LANL property. Fanglomerate is a general term meaning a rock unit composed of conglomerates deposited in an alluvial fan setting. The fanglomerate facies contains angular to subangular cobbles and boulders of latite, quartz latite, dacite, rhyolite, and tuff in a matrix of silts, clays, and sands. Lenses of silt, clay, and pumice are common. It is interbedded with basaltic rocks of the Cerros del Rio volcanic field in the eastern and central part of LANL. The fanglomerate facies is widespread beneath the Pajarito Plateau and caps the prominent cliffs (Puye Escarpment) along the Rio Grande north of Otowi Bridge.

Lacustrine Facies of the Puye Formation

Griggs (1964) included clay-rich lake beds (the lacustrine facies) as the uppermost part of the Puye Formation. He differentiated them from the fanglomerate facies based on the presence of lake siltstones and ancient stream gravels that fill channels cut into the fanglomerates. Basaltic rocks of the Cerros del Rio volcanic field are also found in these channels (Griggs 1964). The lacustrine facies is present in lower Los Alamos Canyon and extends both northward and southward in discontinuous outcrops for several miles. However, it is apparently of limited extent beneath the Pajarito Plateau, being reported only in boreholes near the eastern edge of the plateau. Most likely, these lake beds were one source of clay used for making pottery.

Figure 2.8. The Totavi Lentil is made of sands, gravels, and cobbles, which were deposited by the ancestral Rio Grande. The deposit contains subangular to subrounded clasts from local sources such as the Jemez volcanic field and rounded Precambrian granitic and metamorphic rocks derived from highlands to the north of the Española basin.

Basaltic Rocks of the Cerros del Rio Volcanic Field

The basaltic rocks of the Cerros del Rio volcanic field crop out primarily on the eastern side of the Rio Grande (Griggs 1964; R. Smith et al. 1970) and occur in the subsurface below much of the Pajarito Plateau (Broxton and Reneau 1996; Dransfield and Gardner 1985). Outcrops within LANL property occur in most canyons along the southern and eastern margins of the plateau. The stratigraphic nomenclature for these basalts has varied with different workers (Aubele 1978; Galusha and Blick 1971; Griggs 1964; Kelley 1978; R. Smith et al. 1970). Kelley (1978) mapped four different units of the Cerros del Rio Basalts, one of which (the Cubero Basalts) includes the five units of the basaltic rocks of Chino Mesa (Griggs 1964). Some of the older basalt flows that have been included in this formation may belong to the Santa Fe Group.

The basaltic rocks of the Cerros del Rio volcanic field form thick lava flows separated by interflow breccia, scoria, and ash (Figure 2.9). The lavas were erupted from numerous vents both east and west of the Rio Grande. In the vicinity of the Pajarito Plateau, these basalts form a north-south-trending highland (now buried by the Bandelier Tuff) extending from the western edge of White Rock to the confluence of Los Alamos and Pueblo canyons (Broxton and Reneau 1996). These basalts are interbedded with the upper part of the Puye Formation.

The basaltic rocks of the Cerros del Rio volcanic field include buried remnants of maar volcanoes in White Rock Canyon (Aubele 1978; Heiken et al. 1986). The aprons of fragmental debris surrounding these buried craters consist of thin layers of basaltic ash and sediments. The maar deposits resulted from steam explosions that occurred where basalt erupted through an aquifer or standing body of water.

Figure 2.9. The 2- to 3-Ma Cerros del Rio basalt consists of a thick sequence of massive lava flows separated by beds of breccia, cinder, and sedimentary deposits. The upper photo shows thick Cerros del Rio basalt flows overlain by the Tshirege Member of the Bandelier Tuff. The lower photo shows Cerros del Rio basalt overlain by the Guaje Pumice bed near the confluence of Pueblo and Los Alamos canyons.

Bandelier Tuff

The Bandelier Tuff consists of the Otowi and Tshirege Members, which are stratigraphically separated in many places by the tephra and volcaniclastic sediments of the Cerro Toledo interval (Figure 2.10). The Bandelier Tuff was erupted from the Valles Caldera complex between 1.61 and 1.22 Ma ago. It is perhaps one of the best studied tuff units in the world, and it has been the subject of numerous geological studies since the early 1960s. The tuff is composed of pumice, minor rock fragments, and crystals supported in an ashy matrix. It is a prominent cliff-forming unit because of its generally strong consolidation. In the Tshirege Member, this consolidation is largely due to compaction and welding at high temperatures after the tuff was emplaced. Its light brown, orange brown, purplish, and white cliffs have numerous, mostly vertical fractures (called joints) that show average spacing of between several feet and several tens of feet. The Tshirege Member includes thin but distinctive layers of bedded sand-sized particles, called surge deposits, which demark separate flow units within the tuff.

Most archaeological sites on the Pajarito Plateau are located on the Bandelier Tuff. Archaeological sites include cavates excavated in soft portions of the tuff as well as a variety of structures (e.g., roomblocks, fieldhouses, dams, and terraces) constructed from tuff blocks. Tools such as manos and metates were shaped from tuff blocks. Because the Bandelier Tuff was such an important source of raw material, its detailed stratigraphy is of considerable importance and is discussed further below.

Otowi Member

The Otowi Member crops out in several canyons but is most extensive in Los Alamos Canyon and in canyons to the north. Griggs (1964), R. Smith and Bailey (1966), Bailey et al. (1969), and R. Smith et al. (1970) are important references describing the nature and extent of the Otowi Member. It consists of moderately consolidated (indurated), porous, and non-welded vitric ash-flow tuff (ignimbrite) that forms gentle, colluvium-covered slopes along the base of canyon walls. The Otowi ignimbrites contain light gray to orange pumice supported in a white to tan ashy matrix of glass shards, broken pumice, crystals, and rock fragments (Broxton et al. 1995; Goff 1995).

The Guaje Pumice Bed occurs at the base of the Otowi Member, making it a significant and extensive marker horizon in many boreholes. The Guaje Pumice Bed (Bailey et al. 1969; Self et al. 1986) contains layers of well-sorted pumice fragments whose mean size varies between 2.0 and 4.1 cm (0.8 and 1.6 in.). It has an average thickness of approximately 8.5 m (28 ft) over much of the plateau with local areas of thickening and thinning. The Guaje Pumice Bed's distinctive white color and stratified bedding make it easily identifiable in outcrops.

Figure 2.10. Two major volcanic eruptions from the Valles Caldera complex in the Jemez Mountains produced the widespread and voluminous ash flow sheets of the Otowi and Tshirege Members of the Bandelier Tuff. The Cerro Toledo interval, an interbedded sequence of rhyolitic tephras and sediments, commonly occurs between the two members of the Bandelier Tuff. The upper photograph shows the subunits of the Tshirege Member overlying deposits of the Cerro Toledo interval. The bottom photographs show Otowi Member ash-flow tuffs (left) and a close up of pumices in fall deposits making up the basal Guaje Pumice Bed (right).

Tephra and Volcaniclastic Sediments of the Cerro Toledo Interval

The Cerro Toledo interval is an informal name given to a sequence of volcaniclastic sediments and tephra of mixed provenance that separates the Otowi and Tshirege Members of the Bandelier Tuff on the Pajarito Plateau (Broxton and Reneau 1995; Broxton et al. 1995; Goff 1995). The unit contains primary and reworked rhyolite tephra normally assigned to the Cerro Toledo Rhyolite as described by R. Smith et al. (1970), as well as dacite-rich sediments derived from the Sierra de los Valles. Although it is intercalated between the two members of the Bandelier Tuff, the Cerro Toledo Rhyolite (and the Cerro Toledo interval on the Pajarito Plateau) is not considered part of that formation (see Figure 2.4; Bailey et al. 1969). Outcrops of the Cerro Toledo interval generally occur wherever the top of the Otowi Member appears in Los Alamos Canyon and in canyons to the north. The occurrence of the Cerro Toledo interval is widespread; however, its thickness is variable ranging from several feet to 81 m (266 ft).

The predominant rock types in the Cerro Toledo interval are rhyolitic tuffaceous sediments and tephra (Broxton et al. 1995; Goff 1995; Heiken et al. 1986; Stix et al. 1988). The tuffaceous sediments are the reworked equivalents of Cerro Toledo Rhyolite tephra that erupted from the Cerro Toledo and Rabbit Mountain rhyolite domes located in the Sierra de los Valles. Primary pumice-fall and ash-fall deposits occur in some locations. Cerro Toledo rhyolite, particularly at Rabbit Mountain, was an important source of archaeological obsidian. Although small amounts of obsidian clasts are present in Cerro Toledo deposits on the plateau, these clasts are generally too small to have been a significant source of archaeological obsidian.

Clast-supported gravel, cobble, and boulder deposits made up of porphyritic dacite derived from the Tschicoma Formation are interbedded with the tuffaceous rocks, and in some deposits, the dacitic detritus is volumetrically more important than rhyolitic detritus. These coarse dacitic deposits commonly define the axial portions of paleochannels.

Tshirege Member

The Tshirege Member is the upper member of the Bandelier Tuff and is the most widely exposed bedrock unit of the Pajarito Plateau (Bailey et al. 1969; Griggs 1964; R. Smith and Bailey 1966; R. Smith et al. 1970). Emplacement of this unit occurred during eruptions of the Valles Caldera 1.22 Ma ago (Izett and Obradovich 1994; Spell et al. 1996). The Tshirege Member is a multiple-flow, ash-and-pumice sheet that forms the prominent cliffs in most of the canyons on the Pajarito Plateau. It also underlies the canyon floor in all but the middle and lower reaches of Los Alamos Canyon and in canyons to the north. The Tshirege Member is generally over 61 m (200 ft) thick in the north-central part of LANL and is over 183 m (600 ft) thick near the southern edge of LANL at Technical Area (TA) 49 (Broxton and Reneau 1996).

The Tshirege Member differs from the Otowi Member most notably in its generally greater degree of welding compaction. Time breaks between the successive emplacement of flow units caused the tuff to cool as several distinct cooling units. For this reason, the Tshirege Member is a compound cooling unit, consisting of at least four cooling subunits that display variable physical properties vertically and horizontally (Broxton and Reneau 1995; Crowe et

al. 1978; R. Smith and Bailey 1966). These variations in physical properties reflect zonal patterns of varying degree of welding and glass crystallization that accompanies welding (R. Smith 1960a, 1960b). The welding and crystallization variabilities in the Tshirege Member produce recognizable vertical variations in its properties such as density, porosity, hardness, composition, color, and surface weathering patterns. The degree of welding in each of the cooling units generally decreases from west to east, reflecting the higher emplacement temperatures closer to the Valles Caldera.

The Tsankawi Pumice Bed forms the base of the Tshirege Member. Where exposed, it is commonly 51 to 76 cm (20 to 30 in.) thick. This pumice-fall deposit contains moderately well-sorted pumice lapilli (diameters reaching about 6.4 cm [2.5 in.]) in a crystal-rich matrix. Several thin ash beds are interbedded with the pumice-fall deposits.

Qbt 1g is the lowermost subunit of the thick ignimbrite sheet overlying the Tsankawi Pumice Bed (Figure 2.10). It consists of porous, non-welded, and poorly sorted ash flow tuffs. The "g" in this designation stands for "glass" because none of the glass in ash shards and pumices shows crystallization by devitrification or vapor-phase alteration. This unit is poorly indurated but nonetheless forms steep cliffs because of a resistant bench near the top of the unit that forms a harder, protective cap over the softer underlying tuffs. A thin (10- to 25-cm [4- to 10-in.]), pumice-poor, surge deposit commonly occurs at the base of this unit.

Qbt 1v forms alternating cliff-like and sloping outcrops composed of porous, non-welded, but crystallized tuffs. The "v" stands for vapor-phase crystallization, which together with *in situ* crystallization (devitrification), converted much of the glass in shards and pumices into microcrystalline aggregates. The base of this unit is a thin, horizontal zone of preferential weathering that marks the abrupt transition from glassy tuffs below to crystallized tuffs above. This feature forms a widespread mappable marker horizon (locally termed the vapor-phase notch) throughout the Pajarito Plateau, which is readily visible in many canyon walls. In some locations the transition is marked by a prominent bench developed on top of the glassy tuff (Figure 2.10). The lower part of Qbt 1v is a colonnade tuff that is orange brown, is resistant to weathering, and has distinctive columnar (vertical) joints. The upper part of Qbt 1v consists of white, variably indurated, alternating cliff- and slope-forming tuffs. The tuffs of Qbt 1v are commonly non-welded (pumices and shards retain their initial equant shapes) and have an open, porous structure.

Qbt 2 forms a distinctive, medium brown, vertical cliff that stands out in marked contrast to the slope-forming, lighter colored tuffs above and below (Figure 2.10). A series of surge beds commonly mark its base in the eastern part of LANL, and it displays the greatest degree of welding in the Tshirege Member. It is typically nonporous and has low permeability relative to the other units of the Tshirege Member. Vapor-phase crystallization of flattened shards and pumices is extensive in this unit.

Qbt 3 is a non-welded to partially welded, vapor-phase altered tuff, which forms many of the upper cliffs in the mid to lower reaches of canyons on the Pajarito Plateau (Figure 2.10). Its base consists of a purple gray, unconsolidated, porous, and crystal-rich non-welded tuff that underlies a broad, gently sloping bench developed on top of Qbt 2. This basal, non-welded

portion forms relatively soft outcrops that weather into low, rounded mounds with a white color, which contrast with the cliffs of partially welded tuff in the middle and upper portions of Qbt 3. In the western part of LANL, an additional subunit, Qbt 3t, is present above Qbt 3 (Gardner et al. 2001). Qbt 3t is a moderately to densely welded ashflow tuff that has petrographic and geochemical characteristics that are transitional between Qbt 3 and Qbt 4.

Qbt 4 is a partially welded to densely welded ignimbrite characterized by small, sparse pumices and numerous intercalated surge deposits. This unit caps mesas in the western part of LANL, but it is absent from mesa tops over the middle to eastern portions of the Pajarito Plateau. Devitrification and vapor-phase alteration are typical in this unit, but thin zones of vitric ignimbrite occur within this unit in the western part of LANL.

Valles Rhyolite

The Valles Rhyolite includes rhyolites and associated pyroclastic rocks erupted within the Valles Caldera after its collapse. The Valles Rhyolite is comprised of, in ascending order, the Deer Canyon, Redondo Creek, Valle Grande, Battleship, El Cajete, and Banco Bonito Members (see Figure 2.4). The Valle Grande Member of the Valles Rhyolite is of particular interest because the Cerro del Medio dome complex in the northeast part of the Valles Caldera was an important source of archaeological obsidian. Cerro del Medio is the oldest of the Valle Grande domes that erupted on the floor of the Valles Caldera (1.133 ± 0.011 Ma; Spell and Harrison 1993). Other dome complexes include Del Abrigo, Santa Rosa, Seco, San Luis, San Antonio, South Mountain, and La Jara. Within the Valle Grande Member, Cerro del Medio is the primary source of aphyric to sparsely porphyritic high-silica rhyolite obsidian. Other rocks of the Valle Grande Member were less favorable sources of archaeological obsidian because of their higher phenocryst contents (16% to 35%). Assignment of archaeological obsidian to the Valle Grande Member is facilitated by the unique chemistry of these domes. Selected chemical data for the Valle Grande Member are summarized in Figures 2.11 and 2.12.

Although vents for the Valles Rhyolite are confined to the Valles Caldera, fall deposits and reworked tephra from Deer Canyon, Cerro del Medio, and El Cajete eruptions overlie the Tshirege Member at several locations on the Pajarito Plateau (Figure 2.13). Prevailing winds at the time of these eruptions deposited ash and pumice eastward over the Sierra de los Valles and Pajarito Plateau. Deposited as ash and pumice falls, these tephra were quickly washed from the eastern slopes of the Sierra de los Valles and redeposited as sheets of reworked tephra up to 6 m (20 ft) thick in the western part of the Pajarito Plateau before canyon incision. The interbedded nature of primary fall deposits and volcaniclastic sediments indicates that volcanism and reworking of the tephra was penecontemporaneous. At some locations, the fall deposits and reworked tephra are interbedded with early Pleistocene dacite-bearing alluvial fan deposits.

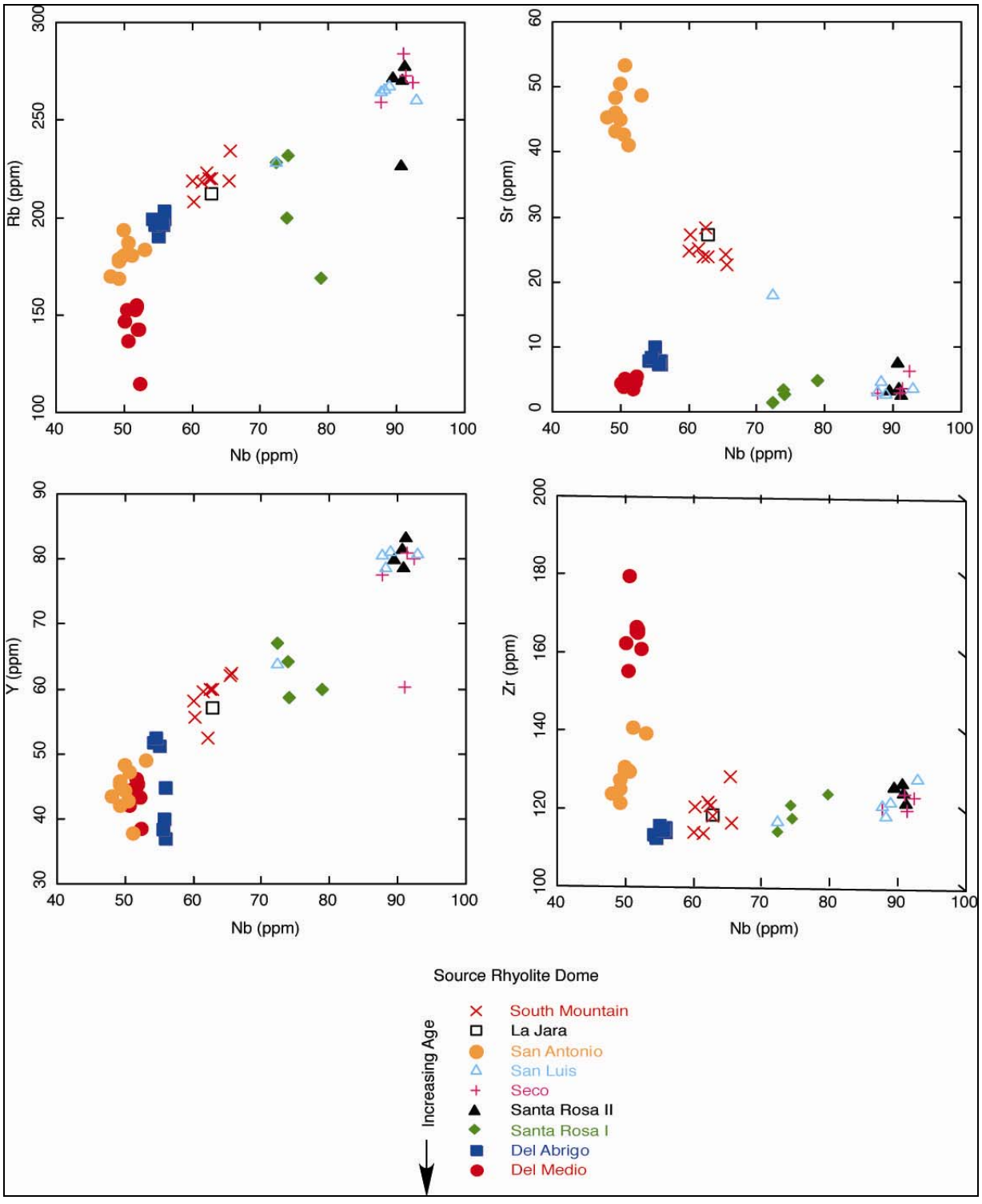

Figure 2.11. Plots of Nd versus Rb, Sr, Y, and Zr for whole rock samples collected from the source domes of Valle Grande Member of the Valles Rhyolite in the Valles Caldera. Data are X-ray fluorescence analyses from Spell (1987).

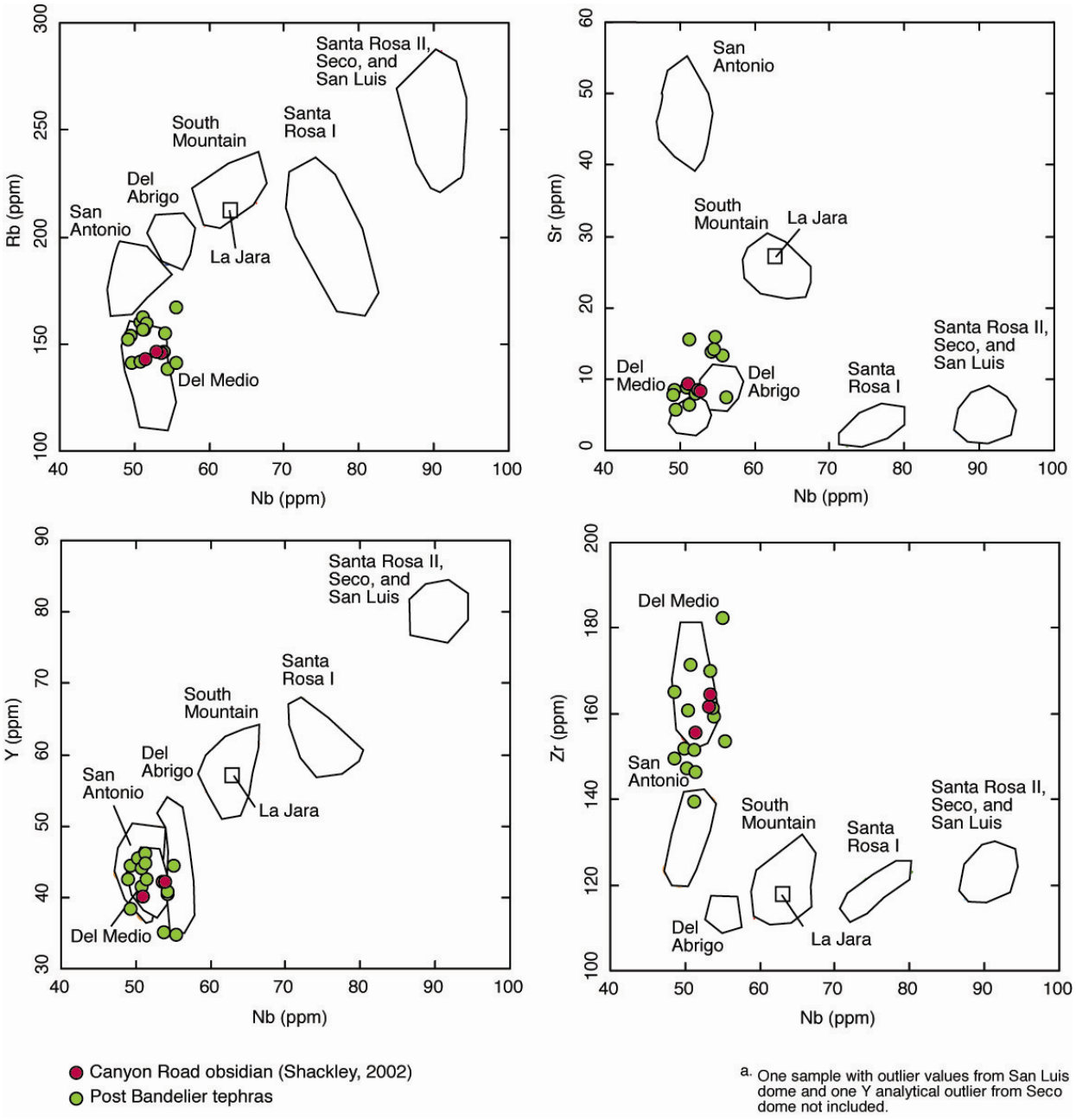

Figure 2.12. Plots of Nd versus Rb, Sr, Y, and Zr for Cerro del Medio tephras collected on the Pajarito Plateau. These data are compared to analyses of source domes (circled areas—see Figure 2.11 for individual analyses; data from Spell [1987]). The tephra data are unpublished X-ray fluorescence analyses (in green) and X-ray fluorescence analyses of obsidian clasts from the Caballo Peaks Apartment site (in red; Shackley 2002).

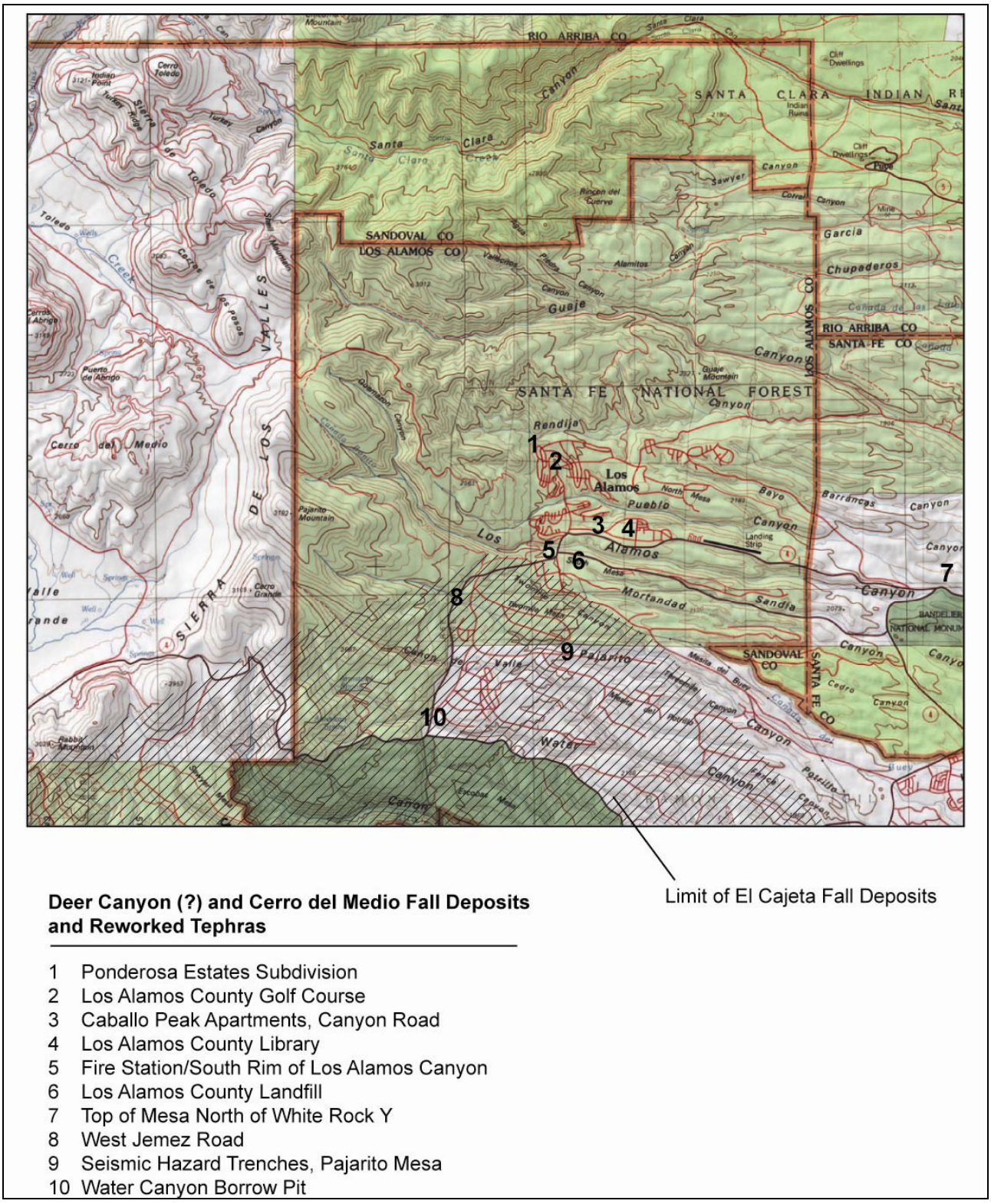

Figure 2.13. Locations where post-Bandelier fall deposits and reworked tephras have been recently recognized on the Pajarito Plateau.

Deer Canyon (?) deposits are the earliest post-Tshirege tephra recognized on the Pajarito Plateau. The best examples of these deposits are found within the Ponderosa Estates subdivision of Los Alamos near Guaje Pines Cemetery. The correlation of these tephra to the Deer Canyon Member is tentative because there is little published information about the chemical and petrographic characteristics of Deer Canyon source areas. Bailey et al. (1969) describe the Deer Canyon Member as petrographically distinct, containing abundant phenocrysts of quartz and sanidine and lacking visible ferromagnesium minerals. The fall deposits and reworked tephra exposed in the Ponderosa Estates subdivision also contain abundant phenocrysts of quartz and sanidine, but also contain visible pyroxenes. These tephra contain 250 to 350 ppm Zr and 90 to 150 ppm Rb, which distinguish them from the rhyolites of the Valle Grande Member (see Figure 2.12), but are similar to analyses for Deer Canyon lavas collected in the southwest part of Valles Caldera (100 to 130 ppm Rb and 236 to 267 ppm Zr; Broxton, unpublished analyses). More work is needed to test the correlation between these tephra and the Deer Canyon Member.

Cerro del Medio fall deposits and reworked tephra overlie the Tshirege Member at a number of locations on the Pajarito Plateau. Good exposures of these deposits occur along Canyon Road on the north side of Caballo Peak Apartments, on the north end of the Los Alamos Canyon landfill, and along Diamond Drive adjacent to the Los Alamos County golf course. Deposits are typically well-bedded and include both primary fall deposits and volcaniclastic sediments made up of aphyric pumice, obsidian and stony rhyolite clasts, and ash (Figure 2.14). Obsidian clasts within these deposits are generally less than 1 cm in diameter and probably were not important sources of archaeological obsidian. Correlation with the Cerro del Medio Member is based on stratigraphic position, the crystal-poor nature of these deposits, and the chemistry of pumices and obsidian clasts, which are similar to the lavas of Cerro del Medio (see Figure 2.12).

El Cajete pumice is widespread in the southwest part of the Pajarito Plateau (see Figure 2.3). Deposits consist of up to 1.5 m of primary fallout pumice with minimal reworking. Pumice clasts are 3 to 5 cm in diameter and are characterized a dense, poorly vesicular structure. El Cajete pumice are easily recognized by their lack of significant weathering, low phenocryst content (<5%), and salt and pepper appearance due to presence of small ferromagnesium phenocrysts.

Alluvium

Discontinuous Quaternary alluvial units overlie Bandelier Tuff as thin deposits on mesa tops and as stream deposits in canyons. Alluvial fans made up of dacite debris are interbedded with, and overlie, Valles Rhyolite tephra in the western part of LANL. Dacite cobbles occur with sandy to gravelly alluvium in canyon-floor sediments of the major drainages crossing the Pajarito Plateau. These alluvial deposits probably served as local sources for dacite cobbles found at some archaeological sites.

Figure 2.14. Cerro del Medio tephra exposed in north parking lot of Caballo Peak Apartments and along Canyon Road. These deposits consist of primary ash and pumice falls and reworked tephras. Lower photograph is a detailed view of deposit and shows white angular pumice, clasts of medium-gray stony rhyolite, and clasts of dark gray and black obsidian; quarter included for scale.

GEOLOGIC STRUCTURE

The Pajarito Plateau is on the western margin of the Española basin of the Rio Grande rift, a tectonically active region. The Pajarito fault system is the major border fault on the west side of the basin, and it delineates the boundary between the eastern Sierra de Los Valles and the western part of the plateau (Gardner et al. 2001). Continuing displacement along this fault system is reflected by Holocene movement and historic seismicity (Gardner and House 1987; Gardner et al. 1990). The Pajarito fault system is characterized by northerly trending normal faults that intertwine along their traces. Down-to-the-east displacement across the fault system produced the series of prominent fault scarps west of LANL. Post-Bandelier vertical throw on this fault system is over several hundred feet south and west of LANL but decreases north of Los Alamos Canyon where the fault system is less prominent.

In addition to the main traces of the Pajarito fault system, other faults cut the Pajarito Plateau. The Rendija Canyon fault is a normal fault trending north-south in the west-central part of the plateau; it crosses Pueblo Canyon near its confluence with Acid Canyon and Los Alamos Canyon near TA-41 but does not have clear surface expression south of Sandia Canyon. The Guaje Mountain fault parallels the Rendija Canyon fault and is projected to cross Los Alamos Canyon near TA-2 although there is no clear offset of the Tshirege Member south of North Mesa. North of LANL both of these faults have down-to-the-west movement and zones of gouge and breccia up to several meters wide and produce visible offset of stratigraphic horizons and recognizable scarps.

CHAPTER 3
OVERVIEW OF PAJARITO PLATEAU GEOMORPHOLOGY

Steven L. Reneau and Paul G. Drakos

INTRODUCTION

Los Alamos National Laboratory (LANL) is located on the Pajarito Plateau in the eastern part of the Jemez volcanic field in northern New Mexico, within the Española basin section of the Rio Grande rift tectonic province (Keller and Cather 1994) (Figure 3.1). The Jemez volcanic field lies along the Jemez lineament, a southwest-to-northeast-trending zone of structural weakness defined by a series of northeast-trending faults and volcanic centers extending from the Springerville volcanic field in Arizona to the Taos Plateau volcanic field and Capulin volcano in northern New Mexico (Laughlin et al. 1982).

The Pajarito Plateau is a dissected landscape of alternating mesas and canyons that is located between the east flank of the Jemez Mountains (the Sierra de los Valles) and White Rock Canyon of the Rio Grande (Reneau and McDonald 1996) (Figure 3.2). The Pajarito Plateau is underlain by the Tshirege Member of the Bandelier Tuff, a massive series of ignimbrites erupted from the Jemez Mountains at ca. 1.22 Ma (million years) and associated with development of the Valles Caldera (Broxton et al., this volume; Izett and Obradovich 1994; Reneau and McDonald 1996; R. Smith and Bailey 1966). The evolution of drainages since the eruption of Tshirege Member of the Bandelier Tuff has produced a landscape with a variety of landforms including gently sloping mesa tops, steep canyon walls, and canyon bottoms. This chapter provides an introduction to the geomorphologic nomenclature, history, and setting for the Pajarito Plateau at LANL.

GEOMORPHIC PROCESSES

Geomorphic processes, or physical processes acting on the earth's surface, play an integral role in determining the nature of the land surface at any point in time, how the land can be used, and whether archaeological sites will be preserved at the surface, eroded, or buried. Changes in climate, including changes in the amount, intensity, and seasonal distribution of precipitation, have strongly affected geomorphic processes and therefore the stability of the land surface (Bull 1991). The nature and density of vegetation are also affected by short-term and long-term changes in climate and by the geomorphic processes acting under that climate. In turn, geomorphic processes are affected by vegetation through their influence on surface runoff and erosion, resulting in complex interrelationships. Results of numerous investigations at LANL and in adjacent areas on the Pajarito Plateau have demonstrated that significant geomorphic changes have occurred in this area over the time period relevant for archaeological investigations, resulting in extensive sediment deposition in some areas and erosion in others (e.g., Reneau and McDonald 1996; Reneau et al. 1996a). Archaeological sites from any time period may thus be either buried or removed by erosion depending on the landscape position.

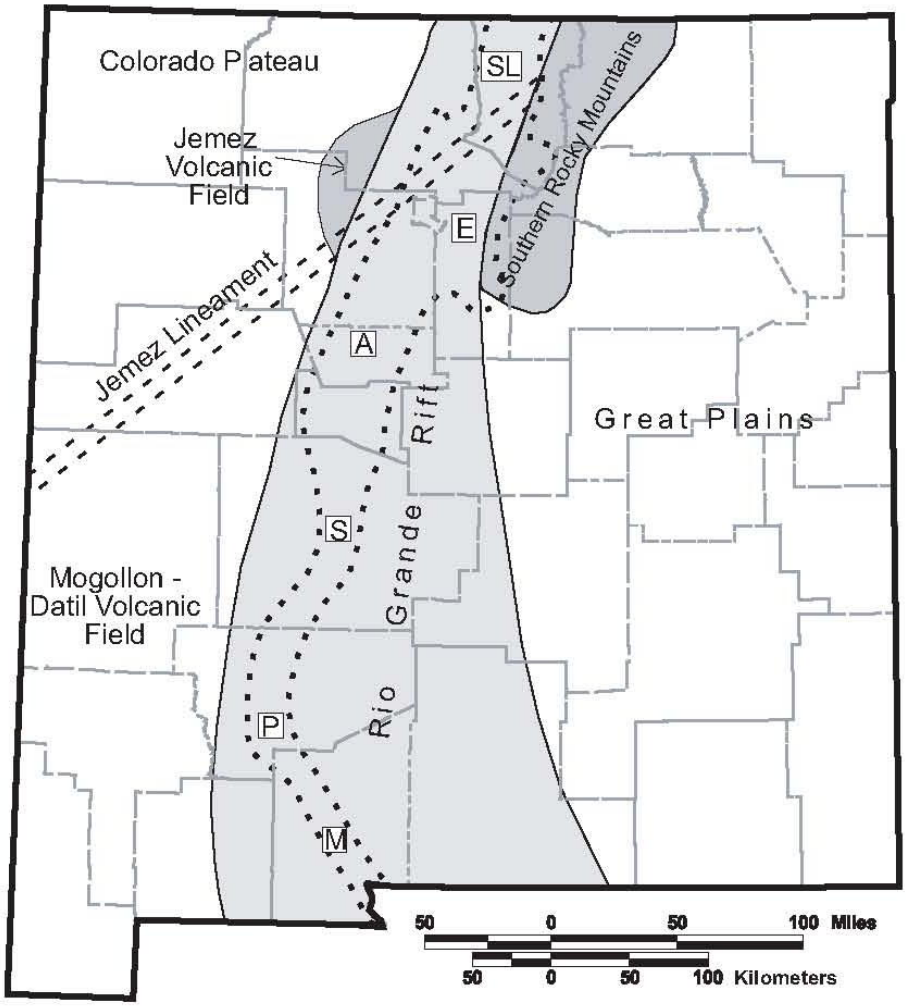

Figure 3.1. Schematic map of New Mexico showing the approximate limits of various physiographic provinces and geographic features. Major basins in the Rio Grande rift from north to south are SL = San Luis, E = Española, A = Albuquerque, S = Socorro, P = Palomas, M = Mimbres. (Modified from Keller and Cather 1994).

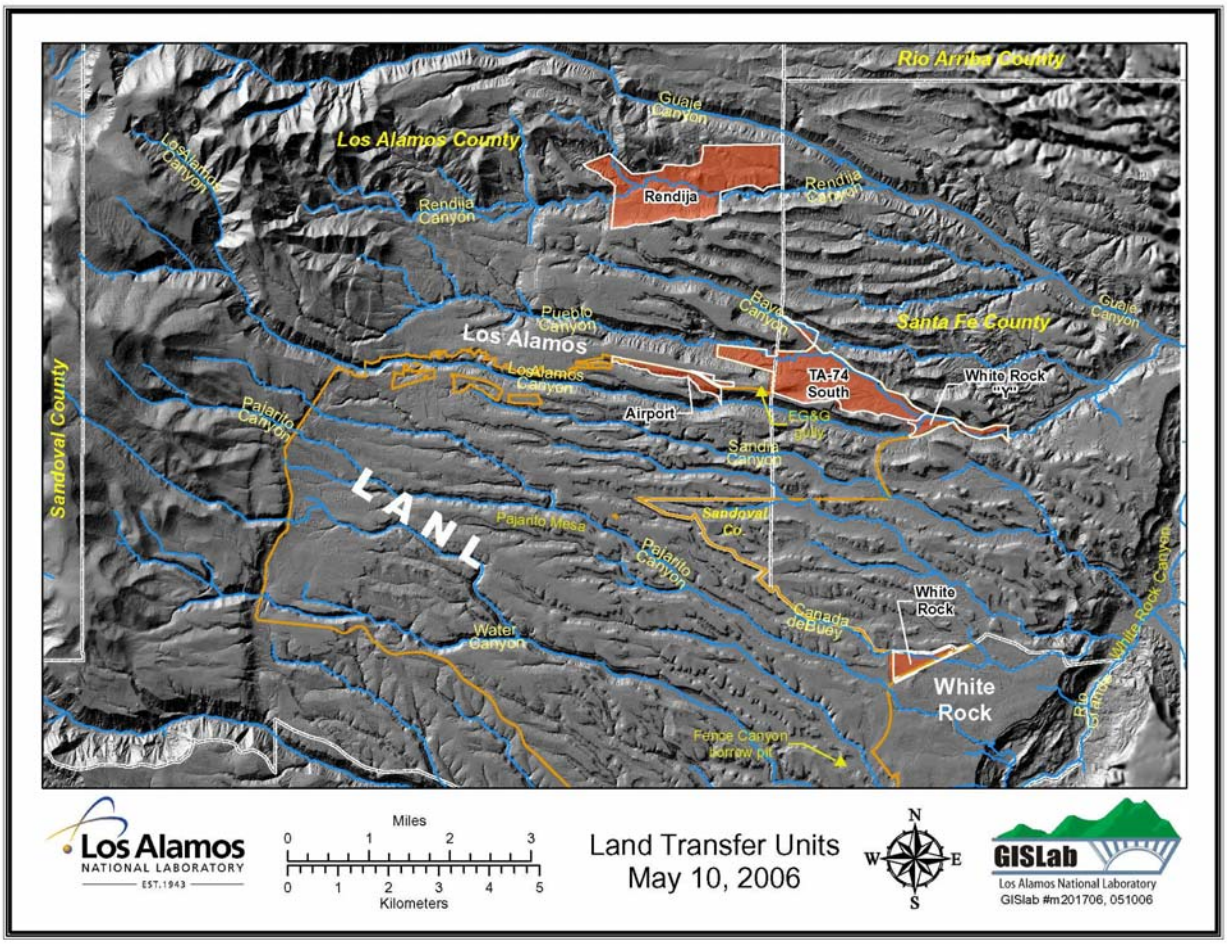

Figure 3.2. Digital elevation map of Pajarito Plateau showing some land transfer parcels.

NOMENCLATURE FOR GEOLOGIC DEPOSITS, SOILS, AND SURFACE PROCESSES

Several basic terms are used in this section for geologic deposits and related surficial materials such as soils and for relevant surface processes. General definitions of geologic terms can be found in Jackson (1997), and the specific usage in this section is discussed below.

Sediment particle size classes have been defined differently in different professions and here we use the basic divisions utilized by geologists and soil scientists. Higher-level subdivisions include "gravel" (particles >2 mm in size), "sand" (0.0625 to 2 mm), "silt" (0.002 to 0.0625 mm), and "clay" (<0.002 mm or <2 μm). Each of these size classes is further subdivided (e.g., very coarse, coarse, medium, fine, and very fine sand). These terms can apply to either individual sediment particles or to sedimentary deposits that are dominated by particles of certain sizes (e.g., sandy gravel or silty sand).

"Alluvium," "alluvial deposit," or "fluvial deposit" refer to deposits from streams or rivers and include a range of sediment texture from gravel to silt. "Channel deposit" refers to alluvium

deposited in the active stream channel at any time and is typically relatively coarse-grained. "Floodplain deposit" refers to alluvium deposited outside the active channel by floods that overtop stream banks and is typically relatively fine-grained. "Stream terrace deposit" refers to alluvium that is older than modern channel and floodplain deposits and generally occurs above the modern channel, underlying surfaces ("stream terraces") that represent channels, or floodplains abandoned following stream incision. "Alluvial fan" refers to generally cone-shaped landforms produced by the deposition of alluvium where streams become unconfined and spread out onto gentler surfaces.

"Colluvium" or "colluvial deposit" refers to generally poorly sorted deposits on hillslopes and includes material with varied origin and grain size. Colluvial deposits can be produced from rockfalls or other forms of mass wasting, such as landslides, and can contain abundant boulders. Colluvial deposits can also be produced by less dramatic processes such as the downslope movement of material on slopes following dislodgment by animals or toppling of trees. As used here, colluvium also includes deposits from shallow, dispersed surface runoff, called "slope wash" or "sheet wash." Note that in this context the distinction between "colluvium" and "alluvium" can be somewhat arbitrary because of a gradual change from dispersed runoff to channelized flow, and stratification resulting from deposition by running water can be locally found on hillslopes.

"Eolian deposit" refers to sediment deposited by wind and is generally in the silt to very fine sand range on the Pajarito Plateau. Eolian deposits dominated by silt are often referred to as "loess." Note that it can be difficult to distinguish thin and/or discontinuous eolian deposits from eolian material that has been locally reworked by surface water, and some deposits with an eolian origin may be included with "colluvium" or "alluvium" for simplicity. Also note that eolian material can be incorporated into soils without producing distinct deposits, and much of the silt, clay, and carbonate in many Pajarito Plateau soils may be supplied by wind (Eberly et al. 1996; McDonald et al. 1996; McFadden et al. 1996; Reneau and McDonald 1996; Reneau et al. 1995).

"Lacustrine deposit" refers to sediment deposited in lakes. Lacustrine deposits are commonly fine-grained and well-laminated, although coarse deposits can also occur near the margins of lakes where coarser sediment is supplied by streams.

"Bioturbation" is a process by which soils and sediments are mixed by biological agents. One common process is animal burrowing, which creates both subsurface tunnels and surficial deposits adjacent to entrances to burrows. The term "krotovina" is commonly used for filled animal burrows. The ingestion and excretion of soil by earthworms is another effective means of bioturbation at smaller scales. The toppling of trees also disrupts soils and sediment, creating "pit and mound" microtopography that gets smoothed over time (Denny and Goodlett 1956). Collectively, these processes can both obscure original sedimentary layers and result in the mixing of material from various depths, affecting the ability to decipher geologic and archaeological records. The effects of bioturbation are most pronounced near the ground surface and become more important over time. Note that some eolian or alluvial deposits on the Pajarito Plateau may be lumped with "colluvium" because bioturbation has created a poorly sorted deposit resembling colluvium whose origin can no longer be determined with certainty.

"Soil" is a term for material at the earth's surface consisting of layers or "horizons" that differ from the parent materials as the result of "pedogenic" or soil-forming processes (Birkeland 1999). At LANL, soils form on a variety of parent materials, including alluvial, colluvial, eolian, and lacustrine deposits. General subdivisions of soil profiles include "A," "B," and "C" horizons, and these horizons can be further subdivided associated with vertical variations in soil properties. "A horizons" are the uppermost soil layers and are characterized by maximum additions of organic matter and often by loss of some material to deeper horizons. "B horizons" are subsurface layers that have generally accumulated clay, iron oxides, or other material translocated from overlying horizons. "C horizons" are deeper layers consisting of generally unweathered parent material. Soil properties change over time, and older deposits have better-developed soils than younger deposits (Birkeland 1999). Soil profiles on the Pajarito Plateau can be complex, reflecting variations in geomorphic processes at the surface (Longmire et al. 1996; McDonald et al. 1996; McFadden et al. 1996; Reneau and McDonald 1996). "Buried soils" are created when significant layers of sediment cover relatively stable surfaces and at some sites several distinct soil profiles can be stacked on top of each other, recording episodic deposition. "Stripped soils" are created by erosion of the upper parts of soil profiles, for example exposing B horizons at the surface. "Cumulative soils" are formed at sites experiencing relatively slow deposition, creating relatively weak but relatively thick A and B horizons. Identification of buried soils and stripped surfaces is integral to identification of occupation surfaces, correlation between sites, and evaluation of relative age of sites based on soil-stratigraphic relationships.

DIVISIONS OF GEOLOGIC TIME

Several general divisions of geologic time are relevant for this discussion. At the highest level, the last 1.8 million years are referred to as the Quaternary period (Van Couvering 1997), which is subdivided into the Pleistocene and Holocene epochs. The term "late Quaternary" includes the late Pleistocene and the Holocene, which is the time period relevant for archaeological investigations in North America. The Pleistocene-Holocene boundary is commonly placed at 10,000 radiocarbon years before present (^{14}C yr BP) (Hopkins 1975), although this is an arbitrarily chosen date within a period of transitional climate and may be subject to change (Morrison 1991). However, 10 ^{14}C ka (ka = thousands of years BP) roughly corresponds to a time of major geomorphic changes on the Pajarito Plateau and is an appropriate boundary for this discussion. When calibrated to a dendrochronological time scale (to correct for variations in the ^{14}C/^{12}C ratio in the atmosphere over time), 10 ^{14}C ka is equivalent to about 11.35 to 11.55 cal (calibrated) ka or about 9400 to 9600 cal BC. (A recent calibration of the radiocarbon time scale is presented in Stuiver et al. 1998, and we use their conversions here.) The Holocene has no formal subdivisions, and here we use the general terms "early," "middle," and "late" to refer to roughly the first third, second third, and last third of the Holocene.

Geomorphic History

In this section we discuss the geomorphic history of the Pajarito Plateau since about 15 ^{14}C ka (ca. 17.4 cal ka), or since the latest Pleistocene, based on available studies. Emphasis is given to

dated deposits and soils from different periods and in different landscape positions and their implications for variations in environmental conditions since 15 ^{14}C ka.

This section uses radiocarbon ages in reference to the geomorphic history of the area because this dating method has provided the most abundant age control for prehistoric deposits on the Pajarito Plateau and in nearby areas. Also, because radiocarbon calibration has changed over time and because many studies utilizing radiocarbon dating have not provided calibrated dates, direct reference to radiocarbon dates allows easier comparison between studies.

Latest Pleistocene

The period between 15 and 10 ^{14}C ka was a time of transitional climate after the peak of the late Wisconsin glaciations in North America and before establishment of the more modern Holocene climate. Paleoenvironmental records in the region, including the record of lake level changes in the Estancia basin (B. Allen 1991), indicate a generally moister climate than at present with significant climatic fluctuations. Deposits dating to the period between 15 and 10 ^{14}C ka on the Pajarito Plateau indicate significantly different geomorphic conditions than during the Holocene that were probably associated with the unique climatic conditions at that time.

Relatively few latest Pleistocene radiocarbon dates have been obtained from the Pajarito Plateau, and available information suggests that the landscape was relatively stable. Some evidence of colluvial deposition has been found, but there was apparently minimal sediment deposition or incision along stream channels. Out of a total of 55 alluvial deposits that had been dated by 1996, only a single site had yielded a date in this range (Reneau and McDonald 1996). This date, 11.6 ^{14}C ka, was obtained from a drill hole sample at a depth of 6.1 m (20 ft) beneath the bottom of the north fork of Ancho Canyon in LANL Technical Area (TA) 39 (Figure 6A of Reneau et al. 1996a). It is similarly expected that in many canyons on the Pajarito Plateau, alluvium of this age, if present, would also be deeply buried.

Dates very close to the Pleistocene-Holocene boundary have been obtained from buried soils at several sites on the Pajarito Plateau and provide evidence for a relatively stable landscape at about 10 ^{14}C ka. Examples include a buried floodplain soil beneath the north fork of Ancho Canyon (9.9 ^{14}C ka, Reneau et al. 1996a, Figure 6A); a buried, organic-rich deposit within a shallow tributary drainage to Cañada del Buey in TA-54 (9.7 and 10.1 ^{14}C ka, Reneau et al. 1996a, Figure 7); an extensive buried soil in a shallow mesa top drainage south of Frijoles Canyon in Bandelier National Monument (10.3 ^{14}C ka, Reneau and McDonald 1996); and a buried soil beneath an alluvial fan at the western margin of LANL in TA-69, between Pajarito Canyon and Two Mile Canyon (10.1 ^{14}C ka, Reneau et al. 2002). McFaul and Doering (1993) report a radiocarbon date of 9.4 ^{14}C ka from humate in a buried soil south of Water Canyon in TA-70, and their sample site is inferred to be analogous to the sites mentioned above.

Slightly older colluvial deposits, dating to the period between 15 and 10 ^{14}C ka, have been identified at several sites on the eastern Pajarito Plateau beneath the buried soils discussed above and suggest at least local deposition of colluvium during this period. One site is along the north wall of Fence Canyon in TA-70, where a 12.3 ^{14}C ka date has been obtained from the upper part

of a buried colluvial deposit (Reneau and McDonald 1996, Figure 1-22). Analogous late Pleistocene units on mesa tops may be recorded by deposits studied by McFaul and Doering (1993) north and south of Water Canyon in TA-70 that are bracketed by dates on humate in buried soils of 9.4 and 15.7 to 16.0 ^{14}C ka (see also Reneau and McDonald 1996:58–60). Additional dates of 11.5 to 13.8 ^{14}C ka have been obtained from buried soils and colluvium in Rendija Canyon and on Pajarito Mesa at TA-67 (McDonald et al. 1996; Reneau et al. 1995), indicating local preservation of colluvium of this age at sites farther west on the plateau.

In contrast to the apparent complacency of geomorphic processes during the latest Pleistocene on the Pajarito Plateau, data from White Rock Canyon indicate a very dynamic landscape along the Rio Grande. In particular, the presence of lacustrine deposits demonstrate that large lakes formed at least three times between ca. 13.7 and 12.4 ^{14}C ka, produced by the damming of the river by landslides (Reneau and Dethier 1996). Unique ecological conditions would have existed along the Rio Grande at these times.

Early to Middle Holocene

Extensive deposits of early to middle Holocene age exist on the Pajarito Plateau in a variety of landscape settings, including alluvial, colluvial, and eolian material. These deposits document a substantial flux of sediment that was apparently derived from extensive erosion in upland areas and on slopes. This sediment supply exceeded the capacity of local transport processes acting under the Holocene climate, resulting in widespread aggradation of canyon bottoms and associated deposition along tributary drainages and on slopes, burying latest Pleistocene soils and stream channels. Significant eolian deposition also apparently occurred at this time. There is also some evidence that larger floods occurred during this period than in the latest Pleistocene, causing relatively high rates of stream incision into bedrock in some canyons.

Channels with drainage areas that range from the smallest first-order basins on mesa tops to the largest watersheds draining the Jemez Mountains have provided evidence for significant sediment deposition in the early to middle Holocene, indicating regional controls on erosion and sedimentation that affected a variety of vegetation communities and terrain (Drakos et al. 1996; Reneau and McDonald 1996; Reneau et al. 1996a). In Frijoles Canyon in Bandelier National Monument, up to 13 m (43 ft) of coarse alluvium was deposited before 6.2 ^{14}C ka, deposits which have now been exposed following stream incision (Reneau 2000). In Mortandad Canyon in TA-5, samples from drill holes indicate that 10 to 12 m (33 to 39 ft) of alluvium has been deposited since 7.2 to 7.8 ^{14}C ka (Reneau et al. 1996a; Figure 6B), and the base of the Holocene section is likely deeper. In Los Alamos Canyon, drill hole data show that alluvial deposits bury El Cajete pumice and indicate that 10 m (33 ft) of aggradation has occurred since ca. 50 to 60 ka (Broxton et al. 1994; Drakos et al. 1996). On the western margin of LANL in TA-69 between Pajarito Canyon and Two Mile Canyon, a trench through a small alluvial fan deposited along a drainage off the Pajarito fault escarpment provided excellent constraints on the timing of initial Holocene aggradation, exposing alluvial deposits at a depth of 2 to 2.5 m that were dated at 9.4 ^{14}C ka, overlying a buried soil dated at 10.1 ^{14}C ka (Reneau et al. 2002). North of Water Canyon, on another alluvial fan at the base of the Pajarito fault escarpment, similar dates of 9.4 to 9.6 ^{14}C ka were obtained from near the top of a 6-m- (20-ft-) thick deposit, providing

additional support for significant deposition at the very beginning of the Holocene (Gardner et al. 2001). Significant early Holocene deposition has also been found along first-order drainages on mesa tops farther east on the Pajarito Plateau, including a location in TA-73 near the Los Alamos town site where deposition began some time before 7.9 to 8.1 ^{14}C ka, burying a shallow channel on bedrock (Longmire et al. 1996; Reneau et al. 1996a:Figure 3). Roughly contemporaneous deposition in White Rock Canyon is documented by a date of 10.0 ^{14}C ka from the lower part of a small alluvial fan above a late Pleistocene Rio Grande terrace (Reneau and Dethier 1996).

Significant deposition of slopewash colluvium in the early to middle Holocene has been documented at several sites. At a borrow pit exposure on the north wall of Fence Canyon in TA-70, about 2.7 m (9 ft) of slopewash material accumulated between 7.9 and ~4 ^{14}C ka (Reneau and McDonald 1996:Figure 1-22). Notably, an Archaic hearth dated at 4.7 ^{14}C ka was exposed nearby within the slopewash deposits, demonstrating prehistoric use of this geomorphic setting and the potential for site preservation by burial (Reneau and McDonald 1996:Figure 1-23). On the mesa south of Frijoles Canyon in Bandelier National Monument, a similar chronology has been obtained, with dates of 8.6 to 8.7 ^{14}C ka obtained from the lower part of a 1.6-m-thick slopewash deposit above a buried soil that yielded a 10.3 ^{14}C ka date (Reneau and McDonald 1996). Early Holocene slopewash deposits dated at 7.0 ^{14}C ka also overlie a buried, organic-rich deposit within a shallow tributary drainage to Cañada del Buey in TA-54 (Reneau et al. 1996a:Figure 7). Although early to middle Holocene deposits are present at several locations, such deposits are typically buried by younger deposits. Early to middle Holocene deposits are likely discontinuously preserved and may be absent from many locations on the Pajarito Plateau.

Evidence for eolian deposition in the early Holocene has been found in one area, where trenches excavated on Pajarito Mesa in TA-67 exposed fine-grained deposits that yielded dates of 9.3 to 9.5 ^{14}C ka overlying older soils (Kolbe et al. 1994; Reneau et al. 1995, 1996a). The texture and the stratigraphic setting of these deposits both argue for an eolian source for the material, and it is expected that similar deposits occur on other mesas. Two of the dated sites on Pajarito Mesa were locations with oxidized tuff clasts that were interpreted as Paleoindian fire pits constructed during a period of mesa top aggradation (e.g., see Figure 2A of Reneau et al. 1996a), indicating the potential preservation of similar sites elsewhere on the Pajarito Plateau.

Evidence for the occurrence of significantly larger floods on the Pajarito Plateau in the early and middle Holocene than in the late Pleistocene is provided by stream terrace sequences in Rendija Canyon and Frijoles Canyon. Stacked Holocene terraces in each canyon record periods of channel stability and lateral cutting that alternate with incision into bedrock. Average Holocene incision rates have been an order of magnitude higher than Pleistocene rates, suggesting recurring large floods capable of stripping gravel from the streambeds and leading to deeper incision (Reneau 2000; Reneau and McDonald 1996).

Late Holocene

Late Holocene deposits on the Pajarito Plateau are generally similar to early and middle Holocene deposits, suggesting similar geomorphic processes, although evidence from several

sites indicates that rates of overall sediment deposition may have decreased in the late Holocene, locally replaced by erosion.

Late Holocene alluvium is widespread in canyons on the Pajarito Plateau, including the lower terraces in Rendija and Frijoles canyons, although in both of these canyons the thickest and/or widest terrace deposits were deposited in the early or middle Holocene (McDonald et al. 1996; Reneau 2000; Reneau and McDonald 1996). Progressive aggradation through the late Holocene is indicated in several canyons that head on the Pajarito Plateau. In Sandia Canyon in TA-53, 4 m (13 ft) of alluvium has been deposited since 2.8 ^{14}C ka (Reneau and McDonald 1996; Figure 1-10), and in Cabra Canyon 4 m (13 ft) has been deposited since about 3.7 ^{14}C ka (Gardner et al. 1990, 2003; Reneau and McDonald 1996:Figure 2-31). The late Holocene section is apparently thinner in other canyons, such as Ancho Canyon in TA-39 where 1.6 m (5 ft) of alluvium has been deposited since 3.0 ^{14}C ka (Reneau and McDonald 1996: Figure 1-29), and the north fork of Ancho Canyon, where a date of 2.9 ^{14}C ka was obtained from a depth of 0.9 m (3 ft) (Reneau et al. 1996a: Figure 6A).

Late Holocene colluvium is present in many areas, including along canyon walls and at the margins of floodplains, demonstrating active erosion and transport of material off hillslopes. Examples include Los Alamos Canyon in TA-62, where 1.4 m (5 ft) of colluvium has accumulated since 3.1 ^{14}C ka (Longmire et al. 1996), and Cañon de Valle in TA-16, where up to 1.9 m (6.2 ft) of colluvium has accumulated since 3.8 ^{14}C ka (Gardner et al. 2001). In other areas, however, colluvial deposits from the early and middle Holocene have been dissected, and erosion has predominated instead of deposition. At the site in Fence Canyon in TA-70 discussed previously, deposition apparently stopped some time after 4.4 ^{14}C ka, and about 4 m (13.1 ft) of incision has subsequently occurred (Reneau and McDonald 1996). Many areas with colluvial soils on the eastern Pajarito Plateau are currently experiencing rapid erosion, including an intensively studied mesa top drainage basin south of Frijoles Canyon in Bandelier National Monument (Wilcox et al. 1996a, 1996b). Erosion is impacting archaeological resources in some of these areas, and 1 liter of potsherds and lithic fragments were collected at a sediment trap in the study area mentioned above after a single runoff event in 1995. Erosion was also apparently active during occupation of some ancestral Puebloan sites, as apparent prehistoric check dams have been seen within a gullied area north of the Tsirege ruins in the Cañada del Buey basin (Reneau and McDonald 1996:54–56).

Late Holocene eolian deposits have been observed at several locations on the Pajarito Plateau. The trenches excavated on Pajarito Mesa at TA-67 provided evidence for thin but extensive late Holocene eolian deposits, averaging about 20 cm thick on the mesa (Kolbe et al. 1994; Reneau et al. 1995, 1996). These deposits date to 0.7 ^{14}C ka or less and cover a series of subsurface archaeological sites near ancestral Puebloan ruins (Reneau et al. 1996a:Figure 2b). Similar thin, discontinuous post-Puebloan age deposits not greater than 20 to 30 cm thick were noted during archaeological excavations on the Mesita del Buey mesa top (Steen 1982). This evidence for young deposition contrasts with evidence for erosion elsewhere on mesa tops, particularly near their margins where tuff bedrock is commonly exposed, and illustrates some of the great variability of surface processes on the Pajarito Plateau.

Late Holocene deposits also occur in White Rock Canyon, in part representing significantly different environments than are found on the Pajarito Plateau. For example, at one location along the Rio Grande 2.1 to 2.6 m (6.8 to 8.5 ft) of fine-grained sediment has been deposited since 2.9 ^{14}C ka directly above a gravel bar along the Rio Grande and may represent Rio Grande floodplain deposits or eolian deposits (Reneau and Dethier 1996; Reneau and McDonald 1996:30). The dated material was in association with fire-cracked stones and indicates burial of an Archaic campsite along the river.

Implications for Site Preservation

Geomorphic processes since the latest Pleistocene on the Pajarito Plateau have resulted in spatially and temporally complex patterns of erosion and deposition that provide abundant opportunities for preservation of archaeological sites of a variety of ages in a range of landscape positions and that also results in destruction of sites by erosion.

The highest potential for site preservation exists along small drainage channels on mesas, on alluvial fans, and in canyon bottoms, where net deposition of alluvium and colluvium has occurred during the Holocene, and on the more stable parts of mesa tops where erosion has been minimal or where deposition of eolian sediment has occurred. Stable parts of fluvial terrace surfaces that have experienced net deposition of colluvium or eolian sediment also have excellent site preservation potential. In contrast, mesa margins have the lowest potential for site preservation due to surface runoff that has eroded soils and exposed bedrock in many areas, and any artifacts in these areas may either have been transported to the site or left as a lag following erosion of associated deposits. Colluvial slopes have variable site preservation potential that is controlled by local geomorphic factors, including slope aspect, relative site position on a particular hillslope, sediment supply, and slope gradient above and below a particular site.

The common presence of a buried soil dating to near the Pleistocene-Holocene boundary beneath early Holocene alluvium or colluvium indicates the potential preservation of Paleoindian sites in many areas, although in canyon bottoms strata of this age may be buried beneath many meters of sediment. The potential for preservation of Paleoindian sites on mesa tops has been demonstrated in an area where apparent fire pits dating to 9.3 to 9.5 ^{14}C ka were found within deposits of inferred eolian material. However, available exposures have indicated great variability in the nature and age of deposits on mesa tops that makes it difficult to predict where sites of a given age might be found. In addition, mesa tops and other relatively stable geomorphic settings where deposition rates are low should be most prone to the mixing of soil and associated artifacts by bioturbation, helping to obscure the archaeological record. This problem should be most severe at older sites that are at or near the ground surface.

The local occurrence of middle and late Holocene alluvial and colluvial deposits also indicates potential preservation of Archaic sites in a range of settings. Buried Archaic sites have been found in colluvial deposits along the margins of canyon bottoms, although these are also commonly areas experiencing erosion in the latest Holocene, contributing to the loss of older sites and preventing burial of younger sites. In comparison to Paleoindian sites, Archaic sites

could be much less deeply buried in areas of deposition and less affected by bioturbation near the surface, although the same caveats apply.

Widespread late Holocene deposits that are contemporaneous with or that post-date Puebloan occupation of the area are more areally extensive than earlier Holocene deposits, providing greater opportunity for site preservation following burial. Significant deposits from this period are in the bottoms of major canyons, and the potential for burial should be highest on late Holocene floodplains and near the base of slopes where late Holocene colluvium has been deposited. Additional deposition has occurred on mesa tops where eolian sediment has accumulated, providing local opportunities for preservation of Puebloan sites. Some colluvial slopes below ridge tops and at slope breaks between steeper slopes above and shallower slopes below have also experienced late Holocene deposition and offer good potential for site preservation. Of interest is the apparent use of some areas by Pueblo people during periods of erosion and landscape dissection, and some sites in eroded areas may provide evidence of how they adapted to and utilized an eroding landscape.

SOIL DEVELOPMENT AND GEOMORPHIC HISTORY

The nature of soils and surficial deposits are controlled by environmental conditions acting during their development, and they can therefore provide various kinds of paleoenvironmental information relevant for archaeological investigations.

The characteristics of surface and buried soils provide primary information about the stability or instability of the land surface at various times and can provide supplemental information about climate and/or vegetation. For example, a strongly developed buried soil indicates an extended period of land surface stability followed by some environmental change that caused sediment deposition at that site. Alternatively, a weakly developed soil or a thickened (cumulative) soil indicates a briefer period of stability or gradual sediment accumulation, respectively. Certain soil characteristics, such as gleying or mottling, can indicate the presence of prolonged periods of saturation or fluctuating water levels and, conversely, the absence of these characteristics can indicate that unsaturated conditions prevailed during soil development (Birkeland 1999). Certain soil properties are some times associated with specific vegetation conditions, and their presence may provide ecological information. For example, mollisols are a type of soil with thick dark surface horizons that generally form under grasslands, whereas other soil types such as alfisols, may form under forest cover. Such lines of evidence have been used to infer changes from forest to grassland at some sites with stacked soils with different characteristics (McFaul and Doering 1993). Weakly developed soils that are likely formed in late Holocene deposits burying Ancestral Puebloan sites are likely entisols or inceptisols. Better-developed soils burying Archaic or Paleoindian sites on the Pajarito Plateau have formed during a predominantly semi-arid climate regime, often have carbonate B horizons, and are likely aridisols.

The characteristics of surficial deposits provide primary information about geomorphic processes during their deposition, and in some circumstances can provide supplemental inferences about other aspects of the environment. For example, particle size and sedimentary characteristics of associated deposits can indicate whether an archaeological site was in or near an active alluvial

or colluvial setting or at a location subject to eolian deposition, or was alternatively at a relatively stable or eroding site on the landscape. Geomorphic processes can be affected by climatic variables that are too short in duration to be preserved in other paleoenvironmental records, such as tree rings, and the record of geomorphic changes may thus provide unique insight into some important environmental characteristics. For example, while tree rings record variations in annual precipitation, particularly precipitation during the winter months, major environmental changes such as channel incision or arroyo cutting can be caused by changes in the intensity of summer thunderstorms that might not be detected in the tree ring record (Leopold 1951).

GEOMORPHIC SETTING OF LAND TRANSFER PARCELS

Five land conveyance parcels located on the Pajarito Plateau at LANL have been the focus of this investigation. Fieldwork was conducted within the Airport (A-3, A-7, and A-5-1), White Rock (A-19), TA-74 (A-18-a), White Rock Y (C-2), and Rendija (A-14) land transfer parcels (Figure 3.2). Geomorphic maps, detailed descriptions of surficial geology, soils, and the geomorphic history of each tract are presented in Reneau and Drakos (Chapter 57, Volume 3). The following is a brief introduction to the geomorphic setting of each tract.

The White Rock Tract is within the Cañada del Buey watershed (Figure 3.2) and includes part of the active stream channel and adjacent floodplains, colluvial slopes, and alluvial fans. Colluvium throughout most of the parcel overlies basalt of the Cerros del Rio volcanic field, and some areas of the parcel comprise stripped basalt bedrock. The Tshirege Member of the Bandelier Tuff, which overlies the Cerros del Rio basalt, is present as an isolated mesa in the western part of the parcel.

The Airport Tract includes a gently east-sloping mesa between a tributary to Pueblo Canyon on the north and DP Canyon, a tributary to Los Alamos Canyon, on the south (Figure 3.2). Bedrock beneath the mesa consists of the Tshirege Member of the Bandelier Tuff. The mesa is capped by eolian sediments and colluvium that thins to exposed bedrock near the mesa edge.

The Rendija Tract is located within the Rendija Canyon watershed and includes part of the active stream channel and adjacent floodplains, tributary drainages, fluvial terraces, colluvial slopes, ridge crests, and mesitas. Rendija Canyon possesses what may be the most extensive and best preserved set of stream terraces on the Pajarito Plateau, locally including at least five Pleistocene surfaces and four Holocene surfaces (McDonald et al. 1996; Reneau and McDonald 1996). The terrace sequence is well-preserved in the central and western part of the tract, whereas the eastern part of the tract includes colluvial slopes below high ridges leading to tributary drainages to Rendija Canyon with narrow strips of young alluvium and relatively poor preservation of terraces. Rendija Canyon has incised below the Tshirege Member of the Bandelier Tuff, and surficial deposits are underlain by Tschicoma Formation dacite lavas Puye Formation fanglomerates, Cerro Toledo interval (unit Qct) pumice beds and alluvium, and non-welded tuff and pumice beds of the Otowi Member of the Bandelier Tuff.

The TA-74 South Tract is located in a relatively broad part of lower Pueblo Canyon (Figure 3.2). TA-74 South Tract geomorphic features include the active stream channel and adjacent floodplains of Pueblo Canyon, higher stream terraces of Holocene and Pleistocene age, and areas of colluvium and alluvial fans on the side slopes and along tributary drainages. The part of Pueblo Canyon comprising the TA-74 South Tract has incised below the Tshirege Member of the Bandelier Tuff, and surficial deposits are underlain by Pliocene fanglomerates of the Puye Formation and non-welded tuff and pumice beds of the Otowi Member of the Bandelier Tuff.

The White Rock Y Tract is located in Los Alamos Canyon and includes the confluence with Pueblo Canyon (Figure 3.2). White Rock Y Tract geomorphic features include the channel of Los Alamos Canyon, incised into basalt bedrock, and an adjacent stream terrace that is overlain by colluvium derived from a higher, Pleistocene-age terrace. The higher terrace is bordered on the south by colluvial slopes that lead up to a Bandelier Tuff-capped mesa south of the tract. Approximately 15-m- (49.2-ft-) high basalt cliffs border the modern stream channel east of the confluence with Pueblo Canyon.

CHAPTER 4
ECOSYSTEMS OF THE PAJARITO PLATEAU AND EAST JEMEZ MOUNTAINS: LINKING LAND AND PEOPLE

Teralene S. Foxx

INTRODUCTION

After the volcanic eruptions in the Jemez Mountains over a million years ago, development of vegetation on the ash-hewn Pajarito Plateau and in the remnant mountains was influenced by relief and climate and, more recently, by human interaction. Volcanism and erosion influenced the development of the soil through factors like rainfall, vegetation, topography, and time. Geofloras were influenced by drying climate and mountain building. Conversely, the developing soils influenced vegetation through chemical make-up, texture, and water availability (Dick-Peddie 1993). As the environment of the Pajarito Plateau and the Jemez Mountains underwent geologic change, various plant communities became established with woodlands at lower, drier elevations and forests at higher, cooler locales (Figure 4.1).

The erosive power of water developed watercourses that incised deep canyons into the plateau. Riparian zones developed in canyon bottoms, dominated by water-loving species that grew within the area mediated by water flowing permanently or ephemerally through the canyons. Throughout the centuries, before humans inhabited the area, a dynamic process of change took place. Fire, windfalls, floods, and changing weather patterns influenced ecosystems—some times within a microhabitat or within the vast landscape. Some 10,000 years ago, humans entered into the ecosystem for the first time. Although their impact was gradual and largely unnoticed until about 1000 years ago, they did bring change. As people aggregated on the land and began to use it more intensively, the landscape was modified. Using data from ethnobotanical, ethnozoological, and archaeological studies, this chapter describes the ways people used the Pajarito Plateau and the adjacent Jemez Mountains and looks at how they impacted their environments.

LOS ALAMOS NATIONAL LABORATORY AND THE PAJARITO PLATEAU

Los Alamos National Laboratory (LANL) is situated on the Pajarito Plateau. The Pajarito Plateau consists of a series of narrow mesas and deep canyons that trend east-southeast from the Jemez Mountains to the Rio Grande. The defining feature of the plateau is the Tshirege Member of the Bandelier Tuff, a massive series of ignimbrites or "ash-flow tuffs" that erupted from the Jemez Mountains caldera. The Tshirege Member buried most of the former topography between the Jemez Mountains and the Rio Grande thereby creating a new landscape. The subsequent erosion of this formation has resulted in the distinctive topography of the Pajarito Plateau and LANL (Broxton et al., this volume; LASL 1976:4–6; Reneau and McDonald 1996:3).

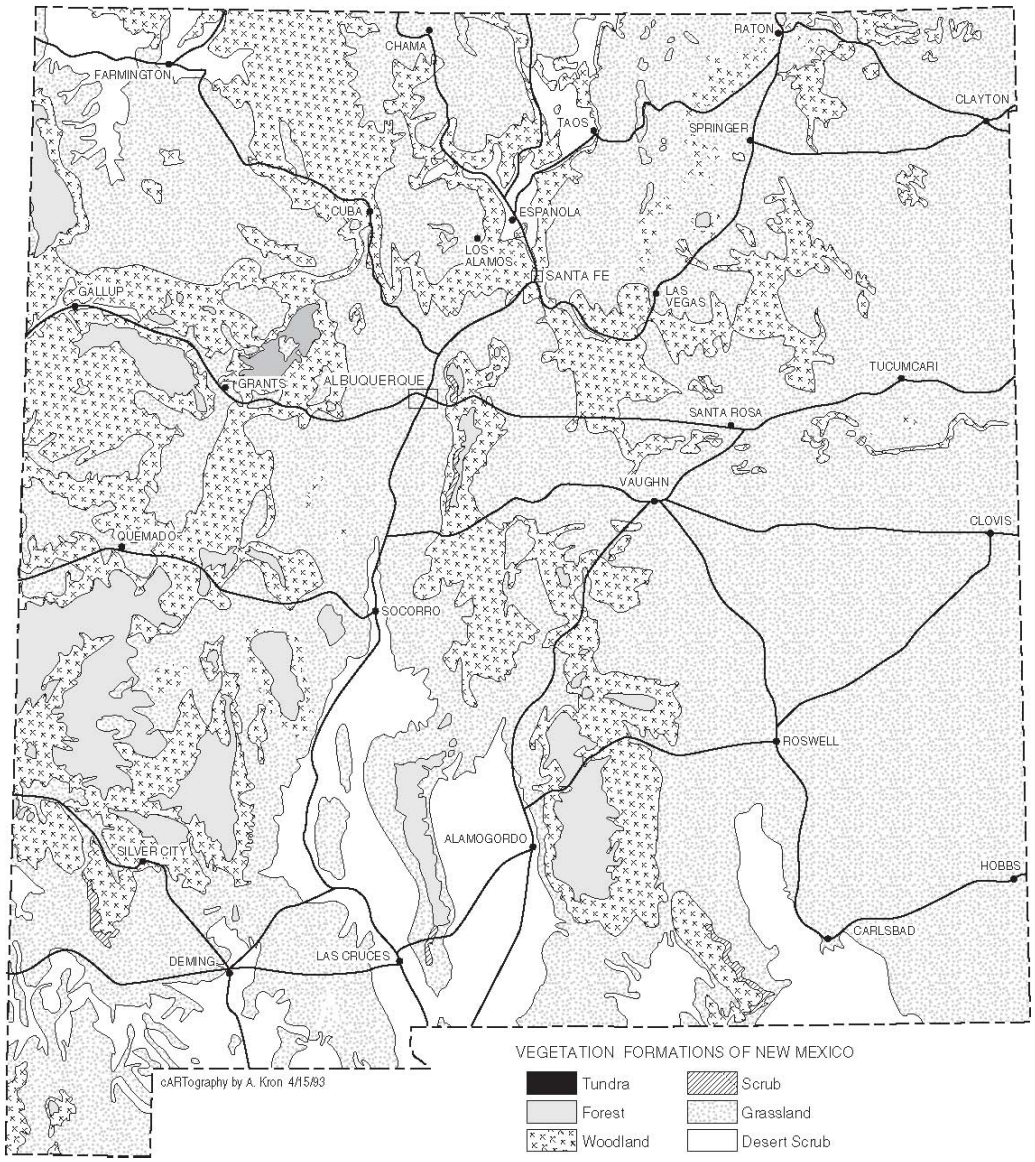

Figure 4.1. Established vegetation types of the Los Alamos area in relation to the rest of New Mexico.

LANL contains several distinct environmental zones. The elevation gradient at LANL is approximately 800 m (2400 ft), ranging from the Rio Grande Valley (1620 m; 5400 ft) to the base of the Jemez Mountains (2340 m; 7800 ft). This elevation change and a complex geologic history have created several different climatic zones, soil types, vegetative zones, and animal habitats within the confines of LANL (Balice et al. 1997:4–6; LASL 1976:2–6; Reneau and McDonald 1996:1–3). Topography is typically rugged and undulating and contains a number of mesa tops and canyon bottoms and their associated steep talus slopes and cliffs. Soils in the canyon bottoms and on the mesa tops of the south and southeastern part of LANL are mostly aridisols and entisols, with an abundance of alluvium on the steep slopes, large tuff rock outcrops, volcanic rock outcrops, talus slopes, and gravelly and sandy loams. Mesa tops are generally associated with areas of high agricultural potential.

Climate of the Pajarito Plateau

Los Alamos has a semiarid, temperate mountain climate. Mean temperatures vary with altitude and average 5°F higher in and near the Rio Grande Valley (1980 m; 6500 ft) and 5°F to 10°F lower in the nearby Jemez Mountains (2600 to 3050 m; 8500 to 10,000 ft) (Bowen 1990:3–17). Mean precipitation values for the Pajarito Plateau over the last 30 years show that higher elevations near Los Alamos receive approximately 48 cm (19 in.) of rain per year, while lower elevations in the piñon-juniper zone near White Rock receive approximately 34 cm (13.5 in.).

Winter temperatures on the Pajarito Plateau range from 15°F to 25°F at night and 30°F to 50°F during the day. Cold Arctic air masses occasionally invade the Los Alamos area from the north and east, but often the shallow layer of coldest air is dammed to the east by the Sangre de Cristo Mountains. Temperatures in the Los Alamos area occasionally will drop to 0°F or below. The freeze-free growing season of 157 days in Los Alamos is relatively short, while the normal growing season in White Rock is even shorter at 145 days. Above 2743 m (9000 ft), frosts can occur during any time throughout the year (Bowen 1990:3–17; Reneau and McDonald 1996:2–3). Summer temperatures are in the 70s and 80s (Bowen 1990, Table 7). Climatic information for the County of Los Alamos extends back to 1910, while that for the community of Española dates back to 1895, and to 1924 for Bandelier National Monument (Bowen 1990; Scurlock 1998).

The normal annual precipitation around Los Alamos, including rainfall and snowfall, totals approximately 46 cm (18 in.). Annual precipitation decreases rapidly toward the Rio Grande Valley, with the normal White Rock precipitation falling somewhere around 33 cm (13 in.). Annual precipitation at higher elevations in the Jemez Mountains is normally around 51 cm (20 in.). In general, the precipitation patterns of the Pajarito Plateau region are characteristic of a semiarid climate where precipitation amounts vary considerably from year to year. Over a 69-year period, the annual precipitation extremes ranged from 17.77 to 77.06 cm (16.08 to 30.34 in.) (Balice et al. 1997:1–12; Bowen 1990:3–17).

Monsoon season on the Pajarito Plateau spans the months of July and August. Convection of warm air over the Jemez Mountains causes thundershowers to develop during the afternoons and early evenings, and these drift over the plateau and cause brief, but intense, rains (Bowen 1990:3–17). Westerly winds push the thunderstorms above the Jemez Mountains towards Los Alamos. The large-scale atmospheric flows transport moisture from the Gulf of Mexico during the summer monsoons, and from the Pacific Ocean during the winter, spring, and fall. Nearly 40 percent of the annual precipitation falls during the monsoon months. Although summer precipitation is heavily weighted toward the monsoons, winter precipitation falls primarily as snow. Accumulations usually approach upwards of 130 cm (51 in.) seasonally, but snowfall levels vary considerably from year to year.

Water Resources

Water is one of the most important elements for permanent habitation. The Pajarito Plateau has both permanent and ephemeral streams and some springs. Few of the canyons of the Pajarito

Plateau have perennial water. Large settlements are associated with canyons that have perennial water (e.g., Frijoles Canyon, Santa Clara Canyon) or springs (e.g., Pajarito Canyon). Pajarito Canyon has a perched aquifer where the water emerges to the surface. Throughout the plateau, there are areas where inhabitants also used water-collecting devices (Steen 1977).

In addition to the permanent and ephemeral streams on the Pajarito Plateau, there are 27 springs that discharge from formations in White Rock Canyon (Purtymun et al. 1980). These springs are habitats for various obligatory and facultative wetland species (Foxx and Tierney 1980), including the giant helleborine orchid (*Epipactis gigantea*).

Water resources and riparian zones are important habitats for many plants and animals. Various plant species were important to the Pueblo and Hispanic residents. Wetland plants were indicators of water; some wetland taxa were used for food and medicine, while others provided building material (e.g., cattail) (Table 4.1). Additionally, wetland and riparian areas attracted greater quantities of game.

Table 4.1. Wetland plants used by Pueblo and Hispanic residents.

Scientific Name	Common Name	Occurrence	Spring	Summer	Habit	Wetland*
Acer glabrum	Rocky Mountain maple	locally common	x		tree	FACW, FAC
Acer negundo	boxelder maple	locally common	x		tree	FAC, FACW
Alnus tenufolia	alder	locally common	x		tree	FACW
Berula erecta	water parsnip	not common		x	perennial	OBW
Betula occidentalis	western water-birch	locally common		x	tree/shrub	FACW
Cyperus aristatus	flatsedge	locally abundant			Perennial	FACW
Equisetum laevigatum	smooth horsetail	locally common			Perennial	FAC, FACW
Forestiera neomexicana	New Mexico olive	common	x		shrub	FAC+
Iris missouriensis	Rocky Mountain iris	locally common	x		perennial	FACW, OBW
Juncus spp.	rush	locally common		x	perennial	FACW, OBW
Mentha arvensis						FACW
Mimulus glabratus	monkeyflower	not common	x		perennial	OBW
Phragmites communis	common reed	occasional			perennial	OBW
Plantago major						FACW

Scientific Name	Common Name	Occurrence	Spring	Summer	Habit	Wetland*
Populus angustifolia	narrowleaf cottonwood	locally common	x		tree	FACW
Populus fremontii	Fremont cottonwood	locally common	x		tree	FACW
Prunus virginiana	chokecherry	locally common	x		shrub	FAC
Rorippa sinuata	yellow cress	locally common	x		perennial	FACW
Rudbeckia lacinata	coneflower	locally common		x	perennial	FACW
Rumex crispus	wild buckwheat					FACW
Salix sp.	willow	locally common	x		shrub	FACW
Scripus sp.	bulrush				perennial	
Typha latifolia	broadleaf cattail	locally common	x		perennial	OBW
Urtica dioca-procera	nettle					FACW

OBW = obligate wetland species; occurs almost always (99%) in wetlands; FACW = Usually occurs in wetlands (67% to 99% of time) but occasionally found in nonwetlands; FAC = Equally likely to occur in wetlands or nonwetlands (34% to 66% of the time).

Plant Communities of the Pajarito Plateau

Mapping and classification of the Jemez Mountains have been done by the US Forest Service for the Santa Fe National Forest (Moir and Ludwig 1979), by Allen (1984, 1989) for Bandelier National Monument, by Potter and Foxx (1981) for the Cerro Grande, by Barnes (1983) for the piñon-juniper woodlands, and by Balice et al. (1997) for LANL and adjacent areas. In the late 1990s, Koch et al. (1996) and Balice et al. (1997) developed a land cover map for the Pajarito Plateau and adjacent east Jemez Mountains. The classification included 10 categories ranging from open water to spruce-fir forests. These classes correspond to the cover types for the land classification map presented in Figure 4.2 (Balice et at. 1997; Koch et al. 1996).

The major cover types were defined by dominant tree species and structural characteristics as follows: juniper savanna, piñon-juniper woodland, ponderosa pine forest, mixed conifer forest, and spruce-fir forest. The relationship between these cover types and elevation is show in Figure 4.3 (Foxx and Hoard 1984). The other cover types—grassland, shrubland, open water, and unvegetated land—are not influenced by topography.

Figures 4.4 through 4.21 show each of the major cover types discussed in Balice et al. (1997), and each are discussed briefly. Additional information concerning plant species that occur in these cover types can be obtained from Foxx and Hoard (1984), Foxx and Tierney (1980), Foxx et al. (1998), and Jacobs (1989).

Open Water, Wetlands, and Riparian Zones

In the arid Southwest, water is essential for survival. On the Pajarito Plateau, springs, perennial and intermittent streams, and the Rio Grande provide life-giving water (Figures 4.4 through 4.9). This cover type includes all land that is periodically flooded (intermittent streams) or is open water (rivers, perennial streams, and ponds). Wetlands are defined as areas with hydric soil and wetland species that either always require water (obligatory wetland species) or must have water part of the time (facultative wetland species). Cattails (*Carex* spp.) are an example of obligatory wetland species and can be found in marshes. Willow and various sedges are examples of facultative wetland species. These species are found on drier sites, sandbars, and mudflats and grass/sedge meadows. Narrow strips along permanent and intermittent rivers and streams are called riparian zones.

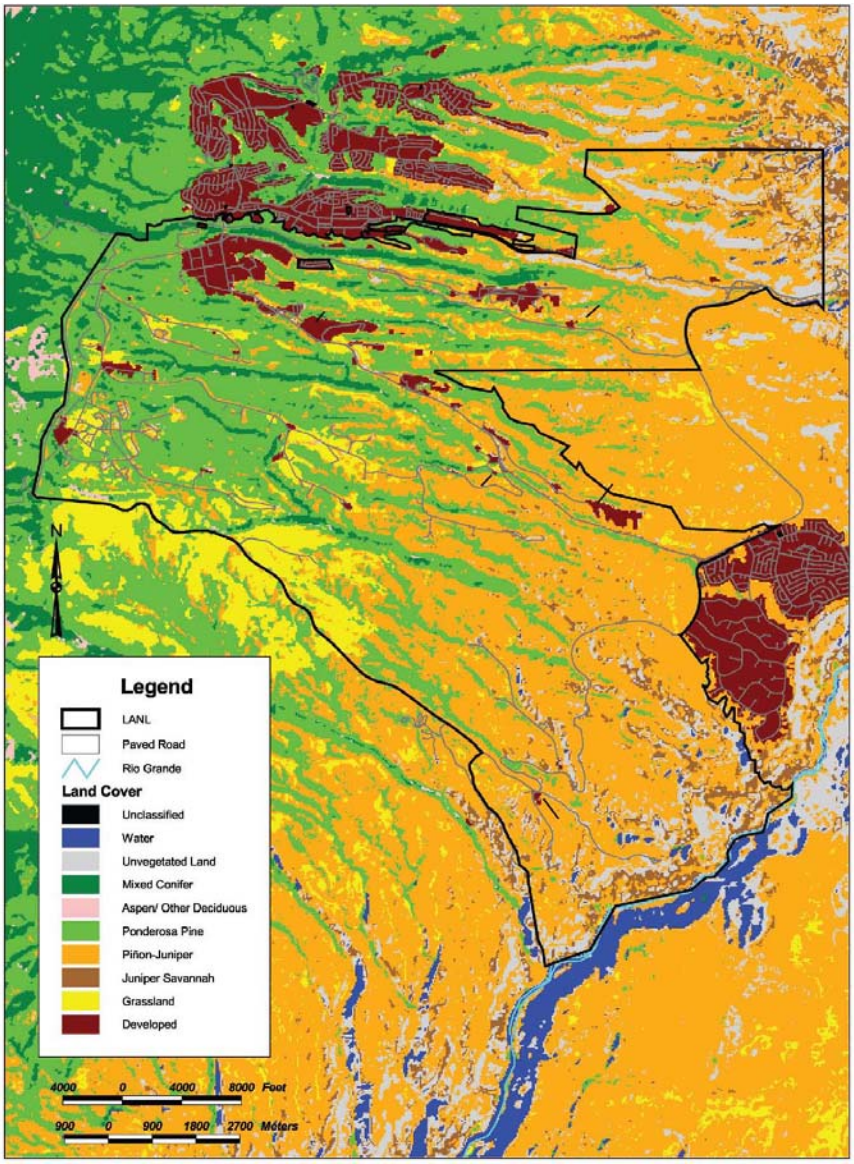

Figure 4.2. Land cover map for LANL and vicinity before the Cerro Grande fire.

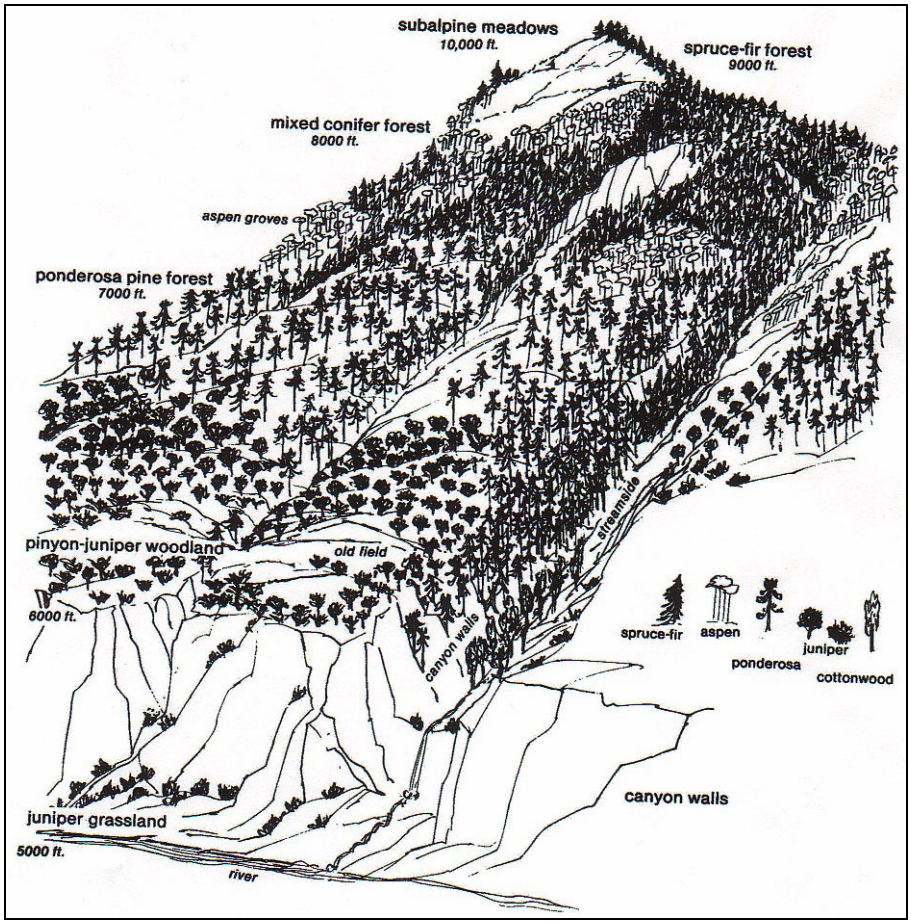

Figure 4.3. Cover types by elevation.

Species within the riparian zones of perennial streams (e.g., Frijoles) include cottonwood (*Populus* spp.) and boxelder (*Acer negundo*). Along the Rio Grande in the vicinity of Bandelier and LANL, tree species have been flooded but were present before construction of Cochiti Dam. Exotic species such as tamarisk (*Tamarix* spp.) and Russian olive (*Elaeagnus angustifolia*) have increased along the Rio Grande, replacing native cottonwoods.

Unvegetated Lands

The unvegetated lands include tuffaceous cliffs, cliff faces, basal cliffs, basalt talus slopes, and felsenmeers. These sites generally have less than 7 percent vegetation, and even though there is not much vegetation, the tuffaceous cliffs and cliff faces were important habitat sites for prehistoric inhabitants. The soft tuff was worked into cavates, and houses and storage areas extended from cliff faces. At lower elevations, the basalt caves provided areas for storage and safekeeping, and petroglyphs are common on the large basalt boulders. Figures 4.10 and 4.11 provide pictures of the tuffaceous and basaltic cliffs around LANL.

Figure 4.4. Intermittent stream in lower Ancho Canyon.

Figure 4.5. Pajarito stream below Pajarito Springs in White Rock Canyon.

Figure 4.6. Sedge/willow marsh in Pajarito Canyon.

Figure 4.7. Perennial stream below Ancho Springs in White Rock Canyon.

Figure 4.8. The Rio Grande at the mouth of Ancho Canyon.

Figure 4.9. The Rio Grande with native willow along the bank.

Figure 4.10. Tuffaceous cliffs in Ancho Canyon.

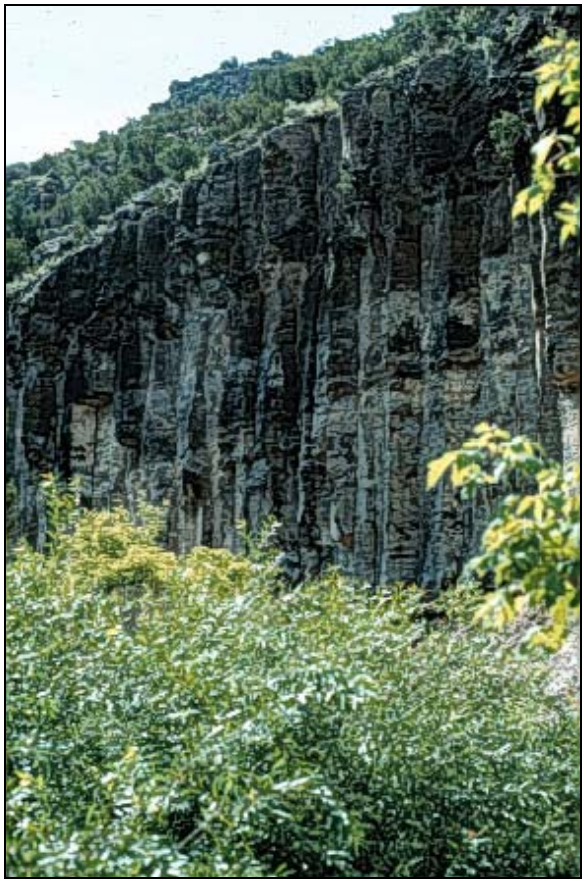

Figure 4.11. Basaltic cliffs in Ancho Canyon.

Juniper Savanna

The juniper savanna is an open grassland that is dominated by one-seed juniper (*Juniperus monosperma*) (Figure 4.12). Land cover in the juniper savanna is between 10 percent and 30 percent. Understory species in this cover type include sideoats grama (*Bouteloua curtipendula*), blue grama (*B. gracilis*), and hairy grama (*B. hirsuta*). The juniper savanna is the primary upland vegetation along the Rio Grande and ranges from 1634 m (5360 ft) to 1951 m (6400 ft) in elevation. There is little evidence of human habitation within this cover type, but evidence of ancient fields and historic animal pens have been found along the upland reaches of the Rio Grande.

Figure 4.12. Juniper savanna in White Rock Canyon.

Piñon-Juniper Woodland

The piñon-juniper woodland consists of open or closed low trees. The dominant tree species are one-seed juniper (*Juniperus monosperma*) and piñon (*Pinus edulis*) (Figure 4.13). One-seed juniper is more abundant at lower elevations, while piñon is more abundant at higher elevations within the zone. These woodlands are between 1890 and 2195 m (6200 and 7200 ft) within the canyons. On the mesa tops these species dominate between 1890 m (6200 ft) and 2195 m (7200 ft). Depending on the altitude, the following species can be found in the understory: blue grama (*Bouteloua gracilis*), Indian ricegrass (*Oryzopsis hymenoides*), and sand dropseed (*Sporobolus cryptandrus*). At higher elevations, mountain muhly (*Muhlenbergia montanus*) is some times present. Most of the habitation sites found on the plateau are located within the piñon-juniper woodland, but many of the homestead sites were located at the ecotone between this type and the ponderosa pine forest.

Figure 4.13. Piñon-juniper woodland.

Ponderosa Pine Forest

This cover type is either a closed or open forest (Figures 4.14 and 4.15). Ponderosa pine (*Pinus ponderosa*) is the dominant species with a cover greater than 7 percent; one-seed juniper and piñon may also be present, but they make up less than 7 percent of the cover.

Figure 4.14. Open ponderosa pine forest.

The ponderosa pine forests can be found at elevations as low as 1890 m (6200 ft) in some protected canyons on the plateau. In more open canyons, ponderosa pine is generally not found below 1921 m (6300 ft). On the mesa tops and lower slopes of the Sierra de los Valles, for example, ponderosa pine forests extend to 2378 m (7800 ft) in elevation.

Understory species in the ponderosa pine forest include blue grama, mountain muhly, mutton grass (*Poa fendleriana*), and little bluestem (*Schizachrium scoparium*). Gambel oak is a common shrub species. A number of fieldhouses and historic homestead sites have been identified in the ponderosa pine forest. Much of the community of Los Alamos and the upper portions of LANL are within this cover type.

Figure 4.15. Closed ponderosa pine forest.

Mixed Conifer/Spruce Fir

Mixed conifer forests typically appear at higher elevations in the mountains and consist of trees that are at least 5 m (16 ft) tall. Douglas fir *(Pseudotsuga menziesii*) and white fir (*Abies concolor*) are the dominant overstory species, although other species such as ponderosa pine may be present in the overstory or midstory (Figure 4.16 and Figure 4.17).

.

Figure 4.16. Mixed conifer forest with Douglas fir and white fir.

Mixed conifer forest intergrades with ponderosa pine communities and as "stringers-on" in north aspects of the canyons and on the canyon bottoms above 2104 m (6900 ft) in elevation. These communities continue to 2591 m (8500 ft) on eastern exposures and on flat areas. Shrubs include ninebark (*Physocarpus monogynous*), wild rose (*Rosa woodsii*), cliffbush (*Jamesia americana*), and dwarf juniper (*Juniperus communis*).

Figure 4.17. Engelmann spruce and white fir dominate high elevations.

Aspen Forest

This cover type occurs in montane and upper montane landscape positions. Trees that are greater than or equal to 5 m (16 ft) tall with coverage greater than or equal to 13 percent are present. Aspen (*Populus tremuloides*) is present in the overstory with at least 20 percent cover (Figure 4.18).

Figure 4.18. Aspen groves are found throughout higher elevations indicating past fire.

Some combination of Douglas fir, ponderosa pine, white fir, or Engelmann spruce (*Picea engelmanni)* are also present but does not dominate the overstory. Aspen communities are common at mid-elevations in the mountains, ranging from approximately 2700 to 3030 m (8900 to 9950 ft). Below 2820 m (9250 ft) aspen stands occupy north and northeast aspects, whereas at upper elevations they are found on the southeast- to southwest-facing positions

Shrublands

Shrublands are identified by the presence of shrub species greater than 0.46 m (1.5 ft) in height with at least 15 percent cover (Figure 4.19 and Figure 4.20). Trees are generally not present or, if they are present, they make up less than 10 percent of the cover. Shrubs include fourwing saltbush *(Atriplex canescans)*, which is often an indicator of prehistoric dwellings, chamisa *(Chrysothamnus nauseosus*), which is often found along roadsides and drainages, New Mexico locust (*Robinia neomexicana)*, which is a common species in burned and/or disturbed areas, and Gambel oak, which is common in ponderosa pine forests and burned areas.

Figure 4.19. Sagebrush (*Artemisia tridentata*) shrubland in White Rock Canyon.

Figure 4.20. Oak shrubland and grassland from the La Mesa fire.

Grasslands and Disturbed Areas

Grasslands are dominated by grasses and grass-like plant species. If shrubs or trees are present in this cover type, then the total percent cover is less than 10. Grasslands can be found on hillslopes in White Rock Canyon or other open sites (Figure 4.21). At the crest of the Sierra de los Valles, subalpine grasslands are conspicuous. They occur at 2743 m (9000 ft) on steep southerly and southwesterly slopes. Montane meadows are found in the mixed conifer and spruce-fir zone. Disturbed areas are found throughout and are recognized by the prevalence of weedy species including Russian thistle, summer cypress (*Kochia scoparia*), snakeweed (*Gutierrezia* spp.), and dandelion (*Taraxacum* spp.).

Figure 4.21. Subalpine grasslands on mountain peaks.

Water Canyon Elevation Gradient

The survey of Water Canyon shows that plant diversity is quite high on the Pajarito Plateau. Almost 300 plant species have been identified (LASL 1976:23). Species diversity among all plants except grasses is elevated at higher elevations (Table 4.2).

Table 4.2. Floral distribution by community type along an elevation gradient.

Overstory-Vegetation Type	Elevation (m)	Numbers of Families	Number of Species*
Fir-spruce	2865	18	28
Subalpine grassland	2865	10	24
Mixed conifer	2560	9	22
Ponderosa pine	2255	12	25
Piñon-juniper	1950	8	17
Juniper-grassland	1645	8	11

*Does not include grasses

A maximum of 18 taxonomic families and 28 non-grass species were recorded in the subalpine grassland (LASL 1976). Members of the composite (Compositae) and grass (Gramineae) families occur with the highest frequency and comprise the highest percentage of ground cover at all elevational sites. Total ground cover reaches a maximum of nearly 100 percent at the higher elevations and decreases steadily to a minimum of 15 percent in the juniper woodland community. As with plant communities, animal communities on the plateau are affected by differences in elevation.

Animal Communities on the Pajarito Plateau

Several invertebrates and vertebrate animal communities are represented at LANL. Many species of small mammals such as deer mice (*Peromyscus* sp.), woodrats (*Neotoma* sp.), moles (*Microtus* sp.), squirrels (Sciuridae), and chipmunks (*Eutamias* sp.) occur in the area, some of which are specific to certain elevation gradients. Other small mammals, such as bats (Chiroptera), are present within the Laboratory boundaries as well, and consist of at least 15 different species (Biggs et al. 1997:1–3; LASL 1976:24–27). The area also contains mule deer (*Odocoileus hemionus*) and elk (*Cervus elaphus*). Little is known about other large and medium size mammals of the area, but based on observations and current studies, a minimum of 12 species of carnivores are present. Among these are black bear (*Ursus arctos*), mountain lion (*Felis concolor*), bobcat (*Felis rufus*), gray fox (*Urocyon cineroargenteus*), and coyote (*Canis latrans*) (Biggs et al. 1997:1–3; LASL 1976:24–27).

Cold-blooded animals in the area include several species of fish found in the Rio Grande. The carp (*Ctenopharyngodon* sp.), chub (*Gila pandora*), and white sucker (*Catostomus commersoni*) are abundant in the waters of the Rio Grande on the eastern boundary of LANL. There are a few brown trout found in the area but not enough to represent a significant population, probably due to the turbidity of the river (LASL 1976:25).

There are approximately nine species of reptiles in the LANL area including small lizards and king snakes (*Lamprapeltis getula*), bull/gopher snakes (*Pituophis melanoleucus*), garter snakes (*Thamnophius* sp.), and rattlesnakes (Crotalidae). The Jemez Mountains salamander (*Plethodon neomexicanus*) is a rare amphibian that is found in the area (LASL 1976:25).

There are some 187 bird species from 44 families reported in the area, some of which are permanent residents and some of which are transient populations. Observed permanent residents include the common raven (*Corvus corax*), pygmy nuthatch (*Sitta pygmaea*), western bluebird (*Sialia mexicana*), gray-headed junco (*Junco caniceps*), and rufus-sided towhee (*Pipilo erythrophthalmus*). Summer birds include the turkey vulture (*Cathartes aura*), red-tailed hawk (*Buteo jamaicensis*), American kestrel (*Falco sparverius*), peregrine falcon (*Falco peregrinus*), chipping sparrow (*Spizella passerina*), and violet-green swallow (*Tachycineta thalassina*) (LASL 1976:25).

The ecological relationships to the topography are interesting. Animals in the lower elevation zone (1700 to 2000 m; 5610 to 6600 ft) include coyote, rattlesnake, bobcat, gray fox, red-tailed hawk, spiny lizard (*Sceloporus magister*), mule deer, deer mouse, and the cottontail (*Sylvilagus* sp.). Animals in the middle elevation zone (2000 to 2400 m; 6600 to 7920 ft), especially in the canyons, include coyote, raccoon (*Procyon lotor*), mountain lion, American black bear, turkey vulture, American kestrel, golden eagle (*Aquila chrysaetos*), gopher snake, rock squirrel (*Spermophilus variegatus*), and mule deer. Animals from the same elevation zone that inhabit the mesa tops include American black bear, mountain lion, common raven, pygmy nuthatch, Colorado chipmunk (*Tamias quadrivittatus*), pine squirrels (*Tamiasciurus* sp.), and mule deer. Animals in the highest elevations (2400 to 3200 m; 7920 to 10,560 ft) include the American black bear, mountain lion, green-tailed towhee, hairy woodpecker (*Picoides villosus*), Rocky Mountain elk, mule deer, western bluebird, and gray-headed junco (LASL 1976:24–26).

PLANTS AND ANIMALS AS INDICATORS OF PAST LAND USE AND CHANGE

Plants

The Pajarito Plateau has a long history of use by different groups of peoples. Archaeological evidence shows that humans were in the area by at least 10,000 years ago (Steen 1977; Vierra 2005a). Agriculture was a common practice on the Pajarito Plateau by about 1000 years ago. Since the 18th century, the plateau has been logged, grazed, and dry-land farmed. Laboratory activities (disposal sites, roads, building) and fires have affected plant and animal communities in the last 50 years. Disturbances, of whatever kind, typically have a general pattern of plant succession after a given period of time: weedy annuals, replacement of annuals with perennial forbs and grass, and invasion of woody species. Plants known as colonizers are usually the first species to grow on disturbed sites since they out-compete the natural species of the original community after the disturbance (Clements 1928; Foxx et al. 1998).

Prehistoric and historic dwellings, agricultural areas, and the surrounding landscape can provide information about past use and activities (Foxx and Tierney 1984, 1999; Foxx et al. 1998). The remains of vegetal and faunal remains within the hearths at an archaeological site can provide information about possible plant and animal uses. Also, the dwellings themselves and the immediate surroundings can provide information about past use and activities. Habitats that had natural or human disturbance are atypical of the surrounding, undisturbed area. These areas of disturbance often have an abundance of plants that were introduced by human activity (Housely 1974; Yarnell 1958). Various categories of these colonizing plants are useful in determining

changes in the environment. There are three categories of species often found in association with natural or human disturbance: invasive weeds (often called pioneer plants), noxious weeds, and camp followers.

Invasive Weeds (Pioneer Plants)

Invasive weeds can be defined as plants that favor an open habitat and thrive in any disturbed area, ancient or contemporary (Lee 1999; Tierney 1973). These plants are called pioneer plants because they are the first arrivals on sites that have been disturbed by human habitation or types of disturbed soils. Most of these species have been introduced from outside the area (e.g., Europe, Africa, or other places within North America) since the time of the European entry into the Southwest and are not native to the landscape. Some species were purposely brought as medicinal or food plants, but others were accidental introductions by seeds clinging to animals or clothing or in goods. Some recent introductions were used as ornamentals (e.g., iris [*Iris missourriensis*]), for repairing spoiled land (e.g., crested wheatgrass [*Agropyron cristatum*]), and landscaping (e.g., Russian olive [*Elaeagnus angustifolia*]). Many of these plants have become naturalized, or have become a common part of the flora of areas in disturbed sites such as archaeological sites, along roadsides, and within floodplains.

Noxious Weeds

Noxious weeds, or a plant that has a negative impact on the environment or the economy, is used in this chapter as defined by the Cooperative Extension Service (Lee 1999). Noxious weeds displace native vegetation, increase soil erosion, and reduce opportunities for land use. In recent years, areas that have been denuded by vegetation after catastrophic wildfires have become prime locations for the growth of noxious weeds such as Canada thistle (*Cirsium arvense*). These weeds are often recent introductions to an ecosystem, and eliminating infestations are important (Lee 1999).

The difference between noxious weeds and invasive weeds is subtle. As the plant becomes common in the environment it may change in its classification. Species such as Russian thistle (*Salsola kali*) have become a common part of the landscape and, although widespread on disturbed soil, is not included in the list of weeds that are noxious in New Mexico. In a Santa Fe New Mexican article dated September 16, 1897, Russian thistle was first reported in the Santa Fe Valley and called a noxious weed. Today, Russian thistle can be found in abundance on some archaeological sites (e.g., Otowi), along roadsides, and in other disturbed sites where subsurface excavation occurred (Yarnell 1958). Since Otowi was excavated in the early 20th century, their presence is to be expected. Unexcavated archaeological sites, however, usually do not have plants like Russian thistle in abundance.

Camp Followers

Camp followers are tolerant of disturbed areas surrounding human activity and, in turn, are tolerated or even encouraged by humans because of their economic or aesthetic value (Tierney 1973). Camp followers have proven to be useful indicators of human activity (Housely 1974; Tierney 1973; Yarnell 1958). They are generally non-native species that were brought along for

a utilitarian use such as food, medicine, or ceremony (e.g., wolfberry [*Lycium pallidum*] and sacred datura [*Datura meteloides*]). Indicator species may be native or non-native species that thrive in the disturbance of habitation sites (e.g., walkingstick cactus [*Opuntia imbricata*], four-wing saltbush [*Atriplex canescans*], and lambs quarters [*Chenopodium* spp.]). Prehistoric agricultural areas can often be located by rock alignments and some times by an anomaly in the existing vegetation, even after 400 years of abandonment. Thus, marks of earlier activities as evidenced by existing vegetation are a legacy of the past.

Floral introductions have occurred since people entered into the environments of the Pajarito Plateau. The presence of introduced species (invasive weeds, noxious weeds, and camp followers) indicates use, changing environments, or accidental introductions. The earliest introductions were probably camp followers brought as people migrated to the plateau. Later introductions may have been purposeful or accidental. Scurlock (1998) listed plants introduced since the entry of the Spanish into the middle Rio Grande Valley with approximate dates. Using Scurlock's list as a starting point, we compared that list of introduced plants with Foxx et al. (1998). Those plants that were found in the Jemez were noted. The list of introduced plants for the Jemez was further extended by other references, including Agricultural Research Service (1971), Crockett (1977), Curtin (1965), Lee (1999), Martin and Hutchins (1980), Phillips Petroleum Company (1957, 1960), Stubbendieck et al. (1989), Tierney (1973), Tierney and Hughes (1983). This list includes primarily "wild" species and does not concentrate on domestic species introduced by the Spanish such as wheat, barley, onions, oats, lettuce, watermelon, or fruit trees, or crops introduced by the Spanish such as tomatoes, chilies, cultivated tobacco, and new varieties of corn and beans (Wozniak 1995).

Animals

Introduction of domestic animals (cows, sheep, goats, pigs, horses, and other species) by the Europeans has had a profound impact on the land and peoples of the Southwest. Migratory societies could move when drought occurred and sedentary groups did not have to depend so much on wild foods. The result was that more trading and raiding was possible. Peace fairs such as those held at Taos in the 18th century between Pueblos, Apaches, Comanches, and the Spanish provided a means to distribute goods (Simmons 1991).

As time passed, some animals were no longer necessary for domestic life. For example, in the mid 20th century, burros were no longer needed for the economy as beasts of burden. Many were released and became feral in Bandelier National Monument and the Santa Fe National Forest. In the mid 1970s and early 1980s, the impacts of these animals on the ecosystem and archaeological sites were addressed in Bandelier National Monument. The animals were removed or exterminated. In recent years there has been one feral burro at LANL.

There have been introductions, extirpations, and extinctions of animal species that have changed the nature of the food chains. One example is the introduction of non-native fish, including brown and cutthroat trout. These fish have reduced the numbers of native fish species (Allen 1989) and make it difficult to determine the use of such groups by early peoples.

Prehistoric Land Use

The landscape of the Pajarito Plateau and east Jemez Mountains remained mostly untouched by human influence until approximately 10,000 years ago when small groups of Paleoindian hunter-gatherers followed game animals up and down the Rio Grande and took trips onto the plateau and into the Jemez Mountains to collect obsidian and other subsistence resources. These people moved often to take advantage of the various resources, and as edible plants became available, the consumers would reposition themselves (Tainter and Tainter 1996). These patterns meant that these hunter-gatherers might be at low elevations for gathering spring greens and at higher elevations for collecting summer and fall berries (Tainter and Tainter 1996; Vierra and Foxx 2002; Vierra 2005a).

From those first few people who wandered the mesas and canyons, the use of the area increased slowly. Archaic hunter-gatherer groups relied on small game such as grouse, as well as various plant species. Later, as maize horticulture became established, agriculturalists used the area for foraging. As the population density increased on the Pajarito Plateau, familiar landscapes were modified. Lands were cleared for agriculture, and every piece of wood within walking distance and that was useful for construction, cooking, or heating was quickly collected. The distribution and abundance of native plants and animal species within that area were altered in a short time. Vegetation communities were influenced by introduced and extirpated plants (Tainter and Tainter 1996).

By the Coalition period (AD 1150 to 1325), humans occupied the Pajarito Plateau on a year-round basis, and environmental impacts were, by extension, greater. During the Coalition and Classic (AD 1325 to 1600) periods, population and associated settlement increased, large, aggregated pueblos were developed, and agriculture, particularly in the lower elevations within the piñon-juniper woodland and juniper savanna, increased into all available arable lands. Though virtually abandoned by the late 1500s because of an extensive period of drought, the plateau continued to be used for foraging and hunting by the occupants who remained to take advantage of the plant and animal resources. In general, human activities on the Pajarito Plateau were closely associated with topography; middle elevations were used primarily for habitation, while upper and lower elevations were used for hunting, foraging, grazing, agriculture, and historic recreational activities.

Plant Resources

The Pueblo people used various plants and animals for daily living, including food, clothing, recreation, and ceremony. Use can be determined in three ways: from literature about ethnobotanical or ethnozoological studies, from surveys of sites to determine availability and camp followers, and from the study of macrobotanical and faunal material from archaeological excavations.

Knowledge of early plant and animal uses has been defined by early ethnologists and, more recently, by interviewers of tribal members. During the early 1900s, interviewed persons from the Keres, Tiwa, and Tewa language groups and Athabascans (the Apache and Navajo) related

folklore about plants and plant usage. Researchers included Castetter (1935), Castetter and Opler (1936), Cook (1930), Elmore (1943), Jones (1931), Robbins et al. (1916), M. Stevenson (1912, 1915), and Swank (1932). Henderson and Harrington (1914) interviewed tribal members about animal uses. These studies have been a basis for much of the understanding about early plant and animal use. Additional information was obtained through excavations and the recovery of plant and animal remains, and from surveys of sites (Ford 1968; Foxx 1982; Lang 1986; Matthews 1990, 1992; Tierney 1977a, b, 1979; Trierweiler 1990, 1992).

Dunmire and Tierney (1995) summarized much of the ethnographic literature and also conducted personal interviews with tribal members of various pueblos. They identified 304 plants known to have uses for food, medicine, cordage, construction, implements, and tanning within the Pueblo Province. The categories they found and percentages of plants within each use category for the Jemez are found in Table 4.3.

Using the list compiled by Dunmire and Tierney, Vierra and Foxx (2002) identified 215 of the 305 species as being present in the Jemez Mountains flora. Of the 215 species, many had multiple uses. Table 4.4 shows the groups of species most commonly used by various groups. Vierra and Foxx (2002) also analyzed the list to determine the plant community where plants used for food and beverages are most likely to occur (Table 4.5).

Table 4.3. Percentage of plants used for different activities (from Dunmire and Tierney 1995).

Activity	Percent
Food and Beverage	42.0
Medicine	59.0
Smoking or Chewing	5.0
Construction	5.0
Coloring, Tanning, Soap, Art, Crafts	12.0
Cordage, Fiber, Fine Matting	3.0
Implements	11.0
Total Number of Identified Plants	**304**

Table 4.4. Plant uses and numbers of plant species used from plant communities.

Activity	Riparian	Juniper Savanna	Piñon Juniper	Ponderosa forest	Mixed Conifer
Medicinal (*n* = 148)	18	82	111	73	35
Food (*n* = 108)	23	41	77	56	30
Implements (*n* = 28)	4	14	20	15	6
Coloring/Tanning (*n* = 37)	6	19	24	16	6
Construction (*n* = 16)	6	7	9	8	4
Smoking (*n* = 13)	0	8	11	3	9
Cordage (*n* = 6)	2	3	2	2	1

Additional information has been gleaned from macrobotanical analysis of remains recovered from archaeological excavations. Information discussed here is limited to two sources (Foxx 1982; Matthews 1990). Foxx (1982) identified macrobotanical material from sites excavated in the Cochiti flood pool, while Matthews (1990) examined materials recovered from Burnt Mesa Pueblo and Casa del Rito. Both charred and uncharred seeds were recovered from flotation samples.

Table 4.5. Species of plants used by multiple Native American cultures of New Mexico.

Plant	Common Name	Number Groups
Achillea lanulosa	yarrow	3
Alnus tenuifolia	alder	3
Amaranthus graezans	pigweed	3
Amaranthus retroflexus	amaranth	6
Artemisia filifolia	sand sage	4
Artemisia frigida	wormwood	3
Artemisia tridentate	big sagebrush	2
Atriplex canescens	four-wing saltbush	7
Croton texensis	doveweed	5
Fallugia paradoxa	Apache plume	4
Hedeoma nana	false pennyroyal	3
Ipomopsis aggregata	scarlet gilia	3
Juniperus monosperma	one-seed juniper	4
Lycium pallidum	wolfberry	4
Mirabilis multiflora	showy four o'clock	3
Monarda menthaefolia	beebalm	4
Cleome serrulata	Rocky Mountain beeplant	8
Pectis angustifolia	lemoncillo	4
Penstemon barbatus	scarlet bugler	3
Pinus edulis	piñon pine	4
Portulaca oleraceae	verdolaga	5
Quercus gambelii	Gambel oak	3
Rhus trilobata	lemonade berry	7
Ribes inebrians	gooseberry	3
Rosa woodsii	wild rose	3
Solanum elaeagnifolium	bullnettle	5
Solanum jamesii	wild potato	4
Yucca spp.	yucca	8

Animal Resources

Compared to plant use, there is far less ethnographic information available for animals. Most of the current knowledge regarding animals comes from analyses of animal remains found in archaeological excavations, from mythology and folk story collections, and through ceremonial uses. Henderson and Harrington (1914) published a comprehensive work on animals of the

Tewa province in the early 20th century. Their work provides one of the earliest listings of animals found in the area and also includes the Tewa names for animals. The purpose of the study was to determine the use and presence of various animal species found in, or that had previously been found, in the areas of El Rito de los Frijoles, the Valle Grande, and Painted Cave in 1910. Their identifications provide a glimpse of species that were common in the area early in the 20th century. Some of these species were extirpated or became extinct since the late 1800s (e.g., bighorn sheep, elk, and wolf). Henderson and Harrington's study was also conducted to help identify various bone fragments that were recovered from archaeological excavations in the Frijoles Canyon area. The taxa identified as a result of their study included deer, rabbit, fox, coyote, wolf, dog, raccoon, badger, wildcat, beaver, small birds, turkey, eagle, hawk, and owl.

Of the 48 mammals Harrington and Henderson (1914) identified, only 15 species were found to have a specific use as food, in ceremony, or within the mythology of the Tewa. Of the 46 bird species noted, only 10 species were used as food, in ceremony, or within the mythology of the Tewa. No reptiles or amphibians were used for food, and only turtles were used for ceremonial purposes. Insects had little importance as a food source, but Henderson and Harrington (1914) identify a number of species referred to by the Tewa.

Extensive excavations for Bandelier were conducted within the Cochiti Lake flood pool in the 1970s. The excavated sites included large multi-room sites, one- and two-room masonry sites, and caves. Guthrie (1982a, b) surveyed the area for present fauna and then identified the various animal remains within the sites. Guthrie determined that many of the faunal remains belong to species that may have used the rocky sites after abandonment by humans and were not used for food or implements. Only a few designated species had charring or knife cuts. Guthrie notes that the bones of other species were a normal part of the fauna of the Rio Grande or were migrants along the river.

During the Bandelier Survey, Trierweiler (1990, 1992) identified the non-human bone assemblages from Burnt Mesa Pueblo (LA 60372) and Casa del Rito (LA 3852), two sites hat were excavated within Bandelier National Monument. Trierweiler identified 16 taxa, including 14 mammal and two bird species. He also noted that although charring on the bones might indicate food preparation, edible species such as antelope, bison, prairie dog, blue grouse, porcupine, skunk, and mule deer did not always contain evidence for burning. Trierweiler identified 10 bone tools made from turkey and mule deer bones.

Faunal assemblages can inform about a number of aspects regarding animal use. The primary result tells of the use of animal resources by people. Another piece of information they can tell about is the occupation or use of a site by an animal after abandonment by humans. And, although a taxon may not be identified in an archaeological faunal assemblage, this does not indicate lack of use by humans. Trading of some remains such as pelts, bones, antlers, and horns may account for some discrepancies.

The list compiled from Henderson and Harrington (1914), and the excavation data were compared to a species list created for the Pajarito Plateau by Biggs et al. (1997) and habitat information by Findley (1987). The kit fox (*Vulpes velox*; reported by Trierweiler 1992) has not been reported for the Pajarito Plateau and because of their habitat requirements they may never

have inhabited areas of the plateau or Jemez Mountains. Similarly, jackrabbits are not presently found in the area. Allen has tabulated the use of various species in 45 different excavations for the Jemez Mountains. Table 4.6 shows the species found in the various ruins and the numbers of faunal remains in descending order.

Table 4.6. Animal species identified from archaeological sites and the numbers of remains in descending order (after Allen 2004).

Common Name	Scientific Name	Number
Turkey	*Meleagris gallopavo*	531
Cottontail	*Sylvilagus audubonii*	460
Jackrabbit	*Lepus californicus*	317
Mule deer	*Odocoileus hemionus*	155
Prairie dog	*Cynomys ludovicianus*	81
Sheep/goat	*Ovis/Capra*	79
Cow	*Bos taurus*	75
Fish	Osteichthyes	53
Quail	*Callipepla/Lophyortyx* sp.	45
Sandhill crane	*Grus canadensis*	33
Bighorn	*Ovis canadensis*	24
Pronghorn	*Antilocapra americana*	24
Kangaroo rat	*Dipodomys* sp.	24
Toad	Bufonidae	10
Bear	*Ursus* sp.	9
Horse/burro	*Equus* sp.	8
Bison	*Bison bison*	7
Owl	Strigidae	5
Elk	*Cervus elaphus*	3
Frog	Ranidae	3
Beaver	*Castor canadensis*	2
Bobcat	*Felix rufus*	2
Pig	*Sus scrofa*	2
Ringtail	*Bassariscus astutus*	2
Dog/coyote	*Canis familiaris/latrans*	2
Sheep	*Ovis aries*	1
Goat	*Capra hircus*	1
Burro	*Equus asinus*	1

Kohler (1990) notes that faunal assemblages from sites excavated in the 1989 and 1990 seasons did not contain elk. Allen (1996) compiled ungulate (hoofed mammals) faunal remains from 45 archaeological sites in the Jemez Mountains. Of the 218 ungulate individuals (based on a total of 646 bones), he found that other ungulate remains—bighorn, pronghorn, and bison—exceeded elk, indicating low population numbers from 1200 to 1500 AD (Allen 1996). It should be noted that elk do not like densely forested sites and generally are found in open meadows like those of the Valle Grande. The last Merriam elk (*Cervus elaphus merriami*) were noted in the Jemez in

the late 1800s. Rocky Mountain elk (*Cervus elaphus nelsoni*) were introduced in 1948 with 28 elk from herds in Jackson Hole, Wyoming; the herds now number into the thousands. The general patterns of movement of elk before the La Mesa fire were different than today and might more closely reflect the migration patterns at the time of prehistoric habitation of the Pajarito Plateau. The elk would summer in the Valle Grande when calving and nursing, and would move down in elevations to the upper mesas (e.g., Burnt and Escobas Mesas) during the winter months (White 1981). The patterns of migration have changed since the La Mesa, Dome, and Cerro Grande fires (Allen 1996; Biggs et al. 1999).

Fire on the Pajarito Plateau

The plant and animal communities discussed in this chapter represent elements of the environment that prehistoric and historic peoples have used and lived in for thousands of years. In the past 20 years there have been several major fires that substantially changed the nature of the plateau landscape:

- The La Mesa fire (1977) burned primarily ponderosa pine forest and some piñon-juniper woodland in Bandelier National Monument, Santa Fe National Forest, and LANL. Areas that were severely burned are now mostly grassland or shrubland; these areas were historically in ponderosa pine forests.

- The Dome fire (1996) burned higher-elevation ponderosa pine and mixed conifer forests in Bandelier National Monument and the Santa Fe National Forest.

- The Oso fire (1997) burned areas within Santa Clara Pueblo land and in the Santa Fe National Forest.

- The Cerro Grande fire (2000) burned much of the ponderosa pine and mixed conifer in the Santa Fe National Forest above 2438 m (8000 ft) behind the town of Los Alamos and Santa Clara Pueblo land. It also burned within LANL between about 2132 and 2438 m (7000 and 8000 ft); these areas were predominantly located within the community of Los Alamos. Much of the area was burned by a medium to low-intensity fire, which changed the overstory from ponderosa pine and mixed conifer to shrubland and aspen stands.

The number of fires on the Pajarito Plateau has been influenced by recent droughts. Table 4.7 shows the droughts in the Historic period in New Mexico. Year numbers in red in Table 4.7 represent fire scar years on tree ring samples collected by Foxx and Potter (1984). The year numbers in green represent recent large fires in the east Jemez Mountains and Pajarito Plateau that are not represented by tree ring sampling, and the year numbers in blue represent the 20 largest fires listed from a regional fire time series developed by Swetnam and Baisan (1996).

Table 4.7. Historic New Mexico droughts, 1542 to 1989 (Scurlock 1998).

16th and 17th Centuries	18th Century	19th Century	20th Century	21st Century
1542	1700 to 1709	1801 to 1803 1801, 1804 1801	1900 to 1904 1900	2000 to 2002 (2000)
1578 to 1580	1707	1805 to 1813 1806, 1814 1806	1907 to 1910 1907, 1908	
1598 to 1606	1714 to 1717 1715 to 1716	1817 to 1822, 1819	1917 to 1918 1919	
1620 to 1623	1719 summer 1724 to 1725	1824 to 1825 1830, 1833	1920 to1925 1921, 1922	
1625 to 1633	1727	1829 to 1830	1927 to 1928 1927	
1635 to 1640	1729 to 1730 1729	1841 to 1843 1842, 1842	1932 to 1937	
1651 to 1672	1734 to 1739	1845 to 1847, 1847	1939 to 1940	
1675 to 1680	1748 to 1759 1748, 1752, 1763, 1765	1849	1942 to 1948 1941, 1944	
1681 to 1680	1768	1851 to 1853 1851, 1861	1950 to 1956 (1954)	
1689 to 1699	1772 to 1774 1773	1873 to 1877 1870, 1878	1971 (1977)	
	1775 to 1785 1786	1877 to 1883 1879, 1883	1980	
	1787 to 1790	1886 to 1890	1989	
	1793; 1797; 1798	1892 Summer 1896 1893, 1896		
		1898 to 1900 1897	(1996, 1998)	

Hunter-gatherer populations actively manipulated vegetation to increase production of useable resources (Pyne 1999). Historically, there is no specific evidence that the native peoples of the upper Rio Grande deliberately set fires for the purposes of attracting game or foraging. There is evidence, however, that fire was used in the Southwest by certain Indian groups. The first Spaniard to enter the region, Cabeza de Vaca, recorded fire practices of the Indians in Texas. Pyne (1999) notes that Bernard DeVoto records that one of the first American columns into the Southwest during the Mexican War found that fire on the mountain was a Southwestern tradition. As their successors learned, it was a fire regime controlled equally by natural and cultural history.

The Apache used broadcast fire as did many tribes living within grasslands. They used smoke signals, burned to cover trails, and burned as an inducement for rain. W. A. Bell noted in 1870 that, "the Apaches also have a very destructive habit … of firing forests of their enemies." Fire frequencies changed after the Apaches were subdued (Pyne 1999). The specific use of fire by

Puebloan peoples has not been recorded. There is some indirect evidence of use of fire through ethnobotanical studies. Lemonade berry *(Rhus trilobata*) has been used in historic Southwestern Indian basketry (M. Stevenson 1915). The branches however are not straight switches and thus ethnobotanists were puzzled by their use for basketry. However, ethnobotanist Vorsilla Bohrer (1983) observed the shrub in a burned area of the Navajo reservation regenerating with vigorous straight new shoots following a fire. She states,

> If ancient hunters were in the habit of burning vegetation to secure raw material for their offerings, they may have served themselves in another way. The burned patches of vegetation would foster increased abundance of game and annual plants like sunflower (*Helianthus*) and bugseed (*Corisperumum*).

Although there is no evidence that peoples of the area specifically set fire for the purposes of hunting or gathering, there is an attitude of understanding the rejuvenating aspects of fire mythology and ritual. At Zuni, fire is used in the rabbit hunt; at Cochiti, Nambe, Zuni, and Isleta, fire has taken the form of fostering new life and growth. Bohrer (1983) states,

> Although, our knowledge of formalized burning practices among Pueblo agriculturalists has been preserved erratically, an attitude toward fire as a fertile force still persists in ritual contexts.

Indeed, fire has a regenerating effect. Almost immediately after fire, shrubs sprout and plant species that have roots or underground stems regenerate quickly. Large game such as elk and deer are attracted to burned areas (Foxx 2001; Whelan 1995).

From fire scar data, it is shown that small and regional fires are correlated with times of drought. Between 1975 and 1977, Foxx and Potter collected 18 fire scarred ponderosa pine samples and calculated the fire frequency for samples dating from the early 1700s. Additionally, Swetnam and Baisan (1996) have extended fire scar data for the New Mexico and Arizona region. From 1709 through 1900 all 20 of the large regional fires identified were in drought years (Tables 4.7 and 4.8).

Because of the regenerating nature of burned areas, Foxx and Potter (1984) speculated that fire could be a source of food items in subsistence cultures. For example, wild onion, known to be collected for food and medicine by most or all Pueblos (Dunmire and Tierney 1995), generally is found as a single plant throughout forested areas. However, after fire large patches can be found within the ponderosa pine zone. Many shrubs are sprouters meaning that young straight shoots would be available (Table 4.9).

Table 4.8. Cross-section from a representative tree on Escobas Mesa sampled after the La Mesa fire (dates courtesy of Craig Allen).

Date	Drought Year	One of 20 Highest Fire Years
1637 Center	Yes	
1725	No	Yes
1737	Yes	

Date	Drought Year	One of 20 Highest Fire Years
1748	Yes	Yes
1757	No	
1763	No	Yes
1773	Yes	Yes
1797 (6)	Yes	
1801 (1)	Yes	Yes
1806 (5)	Yes	Yes
1814 (3)	Year after drought	
1833 (3)	No	
1842 (6)	Yes	Yes
1851	Yes	Yes
1858 (4)	No	
1878 (7)	Yes	
1893 (5)	Yes	
1965	No	
1977	Very early fire season	1977 La Mesa

Information is from one tree with fire scars from 1725 through 1977. Numbers in parenthesis () represent the number out of the other 18 fire scar trees sampled by Foxx and Potter and summarized in Foxx (1982). Column 2 represents those years that correspond to drought years on Table 4.7. Column 3 represents those years determined by Swetnam and Baisan (1996) to be the largest regional fires in New Mexico and Arizona.

Hill and Trierweiler (1986) discuss food stress and drought (Table 4.10). Although fire scar data for the most part is only from trees that were 350 years old (Allen et al. n.d.), extrapolating from available information, it is conceivable that burned areas may have been a source of some species when food stores were dwindling because of drought. Vierra and Foxx (2002) compared the listing of plants used for food, medicine, and other uses with information gained through succession studies after fire. From fire ecology studies we know that before 1900 there were frequent small fires within the ponderosa pine zone (see Table 4.9). We also know from observations and studies (White 1981) that these burned areas attract large game animals like elk and deer and small game animals such as turkey because of new and nutrient-rich forage. Although it presently cannot be proven, there is evidence of the usefulness burned areas might have been to subsistence peoples.

Table 4.9. Early succession plants in burned areas that may have been plant resources for early peoples.

Scientific Name	Common Name	Habitat	Primary Plant Community*				
			MC	PIPO	PJ	JS	Uses
Forbs							
Achillea lanulosa	yarrow	perennial	x	x			medicinal
Allium cernuum	wild onion	perennial	x	x			food/medicine
Amaranthus graezans	prostrate pigweed	annual		x	x		food
Chenopodium album	goosefoot	annual		x	x	x	food
Chenopodium leptophyllum	goosefoot	annual		x	x		food

Scientific Name	Common Name	Habitat	Primary Plant Community*				
			MC	PIPO	PJ	JS	Uses
Euphorbia spp.	thymeleaf spurge	annual			x	x	medicine
Physalis foetens	NM groundcherry	annual		x	x		food
Physalis hederaefolia	groundcherry	perennial		x	x		food
Thelesperma spp.	cota, Indian tea	annual			x	x	food/medicine
Sprouting Shrubs							
Amelanchier sp.	serviceberry	shrub	x				food
Archtostaphylos uva-ursi	bearberry	low shrub	x	x			smoking
Berberis fendleri	Colorado barberry	shrub	x	x	x		food
Berberis repens	Oregon grape	low shrub	x	x			food, coloring
Ceanothus fendleri	buckbrush	shrub		x			food
Quercus gambelii	Gambel oak	shrub					food, medicine, implements
Ribes cernuum	wild currant	shrub		x	x		food
Ribes inebrians	wild currant	shrub	x	x			food
Ribes inerme	gooseberry	shrub	x	x			food
Robinia neomexicana	New Mexico locust	shrub	x	x	x		food, implements
Rosa woodsii	wild rose	shrub	x	x	x		medicine
Rubus strigosus	raspberry	shrub	x				food
Rhus trilobata	Lemonade berry	shrub		x	x	x	food, medicine, smoking, coloring, implements
Prunus virginiana	chokecherry	shrub	x				food, medicine
Salix spp.	willow	shrub					medicine, construction, coloring
Yucca baccata	banana yucca	perennial		x	x		food, medicine, coloring, cordage, implements
Yucca glauca	narrowleaf yucca	perennial			x	x	food, medicine, coloring, cordage, implements
Sprouting Trees							
Acer glabrum	Rocky Mountain maple	tree/shrub	x	x			implements
Populus tremuloides	aspen	tree	x				medicine, construction, coloring

*MC = Mixed Conifer, PIPO = Ponderosa Pine, PJ = Piñon-juniper, JS = Juniper Savanna. Uses from Dunmire and Tierney (1995); Fire species from Foxx and Potter (1984), Foxx (1996); Personal observations in La Mesa, Dome, Oso, and Cerro Grande fires

Table 4.10. Years of severe food stress on the Pajarito Plateau, AD 1150 to 1600* (from Hill and Trierweiler 1986).

Early Coalition	Late Coalition	Early Classic	Middle Classic	Late Classic
1158	1252	1337	1417	1562
		1338	1418	1563
1188			1419	
1189		1342	1420	1581
				1582

Early Coalition	Late Coalition	Early Classic	Middle Classic	Late Classic
1216		1364	1424	1583
1217				1584
1218		1377	1457	1585
1226			1461	
			1475	
			1524	
			1525	

*Each year listed is the third (or later) sequential year of drought when food stores would have been exhausted.

Summary of Fire on the Pajarito Plateau

Today, as when the plateau was first inhabited, fire is a part of the natural cycle. Although the most recent fires (e.g., the Cerro Grande fire) have been caused by human activities, most fires in the mountainous west are caused by lightning. Over a 21-year period in the Santa Fe National Forest, officials recorded 68 lightning-caused fires per year. However, many of these fires remained as ground fires because crown fires only occur when forest and weather conditions are right for fires to get out of control. Studies show that fire was a frequent occurrence before the turn of the 20th century; trees were scarred by fire every five to ten years. The changes resulting from human settlement on, and use of, the Pajarito Plateau in the late 1800s caused suppression of fire, and today many places in the area have not had a fire in over 100 years.

Studies indicate that the last major fire in the 19th century on the Pajarito Plateau was in 1893. Through the ensuing years, without the cleansing of frequent low-intensity fires, forests of the plateau became heavily overgrown. In 1977, environmental and meterological conditions were right for the ignition of a wildfire, and this resulted in the La Mesa fire. This was the first large-scale wildfire on the Pajarito Plateau in the 20th century and burned over 15,000 acres of predominantly ponderosa pine forest. Twenty years later, the Dome fire burned 16,000 acres, and in 1998, the Oso fire burned another 5,000 acres. In May 2000, the Cerro Grande fire burned over 43,000 acres of the eastern slope of the Jemez Mountains. In total, over 80,000 acres of forested landscape on the Pajarito Plateau and in the east Jemez Mountains have been burned by wildfires in the last 23 years; some of these fires have been the result of human activities while others have resulted from natural processes.

METHODS FOR PLANT SURVEYS

During the summers of 2002 and 2003, surveys for the presence of plants within various elevation zones and transfer tracts were conducted for two reasons: 1) to provide plant community information for the archaeological excavations and 2) to provide modern plant information for the pollen identification from the excavated sites. Personnel collected pollen samples in an elevation transect from White Rock to the Pajarito Ski Hill. Photographs were taken at each pollen-collecting site and the major plants recorded. Additionally, the plant communities of the major excavation sites within the land transfer tracts were examined. The plant identification was checked in Foxx and Hoard (1993) and Martin and Hutchins (1984). Since the period of the survey was after the Cerro Grande fire, some areas were within the burn

perimeter. A deepening drought in 2002 and 2003 caused many plants to be stunted (or not fully leafed). Additionally, much of the area was ravaged by the bark beetle and many piñons were dead and dying. These conditions made the diversity of plants normally in the various plant communities stressed and in some cases plants that would have been there were not blooming at the time of year we surveyed. Therefore a general description is based on the present survey information and historic survey information that may be pertinent to each area.

Results of the Plant Surveys for the Conveyance and Transfer Land Tracts

Airport Tract

The Airport Tract (A-3, A-7, and A-5-a) is located at the eastern end of the Los Alamos Airport. It is within the piñon juniper zone and generally has an understory of blue grama. Average rainfall is 12 to 14 inches. The site is relatively narrow and has limited vegetation that includes piñon pine and one-seed juniper with an understory of blue grama. Forbs included bitterweed, snakeweed, and cacti.

White Rock Tract

The White Rock Tract (A-19) is in the piñon-juniper woodland and has an understory of blue grama. The average annual precipitation at this elevation is 12 to 14 inches. The greatest number of edible plants has been found within this zone (Foxx and Tierney 1984; Vierra and Foxx 2002). The tract parallels State Route 4 and is directly across from the town of White Rock. The site is within the vicinity of Tsirege and is within lower Pajarito Canyon. An ephemeral stream flows through the canyon and springs likely provided water for the residents of Tsirege and a watering area for livestock. This tract, when examined, had been particularly hard hit by the bark beetle. Few piñons were still alive. Without an overstory cover the drought had taken a toll on the understory vegetation.

A cereal grain was noted in the vicinity of the site. The plant was most likely sorghum or another cereal grain but was not maize. In addition, some garden sunflowers were identified. Both sorghum and sunflower seeds are common in bird feeders. Scrub jays raid bird feeders for sunflower seeds. They carry the seeds to other trees and seeds also pass through their digestive system. The seeds probably lay dormant until rains provided conditions for sprouting. The thinning and death of so many trees in the area has opened up the tree canopy and such species can grow. There was very little understory vegetation due to the drought and opening of the canopy. To provide a more accurate indication of the plants within the canyon, studies by Foxx and Tierney (1980, 1984) were consulted. These sources also indicate the diversity of plant life when drought is not a factor.

Technical Area 74 Tract

The Technical Area 74 tract is primarily within Pueblo Canyon. The vegetation within this canyon is primarily piñon juniper with some ponderosa pine. There is a wetland area created

from the effluent from the Los Alamos County sewage plant. In June of 2002, we noted plant habitats within Pueblo Canyon.

Rendija Tract

The Rendija Tract (A-14) is on the north side of Los Alamos County above Rendija Canyon. The sites were visited in July of 2003. Photographs were taken and plants were noted at both the Archaic and homestead sites. The homestead site had a large quantity of tomatillo, which usually indicates disturbance and is common on archaeological sites. Tomatillo is considered a camp follower taxon and is often found associated with archaeological sites. The cover found on homesteads within Rendija Canyon and near the pumice mine were used to supplement data collected during the survey (Foxx et al. 1997).

CHAPTER 5
PALEOENVIRONMENTS OF THE SOUTHERN ROCKY MOUNTAINS OF COLORADO AND NEW MEXICO: A SUMMARY FROM LAKE AND BOG SEDIMENTS

R. Scott Anderson

INTRODUCTION

Interest in the long-term history of climate, vegetation, and forest disturbance of northern New Mexico, and specifically the Jemez Mountains/Bandelier National Monument area, has grown steadily over the last decade. This may be due to several important events that have impacted the local area since the late 1990s. One of these—the creation of the Valles Caldera National Preserve (VCNP)—established a focus on preservation and study of a ca. 36,000-ha (88,900-ac) property, formerly part of the privately held Baca Ranch. Bills appropriating funding for, and establishing the boundaries of, the Preserve were passed in 1999 and 2000. Establishment of the Preserve has allowed land managers and scientists to craft management plans that provide for a significant research component in an area that previously existed in private hands.

A second event that focused interest on the region was the Cerro Grande fire, which burned as much as 19,400 ha (48,000 ac) within and near Los Alamos, New Mexico, in May 2000. The effects of this high-severity fire were devastating on ponderosa pine and mixed conifer stands primarily west of Los Alamos and east of the VCNP and focused attention on the history of forest disturbance and its effect on vegetation within the area. A third characteristic bearing directly on the local environmental history is the long record of human habitation within the region (see chapters in Vierra 2005b; Kohler 2004). Therefore, the juxtaposition of interest in understanding local environments and processes that have created those environments, with the history of human habitation and exploitation of this landscape, suggests that the Jemez Mountains may be an ideal location for investigation of the relationship between climate change, human habitation, and forest disturbance.

Former environments and climates can be deduced using a variety of proxies, including pollen and plant macrofossils from lakes, bogs, or meadows; plant macrofossils and pollen from packrat (*Neotoma*) middens; and the tree-ring record of live and dead trees. Each of these proxies has been used primarily to determine climate conditions and/or former vegetation types. Many other proxies exist that are equally as important in determining former environments, including geomorphic and alluvial histories, isotopic analysis of sediments and cave deposits, and the archaeological record of human activities and habitations, among others.

No one proxy can tell the entire story of environmental change; each has its advantages and limitations, and an integration of as many proxy records as possible provides us the best chance to determine the entire picture of former environments. For example, analysis of tree-ring series allows us to determine year-to-year variations of climate (e.g., temperature and precipitation) as well as fire histories for a site. Most often, the record from tree-rings is limited to a few hundreds of years, less often to several millennia (Grissino-Mayer 1996). Packrat midden

deposits provide abundant plant macrofossils that allow us to determine—often to species level—the precise composition of the local flora (Betancourt et al. 1990). Addition of pollen analysis from middens allows for determining characteristics of the regional flora as well (Anderson and Van Devender 1991). But these glimpses of vegetation are most often separated by large blocks of time and are limited to the rocky substrate surrounding the site, as packrats primarily collect within several tens of meters from their nest only. Pollen and plant macrofossils from sedimentary deposits provide a longer, more continuous record than other proxies, but the source area for the pollen is often unclear, especially in areas of high relief (Markgraf 1980).

This chapter explores the history of vegetation change in north-central New Mexico and southern Colorado, centering primarily on the research that has been accomplished in the Jemez Mountains. The data proxies for reconstruction come primarily from analyses of sedimentary deposits that have accumulated in meadows, wetlands, bogs, and lakes over the last 15,000 years. These records document a series of vegetation and environmental changes that span a particularly intriguing time in southwestern North America, including the waning of the last great Laurentide and Cordilleran ice sheets in the northern hemisphere, the establishment of the warmer climates of the present interglacial (the Holocene), and the introduction of *Homo sapiens* into the continent. While the complete picture of paleoenvironmental change in this part of the southern Rockies has yet to emerge, the geographic distribution of sites for reconstructions has rapidly increased. Even so, most of this research on northern New Mexico exists today in the "gray" literature (e.g., project reports, master's theses, and conference abstracts and presentations).

For the general region of interest, Hall (1985) and Brunner-Jass (1999) summarized the paleoecological records from the Southwest and, more specifically, from northern New Mexico and southern Colorado before 2000 (ages presented in calendar years Before Present). A cluster of sites occurred in northwestern New Mexico, including the Chaco Canyon region (Hall 1977, 1985; Betancourt and Van Devender 1981), and the Chuska Mountains (Dead Man Lake region; Bent and Wright 1963; Wright et al. 1973). Other pollen records to the northwest come primarily from archaeological sites, and are of limited temporal extent. Additional sites had been analyzed from the San Juan Mountains of southwest Colorado, including Hurricane Basin (Andrews et al. 1975), Lake Emma (Carrara et al. 1984), Molas Lake (Maher 1963), Twin Lakes (Petersen and Mehringer 1976), and several sites in Mesa Verde (Martin and Byers 1965; Wyckoff 1977). By 1999, virtually nothing was known about the vegetation history of the southern Sangre de Cristo Mountains in New Mexico and Colorado.

From the Valles Caldera itself, a long pollen stratigraphy was recovered from the Valle Grande by Sears and Clisby (1952), which was presumed to be a pre-Wisconsin vegetation record. More recently, a second core was taken from this location, with radioisotope and paleoemagnetic stratigraphies documenting a ca. 50,000-year record spanning the OIS13–OIS14 transition (Fawcett et al. 2005). Closer to the present, Ensey (1997) produced two pollen records of the latest Holocene from Laguna de los Piños and Laguna de la Grulla, of which only the first was included in the report. Brunner-Jass (1999) undertook analysis of a sediment core from Alamo Bog in Alamo Canyon (western portion of the present Preserve), and from Chihuahueños Bog

(immediately north of the Preserve in the Santa Fe National Forest). These records have proven to be the most detailed analysis of vegetation and fire histories for the region to date.

Since 2000 the number of sites within this region has increased substantially. For instance, new records have been produced for the San Juan Mountains (Toney 2004; Toney and Anderson 2006) and the southern Sangre de Cristo range (Armour et al. 2002; Bair 2004), as well as numerous sites stretching northward in highlands west of the Rio Grande (Anderson et al. 2004, 2005). Additional research has been completed on the original Chihuahueños Bog core, while new cores were taken and analyzed from Alamo and Valle Santa Rosa Bogs within the Preserve. With the exception of the last two, most of these records span the entire post-glacial period.

The present chapter is presented in two parts. In Part I, two new records from the Jemez Mountains are presented. These records document Holocene changes in vegetation and fire. Part II presents a summary of the paleoenvironmental data, primarily pollen, macrofossils, and charcoal particles from sediment cores in the Southern Rocky Mountains.

NEW RECORDS FROM THE JEMEZ MOUNTAINS

Alto Alamo Bog

Alamo Bog occurs along Alamo Creek within Alamo Canyon, which is a prominent feature of the western Jemez Mountains of the VCNP. Over the last three decades, several significant research projects have focused on the region, including archaeological investigations (the Baca Geothermal Anthropological Project [Baker 1981]), and an initial study of the vegetation and fire history of the region (Brunner-Jass 1999). The wetland that composes the central core of the bog is located at the intersection of Alamo Creek and an unnamed creek flowing north, at an elevation of 2630 m (8628 ft; location in Figure 5.1).

In 2000 an additional core was obtained from a section of the bog further upstream along Alamo Creek, named Alto Alamo Bog (AAB). Our reasoning for obtaining a second core location was to substantiate and validate the original Alamo Bog record, which suffered from potential problems in sediment dating. This is important because of the long history of human habitation of the region and the potential for human manipulation of the mixed conifer forest there. It was hoped that the AAB core would not be affected by the problems discovered at the site of the original study.

AAB is located at 2658 m (8720 ft) elevation, latitude 35^{o} 54’ 45” N, longitude 106^{o} 34’ 45” W on the Valle San Antonio 7.5’USGS Quad. Vegetation at AAB is much the same as at Alamo Bog proper. The bog surface is dominated by grasses (Poaceae) and sedges (Cyperaceae). Slopes surrounding both bogs are forested and strongly affected by aspect. On north-facing slopes, mixed conifer forests predominate, with Douglas-fir (*Pseudotsuga mensiezii*), white fir (*Abies concolor*), quaking aspen (*Populus tremuloides*), Colorado blue spruce (*Picea pungens*), and southwestern white pine (*Pinus strobiformis*). On xeric south-facing slopes, particularly around Alamo Bog, ponderosa pine (*P. ponderosa*) and Gambel oak (*Quercus gambelii*)

dominates with lesser amounts of the more mesic common juniper (*Juniperus communis*) and many herbaceous species. Terminology follows Martin and Hutchins (1980).

Two Livingstone sediment cores (Wright 1991) were taken from AAB in 2001. Core 1, which was intensively analyzed, yielded a 3.75-m record. Each drive section was described in the lab, noting stratigraphy, sedimentary and organic content, and Munsell color under fluorescent light. Magnetic susceptibility measurements were made using a Bartington MS2E meter at 5-mm intervals. Magnetic susceptibility readings are reported as electromagnetic units per cubic centimeter (emu/cc).

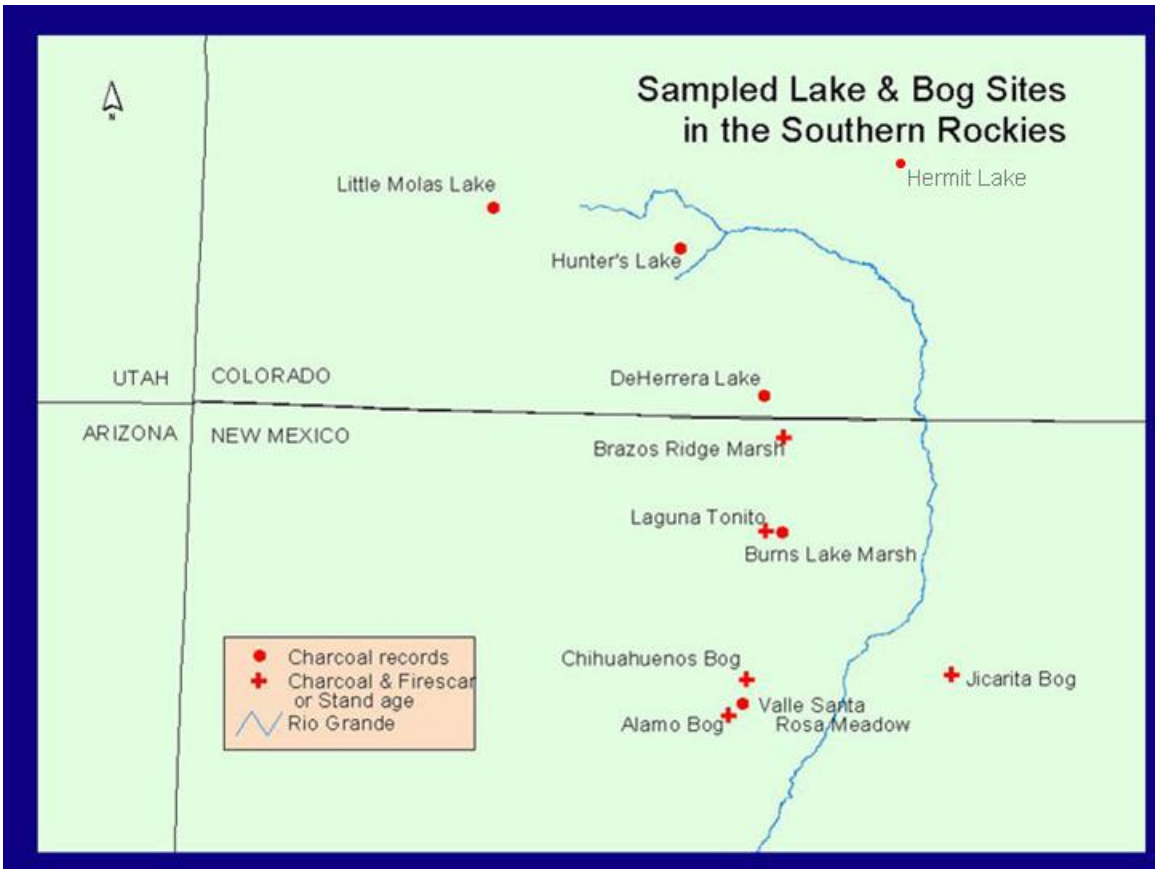

Figure 5.1. Sampled lake and bog sites in the southern Rockies.

Pollen was extracted from the sediments using standard methods (Fægri et al. 1989), including suspension in KOH, HCl, and HF. After acetolysis, pollen residues were stained and suspended in silicone oil. Many of the core samples required a 9-µ sieving step to remove additional clay and fine organics. Pollen counts per sample consisted of a minimum 300 non-Cyperaceae/non-Poaceae grains and a minimum of 50 non-*Pinus* terrestrial grains. *Pinus* grains were identified to subgeneric level when possible (Jacobs 1985a). Wetland (bog/riparian) types, excluding Poaceae, are graphed outside the pollen sum. Plant macrofossil samples for each core were recovered by washing the sample through stacked soil sieves. Macrofossils were also tallied during charcoal analysis (see below). Pollen types and macrofossils were identified using the

comparative collection and manuals in the Laboratory of Paleoecology (LOP) at Northern Arizona University. Pollen data were plotted using Tilia View (Grimm 1992).

For the high-resolution sedimentary charcoal analysis we extracted a 0.5-cc sample from each linear cm of the core length. Sediment samples were sieved into 125-μm and 250-μm fractions. Charcoal particles were identified under a binocular microscope at 10x to 70x. Charcoal was identified by a uniformly black color, an iridescent sheen, and the presence of cellular structure. Macroscopic charcoal counts were standardized to 1-cc volume.

Radiometric ages for this core came from a combination of ^{210}Pb, ^{137}Cs, and ^{14}C analyses. Older sediments (below 42.5 cm depth) were dated by accelerator mass spectroscopy analysis of small sediment samples. ^{14}C ages were converted to calendar ages using CALIB 5.0 (Stuiver et al. 1998). To date the uppermost sediments we used both ^{210}Pb and ^{137}Cs (Appleby et al. 1979; Crusius and Anderson 1995). ^{210}Pb is suitable for dating the most recent 150 years, since its half-life is 22.26±0.22 years (Blais et al. 1995; Olsson 1986). ^{137}Cs has a half-life of ca. 30 years and was produced in great abundance during nuclear atmospheric testing beginning in 1945 (Olsson 1986). The first pronounced increase of ^{137}Cs in sediment dates to AD 1954, with a maximum occurring in AD 1963 to 1964 and a decline by AD 1965.

The Sedimentary Record

The AAB record extends back in time to about 4750 calendar years ago (Figures 5.2 and 5.3), with continuous sedimentation to the present. The sediments consist primarily of silty peats (i.e., colluvium) for most of the record (Figure 5.3), except for a section of sand and pebbles near the core bottom and peat in the upper ca. one meter of the core. Although the sand and pebbles have been graphed as being deposited over several hundred years, this deposit is in all likelihood a nearly instantaneously deposited unit.

The dominant pollen types are pine (*Pinus*) and grass (Poaceae) throughout the record (Figure 5.2), but occurrence of other conifers, especially spruce (*Picea*), fir (*Abies*), Douglas fir (*Pseudotsuga*), and juniper (*Juniperus*) suggests that a rich mixed conifer forest existed adjacent to a grassy meadow for the entire record. The dominant pines were probably ponderosa pine (*Pinus ponderosa*) and southwestern white or limber pine (*Pinus strobiformis* or *P. flexilis*), as shown by macrofossil analysis (Figure 5.3), but macro-remains of spruce and Douglas fir also attest to their local presence. The occurrence of pollen from Colorado piñon (*P. edulis*) and oak (*Quercus*) suggests that these trees may have been present locally as well, or at least were important tree species within the general region, much as they are today.

Small changes in the pollen assemblages suggest that subtle differences in the vegetation history of AAB can be recognized. For instance, before 2200 years ago, herbs were more abundant in the record, including grasses, ferns, and members of the mustard family (Brassicaceae), as well as sedges (Cyperaceae) and meadow-rue (*Thalictrum*) (Figure 5.2). Pollen of spruce and Douglas fir was more common, while pollen of pine (including ponderosa pine) and fir was less abundant than in later time periods. After 2200 years ago, spruce and herb species declined, while pollen of ponderosa pine and fir increased.

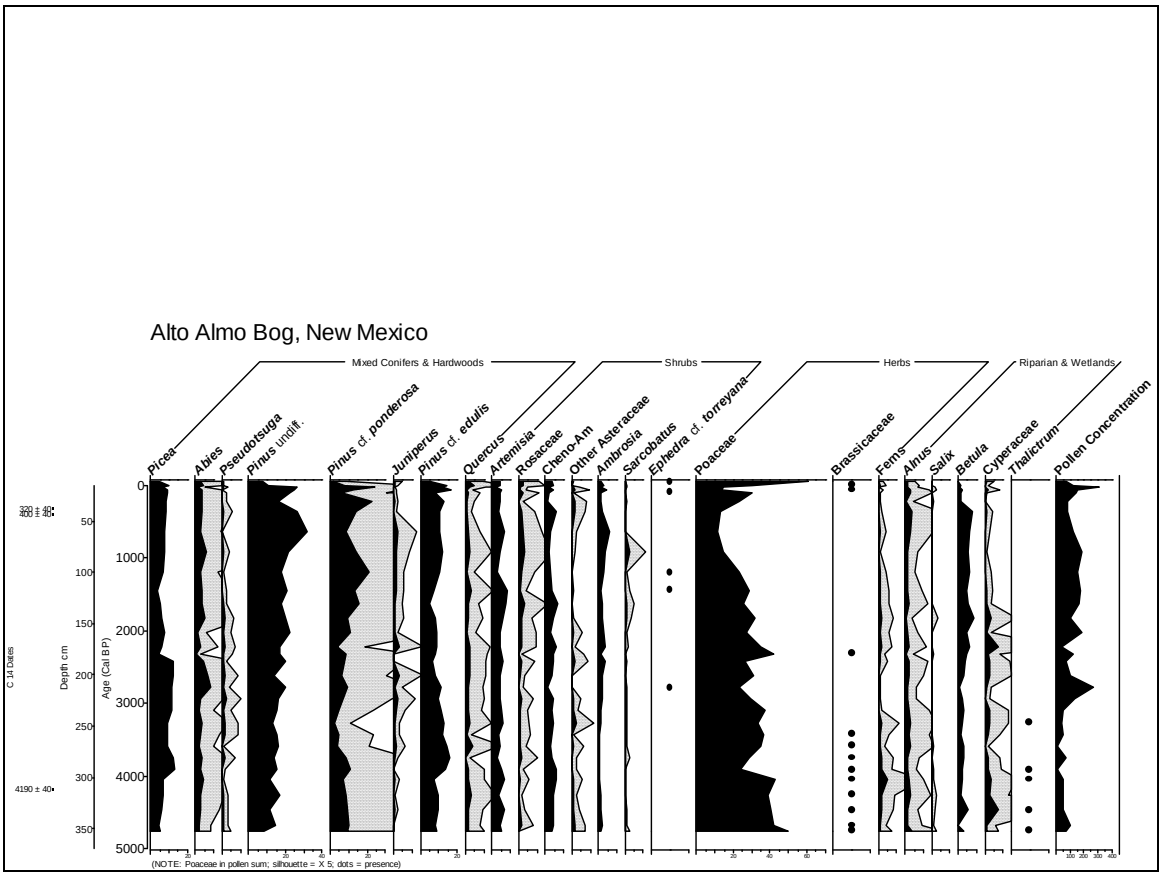

Figure 5.2. Pollen types at the Alto Alamo Bog, New Mexico.

Shrubby taxa, such as members of the rose family (Rosaceae), ragweed (*Ambrosia*), greasewood (*Sarcobatus*), and joint-fir (*Ephedra*) increased after 2200 years ago. Most other taxa do not vary significantly over this transition. Of interest from a biogeographic viewpoint is the occurrence during this period of birch (*Betula*), which is probably bog birch (*B. glandulosa*), whose only known occurrence during the Holocene is here in Alamo Canyon. Pollen changes in the uppermost levels of the core—the Historic period—include declines in pine pollen (especially noted in ponderosa pine) and birch, with increased in grass pollen percentages.

The charcoal stratigraphy (Figure 5.3) approximates the fire history of the site. Abundant charcoal was retrieved from sediments deposited before ca. 4000 years ago, but the amount of charcoal declines substantially between 4000 and 2200 years ago. Subsequently, charcoal concentration increases between ca. 2200 and 400 years ago and declines considerably. Sediments deposited during the 20th century contain virtually no charcoal (Figure 5.3).

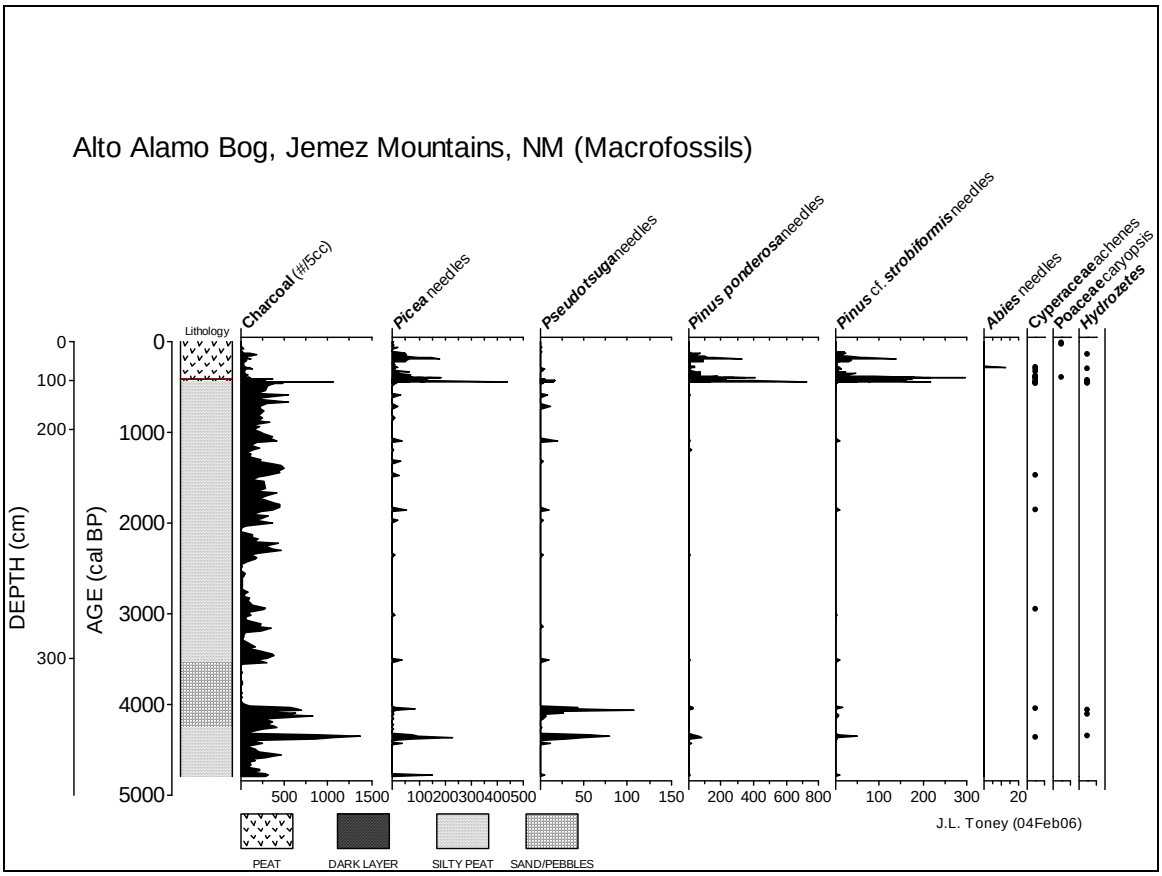

Figure 5.3. Charcoal stratigraphy from the Alto Alamo Bog, New Mexico.

Pollen and charcoal stratigraphies are consistent with an interpretation of occurrence of a mixed conifer forest surrounding an open meadow-like wetland, with frequent fire over the last 4750 years. Before 2200 years ago, however, the local environment may have been moister than subsequently, as shown by the greater abundance of spruce and wetland herbs, such as sedge. The fire record is also consistent with this interpretation for the early part of the record, with smaller concentrations of charcoal, except for the lowermost samples deposited before 4000 years ago. Beginning by 2200 years ago, however, an increase in ponderosa pine in the record, along with an increase in charcoal concentrations, suggests drier conditions with perhaps more frequent fire, at least in portions of the drainage basin. Further support for this comes from the increase in shrubs, although it is unclear if species like greasewood and joint-fir grew locally, or if these types represent long-distance transport of pollen from locations to the west of Alamo Canyon. The Historic period is seen in samples of both pollen and charcoal stratigraphies, with a decline in ponderosa pine pollen—probably due to logging locally—and an increase in grass pollen, which may be due to introduction of exotic grasses due to grazing.

Valle Santa Rosa Bog

A second new study in the VCNP comes from Valle Santa Rosa Bog (VSRB), located in Valle Santa Rosa near its confluence with Valle San Antonio in the northern portion of the VCNP

(location in Figure 5.1). The coring site is located at 2590 m (8500 ft), latitude 35° 57' 45" N, and longitude 106° 31' 00" W, also on the Valle San Antonio 7.5' USGS Quad. Uplands around the bog are fairly open, but common trees include *Picea* sp., quaking aspen (*Populus tremuloides*), and ponderosa pine, with common juniper (*Juniperus communis*) as groundcover. The bog itself is covered by sedges and grasses. On the drier marginal meadow grow blue flag (*Iris missouriensis*), cinquefoil (*Potentilla* sp.), shrubby cinquefoil (*P. fruticosa*), dandelion (*Taraxacum officianale*), yarrow (*Achillea lanulosa*), pussytoes (*Antennaria* sp.), clover (*Trifolium* sp.), buttercup (*Ranunculus* sp.), and members of the pink family (Caryophyllaceae) (terminology after Martin and Hutchins 1980).

Two sediment cores were taken with a Livingstone corer in 2001 on the western margin of the Bog. Core 2 was selected for study and measures 1.8 m long. Our reasoning for studying this site was to obtain a record from the northern portion of the VCNP that could be compared with the Alamo Canyon records.

Essentially the same procedures were followed for analysis of VSRB sediments as for AAB. These included description of core stratigraphy, sedimentary and organic content, and Munsell color, as well as magnetic susceptibility. Pollen and charcoal particle stratigraphy methodology followed the same procedures as for AAB as well (see above). Radiometric ages for this core also came from a combination of ^{210}Pb, ^{137}Cs, and ^{14}C analyses. Older sediments (below ca. 62 cm depth) were dated by accelerator mass spectroscopy analysis of small sediment samples. ^{14}C ages were converted to calendar ages using CALIB 5.0 (Stuiver et al. 1998). ^{210}Pb and ^{137}Cs ages determined the upper 39 cm of the core.

The Sedimentary Record

According to our chronology accepting the bottommost age of the core, the VSRB record extends back in time to over 9000 calendar years ago (Figure 5.4). The upper 8.5 cm of the core is dark brown peat. Below the peat, to ca. 125 cm depth is organic silts (colluvium) alternating with sand layers. Sand units increase below 125 cm, but primarily return to organic silts to the core bottom. Unlike the AAB record, however, sedimentation at this site has not been continuous, and a number of unconformities, or periods of severe drying, are apparent in the pollen record. The most extensive unconformity occurs between 125 and 140 cm depth, encompassing perhaps 1375 to 8500 years ago, or most of the record. Thus, the VSRB pollen record includes only a short period in the late Holocene and one in the early Holocene. Each of these will be treated separately.

As at AAB, the dominant tree pollen type at VSRB is pine (*Pinus*) throughout the record. Unlike AAB however, grass (Poaceae) is not as abundant anywhere in the record. Early Holocene pollen spectra include spruce (*Picea*), ponderosa pine (*Pinus ponderosa*), and other pines, as well as some fir (*Abies*). Shrubs are dominated by sagebrush (*Artemisia*), saltbush-type (*Atriplex*; cheno-am), and other members of the aster family (Asteraceae). Riparian plants, such as willow (*Salix*), carrot family (Apiaceae), and meadow-rue (*Thalictrum*) are most important in this period, suggesting the site may have been a streamside location during the early Holocene.

Pollen deposited during the most recent 1375 years shows that pines, spruce, and fir continued to be important here, and Douglas fir (*Pseudotsuga*) increased in importance during this time (Figure 5.4). Sediments in the upper 40 cm show an increase in juniper (*Juniperus*) and oak (*Quercus*). In addition, pollen indicators of local land clearance and cattle ranching are evidenced here, beginning with the occurrence of introduced species associated with grazing (filaree, *Erodium*; dock, *Rumex*), followed by increased grass (Poaceae) pollen, perhaps a result of non-native introductions. In the uppermost sediments, pine pollen declines although the proportion of ponderosa pine pollen does not. At the same time, an increase is seen in sedge (Cyperaceae) pollen, suggesting higher groundwater tables in the most recent century.

The preliminary charcoal record shows generally highest concentrations of charcoal in the early Holocene section of the core (Figure 5.5). Charcoal concentrations trend to zero during the period encompassing the unconformity, then rebounds in the late Holocene to amounts not exceeding those from the early Holocene. Charcoal declines about 33-cm depth, and falls to zero above 16-cm depth.

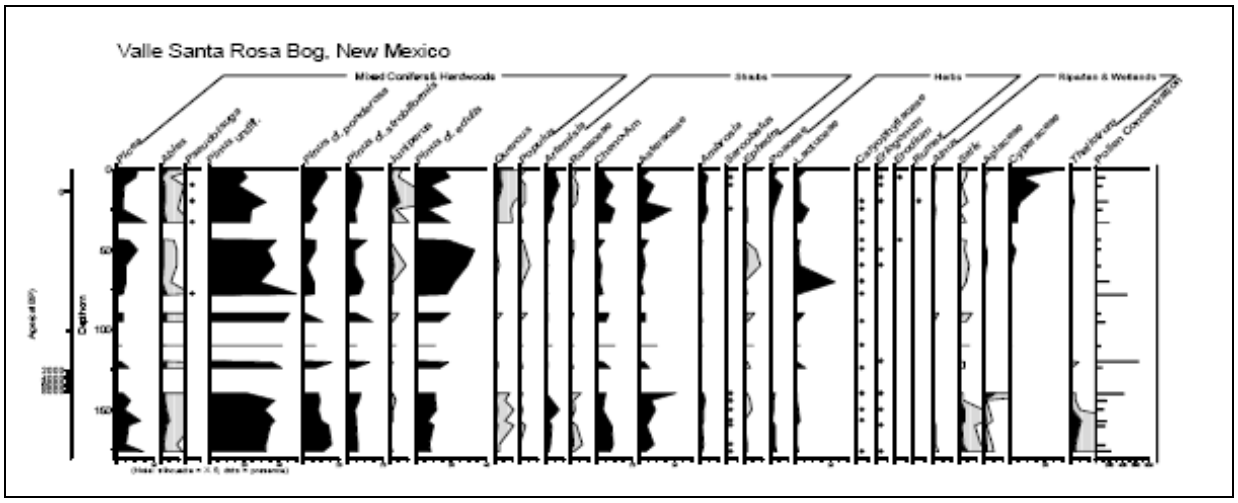

Figure 5.4. Pollen cores from the Valle Santa Rosa Bog, New Mexico.

Pollen and charcoal stratigraphies are considerably more difficult to interpret from VSRB than from AAB due to the considerable portion of the record that is missing. Still, the overall pollen record suggests a similar mixed conifer forest surrounding an open meadow-like wetland for both the early and late Holocene. One major difference between the two sites is the general paucity of grass in the VSRB record compared to the AAB record. This is a little puzzling, since the Valle Santa Rosa today is primarily a grassland, with open forest on the upper-side slopes. The fire history records of the two sites are generally similar, however, with similar amounts of charcoal (on a /cc basis) and a declining amount of charcoal deposited during the 20th century fire suppression period.

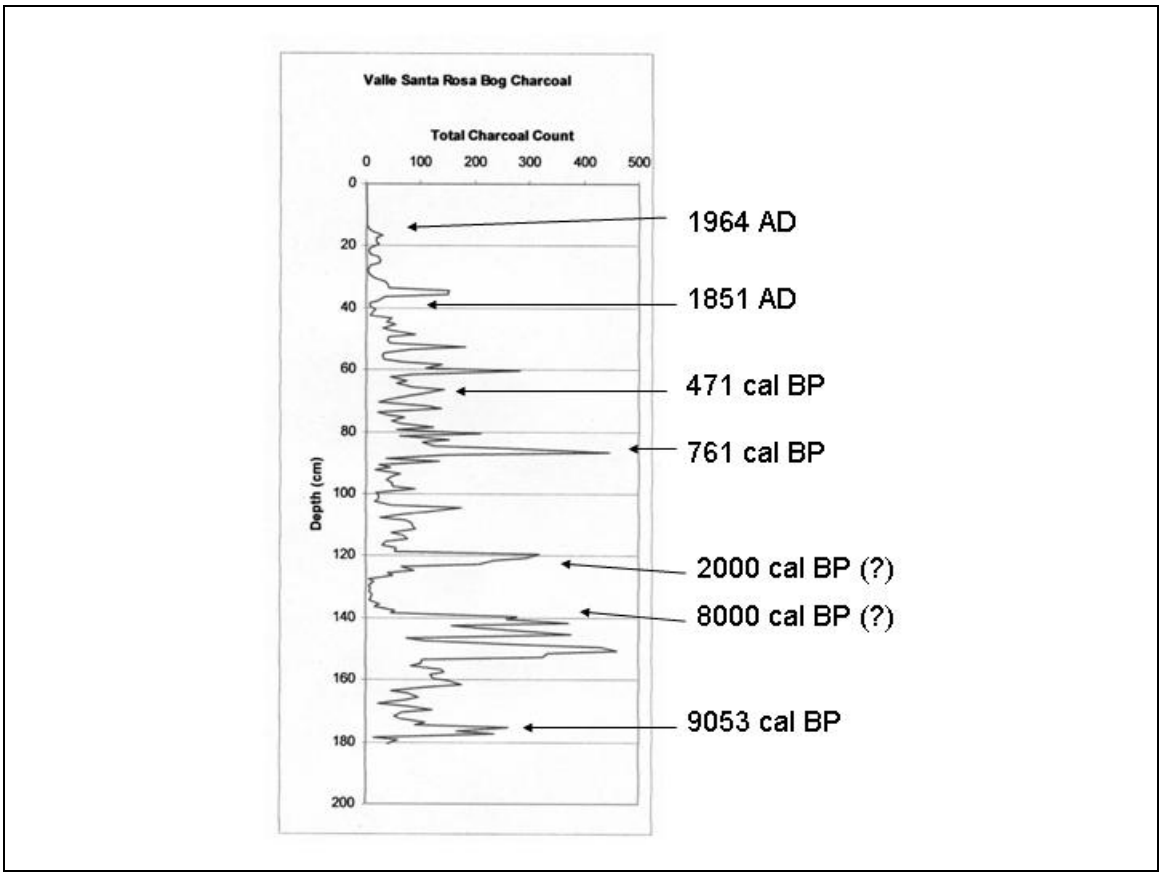

Figure 5.5. The charcoal record from the Valle Santa Rosa Bog, New Mexico.

Vegetation Change in the Southern Rockies

As discussed in the introduction above, our knowledge of the post-glacial paleoenvironmental history of the southern Rockies—including the San Juan and Sangre de Cristo ranges—is meager, but recent efforts have begun to tackle the temporal and spatial history of vegetation change there. Study has tended to concentrate around several themes, including the 1) characteristics of vegetation and climate change during deglaciation in the highlands, 2) understanding the development of the southwestern monsoon and its influence on vegetation, 3) the characteristics of the late Holocene, a time of particular interest in the archaeological record, and 4) fire histories of the present interglacial, among others. In reality, each of these individual subjects is part of a continuum of change that has occurred over the course of the last ca. 15,000 years.

Full- and late-glacial paleoecological studies from the southern Rocky Mountains indicate that treeline was up to 500 m lower during the Pinedale glaciation (Legg and Baker 1980; Maher 1963; Markgraf and Scott 1981). Highest-elevation sites were glaciated, while alpine vegetation found above 3300 m today occupied areas around 2800 m elevation (Legg and Baker 1980). Similarly, subalpine forests found between 2700 and 3300 m elevation today occupied sites below 2300 m elevation (Markgraf and Scott 1981). High-elevation sites reflect late-glacial

conditions with cold winters and increased winter precipitation and drier than present summers (Vierling 1998) and enhanced winter storms originating in the Pacific Ocean (Markgraf and Scott 1981). Models suggest summer precipitation was at a minimum during this period (COHMAP 1988; Kutzbach et al. 1998).

The Late Glacial and Younger Dryas

The southern Rocky Mountains were extensively glaciated during the Pleistocene (Pierce 2004). However, the timing of deglaciation varies from place to place. For instance, in the Park Ranges of northern Colorado, insect assemblages suggest deglaciation before 16,440 cal BP (13,800 yr BP) (Elias 1996), which also suggest mean annual temperatures were only 3 to 4°C cooler than present, but mean winter temperatures were considerably colder (ca. 19 to 21°C cooler than present). Similar evidence (Elias 1996) suggests the Front Range of Colorado underwent deglaciation before ca. 13,860 cal BP (12,000 yr BP) (Elias 1996; Menounos and Reasoner 1997). Deglaciation in the San Juan range may have been somewhat later. Elias et al. (1991) reported ^{14}C basal dates suggesting that deglaciation was complete there by 11,480 cal BP (10,000 yr BP). This was recently confirmed at Little Molas Lake with deglaciation by 11,200 cal BP (Toney and Anderson 2006). In the southern Sangre de Cristo range, near Jicarita Peak, Bair (2004) suggested a much earlier deglaciation, by ca. 15,300 cal BP.

Of great interest has been recent research confirming that the environments of the Southwest were affected by events centered in the North Atlantic during deglaciation. The Younger Dryas stadial (YD; ca. 13,000 to 11,600 cal BP) was a brief period of climatic deterioration in the overall warming of the post-glacial (Yu and Wright 2000). While effects centered primarily on both sides of the North Atlantic, recent evidences suggests that the YD oscillation resulted in rapid vegetation responses at high-altitude sites in the southern Rockies as well. For instance Armour et al. (2002) documented periglacial activity during the YD in the Winsor Creek Basin of the southern Sangre de Cristo Mountains, New Mexico. Nearby at Jicarita Bog on Jicarita Peak, Bair (2004) documented minor vegetation changes associated with cooler conditions at that time. In Colorado at the Sky Pond site, glacio-lacustrine sediments probably associated with a glacial re-advance characterize the YD there (Menounos and Reasoner 1997). Reasoner and Jodry (2000) compared the Sky Pond record with that from Black Mountain Lake in the San Juan Mountains of Colorado and found major vegetation boundaries corresponding with onset and termination of the YD.

The Early to Middle Holocene and Development of the Arizona Monsoon

Subsequent to the YD cooling, extensive warming of climate commenced at the beginning of the present interglacial—the Holocene. The number of sites covering the transition to the Holocene is becoming substantial. Along the Front Range of Colorado, change to organic gyttja deposition with terrestrial macrofossils overlying the YD clastic sediments at Sky Pond signifies elevated biological activity within the lake and increased vegetation cover on land (Menounos and Reasoner 1997). The fossil insect record indicates that the postglacial warming maximum occurred between 12,930 and 10,180 cal BP (11,000 and 9000 yr BP) in the Rocky Mountains. At the La Poudre Pass, Colorado site, the warmest mean July temperatures occurred at 11,255 cal BP (9850 yr BP), and were 3.7 to 6.7°C warmer than present (Elias 1983, 1996). Four sites

above 3000-m elevation in the Front Range show an early Holocene warming between ca. 10,180 to 7830 cal BP (9000 to 7000 yr BP), based on ratios of forest species to tundra species, and the presence of conifer macrofossils (Elias 1985).

In central Colorado, Fall (1997) examined a pollen record from Cottonwood Pass Pond (3670 m), presently above the treeline. However, sediments dating between 9840 and 4480 cal BP (8800 and 4000 yr BP) contains conifer macrofossils and high percentages of *Picea* and *Abies* pollen, indicating a subalpine forest grew at the location then. Climate reconstructions based on modern lapse rates and using an estimated treeline rise of 270 m suggest mean July and mean annual temperatures were ca. 1.9°C and 1.6°C warmer than present, respectively. In south-central Colorado, Anderson et al. (2004) demonstrated establishment of post-glacial, subalpine forests at Hunter's Lake (Wiminuche Wilderness Area, north of Pagosa Springs) by ca. 12,500 cal BP, and at DeHerrera Lake (south-central Colorado) by ca. 13,000 cal BP.

In the San Juan Mountains, Maher (1963) documented fluctuations in pollen ratios of high-elevation conifers—*Picea* and *Pinus*—that suggested higher treeline in the early Holocene at Molas Lake. This was a period of warmer, dry conditions favorable to the upslope migration of trees. Elias et al. (1991) also observed *Picea* and *Abies* krummholz fragments identified by their small size and contorted annual-ring pattern in Lake Emma, Colorado. Sediments indicate that the krummholz vegetation was at least 70 m higher than today throughout much of the early and middle Holocene (Elias et al. 1991), while Toney (2004) and Toney and Anderson (2006) documented early Holocene establishment of spruce forest at Little Molas Lake.

In northern New Mexico, the record from Chihuahueños Bog (north of the VCNP) spans the last ca. 15,000 years (Anderson et al. 2004). Unlike other sites in the region, this area was not glaciated during the late Pleistocene, since it was well below the elevational limit for permanent ice (2925 m). An open spruce forest grew around a small pond until ca. 11,500 cal BP when ponderosa pine became established. Further to the southeast, at Jicarita Bog in the Sangre de Cristo range of New Mexico, warming commenced by 12,000 cal BP and intensified after ca. 11,700 cal BP. Warmest and driest conditions probably existed from ca. 9000 to 4400 cal BP there.

Several studies have documented the establishment of the Arizona Monsoon by the opening of the Holocene. The monsoon is important since it brings moisture to the Southwest during the driest part of the growing season. Anderson (1989) suggested the establishment of ponderosa pine across the southern Colorado Plateau signified expansion of the Arizona Monsoon, since today ponderosa pine is found in locations where summer precipitation is important. Using deuterium (δD) of wood cellulose at Lake Emma, Friedman et al. (1988) suggested that summer monsoonal precipitation dominated in the San Juan Mountains in the early Holocene, but shifted to a greater mix of Pacific frontal storms and monsoons after 4400 cal BP (Carrara et al. 1991). Changes in δD indicate changes in moisture source, the seasonality of precipitation, or a combination of both. Precipitation from air masses originating over the Gulf of California reach the San Juan Mountains without first passing over high mountains; higher D level are expected relative to those originating in the Pacific Ocean that must travel over high mountain ranges before reaching the southern Rocky Mountains. Models suggest that summer radiation decreased from 9000 years ago to the present (COHMAP 1988; Kutzbach et al. 1998). Because

the summer monsoons are driven by heating of land masses, a corresponding decrease in monsoon activity was predicted for the remainder of the Holocene.

Though the early Holocene was warm enough to drive the intensification of the Arizona Monsoon, at least one study from New Mexico suggests that the transition between the early and middle Holocene was particularly dry. Chihuahueños Bog dried out completely between ca. 8500 and 6200 cal BP, as groundwater tables fell in response to warm and dry climates (Anderson et al. 2004). Few other sites have shown such a drastic response to climatic drying. One such site is VSRB (this report), which also shows a lack of sediment accumulation beginning about 8500 years ago. However, the VSRB record does not resume until about 1375 years ago, with most of the Holocene record missing. At Little Molas Lake in the San Juan Mountains, warm conditions prevailed from 10,570 to 6700 cal BP, culminating in a shallow lake phase from 6230 to 5900 cal BP. This falls within the mid-Holocene period of higher treeline documented by Elias et al. (1991).

A site nearby to the Chihuahueños and VSRB—Alamo Bog—also within the VCNP, spans the last 9000 years, but shows a continuous record during this period (Brunner-Jass 1999). Apparently this site had sufficient soil moisture to remain wet during the entire Holocene. The pollen spectra of the entire record is dominated by mixed conifer species, with alder (*Alnus*), sedge (Cyperaceae) and *Spagnum* growing locally on and around the bog.

The Middle to Late Holocene

The middle to late Holocene period is one of substantial transition within the Southwest, and indeed, worldwide. This period is characterized by a general cooling trend relative to the early Holocene, with an increase in effective moisture. Even so, the late Holocene is punctuated by substantial droughts, both recognized in the sedimentary record as well as the tree-ring record.

Physical evidence for effectively cooler conditions is shown in the Winsor Creek Basin cores of northern New Mexico (Armour et al. 2002). The cores document four episodes of magnetic susceptibility spikes congruent with increases in clastic sediment deposition, interpreted as indicative of periglacial activity. These events occur at ca. 5640, 4390, 2870, and 130 cal BP (4900, 3945, 2770, and 120 yr BP, respectively) (Armour et al. 2002).

Palynological evidence of cooling is ubiquitous, but the actual period of transition differs between locations. For instance, effectively more moist conditions occur at Chihuahueños Bog by 6000 to 5000 years ago, as shown by the increase in fir (*Abies*), followed by piñon (*Pinus edulis*) pollen. Moist meadow conditions prevailed at Jicarita Bog, New Mexico, after 5000 years ago, with the development of a sedge meadow at the site. Sediments at Brazos Ridge Marsh (northern New Mexico, 3222 m) did not begin to accumulate in the shallow basin until 5000 years ago, presumably due to lower groundwater tables before that time. At Alamo Bog, grass (Poaceae) expanded at the expense of all other pollen types by ca. 4800 years ago. We interpret this as an expansion of the wet meadow—also due to rising groundwater tables—forcing the mixed conifer forest to grow further away from the middle of the bog as increasingly wetter conditions prevailed. In central Colorado, both the lower treeline (controlled by precipitation) and the upper treeline (controlled by temperature) contracted after ca. 4990 cal BP

(4400 yr BP) (Fall 1997; Markgraf and Scott 1981). And warmer and drier climates than today transition to effectively moister climates at Little Molas Lake in the San Juan Mountains by ca. 4100 years ago. Timberline lowering around Lake Emma in the San Juan range reflected presumed cooling after ~3100 cal BP (Elias et al. 1991). These data document that sites respond to climate changes individualistically, depending upon the sensitivity of sites, and to a lesser extent, the accuracy of the chronology.

Some sites not only document broadscale changes in vegetation and climate during the late Holocene, but the records can be interpreted as being sensitive enough to register drier and wetter periods internal to the long-term late Holocene trend toward cooler conditions. For instance, summer and annual precipitation decreased after 2800 cal BP at Beef Pasture and Twin Lakes in the La Plata Mountains, as indicated by a decrease in *P. edulis* and a narrowing of the *Picea* zone, respectively (Petersen 1981). From 2500 to 1500 cal BP the Twin Lakes data indicate cooler temperatures, but drier summers (Petersen 1981). The upward shift of *Picea* to modern elevations due to warming occurs in the Lost Park record after 1800 cal BP, as higher sagebrush (*Artemisia*) and lower goosefoot (cf. *Atriplex*; Cheno-am) pollen percentages indicate drier summers (Vierling 1998). Modern climate and vegetation conditions were established at Jicarita Bog by 1700 years ago (Bair 2004). Additional evidence for a variable climate during the late Holocene comes from studies of fire histories, as documented below.

Undoubtedly the most detailed tree-ring series published to date for northern New Mexico comes from El Malpais National Monument. Grissino-Mayer (1996) constructed a 2129-year record based on long-lived live and dead Douglas fir (*Pseudotsuga menziesii*) and ponderosa pine (*Pinus ponderosa*) trees in this habitat that was largely protected from grazing and lumbering. Grissino-Mayer's analysis for the last 1900 years documents at least seven major long-term trends in rainfall. Above normal rainfall occurred during the periods AD 81–257, 521–660, 1024–1398, and 1791–1992, while below normal rainfall occurred during AD 258–520, 661–1023, and 1399–1790. The most intense drought during this time period was during AD 258-520. The precision of these data are unmatched by any of the pollen records obtained to date in the Southwest.

Fire Occurrence During the Holocene

Until recently, little was known about the long-term (Holocene-length) fire history of high elevation forests in the Southwest. Anderson et al. (2004, 2005) has reported on a fire history reconstructions from lake and bog sediments from seven sites in southern Colorado and northern New Mexico, which includes data on Little Molas Lake (Toney 2004) and Jicarita Bog (Bair 2004). More recently, Toney and Anderson (2006) have compared the long-term fire history records from Little Molas Lake with several from California to examine sub-continental patterns of burning during the Holocene.

High-resolution sampling—usually every 0.5 to 1.0 cm of linear core—is conducted to deduce the temporal patterns of fire at an individual site. This allows the investigator to construct the raw charcoal record (usually in particles/unit volume). Using the CHAPS program (Long et al. 1998) allows for calculation of charcoal deposition rates (CHAR), and separation of local fires (peaks) from non-local fires (background). This allows for calculation of a metric relating fire

occurrence to time, often number of fires/1000 years. For high-elevation spruce-fir forest types, fire event frequency is usually measured in multiple decades to centuries (Alington 1998; Kipmueller and Baker 2000; Sherriff et al. 2001; Veblen et al. 1994), while for mixed conifer and ponderosa pine forest types it is years to decades (Swetnam and Baisan 1996).

Presently long-term data for the entire Holocene exist for Little Molas Lake, Hunter's Lake, and DeHerrera Lake in southern Colorado and from Jicarita Bog and Chihuahueños Bog in northern New Mexico. Shorter records have been analyzed for Brazos Ridge Marsh, Alamo Bog, and VSRB in northern New Mexico. Two time periods occur in these records where fire event frequency is higher than the Holocene average. Four sites—Little Molas, Hunter's, and DeHerrera Lakes, and Chihuahueños Bog—show higher fire event frequency between ca. 10,000 and 12,000 years ago (Anderson et al. 2004, 2005). The peak in fire activity for Jicarita Bog is displaced to ca. 12,000 to 14,000 years ago. We believe that there are two explanations for this. First, this was the time of highest post-glacial summer insolation, as modeled by Kutzbach and Guetter (1986) and others. This led to much warmer summers, with perhaps 7 percent to 8 percent greater insolation than today. With the initiation of the summer monsoon at this time came an ignition source as well—lightning. Second, this was also a period of rapidly changing vegetation, with the replacement of spruce woodland by spruce-fir forest or of spruce-fir forest by mixed conifer forest. Theoretically, the landscape would have contained abundant dead wood and other necromass for burning, assuming an ignition source was present.

The second period that witnessed a greater than average fire event frequency was during the late Holocene, between ca. 2000 and 1000 years ago. This pattern is present at Hunter's Lake, Brazos Ridge Marsh, and Chihuahueños Bog, with Alamo Bog showing higher fire event frequencies somewhat earlier at ca. 2500 years ago. Several explanations can be advanced for this (Anderson et al. 2004, 2005). First, Mayewski et al. (2004) demonstrated numerous records worldwide that document rapid climate changes as being more frequent during the late Holocene than before. Rapid fluctuations in climate may have placed additional stresses on plant communities that were not as apparent earlier in the record. It is likely that the late Holocene witnessed greater drought frequency. Within the limits of our dating, this late Holocene period is nearly contemporaneous with the AD 258–520 drought period documented from tree-rings at El Malpais (Grissino-Mayer 1996), which also documents additional extended periods of drought in the area during the most recent 2000 years. Second, most of the pollen evidence presented above suggests that mid- to high-elevation forest development reached its maximum extent during the late Holocene. This may have been a result of increased late Holocene winter precipitation, a result of the strengthening of El Niño over the last ca. 5000 years (Anderson and Smith 1997; McGlone et al. 1992; Menking and Anderson 2003; Rodbell et al. 1999). A climatic linkage between drought and climate for the Southwest has been established by Swetnam and Baisan (1996) who clearly showed from tree-ring evidence that the largest fire years are also those with the deepest drought, as measured by the Palmer Drought Severity Index. Therefore, we might expect with increased biomass, periods of drought would witness more frequent fire.

SUMMARY

The number of paleoecological sites with pollen and charcoal data within the southern Rocky Mountains of Colorado and New Mexico has grown considerably in the last decade. Research in this region has been driven by the desires of land managers to understand the history of vegetation change and long-term fire history. For most of the post-glacial period, climate has been the driver of vegetation and fire histories. However, human activities have had an increasingly important impact on the landscape of the region, as shown by the results of the Cerro Grande fire of 2000.

Two new records of vegetation and fire in the Jemez Mountains include AAB and VSRB. Although the record from VSRB is of limited use, the AAB record spans most of the late Holocene, a period of considerable interest to land managers and archaeologists. Pollen and macrofossil evidence demonstrate that forest of this elevation was one of mixed conifers throughout the period, but the characteristics of the forest transitioned about 2200 years ago to one including more ponderosa pine, with greater fire. It is unclear whether an increase in fire frequency allowed for greater ponderosa pine, or vice versa, from these data. It is also unknown at this time whether this change was driven by climatic or human causes. Further investigation is warranted on these issues.

Much of our knowledge of the long-term history of the region remains unpublished, or is found in "gray" literature publications. However, this may soon change, as the numbers of articles from a large USGS-BRD study become published (e.g., Toney and Anderson, 2006). Of great interest to paleoecologists is the occurrence of definitive evidence of a major cooling event—the YD—in the Southwest in several studies. Research has also demonstrated that the Arizona Monsoon developed by the early Holocene and may have been instrumental in providing the ignition source (i.e., lightning) that caused higher fire event frequencies during the major vegetation changes of the early Holocene. At several locations, the late to middle Holocene was the driest time of the record, when lake levels were lower and bogs dried out completely. This phenomenon was not universal, however, and probably depended upon the reliability of sufficient groundwater to maintain moisture in the basin center. Generally cooler climates of the late Holocene allowed an increase in biomass in mid- to high-elevation forests, and favored the expansion of low- (e.g., *Pinus edulis*) and high- (*Abies*) elevation conifers. Climate change during the late Holocene was not unidirectional, though, as the period was punctuated by numerous droughts of centennial duration.

Evidence of human modification of vegetation and fire regimes in the southern Rockies is not obvious until the late 19th and early 20th century. The establishment of grazing is shown at several locations by increases in grasses and introduced herbaceous species. Similarly, the effect of fire suppression is shown at most sites by the cessation of sedimentary charcoal deposition. Paleoecologists continue to examine the record for the impact of native populations on the forests of the southern Rockies, but, with our present understanding of the history of the region, climate appears to be the primary driving force on southwestern forests until the most recent centuries.

CHAPTER 6
MODERN POLLEN ANALOG STUDY, LOS ALAMOS NATIONAL LABORATORY

Susan J. Smith

INTRODUCTION

This report documents the results of a modern pollen study in Los Alamos National Laboratory (LANL). The main goal of this research is to develop an analog that can be used to study archaeological sites. Archaeological pollen data can be compared to natural pollen spectra and unique separated signatures that might reflect cultural activities. The analog is constructed from bulk sediment samples collected during June 2002 from 20 sites arrayed along a vegetation gradient from mixed conifer forests above 9000 ft to piñon and juniper below 7000 ft.

Archaeological sites at LANL are concentrated in transition zone ponderosa pine and piñon-juniper forests, where most of the sites date to the Coalition period (ca. AD 1150–1325) (Vierra et al. 2002a:6–29). The extent and persistence of agriculture on the Pajarito Plateau is impressive and is not limited to the prehistoric period. During the AD 1900s, there were about 35 homesteads on the plateau (Foxx et al. 1997:7). The homesteaders were grazing stock and farming grain, beans, orchards, and vegetables. An important research theme for the modern pollen study is to explore the pollen nature of disturbance. Can past agriculture be recognized from unique pollen assemblages or any key indicator types? A special class of disturbance is created by wildfire, and large tracts of forest have burned in the last 100 years, notably the 2000 Cerro Grande fire. Are there distinct pollen signatures in burned and unburned plots from different forest types? Do pollen spectra from burned sites share any traits with disturbed sites?

MODERN ENVIRONMENT

Detailed information about LANL vegetation is documented in geographic information system databases (Balice et al. 1997; Balice et al. 2000) and a botanical inventory (Foxx and Tierney 1984). LANL is sited on approximately 50,000 ac on the Pajarito Plateau, a broad piedmont off the east slope of the Jemez Mountains characterized by east-west-trending canyons and intervening mesas. The Sierra de los Valles, with three mountain peaks greater than 10,000 ft high, form a dramatic landscape west of Los Alamos and the Rio Grande Valley lies to the east. The elevation gradient from the crest of the Sierra to the Rio Grande (5350 ft elevation) is greater than 5000 ft over a horizontal distance of less than 15 miles.

The regional elevation gradient and diverse local physiography generate a variety of microclimate niches. The corresponding modern vegetation is a complex mosaic that Balice et al. (1997) have categorized into the following five main (Level 1) cover types: juniper savannah, piñon-juniper woodlands, ponderosa pine forests, mixed conifer forests, and spruce-fir forests. Figure 6.1 is a generalized model of the elevation range of the main vegetation types (Balice et al. 1997:13). The boundaries between vegetation communities are diffuse transition zones,

moderated by slope aspect and the many canyons that carry linear stringers of higher-elevation species through lower-elevation communities.

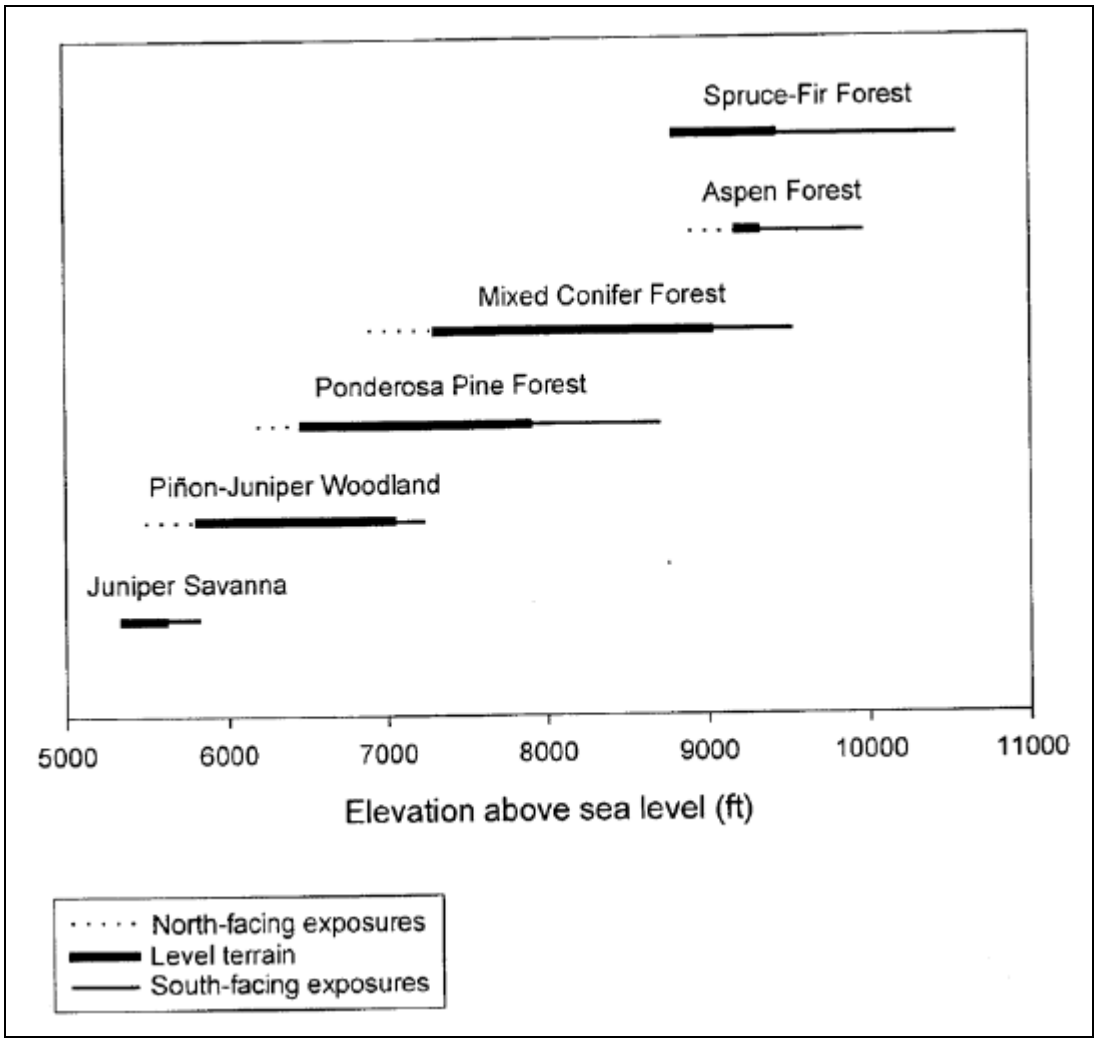

Figure 6.1. Elevational range of main vegetation types (Figure 4 in Balice et al. 1997:13).

During the June 2002 field work, Teralene Foxx identified plant species in the field at 12 of the 20 pollen stations, which is a feat that only an experienced Los Alamos botanist could attempt in the record-breaking drought year of 2002. Several of the herb and forb species were recognized by a stub of stem and a dry piece of curled leaf picked from the soil around the plant base. The plant species identified at each station are listed in Table 6.1. The detailed lists, station descriptions, and pictures for 11 of the stations are documented in Appendix B. A list of all the plant species identified and frequency as a percent of the 20 stations is presented in Table 6.2. A total of 114 plant species were documented, which included 14 species of trees, 25 shrubs, 54 herbs and forbs, 17 grasses, three aquatic species, and one fern. The variety of plants would undoubtedly have been higher, but for the extreme 2002 drought conditions.

Table 6.1. Plant species list for the Los Alamos pollen stations (June 12 to 14, 2002).

Pollen Station Number			**1**	**2**	**3**	**4**	**5**	**6**	**7**	**8**	**9**	**10**	**11**	**12**	**17**	**18**	**19**	**25**	**26**	**27**	**28**	**29**
Plant Taxa Richness (number plant species)			**16**	**17**	**9**	**24**	**7**	**13**	**12**	**20**	**12**	**13**	**10**	**21**	**12**	**14**	**15**	**11**	**11**	**7**	**9**	**7**
Family	**Taxon**	**Common Name**																				
Aceraceae	*Acer glabrum*	rocky mountain maple								x				x								
Betulaceae	*Betula*	Birch												x								
Cupressaceae	*Juniperus monosperma*	one seed juniper	x	x	x							x	x		x		x			x	x	x
Elaeagnaceae	*Elaeagnus angustifolia*	Russian olive						x				x										
Fagaceae	*Quercus gambelii*	gambel oak				x	x	x	x					x	x		x	x				
Fagaceae	*Quercus spp.*	oak	x																	x		
Pinaceae	*Abies concolor*	white fir								x				x								
Pinaceae	*Picea pungens*	blue spruce									x											
Pinaceae	*Pinus edulis*	Colorado piñon	x		x							x	x		x		x			x		x
Pinaceae	*Pinus flexilis*	limber pine							x													
Pinaceae	*Pinus ponderosa*	ponderosa pine		x		x	x	x	x			x	x	x			x				x	
Pinaceae	*Pseudotsuga menziesii*	douglas fir							x	x	x			x								
Salicaceae	*Populus angustifolia*	narrow leaf cottonwood												x				x				
Salicaceae	*Populus tremuloides*	aspen				x				x	x											
Anacardiaceae	*Rhus trilobata*	lemonade berry	x					x				x	x			x				x		
Asteraceae	*Artemisia tridentata*	big sagebrush										x	x						x			
Asteraceae	*Chrysothamnus nauseosus*	rabbitbrush		x								x				x			x		x	
Asteraceae	*Chrysothamnus* sp.	rabbitbrush																	x			

Pollen Station Number			**1**	**2**	**3**	**4**	**5**	**6**	**7**	**8**	**9**	**10**	**11**	**12**	**17**	**18**	**19**	**25**	**26**	**27**	**28**	**29**
Plant Taxa Richness (number plant species)			**16**	**17**	**9**	**24**	**7**	**13**	**12**	**20**	**12**	**13**	**10**	**21**	**12**	**14**	**15**	**11**	**11**	**7**	**9**	**7**
Family	**Taxon**	**Common Name**																				
Asteraceae	*Gutierrezia sarothrae*	snakeweed			x										x	x	x					x
Asteraceae	*Hymenoxys richardsoni*	bitterweed			x	x		x														x
Berberiaceae	*Berberis fendleri*	fendler barberry				x	x							x								
Caprifoliaceae	*Sambucus microbothrys*	elderberry									x											
Celastraceae	*Pachystima myrsinites*	mountain's lover							x													
Cupressaceae	*Juniperus communis*	common juniper				x																
Ericaceae	*Arctostaphylos uvaursi*	bearberry							x													
Fabaceae	*Robinia neomexicana*	New Mexico locust				x		x	x					x				x				
Oleaceae	*Forestiera neomexicana*	New Mexico olive										x										
Ranunculaceae	*Actaea arguta*	baneberry								x												
Ranunculaceae	*Clematis pseudoalpina*	clematis												x								
Rhamnaceae	*Ceanothus fendleri*	buckbrush																				
Rosaceae	*Cercocarpus montanus*	mountain mahogany	x												x		x			x		
Rosaceae	*Fallugia paradoxa*	Apache plume	x																x	x		
Rosaceae	*Rosa spp.*	wild rose				x								x								
Rosaceae	*Rubus strigosus*	raspberry									x											
Salicaceae	*Salix*	willow				x								x								
Saxifragaceae	*Jamesia americana*	cliff bush												x								
Saxifragaceae	*Philadelphus microphyllus*	mock orange												x								

Pollen Station Number			**1**	**2**	**3**	**4**	**5**	**6**	**7**	**8**	**9**	**10**	**11**	**12**	**17**	**18**	**19**	**25**	**26**	**27**	**28**	**29**
Plant Taxa Richness (number plant species)			**16**	**17**	**9**	**24**	**7**	**13**	**12**	**20**	**12**	**13**	**10**	**21**	**12**	**14**	**15**	**11**	**11**	**7**	**9**	**7**
Family	**Taxon**	**Common Name**																				
Saxifragaceae	*Ribes cernuum*	wax currant												x								
Vitaceae	*Parthenocissus inserta*	Virginia creeper												x								
Apiaceae	*Osmorhiza obtuse*	bluntseed cicely								x												
Apiaceae	*Pseudocymoptris montanus*	mountain parsley									x											
Asteraceae	*Achillea lanulosa*	yarrow				x				x												
Asteraceae	*Ambrosia*	ragweed																	x			
Asteraceae	*Antennaria parviflora*	pussytoes				x	x	x														
Asteraceae	*Artemisia carruthii*	wormwood		x																	x	
Asteraceae	*Artemisia dracunculus*	false terragon	x	x	x							x	x							x	x	x
Asteraceae	*Artemisia* spp.	wormwood															x		x			
Asteraceae	*Aster* spp.	aster						x								x	x					
Asteraceae	*Atremisia ludoviciana*	wormwood	x		x						x									x		x
Asteraceae	*Cirsium* spp.	thistle									x			x				x				
Asteraceae	*Conyza canadensis*	horseweed				x																
Asteraceae	*Erigeron divergens*	fleabane				x																
Asteraceae	*Helianthus* sp.	sunflower																				
Asteraceae	*Heterotheca*	golden weed	x													x			x	x		
Asteraceae	*Senecio* spp.	groundsel				x									x	x						
Asteraceae	*Solidago* spp.	goldenrod						x														
Asteraceae	*Taraxacum officinale*	dandelion								x	x			x								
Boraginaceae	Boraginaceae	borage species														x						
Brassicaceae	*Sisymbrium*	tumble mustard																x	x			

Pollen Station Number			**1**	**2**	**3**	**4**	**5**	**6**	**7**	**8**	**9**	**10**	**11**	**12**	**17**	**18**	**19**	**25**	**26**	**27**	**28**	**29**
Plant Taxa Richness (number plant species)			**16**	**17**	**9**	**24**	**7**	**13**	**12**	**20**	**12**	**13**	**10**	**21**	**12**	**14**	**15**	**11**	**11**	**7**	**9**	**7**
Family	**Taxon**	**Common Name**																				
Cactaceae	*Opuntia* spp.	prickly pear	x										x		x		x			x		
Chenopodiaceae	Chenopodium	Cheno-Am															x					
Chenopodiaceae	*Kochia scoparia*	summer cypress		x				x													x	
Chenopodiaceae	*Salsola* sp.	tumbleweed																	x			
Euphorbiaceae	*Euphorbia seryllifolia*	thymeleaf spurge	x																	x		
Fabaceae	*Lupinus caudatus*	lupine		x																	x	
Fabaceae	*Lupinus* sp.	lupine																				
Fabaceae	*Melilotus* spp.	sweetclover		x												x		x			x	
Fabaceae	*Thermopsis pinetorum*	golden pea								x												
Fabaceae	*Vicia americana*	American vetch								x												
Geraniaceae	*Geranium* sp.	wild geranium							x													
Iridaceae	*Iris*	iris (ornamental)				x																
Iridaceae	*Iris missouriensis*	blue flag									x											
Lamiaceae	*Monarda pectinata*	ponymint		x																	x	
Liliaceae	*Allium cernuum*	wild onion				x				x												
Liliaceae	*Yucca baccata*	broadleaf yucca	x												x		x			x		
Loasaceae	*Mentzelia* spp.	blazing star		x																	x	
Malvaceae	Sphaeralcea	globemallow															x		x			
Polemoniaceae	*Ipomopsis aggregata*	scarlet gilia	x													x				x		
Polygonaceae	*Eriogonum cernuum*	buckwheat		x																	x	
Polygonaceae	*Eriogonum jamesii*	antelope sage	x																	x		
Polygonaceae	*Eriogonum racemosum*	buckwheat		x																	x	
Polygonaceae	*Polygonum* sp.	knotweed																x				

Pollen Station Number			**1**	**2**	**3**	**4**	**5**	**6**	**7**	**8**	**9**	**10**	**11**	**12**	**17**	**18**	**19**	**25**	**26**	**27**	**28**	**29**
Plant Taxa Richness (number plant species)			**16**	**17**	**9**	**24**	**7**	**13**	**12**	**20**	**12**	**13**	**10**	**21**	**12**	**14**	**15**	**11**	**11**	**7**	**9**	**7**
Family	**Taxon**	**Common Name**																				
Primulaceae	*Dodecatheon* spp.	shooting star								x												
Ranunculaceae	*Thalictrum fendleri*	meadowrue								x												
Rosaceae	*Fragaria americana*	wild strawberry								x												
Rosaceae	*Potentilla* spp.	cinquefoil				x				x	x											
Rubiaceae	*Galium* sp.	bedstraw								x												
Scrophulariaceae	*Othocarpus purpureo-albus*	purple owlclover			x																	x
Scrophulariaceae	*Penstemon* spp.	penstemon		x					x												x	
Scrophulariaceae	*Verbascum thapsus*	mullein		x		x						x				x		x	x		x	
Solanaceae	*Physalis* sp.	groundcherry														x						
Violaceae	*Viola*	violet								x												
Violaceae	*Viola canadensis*	Canadian violet								x												
Polypodiaceae	*Pteridium* sp.	bracken fern									x	x										
Poaceae	*Agropyron smithii*	wheatgrass				x																
Poaceae	*Aristida* spp.	three awn													x	x						
Poaceae	*Bepharoneuron tricholepis*	pinedropseed							x													
Poaceae	*Bouteloua gracilis*	blue grama	x	x	x								x		x		x			x	x	x
Poaceae	*Bromus* spp.	brome				x				x				x								
Poaceae	*Dactylis glomerulata*	orchard grass										x										
Poaceae	*Danthonia intermedia*	timber oatgrass										x										
Poaceae	*Hilaria* sp.	galleta													x	x						
Poaceae	*Koleria cristata*	june grass				x	x	x	x													

Pollen Station Number			**1**	**2**	**3**	**4**	**5**	**6**	**7**	**8**	**9**	**10**	**11**	**12**	**17**	**18**	**19**	**25**	**26**	**27**	**28**	**29**
Plant Taxa Richness (number plant species)			**16**	**17**	**9**	**24**	**7**	**13**	**12**	**20**	**12**	**13**	**10**	**21**	**12**	**14**	**15**	**11**	**11**	**7**	**9**	**7**
Family	**Taxon**	**Common Name**																				
Poaceae	*Muhlenbergia montanus*	mountain muhly				x	x	x	x					x								
Poaceae	*Muhlenbergia torreyi*	ring muhly											x									
Poaceae	Other Poaceae	other grasses																x				
Poaceae	*Poa fendleri*	bluegrass			x												x					x
Poaceae	*Schizachyrium scoparius*	little bluestem	x	x		x		x							x	x	x			x	x	
Poaceae	*Sitanion hystrix*	squirreltail				x	x															
Poaceae	*Sporobolus* spp.	sand dropseed		x										x							x	
Poaceae	*Stipa (Oryzopsis) micrantha*	littleseed ricegrass											x									
Cyperaceae	*Carex* spp.	sedge								x												
Cyperaceae	*Scirpus* sp.	bulrush																x				
Typhaceae	*Typha*	cattail																x				

Table 6.2. List of plant species.

	Family	Species	Common Name	Frequency as percent of *n* = 20 Stations
	Trees			
1	Betulaceae	*Betula*	birch	5
2	Cupressaceae	*Juniperus monosperma*	one seed juniper	40
3	Elaeagnaceae	*Elaeagnus angustifolia*	Russian olive	10
4	Fagaceae	*Quercus gambelii*	gambel oak	55
5	Fagaceae	*Quercus* spp.	oak	5
6	Pinaceae	*Abies concolor*	white fir	10
7	Pinaceae	*Picea pungens*	blue spruce	5
8	Pinaceae	*Pinus edulis*	Colorado piñon	35
9	Pinaceae	*Pinus flexilis*	limber pine	5
10	Pinaceae	*Pinus ponderosa*	ponderosa pine	55
11	Pinaceae	*Pseudotsuga menziesii*	douglas fir	20
12	Salicaceae	*Acer glabrum*	rocky mountain maple	10
13	Salicaceae	*Populus angustifolia*	narrow leaf cottonwood	10
14	Salicaceae	*Populus tremuloides*	aspen	15
	Shrubs			
15	Anacardiaceae	*Rhus trilobata*	lemonade berry	25
16	Asteraceae	*Artemisia tridentata*	big sagebrush	15
17	Asteraceae	*Chrysothamnus nauseosus*	rabbitbrush	20
18	Asteraceae	*Chrysothamnus* sp.	rabbitbrush	5
19	Asteraceae	*Gutierrezia sarothrae*	snakeweed	25
20	Asteraceae	*Hymenoxys richardsoni*	bitterweed	15
21	Berberiaceae	*Berberis fendleri*	fendler barberry	15
22	Caprifoliaceae	*Sambucus microbothrys*	elderberry	5
23	Celastraceae	*Pachystima myrsinites*	mountain's lover	5
24	Cupressaceae	*Juniperus communis*	common juniper	5
25	Ericaceae	*Arctostaphylos uvaursi*	bearberry	5
26	Fabaceae	*Robinia neomexicana*	New Mexico locust	25
27	Oleaceae	*Forestiera neomexicana*	New Mexico olive	5

	Family	Species	Common Name	Frequency as percent of *n* = 20 Stations
28	Ranunculaceae	*Actaea arguta*	baneberry	5
29	Ranunculaceae	*Clematis pseudoalpina*	clematis	5
30	Rhamnaceae	*Ceanothus fendleri*	buckbrush	0
31	Rosaceae	*Cercocarpus montanus*	mountain mahogany	15
32	Rosaceae	*Fallugia paradoxa*	Apache plume	10
33	Rosaceae	*Rosa* spp.	wild rose	10
34	Rosaceae	*Rubus strigosus*	raspberry	5
35	Salicaceae	*Salix*	willow	10
36	Saxifragaceae	*Jamesia americana*	cliff bush	5
37	Saxifragaceae	*Philadelphus microphyllus*	mock orange	5
38	Saxifragaceae	*Ribes cernuum*	wax currant	10
39	Vitaceae	*Parthenocissus inserta*	Virginia creeper	5
	Herbs and Forbs			
40	Apiaceae	*Osmorhiza obtuse*	bluntseed cicely	5
41	Apiaceae	*Pseudocymoptris montanus*	mountain parsley	5
42	Asteraceae	*Achillea lanulosa*	yarrow	10
43	Asteraceae	*Ambrosia*	ragweed	10
44	Asteraceae	*Antennaria parviflora*	pussytoes	15
45	Asteraceae	*Artemisia carruthii*	wormwood	5
46	Asteraceae	*Artemisia dracunculus*	false terragon	30
47	Asteraceae	*Artemisia* spp.	wormwood	15
48	Asteraceae	*Aster* spp.	aster	15
49	Asteraceae	*Atremisia ludoviciana*	wormwood	15
50	Asteraceae	*Cirsium* spp.	thistle	15
51	Asteraceae	*Conyza canadensis*	horseweed	5
52	Asteraceae	*Erigeron divergens*	fleabane	5
53	Asteraceae	*Helianthus* sp.	sunflower	5
54	Asteraceae	*Heterotheca*	golden weed	15
55	Asteraceae	*Senecio* spp.	groundsel	15
56	Asteraceae	*Solidago* spp.	goldenrod	5
57	Asteraceae	*Taraxacum officinale*	dandelion	15
58	Boraginaceae	Boraginaceae	borage species	5
59	Brassicaceae	*Sisymbrium* sp.	tumble mustard	10
60	Cactaceae	*Opuntia* spp.	prickly pear	20
61	Chenopodiaceae	*Chenopodium* sp.	Cheno-Am	15
62	Chenopodiaceae	*Kochia scoparia*	summer cypress	10
63	Chenopodiaceae	*Salsola* sp.	tumbleweed	10

	Family	Species	Common Name	Frequency as percent of *n* = 20 Stations
64	Euphorbiaceae	*Euphorbia seryllifolia*	thymeleaf spurge	5
65	Fabaceae	*Lupinus caudatus*	lupine	5
66	Fabaceae	*Lupinus* sp.	lupine	5
67	Fabaceae	*Melilotus* spp.	sweetclover	15
68	Fabaceae	*Thermopsis pinetorum*	golden pea	5
69	Fabaceae	*Vicia americana*	American vetch	5
70	Geraniaceae	*Geranium* sp.	wild geranium	5
71	Iridaceae	*Iris* sp.	iris (ornamental)	5
72	Iridaceae	*Iris missouriensis*	blue flag	5
73	Lamiaceae	*Monarda pectinata*	ponymint	5
74	Liliaceae	*Allium cernuum*	wild onion	10
75	Liliaceae	*Yucca baccata*	broadleaf yucca	15
76	Loasaceae	*Mentzelia* spp.	blazing star	5
77	Malvaceae	*Sphaeralcea* sp.	globemallow	15
78	Polemoniaceae	*Ipomopsis aggregata*	scarlet gilia	10
79	Polygonaceae	*Eriogonum cernuum*	buckwheat	5
80	Polygonaceae	*Eriogonum jamesii*	antelope sage	5
81	Polygonaceae	*Eriogonum racemosum*	buckwheat	5
82	Polygonaceae	*Polygonum* sp.	knotweed	5
83	Primulaceae	*Dodecatheon* spp.	shooting star	5
84	Ranunculaceae	*Thalictrum fendleri*	meadowrue	5
85	Rosaceae	*Fragaria americana*	wild strawberry	5
86	Rosaceae	*Potentilla* spp.	cinquefoil	15
87	Rubiaceae	*Galium* sp.	bedstraw	5
88	Scrophulariaceae	*Othocarpus purpureoalbus*	purple owlclover	5
89	Scrophulariaceae	*Penstemon* spp.	penstemon	15
90	Scrophulariaceae	*Verbascum thapsus*	mullein	30
91	Solanaceae	*Physalis* sp.	groundcherry	5
92	Violaceae	*Viola*	violet	5
93	Violaceae	*Viola canadensis*	Canadian violet	5
	Fern			
94	Polypodiaceae	*Pteridium* sp.	bracken fern	5
	Grasses			
95	Poaceae	*Agropyron smithii*	wheatgrass	5
96	Poaceae	*Aristida* spp.	three awn	10
97	Poaceae	*Blepharoneuron tricholepis*	pine dropseed	5
98	Poaceae	*Bouteloua gracilis*	blue grama	40
99	Poaceae	*Bromus* spp.	brome	15
100	Poaceae	*Dactylis glomerulata*	orchard grass	5

	Family	Species	Common Name	Frequency as percent of *n* = 20 Stations
101	Poaceae	*Danthonia intermedia*	timber oatgrass	5
102	Poaceae	*Hilaria jamesii.*	galleta	10
103	Poaceae	*Koleria cristata*	june grass	20
104	Poaceae	*Muhlenbergia montanus*	mountain muhly	25
105	Poaceae	*Muhlenbergia torreyi*	ring muhly	5
106	Poaceae	Other Poaceae	other grasses	5
107	Poaceae	*Poa fendleri*	bluegrass	10
108	Poaceae	*Schizachyrium scoparius*	little bluestem	45
109	Poaceae	*Sitanion hystrix*	squirreltail	10
110	Poaceae	*Sporobolus* spp.	sand dropseed	10
111	Poaceae	*Stipa (Oryzopsis) micrantha*	littleseed ricegrass	5
	Riparian/Aquatic			
112	Cyperaceae	*Carex* spp.	sedge	5
113	Cyperaceae	*Scirpus* sp.	bulrush	5
114	Typhaceae	*Typha latifolia*	cattail	5

POLLEN STATIONS

The modern pollen analog is constructed from 20 stations that sample the main vegetation types, examples of disturbance, meadow and riparian sites, and paired stations in burned and unburned plots from the 2000 Cerro Grande fire. Station descriptions are listed in Table 6.3, organized generally by elevation and vegetation type. The estimated percent cover of three overstory layers (trees, shrubs, and grasses and herbs) and the dominant tree species are included in Table 6.3. Stations selected to represent a burned forest stand, disturbed or riparian site, or meadow are viewed as openings within forest. This perspective is particularly relevant to pollen studies in forests, because conifer trees produce literally tons of wind-dispersed pollen (Fægri et al. 1989:14) that dominate the regional pollen rain. Thus, at the coarsest level, the stations occur in four vegetation types: mixed conifer (*n* = 4), ponderosa pine (*n* = 5), transition ponderosa pine and piñon-juniper (*n* = 5), or piñon-juniper (*n* = 3).

Table 6.3. Modern pollen sampling stations.

Pollen Station (S No.)		Vegetation Type	Description	Elevation		Percent Cover			Ranked Dominant Trees & Plant Taxa Richness[a]
				ft	m	Trees	Grasses	Shrubs	
MC	9	Meadow, High Elevation	Camp May above ski lodge; natural meadow near ski run.	9419	2871		90	10	12

Pollen Station (S No.)		Vegetation Type	Description	Elevation		Percent Cover			Ranked Dominant Trees & Plant Taxa Richness[a]
	12	Riparian (Canyon)	Los Alamos Canyon upstream from ice skating rink	7276	2218	75		25	Douglas Fir, White Fir, Cottonwood, Ponderosa Pine, Birch, Willow, Maple, 21
	8	Mixed Conifer	Pajarito Ski Lodge	9240	2817	90			Douglas Fir, Aspen, White Fir, Maple, 20
	7	Transition Ponderosa Pine to Mixed Conifer	Pajarito Ski Area road, south-facing, steep (60%) slope in mixed conifer. sandy grus-like soils & bedrock (welded tuff). One of few sites within LANL with Limber Pine.	8451	2576	80			Ponderosa Pine, Limber Pine, Douglas Fir, 12
Ponderosa Pine	6	Ponderosa Pine, Burned	Hwy 501 & Pajarito Ski Area junction. Cerro Grande 2000 fire at this station was only ground fire; modern thinning.	7767	2367	50			Ponderosa Pine, 13
	5	Ponderosa Pine	Forest around S 4, old pond site; downslope Cerro Grande fire boundary; history of thinning from 1800s homesteading to 1970s forest management.	7704	2348	70			Ponderosa Pine, 7
	4	Disturbance/Pond Ponderosa Pine	Historic ice house pond now dry & growing wheatgrass. Just downslope of 2000 Cerro Grande fire boundary; pond filled with sheetwash soil & charcoal from July monsoons after May fire. Depression ca. 30 m diameter opening in pine forest (S 5). Cattails used to grow in pond.	7706	2349		100		Ponderosa Pine, Willow, 24
	27	Ponderosa Pine, Burned	Rendija Canyon near gun club. Cerro Grande 2000 fire burn intense near this station with dead stands in canyon	6992	2131	85	40		Ponderosa Pine, 7

Pollen Station (S No.)		Vegetation Type	Description	Elevation		Percent Cover			Ranked Dominant Trees & Plant Taxa Richness[a]
			bottom & fringe of live trees adjacent to road.						
	28	Ponderosa Pine, Unburned	Rendija Canyon near gun club & boundary Cerro Grande 2000 fire (S 27).	6992	2131	85	25		Ponderosa Pine, 9
Transition Ponderosa to Piñon-Juniper	10	Meadow	Pueblo Canyon, sewage effluent area. Water has been reclaimed & diverted to golf course.	6456	1968		100		13
	11	Transition (Canyon) Ponderosa Pine & Piñon Juniper	Pueblo Canyon, forest adjacent S 10.	6468	1972	25	25		Juniper, Piñon, Ponderosa Pine, 10
	17	Piñon Juniper, Burned	Mesa top south of Mortandad Canyon. Cerro Grande 2000 fire burned tree canopy. Oak & yucca second growth form significant cover.	7079	2158	20	70	10	Oak, 12
	18	Disturbed	approx. 1 acre area of mechanical disturbance between S 17 & 18.	7077	2157		80		14
	19	Piñon Juniper, Unburned	Mesa top south of Mortandad Canyon near S 17.	7093	2162	50	35		Piñon, Juniper, Ponderosa Pine, Oak,15
Piñon Juniper	3	Piñon Juniper	Hwy 4 NW of Bandelier Nat. Monument entrance.	6829	2082	65	25		Juniper, Piñon, 9
	1	Piñon Juniper	Highway 4 south of White Rock.	6508	1984	45	5		Equal Piñon & Juniper, 16
	2	Disturbed/Field?	Ancho Canyon, Hwy 4. Possible old field on first terrace. Weeds & grasses dominate gopherized bottomland. Perimeter forest is ponderosa pine with piñon & juniper along canyon bottom to piñon & juniper on side slopes.	6238	1901		100		Ponderosa Pine, Piñon, Juniper, 17
	25	Wetland	Pajarito Canyon wetland, cattails & bulrush ringed by willows.	6669	2033		100		Willow, Ponderosa Pine, 11
	26	Disturbed	Road shoulder adjacent	6675	2034		55	20	11

Pollen Station (S No.)		Vegetation Type	Description	Elevation		Percent Cover			Ranked Dominant Trees & Plant Taxa Richness[a]
			S 25.						
	29	Disturbed/Field	Romero homestead field on Pajarito Mesa. Detailed description and plant list in Foxx and Tierney (1999).	7248	2209		100		7

a. Ranked dominant trees lists all the trees identified at a station in the order of abundance. Plant taxa richness from Appendix B is the number of plant species identified at each station.

Subdivisions within the forest types follow. Stations 11 and 12 represent canyon bottoms characterized by mixed forests, and station 9 is an example of a high-elevation meadow within a mixed conifer forest. There are four examples of disturbance: a road shoulder (S 26), an area of mechanical disturbance (S 18), a possible historic field (S 2), and an historic (ca. AD 1900s) bean field (S 29) at the Romero homestead. The Romero homestead was the subject of a field succession study and archaeobotanical study (Foxx and Tierney 1999; McGehee et al. 2006). There are two sets of paired sites (four stations) sampling the Cerro Grande fire: one pair from burned and unburned ponderosa pine (S 27 and 28) and one set in piñon and juniper (S 17 and 19). Examples of riparian environments were sampled at stations 4, 10, 12, and 25.

METHODS

One to three separate bulk sediment samples were collected at each station by taking 15 to 20 pinches of soil from the top 1.0 to 0.5 cm of soil across an approximately 50- by 50-m area (Adam and Mehringer 1975). The vegetation at each station was characterized by estimating the percent cover of the dominant trees, shrubs, and ground cover. Although only one of the multiple samples from each station was processed and analyzed, the analog could be expanded in future studies to examine the degree of variability between multiple samples.

In the laboratory, subsamples (20 cc volume) were taken from the sample bags, weighed, and spiked with a known concentration (25,084 grains) of tracers (*Lycopodium* spores). Addition of tracers allows pollen concentration to be calculated, which estimates the raw number of pollen grains in a sample. The samples were processed with acids (overnight hydrochloric and hydrofluoric), followed by a heavy liquid gravity separation (zinc bromide 1.9 specific gravity) and acetolysis, which reduces organics. The extracted samples are stored in glycerol.

Pollen assemblages were identified by counting slides from the processed samples on a Reichert, Microstar IV microscope. Entire slides were examined by counting transects at 400x magnification to a 300-grain pollen sum, then scanning remaining transects at 100x magnification to record additional taxa. Pollen aggregates (clumps of grains of the same taxon) were included in the pollen sum as one grain per occurrence and a separate tally made of the number of grains within each aggregate. The occurrence of pollen aggregates in modern surface

samples is generally ignored in ecological studies, but is a useful class of data in archaeological pollen studies (e.g., Gish 1991).

Another type of data documented from the slides is the percent cover of background charcoal particles. Trends in microscopic charcoal abundance from lake core samples have been used to infer fire history. However, the micro charcoal data are generally useful only for long-term regional patterns (MacDonald et al. 1991; Patterson et al. 1987). Pollen extraction procedures filter the possible size range of charcoal to dust or smoke size particles (approximately 200 to <10 µm), which can be blown into a site. Macroscopic charcoal from sediment profiles is a better proxy for local fire history. The purpose in examining the micro charcoal matrix in the LANL samples is to test for any differences at burned and unburned paired sites.

Pollen identifications were made to the lowest taxonomic level possible based on comparison to the Northern Arizona University, Laboratory of Paleoecology pollen reference collection and published references (Faegri et al. 1989; Kapp 2000; P. Moore et al. 1991). The separation between piñon pine and other pines was based primarily on size measurements (Jacobs 1985b). Piñon pine was found to be the least reliable predictor of vegetation in the LANL pollen assemblages. There is significant overlap in the size gradient between small ponderosa pine grains and larger piñon pine (Martin 1963:20–21), and it is likely that there are misidentified grains in both pine categories. Haploxylon pine grains greater than 70 µm were also documented, and these probably represent limber pine (*Pinus flexilis*), a rare conifer growing at higher elevation.

The broad sunflower family group was separated into seven types: sagebrush (*Artemisia*), thistle (*Cirsium*), chicory tribe (Liguliflorae), sunflower family (Asteraceae or Compositae Hi-Spine), the ragweed/bursage type (*Ambrosia* or Low-Spine Compositae), Long Spine, and Broad Spine. The separation between the high and low spine Compositae categories was based on the height of spines, using 2 µm as a cutoff (Hevly et al. 1965). The Long Spine and Broad Spine are unique categories in this analysis.

The Long Spine type is defined as a grain with spines greater than 3.0 µm and a tricolporate aperture system with pores aligned transverse to furrows. The Long Spine probably represents sunflower (*Helianthus*), but other northern Colorado Plateau genera with the same grain morphology include *Layia*, fetid marigold (*Pectus*), coneflower (*Rudbeckia*), marigold (*Tagetes*), crown-beard (*Verbesina*), and *Viguiera*. The broad spine grain morphology is similar to ragweed/bursage, but the spines are distinct with bases twice as wide as long. A possible candidate for the broad spine is *Dicoria*; however, this genus is not listed in Foxx and Tierney (1984), and some other sunflower family member may be represented.

Three numerical parameters were calculated from the pollen counts: taxa richness, pollen percentages, and pollen concentration. Taxa richness is the number of different pollen types identified in each sample. Pollen percentages are a smoothing transformation that represent the relative importance of each taxon in a sample ([pollen counted/pollen sum]*100). Percentages are the main parameter used to discriminate trends in the LANL modern pollen samples.

Pollen concentration is a measure of the absolute number of grains or the density of pollen grains in a sample. Concentration was calculated for each sample by taking the ratio of the pollen count to the tracer count and multiplying by the initial tracer concentration. Dividing this result by the sample weight yields the number of pollen grains per gram of sample sediment, abbreviated gr/g. Concentration may also be calculated by volume—both sample weight and volume are documented in Appendix C. Pollen concentrations can be used to gauge several processes. In natural settings, concentrations can reflect sediment accumulation rates, and in cultural contexts, concentrations can relate to the amount of plant material handled.

RESULTS

All of the pollen data are documented in Appendix C. A total of 43 pollen types were identified, and these are listed in Table 6.4 by common and taxa name and organized into two main categories, trees and shrubs and the ground cover plants (forbs, herbs, grasses, and weeds). The sample frequency for each pollen type is also included. The results are presented in two parts. First, the correspondence between pollen spectra and the main forest types is analyzed, and second, the disturbance, riparian, burned sites, and other unique locations are discussed.

Table 6.4. Pollen types identified and sample frequency.

	Common Name	Taxa Name	Frequency as percent ***n*** **= 20 Samples**
	Trees & Shrubs		
1	Douglas Fir	*Pseudotsuga*	25
2	Spruce	*Picea*	55
3	Fir	*Abies*	100
4	Pine	*Pinus*	100
	Pine Aggregates		55
5	Piñon	*Pinus edulis* type	100
	Piñon Aggregates		10
6	Juniper	*Juniperus*	100
	Juniper Aggregates		10
7	Oak	*Quercus*	100
	Oak Aggregates		10
8	cf. Limber Pine	cf. *Pinus flexilis* = Haploxylon Pine>70 µm	30
9	Mistletoe	Loranthaceae	15
10	Maple	*Acer*	5
11	Walnut	*Juglans*	5
12	Birch	*Betula*	10
13	Willow	*Salix*	10
14	cf. Snowberry	Caprifoliaceae, cf. Symphoricarpos	5
15	Other Rose Family	Roseaceae	10
16	Cliffrose, Mountain	Rosaceae, *Cercocarpus/Purshia*	70

	Common Name	Taxa Name	Frequency as percent *n* = 20 Samples
	mahogany type	type	
17	Buckthorn Family	Rhamnaceae	5
18	Lemonadeberry	*Rhus*	10
19	Mormon Tea	*Ephedra*	45
20	Sagebrush	*Artemisia*	100
21	Yucca	Liliaceae	5
22	Prickly Pear	*Opuntia*	15
23	Greasewood	*Sarcobatus*	15
	Forbs, Herbs, Weeds, & Grasses		
24	Cheno-Am	Cheno-Am	100
	Cheno-Am Aggregates		5
25	Sunflower Family	Asteraceae	95
	Sunflower Family Aggregates		5
26	Bursage/Ragweed type	*Ambrosia*	90
27	Thistle	*Cirsium*	30
28	Long Spine type	cf. *Helianthus*	25
29	Broad Spine type	cf. *Dicoria*	35
30	Grass Family	Poaceae	90
	Grass Aggregates		15
31	Large Grass type	Large Poaceae	10
32	Buckwheat	*Eriogonum*	20
33	Purslane	*Portulaca*	5
34	Spurge Family	Euphorbiaceae	30
35	Mustard Family	Brassicaceae	30
36	Globemallow	Sphaeralcea	5
37	Evening Primrose	Onagraceae	10
38	Pea Family	Fabaceae	10
39	Figwort Family	Scrophulariaceae	10
40	Knotweed	*Polygonum viviparum*	5
41	Four O'clock Family	Nyctaginaceae	5
42	Russian Olive	Elaeagnaceae	5
43	Cattail	*Typha latifolia*	5

Pollen Correspondence to Forest Composition

The stations are grouped by the main forest types: mixed conifer, ponderosa pine, transition forests of mixed piñon-juniper and ponderosa pine, and piñon-juniper. Three stations are grouped separately (S 25, 26, and 29) as unique, primarily disturbed sites. Station 12, a riparian site in Los Alamos Canyon at 2217 m (7276 ft), was listed with the high-elevation mixed conifer sites because the dominant tree is Douglas fir. Station 12 is an example of the more mesic environments created in canyons.

One pattern in the LANL pollen data is the trend for more diverse assemblages at higher elevations, especially in the mixed conifer and ponderosa pine forests. Pollen taxa richness ranges between 15 to 20 pollen types above 2133 m (7000 ft) and less than 15 taxa in the transition and piñon-juniper forests. The exceptions are either high-elevation transition zone sites (S 17, 18, and 19) or unique situations (S 2, 4, 25, 26). This pattern is not evident in the plant species richness at each site (Table 6.1 and Table 6.2), except for a greater number of species from the high-elevation mixed conifer stations. However, the variety of taxa identified in the field is probably low due to the 2002 drought.

The mixed conifer stations produced distinct pollen assemblages, with high values of fir (4% to 34%), high taxa richness (15 to 20), and presence of some rare types, such as honeysuckle, birch, and maple. Low percentages of Douglas fir and limber pine are associated with the mixed conifer stations. Spruce pollen surprisingly was not a good indicator of the higher-elevation stations. Spruce was identified in 11 of the 20 samples analyzed, including S 1 in piñon-juniper.

There is no significant pattern in pollen concentrations, except for low pollen abundance at two disturbed sites (S 26 and 29) and the high-elevation meadow (S 9). Pollen concentration in surface soil is sensitive to the dynamic influx of pollen and sediment. Pollen deposition increases concentration and sediment deposition dilutes pollen density. Generally, pollen concentration is high in the analog samples, which reflects the abundant production from the wind-pollinated conifers.

The distribution of pollen aggregates was not diagnostic of vegetation types. Aggregates from most pollen taxa were rare occurring in only one to three samples, except for pine (Appendix C). Aggregates of pine occurred at 11 of the 20 stations. Oak pollen aggregates were documented at two sites (S 18 and 19), and, at S 18, oak was the primary tree.

The pollen types sensitive to forest composition are fir, pine, and juniper. Piñon pine is included in the summary diagram (Figure 6.2), but this type is not diagnostic, even in the piñon and juniper forest. Disturbed sites and small meadows are generally characterized by high representation of grass or cheno-am, sunflower family, and herb types. The best summary measure of forest types is a ratio between pine (excludes piñon) and juniper. In Figure 6.2, the pine/juniper ratio is highest (19 to 60) from stations in the ponderosa pine forests. Juniper frequencies rise at stations from the transition forests and are highest in the piñon and juniper forests, which is reflected by the minimum pine/juniper ratio of 1. The pine/juniper ratio is suppressed at the high-elevation mixed conifer sites because pine is not the dominant tree at these stations. Pollen taxa that are not particularly good indicator pollen types, with a few exceptions, are oak, rose family, cliffrose/mountain mahogany type, sagebrush, and grass.

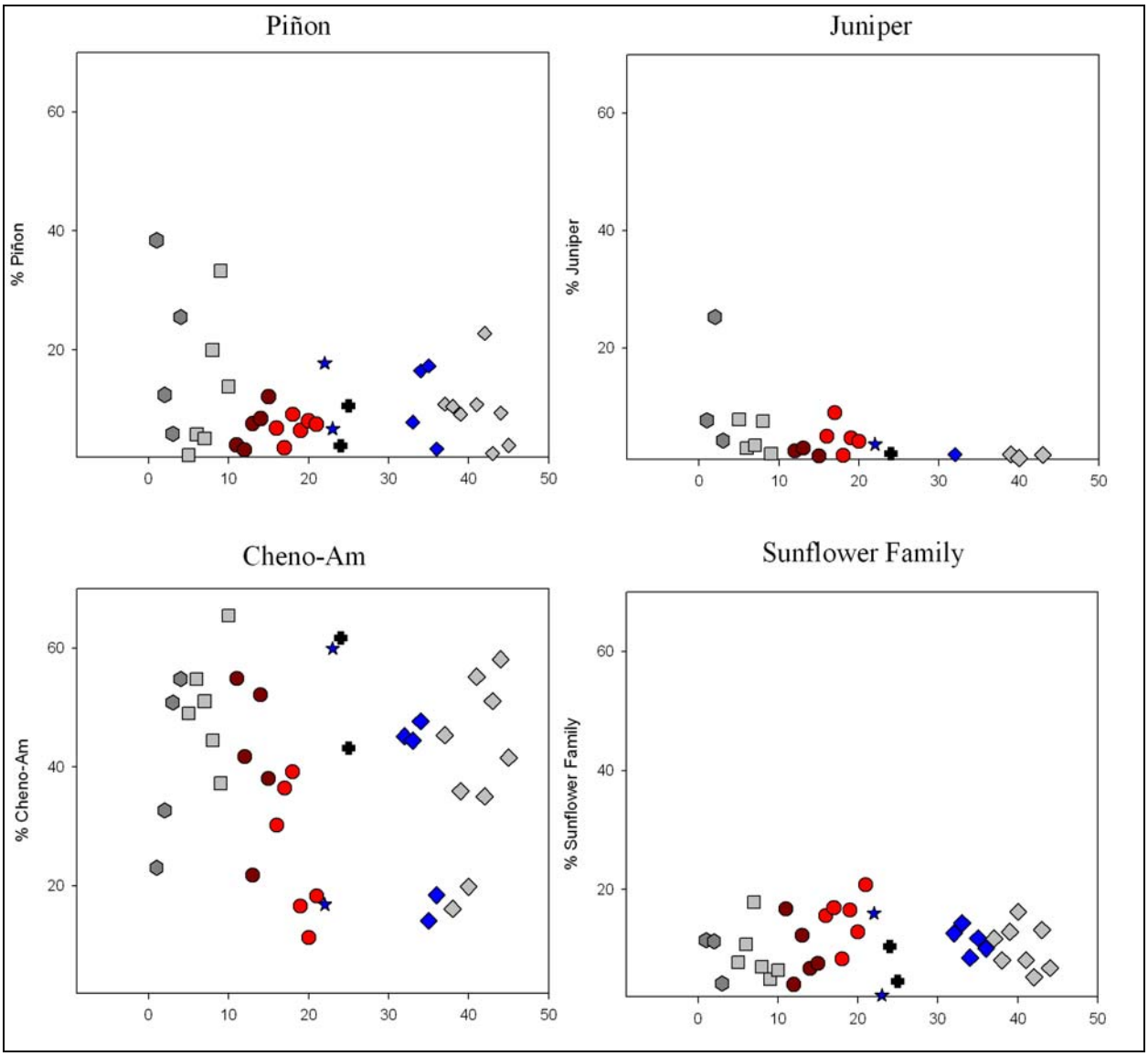

Figure 6.2. Modern pollen analog summary percentage diagram.

Pollen Indicator Types at Disturbance and Riparian Sites

In this section, patterns are discussed that discriminate subdivisions within the main forest types. Summary data for each station are listed in Table 6.5, including general station descriptions, plant taxa richness, pollen concentration, pollen taxa richness, and other key variables.

Table 6.5. Summary pollen results.

Pollen Station (S No.)		Vegetation	Plant Taxa Richness	Elevation ft.	Micro Charcoal[a]	Pollen Concentration gr/gm	Pollen Taxa Richness	Percent Fir	Percent All Trees[b]	Ratio Pine - Juniper	% Cheno-Am & Sunflower Family	Other Key Pollen Types
Mixed Conifer	9	Meadow	12	9419	10 to 20	5785	15	4	46	2	15	Grass 11%, Chicory 6%, Limber Pine
	12	Canyon Riparian	21	7276	<10	24100	15	34	88	13	1	Birch, Douglas Fir, Limber Pine
	8	Mixed Conifer	20	9240	<10	117630	20	11	76	15	6	Douglas Fir, Maple, 6% Spruce, Limber Pine
	7	Ponderosa & Limber Pine	12	8451	<10	444544	16	7	82	14	5	Douglas Fir
Ponderosa Pine	6	Ponderosa Burned	13	7767	<10	122323	15	5	82	30	10	Thistle
	5	Ponderosa	7	7704	10 to 20	68765	15	4	78	31	7	
	4	Pond in Ponderosa	24	7706	20 to 30	40715	11	8	84	28	5	Limber Pine
	27	Ponderosa Burned	7	6992	20 to 30	214926	16	2	83	19	5	
	28	Ponderosa	9	6992	20 to 30	91290	13	1	82	60	8	
Transition Ponderosa Pine to Piñon-Juniper	10	Wet Meadow in Canyon	13	6456	30 to 40	31622	13	2	69	20	10	
	11	Piñon-Juniper & Ponderosa in Canyon	10	6468	<10	92471	13	2	79	4	8	
	17	Piñon-Juniper Burned	12	7079	<10	66647	15	3	70	4	12	
	18	Disturbed Piñon-Juniper	14	7077	10 to 20	154033	22	2	63	11	9	Limber Pine Thistle
	19	Piñon-	15	7093	<10	21762	16	2	86	3	6	Limber

Pollen Station (S No.)		Vegetation	Plant Taxa Richness	Elevation ft.	Micro Charcoal[a]	Pollen Concentration gr/gm	Pollen Taxa Richness	Percent Fir	Percent All Trees[b]	Ratio Pine - Juniper	% Cheno-Am & Sunflower Family	Other Key Pollen Types
		Juniper & Ponderosa										Pine
	3	Piñon-Juniper	9	6829	<10	34570	13	1	73	1	17	Thistle
	1	Piñon-Juniper	16	6508	<10	47093	14	0	76	1	9	
Piñon-Juniper	2	Field in Canyon, Piñon-Juniper & Ponderosa	17	6238	<10	51877	20	2	40	1	40	Thistle
	25	Canyon Wetland in Ponderosa	11	6669	20 to 30	48070	17	5	78	22	4	Cheno-Am
	26	Disturbance Road in Ponderosa	11	6675	<10	11399	17	1	40	2	31	Thistle
	29	Disturbance Romero Field	7	7248	10 to 20	9349	19	2	38	3	18	Sagebrush

a. Micro Charcoal is an estimate of the percent cover of microscopic charcoal in the background matrix of slides made from the processed pollen samples; b. Percent all trees is the sum of pollen percentages from the following trees: Pine, Piñon, Juniper, Douglas Fir, Fir, and Spruce.

Disturbed Sites: Road Shoulder (S 26), Fields (S 2, 29), and Mechanical Disturbance (S 18)

An important research theme explored in this study is the sensitivity of pollen to vegetation changes due to disturbance, which typically occurs in small (1 to 100 acre) areas that have been cleared of trees. Homestead era agriculture during the AD 1900s and modern development at LANL have created a wide range of disturbed sites to choose from. The historic Romero field (S 29) on Pajarito Mesa, a possible historic field (S 2) on the floodplain in Ancho Canyon, a bulldozed area (S 18) on Pajarito Mesa, and a road shoulder (S 26) were sampled. Except for the Romero field (S 29), each disturbed site is matched with samples from adjacent undisturbed forests. Foxx and Tierney (1999) have intensively studied the botany of the old Romero Homestead, including a field succession study in the old bean field. Field succession botany has also been studied at eight other historic fallow fields in the LANL region (Foxx et al. 1997), and these studies provide invaluable information about historic land use and vegetation response to disturbance.

Three of the pollen stations produced pollen signatures distinct from matching samples in surrounding forest. The two field sites (S 2 and S 29) and the road shoulder (S 26) are characterized by the project maximum percentages of cheno-am and sunflower family pollen

(combined values 18% to 40%) and the lowest frequencies of tree pollen (all tree taxa combined range from 38% to 40%). The cheno-am and sunflower family encompass a broad range of weedy plant species, and the high representation from disturbed sites is probably related to opportunistic weeds colonizing new habitat.

The variety of pollen types is also high at disturbed sites; taxa richness ranges from 17 to 22 at stations 2, 18, 26, and 29. This diversity is due to a higher representation of herbs and forbs in open areas, compared to the sparse ground cover plants under forest canopies. Pollen from weedy plants, such as thistle and sunflower (Long Spine *Helianthus* type), is documented more frequently from the disturbed sites. At the Romero field site (S 29), sagebrush pollen was over 20 percent of the pollen count. Two sage plant species, carruth sage and false tarragon (*Artemisia carruthii* and *A. dracunculus*), were identified as good indicators of disturbance in the field succession study completed by Foxx et al. (1997), and both sages are also abundant in the Romero field (Foxx and Tierney 1999). Broad spine, another unknown type from the sunflower family, is more frequent at the disturbed sites than forest sites.

Station 18, the one example of mechanical disturbance, did not produce a pollen assemblage distinct from adjacent forest (S 17 and 19). Station 18 is a small, less-than-one-acre opening in burned piñon-juniper forest that is also within the transition ponderosa pine to piñon-juniper zone. Shrub size oaks that root-sprouted after the Cerro Grande fire killed the piñon and juniper trees common around S 18, and oak pollen is high at S 18 and S 17, which are separated by less than 300 feet. High pollen concentration (greater than 150,000 gr/g) and high percentages of conifer pollen (63% combined from all conifers) indicate the small opening is an efficient collector of abundant pine pollen. Acre-scale clearings will capture more wind-blown conifer pollen than ground inside a forest due to the dynamics between pollen dispersal and wind (Faegri et al. 1989:14–15; Jackson and Smith 1994:191).

Riparian Sites, Stations 4, 10, 12, and 26

Four sites were selected to sample riparian situations; however, wet sites are rare at LANL. The two best examples are the Pajarito Canyon wetland (S 25) and a riparian site in Los Alamos Canyon (S 12). The other two riparian sites are historic wetlands—a pond (S 4) that is now dry and an area in Pueblo Canyon that was a sewage effluent wetland (S 10), but now is dry. The reclaimed water in Pueblo Canyon has been diverted to the golf course.

The pollen assemblage from the dry pond at S 4 did not correspond to the site vegetation. Western wheatgrass was the dominant plant in the old pond site, but grass pollen was only three percent of the pollen assemblage. Pine pollen from the surrounding ponderosa pine forest overwhelmed the assemblage. Sheetwash sediments from burned forest stands upslope of S 4 filled the depression, and the collected pollen sample is probably not representative of pond sediments. Willow trees grow around S 4 and willow pollen was documented from S 5, which represents the pine forest surrounding S 4. The Pueblo Canyon site (S 10) is now a meadow area. The pollen assemblage from S 10 is dominated by tree pollen (69% combined conifers), but there is a component of grass pollen (7%) and cheno-am and sunflower family (10% combined values) that correlate with the wet meadow environment.

The water indicators were cattail and willow pollen recovered from S 25, the Pajarito Canyon wetland. This site is a perennial wetland with bulrush, cattails, and willow. Pine pollen was high from S 25, which reflects the surrounding pine forest in the canyon. No riparian pollen types were identified from S 26, the road shoulder site that is within 100 feet of the Pajarito Canyon wetland. The limited occurrence of cattail pollen is consistent with other research that has shown that, although a wind-pollinated plant, cattail pollen is not dispersed far from source plants (Hevly 1974; Krattinger 1975).

2000 Cerro Grande Fire Paired Pollen Stations

Two pairs of stations were sampled within the Cerro Grande burn, an intense wildfire that burned several thousand acres around Los Alamos in 2000. Stations 27 and 28 are in Rendija Canyon near the gun club and represent burned (S 27) and unburned (S 28) stands of ponderosa pine forest. The fire burned hot in Rendija Canyon, although at S 27, the fire was a ground fire and the trees were not killed. The tree composition and cover are comparable between S 27 and 28, and the main vegetation difference is greater cover of grasses and weeds at the burned site. Stations 17 and 19 represent burned (S 17) and unburned (S 19) transition ponderosa pine to piñon and juniper. The tree canopy was killed at S 17 and there is a greater contrast in the vegetation cover between the two stations (Table 6.3). Shrub size oaks, probably root-sprouted from fire-killed trees, yucca, and grasses and herbs characterize S 17, compared to 70 percent pine, piñon, and juniper tree cover at S 19.

The pollen results from the paired stations show some weak patterns (Table 6.5) that are related to the different plant composition and architecture at the two sites. The percentage of pine pollen was 10 percent less at the burned ponderosa pine S 27 compared to the unburned S 28, but the combined cheno-am and sunflower family percentages were higher at the unburned site S 28, compared to S 27. There is a greater contrast between S 17 and S 19, which is a more mixed forest (Table 6.2). Low percentages of pine and high frequencies of cheno-am and sunflower family were calculated from the burned site (S 17), compared to high pine and juniper values and lower cheno-am and sunflower family at the unburned site (S 19). Oaks are the dominant tree at S 17 and oak pollen was high at 8 percent in the S 17 sample and aggregates of oak pollen were recovered, whereas oak was low (2%) at S 19.

The percent of microscopic charcoal (ca. 200 to less than 10 µm long) in slide preparations was estimated in all 20 LANL modern analog samples to test whether samples from burns had higher amounts of charcoal than unburned sites. The estimated charcoal cover is listed in Table 6.5. Microscopic charcoal was present in all 20 samples at a minimum of less than 10 percent of the background matrix. The maximum percent cover was 30 percent to 40 percent in the sample from S 10, the Pueblo Canyon meadow. Four samples produced charcoal values of 20 percent to 30 percent: S 4 (disturbed pond), S 25 (Pajarito Canyon wetland), and the paired samples S 27 (burned ponderosa pine forest) and S 28 (unburned forest). The samples from S 17 and S 19, the burned and unburned pair in piñon and juniper forest, were characterized by less than 10 percent charcoal. No definitive relationship is interpreted from these data, although there is some indication that charcoal is concentrated in alluvial and sheetwash sediments (S 4, 10, and 25).

CONCLUSIONS

The modern vegetation at LANL is a mosaic that has been modified by a long history of cultural use including prehistoric settlement and agriculture, historic grazing and timber harvest, AD 1900s homesteaders, and modern development and land management practices, such as burning, thinning, and manipulation of water resources. Wildfire is also a significant natural architect of vegetation, as evidenced by the catastrophic effects of recent forest fires. The LANL modern pollen analog developed in this study contributes important baseline information for interpreting pollen data from fossil and archaeological sites. The constructed pollen spectra are sensitive to the natural elevation and vegetation gradient at LANL and to finer-scale compositions that reflect the local site history. However, there is no formula of values that can be applied to filter unique pollen signatures from generic sites—archaeological or natural. The potential for high-resolution pollen analysis can be realized by using the analog to compare to pollen results from specific study sites.

The different forests are characterized by relative differences in fir, pine, and juniper pollen. Cheno-am, sunflower family, and sagebrush (*Artemisia* spp.) characterize old fields. Cheno-am, sunflower family, and grass pollen distinguished the two meadows sampled (S 8 and 10). Riparian sites are rare at LANL, but the only station where cattail was growing (S 25) yielded the only cattail pollen recovered in the study. Other potential indicator pollen types are Douglas fir and cf. limber pine from mixed conifer forests, maple and birch from mesic sites, willow from riparian environments, and sagebrush, thistle, and long spine (cf. sunflower type) from disturbed sites.

CHAPTER 7
THE CURRENT STATUS OF ARCHAEOLOGICAL DENDROCHRONOLOGY AND DENDROCLIMATOLOGY OF THE PAJARITO PLATEAU, NEW MEXICO

Ronald H. Towner

INTRODUCTION

Dendrochronology, or tree-ring dating, has played a significant role in the development of archaeology in the U.S. Southwest; it has also provided important information regarding past environmental variability in the area. This document discusses two subfields of dendrochronology—dendroarchaeology and dendroclimatology—in terms of their impact of studies of human use of the Pajarito Plateau and past environments in the same area. It should be viewed as a summary of what has been accomplished and as a potential guide for further elucidation of human/environment interaction.

Dendrochronology, the science of tree-ring dating, is the most accurate and precise non-documentary dating method available to researchers studying the recent past. Tree-ring dates are accurate and precise to the year, and some times to the season, and have no associated statistical uncertainty or standard error. Other prominent archaeological dating techniques that use natural materials (e.g., radiocarbon, archaeomagnetism, etc.) have been calibrated using dendrochronological samples. It is this precision and accuracy that has allowed archaeologists working in the U.S. Southwest to construct the most detailed chronologies in the world and to explore a plethora of environmental, social, and behavioral questions regarding the past human adaptation to the region.

Dendroarchaeology is the use of tree-ring data from archaeological contexts to provide Christian-calendar dates for archaeological phenomena such as rooms, sites, and cultures, to delineate aspects of past human behavior, such as tool use, wood harvesting and modification practices, and the social strategies used to exploit past wood resources, and to illuminate aspects of past environments, such as species composition of past landscapes and past precipitation and temperature regimes (Dean 1996a; Towner et al. 2001). Dendroclimatology is the use of tree-ring data from living and dead trees—including archaeological timbers—to examine past climate fluctuations and patterns in terms of precipitation and temperature at various temporal and spatial scales (Bradley 1999).

This overview has three main objectives. First, it is a synthesis of all archaeological tree-ring data derived from historic and prehistoric sites on the Pajarito Plateau. Although many of the dates have been published elsewhere (Robinson et al. 1972), this is the most extensive compilation and interpretation of the tree-ring data (not simply dates) from the Pajarito Plateau. Second, it is a synthesis of the existing dendroclimatic data relevant to the area. Such data are not point-specific or constrained by political boundaries and, therefore, the discussion encompasses much of the northern Rio Grande area, not simply the Pajarito Plateau. Finally, the syntheses will be used to suggest possible avenues for future research in the area using both

fields. Therefore, this document will be important both as a detailed summary of the existing data and as a guide for future dendroarchaeological and dendroclimatological research.

A BRIEF HISTORY OF DENDROCHRONOLOGY

Andrew Ellicott Douglass is considered the founder of dendrochronology. Trained as an astronomer, Douglass immigrated to Flagstaff, Arizona, in the late 19th century to develop Percival Lowell's observatory that was designed to explore the possibility of canals on Mars (Webb 1983). Douglass, however, was interested in chronicling sunspot activity as a method to document past and predict future climate. The historical climate records in the Flagstaff area were virtually nonexistent (about 20 years in length), so Douglass searched for some proxy measure of climate with which to compare sunspot cycles. At that time, the great ponderosa pine forests of the Flagstaff area were being actively logged. By examining the stumps, and some times cross-sections, of ponderosa pine trees, Douglass identified the "Flagstaff signature" ring series that contained small rings at specific years in the late 1880s, 1890s, and early 1900s. The first test of Douglass's method occurred in 1904 when he deduced that a tree was cut 10 years previously, in 1894; Douglass checked his deduction with the farmer who had cut the log, who confirmed its cutting date (Towner 2000; Webb 1983).

Douglass continued to develop his chronology from living trees, but in 1914 his research attracted the attention of archaeologists working in the Southwest (Nash 1999). Subsequently, archaeological samples collected by Douglass and others from sites such as Pueblo Bonito in Chaco Canyon and Aztec Ruin on the Animas were cross-dated to form a "floating" or relative chronology some 585 years in length (Douglass 1921). Unfortunately, this chronology did not overlap in time with Douglass' modern tree specimens, and therefore, even though the temporal relationships between the sites were known in annual terms, they were not yet known in terms of the Christian calendar. Archaeologists had learned that Aztec Ruin was approximately 45 years younger than Pueblo Bonito, but whether both sites were built 1,000, 2,000, or 3,000 years ago was still undetermined (Nash 1997, 1999; Webb 1983).

During the 1920s, archaeologists and the dendrochronologist (Douglass) were working to solve the problem of the "gap" between the live-tree and floating chronologies (Haury 1962). Fortunately, archaeologists in the Southwest had developed a pottery seriation based on historic and prehistoric period sites (Colton and Hargrave 1937). Thus, the archaeologists knew the relative temporal position of many sites, if not their absolute ages. Throughout the decade, numerous "beam" expeditions traveled to the Colorado Plateau and Rio Grande area to collect archaeological specimens to further Douglass' tree-ring research (Nash 1999). Using the pottery seriation, these expeditions focused on specific sites thought to represent occupations during the "gap" between the chronologies. Finally, on June 22, 1929, a burned beam (HH-39) from the Whipple Ruin allowed Douglass to combine the two chronologies into a single master record more than 1000 years in length (Haury 1962). After "the gap" was bridged in 1929, dendrochronology experienced a brief florescence with research laboratories established in Tucson, Flagstaff, and Globe, Arizona, and Santa Fe, New Mexico; additional research was conducted on the High Plains in Kansas and North Dakota, in the southeastern United States, and in Alaska.

Dendrohistory in the Northern Rio Grande

As Douglass developed his living tree and archaeological ring sequences for the Four Corners area and Colorado Plateau, he soon realized that the northern Rio Grande area contained a different climatic signal (Douglass letter to Judd date June 24, 1927; cited in Nash 1999:185). Under Douglass' direction, Jeançon and Ricketson collected Rio Grande samples, including some from San Idlefonso, as part of the first Beam Expedition (*El Palacio* 1923a, 1923b). Douglass had worked with samples from Pecos Pueblo excavated by Alfred Kidder, but was unsure of their chronological position. Indeed, the omission of any Rio Grande site, including the famous Pecos Ruin, from his seminal article "The Secret of the Southwest Solved by Talkative Tree-Rings" (Douglass 1929) was glaring (Nash 1999).

After the "gap" in the Central Pueblo chronology was bridged, the most pressing problem in Southwestern dendrochronology became dating the Rio Grande archaeological sequence. Eager to move quickly on the problem, the newly formed Laboratory of Anthropology (LAH) established a tree-ring dating program and Jesse Nusbaum, director of LAH, hired a young Douglass student, W. S. Stallings, to direct it in 1931 (Nash 1999).

Stallings had already collected samples from the area and immediately spent four months in the field collecting living-tree, dead wood, and archaeological tree-ring samples; many of the archaeological samples came from sites on the Pajarito Plateau, such as Puyé, Tsankawi, and Tyuonyi (see below). By the end of 1931, Stallings had collected more than 300 wood and charcoal specimens and by early 1932 had dated the Palace of the Governors and several other historic structures and established a chronology for the Jemez Mountains and Pajarito Plateau back to the early 1500s. Paralleling Douglass' research design, Stallings used the Rio Grande ceramic glazeware sequence established by H. P. Mera (1939) to target specific sites for sampling (Nash 1999).

By the end of 1932, Stallings had developed a ring sequence—predominantly using ponderosa pine—that extended back to AD 1200 and in the process dated Pecos Pueblo for Kidder (Stallings 1933, 1937). In 1934, Stallings and Stanley Stubbs collected numerous samples from Pindi Pueblo that extended the chronology to AD 1100 (Stallings 1934). By 1935, Stallings had established dates for some of the Glaze Wares of the upper Rio Grande and dated numerous historic and prehistoric period sites (Stallings 1937). Thus, within a span of only five short years, Stallings had developed the Rio Grande ring sequence back to AD 1100 and provided Christian-calendar dates for sites and artifact sequence.

This promising beginning, however, soon faltered. Nusbaum's move to Mesa Verde, Stallings' desire to complete his Ph.D. and subsequent military service, and a lack of institutional support resulted in the abrupt decline of tree-ring dating in the northern Rio Grande area. Although additional samples were collected by Stubbs, and E. T. Hall dated many samples from Awatovi, and Stallings even dated some samples for the Taylor Museum in Colorado Springs, dendrochronology at the LAH simply "faded away" in the early 1940s (Nash 1999). Every other tree-ring laboratory in the country except the Tucson Laboratory of Tree-Ring Research (LTRR) facility suffered this same fate. Fortunately, through the foresight of Terah Smiley, the LTRR

acquired the LAH collection and accompanying documentation in the early 1950s. Just as importantly, a young scholar used the collection for his first major dendrochronology project, reanalyzed the samples, and published the Rio Grande chronological sequence—an unfinished goal of Stallings (Bannister, personal communication, 2002; Smiley et al. 1953). All samples collected in the area since the 1950s (see below) have been analyzed and are curated at the LTRR in Tucson, and thus there is a coherent collection available for additional research.

The transfer of collections and expansion of the LTRR in the 1960s resulted in significant advances in dendrochronology and southwestern archaeology (and other fields). Bannister refined the dating of several of the larger ruins in Chaco Canyon and developed theoretical approaches to dendroarchaeology (Bannister 1962, 1965); Robinson began using tree-ring data to examine past human behavior by delineating the impact of stone ax use on Basketmaker III (AD 600-750) society and wood-use practices, and initiated dendroclimatic research using archaeological samples (Robinson 1967; Dean and Robinson 1977). Other researchers examined the dendroarchaeological remains of other southwestern cultural groups (Towner 1996, 1997), refined the theoretical basis of dendroarchaeology (Ahlstrom 1985, 1997) and studied the impact of the field on American archaeology in the 20th century (Nash 1997, 1999).

Jeffrey S. Dean, however, has conducted the most significant research in archaeological dendrochronology in the past few decades. His research on Kayenta Anasazi cliff dwellings used dendrochronological and archaeological data to posit testable hypotheses about the nature of prehistoric social organization and adaptation to southwestern environments (Dean 1969). His 1978 article, "Independent Dating in Archaeological Analysis," elucidated the theoretical basis of various dating techniques and their application to the interpretation of past human events (Dean 1978). Finally, he described three types of information that can be gleaned from tree-ring data: chronological, behavioral, and environmental (see below) (Dean 1996a).

METHODS AND TECHNIQUES OF DENDROCHRONOLOGY

Dendrochronology is based on the fact that many trees, particularly in temperate and high-latitude zones, produce an annual growth layer (cambium). This cambial layer is typically composed of two visually distinct parts—early wood and latewood (Figure 7.1). Early wood consists of large, open, thin-walled trachial cells that appear light in cross-section. Early wood is produced during the first part of the growing season (which varies by species), when the factors that limit growth, such as moisture, temperature, nutrients, and growth hormones are at their optimal levels. Latewood, on the other hand, is comprised of progressively smaller, thicker-walled, trachial cells that appear dark in cross-section. At the end of the growing season, the tree becomes dormant and ceases to produce cambium; a distinct boundary between the previous year's latewood and the current year's early wood is clearly visible, particularly in conifers.

The variability of annual ring width reflects variation in some climatic variable (e.g., precipitation, temperature). In low-elevation conifers, precipitation is the factor most responsible for ring-wide variability. In dry years, trees produce thin cambial layers, but in wet years water ceases to limit growth and a thicker cambial layer is produced. It is this variability in ring width that is the basis of crossdating and dendrochronology. False rings, also known as intra-annual

growth bands, result from a water deficit during the growing season that causes the tree to produce latewood-like cells. If the water deficit is ameliorated, such as by summer monsoon moisture in the Southwest, the tree again produces early wood-like cells until near the end of the growing season. Micro-rings occur in drought years when the tree produces cambium on only specific areas; if samples are taken from areas that lack the cambial layer, the rings appear locally absent or "missing." Crossdating tree-rings, assigning specific years to individual growth rings, accounts for both missing and false rings, and thus is fundamentally different from merely counting rings.

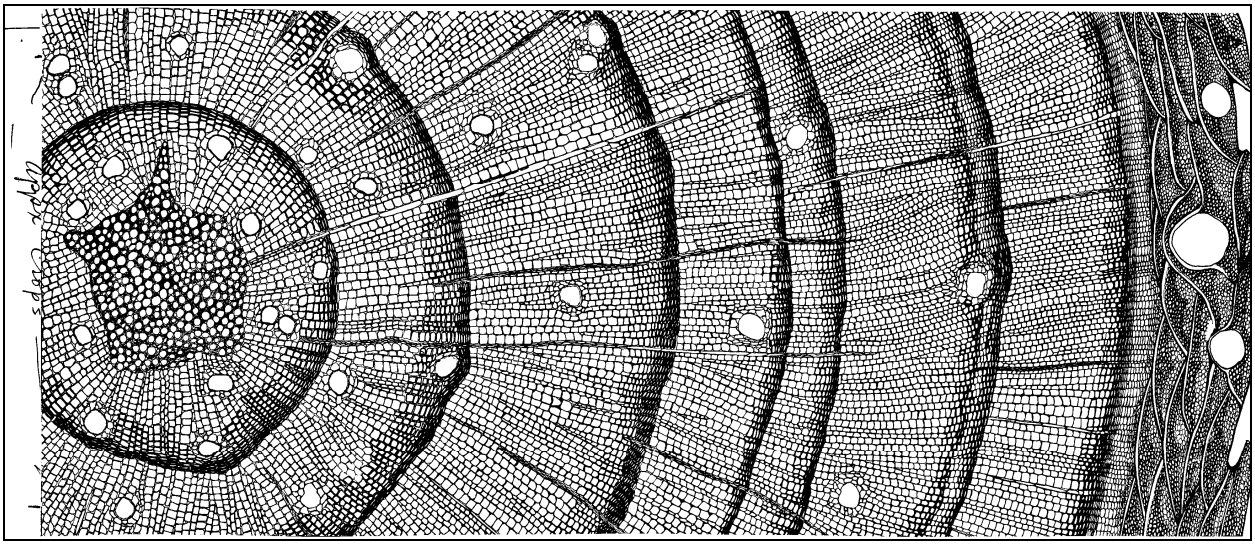

Figure 7.1. Schematic of conifer tree rings.

Crossdating is the most fundamental principle of dendrochronology. If samples do not cross date, temporal control is lost and any interpretations of the tree-ring data become mere estimates. The most common crossdating method used in American archaeology is skeleton plotting. Skeleton plotting is a visual analog technique wherein each ring on a sample is represented by a line on a piece of 1-mm graph paper. The small rings on a sample are noted by drawing a vertical line on the graph paper at the appropriate ring number; the smaller the ring—relative to the surrounding rings—the longer the vertical line drawn on the graph paper. Thus, the skeleton plot visually represents the pattern and "narrowness" of the small rings on a sample. Drawn lines do not represent large and “average” rings. By precisely matching the small-ring pattern between samples, each ring can be assigned to a specific calendar year. Although similar ring-wide patterns have occurred in the past, a sample of 50 to 100 years is usually sufficient for crossdating in the Southwestern United States. An interactive computer crossdating program can be viewed at http://tree.ltrr.arizona.edu/skeletonplot/introcrossdate.htm.

Tree-ring chronologies are built using live trees, dead snags, remnant wood, and archaeological specimens (Figure 7.2). Starting from a known point in time (usually the present), dendrochronologists precisely match and overlap ring-width patterns from successively older samples to create a year-by-year chronology. Typically, chronologies are initiated with a sample of at least 40 increment cores from 20 trees and strengthened with additional specimens and by comparison with other chronologies in the area. When sample depth for any chronology drops

below 10 trees, the dating is considered tentative. The spatial extent of tree-ring chronologies varies according to factors such as topography, elevation, and dominant climatic pattern. For example, extant chronologies from many areas of the Colorado Plateau crossdate with each other even though they are separated by more than 100 miles. In contrast, a chronology from Rayado Creek in the eastern foothills of the Sangre de Cristo Mountains does not crossdate with the Taos chronology less than 30 miles away on the other side of the mountains (Towner 2000). In this case, different climate patterns in each area have resulted in different ring-width patterns in trees on different sides of the mountains.

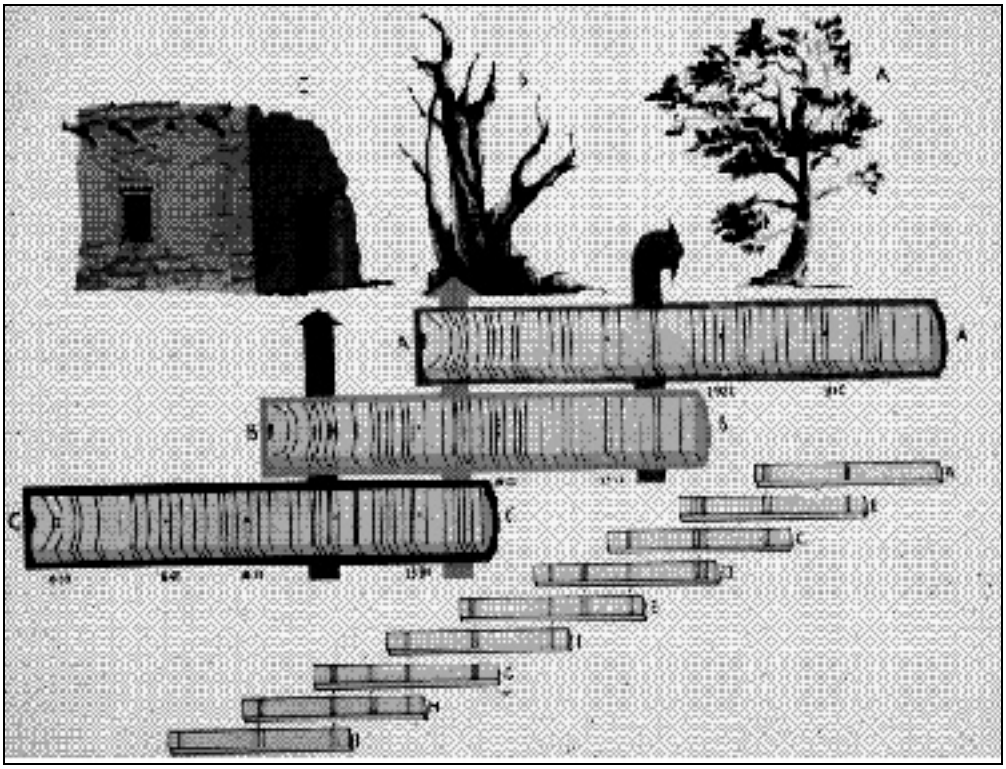

Figure 7.2. Schematic of chronology building with tree rings.

Tree-Ring Requirements

Trees must exhibit four attributes in order to be dendrochronologically useful. First, they must produce distinguishable annual growth layers (rings). Second, an individual ring must grow in a uniform manner around the bole of the tree, or branch (i.e., it must exhibit circuit uniformity). Third, the rings must exhibit some type of annual variability (e.g., ring width, ring density). Finally, a sample must contain a sufficient number of rings to permit the identification of variability patterns; in southwestern conifers, 50 to 100 rings are usually sufficient, but in some areas and with other species like European oak, 200+ rings may be necessary.

Dendrochronology is probably best known as a technique that provides absolute Christian calendar dates for archaeological sites in the American Southwest. The most fundamental principle of dendrochronology is crossdating—matching patterns of annual variability among

local or regional tree populations. In the Southwest, the skeleton plot method of crossdating has been used successfully for decades. If the variability patterns on a sample do not exactly match the tree population, the sample does not crossdate and cannot be used in dendrochronology. In this fundamental respect, crossdating is significantly different than simply counting rings or estimating tree age.

Crossdating allows dendrochronologists to assign a single calendar year to each and every ring on a sample. Unfortunately, not all trees or archaeological samples, even in the Southwest, produce dates. Some trees produce cambium in response to microenvironmental factors that are not reflected in the overall tree population; others respond to non-climatic factors such as nutrient availability, and still others do not produce annual rings.

In order to construct a chronology, the skeleton plotted samples from living trees, standing snags, remnant wood, and archaeological samples are combined into a master skeleton plot. By overlapping the plots of individual specimens, the chronology can be extended backwards in time until a lack of sample depth precludes crossdating. Specific small "marker rings" that occur on a large proportion (usually >75%) of samples in a collection help establish the basic pattern, which is then tested against additional samples and other nearby chronologies. In addition to small size, marker rings may be identified by internal features such as frost-damaged cells, false or double rings, unusually wide or narrow latewood bands, or other microscopically visible attributes.

Collecting and Analyzing Archaeological Tree-Ring Samples

As discussed below, past human behavior is the most significant factor affecting archaeological tree-ring dates. Past people did not select wood for its dendrochronological properties, and not all archaeological specimens will produce dates. Some samples will exhibit little ring-width variability (complacent ring series) and some will show extreme variability outside the range of the normal tree population (erratic ring series) (Stokes and Smiley 1968). Archaeologists and dendrochronologists can mitigate these factors by collecting <u>all</u> samples that display any potential for dating, or, which are the appropriate species and contain 50+ rings (Towner 2000). Even experienced dendrochronologists cannot date samples in the field, however, so selecting only the "best" samples is often self-defeating.

Samples can be collected using several different methods. Live trees are sampled using a Swedish Increment Borer that removes a small pencil-shaped core from the tree (Figure 7.3). Depending on the specific site circumstances, archaeological samples are collected as cross-sections sawn from beams, cores extracted from beams using a specially adapted hole saw, or as charcoal; approximately 80 percent of the 4000 samples annually processed by the LTRR are charcoal from excavated contexts.

Figure 7.3. Photograph of A. E. Douglass collecting a live-tree core near Pinedale, Arizona.

Sample preparation in the laboratory differs depending on the type of material collected. Wood samples, either cores or cross-sections, are sanded with fine-grit sandpaper until the individual cells are visible under a binocular microscope at 10x to 50x magnification. Charcoal is not sanded, but broken to expose a fresh surface. Each sample is then examined under the microscope and the ring series is skeleton plotted on graph paper. The skeleton plots are compared to each other to identify internal crossdating between samples and compared to local and regional master chronologies to determine Christian calendar dates. Discrepancies among

samples are resolved using the wood (or charcoal) as the basic unit of analysis; the paper skeleton plots are only representations of the sample ring series. As the only repository of archaeological tree-ring samples in the western United States, the 300,000 samples and 70,000 dated specimens housed at the LTRR provide an unmatched comparative research collection.

Attributes of Archaeological Tree-Ring Dates

Even when samples produce dates, they must still be interpreted, and not all archaeological tree-ring dates are the same. Because archaeological tree-ring samples are the result of past human behaviors, specific sample attributes and the archaeological context must be considered in any interpretation of the chronological materials. Sample attributes can be used to identify cutting, near cutting, and noncutting tree-ring dates.

Cutting dates, also known as tree death dates, retain the last cambial layer grown by the tree and indicate that the tree was cut in a specific year (assuming tree death resulted from human harvesting). Evidence on the sample that it is a cutting date includes the presence of bark, beetle galleries, a shiny patina, or a continuous ring around the sample (denoted by B, G, L, c, or r in LTRR reports) (e.g., Robinson et al. 1972); a sample can also be considered a cutting date if the symbol "v" accompanies the date—noting that in the opinion of the analyst, the last ring on the sample is the last ring grown by the tree (Ahlstrom 1985). Samples that retain the last cambial layer can also be assigned a cutting (death) season. Samples that exhibit a terminal ring with a full complement of latewood were cut after that growing season for that particular year ended; samples that show only early wood cells were cut during the growing season. Because different tree species have different growing seasons, cutting dates in a structure in the same year from different species can define construction of a building or room to relatively short time period, as little as 4 to 6 weeks in some cases (Dean and Warren 1983; Towner and Dean 1992).

Samples that yield near cutting dates also retain the last ring grown by the tree; however, these particular samples may (or may not) contain a locally absent or missing ring near the end of the sample ring sequence, and are denoted by a "+" symbol (Towner 1997). For example, a sample that dates 1630 to 1748+B retains bark that indicates no exterior ring loss. However, AD 1748 was one of the driest years in the Southwest and the 1748 ring is locally absent on many samples throughout the region. This hypothetical sample may crossdate from AD 1630 to 1744 and contain four additional rings after its last small "marker ring" of 1744. Because 1748 is typically small and often locally absent on other samples, it may also be missing from this hypothetical sample; therefore the last cambial layer on the sample may have actually grown in AD 1749, but there is no way to verify the absence (or presence) of the AD 1748 ring because the ring sequence does not extend far enough beyond AD 1748 to determine if it is locally absent or simply not small on this particular sample. Near cutting dates, therefore, should be considered within a year or two of tree death dates.

Noncutting dates result from two different processes: exterior ring loss or ring counts near the outside of the sample ring sequence (and are denoted by "vv" or "++," respectively). Samples that do not retain the last ring grown by the tree (vv dates) have suffered exterior ring loss either through natural processes, such as erosion, or cultural processes, such as beam shaping. Thus, a

sample dated AD 790 to 957vv could not have been cut before AD 957, but because it may be missing one, 10, or even 100 exterior rings, the harvesting date cannot be determined with any degree of confidence, unless a specific heartwood-sapwood ratio has been developed for a particular species in a particular area (Dean and Ravesloot 1993; Nash 1997). Partially ring counted specimens (++ dates) result from a lack of crossdating on the sample beyond a specific year. Consider again our hypothetical AD 1630 to 1748 specimen. If it cross-dates from 1630 to 1720, it can be dated, but there are an additional 28 rings on the sample that do not match the master ring sequence. In addition to the typically small 1748 ring, many other typically small rings, including 1722, 1724, 1729, 1733, 1735, 1737, 1739, and 1744 may also be missing from the sample. Therefore, it would be labeled 1630 to 1748++B and considered a noncutting date. If all of these rings are missing, the sample would date to at least 1756, but there is no way to determine if all, some, or none of these rings is absent. Ahlstrom (1985) suggests that "++" dates may indicate deadwood use. Such an inference is tenable because as trees die a slow natural death, they respond less and less to macroenvironmental conditions and produce more sporadic cambial growth layers. Noncutting dates (both vv and ++) provide only a *terminus post quem*, a date before which tree death could not have occurred; a noncutting date may predate the actual use of a beam by years, decades, or even centuries.

Deriving Chronological Information from Tree-Rings

The key to interpreting archaeological tree-ring dates is the identification of anomalous dates. Anomalous dates are defined as those dates that do not date the event of interest and are therefore dependent upon the archaeological context and research question (Dean 1978). The tree-ring dates themselves are precise and accurate; they date the last ring on the sample, but may not date the event of interest. For example, if one is interested in dating the construction of Spruce Tree House, the most visited cliff dwelling in the world, the 1932 cutting dates from Kiva C are clearly anomalous. If on the other hand, the event of interest is dating the stabilization work, the 100+ dates in the AD 1200s are considered anomalous. Obviously, dates are only anomalous within a context, and all dates may be anomalous in different contexts.

Identifying anomalous dates requires (a) an adequate sample of dates and (b) defining date clusters. An adequate number of dates is a relative term that depends on the number of samples available for collection, the number of samples collected, and the number of dates derived. A large number of dates certainly increases the probability of identifying date clusters, but may actually increase the difficulty of interpreting them—it will also make the process much more interesting. Ahlstrom (1985) has defined a date cluster as "three or more dates falling in a brief time interval," but definitions vary among researchers and from collection to collection. Ahlstrom has adapted the stem-and-leaf technique to plotting tree-ring dates in order to provide a detailed visual representation of each date in a distribution. Applying the technique to archaeological tree-ring dates, he identified an "ideal" date distribution as a single line on the plot consisting of entirely cutting dates in the same year (Ahlstrom 1985). I enlarged this concept (Towner 1997, 2000) and proposed that different date distributions could be used to identify different wood use behaviors. Although stem-and-leaf plots separate the dates from their archaeological contexts, they delineate the temporal attributes of samples and allow an initial assessment of the relationships among them. Because the stem-and-leaf technique ignores

the archaeological context of tree-ring dates, however, it does not always adequately explain past human behavior.

Deriving Environmental Information from Archaeological Tree-Ring Samples

The precise chronological data provided by tree-ring dates—even well-provenienced cutting date clusters—illuminate more than simply the temporal aspects of an occupation. Embedded in the samples and their interrelationships is also important environmental information. Environmental information can be derived from archaeological tree-ring samples in at least two ways. First, the tree species exploited by past peoples may indicate aspects of local species availability and, thus, environmental composition. Second, archaeological tree-ring samples can be used to reconstruct past precipitation and/or temperature regimes and identify past "extreme" climatic events (see below).

The tree species present in archaeological tree-ring collections are the result of several factors. First, site occupants often exploited the most available species; thus, archaeological samples can be used to assess past species distributions and forest composition (at least at the genus level). For example, the Black Mesa Archaeological Project (BMAP) in northern Arizona collected more than 5000 tree-ring samples from Navajo archaeological sites that were occupied between AD 1800 and 1972. The modern vegetation community of Black Mesa consists predominantly of piñon-juniper forest, isolated stands of ponderosa pine and Douglas fir, and various undatable non-coniferous species. The Navajo BMAP dendroarchaeological samples mirror this distribution both in terms of species availability and spatial distribution (e.g., in areas with higher concentrations of one species, that species is most often used in structure construction; Dean and Russell 1978). These data indicate little ecological change in the composition of Black Mesa forests over the past 200 years.

Species distributions in archaeological collections are affected by more than species availability, however. Human social and economic systems also impact the presence and proportions of species in collections. For example, copious research concerning the Chacoan use of timbers in the Great Houses in Chaco Canyon demonstrates that people may have expended tremendous amounts of labor and energy to acquire and use specific trees for specific structures and functions (Dean and Warren 1983; English et al. 2001).

Deriving Behavioral Information from Archaeological Tree-Ring Data

That chronological and environmental information is present in archaeological tree-ring samples is usually obvious; behavioral information, however, is often overlooked. Data concerning how past people treated wood as a resource by selecting specific tree species or sizes of trees, choosing specific harvesting and beam modification techniques, or using deadwood, stockpiling or reusing beams all reflect how, and some times why, past populations adapted to their physical and social environments.

The behavioral information inherent in archaeological tree-ring samples is directly impacted by two major factors: the behavior of past peoples and the behavior of archaeologists and dendrochronologists. Past peoples must have (a) used wood as a resource for building structures, making artifacts, and as fuel; (b) they must have exploited species that are appropriate for dendrochronological analysis; and (c) they must have used wood in ways that insured its preservation in the archaeological record. Archaeologists influence tree-ring data by (a) selecting sites for study that contain dendrochronological materials, (b) precisely recording the provenience and surface attributes of samples, and (c) properly collecting and submitting the samples for analysis. Dendrochronologists must correctly date the samples and describe their microscopic attributes (e.g., terminal ring characteristics, false and micro-rings).

Certainly, the above-described species selection and economic procurement systems represent past human behaviors. It is at the individual beam, room, structure, and site level, however, that most detailed human behaviors can be identified. Such behaviors include species selection preferences, deadwood use, beam stockpiling, beam reuse, structure repair and remodeling, structure abandonment, and beam harvesting, preparation, and modification. When data from many beams, rooms, and sites are combined, broad-scale patterns of how specific groups treated wood as a resource can be delineated.

This is one area where dendroarchaeology differs from other subfields of dendrochronology. Single samples or site collections are related to specific past human activities and may not contain information relative to larger spatial and temporal issues. For example, the collection and analysis of 130 high-altitude bristlecone pine specimens from the San Francisco Peaks (SFP) of northern Arizona has had important ramifications for reconstructing temperature variability in the entire Southwest and across western North America for the past 2000 years (Salzer 2000a). In contrast, the collection of 1121 archaeological samples from Long House Ruin in Mesa Verde informs us about the activities of a specific group of people in a specific time. Simply put, archaeological tree-ring specimens are part of a specific human behavioral context that may (or may not) be directly related to broader patterns.

The first level of analysis for deriving information about past human behavior is at the individual beam or sample level. Precise provenience and sample attribute information can reveal aspects of beam function, procurement, and preparation (Dean 1969; Towner et al. 2001; Windes and Ford 1996). Beam function includes information about the architectural element and its use (e.g., is the roof beam a primary or secondary beam, a door lintel, or jamb). As in the Chaco case cited above and others, specific species and sizes may have been preferred for specific architectural elements (Windes and McKenna 2001). Beam procurement methods include cutting with a stone or various types of metal axes or saws, breaking, or burning. Noting the procurement method evident on a sample may indicate the use of deadwood (e.g., breaking, burning) or provide a temporal framework for undated samples (e.g., different saw marks relate to technological innovations in saw technology). Beam preparation may include removing limbs, bark, shaping a beam, and preparing the beam ends using various tools. Tools commonly used in beam preparation include various types of axes and saws as well as draw knives, adzes, and grinding tools. Identifying the types of tools used to procure and prepare timbers may have implications for interpreting anomalous dates, distinguishing technological traditions, or recognizing cultural interaction. Other attributes of individual beams that should be recorded, if

appropriate, include the degree of sooting or blackening to recognize potentially reused beams, charring as a potential aid in determining room, structure, or site abandonment mode, the presence of twisted grain or root flares to aid in identifying deadwood use, and any other noticeable attributes.

At the room and structure level, it is necessary to document the architecture as completely as possible. Such characteristics as the bond-abut relationships of walls, changes in wall construction materials or plastering, changes in room function denoted by sealed doorways or covered hearths, and other architectural attributes can help in determining when the room was built (as opposed to when the beams were harvested) and provide clues to the nature of the occupation. When combined with beam attributes and dates, such information can help to identify anomalous dates, the use of deadwood, the reuse of older beams from other rooms or sites, the stockpiling of beams, the repair and remodeling of rooms and structures, and can yield information relative to the duration of occupation and mode of abandonment of a room or structure (Ahlstrom 1997; Dean 1969). Finally, these combined data can help illuminate aspects of human social organization, such as the use of a room or structure by a family or supra-family group; they may also contribute to understanding the dynamics of that group through time, such as changing structure use in response to generational changes in family size, the immigration of new families into a settlement, and many others.

At the site and regional levels, tree-ring data provide the temporal control necessary to delineate broad patterns of human behavior. At the site level, the initial founding of a site can often be determined through tree-ring analysis, and the duration of the occupation may also be delineated. An excellent example of the former is Douglass' dating of the Mesa Verde cliff dwellings. Before the advent of dendrochronology, archaeologists debated whether the structures were hundreds or thousands of years old. Douglass' precise dating of these ruins to the 13th century had profound implications for archaeological and anthropological theories of the rate of human cultural development in the New World (Nash 1999). Similarly, before large-scale sampling efforts and detailed analysis documented the duration of occupation of the Kayenta Anasazi cliff dwelling of Betatakin at less than 40 years, many people assumed such structures had been occupied for hundreds of years. Again, such temporal compression has required anthropologists to reexamine their theories of cultural evolution and has forced archaeologists to consider the importance of settlement mobility patterns in interpretations of population demographics and history.

At the regional level, tree-ring data contribute to understanding population dynamics, culture change, and interaction in a variety of ways. For example, recent dendroarchaeological analysis of several Navajo pueblito structures in Palluche Canyon, New Mexico, reveals very similar initial construction, remodeling, and abandonment dates (Ababneh et al. 2000). These small three- to five-room structures were all apparently constructed, temporarily abandoned, reoccupied, and finally abandoned within a period of about 20 years. The archaeological and dendrochronological data suggest all the sites were occupied by the same extended family group, and this inference is supported by ethnographic data and Navajo oral traditions. Thus, these sites have become much more than simply interesting ruins on the landscape; they can now be related to a specific period in Navajo history, a specific form of social organization, and perhaps to a particular descendent group of Navajos (Ababneh et al. 2000).

On an even larger scale, dendroarchaeological data have been used to illuminate aspects of significant migrations both during the prehistoric period and during the early historic period. As discussed above, the archaeological and climatic information indicate a climatic gradient that may have influenced the timing and direction of the Mesa Verde Anasazi movements out of the Four Corners area and into the Rio Grande Valley (Ahlstrom et al. 1995). More recently, I have suggested that the Navajo emigration out of their Dinétah homeland in northwest New Mexico and into northeastern Arizona during the late 1800s was a social and economic process unrelated to the single-year drought of 1748 (Towner 1997). These large databases enable archaeologists and dendrochronologists to investigate important questions concerning how humans—as individuals, families, and supra-family groups—colonized landscapes, exploited their environments, interacted with their neighbors, and responded to changes in their physical, social, and technological environments.

PREVIOUS ARCHAEOLOGICAL DENDROCHRONOLOGY ON THE PAJARITO PLATEAU

The results of almost 80 years of archaeological tree-ring research on the Pajarito Plateau are presented below. A summary of the dated sites is presented in Table 7.1 and all samples from Pajarito Plateau sites are listed in Appendix D. Before they are discussed, however, a couple of caveats must be offered along with the interpretations. If the two most important factors in a dendroarchaeological date distribution are (a) the behavior of past site occupants and (b) the behavior of archaeologists and dendrochronologists (Dean 1996a; Towner 2000), it is clear that the latter has had a profound influence on the Pajarito Plateau database. Certainly the site occupants' choices of tree species for construction and fuel have helped shape the database. More important, however, has been the research interests, excavation of specific structures and site, and species-specific collection strategies of archaeologists and dendrochronologists, particularly before about 1980.

The interpretations of individual rooms and sites offered below are based on the dendroarchaeological data and minimal provenience information. No site maps or detailed notes are located in the LTRR files, and may not exist for some sites. Because of the limited nature of the accompanying provenience information and site description, however, any such interpretations should be tested against the archaeological and documentary record. Only by placing the tree-ring dates in their archaeological contexts (cf. Towner et al. 2001) can anomalous dates (Dean 1978) be identified and true behavioral events, such as construction, repair, and remodeling, be delineated.

The site presentation is organized in accordance with the LTRR site file system. All sites on the Pajarito Plateau are in the New Mexico "I" quadrangle—a one-degree by one-degree geographic unit, in this case from 35 to 36 degrees N and 106 to 107 degrees W—although the Pajarito Plateau does not encompass this entire range. The archaeological sites included in the synthesis are bounded on the north by Santa Clara Creek, on the south by Borrego Canyon, on the east by the Rio Grande, and on the west by the crest of the Jemez Mountains (Figure 7.4). If known and identified in the LTRR files, sites are also noted by names and LA numbers. Collections with a

large number of dates are also shown as stem and leaf plots (Ahlstrom 1985), where the three-digit column on the left indicates the decade (128 indicates the 1280s, for example) and the numbers on the right indicate individual years.

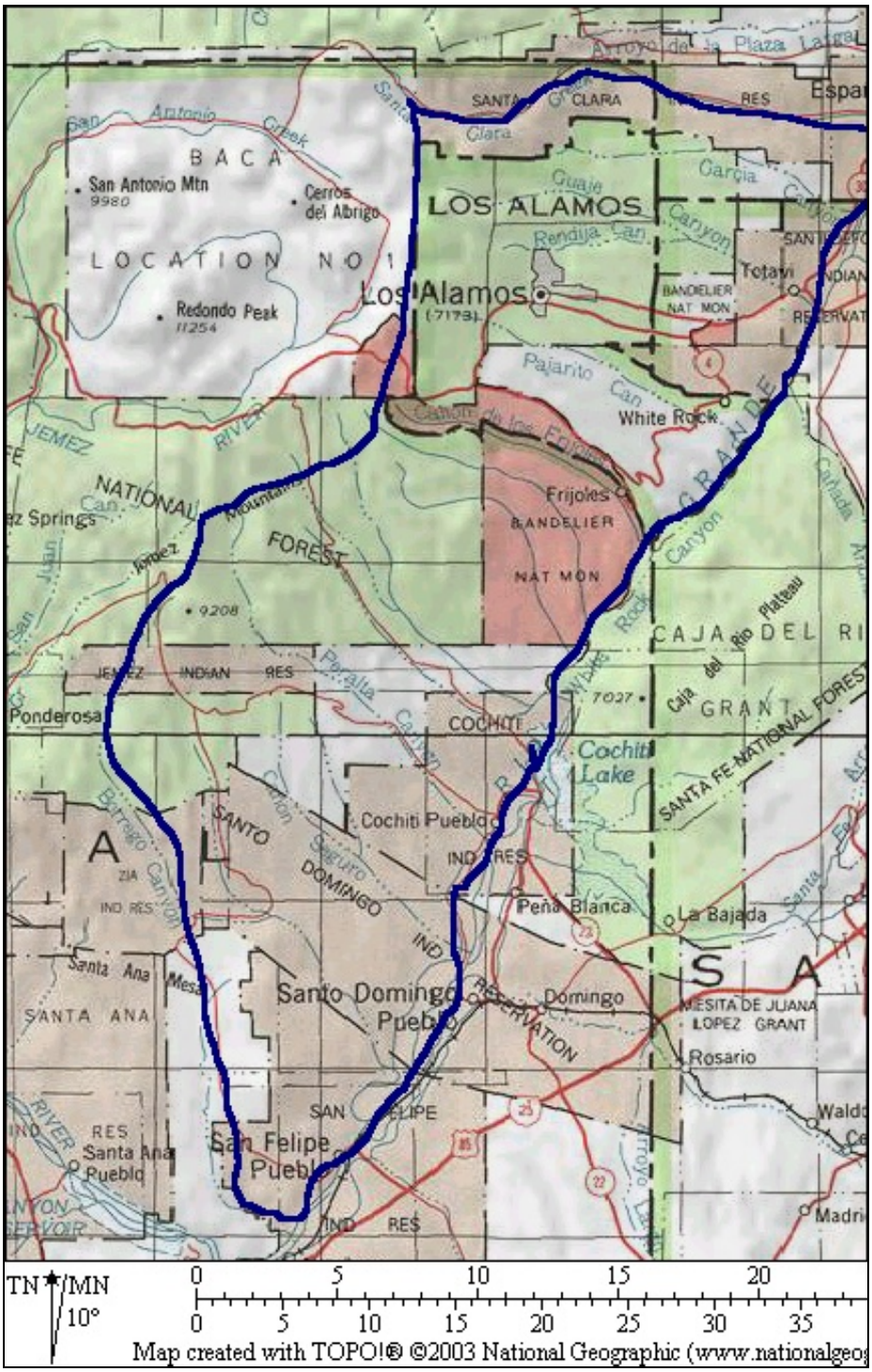

Figure 7.4. Map of the Pajarito Plateau and project area.

Table 7.1. Summary of tree-ring data from all archaeological sites on the Pajarito Plateau.

LTRR Acc#	Site #	Site Name	Number of Samples	Number of Independent Samples	Number of Dates	Submitted by*	Sample Type(s)	Species	Earliest Inside Date	Earliest Cutting Date	Latest Outside Date	Clusters	*Comments*
2	LA 47	Puye	71	71	41	Reuter, Stallings	Char frags	PP, DR, Pnn	1329p	1526v	1577r	1540s, 1570s	*Mostly noncutting*
3	LA 170	Tsirege	59	52	30	Stallings	Char, wd frags	PP, DF, WF	1344fp	1559r	1581vv	1420s, 1510s, 1580s	*Mostly noncutting*
4	LA 8681	Fulton's 190	50	50	20	LAAS (Young)	Char frags	Pnn	1026fp		1218+vv	1190s	*All noncutting*
9		San Ildefonso	2	2	1	1st beam expedition	Wd ½ sects	PP	1661p		1787vv	None	
18	LA 295	Cochiti Church	2	2	2	Kubler/ Taylor Museum	Wd 1" cores	PP	1662np		1745vv	None	*Both noncutting*
25	LA 84/295	Kotyiti	42	41	32	Stallings	Char frags	PP, DF	1487p	1684r	1691v	1650s, 1680s, 1690s	*4 cutting*
30	LA 545	Water Canyon Ruin	28	20	14	Stallings	Char frags	PP, DF	1111fp	1302v	1447v	1300s	*5 cutting*
39	LA 257	Navawi	1	1	0	Stallings	Char frags	PP					
40	LA 708	Los Alamos School	16	16	0	Stallings	Char frags	PP, DF					*All short*
44		Bandelier Group M	5	5	1	Hendron NPS	Char frags	PP	1352fp	1494rG	1494rG comp		*Duplicates?*
45	LA 82	Tyuonyi	125	122	55	Stallings/ NPS	Char frags	PP, DF, Jun	1240np	1386r	1521r comp	1380s, 1420s, 1460s, 1520s	*13 cutting*
46	LA 217	Rainbow House	34	20	18	Worman/ NPS	Char frags	PP	1377p	1449v	1546v	1451	*8 cutting*
47	LA 78	Frijolito	13	13	12	Stallings	Char frags	PP	1315	1426r	1460	1440s	*6 cutting*

LTRR Acc#	Site #	Site Name	Number of Samples	Number of Independent Samples	Number of Dates	Submitted by*	Sample Type(s)	Species	Earliest Inside Date	Earliest Cutting Date	Latest Outside Date	Clusters	*Comments*
48	LA 169	Otowi	11	11	4	Stallings	Char frags	PP	1375fp		1491vv		*1 near cutting*
49	LA 42	Hewett's Ruin 12	7	7	5	Stallings	Char frags	PP	1796fp		1871vv	1830s	*1 cutting*
50	LA 211	Tsankawi	4	4	2	Stallings	Char frags	PP	1373fp		1439vv		*No cutting*
51	LA 3852		3	3	1	NPS	Char frags	PP, Pnn	1006		1085+vv		
	LA 60372	Burnt Mesa Pueblo	25	25	13	WSU/NPS	Char frags	PP, Pnn	1098		1317B		*2 cutting*
	LA 53148		3	3	0	NPS	Wd x-sect	PP					*Branches*
	LA 71155		1	1	0	NPS	Wd x-sect	PP					*Branches*
	LA 71090		3	3	0	NPS	Wd frag	PP, Jun					*Branches*
	LA 84067		1	1	0	NPS	Wd frag	PP					*Branches*
	LA 71081		1	1	0	NPS	Char frag	PP					*Branches*
	LA 4497	Saltbush Pueblo	4	4	3	Snow/MNM	Char frags	Pnn	1151fp		1241vv	None	*No cutting*
	LA 2987		1	1	0	NPS/MNM?	Char frag	Pnn					
	LA 2990		1	1	0	NPS/MNM?	Char frag	Pop					*Navajo midden?*
	LA 2994		1	1	0	NPS/MNM?	Char frag	Jun					
	LA 2998		1	1	0	NPS/MNM?	Char frag						
	LA 3852		1	1	0	WSU/NPS	Char frag	Jun					
	LA 50972	Cavate M 77	1	1	0	WSU/NPS	Char frag	Pnn					
52	LA 70	Pueblo	222	213	163	Lange	Char,	PP,	1184	1401r	1790vv	1420s,	*96 cutting*

LTRR Acc#	Site #	Site Name	Number of Samples	Number of Independent Samples	Number of Dates	Submitted by*	Sample Type(s)	Species	Earliest Inside Date	Earliest Cutting Date	Latest Outside Date	Clusters	*Comments*
		del Encierro					wd frags	DF, Pnn				1440s, 1460s, 1450s	
	LA 34		1	1	0	Lange	Char frag	DF					
	LA 272		6	6	0	Lange	Char frag	PP, Pop					
	LA 3446		5	5	0	Lange	Char frag	Jun, Pop					
	LA 6178		1	1	0	Lange	Char frag	Jun					
	LA 6455	Alfred Herrera Site	137	65	28	Lange	Char frags	PP, DF, Pnn	1197p	1457v	1497 r inc	1490s	*5 cutting*
	LA 6461	Red Snake Hill Site	5	5	0	Bussey	Char, wd frags						
	LA 6462	North Bank Site	258	221	98	Lange	Char, wd frags	PP, Pnn, Jun	1022p	1128r	1280rB	1280	*53 cutting*
	LA 9139		5	4	2	OCA	Char frag	PP	1534fp		1767vv		*No cutting*
56		Bandelier Big Kiva	105	37	15	Stallings/ NPS	Char frag	PP, DF	1320	1522r	1525r	1520s	
61	LA 12121	Alamo Canyon Group	17	17	14	NPS	Char x-sect	Pnn, Jun, PP	1101p	1149v	1177r	1170s	
	LA 13659	Alamo Canyon Group	2	2	0	NPS	Char x-sect	PP					*Short*
	LA 12119	Alamo Canyon Group	36	32	5	NPS	Char x-sect	Pnn, Jun, PP	1116		1419vv		*No cutting*
	LA 12578		1	1	0	NPS	Wd frag	Pnn					
	LA		1	1	0	NPS	Wd frag	Quer					*Oak,*

LTRR Acc#	Site #	Site Name	Number of Samples	Number of Independent Samples	Number of Dates	Submitted by*	Sample Type(s)	Species	Earliest Inside Date	Earliest Cutting Date	Latest Outside Date	Clusters	*Comments*
	12567												*discard*
	LA 12581		1	1	0	NPS	Char x-sect	Jun					*Short*
70		Pajarito Group				UCLA							
		Cavate East Mesa	1	1	1	UCLA	Wd x-sect	PP	1628p		1674vv		
		Site 118 Kiva-I	1	1	1	UCLA	Wd frag	PP	1792	1830r	1830r		
		Site 127 Cavate	2	2	0	UCLA	Char frag	PP					
		Site 128 Cavate	1	1	0	UCLA	Wd x-sect	Pnn					
		Site 252	12	12	1	UCLA	Wd/char frags	PP, Pnn, Jun	1797p		1844+vv		*Also fir and pop*
71		La Mesa Fire Site	3	3	2	Traylor/ NPS	Char frags	PP	1347		1412+vv		*No cutting*
74	LA 3824		7	7	0	Snow/MNM	Char frags	PP, DF					
77		Los Alamos Cabins											
	LA 86643	Gomez Hmstead	8	8	0	LANL	Wd x-sect	Jun, PP					
	LA 16808	Anchor Ranch	10	10	5	LANL	Wd x-sect	PP	1790p	1929 GB comp	1933r LGB comp	1933	
	LA 16808b	D. Romero Hmstead	10		10	LANL	Wd/char frags	PP	1787p	1908rG	1908v	1908	
	LA 70028	Vigil Y Montoya Hmstead	20	19	5	LANL	Wd x-sect	PP, Jun, Pnn	1562		1963++G		
	LA	Hmstead	3	3	1	LANL	Wd x-	PP	1783p		1899++		

LTRR Acc#	Site #	Site Name	Number of Samples	Number of Independent Samples	Number of Dates	Submitted by*	Sample Type(s)	Species	Earliest Inside Date	Earliest Cutting Date	Latest Outside Date	Clusters	*Comments*
	89826	Bridge					sect				rLGB		
	LA 89770	Hmstead Fence	9	9	6	LANL	Wd x-sect	PP	1767p		1890vv		
	LA 21334	Montoya Hmstead	8	7	5	LANL	Wd x-sect	PP, Pnn	1687p		1915++ vv		
	LA 85407	Serna Hmstead	4	4	4	LANL	Wd x-sect	PP	1685		1826vv		
79	LA 16806	Romero Cabin	95	93	79	LANL	Wd s-sect	PP, DF	1644	1894r inc	1966rLB comp	1890s, 19112, 1930s, 1960s	*Same site as above?*
83	LA 51912	Archaic site	8	8	0	MNM/Lent	Char frags	Jun, Pnn					
84	LA 3444	Kuapa	2	2	0	SAR/Haas	Char frags	PP					*Other samples discarded?*
93	LA 3840	Shohakka Pueblo	2	2	1	NPS/ Ruscavage-Barz	Char frags	PP	1387		1441vv		
	LA 118345		2	2	0	NPS/ Ruscavage-Barz	Char frags	PP					
Total			*1528*	*1290*	*700*								

***** LAAS = Los Alamos Archaeological Society; WSU = Washington State University; MNM = Museum of New Mexico; OCA = Office of Contract Archaeology; UCLA = University of California, Los Angeles; SAR = School of American Research.

LTRR NM-I-2, Puyé (LA 47)

A total of 71 samples have been collected from Puyé (Table 7.1; Appendix D), predominantly as a result of Reuter's excavations at the site in the 1930s (Smiley et al. 1953). The samples were initially analyzed by W. S. Stallings at the LAH and dating confirmed by the LTRR in the 1960s. All of the samples are charcoal or wood pieces from excavated contexts. Ponderosa pine (n = 57) dominates the collection, followed by Douglas fir (n = 10), and piñon pine (n = 3). Such dominance by ponderosa (80%) undoubtedly reflects a species preference on the part of the site occupants; selection biases on the part of the collectors, however, may contribute to the species differences, particularly the absence of juniper in the collection.

Forty samples yielded dates, a success rate of 58.6 percent. Douglas fir specimens yielded the highest ratio (9/10), followed by piñon pine (3/4), and ponderosa (29/57). Cutting dates were derived from only eight of the samples; three yielded near cutting dates, and 30 produced noncutting dates. The terminal ring attributes indicate that most tree harvesting occurred in early to mid summer. The mixture of complete and incomplete Douglas fir terminal rings indicates harvesting some time between early May and late June; the ponderosa pine growing season is somewhat later in the summer, but the combination suggests mostly early-season tree procurement (Fritts 1991), although construction may have occurred at any time during the year.

The overall date distribution (Figure 7.5) suggests a site occupation from the late 1400s through the 1570s, although the cutting dates span only 1526 to 1577. The stem-and-leaf plot notes the prefix with year date (e.g., 141 36, represents 1413, 1416). At such a large site, however, the relatively small sample of tree-ring dates probably does not represent the true duration or intensity of the occupation. Although the provenience information for the samples is minimal, if viewed in their archaeological contexts (Towner et al. 2001), the dates suggest the following. First, an initial occupation some time in the late 1400s based on noncutting dates from "the E, S, and W sides of the ruin" (RG-327-12), the "S House 5th N-S line of Rooms from W" (RG-545), the "fill of Deric's Room" (RG-546-3, 15, 22, 23 and RG-547-1, 2), and unprovenienced samples (RG-49, 328, and 625-627). Second, there is a weak cluster of unprovenienced noncutting dates in the 1520s (RG-546-4, 5, RG-653, RG-5306) supported by a 1529v cutting date (RG-48). In addition, a single 1526v cutting date (RG-551) from the "8th N-S line of rooms, 2nd from W," three noncutting dates (1521vv, 1526vv, 1528vv) from the "Fill of Deric's Room," and two noncutting dates (1525vv, 1526vv) from the "E, S, and W sides of Ruin," support the possibility of site expansion in the 1520s. Four areas (E, S, and W sides of Ruin, Fill of Deric's Room, dump, and unprovenienced) contain 1530s noncutting dates—and a 1536+r near cutting date—that indicate a possible site expansion in the 1530s. The mid-1540s are represented by five dates, including three cutting dates from the "dump" (Appendix D), which indicate some activity at the site during that decade. The 1550s and 1560s are represented by single noncutting (1554++vv) and near cutting (1562+v inc) dates, respectively. Five dates, including two cutting and one near cutting date fall in the 1570s. The different proveniences of the samples (E, S, and W sides of Ruin, Fill of Deric's Room, and Dump) suggest tree-cutting activities occurred in several areas of the site in the 1570s.

141 36
***
143 27
144 5
145 24
146 6
147 4
148 8
149 88
***
151 6
152 1156666689
153 14679
154 334678
155 4
156 2
157 22457

Figure 7.5. Stem-and-leaf plot of dates from Puyé (underline indicates cutting or near cutting date).

The small sample size relative to the size of the site, meager provenience information, and paucity of cutting dates make interpretation of the Puyé tree-ring data difficult. Nonetheless, it is probable that (a) the site occupants preferred ponderosa pine for construction, (b) they occupied the site at least as early as the late 1400s, (c) they conducted major expansion of the site between the 1520s and the 1540s, (d) there was little construction in the 1550s and 1560s, and (e) major site expansion occurred in the 1570s. If Walpi Pueblo can be used as a model of wood use at a long-lived pueblo (Ahlstrom et al. 1991), such interpretations would change dramatically with the addition of more tree-ring samples from known proveniences.

LTRR NM-I-3, Tsirege (LA 170)

The tree-ring collection from Tsirege was procured by Stallings in the early 1930s (Smiley et al. 1953). Some provenience information accompanied the samples when they were transferred to Tucson, but it is extremely limited considering the size and complexity of the site. Stallings collected a total of 59 samples from the site, including seven duplicates (Table 7.1; Appendix D); one sample for which there are notes was lost in the transfer of the collection to the LTRR. Thus, 44 independent samples are available from the site. The species distribution includes ponderosa pine (n = 24), Douglas fir (n = 18), and white fir (n = 2). Certainly, Stallings selection bias influenced the species distribution, but the relatively large number of Douglas fir and presence of white fir probably reflect at least some prehistoric selection preferences. It may be important to identify the nearest modern stand of white fir as an estimate of procurement distance.

The 44 samples produced 30 dates, but only three cutting dates (Figure 7.6). The date range is 1411+vv to 1581vv and the cutting date range is 1559r inc to 1581v inc. The overall distribution suggests that there may have been some occupation in the early 1400s (seven noncutting dates before 1427), and additional activity in the 1510s (four noncutting dates 1514 to 1516). The few cutting dates, however, suggest that the occupation was predominately during the 1570s to 1600 timeframe. Other data, such as ceramics and architecture, indicate that the site was occupied for much longer than 30 years. Clearly, sampling in only one area of the site biased the dating toward the end of the occupation.

141 126
142 1236
143 5
144 02
145 7
***
147 79
***
149 226
150 24
151 4556
***
154 0
155 9
***
157 488
158 111

Figure 7.6. Stem-and-leaf plot of dates from Tsirege (underline indicates cutting or near cutting date).

LTRR NM-I-4, Fulton's 190 (LA 8681)

Fifty charcoal samples were collected from Fulton's Site 190 during excavations in the 1950s by the Los Alamos Archaeological Society (Table 7.1; Appendix D). There are no duplicates in the collection. The species exploited include piñon (n = 42), juniper (n = 5), Douglas fir (n = 2), and ponderosa pine (n = 1). The almost total lack of ponderosas makes Fulton's 190 different than most other sites on the Pajarito Plateau, but it may be a result of collection bias. Only the piñon samples yielded dates.

The samples yielded 20 dates, but no cutting dates, and range from 1060vv to 1218+vv. The date distribution (Figure 7.7) shows weak clusters in the 1090s (n = 2), 1160s (n = 3), 1180s (n = 2), 1190s (n = 4) and 1200s (n = 2) that indicate the possibility of a 140+ year occupation. It is most likely, however, that the site was constructed and occupied in the late 1100s until some time in the 1220s. The only date cluster—three noncutting dates of 1190vv, 1191vv, and

1191vv—that supports a late 12th century occupation is from Room 5. No other single provenience contains more than two non-cutting dates within a five-year time span.

```
106     0
***
108     1
109     57
110     6
***
112     4
***
114     9
115     3
116     248
***
118     23
119     0117
120     45
121     8
```

Figure 7.7. Stem-and-leaf plot of dates from Fulton's 190 (underline indicates cutting or near cutting date).

LTRR NM-I-9, San Ildefonso

Only two samples have been collected from San Ildefonso. Both are ponderosa pine cross-sections collected by the First Beam Expedition in 1923 (Nash 1999). Only one sample provided a noncutting date (1661p-1787vv) (Smiley et al. 1953) (Appendix D). Although the sample fits with the known occupation, it is completely inadequate for assessing the occupation of this large, extensive pueblo.

LTRR NM-I-18, Cochiti Church (LA 295)

Two ponderosa pine samples were collected as cross-sections from Cochiti Church by George Kubler of the Taylor Museum in Colorado Springs (Smiley et al. 1953). Both samples dated (1697vv and 1745vv) (Appendix D), but neither yielded a cutting date, probably because they were adzed and missing outside rings. They offer little interpretive value other than that they were not used before the 18th century.

LTRR NM-I-25, Kotyiti (LA 84)

A total of 42 samples, including one duplicate, were collected by Stallings in the 1930s (Table 7.1; Appendix D). All but one of the samples is charcoal; 37 are ponderosa pine, four are

Douglas fir, and the single wood fragment is a juniper specimen. None of the samples is provenienced beyond the site level. Thirty-two of the samples (76%) dated, but only four yielded cutting or near cutting dates. The overall date range is 1547vv to 1691vv, and the cutting date range is 1684r comp to 1690rB inc. Most of the dates, including all of the cutting and near cutting dates, cluster in the 1680s and early 1690s. Obviously, the area of the site where the specimens were collected dates shortly after the Pueblo Revolt but before the Spanish Reconquest.

LTRR NM-I-30, Water Canyon Ruin (LA 545)

Twenty-eight charcoal samples were collected from the site by W.S. Stallings in the 1930s (Smiley et al. 1953). There are eight duplicates in the collection, and thus 20 independent samples (Table 7.1; Appendix D). All but two of the samples were collected from the "Northeast Side of the Court," and the other two were collected from the "Southwest Corner of the Court." The species present include 17 ponderosa pine and three Douglas fir specimens.

The 20 samples yielded 14 dates, including five cutting dates. The dates range from 1165vv to 1447v, and the cutting dates range from 1302rB to 1447v. It is possible, given the small sample size and limited provenience information, that the site was occupied for 150+ years. The current tree-ring data, however, suggest two separate occupational episodes. The first, 1302 to 1303, is denoted by four cutting and one noncutting dates; the second, in 1447, is indicated by a single cutting date and two early 15th century noncutting dates. Such a small, unrepresentative sample, however, makes any inferences somewhat tentative. The mid-1400s activities appear to have been contemporaneous with events at Frijolito.

LTRR NM-I-39, Navawi (LA 257)

A single ponderosa pine sample was collected from Navawi by W. S. Stallings in the early 1930s. The sample did not date (Table 7.1; Appendix D).

LTRR NM-I-40, Los Alamos School (LA 708)

Sixteen charcoal fragments were collected from the site by W. S. Stallings in the 1930s. All but one of the samples is ponderosa pine and the other is a Douglas fir specimen (Table 7.1; Appendix D). None of the samples dated because all contain too few rings for crossdating.

LTRR NM-I-44, Bandelier Group M

Five wood fragment samples were collected from Rooms 1, 2, and 5 of the site by Hendron of the National Park Service (NPS) during stabilization work in the 1930s (Smiley et al. 1953). All the samples are ponderosa pine and only one yielded a date (1352p to 1494rG comp) (Table 7.1;

Appendix D). The date indicates tree procurement in the fall/winter of 1494, but offers little other information about the site occupation.

LTRR NM-I-45, Tyuonyi (LA 82)

The tree-ring collection from Tyuonyi was procured by Stallings, but apparently derived from either Hewett's School of American Research excavations or Hendron's NPS stabilization work in the 1930s and 1940s (Smiley et al. 1953). All of the material was transferred to the LTRR in the 1950s, but one sample (TYU-80) was lost in the transfer.

A total of 125 samples, including only two duplicates, was collected from the site. The 122 independent samples include 97 ponderosas, 16 Douglas firs, five junipers, two *Populus*, and single specimens of piñon and oak (Table 7.1; Appendix D). The species distribution clearly reflects Stallings' collection goals of developing a Rio Grande chronology,

The samples yielded 55 dates, a 45 percent success rate; 20 of the dates are cutting or near cutting dates. The date range is 1327vv to 1521vv and the cutting date range is 1369+r inc to 1521r comp. The date distribution (Figure 7.8) suggests that the site was founded some time in the late 1300s, probably in the 1380s and occupied until the 1520s; most construction appears to have occurred in the 1420 to 1430 period, with repair or remodeling in the 1330s, 1460s, and first two decades of the 1500s.

```
132   7
***
134   0
***
136   69
***
138   356789
139   458
140   0178
141   559
142   1111222236777 7
143   19
144   22237
145   178
146   26679
***
149   46
150   9
151   7
152   11
```

Figure 7.8. Stem-and-leaf plot of dates from Tyuonyi (underline indicates cutting or near cutting date).

Samples were collected from 20 different areas, only four of which did not produce dates (Tier 4, Tier 5, Tier 6, and Trench 1). If the earliest cutting date or cutting date cluster and latest date from each provenience are taken as guides, the following sequence can be inferred. Tier 13, dated 1369+r inc, may be the earliest area sampled. Other areas with their latest (noncutting) dates in the 1300s include Tier 7 (1385vv) and Tier 11 (1386vv), but they probably date to the early 1400s. Several areas indicate construction in the second or third decades of the 15th century, including Tier 12 (1415+vv), Tier 14 (1415+B inc to 1457vv), Tier 10 (1421v to 1496vv), Tier 16 (1419+r comp to 1469vv), Tier 17 (1422+r comp), Tier 18 (1422+r comp), Tier 8 (1431v inc), and Tier 9 (1427r inc to 1451vv). Although not all the areas are supported by cutting dates, it is clear that the 1420s were a period of major site expansion. The 1440s may have also seen some site expansion, particularly in Tier 1 (1443vv), Tier 2 (1442+v), and Tier 3 (1442r comp to 1458vv). Sector C contained a 1466r comp date that indicates activities in the 1460s, contemporaneous with activities in Tier 16 (1466v, 1467r, 1469vv). There may have been some construction at the site in the 1490s, as evidence by a 1496vv date from Tier 10 and a 1494vv date from the site surface. The latest construction at the site was apparently in Tier 15 (1509v inc) and Sector B (1521r comp). It is apparent from both the date distribution and the provenience of different dated timbers that the site was occupied for more than 100 years. Additional samples from different proveniences can be expected to strengthen the existing date clusters and possibly extend evidence of the occupation further.

LTRR NM-I-46, Rainbow House (LA 217)

A total of 34 charcoal samples, including 14 duplicates, was collected from Rainbow House by Worman/NPS in the 1930s (Table 7.1; Appendix D). Nineteen of the independent samples are ponderosa pine and one is Douglas fir, undoubtedly a reflection of the collection bias of the time. One sample is unprovenienced and two were collected from Kiva 1; the remaining 17 samples were excavated from Room 1-18.

Eighteen of the samples yielded dates, including nine cutting dates. The single date from Kiva 1 (1458v) is the latest date from the site. The strong cluster of 1451 cutting dates leaves no doubt that Room 1-18 was built in that year. In addition, the mixture of complete (n = 4) and incomplete (n = 2) terminal rings on the piñon specimens indicates that the structure was built in the late summer/fall of 1451 when some trees had stopped growing and others had not. The subsequent noncutting dates of 1453vv and 1454vv probably represent repair beams procured at the same time Kiva 1 was built (1458). The small cluster of 1420s dates, including two near cutting dates (1422+v and 1427+v) probably represent beams reused from other proveniences or sites. Rainbow House, or at least Room 1-18, appears to be one of the shortest occupations on the plateau and may contribute significantly to ceramic seriation and other studies (Montgomery and Reid 1990).

LTRR NM-I-47, Frijolito (LA 78)

Thirteen ponderosa pine charcoal samples were collected from Frijolito by W. S. Stallings in the early 1930s (Table 7.1; Appendix D); no duplicates were identified in the collection. Five of the samples were collected from a room on the north side of the pueblo, but the remaining samples are unprovenienced. Twelve of the samples dated and six yielded cutting dates. The dates range from 1385vv to 1460r; the cutting dates range from 1426r to 1460r. The distribution of dates suggests some construction in 1426, 1447, 1452 to 1454, and 1460. The limited provenience information suggests that the room on the north side was built in 1447 and repaired in 1460, or built in 1460s with at least one reused timber. Interestingly, all of the dates, except those in 1447, indicate fall/winter tree harvesting. Frijolito was apparently occupied for a relatively brief time—approximately 35 to 40 years (one or two generations), and thus may be an important site for determining ceramic relationships among plateau assemblages. It also appears to be at least partially contemporaneous with the late occupation of Water Canyon Ruin (LA 545).

LTRR NM-I-48, Otowi (LA 169)

Eleven charcoal samples have been collected from Otowi. The site was excavated by L. W. W. Wilson for the Philadelphia Commercial Museum between 1915 and 1917, but the samples were apparently collected by Stallings in the early 1930s. Unfortunately, the data from Otowi are scant and insufficient to asses the internal site dynamics. Five of the samples are duplicates, leaving five independent samples. Four of the samples are ponderosa pine and one is Douglas fir (Table 7.1; Appendix D). Four of the samples yielded dates, including a cutting date of 1414r comp. Although completely inadequate to assess the occupation of such a large complex site, the cutting date of 1409r and noncutting date of 1491vv suggest almost a century of occupation. Additional samples would undoubtedly contribute significantly to understanding the site occupation and external relationships.

LTRR NM-I-49, Hewett's Ruin 12 (LA 42)

The tree-ring laboratory currently curates seven ponderosa pine charcoal samples from Hewett's Ruin 12 that were apparently collected by Stallings in the 1930s. None of the samples is provenienced beyond the site level and two did not date (Table 7.1; Appendix D). The five dated samples yielded four noncutting dates (1830vv to 1871vv) and one cutting date (1867v). Obviously, the samples do not date the prehistoric occupation and there is some suggestion that they came from the "Blumenthal modern house;" they indicate some building activity at the house in the late 19th century (Robinson et al. 1972).

LTRR NM-I-50, Tsankawi (LA 211)

Stallings collected four ponderosa pine charcoal samples from Tsankawi in the 1930s. None of the samples are provenienced beyond the site level and only two dated (Table 7.1; Appendix D).

The two noncutting dates of 1436vv and 1439vv suggest activities in the mid-15th century, but are inadequate for assessing this large pueblo.

LTRR NM-I-51

LA 3852

Three charcoal samples were collected from two structures at the site by NPS (Carlson and Kohler 1989a; Table 7.1, Appendix D). Neither the ponderosa nor the piñon pine sample from Room 6 area 1 dated. A piñon sample (BNM-84) from Pit structure Area 4 yielded a noncutting date of 1006 to 1085+vv and indicates some activity at the site after 1085.

Burnt Mesa Pueblo (LA 60372)

A total of 25 samples, 22 charcoal fragments and three wood fragments, was collected from the site (Kohler 1989; Kohler and Root 1992a, 1992b) (Table 7.1; Appendix D); no duplicates were identified. The majority of the samples are ponderosa pine (n = 16), followed by Douglas fir (n = 7), and piñon (n = 2). It is probable that this species distribution approximates the prehistoric occupants' selection preferences.

The samples yielded 13 dates, including three cutting dates. The overall date range is 1189vv to 1317B inc, and the cutting date range is 1250B inc to 1317B inc. If the dates are combined with their provenience data, the following sequence is inferred. Room 2 appears to be the earliest with a 1250 cutting date; however, other data may indicate this single date is anomalous. Room 1 was constructed some time in the mid-1270s and Room 10 is probably contemporaneous with it. The three noncutting dates from Room 4 only indicate it was occupied some time after 1207; again, archaeological and architectural data may refine the temporal placement of the room. Interestingly, Pit Structure 1, built in 1317, is the latest construction on the site. The dendroarchaeological and provenience data suggest that two separate occupations occurred at the site, one in the mid-1270s and the other approximately 40 years later.

LA 53148

Three wood cross-section samples were collected from the surface of Cavate 1 by NPS. All the samples are ponderosa pine, but none dated (Table 7.1; Appendix D).

LA 71155

A single wood cross-section sample of ponderosa pine was collected from this rockshelter site by the NPS in 1994. It did not date (Table 7.1; Appendix D).

LA 71090

Three wood fragment samples were collected from this cavate and camp site by the NPS in 1994. Two of the samples are juniper and one is ponderosa pine, but none dated (Table 7.1; Appendix D).

LA 84067

A single wood fragment sample of ponderosa pine was collected from a "bedrock pit" at the site by the NPS in 1994. It did not date (Table 7.1; Appendix D).

LA 71081

A single wood charcoal fragment of ponderosa pine was collected from this small surface structure by the NPS in 1994. It did not date (Table 7.1; Appendix D).

Saltbush Pueblo (LA 4497)

Four piñon pine charcoal samples were collected from the site by D. Snow of Museum of New Mexico (Table 7.1; Appendix D). One sample from the "trash" did not date; a sample from the "general fill" dated 1241vv, a sample from the kiva dated 1194vv, and a sample from the kiva floor dated 1215vv. The three noncutting dates indicate activity in the early to mid-thirteenth century, but are inadequate for gleaning any additional temporal information.

LA 2987

A single charcoal sample of piñon pine was collected from the general surface of this site by the NPS or Museum of New Mexico. It did not date (Table 7.1; Appendix D).

LA 2990

A single charcoal sample of *Populus* spp. (probably cottonwood) was collected from this site by the NPS or Museum of New Mexico. It did not date (Table 7.1; Appendix D).

LA 2994

A single charcoal sample of juniper was collected from this site by the NPS or Museum of New Mexico. It did not date (Table 7.1; Appendix D).

LA 2998

A single charcoal sample of *Populus* spp. (probably cottonwood) was collected at this site by the NPS or Museum of New Mexico. It did not date (Table 7.1; Appendix D).

LA 3852

A single charcoal sample of piñon pine was collected from the general surface of this site by Washington State University. It did not date (Table 7.1; Appendix D).

Cavate M 77 (LA 50972)

A single charcoal sample of piñon pine was collected from the general surface of this site by Washington State University (Carlson and Kohler 1989b). It did not date (Table 7.1; Appendix D).

LTRR NM-I-52

Pueblo del Encierro (LA 70)

Pueblo del Encierro was excavated as part of the Cochiti Dam Project by Lange (Table 7.1; Appendix D) and the samples were submitted to the LTRR in the 1960s (Snow 1976). All of the samples are charcoal fragments and all but two are associated with features. A total of 222 samples was collected, including nine duplicates. The 213 independent samples include 94 Douglas fir, 68 ponderosa pine, 39 piñon, seven juniper, three *Populus*, and two non-coniferous specimens that could not be identified to the species level. The species distribution probably reflects prehistoric selection preferences and may indicate some nonlocal procurement of Douglas fir beams. All of the dates were derived from the Douglas fir, ponderosa, and piñon beams; none of the juniper, cottonwood, or other nonconiferous specimens dated.

The 213 samples yielded 163 dates (77%), including 114 cutting dates. The overall date range is 1292vv to 1787vv and the cutting date range is 1401r inc to 1520r inc. The site was certainly not continuously occupied from the late 1200s through the end of the 1700s, but different areas of the site undoubtedly were used at different times. The date distribution (Figure 7.9) suggests that the site was founded in the early 1400s, possibly in the first decade of the century. Major construction began almost immediately in the 1410s and 1420s. Although there is a slight drop in the number of cutting dates in the 1430s, tree harvesting remained relatively constant from the 1440s through the 1480s. The late 15th and early 16th centuries show little activity, but major timber procurement again marked the 1510s until the summer of 1520. The site was probably disused shortly after 1520, and the few, scattered noncutting dates in the 1600s and 1700s may relate to some use in the late 18th century.

```
129     2
***
132     7
****
134     1568
135     07
136     4788
137     4
```

138 11888
***
140 12669
141 123456
142 011222334445566778888
143 4589
144 1113456679
145 01114558
146 2334677888999
147 469999999
148 00666
149 4
150 78
151 33344555555555555555555555555566666689
152 00000000
***
169 1
170 2
***
172 4
***
174 2
***
176 6
177 01
178 67
179 0

Figure 7.9. Stem-and-leaf plot of dates from Pueblo del Encierro (underline indicates cutting or near cutting date).

Tree-ring samples were collected from 41 features and one non-feature area. Samples from 17 of the features did not yield any dates, including Features 29, 33, 42, 62, 78, 79, 90, 93, 100, 107, 123, 140, 167, 179, 181, 229, and 280. Several features yielded single noncutting "vv" dates that may or may not be applicable to construction events. Several potentially early, but poorly dated, features are Feature 92 (1341vv), Feature 87 (1345vv), Feature 213 (1346vv), Feature 223 (1327++vv and 1350vv), Feature 29 (1364vv), and Feature 101 (1381vv); these features may indicate occupation during the 14th century, but the tree-ring evidence is equivocal. By the 15th century, several features contained cutting dates or small date clusters that indicate occupation, including Features 200 (1402+vv), 25 (1416v), 136 (1425+r) , 132 (1427r), 169 (1428vv), 130 (1441r), 292 (1446vv), and 2 (1458vv). Three other features contain disparate cutting dates that are not easily interpreted. Feature 69 contains three dates (1411r, 1423r, and 1427r) from the general fill; they may represent occupation in the 1410s and 1420s, but the earlier beams may have been reused as well. Feature 80 contains four dates (1374vv, 1428r, 1439r, and 1469r) from the general fill; it is unlikely the feature was used for 40+ years, but identifying a construction or repair episode is impossible. Finally, Feature 83 yielded five dates (1388vv,

1406+r, 1412r, 1415r, and 1494r) from the floor fill and general fill; the feature may have been used in the 1410s, but the 1494r date is from the floor fill and may date some repair activity, but it is unlikely that the feature was used for more than 80 years.

Four features contain abundant cutting dates and date clusters and illustrate complex wood use behaviors. Feature 152 yielded 19 dates (Figure 7.10), including 13 cutting dates. The most parsimonious explanation for the date distribution is that CDP-164 (1414r) and CDP-154 (1422r) are reused beams, that the feature was constructed in 1445 using one new and several stockpiled timbers, and that the feature was repaired or remodeled in the summer of 1451 using freshly cut and stockpiled beams. Other interpretations are possible, including construction in 1451 with new, stockpiled, and reused beams and construction over a multi-year period in the 1440s.

135 7
***
138 8
***
140 6
141 4
142 26
143 48
144 113456
145 00111

Figure 7.10. Stem-and-leaf plot of tree-ring dates from Feature 152 at Pueblo del Encierro (underline indicates cutting or near cutting date).

Feature 186 yielded 18 dates, including 14 cutting dates (Figure 7.11). The most parsimonious explanation for the date distribution is that CDP-190 (1455v) is a reused beam, that the feature was constructed in the summer of 1480 using freshly cut timbers and at least seven beams stockpiled from the previous year, and that it was repaired or remodeled in 1486. Alternatively, the structure may have been built in 1486 with mostly reused beams, but it seems unlikely.

134 8
***
144 9
145 5
146 3
147 469999999
148 00666

Figure 7.11. Stem-and-leaf plot of tree-ring dates from Feature 186, Pueblo del Encierro.

Feature 128 yielded the abundant dates (n = 31) and many cutting dates (n = 27), yet is the most complex dating situation at the site. The date distribution (Figure 7.12) suggests at least two major construction episodes with several minor repairs as well. The feature may have been constructed as early as 1401, but initial construction in 1424 with reused (1401, 1409, 1413)

beams, stockpiled timbers (1420, 1421, 1422, 1423), and freshly cut trees (1424) is considered most likely. Repairs were apparently performed in 1428 and again in 1435. A major rebuilding episode occurred in the 1460s, probably in the fall of 1469; freshly cut, stockpiled, and reused beams from other proveniences were apparently used in the remodeling. Additional repairs were then performed in 1513 and some time in the 1520s. Feature 128 is one of the longest-lived individual structures on the Pajarito Plateau with an occupation of quite possibly more than 100 years. Alternative interpretations of the tree-ring data are possible, such as an extended construction time in the 1460s with mostly reused beams, construction earlier than 1424, or even construction in 1513, although the latter is considered extremely unlikely.

136 8
***
140 19
141 3
142 012344488
143 5
144 7
145 45
146 23467788899
***
150 8
151 3
152 0

Figure 7.12. Stem-and-leaf plot of tree-ring dates from Feature 128, Pueblo del Encierro (underline indicates cutting or near cutting date).

Feature 279 was one of the latest construction episodes during the prehistoric occupation of the site. It also yielded the most dates and most cutting dates of any feature on the site (see Table 7.1). Unlike Feature 128, however, the interpretations of Feature 279 are relatively straight-forward. The 1507r cutting date is probably a reused beam. The large number of timbers that date to the summer of 1515 (n = 27) were probably procured and stockpiled for construction in 1516 when and additional six trees were cut. The feature apparently needed minor repairs in the summer of 1518, as evidence by CDP-214. Again, an alternative interpretation of the dates is possible, including a multi-year construction period.

Two other features also date to the early 1500s. Feature 124 contained a single roof beam dated 1515rB inc, and Feature 183 contained a single near cutting date of 1518+r. Both of these features appear to be contemporaneous with Features 128 and 279.

Finally, eight samples from Feature 129 and two samples from the doorway between Features 129/123 date to the late 1780s or 1790s. These are the latest dates from the site and none are cutting dates. Certainly they indicate post-abandonment activities at the site, but their significance remains problematic.

LA 34

A single Douglas fir charcoal fragment was collected from FE 13 of the site by Lange. It did not date (Table 7.1; Appendix D).

LA 272

Six charcoal samples were collected from Feature 1 (CDP-2) and Feature 2 (CDP-3-7) by Lange. Four of the samples are *Populus* spp. (probably cottonwood) and two are ponderosa pine. None of the samples dated (Table 7.1; Appendix D).

LA 3446

Five charcoal samples were collected from Squares 7, 8, 9, 10 or 11, and 13 by Lange. Four of the samples are juniper and one is a ponderosa pine (Table 7.1; Appendix D), but none dated.

LA 6178

A single juniper wood fragment was collected from Feature 21 by Lange. It did not date because it contained too few rings for crossdating (Table 7.1; Appendix D).

Alfred Herrera Site (LA 6455)

The Alfred Herrera Site samples were collected as part of the Cochiti Dam project by Lange (Table 7.1; Appendix D). All of the samples are charcoal collected during the excavations, but some lack detailed provenience information. A total of 137 samples, including 72 duplicates, was collected. The species present include ponderosa (n = 27), piñon (n = 21), Douglas fir (n = 12), juniper (n = 2), *Populus* (n = 2), and one unidentified specimen. The species distribution may reflect prehistoric selection preferences.

The 65 independent samples yielded 28 dates, including five cutting dates (Figure 7.13). The date range is 1281vv to 1497r inc, but the cutting date range is much shorter (1457v to 1497r inc). Thirteen features were sampled, but none of the samples from Features 1, 14, 23, 28, 33, and 59 yielded dates. Likewise, none of the samples from Feature 68 dated, but one is a duplicate of RG-4734, which dates to 1469rB inc. Feature 10 yielded a single noncutting date of 1318vv as did Feature 17, but it is not the same sample. The only date from Feature 24 is 1342vv. The majority of samples and dates were derived from Feature 52, including from rooffall, floor contact, general fill, and floor fill contexts. The latest date, and only cutting date from the floor fill context, is 1457v; there are no dates from the floor contact, but several samples are part of RG-4734, which dates to 1469rB inc. Feature 52 rooffall includes cutting dates in 1469, 1470, 1496, and 1497; it is probable that the roof was constructed in 1469 to 1470 and repaired almost 30 years later. The latest date from Feature 54 is 1478vv and the latest date from Feature 251 is 1382vv.

In general, the dates and proveniences suggest that the entire site was built in the 1470s, possibly as early as 1457, and remodeled or repaired in the late 1490s; the occupation was probably

continuous during that time. The weak cluster of noncutting dates in the 1340s, however, suggests that there may have been an earlier occupation. If the cutting dates are used as a guide, the site occupation was approximately 40 years in duration.

```
128    1
***
130    2
131    488
132    0
***
134    24689
135    7
***
137    02
138    0124
***
140    4
141    0
***
143    9
***
145    77
146    9
147    08
***
149    67
```

Figure 7.13. Stem-and-leaf plot of dates from the Alfred Herrera Site (underline indicates cutting date).

Red Snake Hill Site (LA 6461)

Five charcoals samples, all juniper, were collected from the general fill of Feature 3 at the site by Bussey (1968a; Table 7.1, Appendix D). None of the samples dated and all exhibited erratic ring-growth patterns.

North Bank Site (LA 6462)

The North Bank Site collection was procured as part of the Cochiti Dam Project (Bussey 1968b; Lange 1968a) and contains 258 samples, 37 of which were duplicates (Table 7.1; Appendix D). All of the samples are charcoal fragments and all have at least some provenience information. The species present in the collection include piñon (n = 92), ponderosa (n = 56), juniper (n = 42), *Populus* (cottonwood) (n = 24), Douglas fir (n = 4), two unidentified specimens, and one *Atriplex* spp. (possible saltbush) specimen. The species distribution probably reflects prehistoric selection preferences and local species availability. The paucity of Douglas fir and abundance of both juniper and cottonwood are a result of procurement of low-elevation, local timbers.

The 221 independent samples yielded 98 dates (44%), including 63 cutting or near cutting dates. No dates were derived from Douglas fir, cottonwood, unidentified, or *Atriplex* specimens, and only one juniper sample dated. The low proportion of juniper dates may be related to species growth patterns that create erratic ring series and/or prehistoric selection of small timbers with too few rings for dating.

The overall date range is 1109vv to 1280vv and the cutting date range is 1128r comp to 1280rB inc, approximately a 150-year occupation. The date distribution (Figure 7.14) suggests several episodes of tree harvesting, and probably construction, at the site. The site may have been founded in the late 1120s or 1130 (three cutting dates). There are a few cutting dates in the 1140 to 1174 period that may indicate construction, or they may be reused beams. The first decade of the 13th century saw some construction as evidenced by three 1206 cutting dates and two noncutting dates in 1209. The next significant date cluster occurs in the 1240s and includes cutting dates in 1244, 1246 (n = 2), and 1247. The few cutting dates between 1248 and 1277 may indicate construction, but they are probably reused beams. The largest and tightest date cluster contains 47 cutting dates and two noncutting dates between 1277 and 1280; it clearly indicates construction in 1280 with freshly cut and stockpiled beams. The mixture of complete and incomplete terminal rings in 1280 indicates fall procurement. This large terminal date cluster is not followed by any other dates and thus may indicate abandonment of those areas of the site within a decade of 1280 and almost certainly by 1300.

Tree-ring samples were collected from 24 features at the site and 15 features yielded dates. Samples from Features 21, 27, 30, 33, 41, 43, 87, 88, and 109 did not date. Features 37 and 38 are the earliest features, dating to 1130v and 1128r, respectively; Feature 37 also exhibits some activity in 1146. Six samples from Feature 103 dated, including cutting dates in 1140, 1148, and 1174. Feature 85 produced two dates, the latest date and only cutting date is 1165v. These features, 37, 38, 85, and 103 are the only features that indicate a 12th century occupation, although Feature 84 and Feature 12 yielded noncutting dates of 1118vv and 1191vv, respectively.

The remaining features all date to the 13th century. Feature 106 is relatively well dated with three 1206 cutting dates; the terminal rings (two complete, one incomplete) indicate construction in the fall of 1206. Feature 108 is not well dated, but the latest date is 1223+vv from the general fill. Feature 1 yielded only two noncutting dates, the latest of which is 1239vv. It may be associated with Feature 34, which yielded a single cutting date of 1244rB inc, Feature 10 which yielded a single cutting date of 1246r comp, and Feature 20 which yielded three noncutting dates, the latest of which is 1248vv; the 1246 to 1247 cutting dates from Feature 37 may be part of this same building episode. Feature 99 was apparently built in the 1260s, as evidenced by two cutting and one noncutting date. Feature 65 may be contemporaneous, it contains a single noncutting date of 1275vv, or it may relate to the large construction event in Feature 45. Feature 45 is the best-dated feature with 46 cutting and five noncutting dates. The largest cluster is in 1280 with smaller cutting date clusters in 1277 and 1278. The feature was clearly built in 1280 with freshly cut and stockpiled timbers; the terminal rings indicate it was built in the late summer/early fall of 1280.

110 9
111 788
112 4889
113 000
114 08
115 22
116 358
117 4
118 2
119 1
120 66699
121 5
122 239
123 29
124 1446678
125 5
126 12479
127 25567788888899
128 00000000000000000000000000000000000000

Figure 7.14. Stem-and-leaf plot of dates from the North Bank Site (underline indicates cutting date).

LA 9139

Five charcoal samples, including one duplicate, were collected from Feature 1 of the site by the Office of Contract Archaeology (Table 7.1; Appendix D). Four of the samples are ponderosa and one is piñon. Two of the samples dated, but yielded only noncutting dates of 1675vv and 1767vv, respectively. The duplicate sample from the rooffall of the feature replicates the 1675vv date. The dates suggest some use of the feature in the late 1700s.

LTRR NM-I-56, Bandelier Big Kiva

The Bandelier Big Kiva samples were collected as part of Hewett's excavations and the stabilization of the site by Hendron of the NPS in the 1930s. Initially analyzed by Stallings as part of the Rio Grande chronology, they were transferred to the LTRR in the 1950s. All of the samples are charcoal from the excavations, but some (presumably Hewett's) lack detailed provenience information. A total of 105 samples was submitted, 68 of which are duplicates (Table 7.1; Appendix D). Interestingly, some of the duplicate samples, such as RG-5156 and RG-223, were collected from different proveniences (the west entrance and south fill, respectively); a detailed map of the excavations may indicate the significance (if any) of the duplicates (e.g., multiple uses of the same timber). The species used in the kiva include ponderosa pine (22 independent samples that yielded 8 dates), Douglas fir (14 samples that

yielded 7 dates), and one unidentified specimen (that did not date). Other species were probably present, but were not collected.

The 37 independent samples yielded 15 dates, including six cutting or near cutting dates (Table 7.1; Appendix D). The dates range from 1383vv to 1525+vv; the cutting and near cutting dates are slightly more restricted and span 1505+r to 1525r. Eleven of the dates, and all but one of the cutting or near cutting dates, were procured from the "south fill" of the kiva. The Frijoles Canyon (Hewett?) and "Project 1 West Entrance" samples all yielded "vv" dates that do not date construction episodes. The 1505+r date (RG-5165) from the "West Entrance" may indicate construction, but it may also be a reused beam or piece of dead wood. The dates from the "south fill of the kiva" form a relatively tight cluster in the early 1520s. Based on the terminal cluster, it is most likely that the kiva was built in the fall/winter of 1525, with some freshly cut beams (RG-5191) and timbers that had been stockpiled in 1522 (RG-5178), 1523 (RG-5173, 5206), and 1524 (RG-5193). Another possibility, however, is that the structure was built during three to four consecutive winters, much like Kiva I at Long House in Mesa Verde (Street 2001).

LTRR NM-I-61

Alamo Canyon Group

LA 12121

Seventeen piñon pine samples have been collected from the three different rooms on the site, including charcoal samples and wood cross-sections. Fourteen of the samples yielded dates, including seven cutting dates (Table 7.1; Appendix D). Clearly, Room 4 was built during the growing season of 1177 as indicated by five cutting dates with incomplete terminal rings for that year. The 1162r cutting date probably represents a reused beam and the 1180 noncutting date from the fill indicates that the room was occupied for at least three years. Room 3 was probably constructed in 1150 as indicated by the 1150+v cutting date and three 1149 noncutting dates; the 1154 noncutting date suggests the room was used for a least four years. The only date from Room 2, 1148vv, suggests it may be contemporary with Room 3. It is probable that the site was continuously occupied from 1150 until at least 1180, but it is also possible that there are two separate occupations represented in these rooms. The apparently short-lived nature of the occupation (30+ years) may be important for ceramic seriation and other studies.

LA 13659

Two ponderosa pine charcoal fragments were collected from this cavate site by NPS. Neither sample yielded a date (Table 7.1; Appendix D).

LA 12119

A total of 36 charcoal samples were collected from the site by NPS; four of the samples are duplicates, leaving 32 independent samples from the site (Table 7.1; Appendix D). The species represented include piñon pine (n = 18), juniper (n = 11), ponderosa pine (n = 2), and Douglas fir

(*n* = 1). The preponderance of piñon pine and paucity of ponderosa is somewhat unusual. Only five of the samples dated (three piñons, one juniper, and one ponderosa), and all yielded noncutting dates. The range of dates (1191+vv to 1419vv), lack of cutting dates or date clustering, and different proveniences documented makes interpretation difficult. It is probable, but rather speculative, that both Kiva 1 and Kiva 2 were occupied in the 15th century or later. Room 14 may date somewhat earlier, but the single noncutting date of 1203vv is scant evidence for such an inference.

LA 12578

A single piñon pine wood fragment was collected from the surface of this site by NPS. It did not date (Table 7.1; Appendix D).

LA 12567

A single oak (probably Gambel oak) charcoal fragment was collected from this site by NPS. It did not date (Table 7.1; Appendix D) and has not been curated for future analysis.

LA 12581

A single juniper charcoal fragment was collected from Room 1 of this site by NPS. It did not date (Table 7.1; Appendix D).

LTRR NM-I-70

Pajarito Group

This group of samples consists of those submitted by J. Hill of the University of California, Los Angeles (UCLA) in the 1970s. Limited provenience information is available for the samples and the interpretations are relatively weak.

Cavate East Mesa

A single cross-section of ponderosa pine was collected from this cavate site by UCLA. It yielded a date of 1628p to 1674vv (Table 7.1; Appendix D). Although this is limited chronological information, it indicates use of the structure in the 17th or 18th centuries.

Site 118 Kiva 1

A single ponderosa wood fragment was collected from this cavate site by UCLA. It yielded a cutting date of 1792 to 1830r (Table 7.1; Appendix D). Without detailed provenience information or additional knowledge of the site configuration, interpretation of the date is not possible.

Cavate Site 127

Two ponderosa charcoal fragments were collected from this cavate site by UCLA. Neither sample yielded a date (Table 7.1; Appendix D).

Cavate Site 128

A single cross-section of piñon pine was collected from this cavate site by UCLA. It did not date (Table 7.1; Appendix D).

Site 252

Twelve samples, including three charcoal fragments, four wood fragments, and five wood cross-sections were collected from the site by UCLA. The species represented include five juniper, three *Populus* spp., two fir, and two ponderosa pines (Table 7.1; Appendix D). Only one of the ponderosa samples yielded a noncutting date (1797p to 1844++vv).

LTRR NM-I-71, La Mesa Fire Site

Three ponderosa charcoal fragments were collected from this site by the NPS. Two samples, both "north of Room 1," yielded noncutting dates of 1401+vv and 1412+vv, respectively (Table 7.1; Appendix D). This small sample size suggests some use of the site in the early 15th century.

LTRR NM-I-74, LA 3824

Seven charcoal samples, including four Douglas fir and three ponderosa specimens, were collected from this site by David Snow of the Museum of New Mexico. None of the samples yielded a date (Table 7.1; Appendix D).

LTRR NM-I-77

Los Alamos Cabins

The Los Alamos Cabins samples were collected by LANL archaeologists in 1981, 1990, and 2002. There was apparently some confusion of site names and numbers for the Romero Homestead and two separate LTRR designations were assigned to the site (NM-I-77 and NM-I-79). The entire site is discussed here under the designation NM-I-79.

Gomez Homestead (LA 86643)

Eight juniper samples were collected from the site by LANL archaeologists (Table 7.1; Appendix D). Seven samples are cross-sections and one is a beam end that exhibits metal-ax cut

marks. The samples were apparently collected from the same structure, with the exception of LAC-31, which was a fence post. None of the samples dated.

Anchor Ranch (LA 16808)

Ten independent samples were collected from the site by LANL archaeologists (Table 7.1; Appendix D). All of the samples are ponderosa wood cross-sections. Five samples dated and four are cutting dates. The Ice House was undoubtedly built in the fall/winter of 1933 as indicated by three 1933 cutting dates with complete terminal rings. Sample LAC-57, which dates 1896++LGB, is probably a piece of dead wood; sample LAC-53, which dates 1896++LGB, is a duplicate of LAC-34 from the Homestead Bridge and may have been reused in that structure as a piece of dead wood. The only date from Structure 1, 1929GB comp, indicates tree felling in the fall/winter of 1929. Additional archaeological and tree-ring data are necessary to determine if it represents the building of Structure 1, however.

Vigil y Montoya Homestead (LA 70028)

A total of 20 samples, including one duplicate, was collected as wood cross-sections or beam ends from the site by LANL archaeologists (Table 7.1; Appendix D). The 19 independent samples include 16 ponderosas, one juniper, one piñon, and one Douglas fir specimen. Only five of the samples (four ponderosas and one piñon) yielded dates, all of which are noncutting dates. The latest date from the site, 1963++G, may indicate activity at the site in the 1960s, but its provenience "near the loaf pan" and "++" designation suggest it is a piece of dead wood that may not date the occupation. The 1911++G date from Feature 4 may indicate construction in the 1910s, but again a single, noncutting (possibly dead wood) date is not strong evidence for inferring an occupation of the site. Likewise, the earlier noncutting dates (1720vv, 1830vv, 1855+vv) contribute little to the site interpretation. More samples are needed to delineate the parameters of the Vigil y Montoya site history.

Homestead Bridge (LA 89826)

Three ponderosa wood cross-sections from the Homestead Bridge were collected by LANL archaeologists (Table 7.1; Appendix D). Two of the samples did not date because they contained too few rings (LAC-32) or exhibited erratic growth patterns (LAC-33). Sample LAC-34 yielded a near cutting date of 1783p to 1899+rLGB. Interestingly, the sample is a duplicate of LAC-53, a door lintel in the Ice House at Anchor Ranch (see above). Because the Ice House dates to 1933, there are two alternative interpretations of the bridge. First, it may have been built in 1899 (or 1900) and part of it used to build the Ice House 30 years later. Alternatively, the date may not apply to the bridge, but to some other structure; in which case the bridge and Ice House may have been built in 1933 with a piece of reused or dead wood.

Homestead Fence (LA 89770)

Nine ponderosa samples were collected from the boundary fence by LANL archaeologists. Eight of the samples are beam ends and one is a cross-section. Three samples did not date because they contained too few rings or lacked ring-width variability (Table 7.1; Appendix D). The six

dated samples all yielded noncutting dates because exterior rings have eroded from the samples. The noncutting dates do not form any sort of terminal cluster, so the most parsimonious explanation is that the fence was constructed some time after 1890.

Montoya Homestead (LA 21334)

A total of eight samples, including one duplicate, was collected from the site by LANL archaeologists (Table 7.1; Appendix D). Six of the independent samples are ponderosas and one is piñon; all were collected as wood cross-sections or beam ends. Five samples dated, but none yielded cutting dates. The latest sample (LAC-38) dates 1915++vv and may date the occupation to the 1910s or later. The samples collected from the Canyon Fence provide little data with which to interpret construction other than that the homestead was built some time after 1915.

Serna Homestead (LA 85407)

Four samples, all ponderosa pine, were collected from the site by LANL archaeologists (Table 7.1; Appendix D). Three of the samples are beam ends (one charred) and the other is a wood cross-section. Two samples were collected from the wood pile, one from a structure, and one from a fence. All samples dated, but all yielded noncutting dates that resulted from erosion of exterior rings; indeed, no sapwood rings are present on any of the samples. The noncutting dates indicate construction at the site some time after 1826 and the lack of sapwood rings suggests that the trees were cut some time in the late 1800s or early 1900s.

LTRR NM-I-79, Romero Cabin and Homestead (LA 16806 and 16808B)

The Romero Homestead is the best-dated site on the Pajarito Plateau. A total of 105 samples, including two duplicates, was collected from the site by LANL archaeologists over the past 20 years (Table 7.1; Appendix D). The majority of the samples are wood cross-sections, although a few half-inch cores and charcoal fragments were collected as well. Ninety-nine of the samples are ponderosa pine, three are Douglas fir, and one (a fence post) is juniper. The species distribution clearly reflects (a) preferences by the site occupants and (b) local species availability.

A remarkable 96 percent (n = 94) of the samples dated and 65 samples yielded cutting dates. The overall date range is 1853vv to 1966rB comp and the cutting date range is 1894r inc to 1966rB comp. The date ranges, however, are much less important than the combination of dates and provenience data. Five different proveniences have been sampled: Feature 4, a fence post east of the corral, the corral, the hog pen, and the cabin. The only sample from Feature 4 yielded a noncutting date of 1906vv and the fence post east of the corral yielded a noncutting date of 1894vv. Neither date accurately dates activities at the site.

There are eight dated samples from the corral (Figure 7.15). Although only two are cutting dates, the strong terminal cluster indicates that the structure was built in 1908. Incomplete terminal rings on the two 1908 cutting dates indicate that the corral was built during the ponderosa pine growing season (summer) of 1908.

185 3
***
188 34
189 88
190 6688888

Figure 7.15. Stem-and-leaf plot of dates from the corral at the Romero Homestead (underline indicates cutting or near cutting date).

There are 31 samples from the hog pen, 27 of which dated. The total includes 23 cutting dates (Figure 7.16). The large cluster of cutting dates in 1912 (n = 18) leaves little doubt that the hog pen was built in that year. The mixture of complete (n = 3) and incomplete (n = 15) terminal rings indicates that the structure was built in the late summer/early fall of 1912 when some trees had ceased growth for the year but others had not. The earlier cutting dates in 1894, 1895, 1906, 1908, and 1910 indicate tree harvesting in the area before construction of the hog pen, but do not date the structure itself. The two later noncutting dates (1922++vv, 1933vv) are evidence of structure repair, probably in conjunction with the construction of the cabin (see below).

189 458
190 678
191 00222222222222222222
192 2
193 1

Figure 7.16. Stem-and-leaf plot of dates from the hog pen at the Romero Homestead (underline indicates cutting or near cutting date).

Sixty-one samples have been collected from the cabin, 56 of which dated; fifty-one of the samples yielded cutting or near cutting dates (Figure 7.17). The dates indicate a major construction episode followed by four repair or remodeling events. The single 1913G cutting date is undoubtedly a beam reused from another structure. The cabin was built early in the ponderosa growing season (spring) of 1934. The two 1933 cutting dates exhibit complete terminal rings indicating that they were cut after the 1933 growing season but before the initiation of growth in 1934. All of the 1934 dates, however, exhibit incomplete terminal rings, indicating growing season procurement. The 1935 to 1938 cutting dates (n = 4) suggest a repair episode probably in the summer of 1938; additional provenience and attribute information is necessary to determine if there was one or more repair episodes. The cabin was apparently abandoned for a period of more than 20 years before a reoccupation occurred in the 1960s. Minor repairs were conducted in 1960 to 1961; because all the 1960 and 1961 dates are near cutting "+" dates, it is possible, indeed probable, that these beams were procured during the growing season of 1961. The nine 1966 cutting dates all exhibit complete terminal rings and indicate a major remodeling episode in the fall/winter of 1966.

Interestingly, the three well-dated structures at the Romero Homestead date to different years. Although there are several cutting dates that indicate tree felling in the 1890s and early 1900s,

construction occurred only in 1908, 1912, and 1934—and the cabin was the last structure built. Where people were living before construction of the cabin should be investigated using archaeological and documentary sources. Repairs to the cabin in 1938 suggest the occupation lasted more than five years, but the precise duration cannot be determined from the tree-ring data. The 1960s repair and remodeling episodes indicate reuse of the cabin, but not necessarily reuse of the site as an economic entity. Additional tree-ring data from other features may contribute to understanding the internal site dynamics of the Romero Homestead, but more detailed archaeological and historical data are needed as well.

189 2
190 88
191 3
192 6
193 2334444444444444444444444444445778
***
196 00011666666666

Figure 7.17. Stem-and-leaf plot of dates from the cabin at the Romero Homestead (underline indicates cutting or near cutting date).

LTRR NM-I-83, Archaic Site (LA 51912)

Eight charcoal samples, six juniper and two piñon, were collected from the site by Steve Lent of MNM in 1988. Features 1, 12, 14, and 18 were sampled, but none of the specimens dated.

LTRR NM-I-84, Kuapa (LA 3444)

Two ponderosa pine charcoal samples were collected from the site by Haas. Neither sample yielded a date (Table 7.1; Appendix D).

LTRR NM-I-93

Shohakka Pueblo (LA 3840)

Two ponderosa charcoal samples were collected from Feature 3, Area 1 of the site by Ruscavage-Barz of NPS. One sample yielded a noncutting date of 1387 to 1441vv and the other sample did not date (Table 7.1; Appendix D).

LA 118345

Two ponderosa pine charcoal samples were collected from FE 1 Area 1 of the site by Ruscavage-Barz of NPS. Neither sample yielded a date (Table 7.1; Appendix D).

A SUMMARY OF DENDROARCHAEOLOGICAL DATA FROM THE PAJARITO PLATEAU

Tree-ring samples have been collected from archaeological sites on the Pajarito Plateau for almost 80 years and the results are presented below. Before they are discussed, however, a couple of caveats must be offered along with the interpretations. As mentioned above, the two most important factors in any dendroarchaeological date distribution are (a) the behaviors of past site occupants and (b) the behaviors of archaeologists and dendrochronologists (Dean 1996a, 1996b; Towner 2000). It is clear that the latter has had a profound impact on the structure of the Pajarito Plateau dendroarchaeological database.

Certainly the site occupants' choices of different tree species for construction and fuel have helped structure the distribution. We need only examine the species differences between the Romero Homestead, where ponderosa pine was used almost exclusively and the North Bank Site, where there is a mixture of piñon, juniper, ponderosa, Douglas fir, and even cottonwood, to see that the site occupants influenced the date distribution. It is abundantly clear, however, that, particularly for the large prehistoric pueblos that were sampled before the Cochiti Dam Project, the species-specific collection strategies and minimal recording efforts of the archaeologists and dendrochronologists have structured the data far more than the site occupants' behaviors. Therefore, the summaries presented below should be viewed as preliminary and subject to testing with archaeological, documentary, and other data.

A total of 1528 samples have been collected from Pajarito Plateau archaeological sites, including 238 duplicates (Table 7.1; Appendix D). The 1290 independent samples include 678 ponderosa, 253 piñon, 197 Douglas fir, 108 juniper, 40 cottonwood, and many fewer oak (n = 2), fir (n = 2), white fir (n = 2), undifferentiated non-coniferous species (n = 2), unidentified species (n = 5), and a single *Atriplex* spp. specimen. Only the Douglas fir, piñon, ponderosa, juniper, and white fir yielded dates. The Douglas fir had the highest ratio of dates/samples (68.9%), followed by the piñon (65.4%), ponderosa (59.7%), white fir (50%, but n = 2), and juniper (1.8%). Most of the lack of dating in the pines and Douglas fir is probably a result of samples with too few rings for crossdating. The extremely low proportion of juniper dates, however, is probably a result of small samples with too few rings and erratic growth patterns. As discussed below, however, a more carefully designed research and sampling strategy should enable us to delineate the juniper growth patterns and date many more samples. In many other areas of the Southwest, juniper dates well and in some cases the proportion of juniper dates exceeds that of ponderosa (cf. Towner 1997).

Figure 7.18 presents all the dates, cutting and noncutting, derived from Pajarito Plateau archaeological samples. The distribution of cutting and near cutting dates (see below) certainly can be used to infer tree-harvesting activities. The overall date distribution, however, provides additional information concerning the use of the area.

106 0
***
108 155

109 57
110 69
111 788
112 44889
113 000
114 0889999
115 022234
116 22345588
117 477777
118 02239
119 01111347
120 3445666799
121 558
122 2239
123 29
124 11446678
125 05
126 1245677789
127 012255556778888888999
128 00000000000000000000000000000011
129 12
130 1222233
131 46788
132 077
***
134 24566889
135 077
136 467889
137 024
138 01112334556788889
139 4568
140 01112466788999
141 00112222334455566999
142 011111112222222223333444556666667777777788889
143 11124555677899999
144 01111122223345566677777799
145 011111111112234444557777888
146 022334666677788899999
147 004467899999999
148 006668
149 12244446667888
150 244578 9
151 333444555555555555555555555555556666666788889
152 00000000111112334555666668 9
153 14679
154 03346778

```
155   49
156   2
157   22445788
158   111
159   9
160   5
161   6
***
164   2
165   12479
166   16
167   45
168   000123334455558 89
169   01117
170   2
***
172   04
173   7
174   256
***
176    67
177    017
178    677
179     012
***
181     59
182      26
183   0012347
184   048
185   35
186   7
187   1
188   34
189   04568889
190   66678888
191   00122222222222222235
192   29
193   133344444444444444444444444445778
***
196   0001136666666666
```

Figure 7.18. Stem-and-leaf plot of all Pajarito Plateau tree-ring dates (underline indicates cutting or near cutting date).

Although there are a few dates in the AD 1000s, the first dendroarchaeological evidence of pueblo construction is in the early to mid-1100s. A small "bulge" in the distribution between

approximately 1130 and 1210 supports this inference. A large peak in the 1260 to 1280 period indicates significant construction in the area; whether this peak is related to the immigration of people into the area (cf. Ahlstrom et al. 1995), or is an artifact of sampling bias, is an archaeological question.

The low number of dates in the 1281 to 1380 period (n = 37, or one date every three years) indicates little tree harvesting activity. The tree-ring data certainly do not support the concept of a large immigration of people onto the Pajarito Plateau immediately following the depopulation of the Four Corners area (cf. Ahlstrom et al. 1995).

The tree-ring data indicate that the major occupation of pueblos on the Pajarito Plateau began in the late 1300s and continued at least until the 1540s. The majority of dates fall between the late 1300s and early 1540s and suggest major construction and expansion of pueblos. The slight drop in the number of dates between ca. 1480 and 1510 may indicate a slowing of site expansion, but is not an indication of depopulation or abandonment of the area.

With the exception of a small peak in the 1570s, the period from 1545 to 1680 shows very few tree harvesting episodes. The paucity of dates in the early part of the period, perhaps 1545 to 1610, may be a result of epidemic disease inhibiting new construction (Dobyns 1983; Ramenofsky 1987; Reff 1991); the low level of activity during the latter era—speculatively 1610 to 1680—may be a result of the Spaniards' demands for tribute and labor from the pueblos (Kessell 1979; Scholes 1937).

The sharp peak in the 1680 to 1690 period is probably related to the Pueblo Revolt of 1680 and Spaniards' reconquest the following decade. The low number of dates in the 1700s and early 1800s indicates a cessation of construction and probable depopulation of many sites in the area.

The next peak in the dendroarchaeological data relates to the Hispanic expansion onto the Pajarito Plateau in the 1890s. Interestingly, after significant activities ca. 1890 to 1913, there is apparently a 20-year gap in the data until the early 1930s. Similarly, more than 20 years passed before additional dates indicate activities in the early to mid-1960s. The tree-ring data for the Hispanic occupation indicate that individual families, not larger corporate groups, exploited the area during the 20th century.

The distribution of cutting dates from the Pajarito Plateau (Figure 7.19) shows similar, but more restricted, trends. The earliest cutting date is 1128 and the tree-ring data cannot be used to infer an earlier occupation of the area. Minor levels of tree cutting in the early to mid-1100s suggest that the area was initially settled at that time. There is no substantial increase until the 1170s. The 1170s tree-cutting episodes were followed by almost 30 years of no activity; likewise, the three trees cut in 1206 were followed by an almost 40-year gap in the distribution. Thus, with the possible exception of the 1170s and 1206, the dendroarchaeological evidence suggests small, discontinuous use of the Pajarito Plateau from the early 1100s until the 1270s. The distribution shows a major expansion of tree felling activities in the late 1270s and 1280, but it should be remembered that those cutting dates were derived from a single feature at the North Bank Site. After 1280, there are only eight cutting dates until the turn of the 15th century. This extremely

low number of tree-harvesting events—an average of one every 15 years—indicates that there was not a major influx of people onto the Pajarito Plateau during the 1300s.

112 8
113 00
114 08
115 0
116 25
117 477777
***
120 666
***
124 46667
125 0
126 16
127 2778888889
128 00000000000000000000000000000000
***
130 2233
131 67
***
136 9
***
138 6
***
140 169
141 123445569
142 0111222222664445578
143 159
144 1112234577779
145 01111111112445578
146 02346667778889999
147 069999999
148 00666
149 44678
150 579
151 3555555555555555555555555555666668889
152 000000012334569
153 16
154 334
155 9
156 2
157 4457
158 1
***
168 49

```
169    01
183    0
***
186    7
***
189    459
190    6888
191    02222222222222222223
192    9
193    333444444444444444444444444445778
***
196    00011666666666
```

Figure 7.19. Stem-and-leaf plot of all Pajarito Plateau cutting and near cutting dates.

The major prehistoric occupation of the area was clearly during the 1400s and early 1500s. Beginning in the first decade of the 15th century, tree cutting reached substantial levels in every decade of the century, except the 1430s. The lower level of activity in the 1430s may be a result of sampling bias, a pause in site founding or growth, or some other factor; it is an archaeological issue that deserves further scrutiny. The end of the 1400s witnessed a slow decline in tree harvesting that may be related to out-migration, a lack of site expansion, or both. The large "bulge" in the distribution in the 1510s and 1520s indicate significant tree harvesting in the early 16th century. This bulge, unlike the 1280s one, includes a number of large sites, including Puyé, Tsirege, Tyuonyi, Pueblo del Encierro, and the Bandelier Big Kiva.

The low number of dates from 1530 to 1870 (n = 18, or 1 every 14 years), indicates limited occupation and/or use of the area. There may have been a minor resurgence in the 1570s and reuse of the area in the 1680s in response to the Pueblo Revolt, but in general the area appears to have been little used until the Hispanic occupation of the 20th century.

The Hispanic occupation was fundamentally different, however. These single-family groups selected different tree species, mostly ponderosa pine, and constructed different types of structures to accomplish different economic goals (e.g., the hog pen). The 20-year gap between the different structures at the Romero Homestead (and some of the other sites) should be investigated with documentary and oral history sources. Perhaps the most interesting aspect of the Hispanic tree-ring data are the cutting date clusters in the 1960s, after the area became restricted due to LANL priorities. How, who, and why the Romero Homestead was remodeled are interesting questions.

DENDROCLIMATOLOGY AND PAST ENVIRONMENTAL VARIABILITY IN THE PAJARITO PLATEAU AREA

Dendroclimatology is the use of tree-ring data to retrodict past climate patterns. The subfield has a long history within dendrochronology, but has grown exponentially in the past few decades. In part because of Douglass' interest in sunspot activity, tree-rings and climate have been linked

since the beginning of dendrochronology. Indeed, one of the obstacles to "bridging the gap" was the severe drought of the late 1200s on the Colorado Plateau. Douglass (1935) was the first scientist to suggest a connection between the "Great Drought" and the Anasazi abandonment of the Four Corners area, a question that is still debated in southwestern archaeology. Schulman (1956) was actually the first dendrochronologist to develop a climate reconstruction, but it was not until Fritts' (1976, 1991) efforts that dendroclimatology became a quantitative endeavor. It was not until the 1970s, however, that dendroclimatology was used in the northern Rio Grande region.

A dendroclimatic reconstruction involves developing a mathematical model of the relationship between the environment and the cambial growth of trees (LaMarche 1974; Schulman 1954, 1956). Trees are natural archives of information about past environments, and because many are older than the oldest historical documents, they can be used to illuminate aspects of prehistoric climate (Dean 1988; Swetnam and Betancourt 1998). Such archives, however, contain information on a number of different aspects of the environment, and it is necessary to isolate the variables one wishes to study. Specific field collection, laboratory analysis, and statistical procedures are designed to eliminate the "noise" in the tree-ring series and highlight the environmental "signal of interest" (Fritts 1991; Salzer 2000a). In some instances, the signal of interest is long-term trends in precipitation, in others it is long-term temperature variability, and in still others it is the short-term spatial differences and identification of extreme events, such as floods or very dry years in specific areas (Graybill 1989). For detailed discussions of the methods and techniques of dendroclimatology, see Fritts (1976, 1991).

Dendroclimatic reconstructions can provide annual estimates of various climatic variables and are the most precise method for doing so. Dendroclimatology, however, is not without its limitations. First, the technique can only be used for those time periods encompassed by the tree-ring samples; in the Southwest, the time frame is limited to the past two and one-half millennia. Climate variation before about 2600 years ago must be examined using other methods. Second, dendroclimatic reconstructions tend to underestimate the extreme values of particular years. Tree rings tend to underestimate the magnitude of high-precipitation (wet) years because in those years water ceases to become the most limiting factor in cambial growth (Fritts 1991). In other words, trees have an adequate supply of water, but some other factor (e.g., temperature, nutrient supply, genetics) prevents uncontrolled cell division and cambial growth (Fritts 1976). In extremely dry years, something of the opposite problem occurs in the Southwest. If a tree does not receive adequate moisture to initiate growth, the result is a locally absent or "missing" ring. The tree, in effect, has recorded "0" moisture for that year even if some precipitation may have fallen. Another potential problem is the 'short-segment' curse (Cook et al. 1995; Sheppard et al. 1997). In some instances, it appears that trees have adapted their growth patterns to "short-term" climatic norms, that is, conditions prevalent during their lifetimes. Thus, it is best to collect extremely long-lived trees (Grissino-Mayer 1996; Salzer 2000a), but that strategy is not always possible. In many cases, including the northern Rio Grande region, archaeological chronologies have been combined with live-tree chronologies to extend the dendroclimatic record into the first millennium AD (Rose et al. 1981). Despite these caveats, tree-ring based reconstructions of climate are the most accurate and precise methods available for examining the past climate variability of the Pajarito Plateau during the past two millennia.

Reconstructions of Precipitation in the Northern Rio Grande

The first dendroclimatic reconstruction in the Southwest was developed by Dean and Robinson in 1977. As a dendroclimatic reconstruction for the Colorado Plateau, this early work is not a reconstruction of annual temperature or precipitation. It is a reconstruction of decadal departures from mean ring-widths for 25 specific tree-ring stations, including the Jemez Mountain chronology. The modern and archaeological tree-ring data used span the period AD 623 to 1978, and have been used predominantly to reconstruct relative variability in annual ring-width on a decadal scale (Appendix E). No climate data were used in this qualitative reconstruction. The reconstruction was certainly adequate for its time and purpose. The qualitative nature of the reconstruction was based on the relative change in decadal ring-width averages; thus, it indicated that tree-growth at the Jemez Mountain locality in the AD 960s, for example, was 1.3 standard deviations greater (Figure 7.20) than the mean and that growth in the AD 1420s was 1.2 standard deviations below the mean at the same site (Figure 7.21).

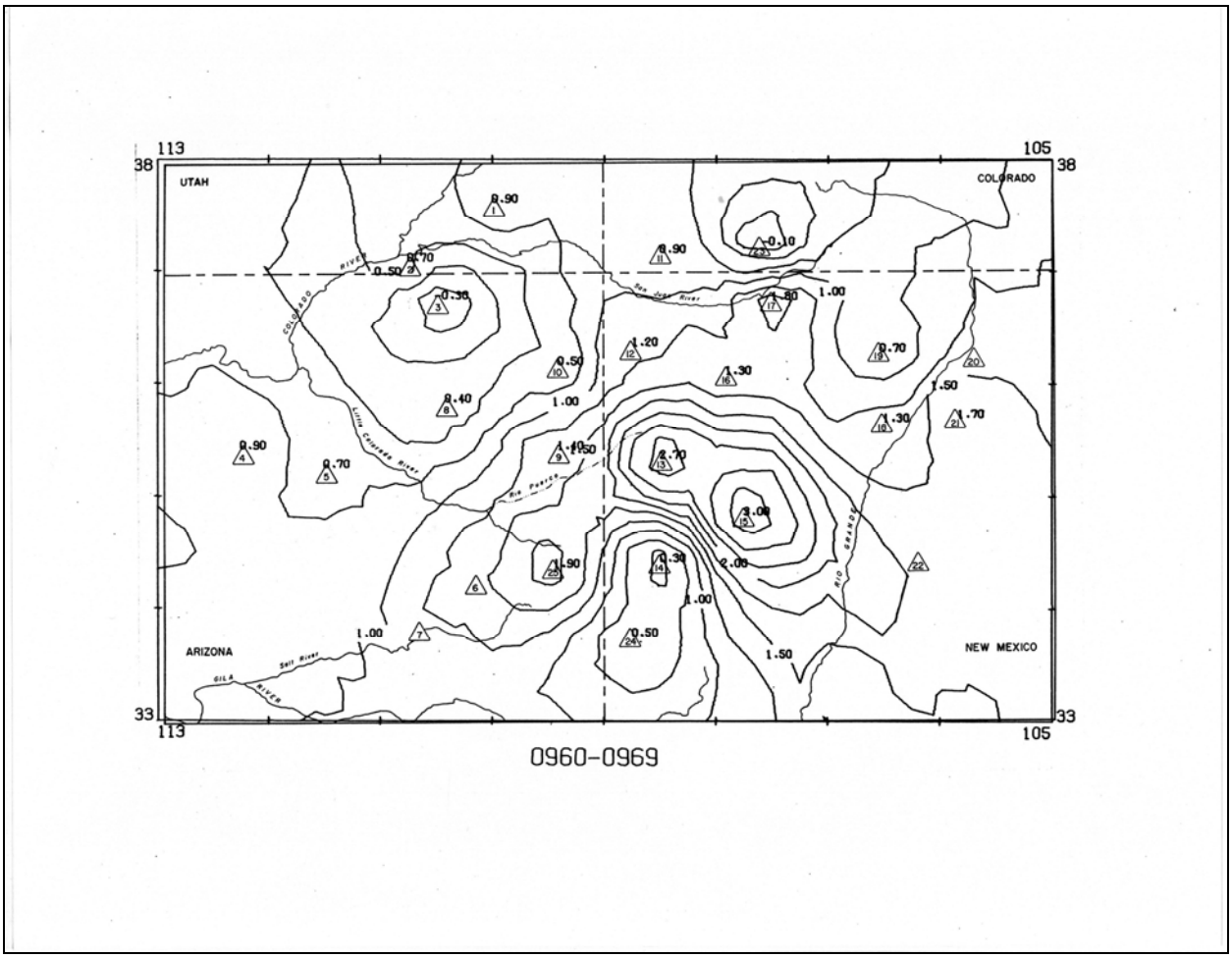

Figure 7.20. Isopleth of growth anomalies in the 960s (from Dean and Robinson 1977).

It did not, however, estimate the environmental factors responsible for the growth departures. Certainly, precipitation is major component of growth in southwestern conifers, but it is by no means the only factor in tree growth (Fritts 1991). The decadal summaries, based on Christian calendar decades, undoubtedly smoothed some between-decade variation and minimized high-frequency annual values. Thus, Dean and Robinson's (1977) research illuminated broad temporal and spatial patterns of ring-width change, but provided no quantitative data concerning annual precipitations or temperature responsible for those changes.

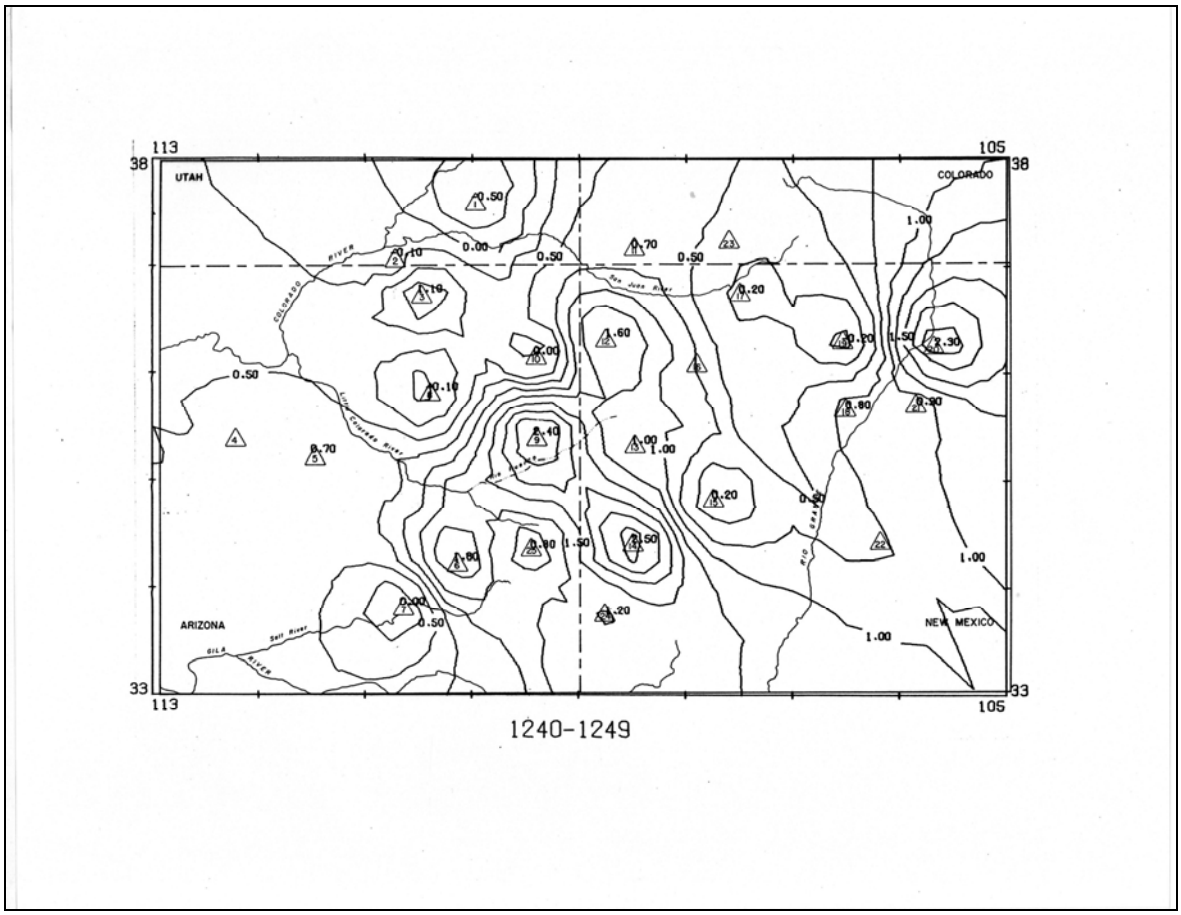

Figure 7.21. Isopleth of growth anomalies in the 1420s (from Dean and Robinson 1977).

Shortly thereafter, Rose et al. (1981) produced a quantitative reconstruction in the northern Rio Grande that extended back to AD 985. Rose and his colleagues used live piñon samples from Glorieta Mesa and archaeological samples from Arroyo Hondo and other sites to reconstruct both annual and spring (March-June) precipitation in the area. Because of the uncertainty as to whether the living trees and archaeological specimens reflected the same climatic variables (e.g., were derived from the same population), Rose et al. (1981) conducted extensive statistical analyses to demonstrate the coherence of the database.

The resulting reconstructions (Appendices F and G) indicate important aspects of precipitation in the area as well as illuminate trends over long time scales. The Arroyo Hondo analysis indicates

that the mean annual precipitation for the area is 13.337 inches and the standard deviation is 2.16; the spring mean is 4.21 and spring standard deviation is 1.81. Probably most importantly, their analysis of both the tree-ring and modern climate data indicates that spring precipitation is more variable than annual precipitation. In short, the late-summer (monsoonal) and early-winter precipitation is somewhat consistent—and therefore predictable over the long term—but spring precipitation varies from year to year, decade to decade, and probably century to century. Thus, spring precipitation typically accounts for approximately one-third of the annual rainfall. As they state, "spring is the period of seed germination of traditional Pueblo crops.... And if late summer rainfall is stable as suggested, germination may have been the controlling factor in successful farming..."(Rose et al. 1981:106).

The period from AD 990 to 1430 was characterized by high-amplitude and high-frequency changes in both spring and annual precipitation. Such a trend may have facilitated adaptational strategies such as storage, trade, and "alliance formation" as mechanisms to mitigate the effects of rapid and severe fluctuations in rainfall. The period from AD 1430 to 1735 was somewhat the opposite with low frequency, low amplitude fluctuations; and the period from AD 1735 to 1970 exhibited low frequency changes of somewhat moderate amplitude.

On a more detailed level, the 1295 to 1335 period was consistently above average and 1335 to 1400 was variable with high amplitude in 1335 and 1370 but low amplitude in 1365 and 1380. Consistently high precipitation characterized the 1400 to 1415 years, but there was a very low point in 1420. The early 1500s were consistently high, with a low in 1520, and a return to high precipitation until about 1560. The "mega drought" of the late 1500s was particularly severe. Low precipitation characterized the early Hispanic period, 1875 to 1900, but consistently high precipitation persisted from about 1900 to 1950. The 1950s drought was severe in the northern Rio Grande, but not as severe as in the south.

Although the Dean and Robinson (1977) qualitative reconstruction included a spatial component (see above), it was not until the 1990s that an extensive, quantitative precipitation reconstruction of the spatial and temporal variability within the Southwest was developed. Dean and Funkhouser (1995) used 27 tree-ring chronologies spread from the Grand Canyon to the Pecos River and central Utah to the Gila River to characterize precipitation over the past 1400+ years. They identified two spatially discrete principal components, predominantly to the north and west and the other to the south and east (Figure 7.22). This configuration resembles the modern precipitation regime whereby the north and west is characterized by bimodal distribution with both winter and summer precipitation, and the southeast area exhibits a unimodal, summer-dominant precipitation pattern. The same pattern characterizes much of the prehistoric period, except the 1250 to 1450 period when the northwest area experienced "a totally aberrant" pattern. "The only stable characteristic of this period is the persistence of the southeastern component" (Dean and Funkhouser 1995:94), which includes the Pajarito Plateau. The relationship of this aberrant climatic pattern on the Puebloan peoples of the Colorado Plateau and Rio Grande area has not yet been delineated.

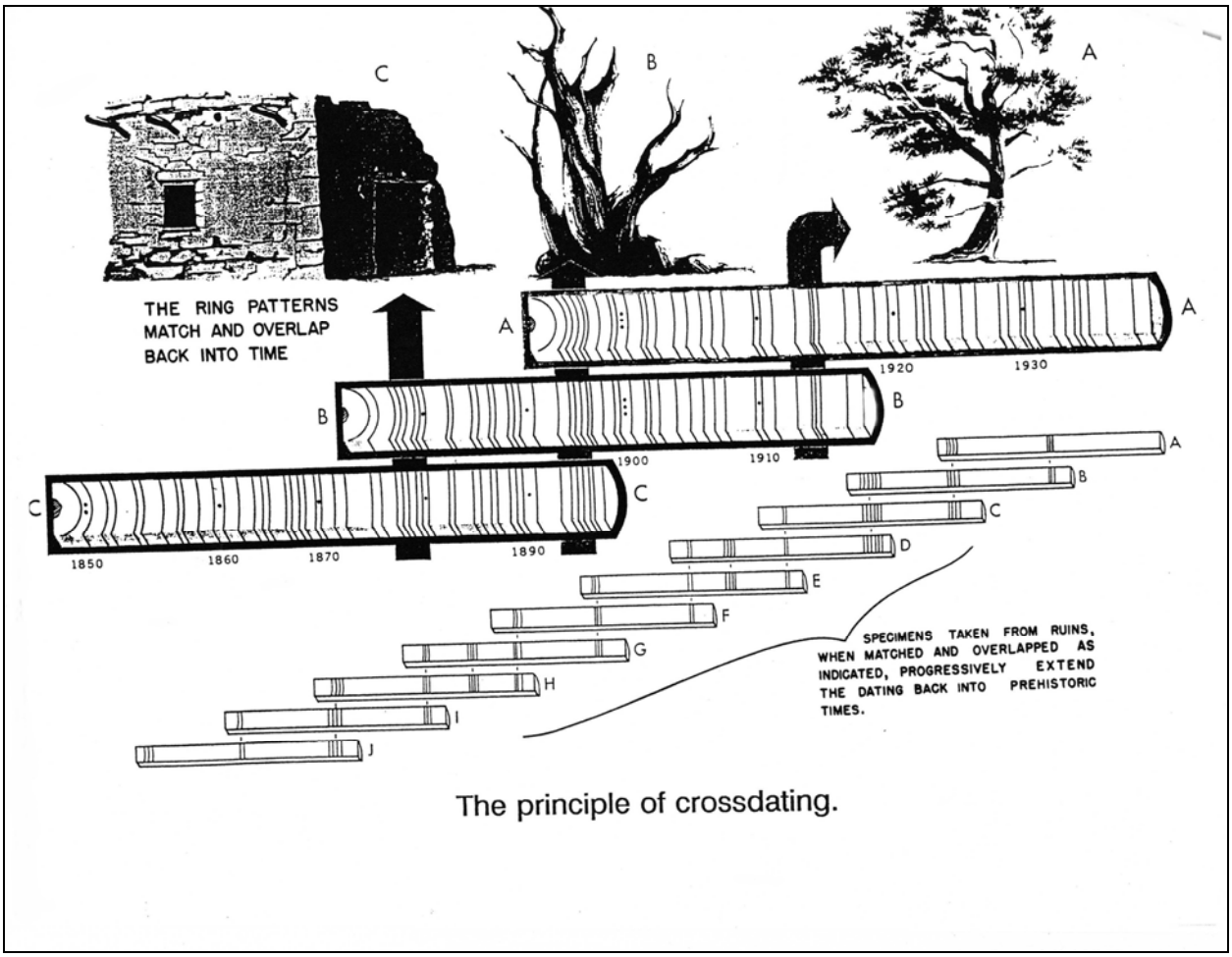

The principle of crossdating.

Figure 7.22. Map showing principal components of southwestern precipitation (from Dean and Funkhouser 1995).

Reconstructions of Temperature in the Southwest

Salzer (2000a) had developed the only tree-ring based, quantified temperature reconstruction currently available in the Southwest. Using high-altitude bristlecone pine trees from the SFP in northern Arizona, he retrodicted monthly mean-maximum annual temperature from 663 BC to AD 1997; only the AD 660 to 1997 period is used herein. Details of the reconstruction methods and results can be found in Salzer (2000a) and subsequent articles (Salzer 2000b).

A few comments about Salzer's reconstruction are necessary, however. As mentioned above, relative temperature is more or less uniform across the Colorado Plateau, although extremely local micro-environments may be exceptions to the trends. The Rio Grande and other areas east of the Continental Divide undoubtedly have different temperature influences, so the Colorado Plateau temperature record may only weakly reflect conditions in the northern Rio Grande. Temperature also varies with elevation. The SFP reconstructed temperature values represent temperatures at 2240 m above sea level. Using modern temperature data from several different

climate stations and published regression equations, Salzer (2000a) suggests an adjustment of 2 degrees centigrade per 305 m change in elevation. Finally, mean-maximum temperature is an indicator of daily high temperatures. Salzer's (2000a) analysis indicates that the highest correlation of temperature with tree growth is during January to December of the year before the growth year (Year t-1). Thus, a lag of t-1 was used in his reconstruction.

Temperature may be a very important variable to reconstruct in terms of understanding the adaptation of agriculturalists to the Pajarito Plateau. Particularly, if a seasonal (spring) temperature signal can be obtained, we may be able to elucidate more clearly the maize growing season in specific years and over longer time spans.

RECOMMENDATIONS AND CONCLUSIONS

Dendroarchaeology

Dendroarchaeology has made significant contributions to the understanding of past human behavior, occupation, and adaptation to the Pajarito Plateau environment. The dendroarchaeological resources can continue to contribute important information concerning past human/environment interaction in the area if various types of data collection and research are targeted toward specific goals. The information contained in dendroarchaeological samples is a non-renewable resource that is at risk from natural threats, such as fire and erosion of exterior rings, and cultural impacts, such as vandalism and illegal collecting. The following recommendations provide a strategy for more fully exploiting the dendroarchaeological resources of the Pajarito Plateau.

First, all available tree-ring samples from previously excavated and unexcavated contexts should be submitted for analysis. Samples may exist in archaeological collections curated at various museums around the country, and analyzing the samples may yield new information without any additional fieldwork or impact to the resources. Such a strategy was recently used by the field Museum of Natural History in reassessing their Paul S. Martin Collection, and the reanalysis resulted in the dating of previously undated sites and a substantial increase in the number of data and other information from the samples. Many different institutions and individuals have been involved in archaeological excavations on the Pajarito Plateau over the past 100+ years, and it is unlikely that all of the wood or charcoal specimens collected have been submitted for analysis. Analyzing these "old" samples, therefore, may have tremendous benefits.

Second, all newly collected samples should be submitted for analysis. Whether through research projects or Cultural Resource Management-mandated testing and excavation, all such samples need to be analyzed. Pre-selection of samples in the field (e.g., choosing those that "look best") is often a self-defeating exercise. Although trained dendrochronologists may be able to tell if a sample dates in the field, not even they can be certain if a sample will not date. All such samples should be treated as cultural artifacts, which they are, and recorded properly, including precise provenience information, assumed function, size, and tool marks present. The LTRR requires

that specific information accompany the samples (Figure 7.23) and additional information (Figure 7.24) is critical for properly interpreting the samples.

TREE-RING SAMPLES SUBMISSION FORM

Date:

Site Name/Number	**Total Number of Samples**

UTM Zone: **Elevation:**
Easting:
Northing:
Map Reference:
Site Location

Estimate of Total Number of Architectural Units:
Type of Architecture (surface masonry, pithouses, etc):
Aspect of Site (open or sheltered):
Phase/Period:
Site Description

Name:
Institution:
Address:
City, State, ZIP:
Send Results to

Figure 7.23. Laboratory of Tree-Ring Research sample submission form.

TREE-RING SAMPLE INVENTORY Page of

Date:

_____
(Site)

		For TRL Use ONLY		
Provenience	Field Sample No(s)	TRL #	Species	Comment

Figure 7.24. Laboratory of Tree-Ring Research tree-ring sample inventory.

Third, a concerted effort should be made to more adequately develop the juniper ring sequence in the area. Traditionally, juniper was not collected because it was difficult to crossdate and not valuable for dendroclimatic purposes. Indeed, the low proportion of dates (2/113) from Pajarito Plateau juniper samples attests to its difficult nature. Many of those samples, however, were collected in the 1960s when the ring sequences had not been intensively analyzed. In other areas, new juniper chronologies are contributing important chronometric data to understanding the past. The development of juniper chronologies and reanalysis of samples from Long House in Mesa Verde, for example, has resulted in a more than threefold increase in the number of dates from that structure (Street 2001). Certainly, such a task will not be easy or quick, but the dividends will be substantial.

Fourth, a serious effort should be made to exploit the "arboreal" dendroarchaeological record. Isolated cultural features, such as ax-cut limbs and stumps, peeled trees, and intentionally burned stumps have been used elsewhere (Montorano 1988; Swetnam 1983; Towner et al. 1998) to date past human activities, even in the absence of high-quality architectural samples. The inhabitants of the Pajarito Plateau, both prehistoric and historic, have exploited the wood resources of the area in various ways. Sampling such features (Figure 7.25) will have at least two benefits (a) it will increase the number of juniper samples and aid in the development of a juniper ring sequence and (b) it will help date land-use patterns through time by the different occupants of the area.

Figure 7.25. An axe-cut juniper limb in the Rio Puerco Valley.

Finally, samples should be collected from all extant historic and prehistoric structures and features exposed to the elements. Such samples can be collected as half-inch or five-eighth-inch cores with minimal impacts to the resource. The wood in these structures is seriously threatened by natural erosion of the outer rings, fire, vandalism, insect infestations, and a variety of other natural and cultural factors. As a non-renewable resource, the information contained in these wood samples is in danger of being lost forever if action is not taken to preserve it.

Dendroclimatology

Dendroclimatology has been used for more than 20 years to characterize past precipitation on the Pajarito Plateau and throughout the northern Southwest. Live-tree and archaeological samples have been combined in various ways to delineate (a) patterns of annual precipitation for more than 1000 years, (b) patterns of spring precipitation in the northern Rio Grande for more than 1000 years, and (c) changes in the spatial distribution of precipitation for almost 1500 years. Reconstructing temperature, on the other hand, has been much more difficult. Only a single temperature reconstruction, albeit 2600 years long, exists for the entire Southwest. Unlike archaeological tree-ring data, dendroclimatological samples do not reflect "points" on the landscape, they reflect broad-scale patterns. Therefore, the recommendations for future research below extend beyond LANL and the Pajarito Plateau.

The most pressing need in southwestern dendroclimatology is another temperature reconstruction with which to compare Salzer's (2000a) SFP reconstruction. Certainly, temperature is more spatially coherent than precipitation, but the SFP are located west of the Continental Divide in the northwest part of the Colorado Plateau and therefore may not accurately reflect temperature trends in the Rio Grande area. Trees that contain a temperature signal, however, are unlikely to be found in the Jemez Mountains or LANL lands. The most likely area to search for such trees is at extreme timberline in the Sangre de Cristo Mountains east of the Rio Grande.

A second important issue for archaeological and other research is more adequately delineating the seasonal patterns of precipitation on the Pajarito Plateau. Annual precipitation patterns have been well documented and Rose et al. (1981) identified spring precipitation variability. Identifying additional seasonal variability in precipitation will aid not only archaeological research, but other fields as well. One possible way to accomplish this goal is to (a) reassess the dendroarchaeological collections for suitable samples and (b) develop chronologies from different tree species along an elevational gradient from the Rio Grande to the crest of the Jemez or Sangre de Cristo Mountains. If appropriate trees are located, we may be able to reconstruct variables such as winter snowpack, as has been done elsewhere (Woodhouse 2002).

Finally, one task that has not been accomplished, but which had important implications for human use of the area, past, present, and future, is the reconstruction of stream flow for rivers in the area. Stream flow depends on many factors (Stockton 1990), but can be modeled using tree-ring data. Three rivers in the area might be amenable to stream flow reconstructions: the Jemez, the Chama, and the Rio Grande. The Jemez may be the easiest to reconstruct because it has a limited watershed with few major tributaries. The Rio Chama, although larger, may be amenable

to reconstructions if trees in the upper portions of the watershed and its tributaries can be located. Stream flow in the upper Rio Grande would be the most difficult to model because of the length and numerous climatic factors that influence its flow—trees from the San Juan and Sangre de Cristo Mountains in Colorado, as well as those in New Mexico would be needed to develop such a reconstruction.

Tree-ring reconstructions of various climatic parameters—precipitation, temperature, snowpack, stream flow-- can contribute significantly to archaeological research on LANL properties, the Pajarito Plateau, and the northern Rio Grande in general. As noted above, however, dendroclimatological data are not point data and they have broad interdisciplinary applicability. It is unrealistic, therefore, to expect archaeological or Cultural Resource Management-related projects to fund such research. A broad coalition of pubic and private interest groups is needed to identify the variability in climate that has and will continue to impact the human and non-human populations of the Pajarito Plateau.

CONCLUSIONS

Dendrochronology has a long and distinguished history on the Pajarito Plateau. Beginning with the 1st Beam Expedition and Stallings' development of the Rio Grande chronology, tree-ring data have helped date many archaeological sites and cultural phenomena. Beginning in the 1970s, archaeological and live-tree samples have been used to illuminate various aspects of past climate variability. Pan-southwestern tree-ring data have helped identify aspects of past population movements and adaptations to local and regional environments, as well as help us understand past climate variability over the past two millennia.

Despite the successes of the past 80 years, much work remains to be done. The reanalysis of previously collected archaeological samples, more detailed documentation of new samples, development of an adequate juniper chronology, and collection of non-architectural samples will materially enhance our understanding of the human use of the Pajarito Plateau landscape. New, geographically dispersed live-tree collections, combined with carefully selected archaeological samples will help us document past seasonal precipitation patterns, snowpack amounts, temperature fluctuations, and stream flow in the rivers of the area. These are ambitious goals, but they can be accomplished with dedicated researchers, adequate public and private funding, and continued institutional support.

CHAPTER 8
DENDROCLIMATIC RECONSTRUCTIONS IN THE NORTHERN RIO GRANDE

Ronald H. Towner and Mathew W. Salzer

INTRODUCTION

One of the goals of archaeology is to provide a long-term perspective on human/environment interaction. Humans, like all other species, live in and interact with the environment, and these interactions involve the extraction of both biotic and abiotic resources and respective adaptations to them. The environment—both biotic and abiotic—is constantly changing and does so at many difference scales (e.g., day, month, year, decade, century, and millennium). Through the medium of culture, humans have the ability to modify their environment, but they must also cope with both long- and short-term trends and perturbations in that environment. Thus, understanding past environments helps us understand how past human groups adapted to the ever-changing environment using technology, social organization, and even ideology. This chapter uses recent data to develop new paleoclimatic reconstructions for the Pajarito Plateau in an effort to better understand prehistoric interactions between Pajaritans and their environment (Figure 8.1).

Understanding the past environment of the area is critical for comprehending the adaptations of the past inhabitants to their physical environment. This chapter examines only one aspect (precipitation) of past environments on the Pajarito Plateau. The data and interpretations presented herein have important implications for understanding the Ancestral Puebloan, Puebloan, Hispanic, and Anglo occupations of the area. They may also help illuminate aspects of the AD 700–1100 period when few people lived in the area and will provide insights into the modern climate variability as well. The dendroclimatic reconstruction data presented here are only one component of the human/environment interaction matrix, and it is hoped that it will spur other researchers to investigate other aspects of the matrix.

BACKGROUND AND PREVIOUS RESEARCH

Dendroclimatology was chosen as the method to examine paleoclimate in the project area for several reasons. First, the project area is part of the vast piñon-juniper forest of the Colorado Plateau and Rio Grande (Figures 8.2 and 8.3). In addition, the appropriate tree species such as ponderosa pine (*Pinus ponderosa*), Douglas fir (*Pseudotsuga menziesii*), piñon pine (*Pinus edulis*), and Southwestern white pine (*Pinus reflexa*) are plentiful in the project area, and are excellent natural archives of past environmental and climatic information. Thus, the wood resources are available for many kinds of analysis. Second, dendroclimatology, the study of climate based on annual growth rings in trees, is the most precise and accurate method of reconstructing climate in the prehistoric period. Dendroclimatic reconstructions provide statistically reliable estimates of annual precipitation and/or temperature for each and every year in the study. No other method of studying long-term climate variability can make such a claim.

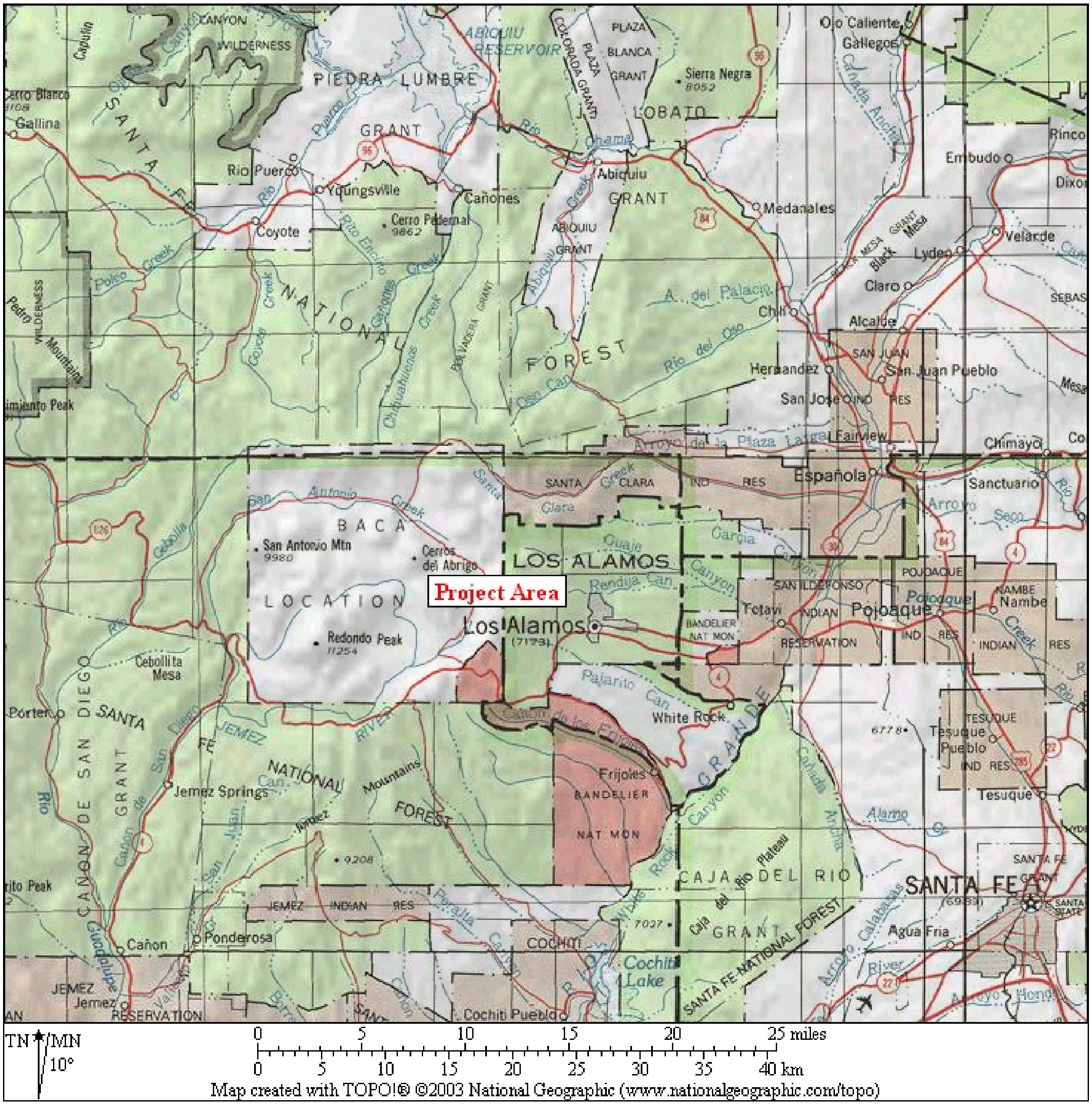

Figure 8.1. Map of the project area.

Figure 8.2. Photo of project area.

The trees of the project area have proven to be quite useful in dendrochronology (tree-ring dating) because they add a single annual layer of cambium (a tree ring) that varies in width depending on climatic conditions in a particular year. The presence of these environmentally sensitive tree species in both the modern vegetation mosaic and archaeological record of the area enables us to use dendroclimatology to examine aspects of past precipitation variation. This study will significantly enhance understanding of past climatic change in the project area and allow archaeologists to better incorporate climatic variations into their interpretations of past cultural adaptations.

A dendroclimatic reconstruction involves developing a mathematical model of the relationship between the environment and the cambial growth of trees (LaMarche 1974; Schulman 1956). Trees are natural archives of information about past environments, and because many are older than the oldest historical documents, they can be used to illuminate aspects of prehistoric climate (Dean 1988; Swetnam and Betancourt 1998). Such archives, however, contain information on a number of different aspects of the environment, and it is necessary to isolate the variables one wishes to study. The specific field collection, laboratory analysis, and statistical procedures described below are designed to eliminate the "noise" in the tree-ring series and highlight the "signal of interest." In some instances, the signal of interest is long-term trends in precipitation,

in others it is long-term temperature variability, and in still others it is the short-term spatial differences and identification of extreme events, such as floods or very dry years in specific areas.

Figure 8.3. Photo of project area.

Dendroclimatic reconstructions can provide annual estimates of various climatic variables and are the most precise method for doing so. Dendroclimatology, however, is not without its limitations. First, the technique can only be used for those time periods encompassed by the tree-ring samples; in the Southwest, the time frame is limited to the past two and one-half millennia (Salzer 2000a). Climate variation before about 2600 years ago must be examined using other methods. Second, dendroclimatic reconstructions tend to underestimate the extreme values of particular years. Tree rings tend to underestimate the magnitude of high precipitation (wet) years because in those years water ceases to become the most limiting factor in cambial growth (Fritts 1991). In other words, trees have an adequate supply of water, but some other factor (temperature, nutrient supply, genetics, etc.) prevents uncontrolled cell division and cambial growth (Fritts 1976). In extremely dry years, something of the opposite problem occurs in the Southwest. If a tree does not receive adequate moisture to initiate growth, the result is a locally absent or "missing" ring. The tree, in effect, has recorded "0" moisture for that year even if some precipitation may have fallen. Despite these caveats, tree-ring based reconstructions of

climate are the most accurate and precise methods available for examining the past climate variability of the Rio Grande and Colorado Plateau during the past two millennia (Grissino-Meyer 1996; Salzer 2000b).

Dendroclimatology has been used for more than 20 years to characterize past precipitation throughout the northern Southwest (see Chapter 7, this volume for a detailed discussion of past efforts in the northern Rio Grande). On a local and archaeologically oriented level, Orcutt (1999) used many of the previously collected data to retrodict the Palmer Drought Severity Index (PDSI) in the Bandelier area as part of the Bandelier Archaeological Survey. Although not strictly a dendroclimatic reconstruction, Orcutt's detailed examination of the AD 1150–1610 period and use of proxy paleoclimate data have been a major contribution to studies of human/environment interaction in the northern Rio Grande. Orcutt's Agricultural Risk Model is discussed in more detail below.

The following are reasons why a new climate reconstruction was needed:

1. Both the tree-ring and climate data for the previous reconstructions end in the late 1970s (Dean and Robinson 1977; Rose et al. 1981). The addition of 30 years of both tree-ring and climate data resulted in an almost 20 percent increase in the period of overlap needed to calibrate the tree-ring/climate relationship. This longer period of overlap is critical and resulted in much stronger correlation coefficients and increased our confidence in the results significantly.
2. By using climate data from individual stations, instead of divisional data, the reconstruction much better reflects the conditions in the local project area.
3. Using these climate station data and new tree-ring chronologies also enabled us to document spatial variability within the project area.

THE PAJARITO DENDROCLIMATIC RESEARCH DESIGN

Developing new chronologies and retrodictions of past precipitation were the bases of this project. Certainly, other aspects of past climate, such as temperature, played a role in human use of the Pajarito Plateau. Precipitation, however, is the most direct measure available and was probably the most important for prehistoric and historic period agriculturalists.

This project had four specific goals for elucidating past aspects of human/environment interaction through the retrodiction of past precipitation: low-frequency variation, high-frequency variation, spatial variability, and evaluating agricultural risk. We wanted to

1. Examine the low-frequency variability in the precipitation signal. Low-frequency variation is important because it is the climatic condition adapted to by human groups;
2. Examine high-frequency variation in the dendroclimatic record. High-frequency variation is important because it contains the signal of extreme events that may have seriously impacted local populations on a short-term basis;
3. Document the spatial variability in precipitation within the project area. For example, we wish to examine geographic areas that were affected differently than others;

4. Evaluate the climatic variability aspects of the Agricultural Risk Model developed for the area by Orcutt (1999).

METHODS AND PROCEDURES

Field Research and Methods

An important component of this project was to collect samples from living trees in the project area. Initially, our goals were to collect long-lived trees throughout the project area in order to provide data relevant to both past temporal and spatial retrodictions of two climate parameters: precipitation and temperature. As we conducted the field work, however, it became clear that we would have to modify our goals.

Our first problem is that there are very few long-lived trees in the area; most trees are less than 500 years old. We observed few trees that exhibit characteristics of old age, such as stripped bark, spiral grain, and spiked tops (cf. Schulman 1954). Indeed many of the trees in the area appear to have germinated in the early 1600s following a massive die-off during the mega-drought of the 1560s to 1590s (Swetnam and Betancourt 1998). This pattern, massive die-off in the late 1500s and extensive tree recruitment in the early 1600s, has been documented in many areas of the Southwest (Allen et al. 1998; Betancourt et al. 1993; Savage et al. 1996).

Second, the lack of high-altitude temperature-sensitive trees prevents us from retrodicting Pajarito temperature variability. Salzer's (2000b) San Francisco Peaks, Arizona, retrodiction may be relevant, but a Rio Grande area temperature retrodiction is badly needed.

Field Methods

The field work component of the project included extracting 318 cores and cross-sections from 166 climatically sensitive old trees at 11 sites (Table 8.1).

Table 8.1. Description of live-tree collections.

Collection Site	Species	Trees	Cores	Date Range	Measured?	Previous Chronology	Old Measurements?	Used in Reconstruction
Alta Mesa DF	DF	16	26	1652–2005	Y	N	N	YES
Alta Mesa PP	PP	15	30	1621–2005	N	N	N	NO
Alta Mesa WP	WP	15	31	1540–2005	Y	N	N	NO
Alta Mesa PNN	PNN	18	35	1533–2005	Y	N	N	YES
Bland Canyon	PP	12	23	n/a	N	Y	Y	NO
Los Alamos Canyon	PP	20	41	1786–2005	Y	Y	Y	YES

Collection Site	Species	Trees	Cores	Date Range	Measured?	Previous Chronology	Old Measurements?	Used in Reconstruction
Caja del Rio	PNN	5	4	n/a	N	Y	Y	NO
Upper Los Alamos	PP	16	32	1658–2005	Y	N	N	YES
Paliza Campground	PNN	16	31	1645–2005	Y	Y	Y	YES
Rio de los Frijoles	PP	16	31	n/a	N	Y	Y	NO
Pine Springs Resample	PP	17	34	1767–2005	Y	Y	Y	YES
Totals		**166**	**318**					

No juniper trees were sampled as part of this project because they exhibit more variability within individual rings and are much more difficult to measure accurately. Using a Swedish increment borer (Figure 8.4), cores were taken from the lowest practical location on the tree bole in order to maximize the number of rings available for analysis.

Figure 8.4. Photo of sampling with increment borer.

When possible, two cores were collected from each tree in order to minimize the within-tree variation in ring width; likewise, multiple trees were sampled at a single site (always more than 10 trees if possible) in order to reduce the between-tree variation in growth. These sampling strategies help ensure that the resulting site-specific ring sequences reflect a common growth parameter, in our particular case, precipitation, and that other "noise" is averaged out of the chronologies (Fritts 1976).

Collected during November 2005, our samples are distributed on and around the Pajarito Plateau (Figure 8.5). Six of the live-tree sites have been collected previously but the data were never used due to funding shortages; the data, however, existed in paper form at the Laboratory of Tree-Ring Research (LTRR) and were entered into a computer database for use during this project. Our re-sampling at these sites was designed to update the ring sequences and provide an additional 30 years of ring-width data against which to calibrate the precipitation data.

Our five new chronologies were distributed throughout the project area, although four species-specific chronologies are all located on Mesa Alta; the only new chronology on the Pajarito Plateau is Upper Los Alamos. Table 8.1 presents some descriptive data for these chronologies and merits additional explication. Although we attempted to collect two cores per tree, some cores were unsuitable because of breakage, interior heartwood rot, pitch pockets, or other idiosyncratic abnormalities. The table also illustrates that trees greater than 500 years old are difficult, if not impossible, to locate in the project area. In addition, the Caja del Rio live tree site could not be adequately re-sampled because the trees died during the recent drought and beetle infestation.

Laboratory Research and Methods

After the end of field work, the first step in chronology development and climatic reconstruction is cross-dating each of the live-tree samples. Each of the chronologies used in the reconstruction was developed completely independently of the others; thus, each can be considered an independent test of the cross-dating method. By cross-dating the cores against each other and the "New Mexico I" master chronology (Robinson et al. 1972), we were able to determine the year each and every ring grew. Although different cross-dating methods are used in different parts of the world, the LTRR uses the ‘skeleton plot’ method of cross-dating (Stokes and Smiley 1968). Skeleton plotting is an analog method of representing the narrow rings on a sample using graph paper (Figure 8.6). By comparing skeleton plots of many different samples, a master skeleton plot can be developed that extends further back in time and contains more information than any single sample. Area l master plots are developed and extended further back into the past by overlapping samples from living trees, dead snags, and archaeological specimens (Figure 8.7).

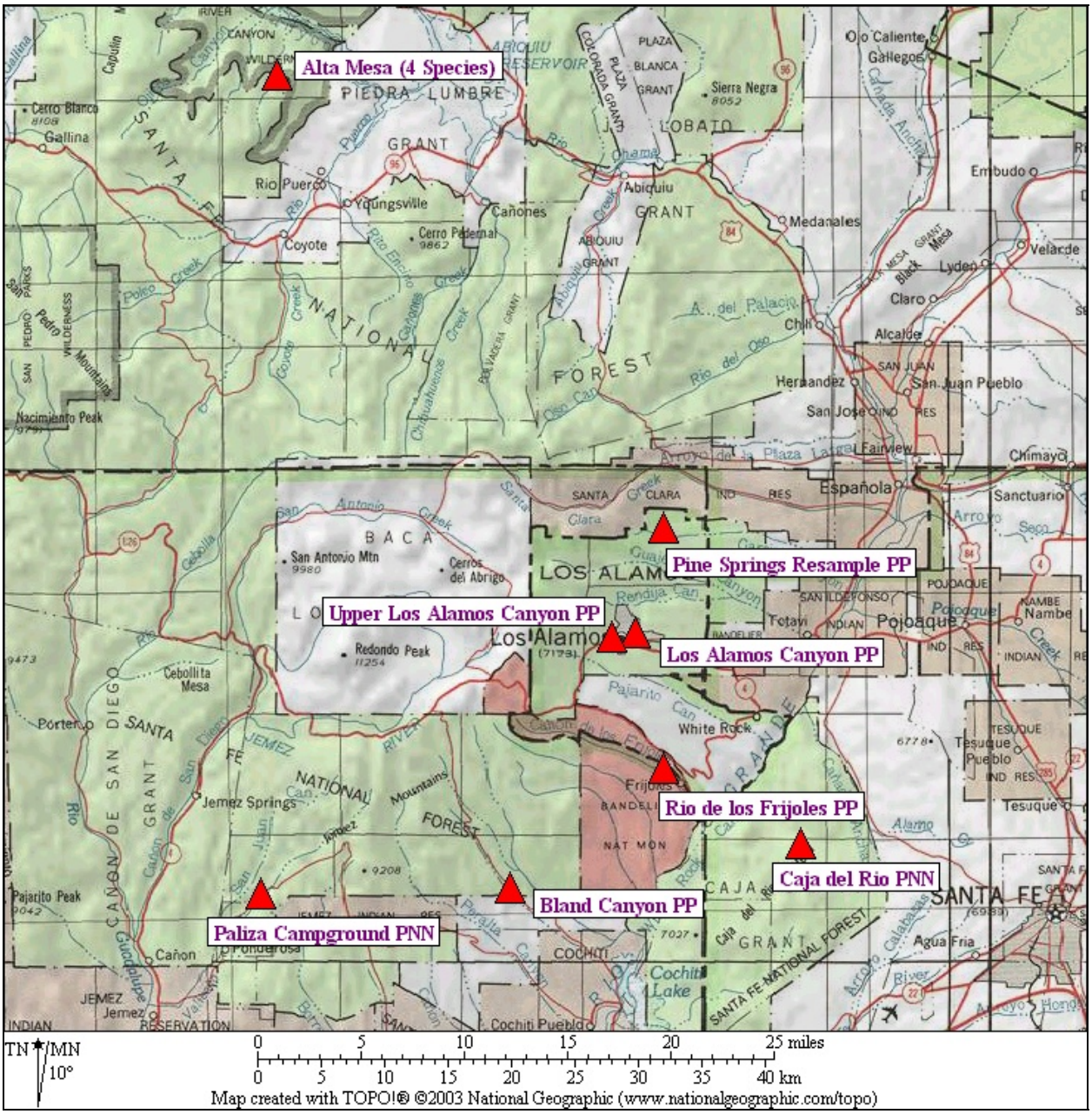

Figure 8.5. Map of live-tree sample locations.

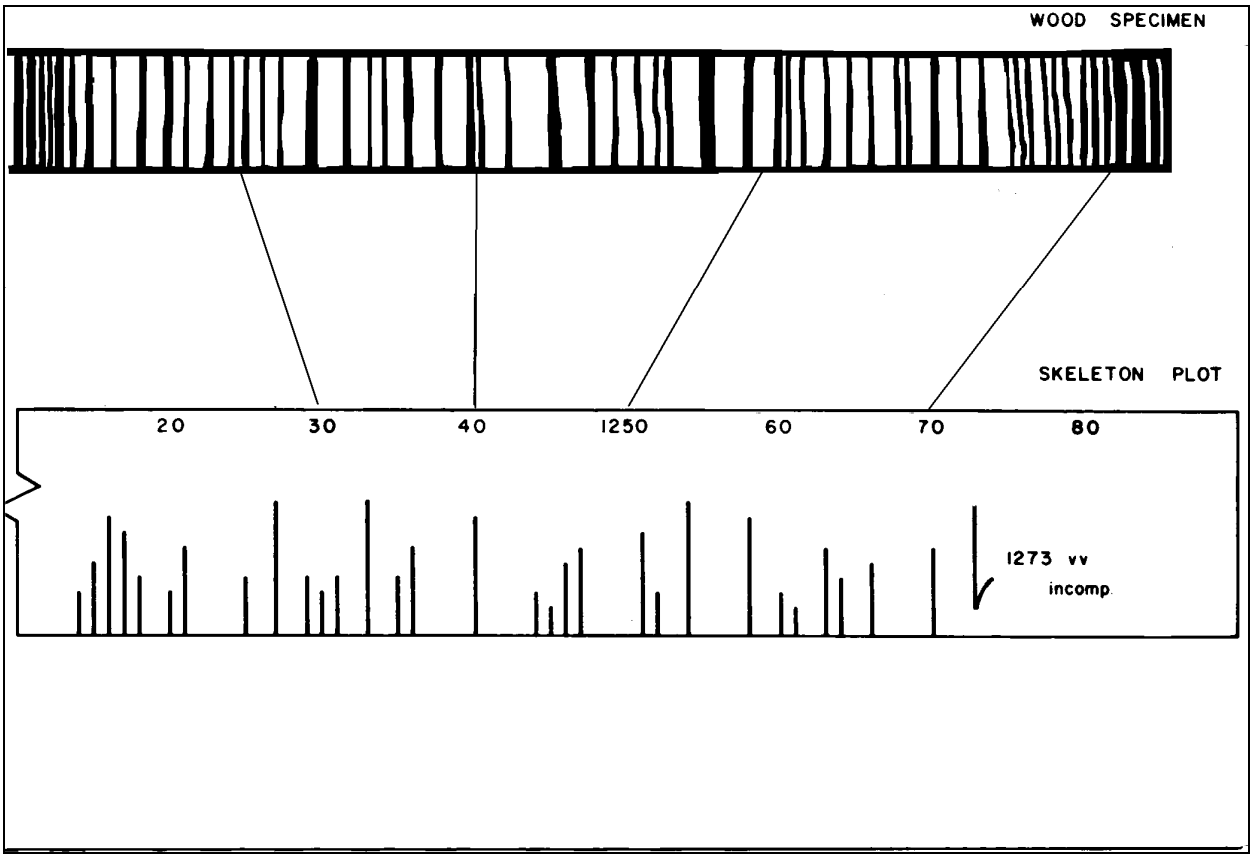

Figure 8.6. Skeleton plotting technique.

Statistical Methods: Building Quantitative Tree-Ring Chronologies

A master skeleton plot is not a tree-ring chronology, however; it is simply a graphical representation of relative ring widths—very useful for dating, but less useful for reconstructing climate. In order to develop a quantitative chronology of the cross-dated ring series, each ring on each sample must be measured to the nearest 0.01 mm. The LTRR uses a Velmax microscopic measuring system (Figure 8.8) that automatically inputs the measurements onto a computer disk. For this project, we measured 33,004 individual rings from the live-tree samples (Table 8.2); other samples used in the reconstruction (see below) had been measured previously.

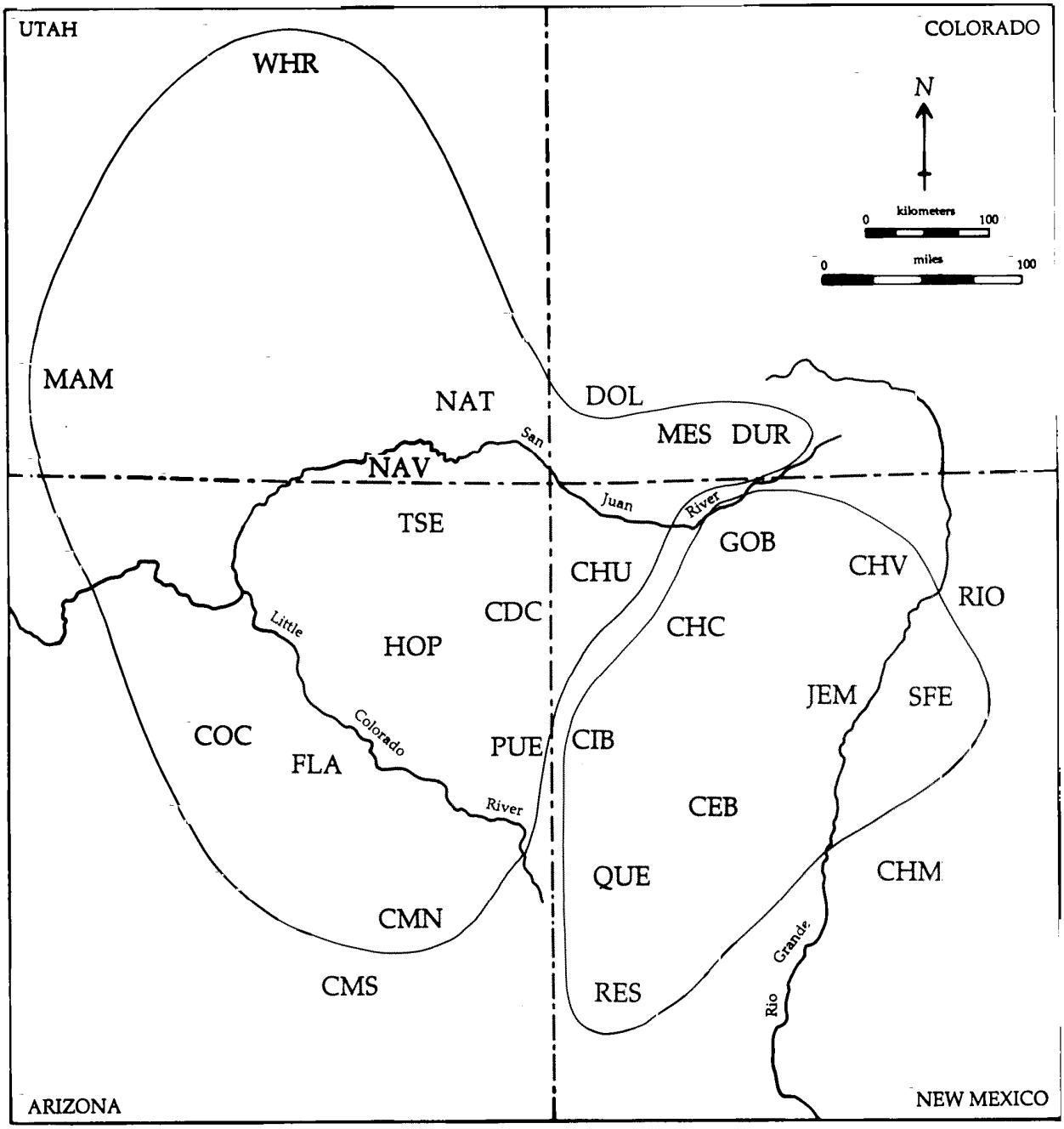

Figure 8.7. Chronology building process.

Figure 8.8. Measuring tree rings.

Table 8.2. Descriptive statistics of the live-tree chronologies.

Chronology Name	Elevation	Aspect	Species	Number of Samples	Dates	Number of Measured Rings	Series Intercorrelation	Mean Sensitivity	Percent Missing Rings
Alta Mesa PNN	8000'	WSW	PNN	24	1534–2005	7140	0.779	0.426	2.52
Alta Mesa DF	8000'	WSW	DF	19	1652–2005	3258	0.882	0.599	1.16
Pine Springs PP	7260'	N	PP	24	1777–2005	4418	0.805	0.609	4.54
Upper Los Alamos PP	7250'	SSE	PP	27	1659–2005	6238	0.824	0.499	1.96
Los Alamos C PP	6680'	N	PP	30	1786–2005	5693	0.833	0.511	1.58
Paliza CG PNN	6750'	SE	PNN	25	1645–2005	6257	0.773	0.559	4.24
Totals				**149**		**33004**			

Measuring the samples provides more information than simply ring width. By using the computer program COFECHA we were are able to evaluate the accuracy of our cross-dating and determine the strength of our chronologies (Holmes 1983). The computer program also enables us to measure the within- and between-tree variation, and compare the mathematical correspondence of each of our chronologies.

Table 8.2 shows the descriptive quantitative data that guided our sample and chronology selection. The variables shown in the last three columns of the table show the utility of the chronologies for dendroclimatic purposes. The series intercorrelation is a measure of how much variability in individually dated rings exists in the chronology (i.e., how much variability is seen in the AD 1729 ring among the trees at the same site). Simply put, the series intercorrelation indicates how much ring-width variation in the series is common to all trees—and presumably due to climate. Therefore, the higher the series intercorrelation, the stronger the climate signal in our chronologies. The correlations are similar, but the Alta Mesa Douglas-firs show the highest correlation.

Mean sensitivity is a statistic developed in dendrochronology that considers the frequency of missing rings, series intercorrelation, and other factors. In theory, mean sensitivity can vary between "0" and "2." A mean sensitivity of "0" indicates no ring-width variability meaning that all rings are exactly the same size. Conversely, a means sensitivity of "2" indicates that every other ring in the series is missing (50% missing rings). In practice, neither of these extremes is reached because such samples cannot be cross-dated—the "0" series because there is no variability and the "2" series because there is too much variability. Typically, mean sensitivity varies between 0.25 and 0.75, depending on the species, tree age, and site location. Again, our chronologies are similar, although the Pine Springs chronology is the most sensitive.

The percent of missing rings is also a general indicator of site growing conditions and contributes to mean sensitivity. Whereas Upper Los Alamos, Los Alamos Canyon, and Alta Mesa are relatively mesic sites, Pine Springs and Paliza Campground are relatively arid and the trees are subject to more water stress. Finally, Douglas-firs tend to have fewer missing rings than other tree species. This attribute of Douglas-firs is important because it allows us to cross-date more samples and verify the cross-dating of samples with more missing rings. After initial evaluation using COFECHA, some trees and cores were deemed unsuitable for quantitative analysis and were not included in the reconstruction.

Standardization

The next step in the reconstruction process is to standardize each ring series and create tree-ring indices for the samples. Standardization is accomplished using a curve-fitting equation and results in all series having a mean of "0" and a standard deviation of "1." This process eliminates the size- and age-related ring-width variability (i.e., rings near the pith are larger than those near the outside of the tree), retains the climate signal, and makes the ring series comparable. In the initial chronology building procedure, we standardized the ring series using the computer program ARSTAN. All measured ring-width series were standardized conservatively through the fitting of a modified negative exponential curve, a straight line, or a negatively sloped line to

the series. This process removes the age/size related growth trend and transforms the ring-width measurement values into ring-width index values for each individual ring in each series (Fritts 1976). By averaging the annual standardized indices of tree growth, we created mean site chronologies for each site. In general, these conservative standardization techniques and the use of long series preserve low-frequency information in the resulting chronologies (Cook et al. 1994). This process resulted in six independent, quantitative tree-ring chronologies that could be selected for the climate reconstructions**.**

Calibration of the Tree-ring/Climate Relationship

The next step in the reconstruction is calibrating the tree rings against modern climate data and assessing the strength of that relationship. This step necessitates (a) testing the association between the modern part of the chronology and instrumental climate data to determine the strength and seasonality of the climatic influence on tree growth with correlation analysis; (b) calibrating the climate data and the tree-ring chronology using a statistical scaling technique; and (c) retrodicting past climate for the length of the tree-ring chronologies. See Fritts (1976) for more details on developing dendroclimatic reconstructions. Two calibrated and verified reconstructions of wet-season (previous October through June) precipitation were developed from the tree-ring chronologies—one for the northern region (Chama) and one for the southern region (Jemez Springs). Each of these reconstructed time-series of past precipitation was then smoothed using a 20-year cubic smoothing spline. The final products are four time series: two for the northern part of the study area (one to emphasize high-frequency [annual] variability and one to emphasize low-frequency variability) and two for the southern part of the study area (similarly, one high frequency [annual] and one low frequency).

We compared the tree-ring indices for the modern period with instrumental precipitation data from the United States Historical Climatology Network (USHCN). These data are part of a quality-controlled network and are considered highly reliable. In the southern section, we compared four tree-ring series to USHCN data from Jemez Springs, New Mexico. In the northern section, we compared USHCN data from Chama, New Mexico, to the two tree-ring series. In both cases, correlation analysis showed a strong positive correlation between wet-season (previous October through June) precipitation and tree-ring index. There is negligible correlation between summer precipitation and tree growth. This is consistent with other tree-ring based precipitation reconstruction studies in the U.S. Southwest ((D'Arrigo and Jacoby 1991). For each "year" the precipitation amounts for previous October to June were totaled. These amounts form the basis for the calibration with the tree-ring data.

Growth processes of lower-elevation trees in the Southwest often are limited by climatic conditions during a period before the actual growing season (Fritts 1976). Ring-width variability can reflect changes in precipitation amounts from the fall/winter seasons before the trees' growing season through the growing season of ring formation. The period from the previous October through June of the growing season is the seasonal climatic interval most highly correlated with annual tree-ring width and was determined to be the interval when precipitation had the greatest effect on tree growth. Monthly values for this period were summed for the individual years to create the final climate series used in the reconstructions. Consequently, the variable being reconstructed is prior-October through current June precipitation.

In total, there are six new (seven modern living-tree) and two archaeological tree-ring series used in the reconstructions. Because of the absence of long-lived trees in the project area, previously measured ring-width series of beams from archaeological sites (LTRR files) were appended to the earlier portions of measured series from living trees near the sites in order to substantially lengthen the records. In both the northern and southern portions of the study area, the archaeological chronologies are shown to be consistent with the modern living-tree chronologies used in the calibration (Figures 8.9 and 8.10). This is an important point and suggests that the new living-tree chronologies are an adequate analog for what occurred in the past—the earlier portion of the reconstructions. The southern and northern chronologies were lengthened in the following manner.

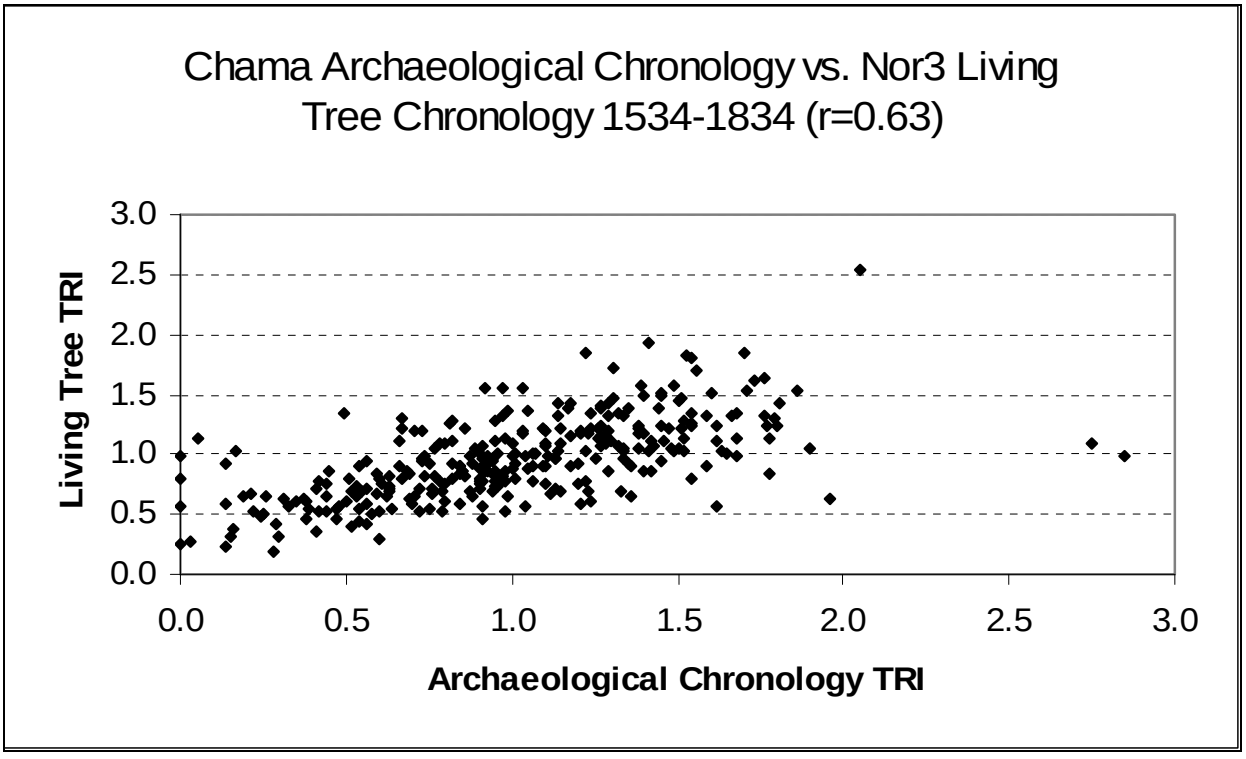

Figure 8.9. Correlation of archaeological and living tree samples from Chama.

At Jemez, we took an average of the tree-ring indices from four new sites: Paliza Campground (piñon), Upper Los Alamos, Los Alamos Canyon, and Pine Springs (all ponderosa pine). This process of combining or compositing several chronologies into a single series reduces non-climatic "noise" in the tree-ring data and strengthens the climatic signal. The new tree-ring average chronology extends back to AD 1645 and correlates very well with the Jemez Springs USHCN previous October to June precipitation series (r = 0.78, 1911–2002). Before AD 1645 (AD 598–1644), the Jemez archaeological chronology was used.

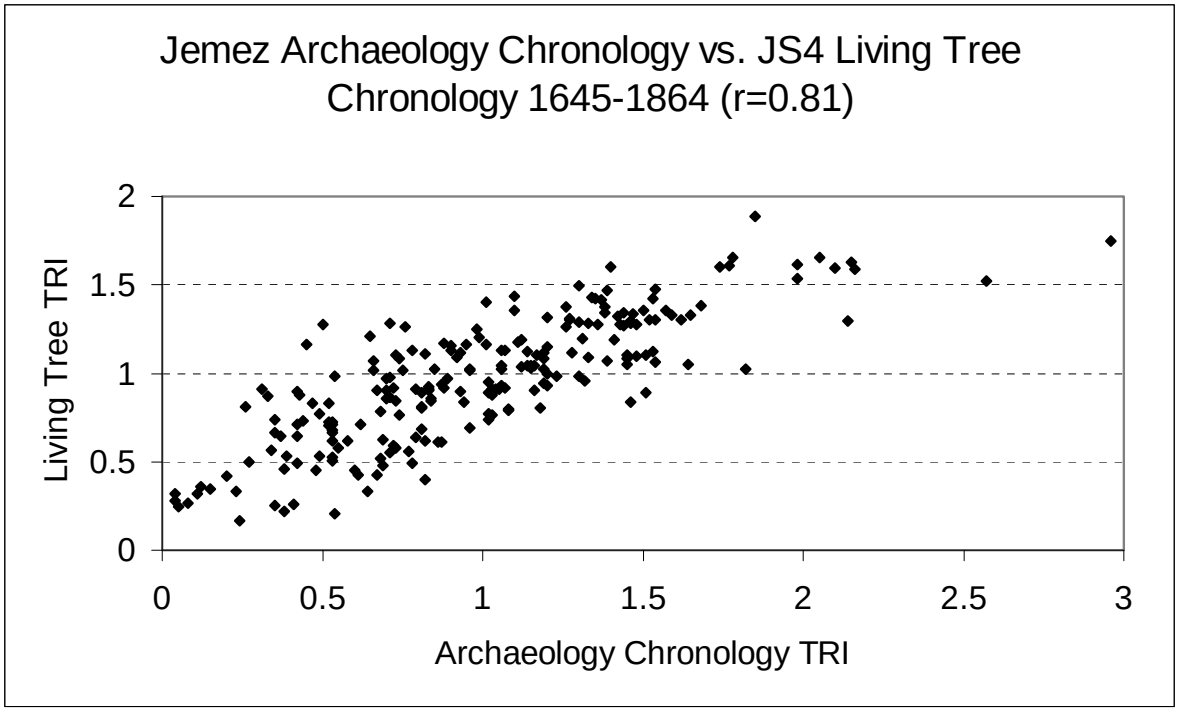

Figure 8.10. Correlation of archaeological and living tree samples from the Jemez.

For the northern reconstruction at Chama, we used two new tree-ring chronologies, both from Alta Mesa, New Mexico (Douglas-fir and piñon). These extend back to AD 1534 and correlate well with modern USHCN precipitation data from Chama (r = 0.66, 1889–2002). The tree-ring series used in the northern reconstruction is a more complicated composite than that used in the southern reconstruction. In the earliest part, AD 759–1361, it consists only of the Chama archaeological chronology (LTRR files); from 1362 to 1533, it is the archaeological chronology combined with the Echo Amphitheatre living tree chronology collected in the 1970s (Dean and Robinson 1977); from 1534 to 1834 it is an average of the new Alta Mesa chronologies and the Chama/Echo chronologies; from 1835 to 1972 it is an average of the Alta Mesa and Echo chronologies without any archaeological wood; and from 1973–2002 only the new Alta Mesa average was used.

For both Jemez and Chama, we scaled the tree-ring width index values to the previous October to June precipitation instrumental data for the period of record to equate their means and standard deviations (Figures 8.11 and 8.12). Scaling in this manner has been used as a calibration device in some recent multi-proxy reconstructions of past temperature (Moberg et al. 2005). This type of calibration, as opposed to regression techniques, tends to maintain rather than suppress amplitudes. It is clear that the ring-width variability and reconstructed precipitation anomalies co-vary in both their interannual and decadal-scale frequencies.

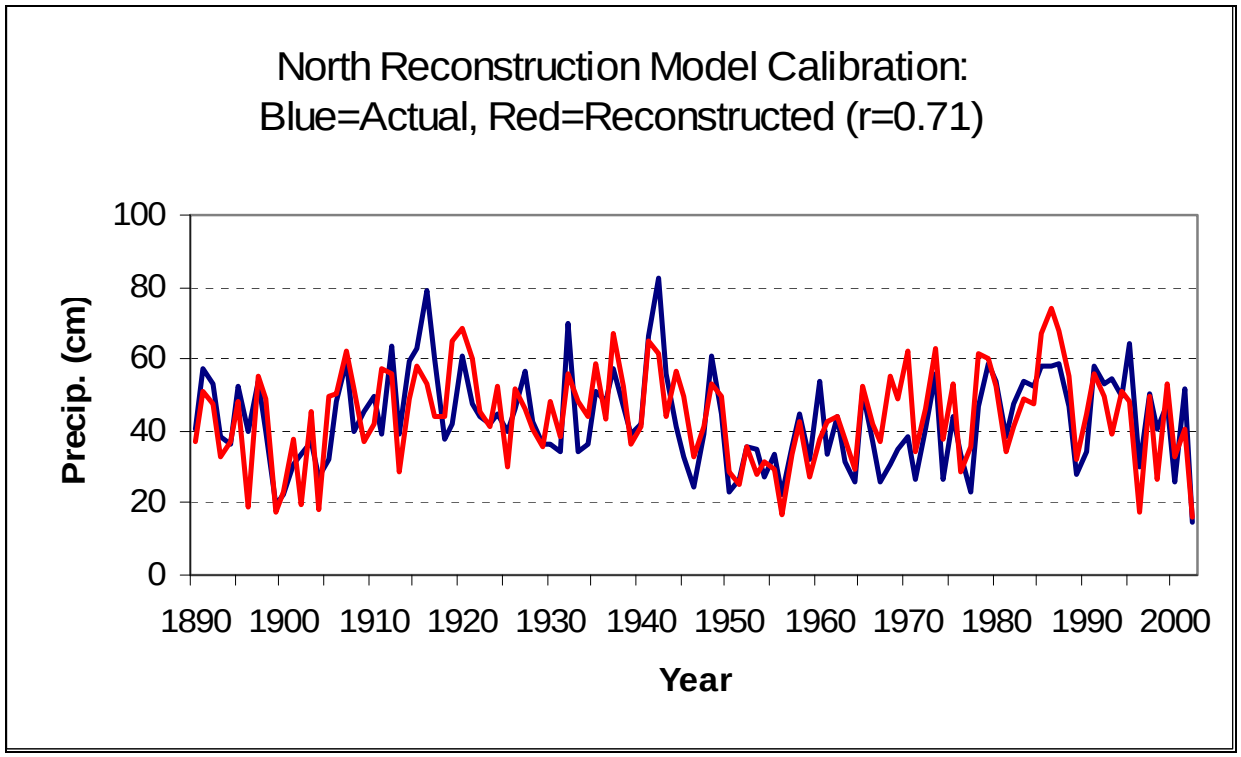

Figure 8.11. Calibration period comparison of Chama tree growth and historical data.

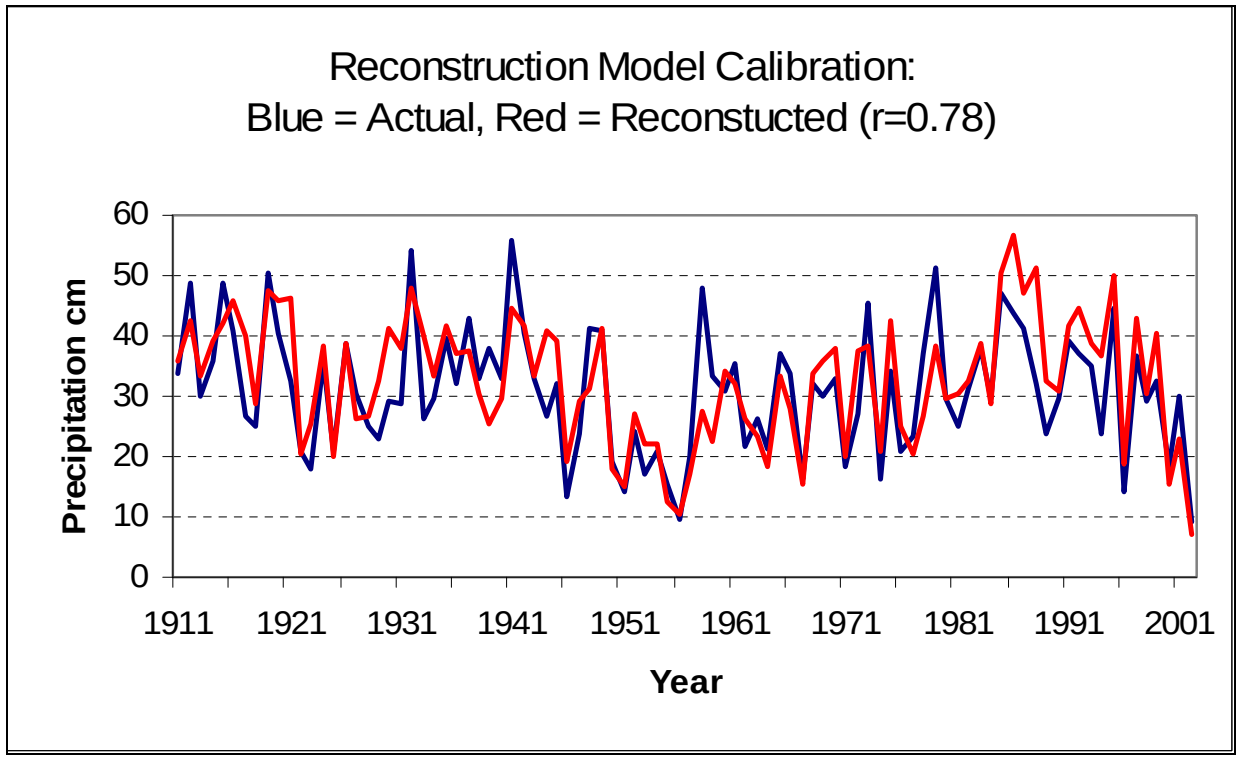

Figure 8.12. Calibration period comparison of Jemez tree growth and historical data.

The calibration followed Moberg et al. (2005) and can be formally expressed as follows:

$$P(t) = f \cdot R(t) + c \ ,$$

where P is the instrumental precipitation data, R is the ring-width index chronology, f is a variance scaling factor, c is a constant that adjusts the mean, and t is time. The factor f and constant c are derived by:

$$f = S_P/S_R \qquad \text{and} \qquad c = P_{(mean)} - f \cdot R_{(mean)}$$

where S_P and S_R are the respective standard deviations of the instrumental precipitation data and the ring-width index chronology in the overlapping interval and $P_{(mean)}$ and $R_{(mean)}$ are the corresponding means. The long Jemez and Chama tree-ring chronologies were scaled in this manner to produce the southern (Jemez) and northern (Chama) precipitation reconstructions (see below).

RESULTS

Jemez Chronology: Long-Term, Low-Frequency Precipitation Trends

The Jemez reconstruction of low- and high-frequency trends in precipitation in the Pajarito Plateau area is shown in Figure 8.13; the raw data are presented in Appendix H. The long-term precipitation mean for the area is 31.32 cm per tree-year, and the standard deviation is 10.49 cm per year. For any substantial period of time (100+ years) over the course of the reconstruction, the mean changes very little. Several aspects of the reconstruction merit detailed discussion.

First, overall, Figure 8.13 shows the most variable precipitation between AD 600 and approximately AD 900; the extremes are both higher and lower during this period than during most other periods. Another period of significant variability is the late 1400s through the early 1600s. Extreme highs in the early and late 1500s are contrasted with deep lows in the mid to late 1500s. In contrast, periods of generally low variability include the late 1200s through the early 1400s and the 1700s and early 1800s.

If variability is measured in overlapping 20-year increments, however, a different picture emerges. The AD 600 to 900 period shows variability, but most of the fluctuations are near or above the mean. Beginning in the late 800s, a significant decline in precipitation lasts through the early 10th century. Temporal variability changes about AD 1000 and lasts until the beginning of the 15th century. The peaks and valleys of the graph are farther apart, indicating precipitation was variable at longer time scales, even if mean precipitation was lower. This low-frequency variation is typically the type of change to which human societies adapt (Doyel and Dean 2006; Dean et al. 1994). The period from about 1500 though the late 1800s is characterized by higher frequency changes, particularly after AD 1700. Lower-frequency changes returned in the 20th century.

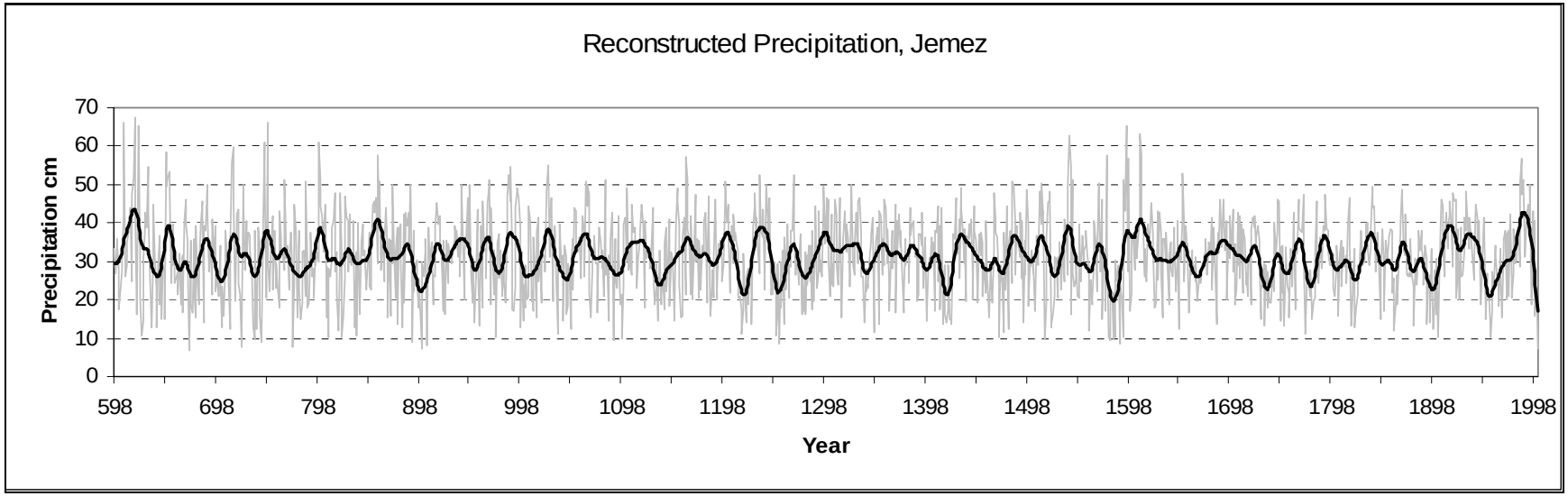

Figure 8.13. Annual and splined precipitation graph for the Jemez chronology.

In terms of absolute precipitation, high precipitation periods tend to be slightly more common in the early part of the reconstruction and low precipitation periods more common after AD 1200. Notable droughts are centered on the late 800s, the late 1000s to early 1100s, the late 1200s, the early 1400s, the late 1500s, the late 1800s, and the mid-1900s. Wetter intervals include the early 600s, the late 700s, the mid-800s, the early 1200s, the early 1400s, the early 1600s, the early 1900s, and the late 1900s.

Jemez Chronology: High-Frequency Variation

By statistical definition, any year within one standard deviation of the mean (e.g., between 20.83 and 41.81 cm of precipitation per year) would be considered normal. Embedded in the annual precipitation values is information concerning high-frequency variation and extreme years that may have significantly impacted human groups in the Pajarito area. If a year with a precipitation value within a single standard deviation of the mean is considered normal, those outside of the range can be considered extreme to some degree. Towner (1997) suggests that "Good" and "Bad" years can be defined as more than one standard deviation from the mean and "Very Good" and "Very Bad" years defined as two standard deviations above or below the mean, respectively.

Most century-long periods exhibit similar numbers of extremely good and extremely bad years. This pattern is an illustration of the variability and short-term unpredictability of precipitation on the Colorado Plateau (cf. Euler et al. 1979). Indeed, over the length of the reconstruction, slightly more than 30 percent of the annual values are more than one standard deviation from the long-term mean. In human terms, these data indicate that almost one in every three years was either ‘Good,’ ‘Bad,’ ‘Very Good,’ or ‘Very Bad.’ Given the human propensity for remembering stressful times, it is not surprising, therefore, that historical documents and even oral traditions have recorded more "drought" times than times of plenty (Reeve 1958, 1959).

It is instructive to examine extreme years on a century by century basis (Table 8.3) keeping in mind that the century designation are an artificial division based on the Christian calendar. Several centuries stand out as unusual.

Table 8.3. Extreme years by century, Jemez chronology.

Century	Century Mean	Very Good	Good	Average	Bad	Very Bad
600–699	32.62	7	12	62	18	1
700–799	30.42	5	8	67	16	4
800–899	32.43	3	12	69	13	3
900–999	31.82	2	15	62	18	3
1000–1099	30.24	1	11	66	20	2
1100–1199	31.47	1	10	72	17	0
1200–1299	30.83	1	14	67	17	1
1300–1399	32.27	0	13	77	10	0
1400–1499	30.89	0	11	69	19	1
1500–1599	30.83	**6**	**13**	**59**	**17**	**5**
1600–1699	32.34	3	4	82	11	0
1700–1799	30.27	0	8	77	17	0

Century	Century Mean	Very Good	Good	Average	Bad	Very Bad
1800–1899	29.77	0	6	81	13	0
1900–1999	32.69	1	14	69	16	0
2000–2002	n/a	0	0	1	1	1
Total		**30**	**151**	**980**	**223**	**21**

The 600s exhibited the second highest century mean and had equal numbers of extreme years. The high number of 'Very Good' years (n = 7) were all concentrated in the first 52 years of the century. Strings of consecutive 'Good' years occurred in 616–619 and 649–653, and only one consecutive string of 'Bad' years occurred (627–628).

The 700s were below the long-term precipitation average and experienced 20 'Bad' or 'Very Bad' years and five 'Very Good' years (all in the first half of the century). Consecutive 'Good' years occurred in 714–716 and there was never a string of three consecutive 'Bad' years. Thus, the last half of the AD 700s were certainly not optimal for rainfall-dependent agriculturalists. We leave it to Pajarito area archaeologists to discuss the potential cultural adaptations to this extremely dry period.

The following century (AD 800s) is notable for a return to higher precipitation values, and a "normal" number of extreme years. 'Good,' 'Bad,' 'Very Good,' and 'Very Bad' years occurred in almost the same frequency and were more or less evenly distributed throughout the century. Three 'Good' years (AD 800–802) started the century and is the only three-year period of either extreme.

The AD 900s had a relatively high number of extreme years (n = 38) and slightly above average precipitation. Consecutive extreme years occurred three times, all late in the century (AD 966–968, AD 986–989, and AD 994–997). In general, the century was drier early and wetter late.

The AD 1000s were, on average, the driest century in the reconstruction period, and contained 34 extreme years; there were only two 'Very Bad' years, but 20 'Bad' years. All but one of the 'Good' years occurred before AD 1067, but there were two 'Good' consecutive-year periods (AD 1024–1026 and AD 1063–1066). In general, the latter half of the century was drier than the first half.

The AD 1100s exhibit near mean precipitation and slightly fewer extreme years; no consecutive-year extremes were noted in the century. The mid-1130s were dry. Six of the 10 years in the decade were 'Bad,' but in general, extreme years were distributed more or less evenly throughout the century. This period coincides with the "Chaco drought" farther west, but does not appear to have been extreme in the northern Rio Grande area

The AD 1200s exhibited below average precipitation, some extreme years (n = 33), but positive and negative departures from the mean were more or less equal. The only string of 'Good' years occurred in AD 1216–1218, and no bad strings were identified. In general, the AD 1230–1250 period was wet, as was the AD 1290–1299 period, but the middle of the century was dry. The Great Drought (AD 1276–1299) of the Four Corners area appears to have been much shorter and less severe in the Pajarito area

The AD 1300s present a very different story. They were one of the wettest centuries in the reconstruction, had the most average years, and contained no 'Very Good' or 'Very Bad' years; nor were there any consecutive three-year periods of extreme precipitation. In short, the AD 1300s were relatively wet and consistent. Extreme years, 'Good' or 'Bad,' were distributed more or less evenly and never occurred for long periods of time.

The AD 1400s were much drier and experienced more 'Bad' years than 'Good' and there were two multi-year extreme periods (AD 1418–1420 and AD 1422–1424). In particular, the early part of the century was much drier than normal, and wet years occurred only infrequently.

The AD 1500s were also quite dry, but contained the highest frequency of extreme years in the entire reconstruction ($n = 41$). 'Very Good' years were offset by 'Very Bad' years. Consecutive multi-year 'Good' periods include AD 1519–1521, AD 1539–1541, and AD 1594–1597; 'Bad' periods include AD 1522–1524 and AD 1579–1561. It is interesting to note that some of the wettest years in the entire reconstruction occurred when Coronado was encamped in New Mexico (AD 1539–41) and just before Oñate's colonization of the Rio Grande (AD 1594–1597). The megadrought of the AD 1570s–1590s noted elsewhere appears to have been shorter (AD 1573–1593) and less severe in the Pajarito area; it contained six 'Bad' and three 'Very Bad' years that were only partially mitigated by one 'Very Good' year. Because the annual means were consistently low, even if not extreme, the dry years probably had a more deleterious effect on the local environment.

The AD 1600s contained fewer extreme years than any other century in the reconstruction and there were no three-year extreme periods. The latter half of the century was certainly more variable than the early part, but exhibited many 'Good' years. The idea that a drought played a major role in the Pueblo Revolt of 1680 is not supported by the dendroclimatic data. The year of the revolt (AD 1680) was an average year (41.55 cm) in the Pajarito area, and no 'Bad' years occurred between AD 1676 and AD 1684. Historical references to drought, therefore, are probably better interpreted as food shortages caused by severe disruptions in trade, labor, scheduling, and tribute responsibilities of the Rio Grande pueblos. Clearly, the causes of the Pueblo Revolt lie in the social and economic policies of the Spanish Colony, not in environmental perturbations

The AD 1700s were relatively dry; mean precipitation was 30.27 cm, but the century contained neither 'Very Good' nor 'Very Bad' years. 'Bad' years ($n = 17$) far outnumber 'Good' years ($n = 8$), and there were two strings of 'Bad' years (AD 1737–1739 and AD 1779–1782), but no strings of 'Good' years. The latter half of the century was probably drier than the first half, but some wet years did occur.

The AD 1800s were the driest century in the reconstruction (mean precipitation 29.77 cm), but contained neither 'Very Good' nor 'Very Bad' years. The only consecutive string of extreme years was the AD 1839–1841 dry period.

The AD 1900s are notable for two trends. The century mean is the highest in the reconstruction (32.69 cm), and there was significant variability. The first few years of the AD 1900s were marked by drought as were the mid-1950s. In contrast, the late 1910s and mid-1980s were wet.

Jemez Chronology: Extreme Events

Extreme events can have serious impacts on human societies. Extreme droughts may lead to crop failures, changes in storage technologies and agricultural strategies, site abandonments and migrations, and many other sociological and technological changes. Likewise, high precipitation years or events may lead to flooding and crop failure, increased erosion and arroyo cutting, and even such phenomenon as increased disease-carrying rodent populations (e.g., hantavirus).

Table 8.4 presents the 25 highest and 25 lowest precipitation years in the Jemez reconstruction. The range of precipitation is quite impressive, ranging from a low of 6.91 cm in AD 672 to a high of 67.42 in AD 618. Nine of the driest years and eight of the wettest years fall within the Bandelier chronology periods defined by Orcutt (1999; see below).

Table 8.4. Twenty-five wettest and driest years in the Jemez reconstruction.

Jemez		Jemez	
Year	**Driest**	**Year**	**Wettest**
672	6.91	618	67.42
901	7.15	608	66.20
2002	7.15	749	65.96
723	7.89	622	65.47
774	7.89	1596	65.47
907	8.13	621	63.27
1254	8.62	1610	63.03
1590	8.62	1540	62.79
743	9.11	800	61.08
892	9.11	746	60.83
1580	9.35	715	59.61
1090	9.59	649	58.64
736	9.84	858	57.66
1099	9.84	1611	57.66
1516	9.84	1577	57.42
1583	9.84	1162	57.17
823	10.08	1599	56.93
975	10.08	1986	56.64
1585	10.08	714	55.95
1904	10.32	1026	54.98
809	10.33	989	54.73
1471	10.33	631	54.49
1579	10.33	1541	54.49

Jemez		Jemez	
Year	**Driest**	**Year**	**Wettest**
1593	10.33	1597	53.76
1956	10.43	652	53.27

In terms of centuries, the AD 1500s stand out as unique with seven of the 25 driest years as well as six of the 25 wettest years. Such variability almost certainly was a challenge for the Puebloan occupants of the area. However, the centuries from AD 800–1500 were relatively free of these extreme years; particularly the period from AD 1100–1500, which experienced two extremely dry years and a single extremely wet year. As noted above, critical years of the Spanish exploration and colonization of New Mexico were quite favorable. Coronado experienced two wet years in AD 1540 and AD 1541; Oñate marched up the Rio Grande on the heels of wet years in AD 1596 and AD 1587 and experienced a wet year in AD 1599; later, he moved the capital during the two wettest years, AD 1610–1611, of the 17th century. We present the raw data in Appendix H so that Pajarito area archaeologists may explore any possible relationships between extreme events and cultural changes.

Jemez Chronology: The Bandelier Archaeological Periods

Orcutt (1999) developed an archaeological chronology of the Bandelier area based primarily on seriation of ceramics. Because we are interested in the entire human occupation of the area, we added several periods to the Orcutt chronology (see below). These periods are defined based on political events in New Mexico history and may or may not correlate with the archaeological or climatic records.

Period 1 (AD 1150–1190)

This period is defined as the Early Coalition and represents the initial settlement of the Bandelier area (Orcutt 1999). The period has a mean of 31.91 cm and standard deviation of 11.26 cm, both of which are greater than their long-term counterparts. 'Bad' years outnumber 'Good' years and there is only one 'Very Good' year (AD 1162), which ranks as the 16th wettest year in the chronology. 'Good' and 'Bad' years are distributed about evenly throughout the period and there are no consecutive strings of extreme years. In general, the period was slightly wetter than normal, but had more variable precipitation than normal as well.

Period 2 (AD 1190–1220)

This period remains part of the Early Coalition in Orcutt's (1999) archaeological chronology. It has a period mean of 31.24 cm and standard deviation of 9.85 cm, both of which are lower than the long-term values. The only consecutive string of extreme years is the AD 1216–1218 period; however, the initial years of the 13th century (AD 1200–1203) include three 'Good' years and a normal year, but the AD 1214–1218 period includes four 'Bad' years and one normal year. The period was slightly drier than normal and exhibited less variability than normal.

Period 3 (AD 1220–1235)

This short period is still part of the Early Coalition. It has a mean of 31.05 cm, slightly lower than the long-term mean and a standard deviation of 11.63 cm, which is substantially higher than the long-term standard deviation. 'Good' years and 'Bad' years were equal in frequency and there were no signs of extreme years. In general, the period was slightly drier than normal, but had a wider variation in precipitation. With such a short period, however, these statistics may not be very meaningful.

Period 4 (AD 1235–1250)

This period brings the Early Coalition to a close. It has a mean of 35.40 cm and a standard deviation of 10.48. There were no 'Bad,' 'Very Bad,' or 'Very Good' years, and four 'Good' years, but not in a consecutive string. All four 'Good' years occurred before AD 1245, however. The period appears to have been the wettest period in the reconstruction, but its small size makes such an inference uncertain.

Period 5 (AD 1250–1290)

This is the first period in the Late Coalition (Orcutt 1999). It has a mean of 28.15 cm and a standard deviation of 9.52, both of which are substantially lower than their long-term values. 'Bad' and 'Very Bad' years outnumber 'Good' and 'Very Good' years 11 to 2, but there are no consecutive strings of extreme years. The early part of the period (AD 1251–1258) had four 'Bad,' one 'Very Bad,' and three normal years (all of which were low precipitation years); the 'Very Bad' year (AD 1254) ranks as the seventh driest year in the chronology. The late part of the period encompasses much of the Great Drought (AD 1276–1299) and contains five 'Bad' years. In general, the period was dry and not variable.

Period 6 (AD 1290–1325)

This period represents the end of the Late Coalition. It has a mean of 34.43 cm and a standard deviation of 9.97. 'Good' years far outnumber 'Bad,' but there are neither 'Very Good' nor 'Very Bad' years, nor are there any consecutive strings of extreme years. The early portion of the period, AD 1290–1302, contained six 'Good' years and seven normal years, but the remainder of the period was mostly within the normal range of variation. The period was wet and not extremely variable.

Period 7 (AD 1325–1375)

This period encompasses much of the Early Classic (Orcutt 1999). It has a mean of 32.26, higher than the long-term mean, and a standard deviation of 9.15, lower than the long-term value. The frequency of 'Good' and 'Bad' years is about equal, and there are no 'Very Good' or 'Very Bad' years; neither are there any consecutive strings of extreme years. The period was slightly wetter than normal with less variability, but the measures are not extreme.

Period 8 (AD 1375–1400)

This short period marks the end of the Early Classic period of the archaeological chronology. It has a mean of 30.23 cm and a standard deviation of 8.57, both of which are substantially lower than the long-term values. There are four 'Bad' years and one 'Good' year, but no consecutive strings of 'Very Good/Very Bad' years. The period was apparently dry with little variability, but the short duration of the period makes such measures suspect.

Period 9 (AD 1400–1440)

This period is the early part of the Middle Classic period. It has a mean of 29.90 cm and a standard deviation of 10.27, both of which are lower than the long-term values. 'Bad' years (n = 10) outnumber 'Good' (n = 5) and there were two strings of 'Bad' years, AD 1418–1420 and AD 1422–1424; indeed, the AD 1415–1424 period contained seven 'Bad' years and three normal years (all of which were below the period mean). The period was generally dry and not very variable.

Period 10 (AD 1440–1525)

This is a large portion of the Middle Classic period in the archaeological chronology. It has a mean of 31.44 cm and a standard deviation of 10.54, both of which are very close to the long-term values. There are only two consecutive strings, both near the end of the period; AD 1519–1521 was 'Good,' but AD 1522–1525 was 'Bad.' In general, the early two-thirds of the period was dry or normal, and only the AD 1510–1521 period was wet. One of the 'Very Bad' years (AD 1516) ranks as the 15th driest year in the chronology.

Period 11 (AD 1525–1610)

This period encompasses the end of the Late Classic period and beyond in the archaeological chronology. It has a mean of 30.46 cm, substantially lower than the long-term mean, and a standard deviation of 13.07 cm, significantly greater than the long-term value. The period is notable for the greatest frequency of 'Very Good' and 'Very Bad' years of any period in the chronology. Consecutive 'Good' years occurred in AD 1539–1541 and AD 1594–1597, and consecutive 'Bad' years occurred in AD 1579–1581. All six 'Very Bad' years in this period (AD 1579, AD 1580, AD 1583, AD 1585, AD 1590, and AD 1593) rank in the top 25 driest years in the chronology, and likewise, all six 'Very Good' years (AD 1540, AD 1541, AD 1577, AD 1596, AD 1597, AD 1599, and AD 1610) rank in the top 25 wettest years in the chronology. In general, the period was dry but highly variable.

Period 12 (AD 1610–1680)

This period is defined by the founding of the Spanish capital in Santa Fe and ends with the Pueblo Revolt. As such, it encompasses much of the early Spanish colonization era. The precipitation mean for the period is 32.11 cm, which differs from the long-term mean by +0.79 cm, and the period standard deviation is 9.11, which differs from the long-term standard deviation by –1.38. There are no three-year strings of extreme years (see Table 8.4). The first

two years of the period (AD 1610–1611) were 'Very Good,' however, and may have facilitated the Spaniards' move to Santa Fe. Indeed, both AD 1610 and AD 1611 rank in the top 14 wettest years in the chronology. Two two-year periods (AD 1624–1625 and AD 1666–1667) were 'Bad,' but in general much of the period experienced normal amounts of precipitation. 'Bad' years were distributed relatively evenly throughout the period. Notably, AD 1680 was relatively wet (41.55 cm), but is not classified as a 'Good' year (41.71 cm); in addition, none of the 12 years before AD 1680 was 'Bad.' Thus, a precipitation deficit probably had little to do with the Pueblo Revolt.

Period 13 (AD 1680–1692)

This short period is defined by the Pueblo Revolt and ends with the Spaniards' return to the north. The period mean is 33.94 cm, compared to the long-term mean of 31.32, and the period standard deviation is 8.95, compared to the long-term standard deviation of 10.49. There was only one 'Bad' year (AD 1685) and two 'Good' years (AD 1689 and AD 1692). The later good year may have impacted de Vargas' return to New Mexico in some fashion.

Period 14 (AD 1693–1753)

This period is defined by the Reconquest and ends with the rise of Ute and Comanche threats in the north and the attack on Abiquiu. The period mean is 30.0 cm, compared to the long-term mean of 31.32, and the period standard deviation is 8.97 compared to the long-term standard deviation of 10.49. There is one period of consecutive extreme years, the 'Bad' years of AD 1737–1739; in addition, the AD 1729–1739 period included six 'Bad' and five normal years. Thus, the period was generally drier and less variable than normal.

Period 15 (AD 1754–1821)

This period is defined by the rise of the Ute/Comanche threat and ends with Mexican independence. The period mean is 30.29 cm and standard deviation is 8.63; both measures are below their long-term counterparts. There is only one string of extreme years—the 'Bad' years of AD 1779–1782. There were no 'Very Good' or 'Very Bad' years, and 'Good' and 'Bad' years are distributed throughout the period. In general, the period was dry and not very variable.

Period 16 (AD 1822–1849)

This is the period from Mexican independence until the U.S. acquisition of New Mexico. The period mean is 31.49 cm, slightly above the long-term mean, and the standard deviation is 8.65, significantly below the long-term measure. There is only one consecutive string of extreme years—the 'Good' years of AD 1839–1841; the first two years of the period (AD 1822–1823) were 'Bad' years.

Period 17 (AD 1850–1912)

This period is defined by the US acquisition of New Mexico and ends with Statehood. The period mean is 29.43 cm , significantly lower than the long-term mean, and the standard

deviation is 9.00, also below the long-term measure. There were no consecutive strings of extreme years, but 'Bad' years (n = 11) outnumbered 'Good' (n = 4), and most of the 'Bad' years occurred between AD 1861–64 (three 'Bad' and one normal) and between AD 1893–1904 (six 'Bad' years and six normal years). The 'Very Bad' year of AD 1904 ranks as the 20th driest year in the chronology.

Period 18 (AD 1913–2002)

This period is defined by New Mexico statehood and ends with the end of the reconstruction. The period mean is 32.45 cm and the standard deviation is 10.40. There were two 'Good' strings (AD 1919–1921 and AD 1985–1988) and one 'Very Bad' string (AD 1955–1957). The 1950s included five 'Very Bad' and five normal years. In general, the period was normal or wet until the 1950s, dry from the 1950s through early 1970s, and wet throughout the remainder of the 20th century. The drought of the 2000s has included two 'Very Bad' years (AD 2000 and AD 2002). Two 'Very Bad' years (1956 and 2002) and one 'Very Good' year (1986) rank in the top 25 driest and wettest years, respectively (Table 8.5).

Table 8.5. Extreme years in the Bandelier archaeological periods, Jemez reconstruction.

Period	Dates	Mean	Standard Deviation	Very Good	Good Year	Average Year	Bad Year	Very Bad	Consecutive Strings
1	1150–1190	31.91	11.26	1	5	25	9	0	None
2	1190–1220	31.24	9.85	0	3	23	4	0	1216–1218 (-)
3	1220–1235	31.05	11.63	0	3	9	3	0	None
4	1235–1250	35.40	10.48	0	5	10	0	0	None
5	1250–1290	28.15	9.52	1	1	27	10	1	None
6	1290–1325	34.43	9.97	0	10	24	2	0	None
7	1325–1375	32.26	9.15	0	7	38	5	0	None
8	1375–1400	30.23	8.57	0	1	20	4	0	None
9	1400–1440	29.90	10.27	0	5	25	10	0	1480–1422 (-) 1422–1424 (-)
10	1440–1525	31.44	10.54	0	12	57	14	2	1519–1522 (+) 1522–1524 (-)
11	1525–1610	30.46	13.07	7	7	83	12	6	1539–1541 (+) 1579–1581 (-) 1594–1597 (+)
12	1610–1680	32.11	9.11	3	2	57	8	0	None
13	1681–1694	33.94	8.95	0	2	10	1	0	None
14	1695–1753	30.00	8.97	0	4	43	11	0	1737–1739 (-)
15	1754–1821	30.29	8.63	0	5	52	9	0	1779–1782 (-)

Period	Dates	Mean	Standard Deviation	Very Good	Good Year	Average Year	Bad Year	Very Bad	Consecutive Strings
16	1822–1849	31.49	8.65	0	3	21	3	0	1839–1841 (-)
17	1850–1912	29.43	9.00	0	4	46	11	0	
18	1913–2002	32.45	10.40	1	12	61	14	1	1919–1921 (+) 1957–1955 (-) 1985–1988 (+)

Chama Chronology: Long-Term, Low-Frequency Precipitation Trends

The Chama reconstruction of low- and high-frequency trends in precipitation in the northern area is shown in Figure 8.14; the raw data are presented in Appendix I. The long-term precipitation mean for the area is 43.34 cm per tree-year, and the standard deviation is 11.42 cm inches per year. For any substantial period of time (100+ years) over the course of the reconstruction, the mean changes very little. Although the Chama mean is substantially higher than the Jemez mean, the trends in the two chronologies are similar—as one would expect. There are however, some important differences that are discussed below.

The Chama reconstruction shows relatively consistent variability (i.e., the low-variability and high-variability periods are usually short). High-variability predominates in the late 800s and early 900s, and again in the late 1400s to early 1500s, whereas low variability is typical in the mid-1300s and late 1500s/early 1600s periods.

Using 20-year overlapping periods, however, shows a different trend. From the beginning of the chronology through the late 900s, variability over this longer term is relatively low. A period of high variability begins about AD 1000 and continues until the early 1100s. Low long-term variability again predominates from about AD 1150 through the mid-1400s. High variability typifies the period from the 1700s to the present.

In terms of absolute precipitation, there are several periods of high and low precipitation. High precipitation periods occur in the early 1000s, mid-1000s, mid-1300s, early 1600s, and throughout much of the 20th century. Low periods include late 1000s, early and mid-1200s, mid-1400s, late 1500s, and mid-1900s. Several well-known periods are different in the Chama area. For example, the "Chaco drought" of the mid to late 1100s shows low variability, but mostly average precipitation. The "Great Drought" of the late 1200s was neither lengthy nor severe in the Chama area. The most prolonged downturn in rainfall occurred during the 1400s—a drought that was long, but not extremely severe and extremely favorable precipitation dominated in the 1600s, a factor which may have aided the Spaniards colonization of northern New Mexico. Likewise, with the exception of the 1950s, which was the most severe drought in the

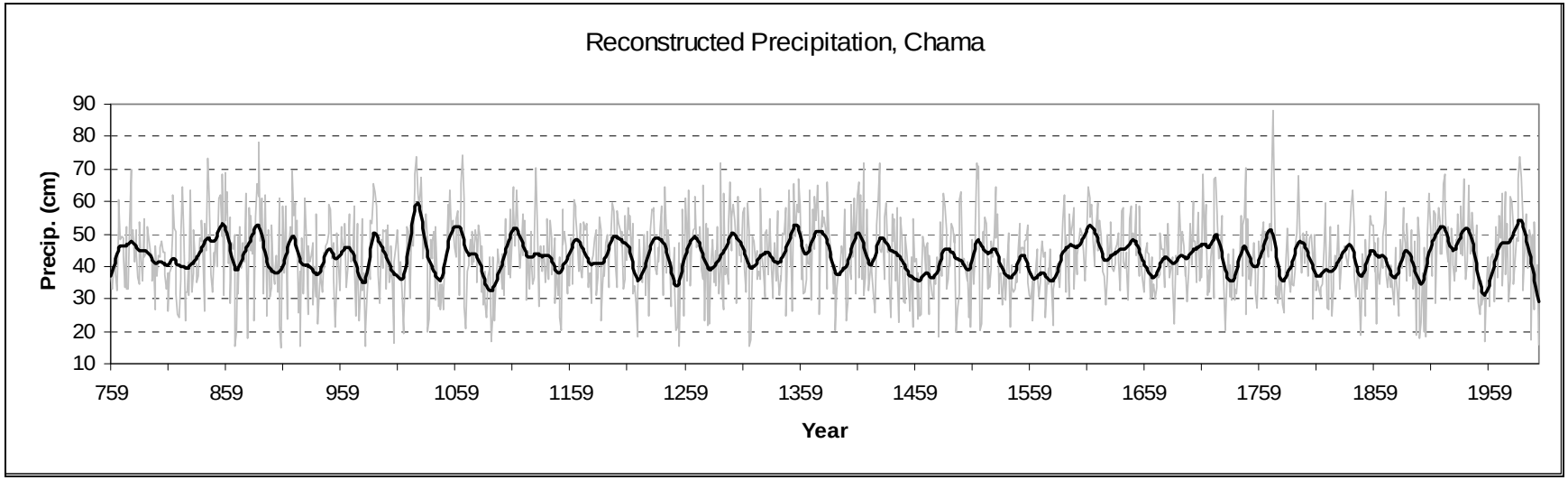

Figure 8.14. Annual and splined precipitation graph for the Chama chronology.

reconstruction, the 20th century shows high precipitation that many Anglos have come to regard as "normal" conditions.

Chama Chronology: High-Frequency Variation

Examining the Chama chronology in terms of individual centuries yields additional interesting results (Table 8.6). Because the reconstruction does not begin until AD 759, however, the AD 700s are not included in the discussion.

Table 8.6. Extreme years per century, Chama reconstruction.

Century	Century Mean	Very Good	Good	Average	Bad	Very Bad
600–699	--	n/a	n/a	n/a	n/a	n/a
759–799	--	0	2	37	1	0
800–899	44.63	4	17	61	15	3
900–999	42.48	1	15	69	12	3
1000–1099	43.04	4	11	68	13	4
1100–1199	44.16	1	14	75	9	1
1200–1299	43.40	1	16	67	14	2
1300–1399	44.98	1	23	63	10	3
1400–1499	42.54	2	17	60	19	2
1500–1599	41.09	3	6	76	14	1
1600–1699	44.01	0	12	80	8	0
1700–1799	43.58	6	9	68	16	1
1800–1899	41.07	0	7	81	10	2
1900–1999	45.17	5	15	64	12	4
2000–2002	--	0	0	2	0	1
Total		**28**	**164**	**871**	**153**	**27**

In terms of individual years, the AD 800s are the second-most variable century in the Chama reconstruction; they also have a relatively high century mean. The AD 840s to AD 860s period was wet, as was the AD 880s, although the only consecutive string of above average years was AD 885–888. Below average years were spread more or less evenly throughout the century and the only string of bad years was AD 816–818; the AD 867–870 period, however, included two 'Very Bad,' an average, and a 'Bad' year.

The AD 900s have a relatively low century mean and about an average number of extreme years. After a string of 'Good' years (AD 917–919), most of the century was relatively dry, including the 'Very Bad'/'Bad' string of AD 980–982—until the upturn of four 'Good' years in AD 987–990.

The AD 1000s may be the most "average" century in the reconstruction. The century average (43.04 cm) is very close to the long-term mean and the number of extreme years (n = 32) is about average. The only consecutive strings of extreme years are both 'Good' (AD 1063–1066) and include the longest and wettest series of years in the entire reconstruction (AD 1023–1029).

After AD 1066, however, there were no 'Good' years, seven 'Bad' years, and one 'Very Bad' year. Thus, the first two-thirds of the century were wet, but the last three decades were either "normal" or dry.

The 1100s also had a relatively high century mean (44.16 cm) and a relatively low number of extreme years (n = 25). 'Good' years (n = 14) outnumber 'Bad' (n = 9), although 'Very Good' and 'Very Bad' years are equal. The only three-consecutive year strings were both wet (AD 1162–1164 and AD 1195–1197), although the AD 1146–1151 period includes three 'Bad,' two average, and one 'Very Bad' year. The first half of the century was mostly average or 'Good,' the middle average or 'Bad,' and the end was average or 'Good.'

The 1200s had a low century mean (43.40 cm) and 33 extreme years—about evenly split between 'Very Good/Good' (n = 17) and 'Bad/Very Bad' (n = 16). The only consecutive string of extreme years was wet (AD 1230–1232). The first half of the century was above average with the exception of the AD 1214–1217 period, which had a 'Bad,' average, 'Bad,' and 'Very Bad' string of years. The early AD 1250s were 'Bad,' but most of the rest of the century was average or 'Good.' This reconstruction is notable because the Great Drought (AD 1276–1299) of the Colorado Plateau does not appear to have seriously impacted the Chama area.

The 1300s had the second-highest century mean and third-highest number of extreme years in the reconstruction. The century had the highest number of 'Good' years (n = 23) of any century in the reconstruction, but only one 'Very Good' year. The only string of consecutive extreme years was AD 1356–1359, which included three 'Good' and one 'Very Good' year. Importantly, AD 1353 and AD 1354 were also 'Good' years, and AD 1355 was an average year. In short, the AD 1350s were wet. There were no consecutive strings of 'Bad' years. Overall, the AD 1300s experienced several average and 'Good' periods and no serious downturns in precipitation.

The AD 1400s exhibited the most variability of any century; only 60 years were classified as "normal." The mean is somewhat low, but not extremely so. 'Good' (n = 17) and 'Very Good' (n = 2) years almost equal the number of 'Bad/Very Bad' years (n = 21). The only consecutive string of extreme years is the AD 1495–1497 'Bad' period. The AD 1404–1414 period, however, includes six 'Good,' one 'Very Good,' three normal, and only one 'Bad' year; on the other hand, the AD 1449–1464 period includes seven 'Bad' years, eight normal years, and one 'Good' year. In general, the early part of the century was relatively wet and the last half was much drier.

The AD 1500s had a low century mean and relatively few extreme years. 'Bad' years (n = 14) outnumber 'Good' (n = 6), but 'Very Good' years (n = 3) outnumber 'Very Bad' (n = 1) years. The only consecutive string of extreme years is the AD 1513–1515 period when all three years were 'Very Good.' The first 30 years of the century were relatively wet or normal, but the AD 1532–1588 period contains only normal or 'Bad' years. The mega-drought of the late AD 1500s may have affected the area, but probably not as severely as areas farther south.

The AD 1600s had a high century mean and neither 'Very Good' nor 'Very Bad' years; indeed, the century was the second least variable in the reconstruction in terms of extreme years (n = 20). The only consecutive string of extreme years was the AD 1610–1613 wet period. In general,

extreme years were somewhat evenly distributed throughout the century with neither prolonged wet or dry periods.

The AD 1700s had a century mean near the long-term mean, but had the highest number of 'Very Good' (n = 6) years in the reconstruction. The only consecutive strings of extreme years were the AD 1720–1722 and AD 1770–1772 periods; dry periods include the AD 1733–1739 period with four 'Bad' and three normal years, and the AD 1773–1781 period with six 'Bad' and three normal years. The early part of the century was somewhat wet, but after AD 1729, most years were either normal or 'Bad' with a couple of exceptions.

The AD 1800s had the lowest century mean in the reconstruction. They also had the highest number of normal years (n = 81); 'Bad' (n = 10) and 'Very Bad' (n = 2) years outnumber 'Good' (n = 7) and 'Very Good' years (n = 0). No strings of consecutive extreme years were identified.

The AD 1900s had the highest century mean in the reconstruction (45.17) and a relatively high number of extreme years (n = 36). Extremely wet periods include 1919–1921 and 1985–1988 (three 'Very Good' and one 'Good' year); only one string of 'Bad' years was identified (1954–1956). In general, the 1905–1950 period was wet or normal, the 1950s with six 'Bad,' one 'Very Bad,' and three normal years were extremely dry, and the last 40 years of the century were relatively wet or normal.

Little can be said about the 2000s, except that 2002 was an extremely dry year.

Chama Chronology: Extreme Events

The 25 most extreme years (Table 8.7) show an impressive range of precipitation from a low of 14.70 cm in AD 907 to a high of 88.11 cm in AD 1771. In terms of centuries, the AD 1900s and AD 1000s both contain four of the driest and four of the wettest years. The AD 800s also contained a high number of these extreme years. Interestingly, the AD 1100–1600 period of the most intense Puebloan occupation of the area contains only six of the wettest and six of the driest extreme years. In historical terms, the only significant correlation is the very wet year of AD 1793, which may have aided de Vargas' reconquest of New Mexico.

Table 8.7. Twenty-five wettest and driest years in the Chama reconstruction.

Year	Driest	Year	Wettest
907	14.70	1771	88.11
867	15.28	888	78.29
924	15.57	1065	74.53
980	15.57	1986	74.04
1254	15.57	1025	73.66
1315	15.57	843	73.37
2002	15.81	1290	71.93
1005	16.15	1414	71.93
1956	16.82	1428	71.64

Year	Driest	Year	Wettest
1090	17.01	1513	71.64
1996	17.29	1515	70.77
1316	17.59	1747	70.29
1899	17.76	1129	70.19
878	17.88	776	69.90
1217	18.17	917	69.62
1480	18.17	858	68.75
1904	18.23	856	68.46
1847	19.00	1024	68.46
1896	19.02	1710	68.26
1013	19.32	1920	68.24
1902	19.75	1793	67.93
868	19.90	1987	67.52
981	19.90	1721	67.38
1035	19.90	1029	67.30
1495	19.90	1937	67.13

COMPARING THE JEMEZ AND CHAMA RECONSTRUCTIONS: SPATIAL DIFFERENCES IN PAJARITO AREA PRECIPITATION

One of the goals of this project was to explore the possible spatial differences in precipitation in the Pajarito area. Such differences may help archaeologists elucidate differences in settlement and subsistence patterns in different areas at different times and address issues such as mobility and migration. By using the chronologies and correlating them with the Chama and Jemez Springs weather stations, respectively, we are able to provide estimates for past precipitation in both the northern and southern portions of the project area (Figure 8.15).

There are several ways to examine and compare the two reconstructions, including by annual values, smoothed annual values, frequency and severity of extreme events, and Z-scores. Appendices H and I present the annual and smoothed basis for every common year in both chronologies. The reconstruction graphs typically track each other very well—when it is wet/dry in Chama, it is wet/dry in Jemez and vice versa. The Chama area typically received about 10 cm more precipitation than the Jemez area (Figure 8.15) on an annual basis. This difference is certainly real, although the magnitude of the difference may be impacted by our use of the Chama modern data in the calibration. Chama is farther north than our tree collection sites, but the live-tree sites are approximately 1000 ft higher in elevation than the weather station. Both of these factors may inflate the absolute quantities for the northern Pajarito area, but we believe they represent increased precipitation in the north and that the trends are accurate. One interesting aspect of Figure 8.15 is those years when the Jemez area shows higher absolute values than the Chama reconstruction. Given that Puebloan societies developed a three-year storage strategy (Schlanger 1985), such single-year discontinuities probably had little effect on long-term adaptive strategies. It would be interesting, however, to determine whether or not hunting, gathering, trading, or raiding changed during those years.

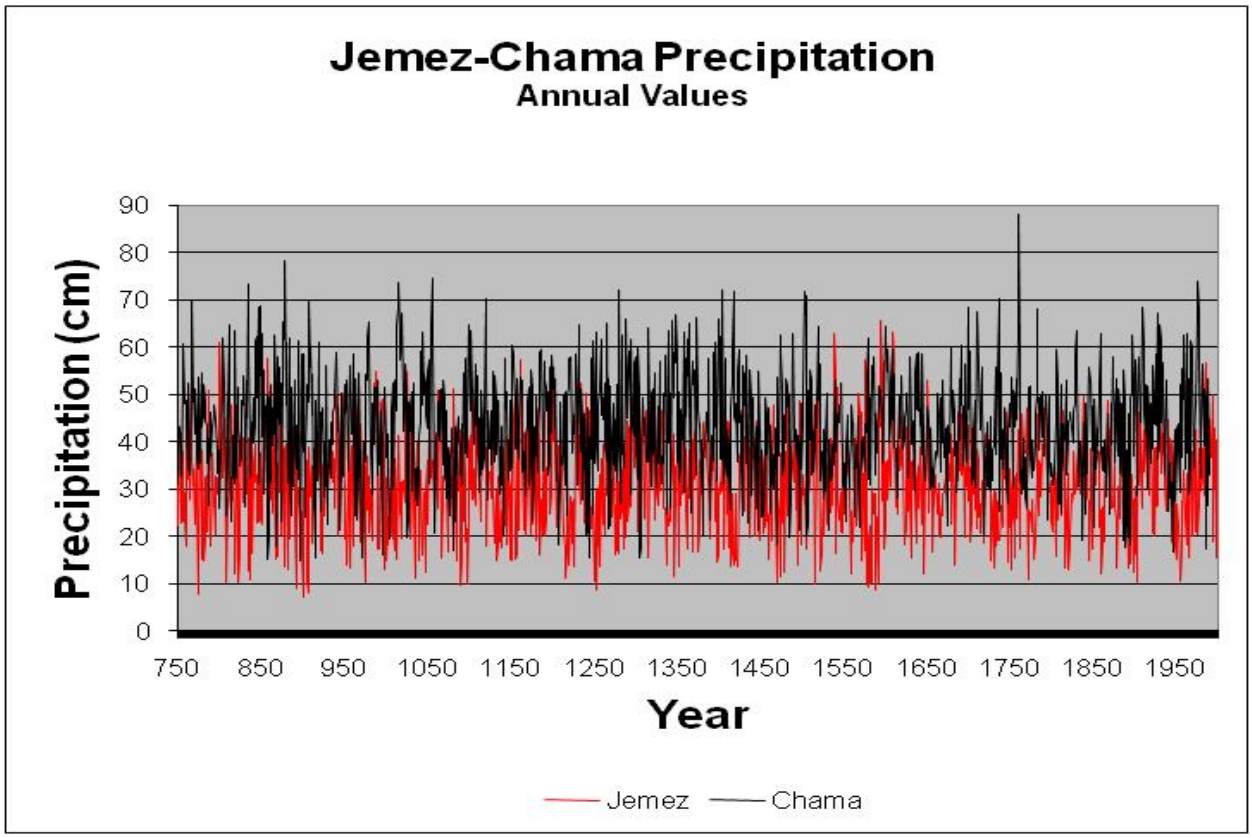

Figure 8.15. Annual precipitation values for both Jemez and Chama chronologies.

Another way to compare the two reconstructions is by plotting the 20-year smoothed absolute values for each year (Figure 8.16). This approach helps remove the individual annual variation in each reconstruction. The Chama reconstruction almost always retrodicts higher precipitation values than the Jemez reconstruction using the 20-year spline. There is one short span in the entire 1241 years of both reconstructions when the Jemez was more well-watered than the Chama area. The AD 1538–1542 period shows the Jemez with absolutely more precipitation than the Chama; in addition, during AD 1543–1544 the two areas are nearly equal. Significantly, this trend is not due to droughts when both areas were dry and the Jemez simply less arid. Included in the 25 wettest years of the Jemez reconstruction are AD 1540, AD 1541, and AD 1543 (see below); none of the years between AD 1530–1550 in the Chama area was unusually wet. As shown in Figure 8.17, even the absolute differences are highest during this time period. From this perspective, Coronado's trip from Hawikuh and sojourn in the Rio Grande Valley could not have come at a better time for the Spaniards.

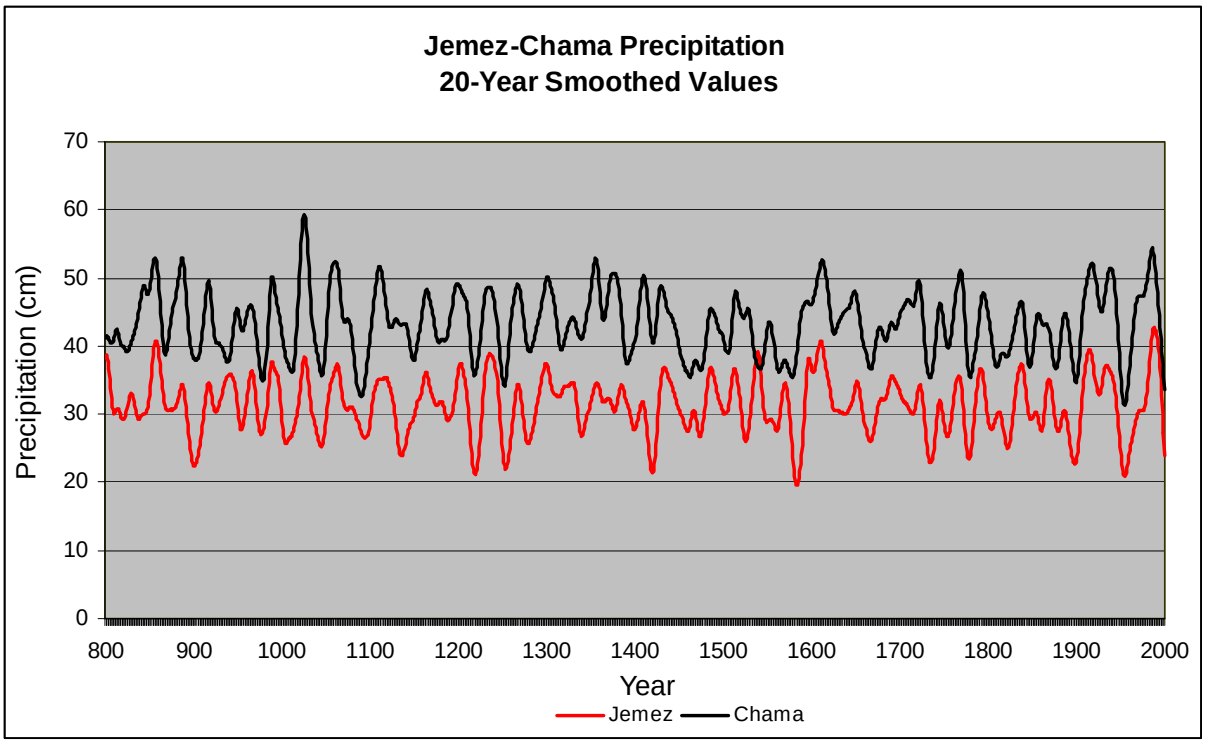

Figure 8.16. Splined precipitation values for both Jemez and Chama chronologies.

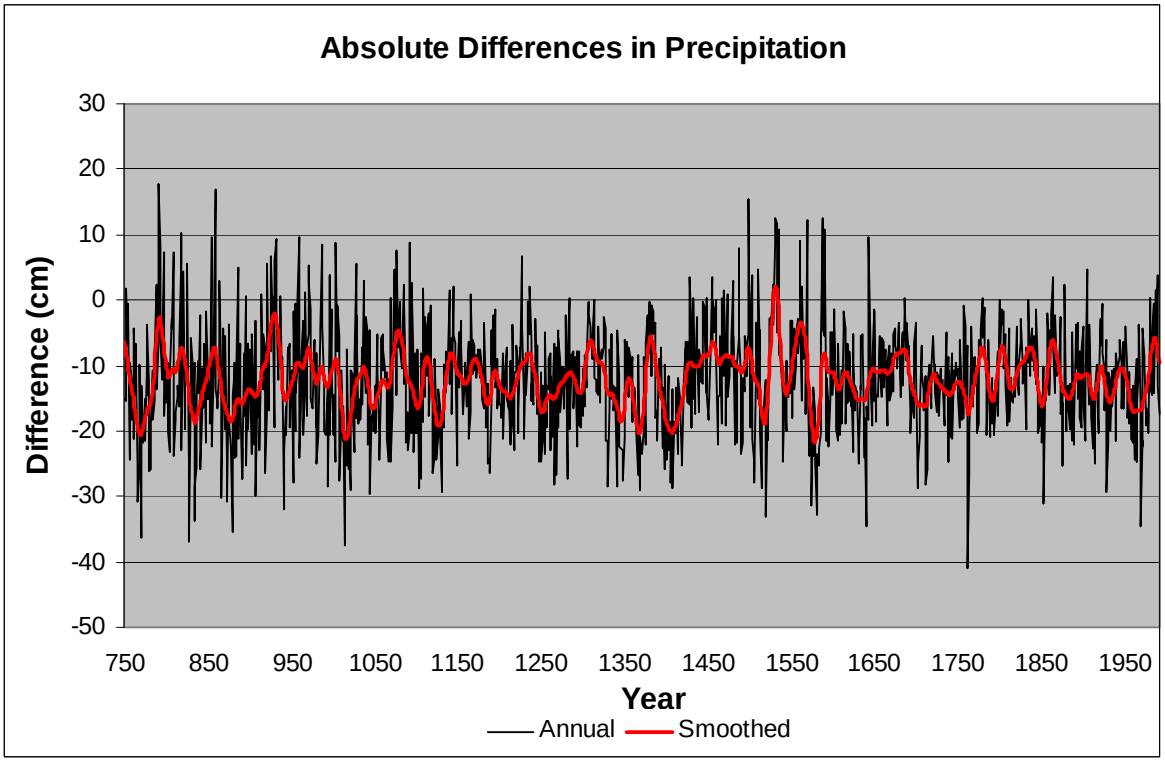

Figure 8.17. Graph of precipitation value absolute differences, both chronologies.

Extreme Events

Another factor that may have been important in land-use strategies of the area is the frequency and magnitude of extreme events. The chronology-specific extreme events have been discussed above, but here we examine the temporal relationships in each area.

Table 8.8 presents the extreme (very good, good, bad, and very bad) years in each reconstruction. These classifications are based on each chronology's mean and standard deviation; thus, a 'Bad' year in Chama may not necessarily be a 'Bad' year in Jemez and vice-versa. Because the Chama retrodiction is shorter, only the 9th to 20th centuries are compared.

Table 8.8. Comparison of extreme years in each reconstruction.

Century	Jemez Very Good	Chama Very Good	Jemez Good	Chama Good	Jemez Average	Chama Average	Jemez Bad	Chama Bad	Jemez Very Bad	Chama Very Bad
800–899	3	4	12	17	69	61	13	15	3	3
900–999	2	1	15	15	62	69	18	12	3	3
1000–1099	1	4	11	11	66	68	20	13	2	4
1100–1199	1	1	10	14	72	75	17	9	0	1
1200–1299	1	1	14	16	67	67	17	14	1	2
1300–1399	0	1	13	23	77	63	10	10	0	3
1400–1499	0	2	11	17	69	60	19	19	1	2
1500–1599	6	3	13	6	59	76	17	14	5	1
1600–1699	3	0	4	12	82	80	11	8	0	0
1700–1799	0	6	8	9	77	68	17	16	0	1
1800–1899	0	0	6	7	81	81	13	10	0	2
1900–1999	1	5	14	15	69	64	16	12	0	4

In general, the frequency of extreme years are similar in the two areas through time. The Jemez area has experienced fewer 'Very Bad,' 'Very Good,' and 'Good' years, but more 'Bad' years. Most centuries were similar in that most had an equivalent number of normal years, but there were exceptions.

In the AD 800s, the Chama area experienced more 'Good' years; in the AD 900s, the Jemez area suffered through more 'Bad' years; in the AD 1300s, the Chama area had more 'Good' years, but also more 'Very Bad' years; in the AD 1400s, the Chama area also had more 'Good' and 'Very Good' years. The AD 1500s were unusual in that the Jemez area had more 'Very Good' and 'Good' years, but also more 'Bad' and 'Very Bad' years—obviously, precipitation was more variable in that area at that time. The AD 1900s were also somewhat unusual in that the Chama area experienced more 'Very Good,' 'Good,' and 'Bad' years, but also more 'Very Bad' years.

These data suggest that differences in extreme years most often, but not always, were the result of wetter years in the north. The impacts of these inferences on past human settlement and land-use practices remain to be explored by area archaeologists.

Z-Scores

Perhaps the most efficient way of comparing the two retrodictions on both short- and long- term time scales is by transforming the data into Z-scores. This transformation allows us to compare the chronologies using the same quantitative and temporal scales regardless of the absolute values. Table 8.9 summarizes these differences for each century in the reconstructions. It should be remembered, however, that the absolute values in the reconstruction are estimates with associated statistical errors and that they should not be interpreted as absolutely measured precipitation amounts.

Table 8.9. Comparison of Z-scores.

Time Period	Jemez	Chama	Comments
770–790	decreasing	increasing	Values moving in opposite directions; possibly related to sample size (?)
795–807	increasing	flat	Jemez wetter, Chama relatively flat just below mean
836–848	flat	increasing	Chama wetter, Jemez flat around mean
875–893	increasing	increasing	Both wet; Chama much wetter
895–910	decreasing	decreasing	Both dry; Jemez much drier
929–945	increasing	decreasing	Values moving in opposite directions; Chama much drier
972–984	decreasing	decreasing	Both dry; Chama drier
1019–1033	increasing	increasing	Both wet; Chama much wetter
1078–1096	decreasing	decreasing	Both dry; Chama drier
1107–1114	increasing	increasing	Both wet; Chama wetter
1128–1152	decreasing	decreasing	Both dry; Jemez drier; Chama offset 1133–1157
1211–1227	decreasing	decreasing	Both dry; Jemez drier
1230–1244	increasing	increasing	Both wet; Jemez wetter
1311–1325	increasing	decreasing	Jemez wet above mean; Chama dry
1349–1361	increasing	increasing	Both wet; Chama wetter
1372–1383	flat	increasing	Chama wet; Jemez at mean
1386–1402	decreasing	decreasing	Both dry; Jemez offset 1393–1406
1411–1426	decreasing	decreasing	Both dry; Jemez much drier; Chama offset 1417–1424
1480–1497	increasing	increasing	Both wet; Jemez wetter
1525–1530	decreasing	increasing	Jemez dry; Chama around mean
1533–1545	increasing	decreasing	Chama dry; Jemez much wetter
1566–1574	increasing	decreasing	Chama dry; Jemez wetter
1579–1592	decreasing	decreasing	Both dry; Jemez much drier
1593–1622	increasing	increasing	Both wet; 1593–1613 Jemez wetter

Time Period	Jemez	Chama	Comments
1676–1698	increasing	decreasing	Jemez wet; Chama dry
1710–1717	decreasing	increasing	Jemez average; Chama wet
1806–1813	decreasing	decreasing	Chama dry; Jemez not as dry
1830–1844	increasing	increasing	Both wet; Jemez wetter
1845–1854	decreasing	decreasing	Both dry; Chama drier
1866–1871	decreasing	decreasing	Both dry; Chama drier

Figure 8.18 shows the smoothed Z-scores for the common years in both chronologies. As can be seen, both chronologies track each other relatively well—again, not surprising. During periods such as the AD 850s, mid-900s to mid-1000s, mid-1100s to early 1300s, and much of the post-1700 era, the chronologies are very similar in terms of trends, if not magnitudes of change. Certainly there were more severe droughts and more precipitation in one area or another, but the changes were, for the most part, synchronous.

The most interesting periods, on the other hand, are those that are asynchronous—drought in one area offset by wetter conditions in the other. Table 8.9 describes the graph in detail and the raw data are presented in Appendix J. Again, the most dramatic difference between the two areas occurs in the AD 1530s and early 1540s when Jemez was wet and Chama dry.

Finally, we have also developed quantitative methods for comparing the periodicity of the two time series (Cook and Peters 1981; Johnson 1994; Salzer 2000a). We use these techniques to characterize each reconstruction and compare the high and low precipitation periods in each area.

The quantitative method involves several steps. First, a 10-year smoothing spline was applied to the reconstructed precipitation values (Cook and Peters 1981); the spline functions as a low-pass filter and preserves the high-frequency variation in the data. Second, the original and splined data were converted to Z-scores, which quantified the deviations from the long-term mean. Third, we used the splined (Z-score) data to identify periods that deviated from long-term mean conditions by at least 1.1 standard deviations, the value proposed by Dean (1988) as significant in influencing past human adaptive behavior. The initial and terminal years of each period were defined using non-smoothed data because the splined data are influenced by preceding and succeeding amounts. The minimum length for any period was defined as five years. Finally, the beginning of a period was defined as the year when the reconstructed value first substantially deviated from mean conditions (<0.5 sad or >0.5 sad), and the end of a period was defined as that point when conditions returned for two consecutive years.

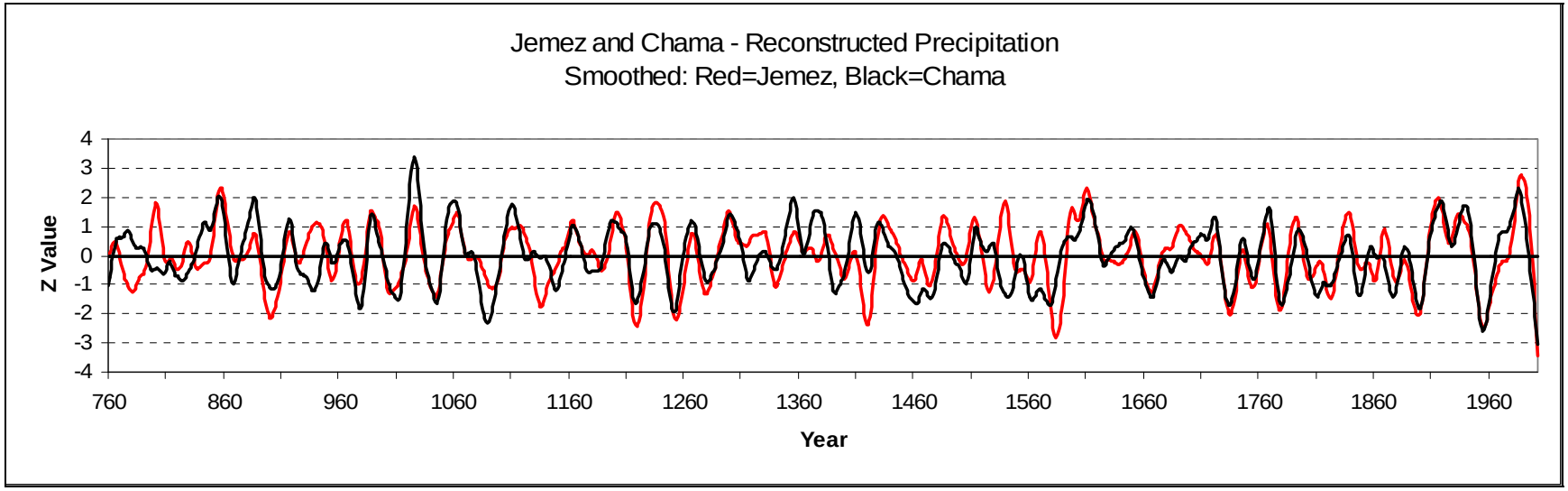

Figure 8.18. Z-scores of both chronologies.

Table 8.10 lists the wet and dry periods for both areas using quantitative criteria. There are several interesting aspects of these data. First, the only absolutely contemporaneous dry periods in both chronologies are near the recent end—the 1899–1904 drought, the 1950s drought, and the current drought. Conversely, four absolutely contemporaneous wet periods all occurred before AD 1302. Six wet periods overlap substantially, but are offset by a year or more; three occurred before AD 1029 and three occurred after AD 1608. There are also seven near-contemporaneous dry periods—three occurred before AD 1000 and three occurred after AD 1664. These short differences in periodicity may be the result of the use of different tree species in various parts of the chronologies and deserves additional research. The distribution of these periods in different centuries may also be important; there were no wet periods in the 1800s in either chronology, no dry periods in the 1300s at Chama, and no wet periods in the 1500s at Chama.

Table 8.10. Quantitative comparison of wet/dry periods in each reconstruction.

Jemez Wet	Chama Wet	Jemez Dry	Chama Dry
612–619	--	639–648	--
628–632	--	658–666	--
649–655	--	672–681	--
800–806	841–844	698–706	939–943
853–860	858–862	778–783	975–984
885–890	**885–890**	807–811	999–1005
915–919	915–921	897–903	1010–1014
985–989	985–990	950–955	1044–1049
994–998	1023–1029	999–1006	1081–1087
1024–1029	1052–1057	1131–1140	1090–1094
1060–1066	1109–1114	1214–1224	1146–1151
1162–1167	**1162–1167**	1248–1258	1214–1227
1200–1204	1207–1213	1276–1288	1426–1256
1228–1232	**1228–1232**	1335–1342	1461–1465
1241–1245	1266–1270	1396–1400	1471–1477
1297–1302	**1297–1302**	1415–1424	1504–1510
1330–1334	1353–1359	1455–1461	1542–1548
1383–1387	1370–1374	1470–1477	1573–1581
1431–1437	1377–1384	1579–1587	1664–1672
1484–1488	1409–1414	1666–1670	1729–1739
1511–1515	1608–1613	1733–1742	1773–1781
1536–1541	1617–1621	1773–1782	1806–1814
1609–1613	1646–1651	1818–1824	1842–1848
1651–1655	1743–1747	1859–1864	1871–1876
1766–1771	1768–1772	**1899–1904**	**1899–1904**
1790–1795	1792–1797	**1950–1959**	**1950–1959**
1912–1921	1941–1945	**2000–?**	**2000–?**
1930–1937	--	--	--
1983–1988	--	--	--

Also of interest may be those near-sequential periods with similar conditions. For example, the Jemez wet period of AD 1200–1204 was followed shortly thereafter by a Chama wet period from AD 1207–1213; other wet sequences include AD 1377–1384 (Chama) and AD 1383–1387 (Jemez), and AD 1646–1651 (Chama) and AD 1651–1655 (Jemez). There are only two near-sequential dry periods in the reconstructions; AD 1455–1461 (Jemez) and AD 1461–1465 (Chama), and AD 1573–1581 (Chama) and AD 1579–1587 (Jemez). Although few in number, these near-sequential periods may have influenced land-use patterns on the Pajarito Plateau and in surrounding areas. All but the latest wet episode in the mid-1600s occurred during the Bandelier archaeological periods and may be amenable to archaeological research using those data.

It is probable that the differences between the Chama and Jemez, particularly on a seasonal basis, are related to the fluctuating, sinuous line that separates two different climatic regimes in the Southwest (Ahlstrom et al. 1995; Dean and Funkhouser 1995). North and west of the line, precipitation has generally been unimodal; that is, winter snow pack has been the major component of annual precipitation. South and east of the line, a bimodal regime of winter rains and summer monsoons has predominated. Over the centuries, this fluctuating pattern has moved back and forth between the New Mexico-Colorado border and approximately the northern Chama Valley area (Dean 1996b; Dean and Funkhouser 1995), except during the chaotic period of ca. AD 1225–1450. Therefore, combined with the archaeological record of the area, the Pajarito area is an ideal locale to investigate the impacts of changing seasonal precipitation patterns on the cultural adaptations of subsistence agriculturalists, hunter-gatherers, and pastoralists.

Evaluation of the Agricultural Risk Model

Orcutt (1999) developed a detailed model of agricultural risk in the Bandelier area in order to explain such archaeological phenomena as mobility, aggregation, and the degree of commitment to agriculture during the AD 1150–1610 period. Orcutt's detailed study used the July PDSI (Palmer 1965) and exhaustive archaeological data (Powers and Orcutt 1999b) to elucidate many aspects of the prehistoric and protohistoric occupation of the area. The PDSI data were derived using the Rose et al. (1981) Arroyo Hondo tree-ring reconstruction of precipitation.

One of the major goals of this study was to evaluate the climatic aspects of the model; we are not reevaluating or using the archaeological data. This evaluation should in no way be construed as a criticism of Orcutt's efforts. We have developed new databases and used previously collected data that were not available at the time of her study.

The basic theoretical underpinnings of the Orcutt model are sound and we use them here. The mean and variability of moisture during each archaeological period are critically important to the success of argriculturalists in the Southwest. We use these same measures, but in different ways, to compare all three data sets: the Jemez reconstruction, the Chama reconstruction, and the Orcutt model.

The Jemez Reconstruction

Table 8.11 presents the precipitation mean and standard deviation for each period in the Bandelier chronology. It also lists the period deviation from the long-term mean and standard deviation (columns 4 and 6); Figure 8.19 summarizes these data using box-and-whisker plots.

Table 8.11. Jemez reconstruction wet/dry periods compared to Bandelier archaeological chronology (non-overlapping).

Period	Years	Mean	Deviation from Long-Term Mean	St Dev	Deviation from Long-Term Value
1	1150–1190	31.91	0.59	11.26	0.77
2	1190–1220	31.24	-0.08	9.85	-0.64
3	1220–1235	31.05	-0.27	11.63	1.14
4	1235–1250	35.40	4.08	10.48	-0.01
5	1250–1290	28.15	-3.17	9.52	-0.97
6	1290–1325	34.43	3.11	9.97	-0.52
7	1325–1375	32.26	0.94	9.15	-1.34
8	1375–1400	30.23	-1.09	8.57	-1.92
9	1400–1440	29.90	-1.42	10.27	-0.22
10	1440–1525	31.44	0.12	10.54	0.05
11	1525–1600	30.46	-0.86	13.07	2.58

Long-term mean = 31.32; standard deviation = 10.49

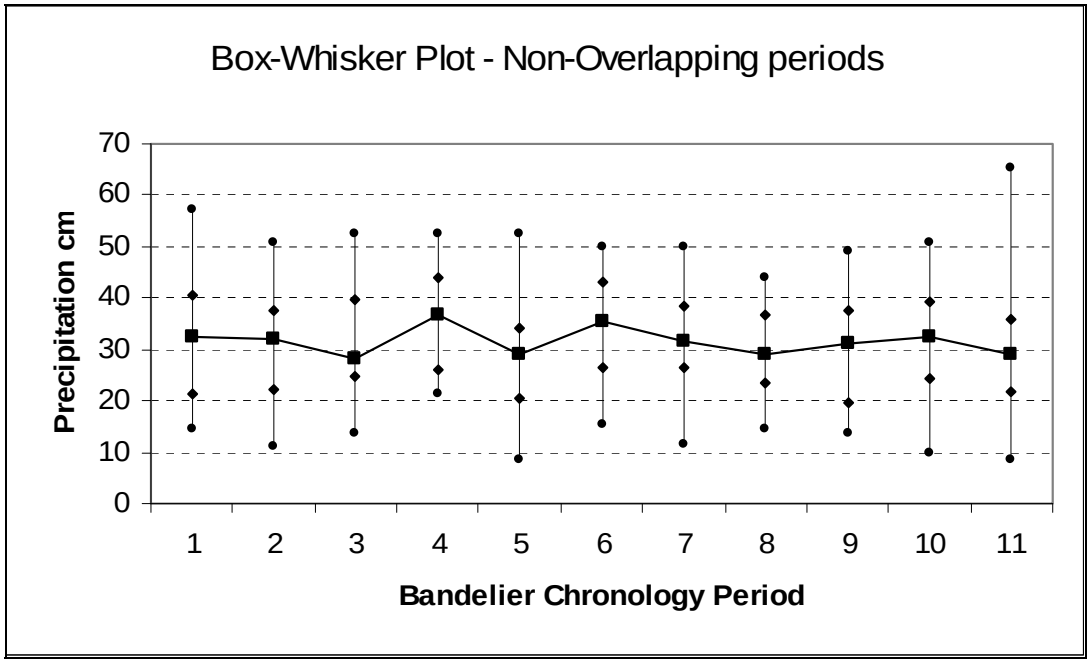

Figure 8.19. Jemez box-and-whisker plot of Bandelier chronology (non-overlapping).

Most of the periods exhibit similar precipitation means and standard deviations. Periods 4, 5, 6, and 9, however, are clearly different. Periods 4 and 6 had much higher mean precipitation than other periods, and Period 5 was much lower. Period 9 was also dry, but not as dry as Period 5. The dramatic differences, or alternations, between Period 4, 5, and 6 may have had important impacts on the area occupants. We leave such interpretations to Pajarito archaeologists.

The standard deviations within each period are also informative. Periods 3, 7, 8, and 11 have the highest standard deviations, although Period 5 could also be considered somewhat high. We believe it important that the "alternating" Periods 4, 5, and 6, which have very different precipitation means, have relatively low standard deviations. It may also be important that the highest standard deviation is in Period 11, which exhibits a relatively low mean precipitation. How this precipitation regime impacted the Puebloan and Spanish populations in the area remains an important question.

Orcutt uses 10-year overlaps for each period because the period boundaries are uncertain and because there is usually a lag between environmental stress and human behavior (Orcutt 1999:231). Table 8.12 presents the 10-year overlapped Jemez data and Figure 8.20 shows these data graphically.

Table 8.12. Jemez reconstruction wet/dry periods compared to Bandelier archaeological chronology (overlapping).

Period	Years	Mean	Deviation from Long-Term Mean	St Dev	Deviation from Long-Term Value
1	1140–1200	31.57	0.25	10.36	-0.13
2	1180–1230	30.59	-0.73	10.32	-0.17
3	1210–1245	31.80	0.48	11.14	0.65
4	1225–1260	31.36	0.04	11.41	0.92
5	1240–1300	30.32	-1.00	10.18	-0.31
6	1280–1335	33.29	1.97	9.56	-0.93
7	1315–1385	31.92	0.60	9.12	-1.37
8	1365–1410	31.71	0.39	8.26	-2.23
9	1390–1450	30.15	-1.17	9.88	-0.61
10	1430–1535	31.64	0.32	10.03	-0.46
11	1515–1610	30.95	-0.37	13.39	2.90

Long-term mean = 31.32; standard deviation = 10.49

Examining the data in this way indicates that only Periods 5, 6, and 9 were different from the long-term mean in any meaningful way. Period 4, which is the most different period in the non-overlapped analysis, is very close to the long-term mean. Period 9 also stands out in both analyses as below the mean. If we examine the overlapped periods in terms of standard deviations, Periods 7, 8, 11, and possibly 6 are clearly different. Period 11 was clearly more variable, as well as relatively dry.

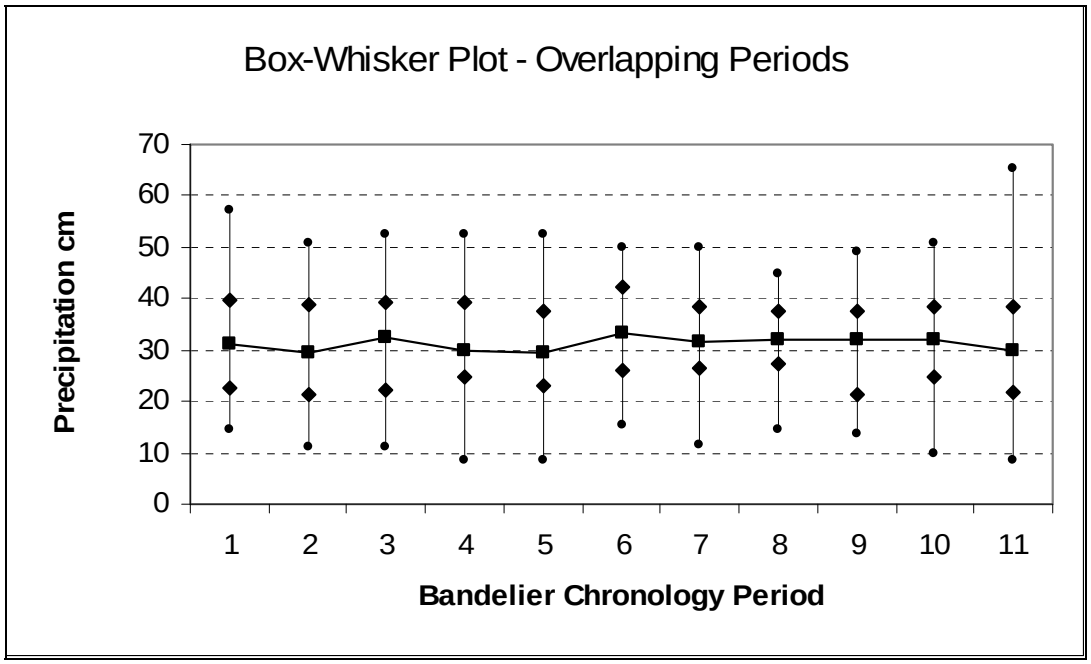

Figure 8.20. Jemez box-and-whisker plot of Bandelier chronology (overlapping).

The Chama Reconstruction

Table 8.13 presents the Chama precipitation mean and standard deviation for each period in the Bandelier chronology. It also lists the period deviation from the long-term mean and standard deviation (columns 4 and 6); Figure 8.21 summarizes these data using box-and-whisker plots.

Table 8.13. Chama reconstruction wet/dry periods compared to Bandelier archaeological chronology (non-overlapping).

Period	Years	Mean	Deviation from Long-term Mean	S.D.	Deviation from Long-term S.D.
1	1150–1190	42.79	-0.55	10.16	-1.26
2	1190–1220	44.68	1.34	10.73	-.69
3	1220–1235	43.57	0.23	10.25	-1.17
4	1235–1250	44.45	1.11	9.81	-1.61
5	1250–1290	42.39	-0.95	13.43	2.01
6	1290–1325	45.22	1.88	13.29	1.87
7	1325–1375	46.58	3.24	11.85	.43
8	1375–1400	42.39	-0.95	11.30	.12
9	1400–1440	45.47	2.13	12.56	1.14
10	1440–1525	41.18	-2.16	12.15	.73
11	1525–1600	40.55	-2.79	9.01	-2.41

Long-term mean = 43.33731; standard deviation = 11.42

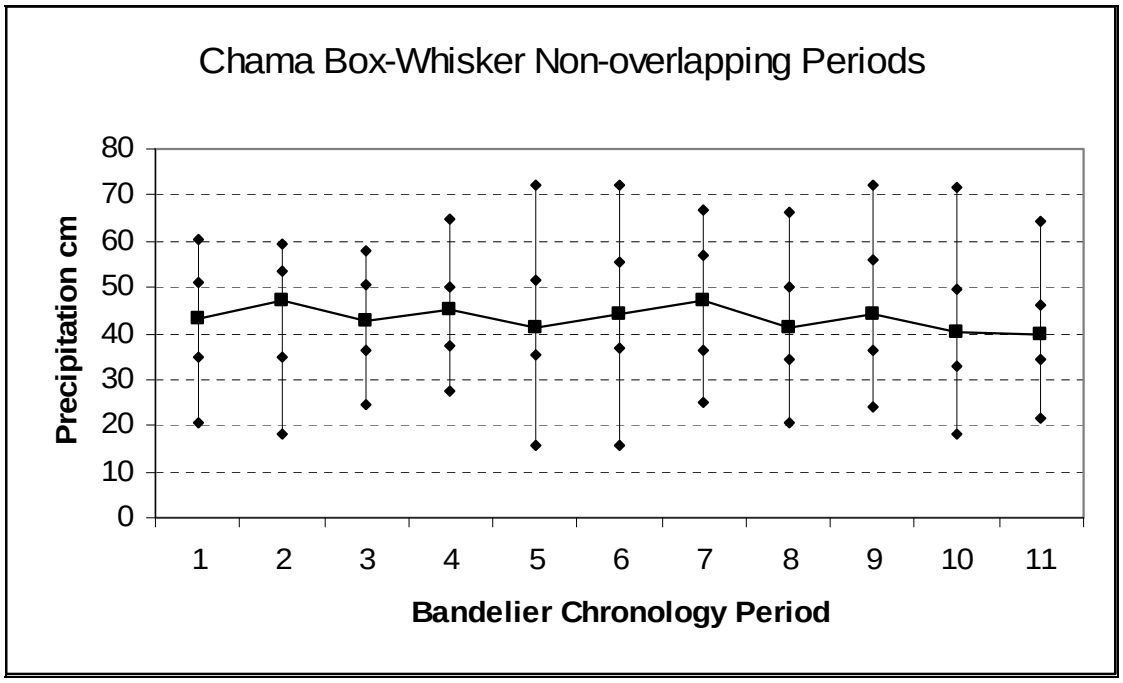

Figure 8.21. Chama box-and-whisker plot of Bandelier chronology (non-overlapping).

The Chama reconstruction period means present an interesting pattern. After below-average precipitation in the AD 1150–1190 period, there was above-average precipitation in Periods 2 to 4, from AD 1190–1250. After low precipitation from AD 1250–1290 (Period 5), above average precipitation prevailed throughout Periods 6 and 7 (AD 1290–1375). Periods 8 and 9 alternated between below and above-average precipitation, but the final two periods (10 and 11) experience the lowest precipitation means in the reconstruction. In short, the archaeological chronology begins dry, is somewhat wet for 60 years, drier for 40 years, wetter for 85 years, drier for 25 years, wetter for 40 years, and finally drier for the last 160 years of the chronology.

The Chama period standard deviations also present an interesting pattern. The first four periods (AD 1150–1250) experienced variability below the long-term average; the next six periods were all above the long-term standard deviation, and the final period (AD 1525–1610) was the least variable in the entire archaeological chronology.

Viewing the Chama chronology using 10-year overlapped periods (Table 8.14; Figure 8.22) changes the interpretation slightly.

Table 8.14. Chama reconstruction wet/dry periods compared to Bandelier archaeological chronology (overlapping).

Period	Years	Mean	Deviation from Long-term Mean	S.D.	Deviation from Long term S.D.
1	1140–1200	43.32	-0.02	9.94	-1.48
2	1180–1230	43.53	0.19	10.58	-.84
3	1210–1245	43.68	0.34	10.94	-.48

Period	Years	Mean	Deviation from Long-term Mean	S.D.	Deviation from Long term S.D.
4	1225–1260	42.83	-0.51	12.59	1.17
5	1240–1300	42.92	-0.42	12.89	1.47
6	1280–1335	43.70	0.36	12.00	.58
7	1315–1385	45.49	2.15	12.20	.78
8	1365–1410	45.53	2.19	11.90	.48
9	1390–1450	43.76	0.42	12.47	1.05
10	1430–1535	41.83	-1.51	11.92	.5
11	1515–1610	41.57	-1.77	9.94	-1.48

Long-term mean = 43.33731; Standard deviation = 11.42

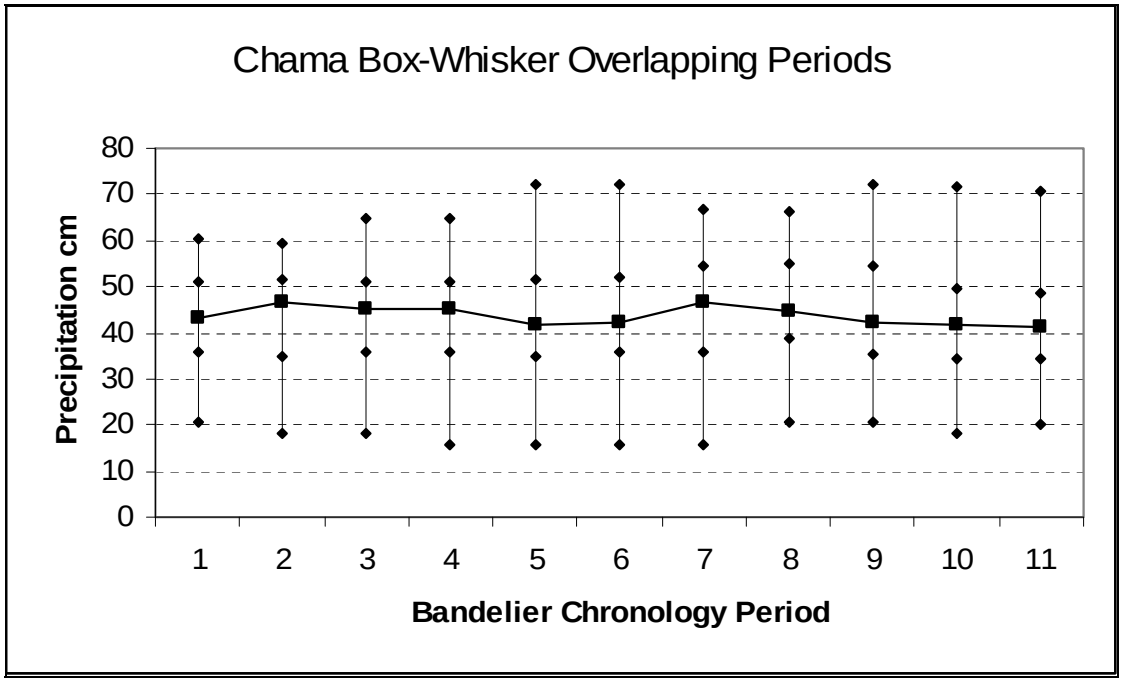

Figure 8.22. Chama box-and-whisker plot of Bandelier chronology (overlapping).

In terms of mean precipitation, Period 4 (AD 1225–1260) is below average and Period 8 (AD 1365–1410) is now above average; the other periods change in terms of absolute values, but not whether or not they are above or below the long-term mean. In terms of standard deviations, only Period 4 changes from less variable to above the long-term standard deviation.

The Jemez and Chama reconstructions and the Orcutt model provide three different views of past moisture availability in the Pajarito Plateau area between AD 1150–1610. There are, of course, differences. This project retrodicted precipitation using tree-ring data and Orcutt retrodicted soil moisture based on different tree-ring data. There are also spatial differences in these approaches—our Jemez retrodiction is calibrated on the Jemez Springs HCN data, our Chama retrodiction is based on the Chama station data, and the Orcutt model is ultimately based on the

Arroyo Hondo tree-ring series. Nevertheless, we believe the different reconstructions are broadly comparable.

Orcutt developed a matrix that partitioned her period data into four possible moisture and variability combinations: high mean/high variation, high mean/low variation, low mean/high variation, and low mean/low variation. She then plotted each archaeological period in the matrix (Figure 8.23) and posited behavioral responses to these variables that should be visible in the archaeological record.

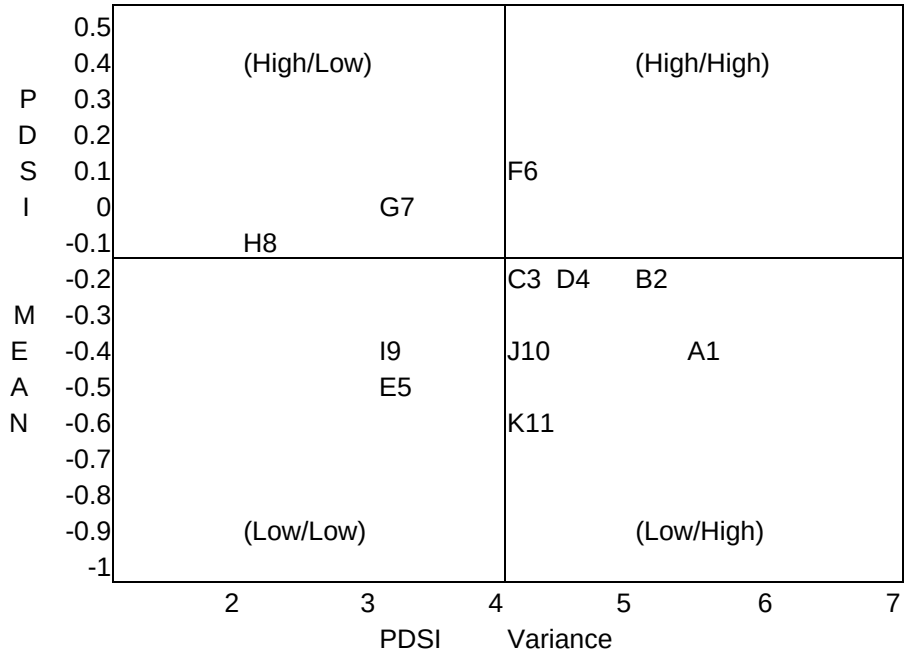

Figure 8.23. Orcutt's quadrats of precipitation variability.

As a comparative exercise, we have partitioned the Jemez and Chama data into similar combinations and plotted them (Figures 8.24 and 8.25). When we compare all three models (Table 8.15), there are important similarities and differences.

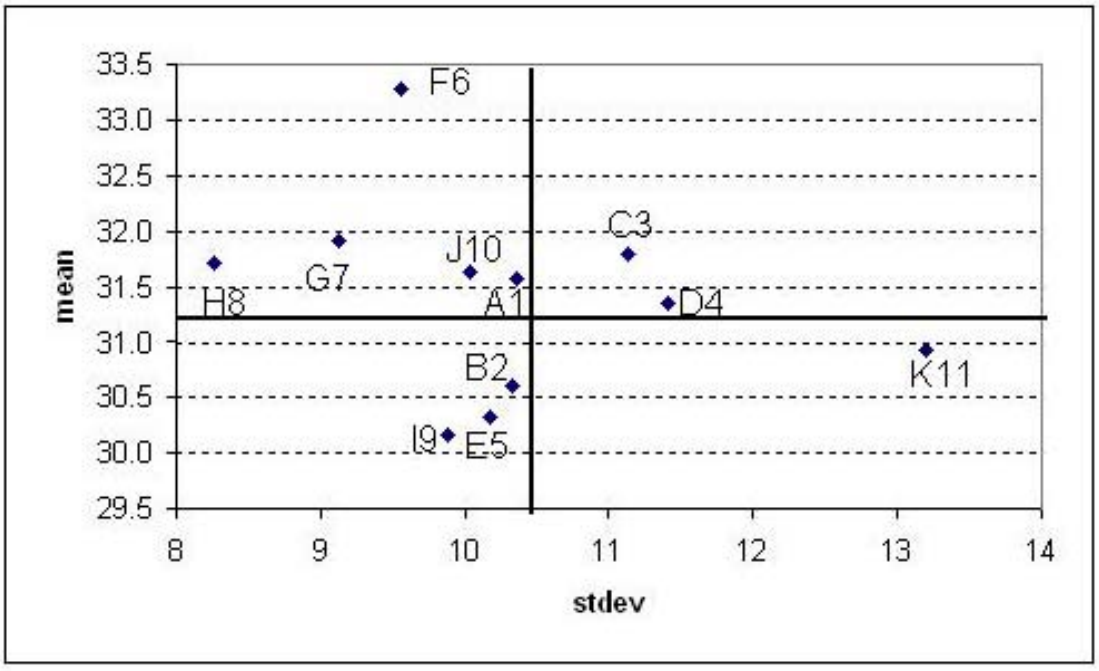

Figure 8.24. Jemez chronology quadrats of precipitation variability.

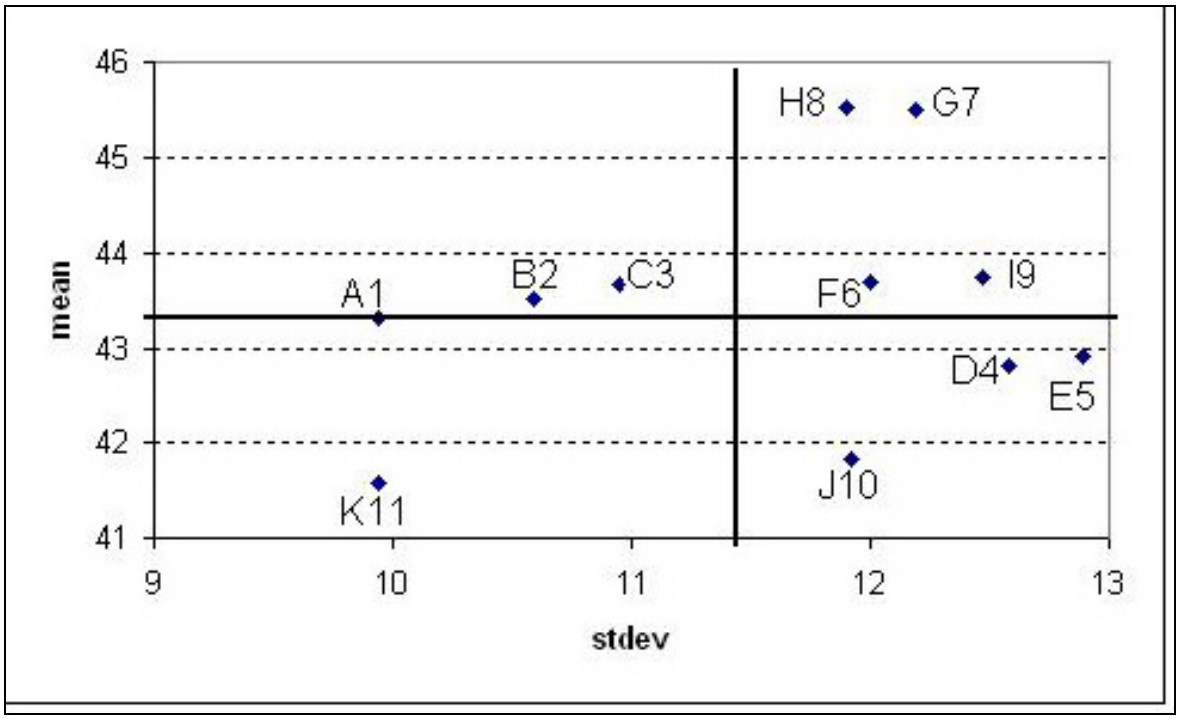

Figure 8.25. Chama chronology quadrats of precipitation variability.

Table 8.15. Comparison of three models' mean and variance.

Period	Orcutt Model		Jemez		Chama	
	Mean	Variance	Mean	S.D.	Mean	S.D.
1	L	H	H	L	H	L
2	L	H	L	L	H	L
3	L	H	H	H	H	L
4	L	H	H	H	L	H
5	L	L	L	L	L	H
6	H	H	H	L	H	H
7	H	L	H	L	H	H
8	H	L	H	L	H	H
9	L	L	L	L	H	H
10	L	H	H	L	L	H
11	L	H	L	H	L	L

Interestingly, there are no periods in which all three models agree on both variables. Sometimes they all agree on one variable, and some times two reconstructions agree on both, but disagree with the other model. The possible reasons for these similarities and differences are explored below.

In Period 1 (AD 1150–1190), the Jemez and Chama datasets agree (High mean/Low standard deviation) and are opposite of the Orcutt model (Low/High). These differences may be more perceived than real. The Jemez and Chama High means are only slightly above their long-term values, and the Jemez standard deviation is only slightly below its long-term value. Clearly, however, the Chama and Orcutt variability value are much different.

During Period 2 (AD 1190–1220), all three reconstructions are different: Orcutt is Low/High, Jemez is Low/Low, and Chama is High/Low. Again, the absolute values may be important—the Chama mean is only slightly above the long-term average, the Orcutt mean is slightly below, and the Jemez standard deviation is slightly below. Thus, the major differences between the Orcutt model variance and Chama standard deviation.

All three reconstructions show different results in Period 3. The Jemez (High/High) and Chama (High/Low) agree about above-average precipitation, and the Orcutt model (Low/High) and Jemez agree about above-average variability. A closer look at the plots, however, shows that all three reconstructions place the period near both central axes of the quadrants; thus, the differences are simply not great.

Period 4 (AD 1235–1250) shows significant agreement in that all three models indicate high variability; the Orcutt model and Chama also indicate low mean moisture availability. Like the previous periods, however, the mean values are all very near the long-term value and the differences are probably not behaviorally important. The period obviously experienced highly variable conditions as indicated by all three datasets.

With only one exception, Period 5 (AD 1250–1290) is characterized as Low mean/Low variability; the Chama reconstructions recorded very high variability. The period was clearly dry throughout the northern Rio Grande, but the Chama area was less arid and experienced more wet years. The implications of this difference deserve more scrutiny by area archaeologists.

Conditions changed significantly during Period 6 (AD 1290–1325). All three models indicate high mean moisture, and the Orcutt and Chama data indicate high variability as well. The Orcutt and Jemez data suggest that this period had the highest mean precipitation during the archaeological chronology. Apparently, the Jemez/Bandelier area was wet and somewhat variable; the Chama area was only slightly above average and somewhat more variable. All in all, Period 6 should have been very productive throughout the northern Rio Grande area.

The good times continued during Period 7 (AD 1325–1375) with high means and low variability, except in the Chama area which also experienced high variability. The high variability in the Chama area was probably offset by one of the highest means in the entire reconstruction.

Period 8 (AD 1375–1400) is identical to Period 7 in terms of the category classifications; Orcutt and Jemez (High/Low) and Chama (High/High). The high means in all three reconstructions are very similar and the variability is lower in all three models than in Period 7. Indeed, Period 8 may have been the most optimal period in the entire archaeological chronology.

Things changed dramatically in Period 9 (AD 1400–1440). Mean moisture availability was low in both the Orcutt and Jemez models, but slightly above average in the Chama dataset. Variability was low in the Jemez/Bandelier area, but still high in the Chama area. These spatial differences may have had important implications for settlement and subsistence throughout the area and should be explored by area archaeologists.

The Orcutt and Chama reconstructions agree that Period 10 (AD 1440–1525) experienced low mean/high variability; the Jemez, on the other hand, indicates high mean/low variability. Examination of the raw data, however, indicates that the Jemez High/Low configuration is a result of classification; the mean is only slightly above the long-term value and the standard deviation is only slightly below the long-term value. Thus, all three models are telling similar stories—times were not great.

The final archaeological period (AD 1525–1610) continued to be relatively poor. The Orcutt and Jemez models indicate Low mean and High variability, and the Chama data indicate Low mean and Low variability.

Finally, we also used quantitative methods to evaluate precipitation periodicity during the years of the Bandelier archaeological chronology. Our methods are similar to those used above to identify wet/dry periods in each reconstruction. In this evaluation, however, every year's value was forced into a wet/dry category based on its relationship to the long-term mean and splined values around it. In this way, the method is similar to those of a PDSI analysis.

Table 8.16 presents our wet/dry years, the Bandelier periods, and comments regarding the precipitation during those periods. Only two periods, Period 1 (AD 1150–1190) and Period 6

(AD 1290–1325), did not experience changes in the precipitation regime. Interestingly, both Periods 1 and 6 experienced above-average precipitation. All the other archaeological periods experienced at least one, and some times more, shifts from wet or dry conditions to the opposite.

Table 8.16. Quantitative evaluation of precipitation periodicity compared to Bandelier archaeological periods.

Years	Condition	Bandelier Period	Bandelier Years	Comments on Period Precipitation
1131–1151	DRY	--	--	n/a
1152–1213	WET	1	1150–1190	wet all period
1214–1227	DRY	2	1190–1220	wet early, dry late period
1228–1245	WET	3	1220–1235	dry early, wet late period
1246–1264	DRY	4	1235–1250	wet early, dry (very) late period
1265–1275	WET	5	1250–1290	dry early, wet middle, dry late period
1276–1289	DRY	5	1250–1290	dry early, wet middle, dry late period
1290–1334	WET	6	1290–1325	wet all period
1335–1350	DRY	7	1325–1375	wet early, dry middle, wet late period
1351–1388	WET	7	1325–1375	wet early, dry middle, wet late period
1389–1403	DRY	8	1375–1400	wet early, dry late period
1404–1414	WET	9	1400–1440	dry (very) early, wet early, dry middle, wet late period
1415–1425	DRY	9	1400–1440	dry (very) early, wet early, dry middle, wet late period
1426–1448	WET	9	1400–1440	dry (very) early, wet early, dry middle, wet late period
1449–1483	DRY	10	1440–1525	wet (very) early, dry early middle, wet late middle, dry early late, wet late period
1484–1494	WET	10	1440–1525	wet (very) early, dry early middle, wet late middle, dry early late, wet late period
1495–1510	DRY	10	1440–1525	wet (very) early, dry early middle, wet late middle, dry early late, wet late period
1511–1541	WET	11	1525–1610	wet early, dry middle, wet late period
1542–1593	DRY	11	1525–1610	wet early, dry middle, wet late period
1594–1655	WET	11	1525–1610	wet early, dry middle, wet late period

DISCUSSION

The three models all provide important data regarding precipitation and the availability of moisture during the AD 1150–1610 period. One of the major problems with using the quadrant classification system, however, is that it ignores the range of data. Several periods in all three models cluster near the quadrant axes, and slight changes in one variable would change their classification. For example, the long-term standard deviation of the Jemez reconstruction is 10.49; the standard deviation for the smoothed Period A1 data is 10.36—a difference of only 0.13. Likewise, the Period A1 mean is 31.57 and the long-term mean is 31.32. Thus, the Jemez period A1 is classified as High/Low, but with minor adjustments—either in the real precipitation or in analysis techniques, could just as easily be classified as High/High, Low/High, or even Low/Low.

In the Jemez reconstruction, five, and maybe more, of the periods could be subject to change due to minor variations (A1, B2, C3, D4, and J10); only Periods E5, F6, K11, and G7 appear to be truly different than the others. In the Chama reconstruction, Periods G7, H8, J10, and K11 appear different, although others could be included as well. In the Orcutt model, all the periods cluster more tightly near the central axes, but Periods F6, H8, G7, K11 and possibly some others appear different.

The quantitative evaluation of precipitation during the Bandelier archaeological periods suggests little correlation between precipitation amounts and variability and cultural sites. This is not to imply that precipitation had no impact on cultural trajectories on the Pajarito Plateau; it most certainly did on both long and short time scales. What we infer is that precipitation was but one factor in the decisions of people to settle, use, and depopulate the plateau over the centuries.

We are not suggesting that there has been no variability between the archaeological periods; clearly other data in this chapter indicate that precipitation has varied over time and across space during the prehistoric and protohistoric occupation of the northern Rio Grande. We do question whether this variability coincides with the Bandelier archaeological periods and if the human responses to the variability are reflected in the archaeological record at such fine temporal scales. In general, we believe the archaeological periods, particularly if overlapped, are too short to capture either the climatic or cultural variation.

CHAPTER 9
A CONTEXT FOR THE INTERPRETATION OF ARCHAEOMAGNETIC DATING RESULTS FROM THE PAJARITO PLATEAU

Eric Blinman and Jeffrey Royce Cox

INTRODUCTION

Archaeomagnetic dating is one of several dating techniques that can be applied to the development of detailed archaeological chronologies. In the context of archaeological investigations on the Pajarito Plateau, the alternate tools include tree-ring dating, radiocarbon dating, ceramic dating, and a variety of luminescence techniques. This summary of archaeomagnetic dating was requested in order to accomplish three goals. The first was to provide an explanatory guide to the theoretical and practical foundations of archaeomagnetic dating. The second was to evaluate existing archaeomagnetic curves that are relevant to the dating interpretation of Pajarito Plateau samples, specifically looking at the strengths and weaknesses of the curves as revealed using sample results from Dr. Robert DuBois, University of Oklahoma. The third was to catalog the archaeomagnetic results from the northern Rio Grande region that can be used for comparison with results from the Pajarito Plateau.

The basic elements of archaeomagnetic dating were developed in the 1930s by Emile Thellier and his students (Wolfman 1990). Despite this early start, research and development have proceeded sporadically compared with other dating techniques in the face of theoretical and practical limitations (Eighmy 1991). Progress has been greater in the Southwestern United States than elsewhere in North America, but archaeomagnetic dating remains of secondary importance to archaeologists compared with other natural science techniques such as dendrochronology and radiocarbon assays. Luminescence dating techniques (Feathers 2000) are showing promise as well, although confidence in its strengths and weaknesses will be dependent on additional case studies (e.g., Dykeman et al. 2002).

The ambiguous position of archaeomagnetic dating is due to a mixture of advantages and disadvantages. Archaeomagnetic dating records the time of the last exposure of archaeological features to a source of heat. Archaeomagnetic dating is most effective when the feature is heated above 580 to 680° C (the Curie points for the most common magnetic materials in soils), but lower temperatures can also produce datable samples (Smith 1990). For features such as hearths or burned structures, archaeomagnetic dating is one of only two techniques that can provide last-use or abandonment dates as opposed to construction dates (luminescence dating can also provide last-use dates in some contexts). Another advantage is that since archaeomagnetic dating is based on geophysical properties (Sternberg 1990) rather than cultural behavior, dating results can be more reliable in some contexts. This is particularly true when dead wood is harvested for fuel or building material, skewing radiocarbon or tree-ring samples toward dates that are too old (Smiley 1985). Finally, when high-quality samples are available, and for some time periods when dating curves are robust, archaeomagnetic dating accuracy and precision can be excellent, falling within the range of 20 to 40 years.

Disadvantages of archaeomagnetic dating are both methodological and contextual. The underlying basis for the technique is the year-to-year variation in the geographic position and strength of the earth's geomagnetic field. There is no theoretical model that can accurately describe geomagnetic field variation, and calibrated virtual geomagnetic polar curves for dating purposes must be developed from paleo- and archaeological samples (or from historic records). The pole positions of these samples and often their calibrating dates are measured with error, and the uncertainties result in archaeomagnetic dating curves that are tentative approximations of the true curve. Also, curves follow an overlapping path, resulting in the possibility of multiple date interpretations for a single sample result. In this respect, final date interpretations are often dependent on the expectations of the archaeologist, reducing the independence of archaeomagnetic dating's contribution to the resulting cultural chronologies. Finally, sample quality can be affected by both systematic and idiosyncratic factors of sampling technique and local magnetic anomalies, resulting in either imprecision or inaccuracy in individual cases.

PRINCIPLES OF ARCHAEOMAGNETIC DATING

The underlying basis for archaeomagnetic dating is the year-to-year variation in the geographic position and strength of the earth's geomagnetic field (Sternberg 1990). This field consists of a dipole component that is usually oriented near the rotational axis of the earth and non-dipole components that are regional and local in nature. At any given point on the earth's surface, these components combine to create an apparent or virtual geomagnetic pole (VGP) location. As the strength and orientation of the dipole and non-dipole fields vary through time, the VGP location changes, describing a VGP curve. Because of the influence of non-dipole fields, VGP curves will not be the same from region to region, although there are greater similarities between regions that are adjacent east-west than north-south (Sternberg 1990:9–10).

Magnetic material in soil (primarily magnetite and hematite) is affected by the prevailing geomagnetic field. When this magnetic material is heated to and above its Curie point (580° C for magnetite and 680° C for hematite), it acquires a field direction that is influenced by the orientation of the earth's field as the material cools. This is known as the thermal remnant magnetism, or TRM. Although subsequent events can weaken or alter this TRM, such as a nearby lightning strike, in most cases the TRM orientation persists until the soil is subjected to another heating episode that exceeds the previous temperature or the Curie point.

An archaeomagnetic sample usually consists of a set of up to 12 specimens collected from the soil lining a hearth, kiln, oven, or other type of burned feature. Fired rocks, such as sandstone, can also be sampled if care is taken during collection. The orientation of each specimen is carefully measured, and magnetic properties of each specimen are subsequently measured in the laboratory. Measurement usually includes progressive alternating field (AF) demagnetization to reduce the influence of any secondary magnetic components that might have been acquired since the feature was last fired. Results of the individual specimen measurements are compared, and data from the best specimens are combined to characterize the earth's magnetic field at the time the feature was burned. The mean orientation of the specimens is the estimate of the VGP location, and the dispersion of the specimen orientations provides an error term that is expressed as an ellipse or oval of confidence (two standard deviations) around the VGP center point.

Inconsistent specimen orientations result in samples with large ellipses, reflecting greater uncertainty about the true VGP location.

Date interpretations are made by comparing each sample plot with a regional VGP curve (also called a secular variation curve). Points of intersection of the ellipse with the curve determine the beginning and end points of the date range. Since the calibration curve is only an approximation of the real curve, when a sample centerpoint falls off of the curve, a common convention is to move the centerpoint to the nearest point on the curve for the calculation of the date range. Where the ellipse intersects more than one segment of the calibration curve, the centerpoint is moved in turn to the closest point of each segment, resulting in as many date range estimates as the number of curve segments that fall within the original ellipse.

Because of the influence of non-dipole components on the geomagnetic field, calibration curves must be established for each region of the earth's surface. The U.S. Southwest curves have been developed for a relatively large region of 500 to 1000 miles in diameter. For this reason, the calibration curves are best thought of as bands within which the true curve lies, varying slightly depending upon the location of the project area within the region. As an arbitrary compensation for this additional uncertainty, date range estimates are usually rounded five years beyond either end of the points where the ellipse intersects the curve.

For regions or time periods where a calibration curve does not exist, sample results can be used to construct a curve. In the absence of independent dates for samples, seriation principles can be used to develop a first approximation of the true curve. Where independent dates are available, they can serve both to validate the direction of the curve and to calibrate the curve to the modern time scale. For regions and time periods where calibration curves have been established, sample results are used not only to produce date estimates but also to validate and refine the existing approximation of the true curve.

SAMPLING AND MEASUREMENT PRACTICE

Burned sediments are collected as carefully oriented specimens approximating the volume of a sugar cube. Ideally, specimens are cut from portions of the feature that are well burned, show no erosion, and show no evidence of cracking or slumpage. Ideal sampling material is rare due to the actions of roots, insects, small mammals, mass slumpage, and repeated exposure to wetting and drying. To the extent that disruptive agents cause small random reorientations of the material, the ultimate sample result will be less precise but still accurate. To the extent that slumpage causes the systematic reorientation of large blocks of the material to be sampled, results may be precise but may be inaccurate. Most of these sources of error can be detected and avoided or minimized during specimen collection. Where cracked and potentially displaced material must be sampled (as in many Pajarito Plateau fire hearths where hearth lining material has cracked), field judgments must identify the most stable material. Where there is ambiguity in the integrity of any particular block of burned sediment, multiple specimens from multiple blocks are necessary to evaluate the potential effects of slumpage on the orientations. A sample or set usually consists of eight to 12 specimens. Fewer than eight weakens the statistical confidence measure of the result. More than eight specimens do not materially improve the

statistical precision, but more than eight may be required to cope with sample quality issues that are noted during the collection process.

When columns of burned material have been isolated, they are enclosed within high-precision brass or aluminum molds. The molds are set on bases of modeling clay, which both seal the bottom of the mold to the burned feature and allow the mold to be precisely leveled. After leveling, the mold is filled with a fast-setting plaster, and the contemporary magnetic orientation of the mold is measured with a vetted Brunton compass. Vetting is necessary because of inherent imprecision in the compass manufacturing process; up to seven of every 12 compasses are rejected for inaccuracies that are greater than is acceptable for archaeomagnetic sampling. When the plaster has set, the mold and contents are detached from the feature, the ends of the specimen are trimmed, the base is capped with plaster, and the specimen is labeled so that the mold orientation can be associated with the specimen during measurement.

After collection, samples are transported to the measurement laboratory. At the Archaeomagnetic Dating Laboratory (ADL) at the Museum of New Mexico in Santa Fe, samples are stored under shielded conditions and are measured within Helmholtz coils that are adjusted to create a zero magnetic field around the spinner magnetometer. Storage within a zero field allows weak viscous contaminating magnetic components to dissipate before measurement. Under conditions of a zero magnetic field, measurement accuracy and precision are increased, especially for weak samples. Samples are assigned sequential laboratory numbers. Declinations are assigned to each sample based on the date of collection and the latitude and longitude of the site using either maps of geomagnetic declination or the MagCalc program (1993). The declination allows the magnetic specimen orientation taken during sampling to be translated into an azimuth relative to true north.

Magnetic orientation and strength are first measured for samples (sets of specimens) at their natural remnant magnetism (NRM). The NRM is a combination of the TRM vector of interest and any other vectors that may be present. “Contaminating” vectors can include magnetized pebbles whose size precluded reorientation on heating and viscous magnetic fields that are slowly subject to reorientation by the prevailing earth’s magnetic field. In an effort to remove these contaminating vectors, the specimens are remeasured after progressive AF demagnetization steps. Standard demagnetization and remeasurement are carried out at the following intervals: 50, 100, 150, 200, and 300 Oe (Oersteds). Demagnetization effectively eliminates weakly held magnetic components, from both the TRM and other sources. These secondary components are generally not random and therefore affect both the apparent direction of magnetization and the dispersion of the specimen directions, influencing both the accuracy and precision of pole locations and date estimates. Under ideal conditions, the TRM of interest is the strongest contributor to NRM, and demagnetization eliminates the unwanted components, leaving a residual component that accurately reflects the orientation of the earth's magnetic field at the time of cooling. Under poor conditions (usually extremely weak samples), demagnetization can eliminate the TRM as well as any secondary components before a defensibly “best” orientation is identified.

Since the magnetic history of a sample is unknown and since the strength of spurious magnetic components can vary widely, selection of the "best" demagnetization level for an individual

sample can't be predicted in advance. The best demagnetization level for a sample is identified by the analyst when the direction and dispersion measurements of a specimen suite stabilize, and when the analyst is confident that the direction is appropriate for a TRM result. The latter criterion inserts an undesirable but unavoidable subjectivity into the archaeomagnetic dating process. Since the TRM vector of interest must by definition be a point on the VGP curve, demagnetization results that move the centerpoint toward the curve are judged more likely to accurately reflect the TRM than are results that move the centerpoint away from the curve. The field archaeologist's expectations of sample age influence the archaeomagnetic technician's decisions, as do the currently accepted version of the VGP curve. In the absence of any theoretical model that can distinguish the non-TRM vector contributions to the overall result, the judgment, experience, and biases of the technician are a necessary part of the measurement and dating process.

In some instances, individual specimen measurements deviate markedly from the other specimens of the sample. These outliers are usually defined as specimens that fall beyond two standard deviations of the sample mean. Outliers can be caused simply by sampling error, by unwanted heterogeneity in the specimens (such as magnetized pebbles), or by mistakes in field collection and documentation. The usual procedure is to use Fisher statistics to identify outliers and to progressively eliminate outliers from the set result until the results of the remaining specimens fall within two standard deviations of the new sample mean. If only sampling error were contributing to the dispersion of specimen vectors, 1 out of 20 samples would have a result where a single specimen was eliminated. In practice, more samples than expected have one or more specimens dropped from the final result, reflecting the presence of more potential sources of error than simply the measurement process.

Mean vector direction (recorded as the inclination and declination of the sample) and the dispersion (recorded as an angular expression of alpha 95 or $\acute{\alpha}_{95}$) are used to calculate a VGP for the selected sample result and an oval of confidence around the VGP centerpoint. Where the $\acute{\alpha}_{95}$ dispersion value exceeds 4.0°, the confidence oval is so large that its overlap with dating curve segments generally yields large date ranges that are not useful for the archaeologist. Also, as the α_{95} exceeds 4.0°, there is less and less confidence that the result is exclusively representative of the TRM as opposed to other sources of a magnetic orientation. Although results with α_{95} values of more than 4.0° can be interpreted, the ADL does not routinely assign date ranges to those results. As $\acute{\alpha}_{95}$ values decrease, precision of the VGP location increases. A "good" result generally has an $\acute{\alpha}_{95}$ of less than 2.0° and an excellent result has an $\acute{\alpha}_{95}$ of 1.0° or less. However, measurement precision applies to the estimate of the sample VGP location only, and its extension to a subsequent dating interpretation is dependent on all of the assumptions of the dating technique being correct.

Calibration Curves

Archaeomagnetic dates are estimated by comparing sample results with a calibration or VGP or dating curve. However, as discussed above, VGP curves are approximations since there is no theoretical model for polar movement. We can assume that the true curve is continuous, it can change in its rate of movement, it can turn abruptly or slowly, and it can loop back upon itself in

either short or long time periods. Any attempt to derive a true curve with these qualities from ancient records faces three problems. First is the degree to which the material being sampled is continuously recording the changing VGP and that the material will support a sampling interval that is fine enough that all significant inflection points of the curve are represented in the dataset. Second, since VGPs are measured with error, sample density at each time point must be high enough that a mean VGP location is a valid representation of the curve position. Third, the independent chronology of the samples must be sufficiently robust that samples are not mis-sequenced or mis-dated.

Lake or ocean sediment cores can provide a relatively continuous record of polar movement through detrital remnant magnetism, in which minute magnetized particles are influenced by the prevailing earth's magnetic field as the particles fall through water (Sternberg 1990:18). The particle orientations are set as the sediment gels and compacts, and the sediment sequence becomes a continuous record of secular field variation. Such records would be ideal for VGP curve development, but the theoretical potential runs into practical limitations. Even small variations in sedimentation rates stretch and shrink the record, limiting the simple use of depth as a proxy for an interval or ratio time scale. The physical process of core collection is challenging, and it is difficult to maintain core orientation precisely. Relative declination variation within a core is generally reliable, but the absolute orientation of a core to the modern geomagnetic field is only an approximation. Rapid sedimentation rates are ideal, but core lengths are limited (generally 2 to 3 m), so that long records must be collected by multiple overlapping cores, introducing the problem of core matching, both in a stratigraphic sense and in the sense of consistent specimen orientation. Dating calibration is limited to radiocarbon assays of the organic constituents of the sediments, with the inherent ambiguities of the calibration process (Stuiver and Reimer 1983) and the expense of having to submit multiple and close interval samples to calibrate changes in deposition rates as well as to establish age. Also, detrital magnetism studies have been limited in number, and their geographic positions have been peripheral to the Southwest (e.g., Verosub et al. 1986). Similarities with the Southwestern archaeological VGP curves have been used to validate the detrital curves, rather than the opposite.

At the present time, approximations of the Southwestern VGP curve must be built from large numbers of results from archaeological contexts, using independent sources of dating both to establish the relative sequence of pole positions and the calibration of the resulting curve to the modern time scale. This task is not simple, either in theory or in practice. Archaeological samples are dependent on cultural burning events and on the archaeologists' decisions of what sites will be excavated. There is no guarantee that the cultural burning events are sampling the entire sequence of VGP variation with the same richness, and of the universe of culturally burned sediments, only a small portion has been excavated let alone sampled for archaeomagnetic information. Independent chronological control can be highly variable, from the precision of tree-ring dates to the ambiguity of radiocarbon assays to the generality of phase or ceramic period assignments. Given these limitations, it is remarkable and gratifying that the calibration curves that have been proposed through the years by Robert DuBois, Jeffrey Eighmy, Robert Sternberg, and Daniel Wolfman have been so robust and effective, despite their status as approximations and despite their differences.

Two contrasting approaches have been used for constructing VGP curves in the Southwest (Sternberg and McGuire 1990a, b; Eighmy 1991). One is a moving-window averaging technique. In this method, sample results are arranged by estimated archaeological age (based on independent judgments of the excavators). A weighted average is calculated of the sample results that fall or could fall within a given range of years, and that average is used to define the calibration point for the midpoint of the range. The "window" is advanced by an interval (such as one-half the length of the time window), and another average is calculated and plotted. The calibration curve is then constructed by joining these points.

The second method is a visual or freehand approach. In this method, sample centerpoints are placed on a polar plot, including both independently dated and undated samples. A freehand approach is then used to sketch in a curve, assuming that all samples, whether independently dated or not, should be on or near the curve. Independently dated samples are used to confirm the direction of the curve, to differentiate crossover points and loops, and to calibrate the curve to the modern time scale. Knowledge of the behavior of calibration curves in adjacent regions can also be applied to develop the curve in time periods where sample points are thin or trends are ambiguous.

Both techniques have strengths and limitations. The moving-window approach is replicable and explicit, and it is amenable to computer manipulation so that revised curves are easily constructed as additional calibration data become available. Weaknesses are a reduced sample size, susceptibility to error in archaeological date assignment, and artificial smoothing of variation. Smoothing poses two related problems. Window lengths are set arbitrarily, usually in the range of 40 to 100 years, or can be variable based on data density (Sternberg and McGuire 1990; Eighmy and Klein 1990). VGP variation that occurs at time scales below the window size and interval is effectively lost. In most instances this is inconsequential due to the size of most error ellipses, but it also partially explains the disconcerting consequence that an unusually large number of excellent results ($\acute{\alpha}_{95}$s of 1.0° or less) fall off of the resulting curve. The second and more important problem is that changes in the direction of VGP movement are artificially foreshortened, with the magnitude of the effect proportional to the abruptness of the direction change. Foreshortening is a mathematical consequence of the averaging technique, and the degree and significance was first demonstrated by Cox and Blinman (1999) and then confirmed by Lengyel (1999). The moving window average technique is also susceptible to distortion if archaeologists have misinterpreted the chronology of the calibration samples or if inaccurate VGPs are included in the calibration dataset.

Subjectivity is the principal weakness of the freehand approach to calibration. Because paleomagnetic curves commonly contain loops and intersections, sample results that are not independently dated can be interpreted based on preconceptions of curve direction. Also, familiarity with individual samples or suites of samples can lead to over-interpretation of small (<2°) curve features such as loops and kinks. As a result, two researchers given the same data are unlikely to produce precisely the same curve. Strengths of the technique are that it makes use of a large amount of data and that it need not systematically dampen variation. The large number of data points has the potential to increase the resolution of the curve, especially if there are cultural factors that reduce the number of independently dated samples for specific time periods. Perhaps more important is that there is no systematic foreshortening bias built into the technique,

so that there is an opportunity for more accurate representation of loops and short term deflections of the curve. However, due to the subjectivity of curve construction, there is no internal standard against which the accuracy of the curve can be measured.

Three calibration curves are currently available for the interpretation of dates from Southwestern sample results (Figure 9.1). Robert DuBois' Southwest curve (1989) is a freehand compilation based on four decades of research on Southwestern archaeomagnetic dating. His curve is unique in including a pre-AD 600 component, but its calibration is more general than the other curves, and it is rarely used by other researchers for date interpretation except in the pre-AD 600 period. Stacey Lengyel and Jeffrey Eighmy's SWCV2000 curve is the latest revision of a long series of moving average-based curves produced by Eighmy's Archaeometric Laboratory at Colorado State University (Eighmy 1991; Eighmy and Klein 1990; LaBelle and Eighmy 1995). The Eighmy curves have generally superceded the curves developed by Robert Sternberg (1990) using the same averaging technique. The SWCV2000 curve is a methodological departure in that it incorporates modifications to the moving average results. Simulations were used to estimate and correct for the magnitude and direction of foreshortening at inflection points, and non-calibration data were used to modify the location of the curve in the AD 900 to 1025 segment. Daniel Wolfman's curve is a freehand compilation based on his interpretation of his own data. He lacked data to improve on the various Eighmy curves or on the DuBois curve for the AD 400 to 1000 and post-AD 1450 time periods. Wolfman's curve has been in use for some time (Windes 1991:297–304), but formal publication of the curve was posthumous (Cox and Blinman 1999). The data Wolfman used to construct the curve have never been completely reconstructed.

Differences between the three curves are both minor and dramatic, depending on the time period. This reflects the tentative nature of our understanding of the Southwest VGP curve as well as the different methodological approaches to curve construction. Small discrepancies in both path and calibration characterize the AD 400–1150 period segments of the three curves, but the discrepancies by and large have little effect on date interpretations. In contrast, there are large and significant differences in the AD 1150–1800 period, and in particular the AD 1150–1400 period. The DuBois and Wolfman freehand curves are similar, but the more explicitly developed SWCV2000 differs markedly. These differences are incompatible with the magnitude of many sample error terms, resulting in an inordinately large number of precise results (α_{95}s of 2.0° or less) that fall significantly off of one or more of the curves. These differences have also been evident in a number of incorrect date interpretations, where demonstrably post-AD 1150 samples were being given pre-AD 1150 date assignments, and vice versa. Since only one true curve exists, portions or all of each of the three extant curve models are probably incorrect for the AD 1150–1400 time period.

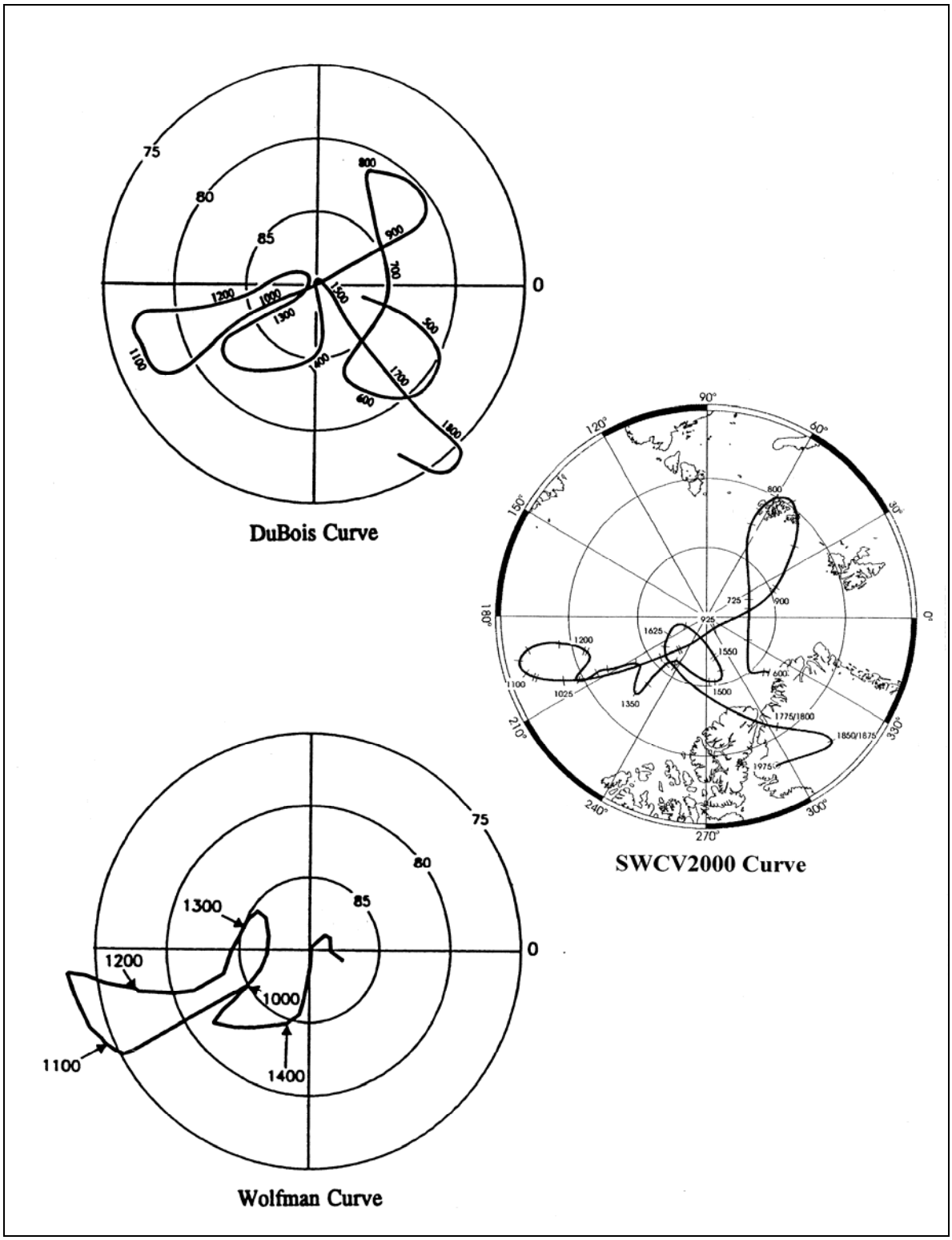

Figure 9.1. Current archaeomagnetic dating curves for the Southwestern United States. The DuBois curve is adapted from DuBois (1989), the SWCV2000 curve is from Lengyel and Eighmy (2002), and the Wolfman Curve is from Cox and Blinman (1999).

This significant weakness in the calibration curves for archaeomagnetic dating coincides, unfortunately, with the period of interest in Pajarito Plateau chronology (Vierra et al. 2002a). The initiation of the Coalition period is placed around AD 1150 (Vierra et al. 2002a) or AD 1200 (Powers and Van Zandt 1999). Trajectories of population growth and aggregation are demonstrable through the Coalition period, but the dynamics of those trajectories are still poorly understood for lack of a robust chronology through the 13th and 14th centuries. Significant regional changes in population aggregation (nucleation) define the onset of the Classic period at AD 1325, and large pueblo-based or village-based settlement patterns persist until the onset of the Spanish Colonial period at AD 1600.

CURVE PERFORMANCE EVALUATION

Ambiguities surrounding the AD 1150–1400 VGP curve segments can be explored with a performance evaluation of the proposed curves. The template for this approach was developed in an evaluation of the AD 650–950 portion of the SWCV590 curve (Cox and Blinman 1999). The underlying assumption is that archaeomagnetic results are all valid "samples" of the true curve position. Each will reflect a location of the earth's geomagnetic pole at the time of cooling, with an error that stems principally (although not entirely) from measurement uncertainties. Additional sources of error may be present, and those must be considered during data interpretation. The method of curve evaluation is most easily characterized as a study of residuals. Samples are reviewed for relevance to a particular curve segment. Sample centerpoints are plotted in relation to the curve, residual distances are calculated between the centerpoints and the curve, and the magnitude and sign of the residuals are evaluated for the presence of any systematic patterns. If the curve is a valid approximation of the true curve, residuals should be randomly distributed around the curve, and most sample error terms (α_{95}s) should overlap with the curve. In the AD 650–950 curve evaluation, we were able to demonstrate that the moving average technique used to develop the SWCV590 curve systematically biased the curve at its inflection points (Cox and Blinman 1999), resulting in confirmation of our conclusions with a simulation approach (Lengyel 1999), and revision of the Eighmy curve to begin to correct the problem (Lengyel and Eighmy 2002).

The original residual study was conducted by hand using graphic techniques (Cox and Blinman 1999). The steps have now been automated using the capabilities of Surfer and custom programs written in C++. The steps in the analysis consist of 1) rendering the curve to be evaluated as a "string of pearls," 2) development of a dataset of relevant (or possibly relevant) archaeomagnetic results, 3) residual calculation, and 4) data analysis and interpretation.

Curve rendering was accomplished by digitizing a proposed curve and replacing the table of digitized points with points that are evenly distributed along the path of the curve (a "string of pearls"). The calibration points (dates) proposed by the curve authors were added to the table at the appropriate points along the curve, and intervening dates were interpolated for each point. As the most widely used curve in the interpretation of contemporary archaeomagnetic results, the SWCV2000 curve was used for segment definition. Arbitrary break points were defined along the curve, each representing both a discrete period of time and a distinctive feature of the curve. The segment definitions are provided in Table 9.1.

Table 9.1. Segment definitions for curve performance evaluation.

Segment number	Beginning date (AD)	Ending date (AD)
1	NA	400
2	400	600
3	600	800
4	800	950
5	950	1125
6	1125	1225
7	1225	1300
8	1300	1400
9	1400	1500
10	1500	1600
11	1600	1900

The datasets chosen for comparison with the curve segments in this study come from data provided by Robert DuBois. These archaeomagnetic results were not used in producing either the SWCV2000 or the Wolfman Curve, and therefore they can be viewed as independent comparative information. Only results with $\acute{\alpha}_{95}$ values of 3.0° or less were selected for use in the comparison. Independent chronological information for many of the results is sketchy, but most samples could be assigned to one or more segments after researching site notes and interviewing archaeologists. We expect that additional research will improve the precision in the assignments of individual samples to the segments. Segments 5 through 9 are most relevant to the culture history of the Pajarito Plateau, and only those segments are treated in the following discussion.

AD 950–1125 (Segment 5)

Segment 5 of both the SWCV2000 and Wolfman Curves are generally similar in path location and pace (Figure 9.2). The Wolfman Curve begins at AD 1000 rather than 950, explaining part of the apparent discrepancy at the early end of the curves. The most significant difference is the extension of the Wolfman Curve to below 74° N latitude at its most extreme, while SWCV2000 loops back at about 76° N latitude. The Wolfman Curve also remains at higher longitudes in the decades before AD 1100 than SWCV2000.

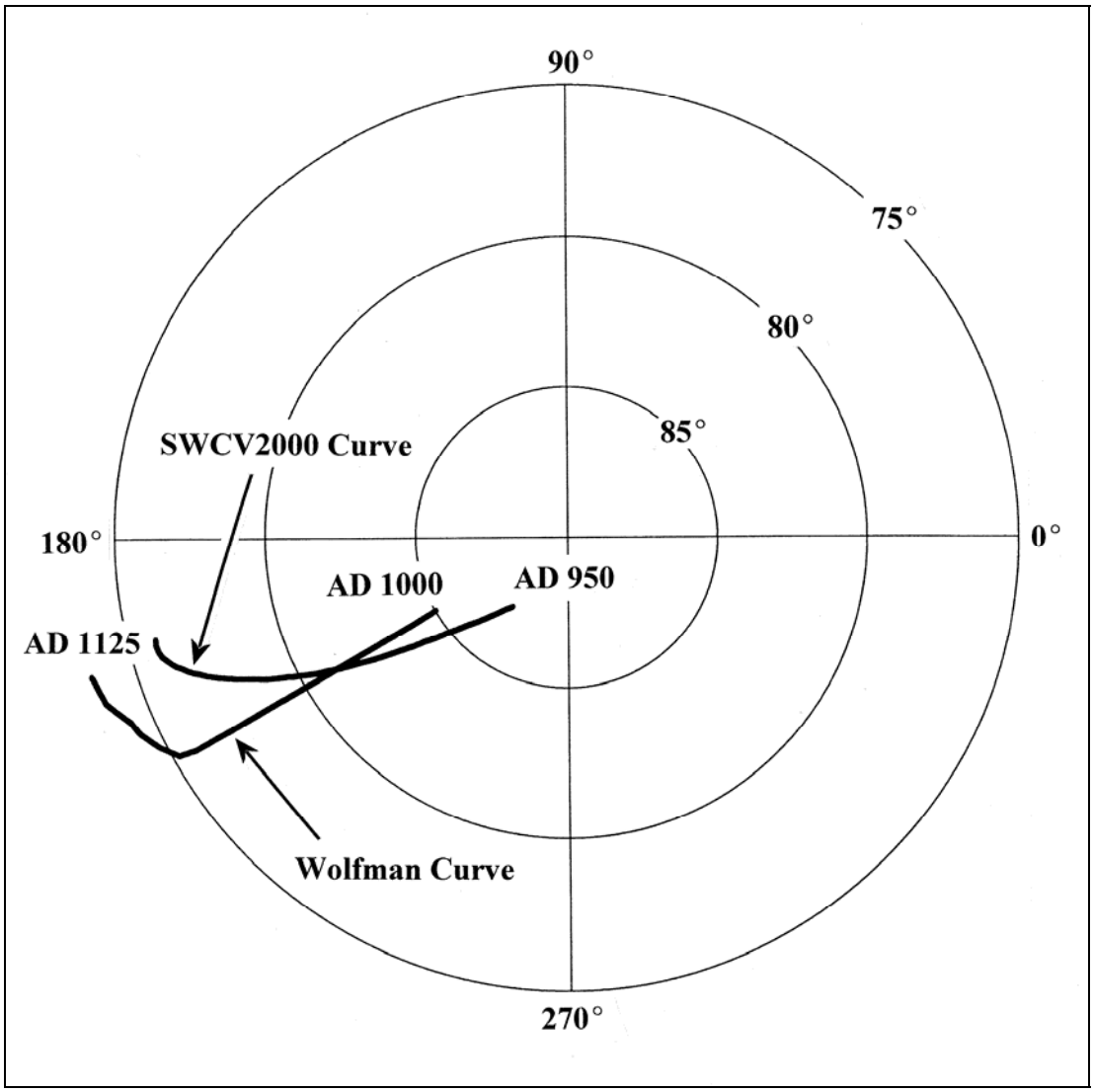

Figure 9.2. AD 950 to 1125 and AD 1000 to 1125 segments of the SWCV2000 and Wolfman VGP curves.

SWCV2000 is compared with results from the DuBois database that might date to the AD 950–1125 period in Figure 9.3. Samples that might date within the AD 950–1125 segment or earlier are indicated with circles. Open circles are results that could date as much as two segments earlier, while solid circles are probably either associated with this segment or one segment earlier. Results marked with "+" signs are assigned exclusively to this segment with relatively strong confidence. Results identified with square symbols either date to this segment or to a later segment. Solid squares could date in the next segment, while open squares could be relevant to either of the next two segments as well as perhaps being associated with Segment 5. Three results (all circles) are located between 0 and 90 longitude and clearly are related to pre-AD 950 segments of the curve. Two other possibly early results are located along this segment of VGP curve and probably date to this period. All of the sample results that were confidently expected to be along this segment are generally in the curve vicinity, validating their temporal placement. The results that might be either contemporary with or slightly later than this segment include a

number of centerpoints that extend to both lower longitudes and latitudes than the AD 1125 end of the curve. Otherwise they cluster relatively evenly around the VGP path. The most temporally ambiguous of the later samples (the open squares) tend to cluster within the limits of the curve but are relatively consistently above the curve.

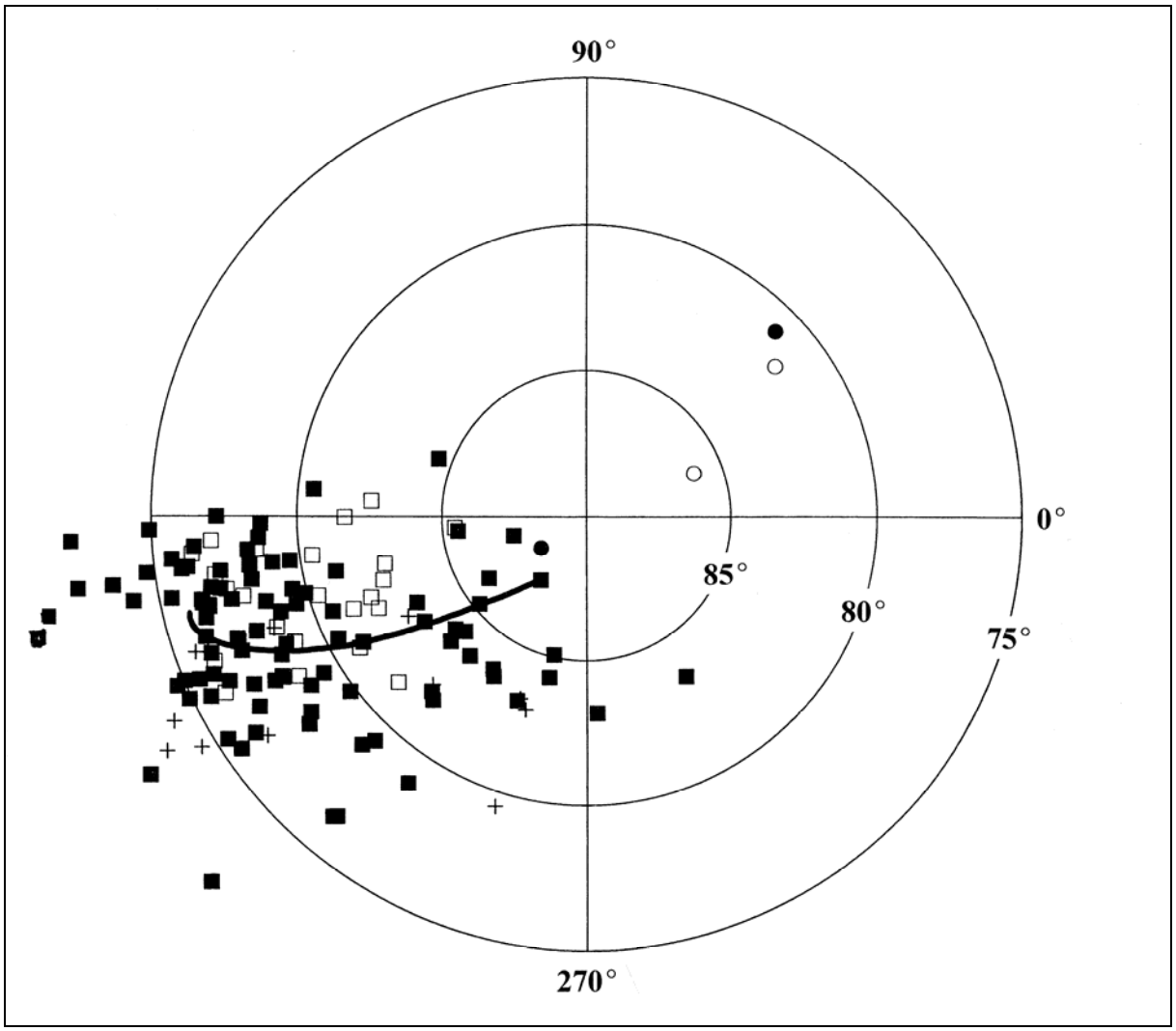

Figure 9.3. Archaeomagnetic result centerpoints from the DuBois database that could date to the AD 950 to 1125 period. Open circles denote samples that are believed to date within the AD 600 to 1125 period. Solid circles denote samples that are believed to date with the AD 800 to 1125 period. Samples denoted by a "+" are exclusively dated to the AD 950 to 1125 period. Solid squares denote samples that are believed to date within the AD 950 to 1225 period. Open squares denote samples that are believed to date within the AD 950 to 1300 period. All centerpoints are associated with α_{95} values of 3.0° or less.

Only those results that are exclusively and confidently associated with the AD 950–1125 period are presented in Figure 9.4.

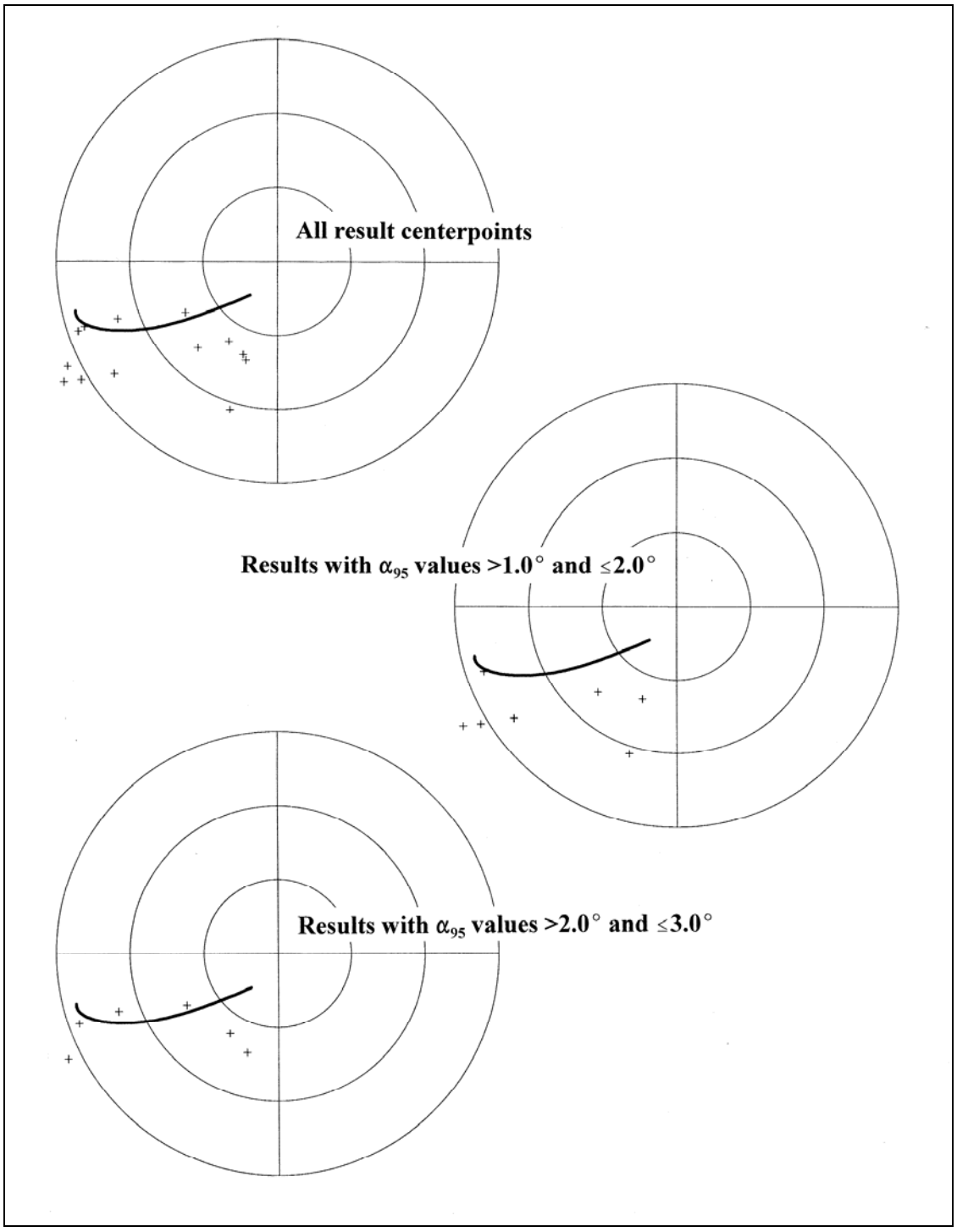

Figure 9.4. DuBois archaeomagnetic results that are confidently and exclusively associated with the AD 950 to 1125 period, contrasted with the SWCV2000 VGP curve. The upper figure includes all results, regardless of precision. The lower plots include only moderate and low precision results, respectively.

All results are plotted together, and additional plots are provided that present the same results by precision categories. These overall results strongly suggest that the SWCV2000 segment is placed too low in longitude, and this is confirmed by looking only at the moderate precision results ($\alpha_{95} \leq 2.0°$). Residuals calculated for these samples are overwhelmingly negative for the entire length of the curve segment, as graphed against time (date of the closest point on the SWCV2000 curve) in Figure 9.5. This discrepancy in curve path is consistent with the observation by Lengyel and Eighmy (2002) that there is anecdotal evidence for a lower latitude path than was produced by the moving average technique using the independently dated samples alone.

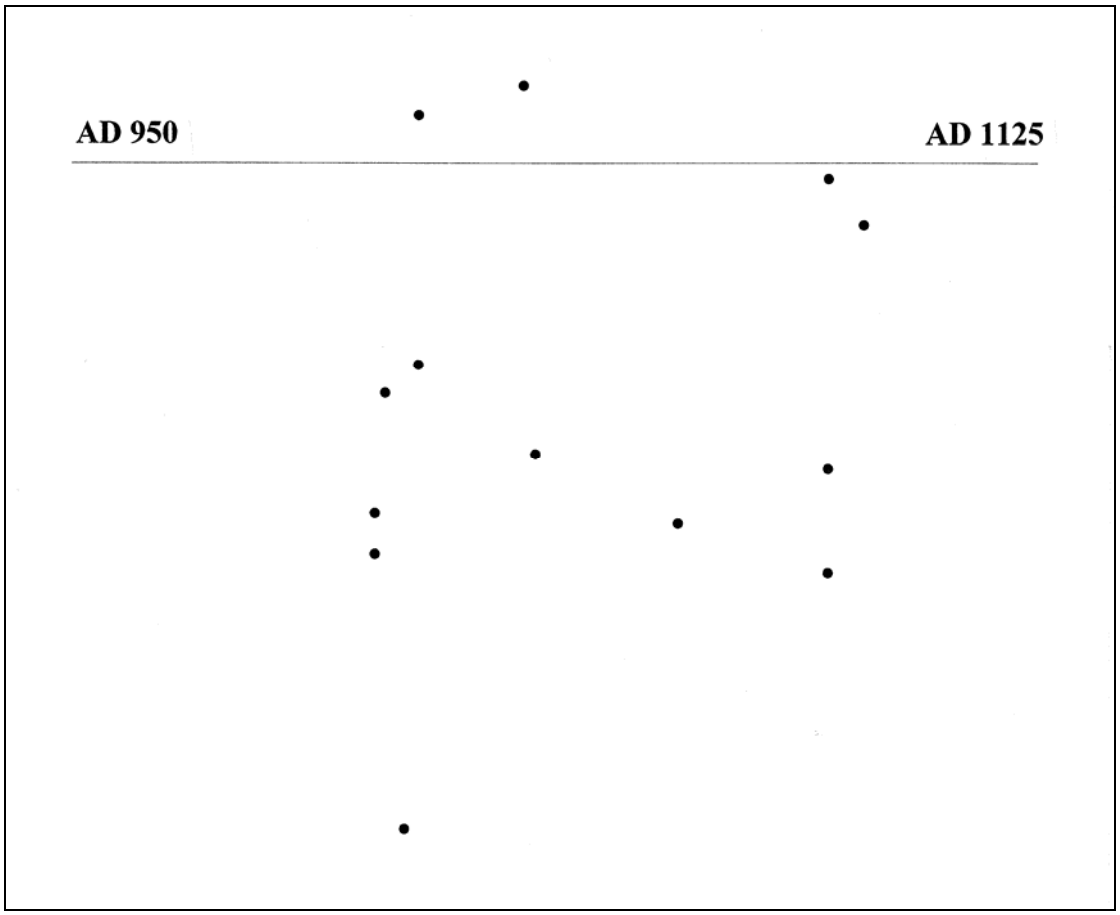

Figure 9.5. Plot of residual distances from confidently attributed AD 950 to 1125 sample centerpoints and nearest points along the AD 950 to 1125 segment of SWCV2000.

The same DuBois AD 950–1125 result dataset is contrasted with the Wolfman Curve in Figure 9.6. Although the Wolfman Curve begins at AD 1000 rather than 950, as with the SWCV2000 curve, four of the potentially early samples (solid and open circles) fall off the curve at the younger end. The potentially contemporary or slightly later samples (solid squares) are clustered both around the curve and off of the later end of the curve, while the potentially contemporary and much later samples (open squares) tend to fall above the curve (lower longitudes).

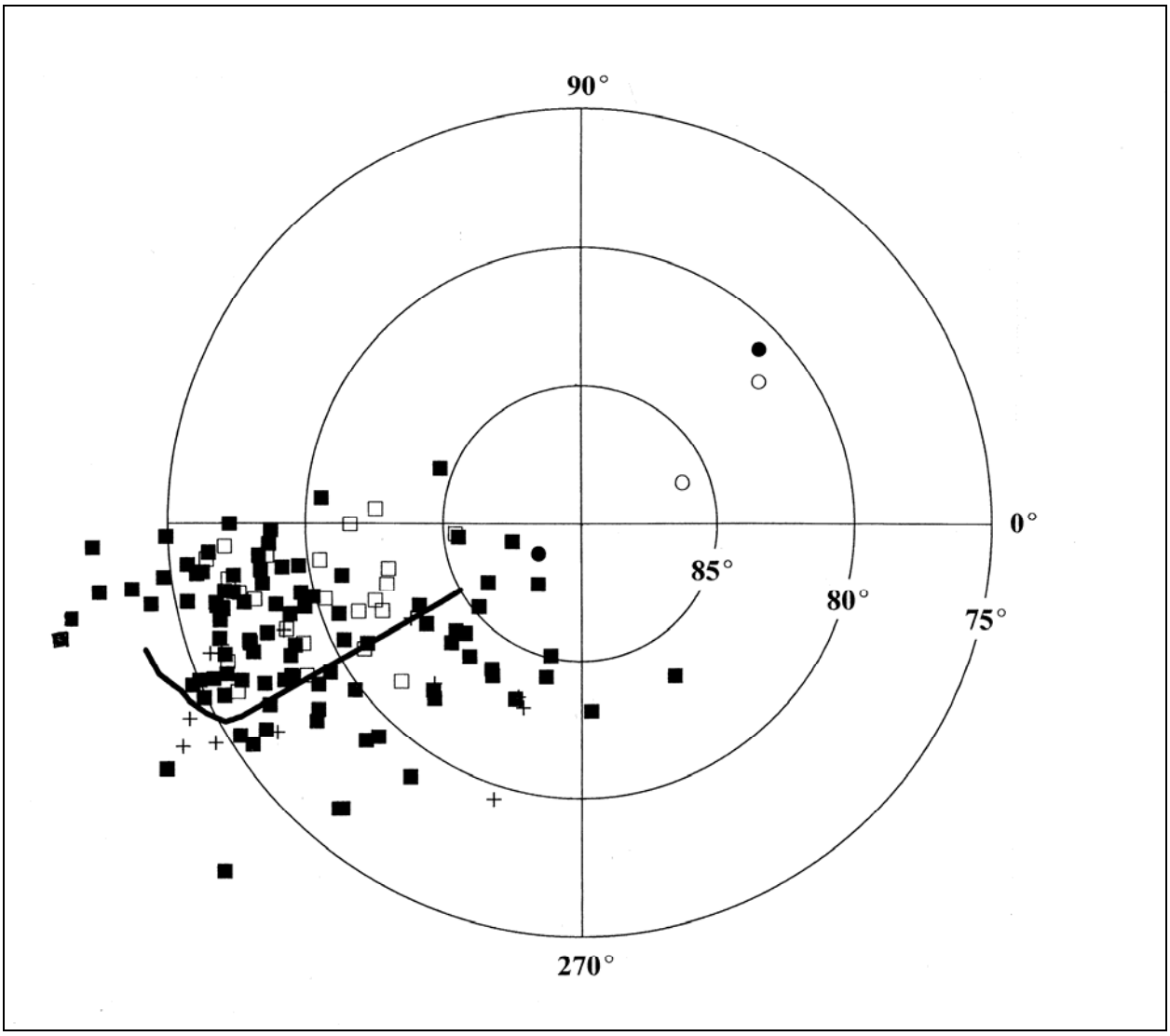

Figure 9.6. The AD 1000 to 1125 segment of the Wolfman Curve and archaeomagnetic result centerpoints from the DuBois database that could date to the AD 950 to 1125 period. Open circles denote samples that are believed to date within the AD 600 to 1125 period. Solid circles denote samples that are believed to date within the AD 800 to 1125 period. Samples denoted by a "+" are exclusively dated to the AD 950 to 1125 period. Solid squares denote samples that are believed to date within the AD 950 to 1225 period. Open squares denote samples that are believed to date within the AD 950 to 1300 period. All centerpoints are associated with α_{95} values of 3.0° or less.

The 13 results that are confidently associated with the AD 910–1125 time period (+) are presented without the more ambiguous data points in Figure 9.7. The scatter suggests that the Wolfman Curve is more consistent than the SWCV2000 curve in representing the results, but only slightly more consistent and only in the last half of the curve segment. The first half of the curve segment appears to be at a lower latitude than is suggested by the locations of the DuBois centerpoints, a suggestion supported by both the moderate and low precision results. This conclusion is clearly evident in the residual plot for the pre-AD 1050 period (Figure 9.8).

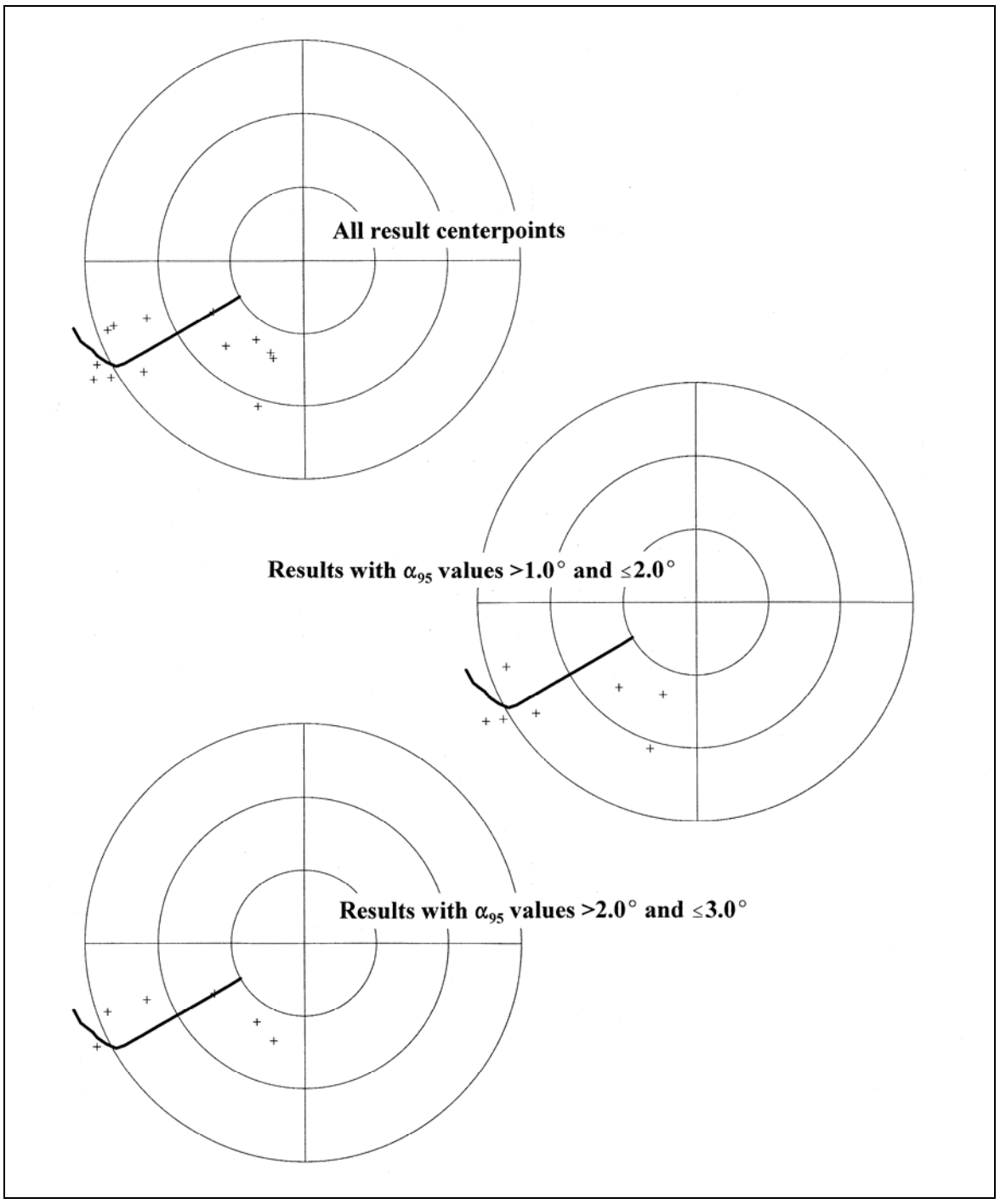

Figure 9.7. DuBois archaeomagnetic results that are confidently and exclusively associated with the AD 950 to 1125 period, contrasted with the Wolfman VGP curve from the AD 1000 to 1125 period. The upper figure includes all results regardless of precision. The lower plots include only moderate and low precision results, respectively.

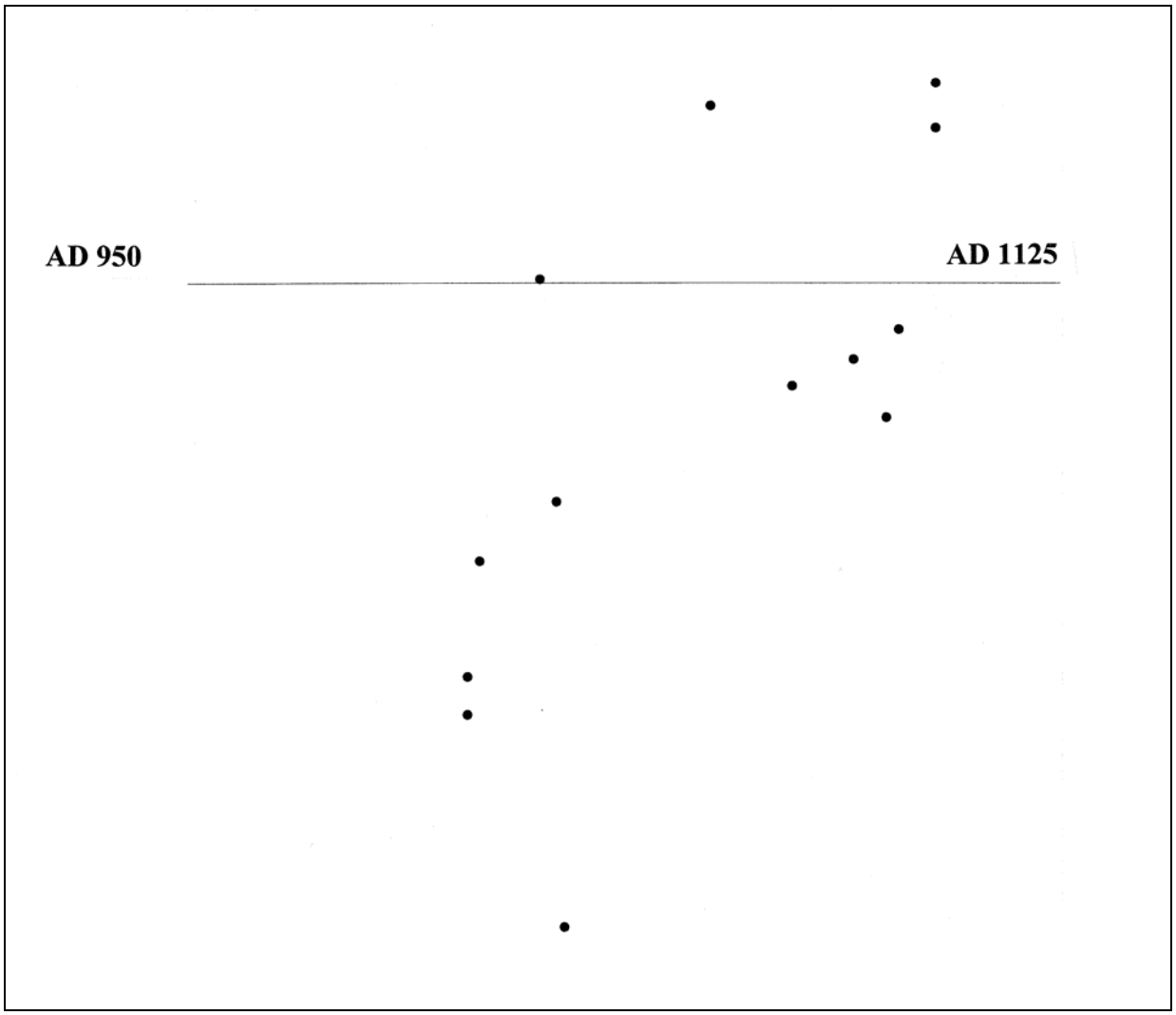

Figure 9.8. Plots of residual distances from confidently attributed AD 950 to 1125 sample centerpoints and nearest points along the AD 1000 to 1125 segment of the Wolfman Curve.

The post-AD 1050 segment has a more normally distributed pattern of residuals, but the termination of this curve segment may be slightly too extreme (too low in both latitude and longitude). The latter observation is weak simply because there are too few points in the DuBois dataset to be confident, and there are a number of potentially contemporary or later results (solid squares) that are at lower latitudes and longitudes.

This tentative evaluation of Segment 5 suggests that neither the SWCV2000 nor Wolfman Curves adequately represent a VGP path that would best account for the samples in the DuBois dataset. The post-AD 1050 segment of the Wolfman Curve may be more accurate, while the paths of both curves appear to need adjustment toward higher longitudes in the pre-AD 1050 period.

AD 1125–1225 (Segment 6)

The VGP path reverses itself in a loop at some time near or after AD 1125. The SWCV2000 and Wolfman approximations of the AD 1125–1255 VGP path are presented in Figure 9.9. The VGP curves are in relatively close agreement of the pole position at about AD 1225, but they disagree at AD 1125 and for the subsequent 50 to 60 years. The Wolfman Curve begins at a lower latitude and remains below 76° latitude until shortly after AD 1180. Where SWCV2000 presents the inflection point of the reversal at AD 1125, the Wolfman Curve proposes that the inflection is delayed until approximately AD 1150.

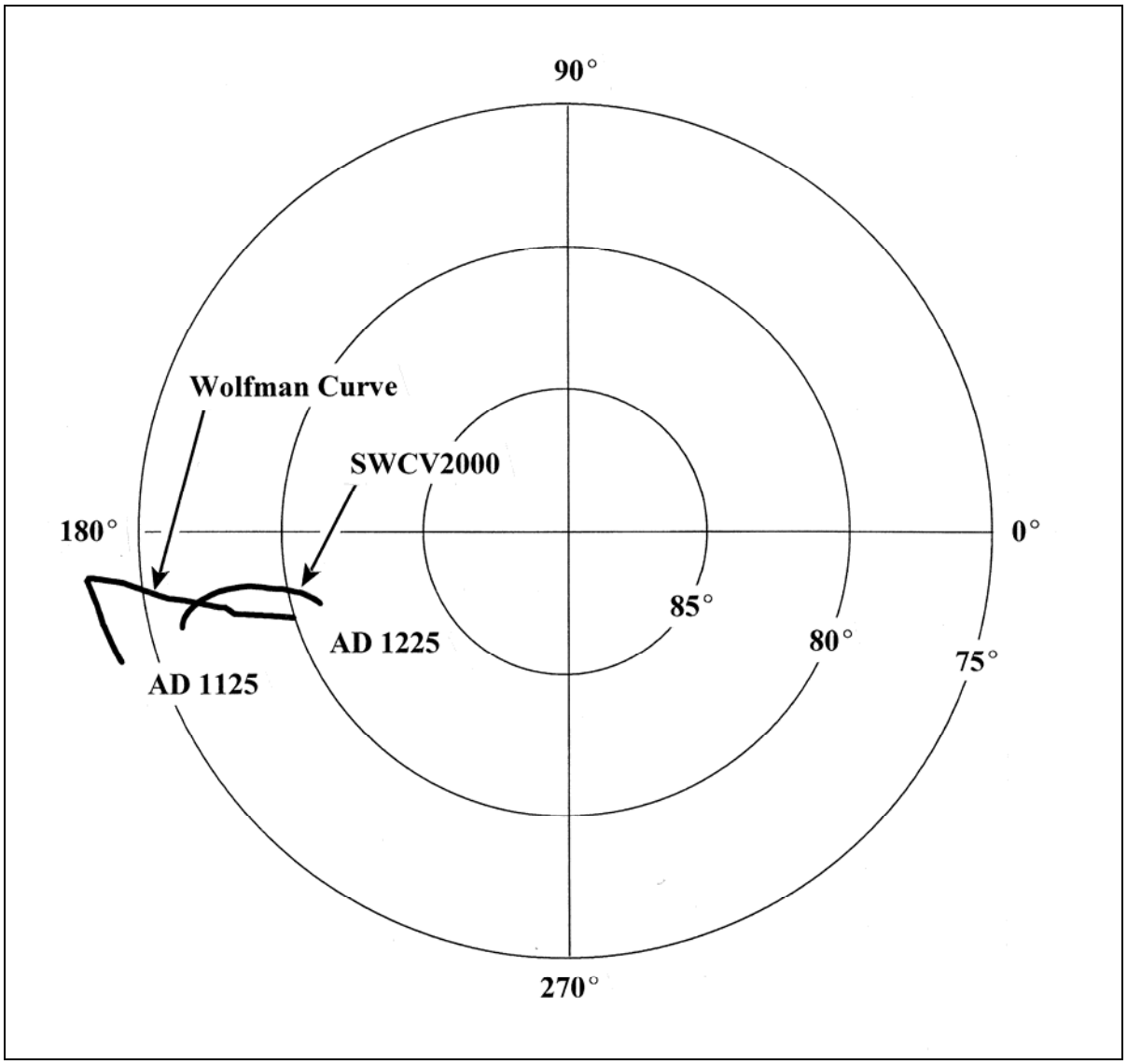

Figure 9.9. AD 1125 to 1225 segments of the SWCV2000 and Wolfman VGP curves.

Sample results from the DuBois database that could be contemporary with the AD 1125–1225 period are plotted with the AD 1125–1225 segment of SWCV2000 in Figure 9.10. Those results whose independent dating suggests that they are contemporary with or earlier than the segment

(solid circles) are scattered around the segment, with the majority below (at higher longitudes) where earlier samples might be expected to fall. A small number are located off the early end of the curve, at lower latitudes. Results whose independent dating could be contemporary with or either slightly later (solid squares) or significantly later (open squares) tend to be located around the curve, below the curve (lower longitudes), or to the right (higher latitudes).

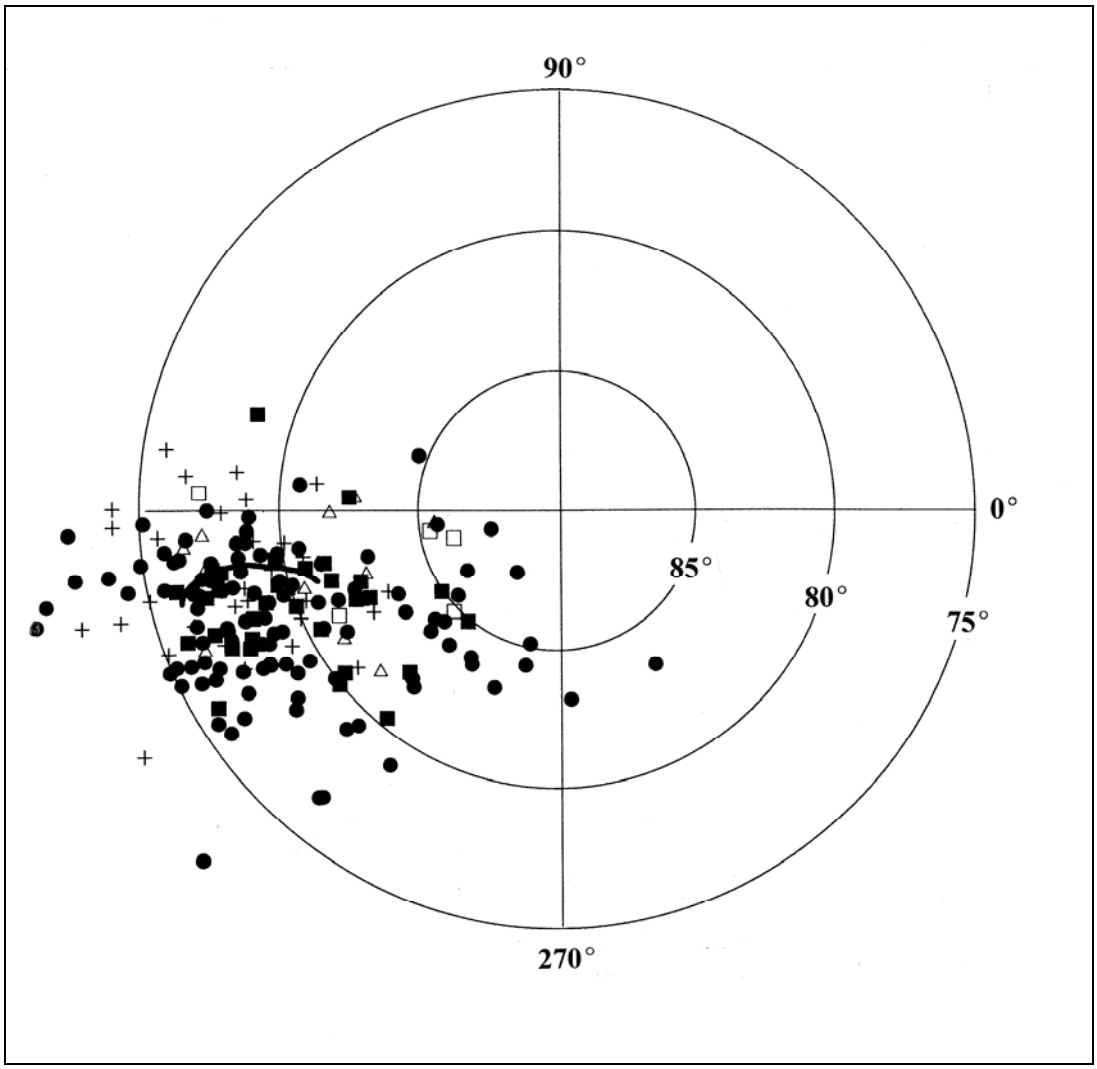

Figure 9.10. SWCV2000 and archaeomagnetic result centerpoints from the DuBois database that could date to the AD 1125 to 1225 period. Open circles denote samples that are believed to date within the AD 800 to 1225 period. Solid circles denote samples that are believed to date within the AD 950 to 1225 period. Samples denoted by a "+" are exclusively dated to the AD 1125 to 1225 period, while samples marked with an open triangle are dated to the broader AD 950 to 1300 period. Solid squares denote samples that are believed to date within the AD 1125 to 1300 period. Open squares denote samples that are believed to date within the AD 1125 to 1400 period. All centerpoints are associated with α_{95} values of 3.0° or less.

Those samples that are confidently and exclusively associated with AD 1125–1225 period based on independent evidence are illustrated without the less precisely dated results in Figure 9.11.

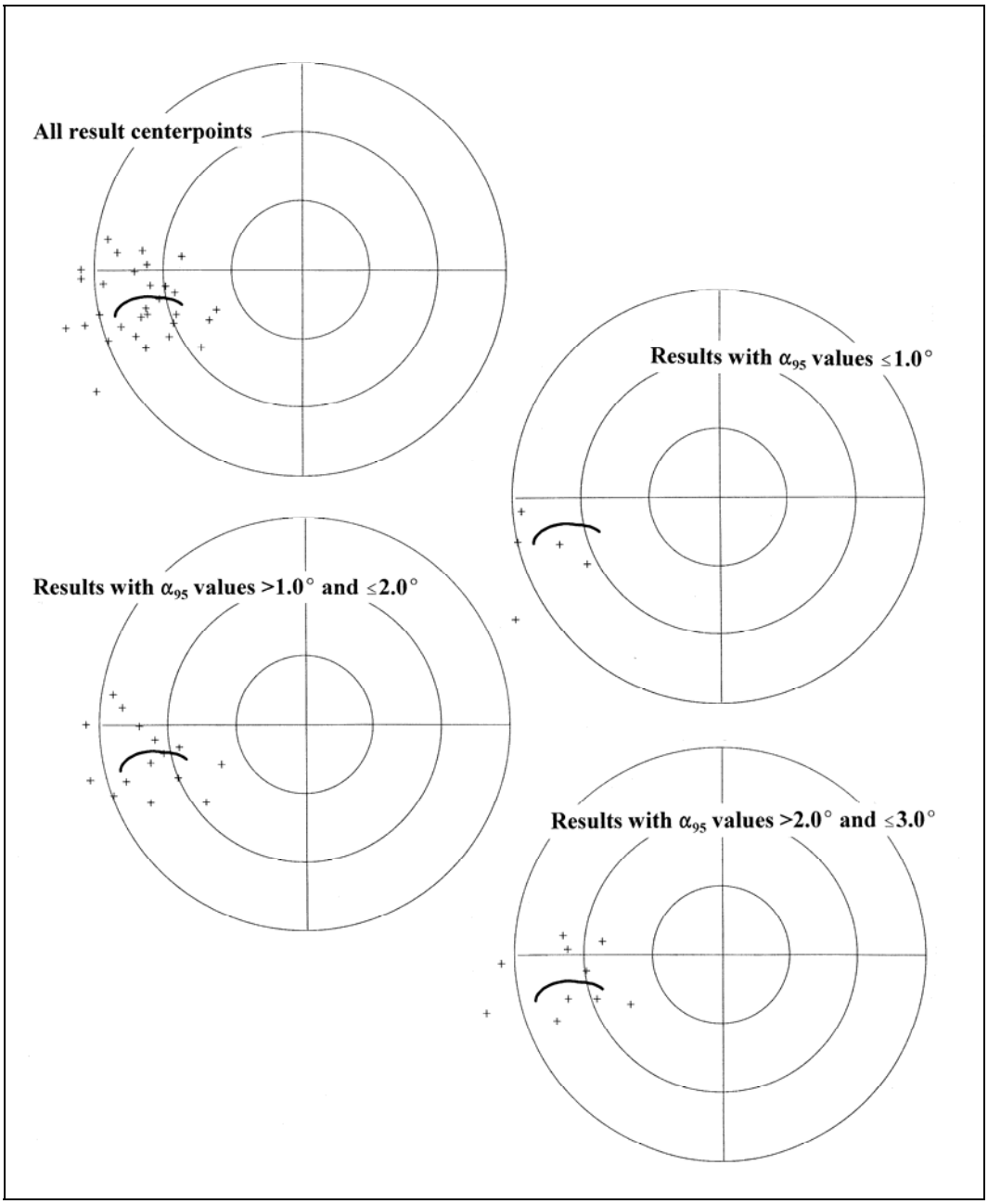

Figure 9.11. DuBois archaeomagnetic results that are confidently and exclusively associated with the AD 1125 to 1225 period, contrasted with the SWCV2000 VGP curve. The upper plot includes all results, regardless of precision. The other plots distinguish high, moderate, and low precision results.

One extremely precise result (α_{95}<1.0°) falls at a considerable distance from the curve at higher longitudes and latitudes. Moderately precise results (1.0°<α_{95}<2.0°) include several that fall at

lower longitudes and lower latitudes. The low precision results are all closely within their errors of the SWCV2000 segment. A plot of the residual distances of these high precision results from their closest points on the curve is presented in Figure 9.12.

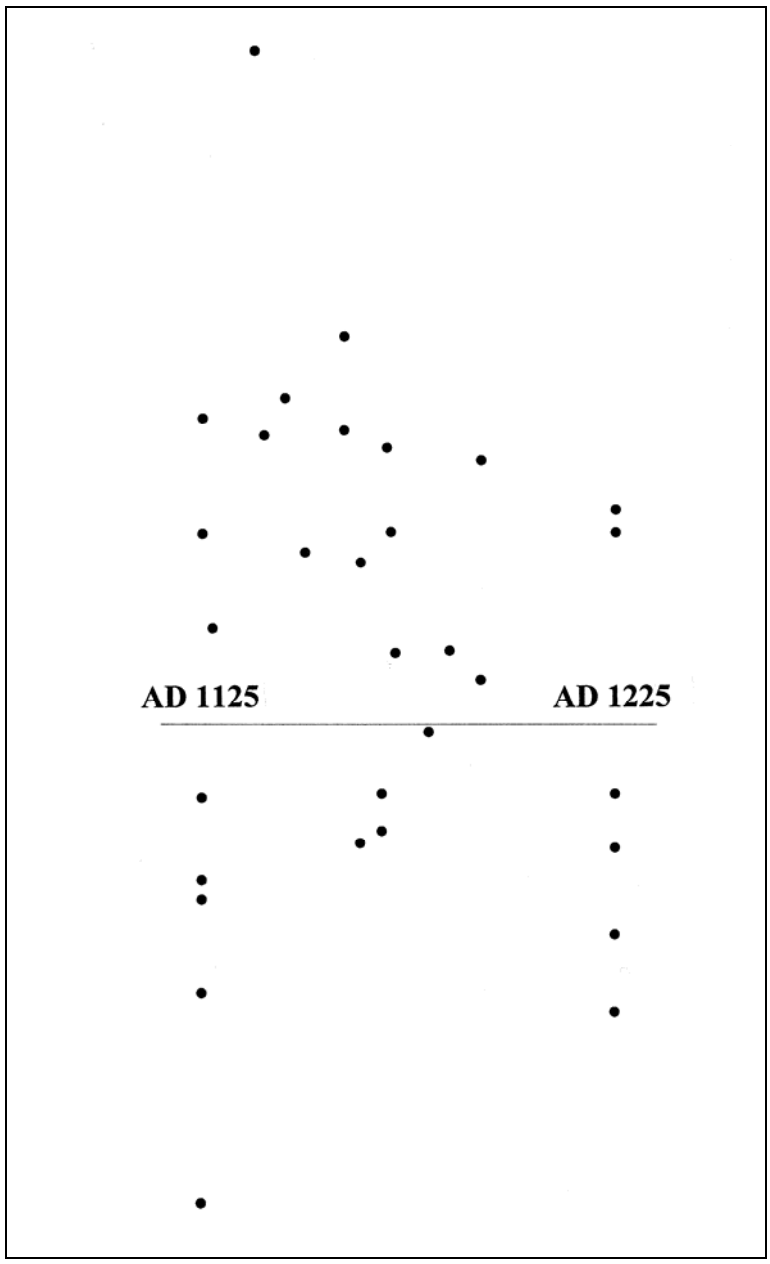

Figure 9.12. Plot of residual distances from confidently attributed AD 1125 to 1225 sample centerpoints and nearest points along the AD 1125 to 1225 segment of SWCV2000.

Unlike the previous segment, residuals are not patterned on either side of the curve, but there are concentrations of large residuals at the ends of the segment. The three results that are substantially distant from the AD 1225 end of the segment are associated with moderate and low

precision VGP estimates. A larger number of results, including high precision estimates, are at a distance from the AD 1125 end of the segment.

The same DuBois results are contrasted with the Wolfman Curve for the AD 1125–1225 period in Figure 9.13.

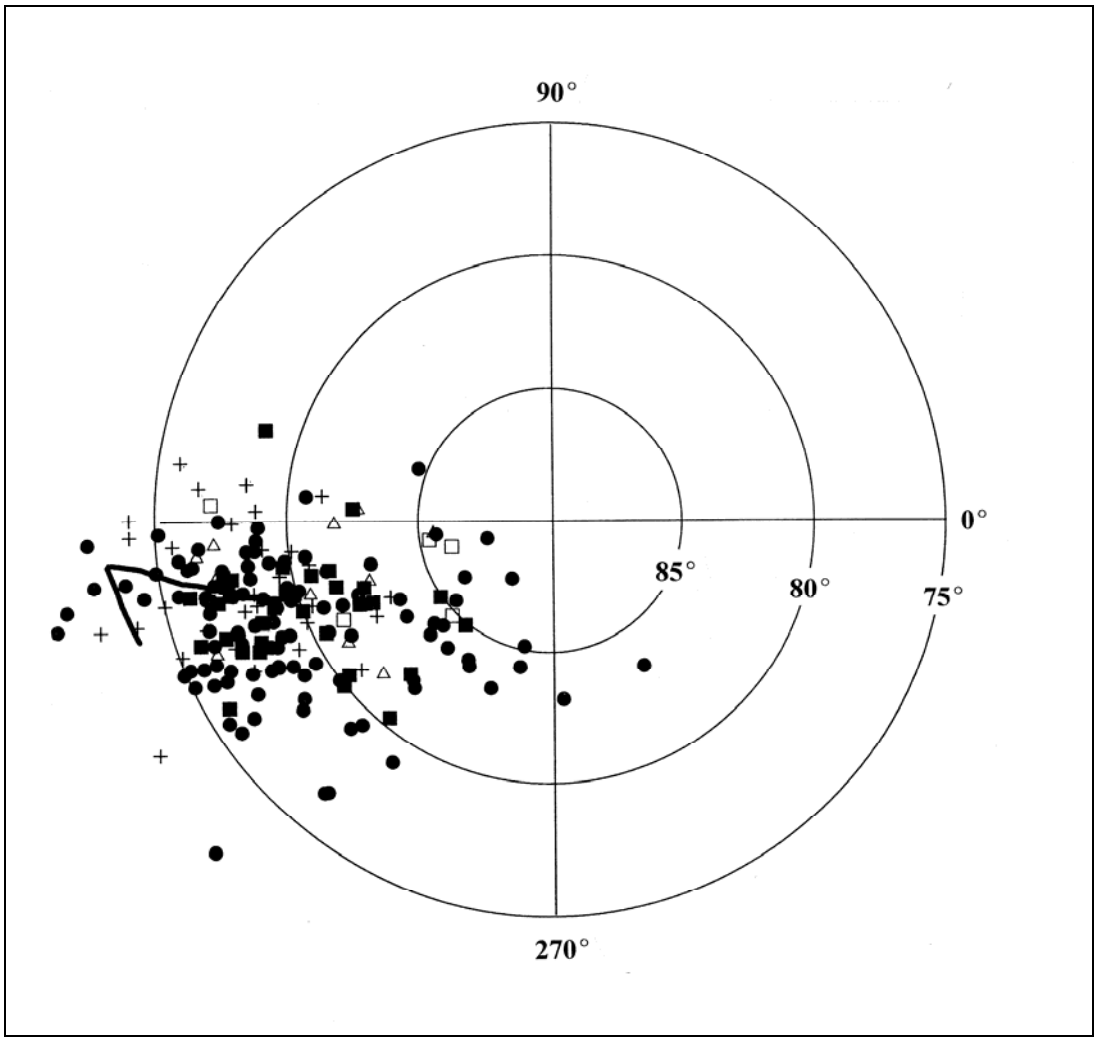

Figure 9.13. The AD 1125 to 1225 segment of the Wolfman Curve and archaeomagnetic result centerpoints from the DuBois database that could date to the AD 1125 to 1225 period. Open circles denote samples that are believed to date within the AD 800 to 1225 period. Solid circles denote samples that are believed to date within the AD 950 to 1225 period. Samples denoted by a "+" are exclusively dated to the AD 1125 to 1225 period. Solid squares denote sample that are believed to date within the AD 1125 to 1300 period. Open squares denote samples that are believed to date within the AD 1125 to 1400 period. All centerpoints are associated with α_{95} values of 3.0° or less.

In general, the same comparisons hold for the samples that could be earlier and the samples that could be later. There is, however, a slightly better fit between the Wolfman Curve segment and

the results that can be confidently and exclusively attributed to this period (Figure 9.14). A single high precision result is significantly off the AD 1125 end of the curve, but the discrepancy is less than that associated with the SWCV2000 curve. The late end of the segment seems to be at an appropriate longitude, although there is a slight suggestion in the moderate precision results that the AD 1225 point should be extended to a slightly higher latitude. There is less support for the low latitude path of the portion of the curve between AD 1125 and 1150, and there is even some suggestion that the inflection point should be closer to 76° latitude and 180° longitude.

Because of the inflection of this segment of the Wolfman Curve, the residual plot is somewhat less useful than it might be, especially for the pre-AD 1175 portion of the curve (Figure 9.15). However, a slight dominance of positive residuals along the last half of this segment supports the suggestion that a slightly lower latitude path from the inflection point may be appropriate. Also, the cluster of residuals that fall off the AD 1225 end of the curve segment support the need to extend this portion of the curve to higher latitudes.

In comparing the performance of the two curves for the AD 1125–1225 period (see Figures 9.9, 9.11, and 9.14), a compromise between the two paths would seem to be called for. The DuBois dataset does not support the excursion of the early portion of the Wolfman Curve along such a low latitude path, but it does suggest that the path needs to extend to lower latitudes than is represented by SWCV2000. A very slightly wedge-shaped distribution of points along the low latitude end of the scatter provides weak support for an inflection point in the early portion of this time period (as represented in the Wolfman Curve), but that point would need to be closer to 76° latitude and 180° longitude than where the inflection point is currently drawn. The slightly lower (higher longitude) termination path of the Wolfman Curve for the period is supported by the high and moderate precision results of the confidently and exclusively attributed samples, but that support fades when the low precision results are added to the evaluation. Regardless, the comparison suggests that the AD 1225 extension of the SWCV2000 curve is probably more accurate and that the AD 1225 point may even need to be pushed to a slightly higher latitude.

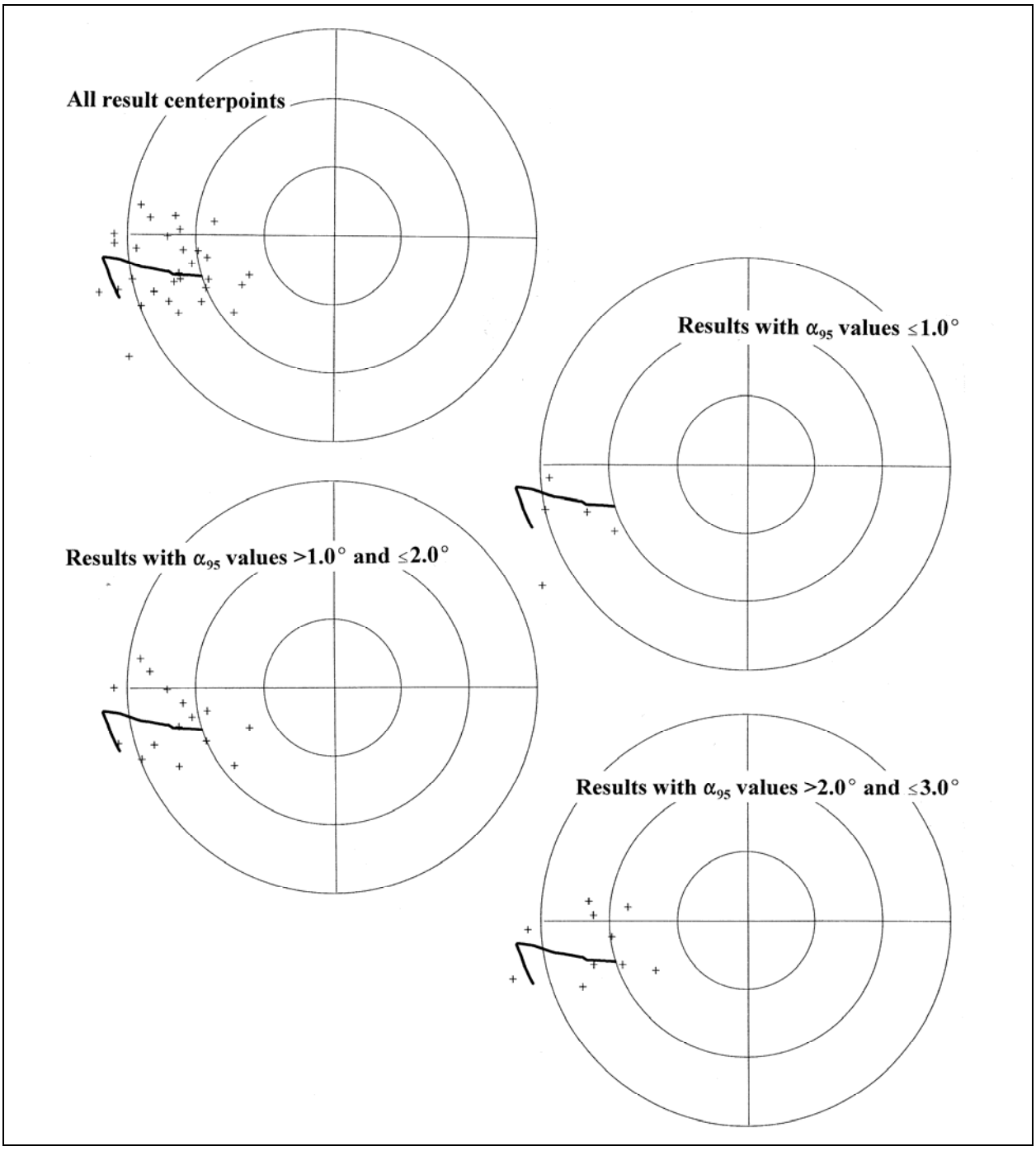

Figure 9.14. DuBois archaeomagnetic results that are confidently and exclusively associated with the AD 1125 to 1225 period, contrasted with the Wolfman VGP curve for the AD 1125 to 1225 period. The upper figure includes all results, regardless of precision. The lower plots include only moderate and low precision results, respectively.

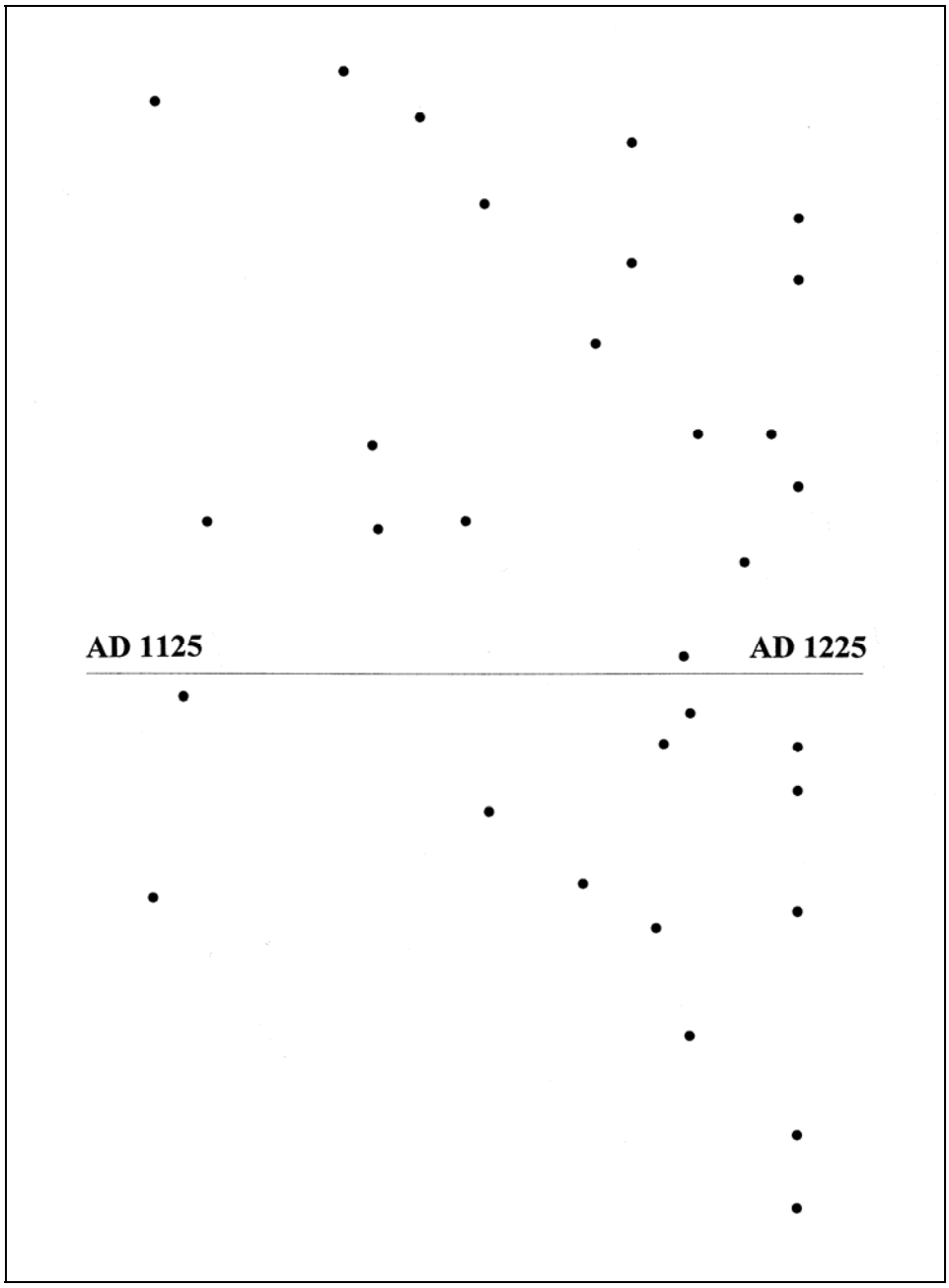

Figure 9.15. Plot of residual distances from confidently attributed AD 1125 to 1225 sample centerpoints and nearest points along the AD 1125 to 1225 segment of the Wolfman Curve.

AD 1225–1300 (Segment 7)

The greatest discrepancies between current Southwest VGP curves begin at AD 1225. The SWCV2000 and Wolfman Curve segments for the AD 1225–1300 period are presented in Figure 9.16. Both begin at approximately the same position, but the end points differ radically. SWCV2000 portrays the VGP movement as extremely slow and in the form of a relatively tight

loop. The progression of the curve is so slow that only samples with remarkably precise results ($\alpha_{95} \leq 0.5°$) could distinguish features that dated to the extreme ends of the period. The Wolfman Curve is radically different, suggesting polar movement at approximately the same rate as the preceding period, and with a termination point significantly distant from the starting point.

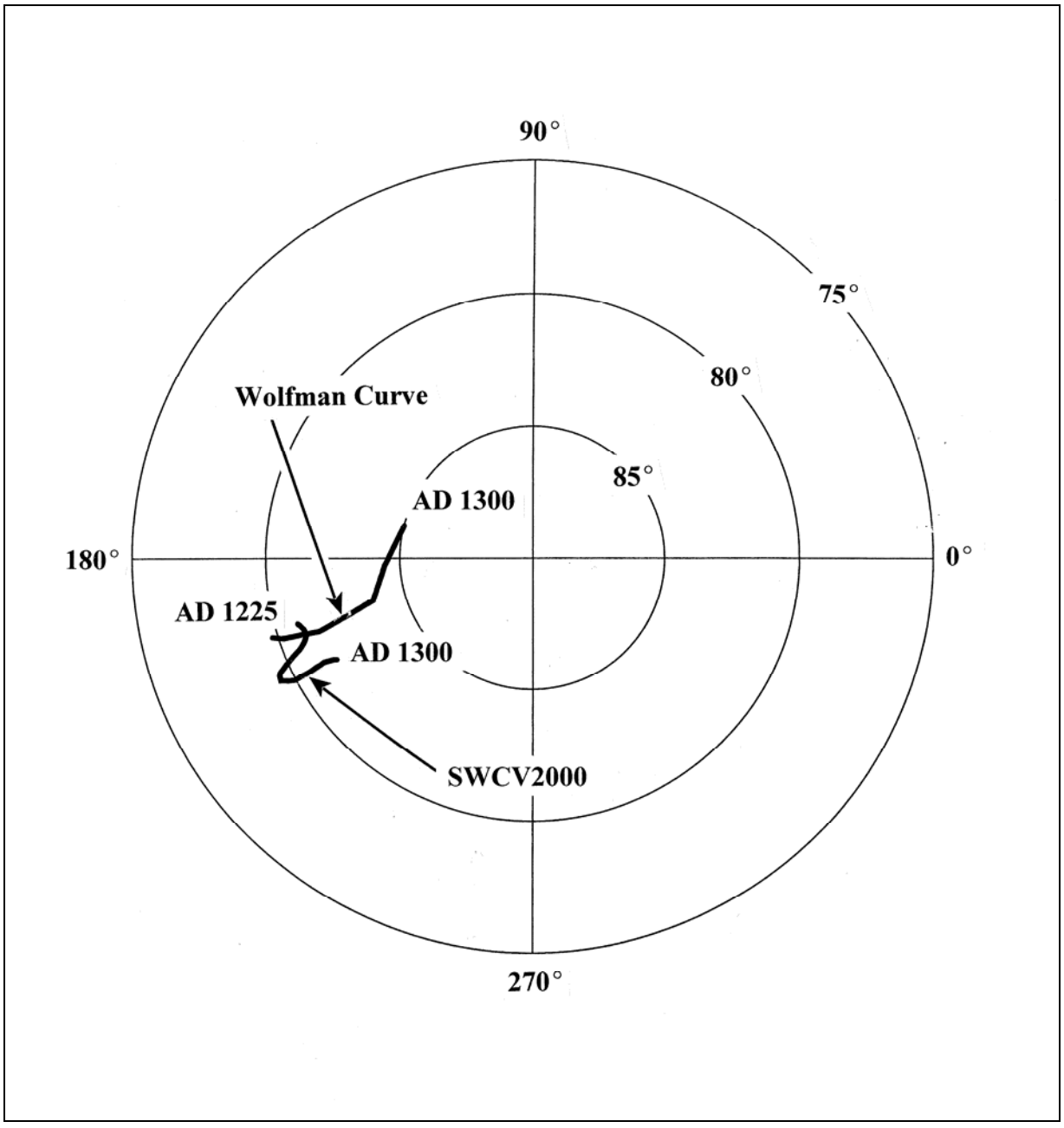

Figure 9.16. AD 1225 to 1300 segments of the SWCV2000 and Wolfman VGP curves.

The DuBois dataset is contrasted with the SWCV2000 curve in Figure 9.17. Contemporary or potentially earlier results (solid and open circles) tend to be scattered both around the curve segment and toward lower latitudes (in the area of the AD 1125–1225 segment). Contemporary

or potentially later results (solid and open squares) are much more dispersed, with clusters both around the segment and at higher latitudes and slightly higher longitudes.

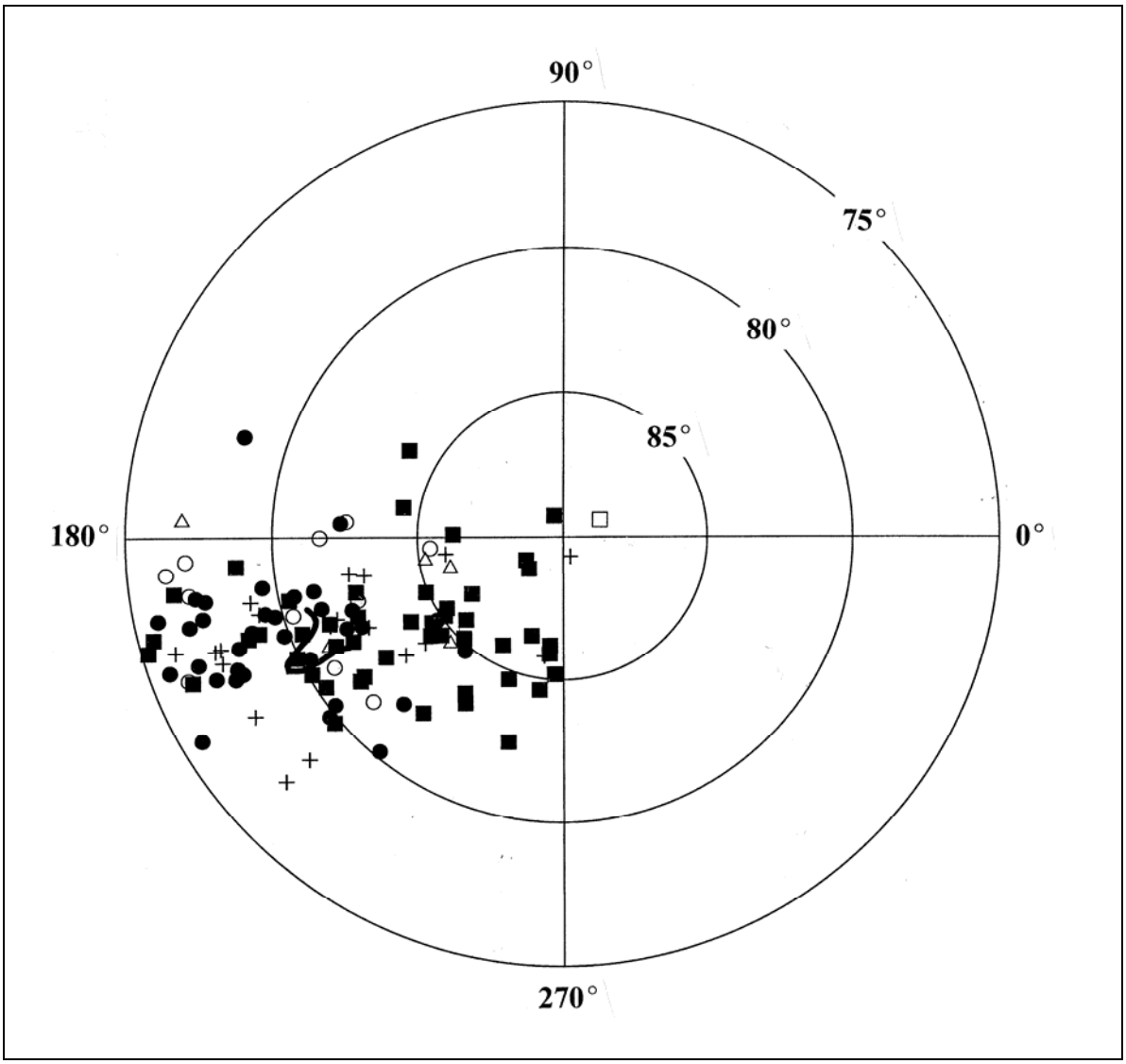

Figure 9.17. SWCV2000 and archaeomagnetic result centerpoints from the DuBois database that could date to the AD 1225 to 1300 period. Open circles denote samples that are believed to date within the AD 950 to 1300 period. Solid circles denote samples that are believed to date within the AD 1125 to 1300 period. Samples denoted by a "+" are exclusively dated to the AD 1225 to 1300 period, while samples marked with an open triangle are dated to the broader AD 1125 to 1400 period. Solid squares denote samples that are believed to date within the AD 1225 to 1400 period. Open squares denote samples that are believed to date within the AD 1225 to 1500 period. All centerpoints are associated with a α_{95} values of 3.0° or less.

Results that are confidently and exclusively attributed to the AD 1225–1300 period are isolated from the less-well-dated results in Figure 9.18.

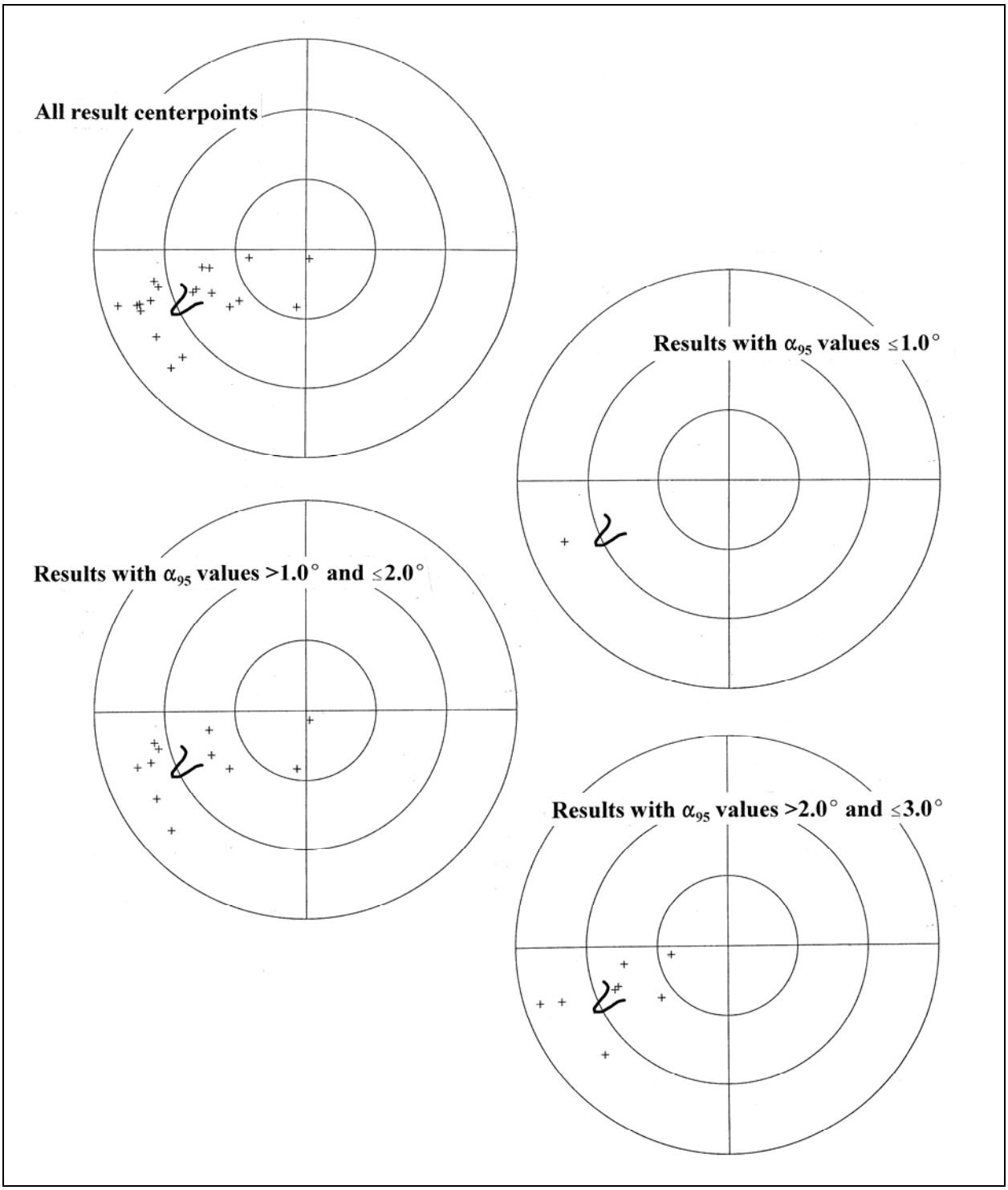

Figure 9.18. DuBois archaeomagnetic results that are confidently and exclusively associated with the AD 1225 to 1300 period, contrasted with the SWCV2000 VGP curve. The upper plot includes all results, regardless of precision. The other plots distinguish high, moderate, and low precision results.

Only one of the results is extremely precise, and it lies off of the curve at a lower latitude. Moderately precise results both cluster around the curve and tend to spread linearly, toward and away from the North Pole. The centerpoints associated with low precision results are similar in dispersion to the moderate precision results. Residual distances between the centerpoints and the curve are less useful as an analytic tool for this segment due to the short and reflexive nature of the curve segment. The distances were divided into those for centerpoints that are closer to the North Pole (positive) and those centerpoint distances that are further away (negative), and the distances are plotted in Figure 9.19. Positive residuals tend to be greater in magnitude, reflecting an apparent longitudinal linearity that is not captured by the SWCV2000 curve.

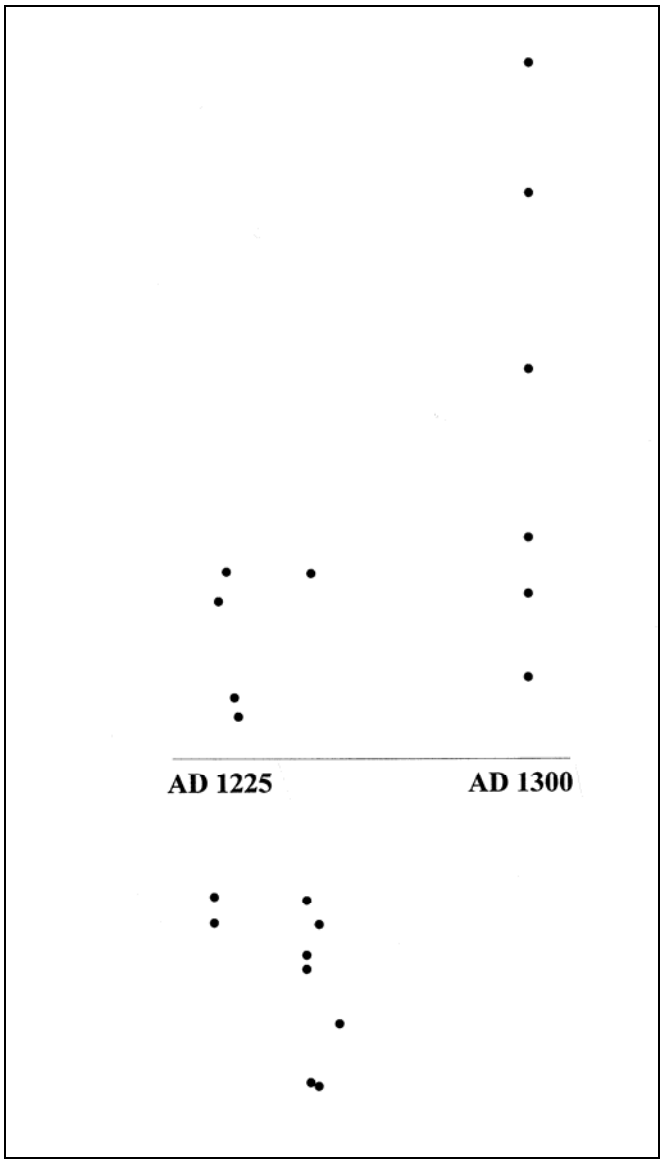

Figure 9.19. Plot of residual distances from confidently attributed AD 1225 to 1300 sample centerpoints and nearest points along the AD 1225 to 1300 segment of SWCV2000.

The same Dubois AD 1225–1300 dataset is contrasted with the Wolfman Curve in Figure 9.20.

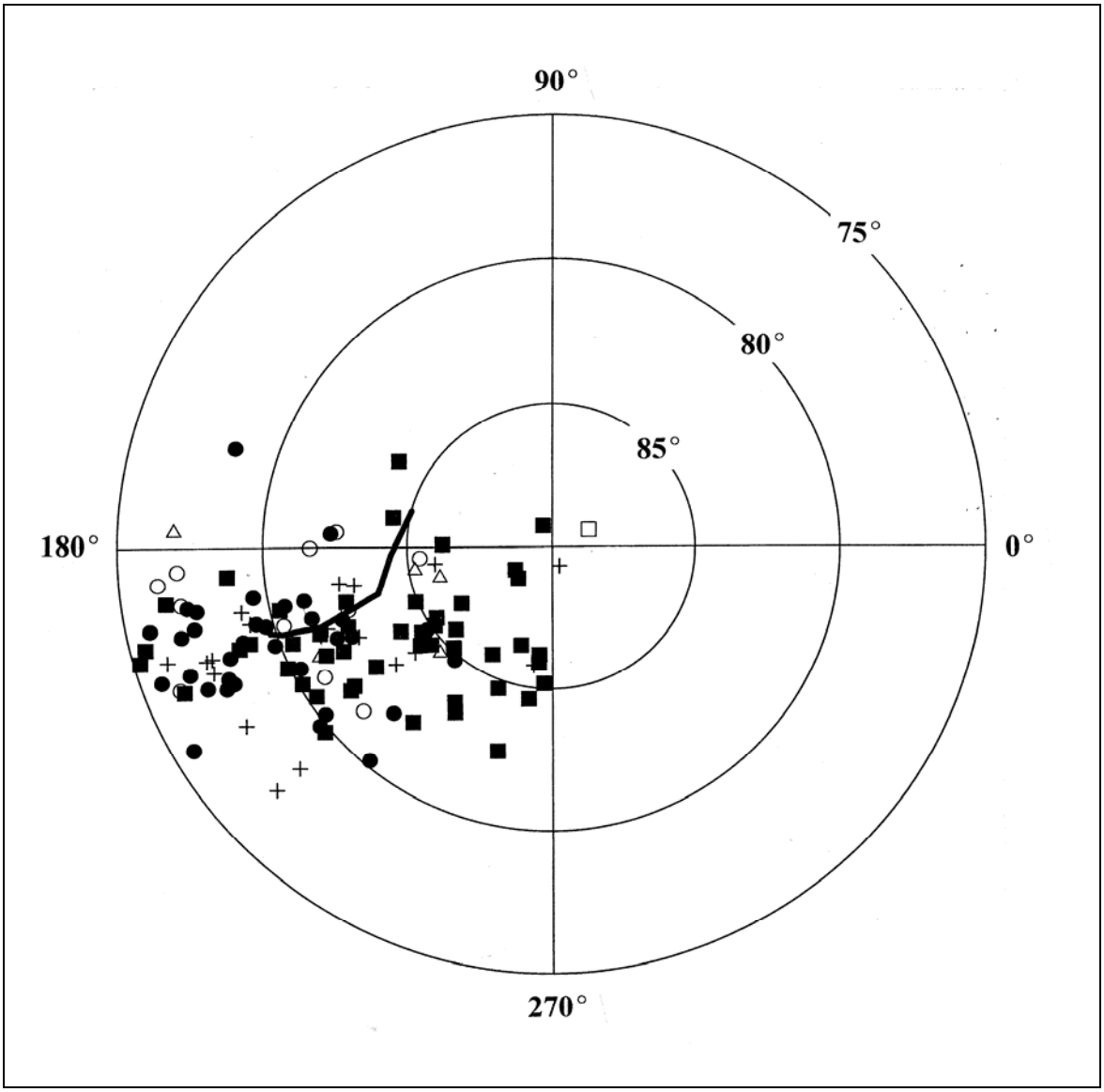

Figure 9.20. The AD 1225 to 1300 segment of the Wolfman Curve and archaeomagnetic result centerpoints from the DuBois database that could date to the AD 1225 to 1300 period. Open circles denote samples that are believed to date within the AD 950 to 1300 period. Solid circles denote samples that are believed to date within the AD 1125 to 1300 period. Samples denoted by a "+" are exclusively dated to the AD 1225 to 1300 period, while samples marked with an open triangle are dated to the broader AD 1125 to 1400 period. Solid squares denote samples that are believed to date within the AD 1225 to 1400 period. Open squares denote samples that are believed to date within the AD 1225 to 1500 period. All centerpoints are associated with α_{95} values of 3.0° or less.

Contemporary or potentially earlier results (solid and open circles) tend to cluster around the earlier one-third of the Wolfman Curve segment and extend to lower latitudes in the approximate

area of the AD 1125–1225 segment. Samples that are contemporary or potentially later (solid and open squares) are more broadly distributed, again clustering around the earlier half of the Wolfman Curve segment as well as filling an area toward higher latitudes and slightly higher longitudes. A few of the contemporary or potentially later sample results are near the AD 1330 end of the curve segment, but much fewer than are in the other areas of the scatter.

Only the results that are confidently and exclusively attributed to the AD 1225–1300 period are included in the plots of Figure 9.21. The single high precision result is just outside the early end of the curve. The moderate precision results are scattered mainly below the curve (higher longitudes), and a cluster of results extends beyond the early end of the segment. No samples cluster around the later one-third of the segment, while two centerpoints are much closer to the north pole. Low precision results mirror the moderate precision scatter, and the total distribution suggests that a slightly longer path at higher longitudes would better match the DuBois data. The residual distance between the centerpoints and the nearest points on the curve segment support this conclusion (Figure 9.22), with an inordinately high proportion of negative residuals and a large numbers of and magnitudes for residuals associated with the end points of the segment.

If the samples in the DuBois dataset are representative of the AD 1225–1300 time period, neither curve adequately reflects the true VGP path. There appears to be greater linearity to the path than is represented by the reflexive and short SWCV2000 segment. The Wolfman segment is too low in longitude, and there is little support for the even lower longitude termination of the segment. In both cases, a path toward the north pole would more completely account for the available data.

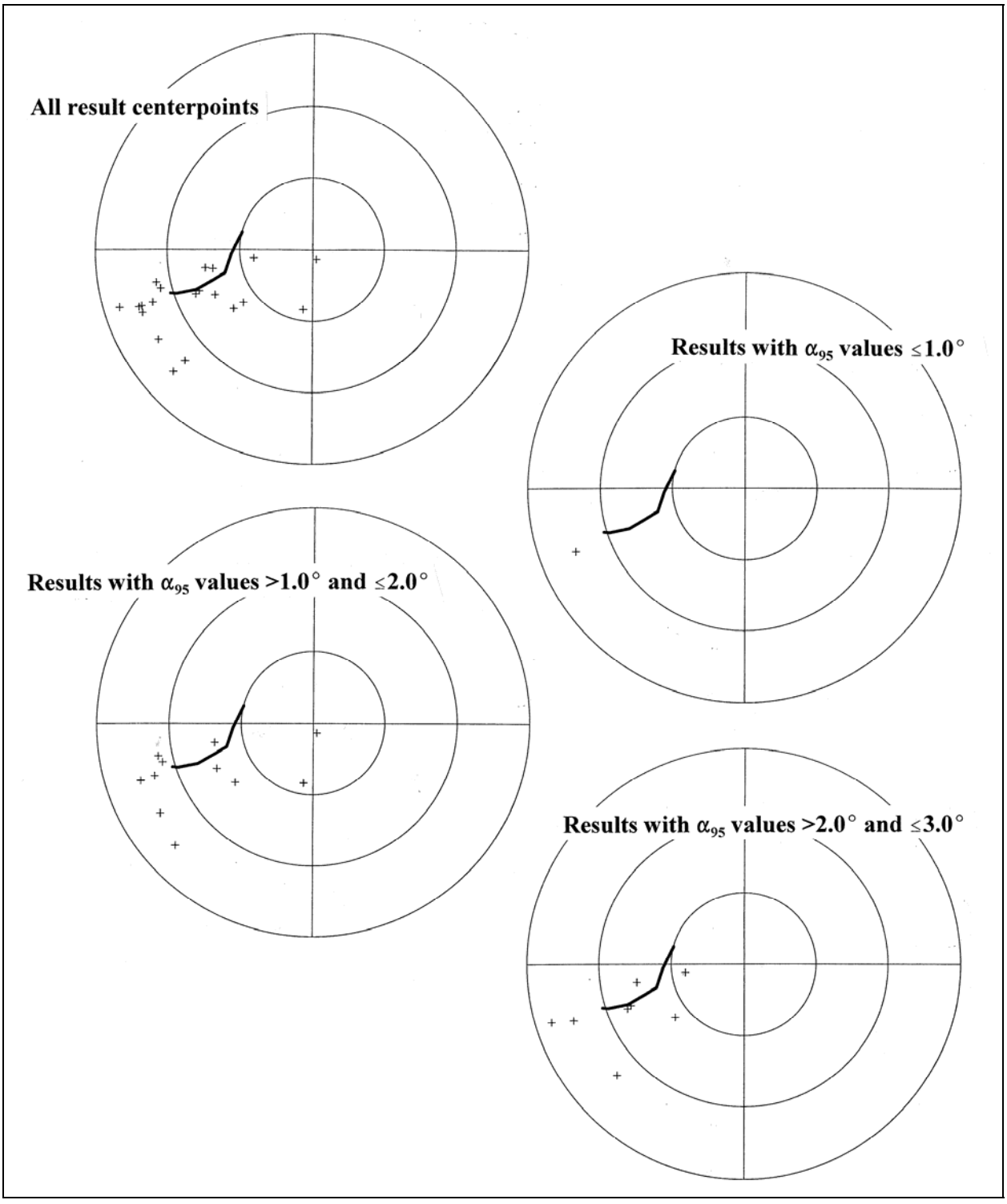

Figure 9.21. DuBois archaeomagnetic results that are confidently and exclusively associated with the AD 1225 to 1300 period, contrasted with the Wolfman VGP curve for the AD 1225 to 1300 period. The upper figure includes all results, regardless of precision. The lower plots include only moderate and low precision results, respectively.

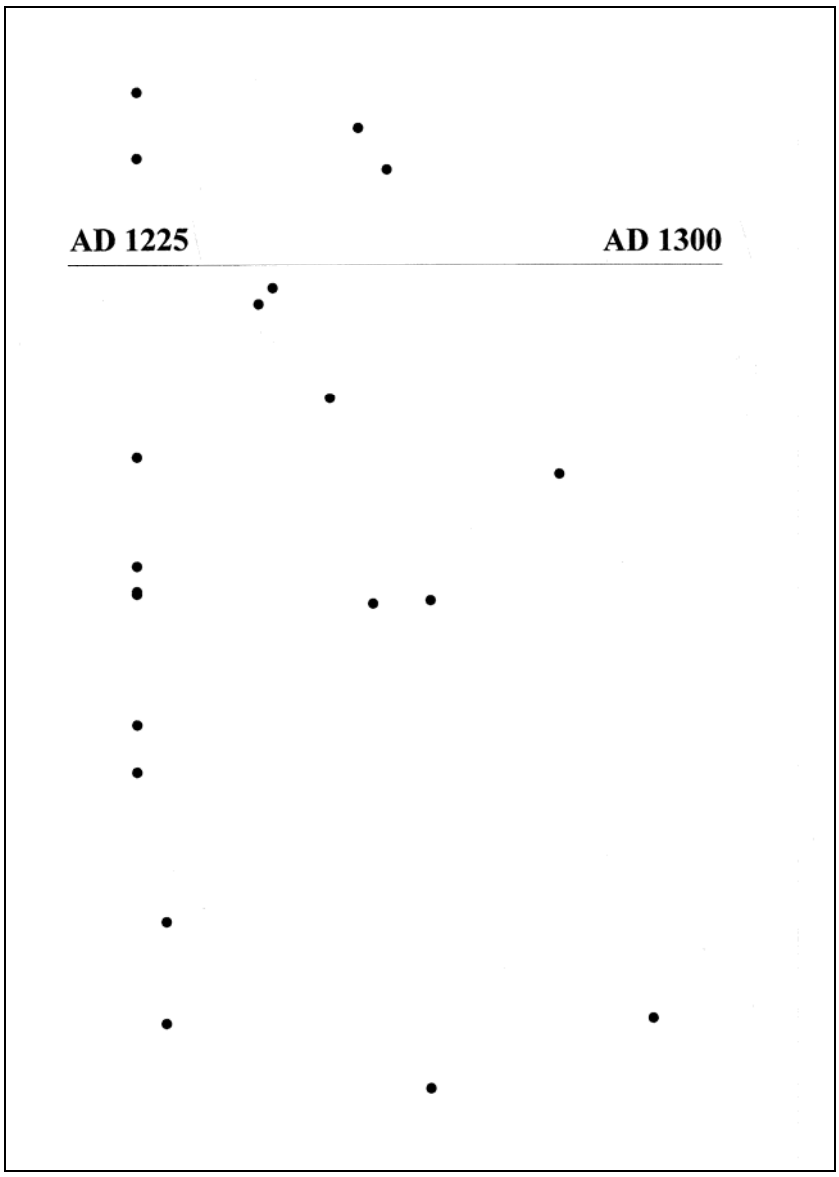

Figure 9.22. Plot of residual distances from confidently attributed AD 1225 to 1300 sample centerpoints and nearest points along the AD 1225 to 1300 segment of the Wolfman Curve.

AD 1300–1400 (Segment 8)

Differences between the SWCV2000 and Wolfman approximations of the AD 1300–1400 curve segment are extreme, although both segments terminate at approximately the same location (Figure 9.23). The SWCV2000 VGP path is relatively short and has a kink or inflection in the middle of the period. High precision results could conceivably discriminate events at either end of the period, but moderate precision results could encompass the entire segment. The Wolfman Curve represents a path more than twice as long, beginning with an excursion to longitudes of less than 170E, significantly distant from the nearest point on the SWCV2000 curve. For nearly

the first half of the period, the Wolfman segment remains at latitudes greater than 85E, returning to the vicinity of the SWCV2000 curve for the post-AD 1350 portion of the segment. The Wolfman Curve segment terminates at a higher longitude than SWCV2000, but they are similar in latitude.

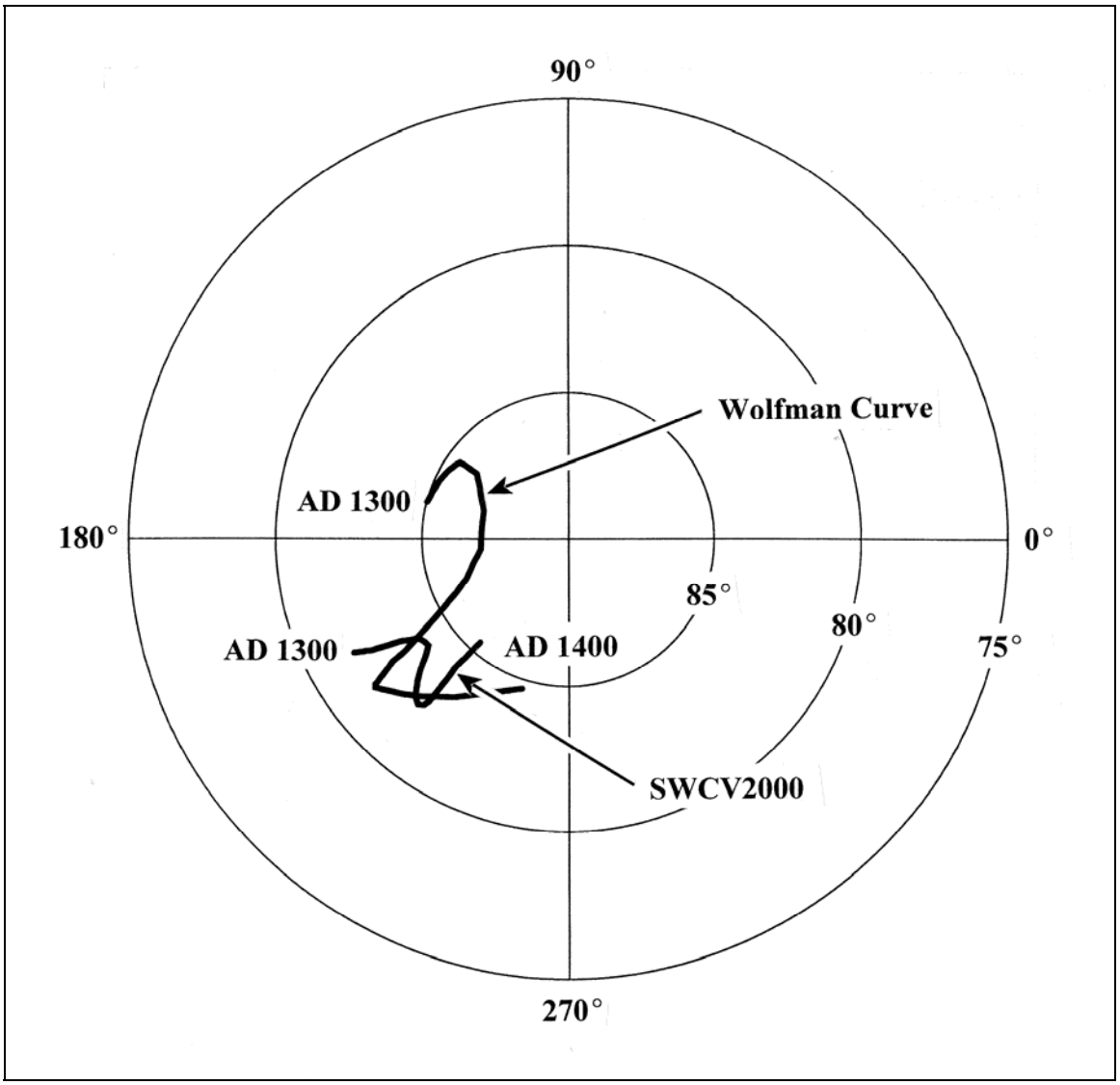

Figure 9.23. AD 1300 to 1400 segments of the SWCV2000 and Wolfman VGP curves.

The DuBois dataset is contrasted with the SWCV2000 curve in Figure 9.24. Contemporary or potentially earlier results (solid and open circles) tend to be scattered both around the curve segment, above it (toward lower longitudes), and toward lower latitudes. Contemporary or potentially later results (solid and open squares) are more tightly clustered, both around the later half of the segment and at higher longitudes.

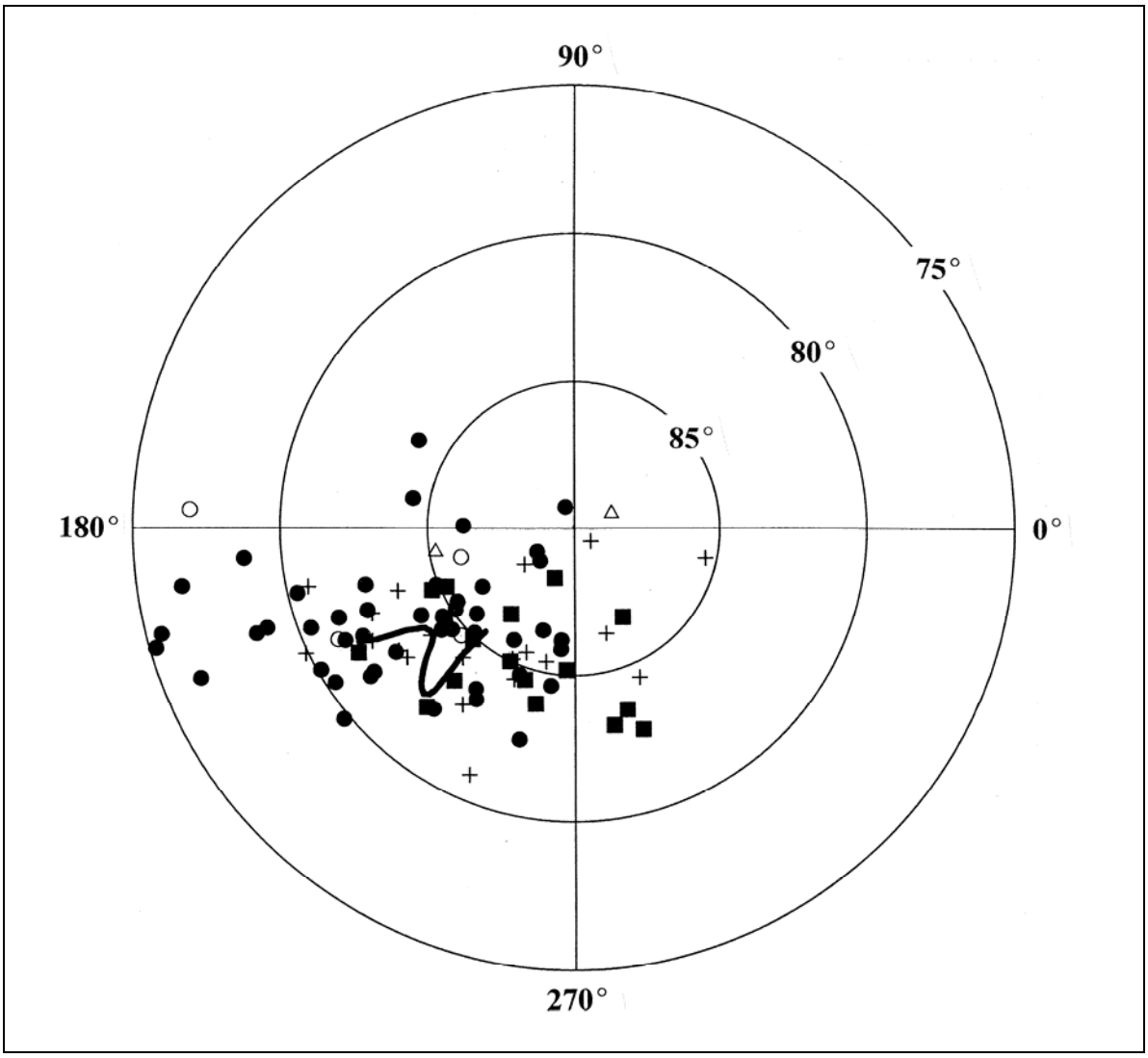

Figure 9.24. SWCV2000 and archaeomagnetic result centerpoints from the DuBois database that could date to the AD 1300 to 1400 period. Open circles denote samples that are believed to date within the AD 1125 to 1400 period. Solid circles denote samples that are believed to date within the AD 1225 to 1400 period. Samples denoted by a "+" are exclusively dated to the AD 1300 to 1400 period, while samples marked with an open triangle are dated to the broader AD 1225 to 1500 period. Solid squares denote samples that are believed to date within the AD 1300 to 1500 period. All centerpoints are associated with α_{95} values of 3.0° or less.

Results that are confidently and exclusively attributed to the AD 1300–1400 period are isolated from the less precisely dated results in Figure 9.25. The scatter of all results clusters around the curve and also extends to higher longitudes. These higher longitude points extend the late end of the segment, and they include results of high, moderate, and low precision.

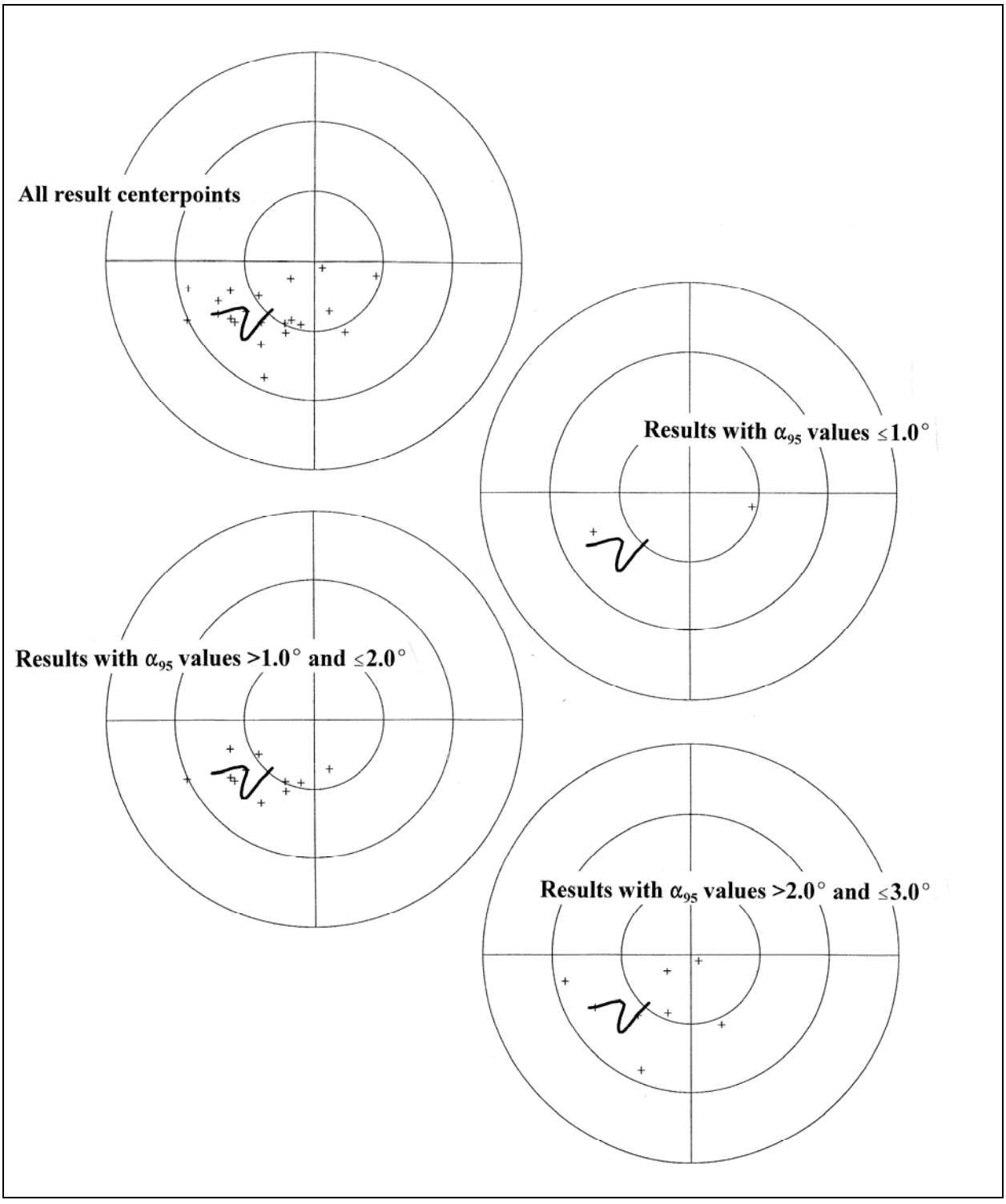

Figure 9.25. DuBois archaeomagnetic results that are confidently and exclusively associated with the AD 1300 to 1400 period, contrasted with the SWCV2000 VGP curve. The upper plot includes all results, regardless of precision. The other plots distinguish high, moderate, and low precision results.

Residual distances between the result centerpoints and the nearest points along the curve segment (Figure 9.26) are less meaningful due to the relatively nonlinear nature of the curve segment. The distances were divided into those for centerpoints that are graphically above the curve as extended (positive) and those centerpoints that are below the curve segment (negative). Negative residuals are more common than positive residuals, and there is an unusually large number of large residuals at the end of the segment (AD 1400).

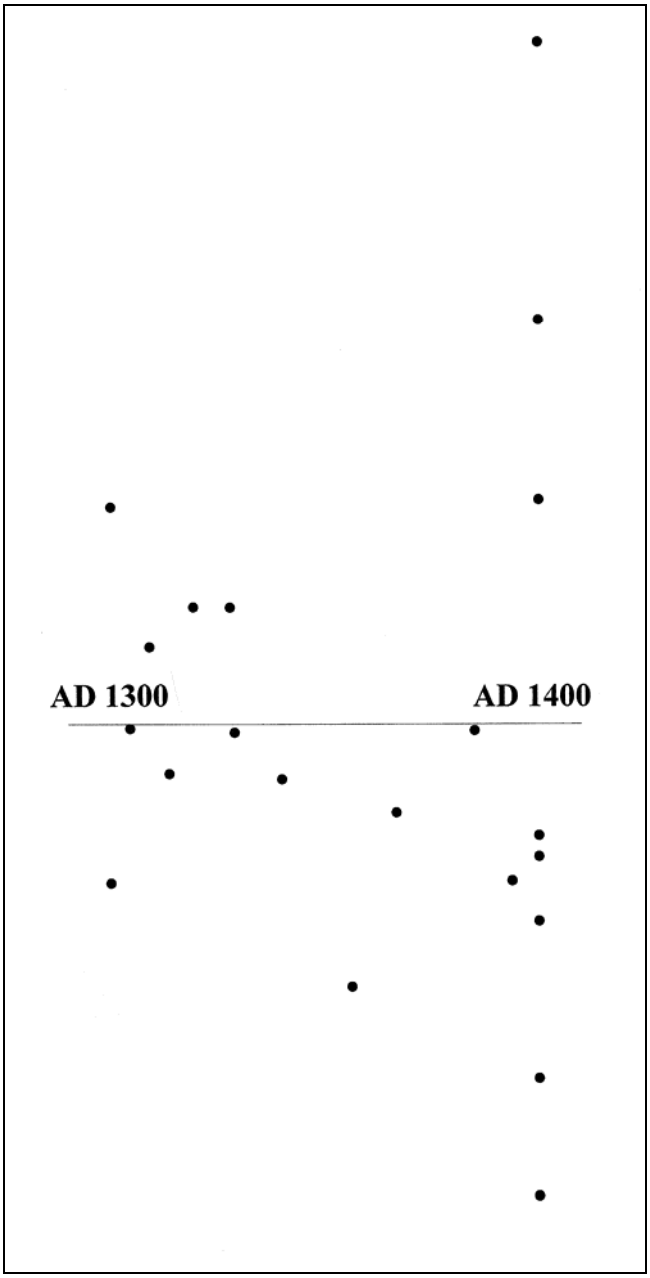

Figure 9.26. Plot of residual distances from confidently attributed AD 1300 to 1400 sample centerpoints and nearest points along the AD 1300 to 1400 segment of SWCV2000.

The same DuBois dataset is contrasted with the AD 1300–1400 segment of the Wolfman Curve in Figure 9.27.

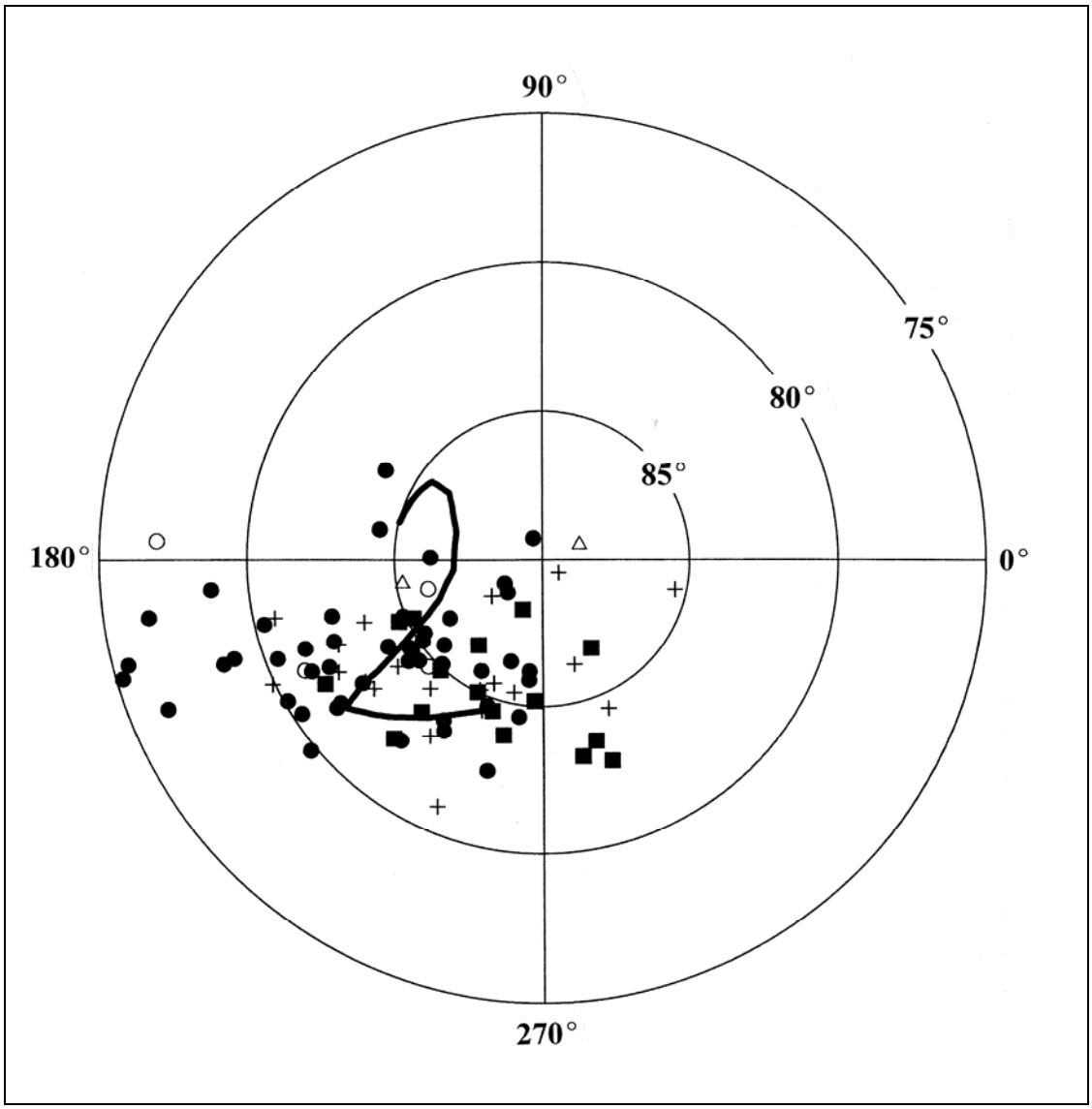

Figure 9.27. The AD 1300 to 1400 segment of the Wolfman Curve and archaeomagnetic result centerpoints from the DuBois database that could date to the AD 1300 to 1400 period. Open circles denote samples that are believed to date within the AD 950 to 1300 period. Solid circles denote samples that are believed to date within the AD 1125 to 1300 period. Samples denoted by a "+" are exclusively dated to the AD 1225 to 1300 period, while samples marked with an open triangle are dated to the broader AD 1125 to 1400 period. Solid squares denote samples that are believed to date within the AD 1225 to 1400 period. All centerpoints are associated with α_{95} values of 3.0° or less.

Results that are either contemporary with or earlier than the segment (solid and open circles) cluster either around the curve or at lower latitudes. Several of these results are proximate to the early third of the curve segment (180° longitude or less). Sample results that are either

contemporary with, or later than, the segment (solid and open squares) cluster around the segment or lie at higher longitudes off of the late end of the segment.

The results that are confidently and exclusively attributed to the AD 1300–1400 period are plotted with the Wolfman Curve segment in Figure 9.28. One high precision result is near the curve while the other is significantly removed off of the late end of the segment. Moderate precision results are all clustered in the area of the later two-thirds of the curve, as are the low precision results albeit with a slightly more diffuse scatter. None of the precisely attributable results falls proximate to the early one-third of this segment. The residual distances are defined as positive if the centerpoint lies to right of the curve segment, while negative distances denote centerpoints to the left of the curve (Figure 9.29). One large positive residual is the single high precision result, but the most significant observation is the scarcity of results that are linked to the first quarter of the curve path.

The DuBois dataset suggests that some revision of these segments is warranted. The resolution (precision) of the DuBois results is insufficient to evaluate the validity of the recurved path represented in SWCV2000, but the scatter does suggest that the segment may need to be extended toward lower latitudes. The Wolfman Curve is more ambiguous. There are no results in the well-dated DuBois samples that can validate the extension of the early one-third of the curve segment to the lower longitudes. Either this extension is invalid or the early 14th century is not represented by the results in the database.

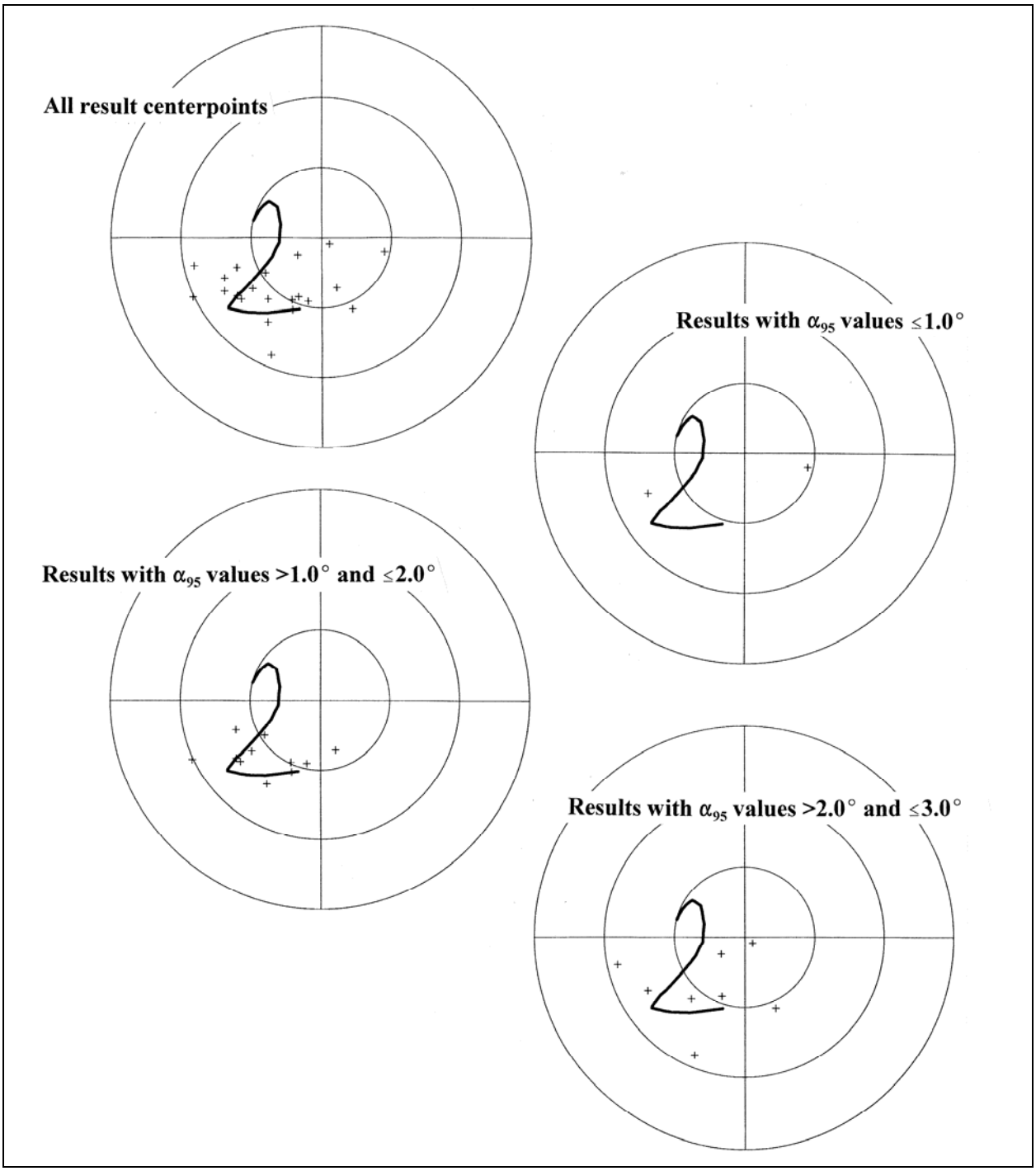

Figure 9.28. DuBois archaeomagnetic results that are confidently and exclusively associated with the AD 1300 to 1400 period, contrasted with the Wolfman VGP curve for the AD 1300 to 1400 period. The upper figure includes all results, regardless of precision. The lower plots differentiate high, moderate, and low precision results, respectively.

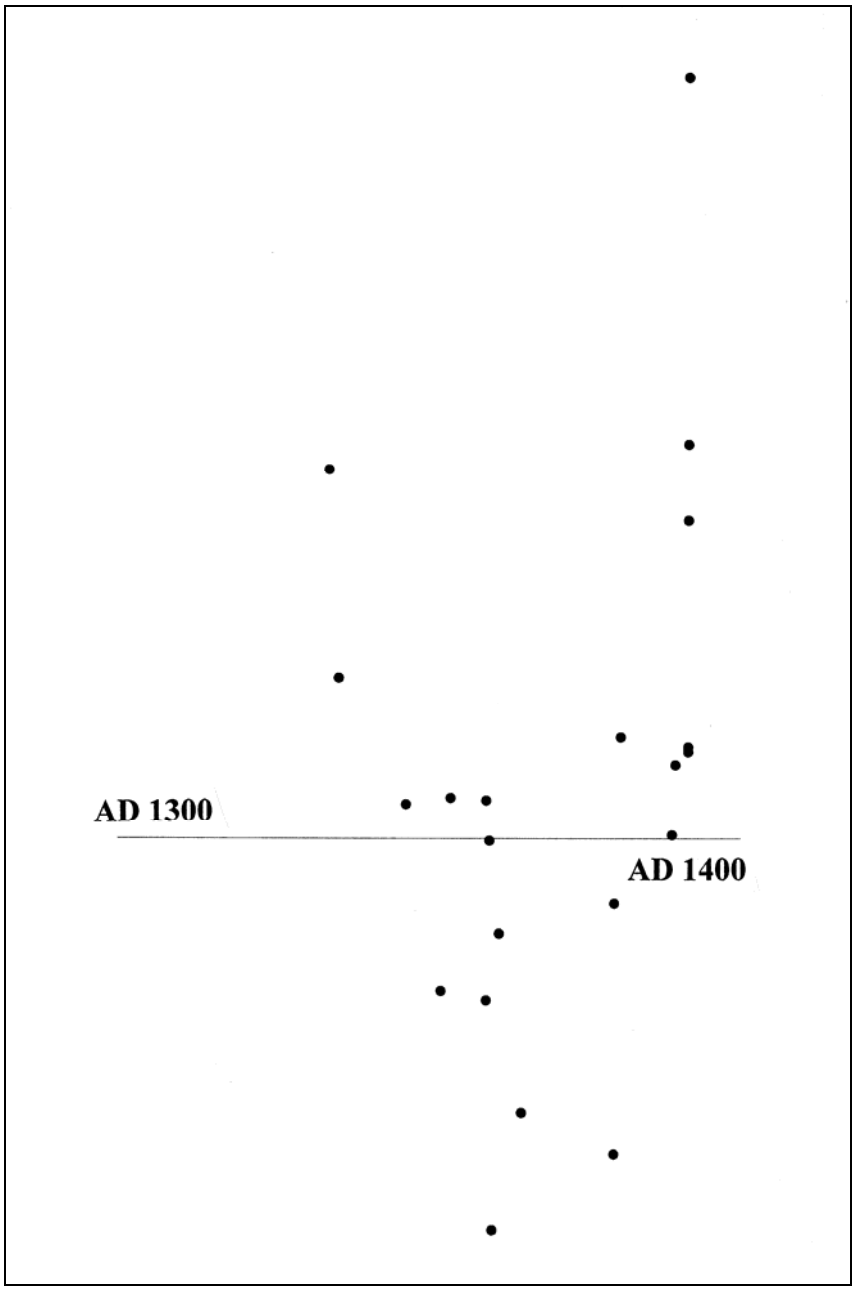

Figure 9.29. Plot of residual distances from confidently attributed AD 1300 to 1400 sample centerpoints and nearest points along the AD 1300 to 1400 segment of the Wolfman Curve.

AD 1400–1500 (Segment 9)

The final segment of this study covers the AD 1400–1500 period. The SWCV2000 and Wolfman Curves for the period are presented in Figure 9.30. The two curve segments have approximately the same starting point, but they again diverge radically, and high precision results would easily distinguish the two proposed AD 1500 positions. The difference between the proposed VGP segments lies in the abrupt excursion of the Wolfman Curve toward the pole,

followed by movement to lower latitudes in the area between 10° and 350° longitude. The Wolfman Curve implies polar movement at nearly twice the rate implied by the SWCV2000 path.

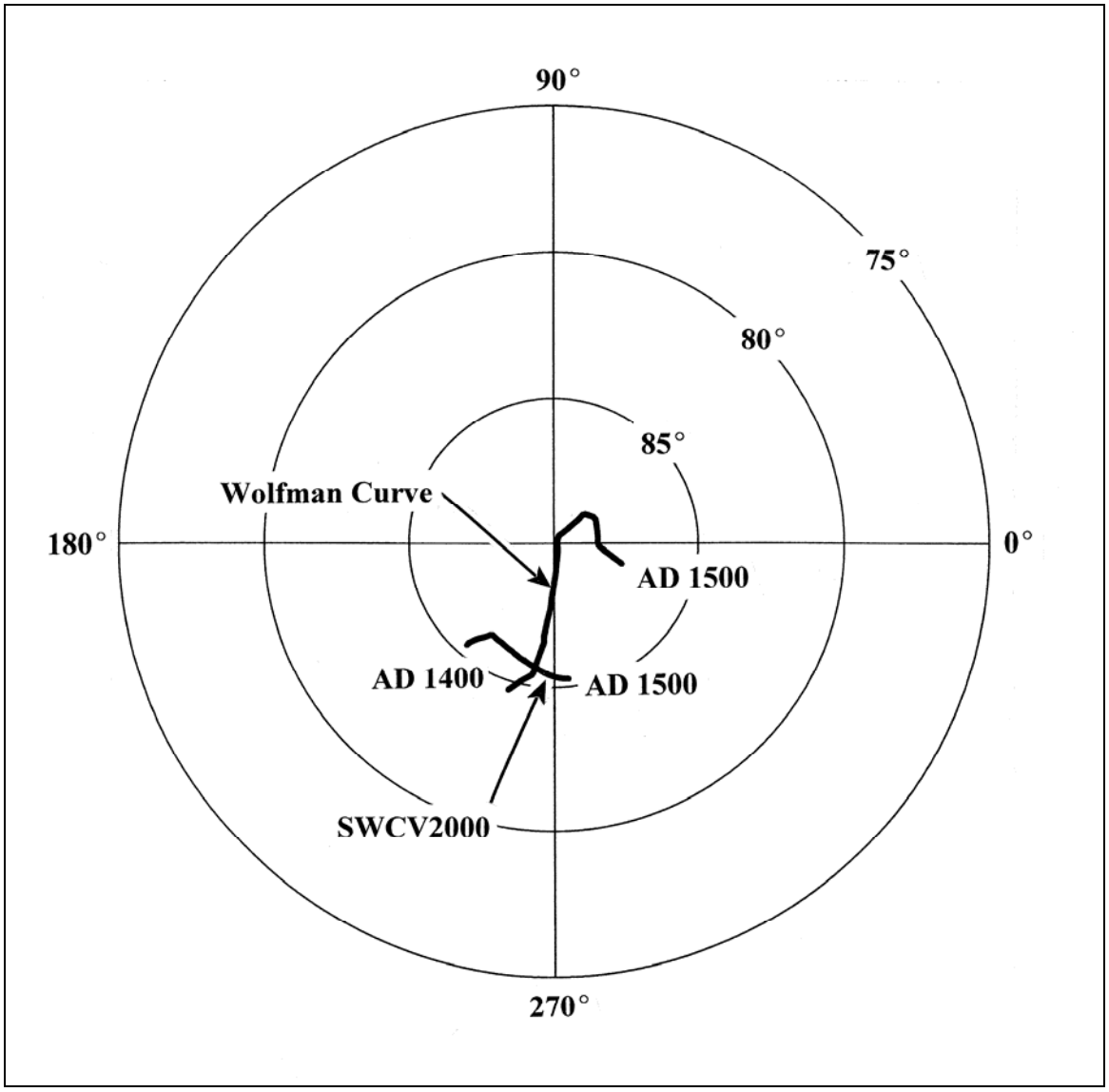

Figure 9.30. AD 1400 to 1500 segments of the SWCV2000 and Wolfman VGP curves.

Potentially relevant results from the DuBois dataset are contrasted with the SWCV2000 curve in Figure 9.31. Contemporary or potentially earlier results (solid and open circles) tend to be clustered around the curve segment, with slightly more results at lower latitudes. Contemporary or potentially later results (solid squares) are restricted to higher longitudes.

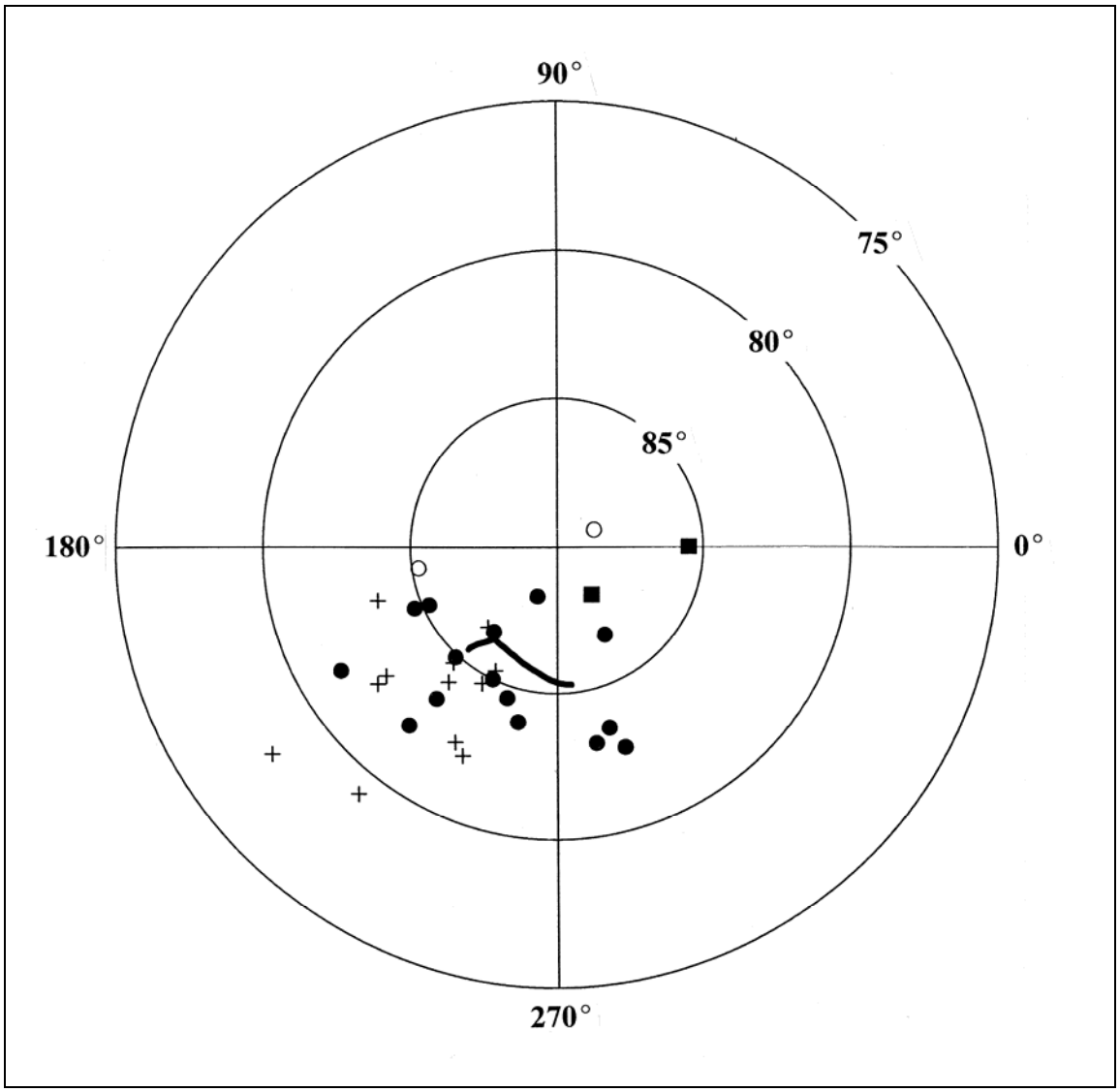

Figure 9.31. SWCV2000 and archaeomagnetic result centerpoints from the DuBois database that could date to the AD 1400 to 1500 period. Open circles denote samples that are believed to date within the AD 1225 to 1500 period. Solid circles denote samples that are believed to date within the AD 1300 to 1500 period. Samples denoted by a "+" are exclusively dated to the AD 1400 to 1500 period. Solid squares denote samples that are believed to date within the AD 1400 to 1600 period. All centerpoints are associated with α_{95} values of 3.0° or less.

Results that are confidently and exclusively attributed to the AD 1400–1500 period are isolated from the less precisely dated results in Figure 9.32. Where potentially earlier results were scattered around the curve segment, the AD 1400–1500 result centerpoints barely overlap the curve path. All but one are located at lower latitudes and at equivalent or lower longitudes. This is true of both moderate and low precision results, although the scatter of low precision result centerpoints is greater. The systematic offset of these results from the curve segment prompted a cursory examination of the source of these samples.

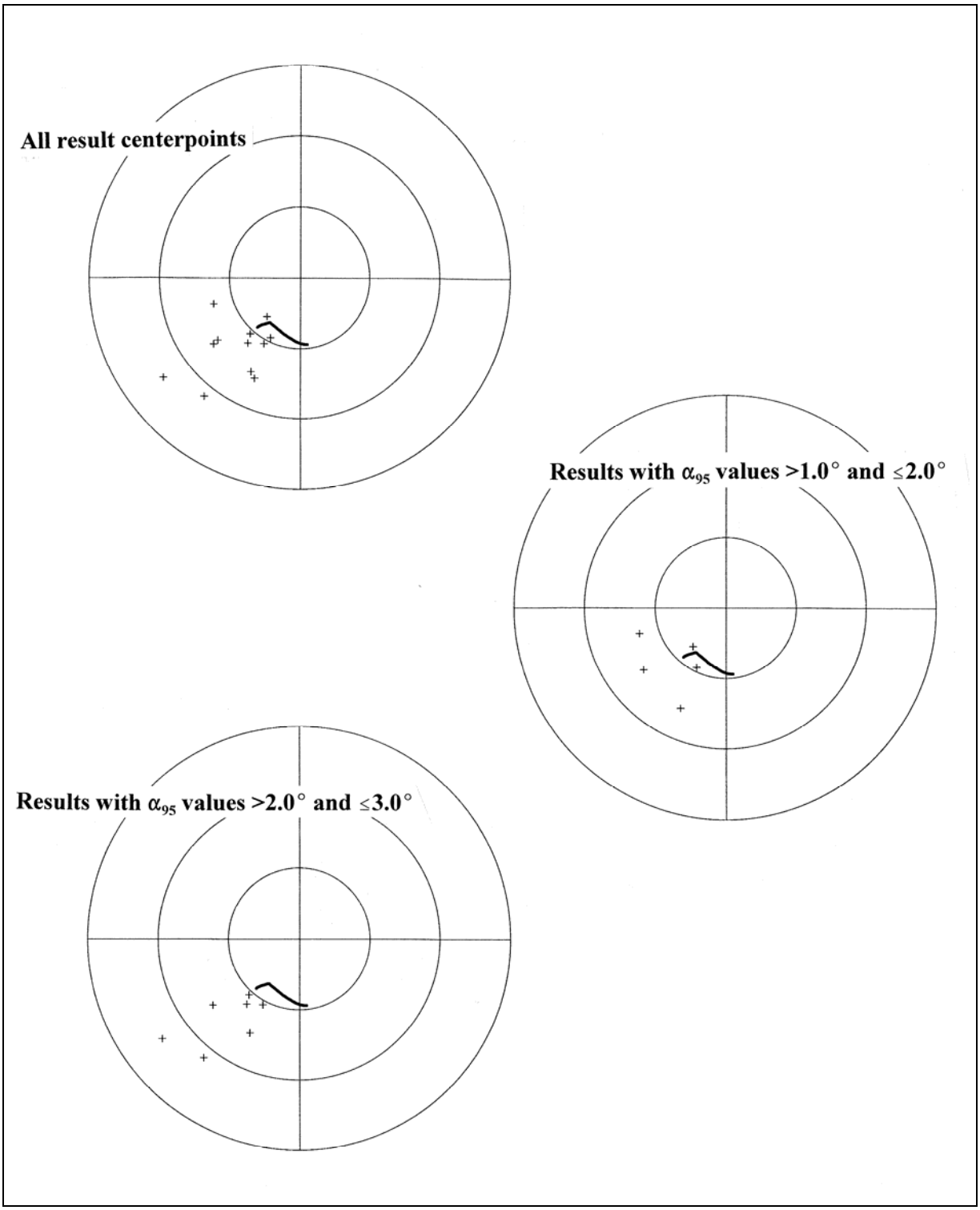

Figure 9.32. DuBois archaeomagnetic results that are confidently and exclusively associated with the AD 1400 to 1500 period, contrasted with the SWCV2000 VGP curve. The upper plot includes all results, regardless of precision. The other plots distinguish moderate and low precision results.

All but two of the exclusively attributed results are from Component II at Arroyo Hondo (LA 12). This component is given an initiation date of AD 1388 and an abandonment date of shortly after AD 1410. An additional sample is dated by the 15th century by non-cutting tree-ring dates of 1401 and 1412, while the final sample is dated by the presence of Glaze C to the early 15th century. All of these results could conceivably fall within the first 25 years of the AD 1400–1500 period, explaining their placement near the early end of the SWCV2000 curve segment, but they are sill falling off of the curve. Residual distances between the result centerpoints and the nearest points along the curve segment (Figure 9.33) reflect this relationship in both their magnitude and their date associations.

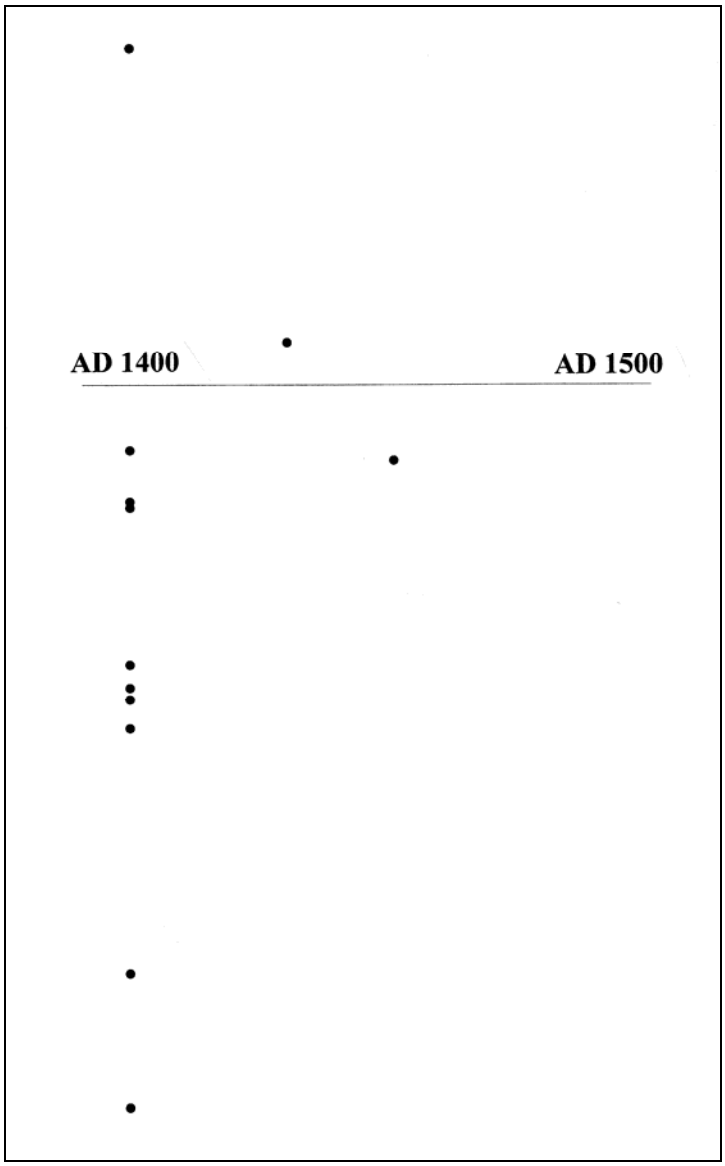

Figure 9.33. Plot of residual distances from confidently attributed AD 1400 to 1500 sample centerpoints and nearest points along the AD 1400 to 1500 segment of SWCV2000.

The same DuBois data are contrasted with the Wolfman Curve segment for the 1400–1500 period in Figure 9.34. Contemporary or potentially earlier results (solid and open circles) tend to be clustered around the early one-half of the curve segment, with slightly more results at lower latitudes. Contemporary or potentially later results (solid squares) are both located near the termination of the curve segment.

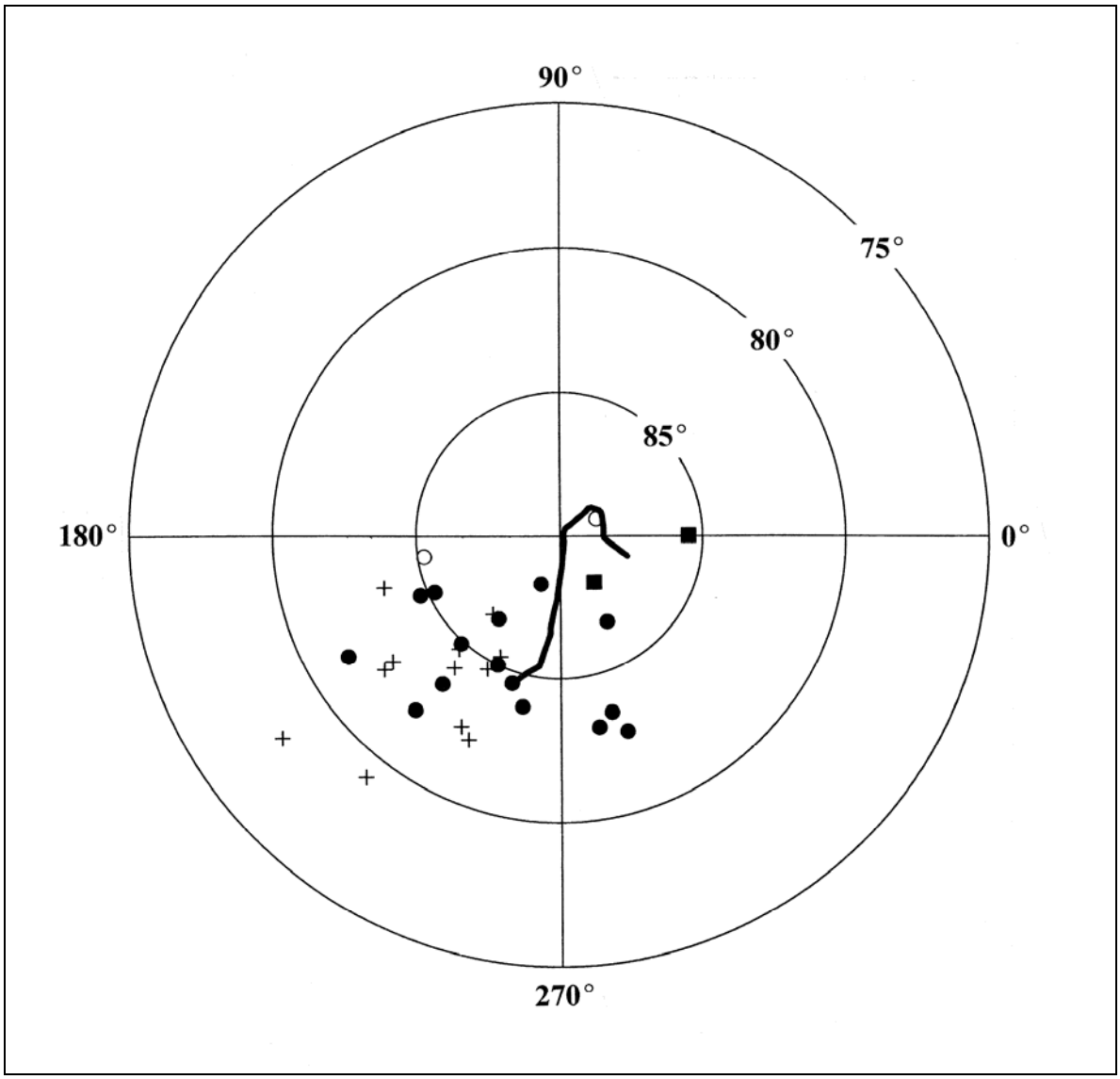

Figure 9.34. The AD 1400 to 1500 segment of the Wolfman Curve and archaeomagnetic result centerpoints from the DuBois database that could date to the AD 1300 to 1400 period. Open circles denote samples that are believed to date within the AD 1225 to 1500 period. Solid circles denote samples that are believed to date within the AD 1300 to 1500 period. Samples denoted by a "+" are exclusively dated to the AD 1400 to 1500 period. Solid squares denote samples that are believed to date within the AD 1400 to 1600 period. All centerpoints are associated with α_{95} values of 3.0° or less.

The results that are exclusively dated to the AD 1400–1500 period are contrasted with the curve segment in Figure 9.35.

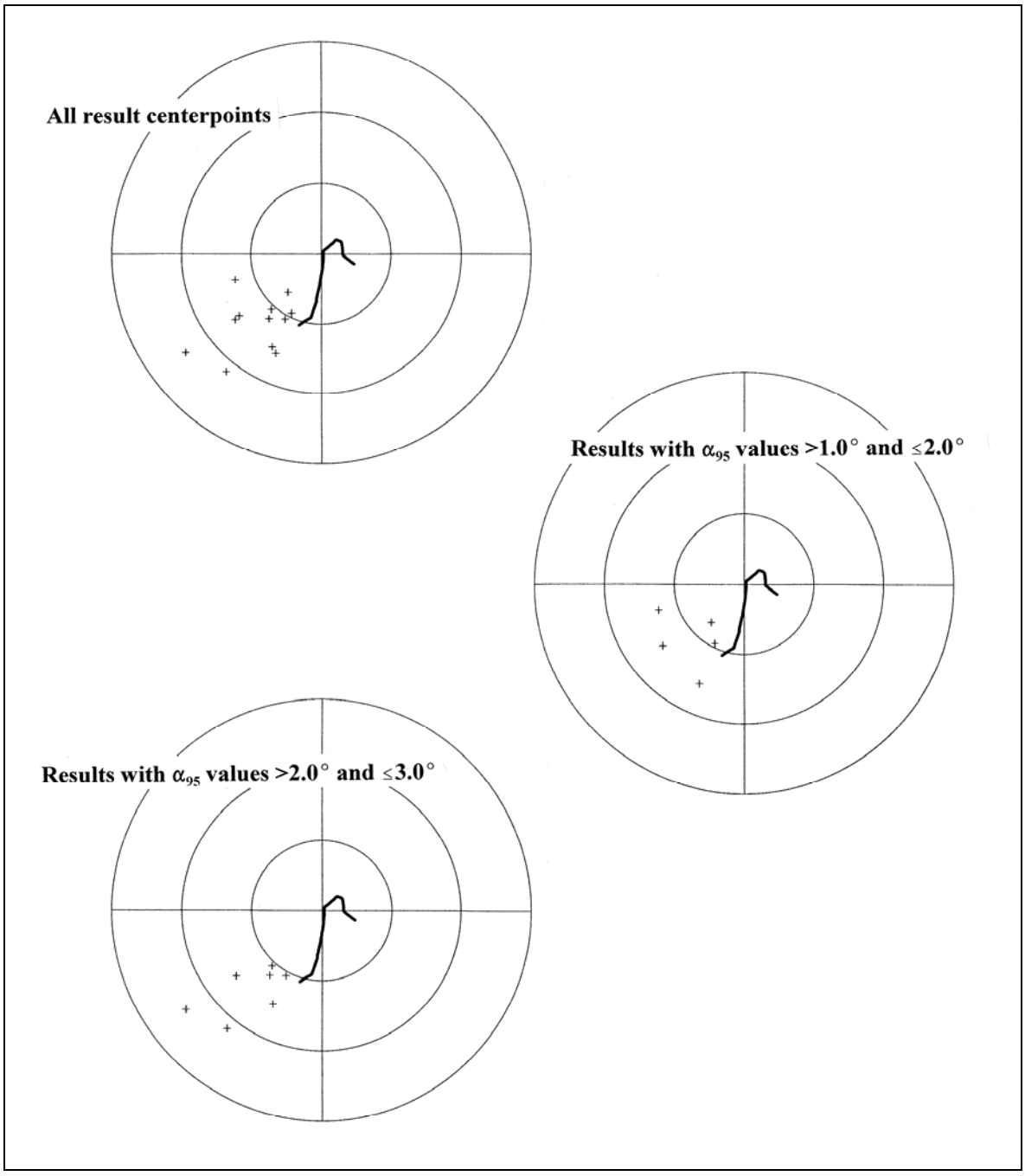

Figure 9.35. DuBois archaeomagnetic results that are confidently and exclusively associated with the AD 1400 to 1500 period, contrasted with the Wolfman VP curve for the AD 1400 to 1500 period. The upper figure includes all results, regardless of precision. The lower plots differentiated moderate and low precision results, respectively.

There is slight overlap between the moderate precision results and the early portion of the curve segment, but the majority of the results are located at lower latitudes and slightly lower longitudes than the AD 1400 end of the curve. Since these results are biased toward the AD 1400–1425 period, overlap with the early end of the curve only would be expected, but they clearly tend to fall off of the early end of the curve. This is reflected in the residual pattern (Figure 9.36), which is similar to that for the SWCV2000 curve.

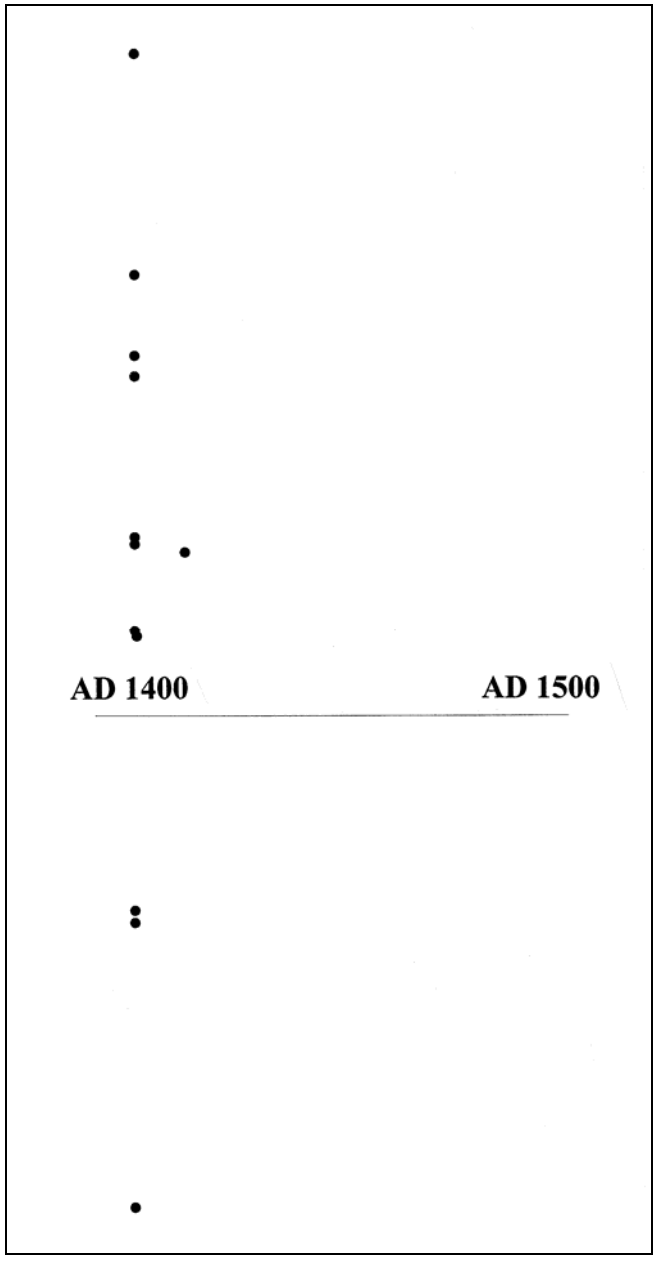

Figure 9.36. Plot of residual distances from confidently attributed AD 1300 to 1400 sample centerpoints and nearest points along the AD 1300 to 1400 segment of the Wolfman Curve.

Neither the SWCV2000 nor Wolfman VGP paths appear to be accurate for the AD 1400–1500 period, but the DuBois dataset for this period is an incomplete basis for evaluation. Both curves appear to be too high in latitude for their representations of the first few decades of the 15th century, but after about AD 1425, we have no DuBois data to compare with the remaining 75 years of polar movement. Two "contemporary or later than" sample results (solid squares in Figure 9.34) are the only suggestions that the Wolfman Curve may be correct in proposing an excursion toward the pole in the later half of the 15th century. Otherwise, the differences between the two proposed paths cannot be resolved at this time.

Summary

The DuBois dataset has provided a relatively unique opportunity to evaluate the SWCV2000 and Wolfman VGP dating curve performances with an independent body of archaeomagnetic results. Neither of the curves appears to be validated for their entire path, some segments appear to be more valid than others, and a hybrid curve will probably prove to be a stronger approximation of the true curve. The weakest areas of the curve are, unfortunately, in the very segments of interest for the interpretation of Pajarito Plateau archaeomagnetic dating results (AD 1125–1500). In most cases, even the more extreme differences in the curves will not result in serious chronological errors, as long as the full date ranges of archaeomagnetic date ranges are used in archaeological interpretations. However, there is one ironic consequence of the differences between the curves and the weaknesses in both that have been suggested by the DuBois dataset. For some time periods, the discrepancies are large enough that precise samples (small $\downarrow_{95}$ values) will fall off the dating curves and are in greater jeopardy of misinterpretation than are less precise results.

The extent to which the DuBois dataset is representative of the full time periods used in the segment analysis has yet to be studied, but in one case (AD 1400–1500) it is clear that cluster effects (many samples from one site or one component) must be investigated before the trends noted in this evaluation can be acted on. The next steps in this study of curve performance will be the integration of the individual Colorado State University results that were used to develop SWCV2000, a more detailed evaluation of within-segment chronology, and an evaluation of the calibration of the curves. These efforts can be compared with the summaries of Deaver (1997) for the Hohokam region, ultimately resulting in the proposal of a hybrid curve that can be applied as the next approximation for dating purposes.

ARCHAEOMAGNETIC RESULTS FROM THE NORTHERN RIO GRANDE REGION

In addition to chronological interpretation based on regional VGP curves and date ranges, archaeomagnetic results can be used directly in both intra-site and inter-site comparisons. Toward this end, we have compiled the DuBois dataset archaeomagnetic results from sites within the broadly defined northern Rio Grande region. The region has been defined as the area within 35.0 to 36.5° north latitude and 105 to 107° west longitude (253 to 255° longitude). These results have been previously distributed as date ranges based on various generations of the DuBois curve, but the VGP positions and error ellipses have not been published. The individual

and grouped results are presented in Table 9.2, plotted with either the Wolfman Curve or with the pre-AD 950 portion of the SWCV2000 curve for comparison. The samples are listed with available contextual information in Table 9.2.

Table 9.2. Robert DuBois dataset for the northern Rio Grande region.

Curve segment	Sample number	Multiple segments?	Independent dating implications	Comments
AD 400–600	? 11	AD 600–800	Field = BM III	1963 UNM Anthro Club excavations
AD 600–800	? 11	AD 400–600	Field = BM III	1963 UNM Anthro Club excavations
AD 800–950	? 30	AD 950–1125	Field = 1000	LA 70, Room 126; Snow 1976
	1854		Pottery late 9th thru early 10th century	LA 25852, Pithouse, fire pit; Hammack et al. 1983
	1857		Pottery mid 9th thru early 10th century	LA 25860, Pithouse 2, hearth; Hammack et al. 1983
	1858		Pottery mid 9th thru early 10th century	LA 25860, Pithouse 1, hearth; Hammack et al. 1983
	1859		Pottery late 9th thru early 10th century	LA 25860, Pithouse 3, hearth; Hammack et al. 1983
AD 950–1125	30	AD 800–950 ?	Field = 1000	LA 70, Room 126; Snow 1976
	? 167	AD 1125–1225	Valdez Phase	LA 9206?; Loose 1974; Boyer 1997
	905	AD 1125–1225 ?	Field = 850–1125	Nambe Falls, 29SF18, Pithouse, Feature 151, hearth; Skinner et al. 1980
	? 1075	AD 1125–1225 ? AD 1225–1300 ?	Field 1000–1300	LA 12054 (LG77-P), Gallina pithouse, circular hearth; Mackey and Holbrook 1978
	? 1076	AD 1125–1225 ? AD 1225–1300 ?	Field 1000–1300	LA 12056 (LG42), Gallina unit house, slab-lined hearth; Mackey and Holbrook 1978
	? 1904	AD 1125–1225 ?	Valdez Phase	Cerrita Ridge Site, Pithouse, Floor 2, Hearth; Woosley 1986; Boyer 1997
AD 1125–1225	167	AD 950–1125?	Valdez Phase	LA 9206?; Loose 1974; Boyer 1997
	? 905	AD 950–1125	Field = 850–1125	Nambe Falls, 29SF18, Pithouse, Feature 151, hearth; Skinner et al. 1980

Curve segment	Sample number	Multiple segments?	Independent dating implications	Comments
	? 1075	AD 950–1125 ? AD 1225–1300 ?	Field 1000–1300	LA 12054 (LG77-P), Gallina pithouse, circular hearth; Mackey and Holbrook 1978
	? 1076	AD 950–1125 ? AD 1225–1300 ?	Field 1000–1300	LA 12056 (LG42), Gallina unit house, slab-lined hearth; Mackey and Holbrook 1978
	? 1113	AD 1225–1300 ?	Field, Pueblo III	Cochiti, LA 12522, Pithouse 1, central fire pit; Laumbach et al. 1977
	1183		TR 1148 in fill below; roomblock const thru 1177	Bandelier, LA 12121, Room 7, Hearth 1; Hubbell and Traylor 1982
	? 1185	AD 1225–1300 ?	Const in late 1100s to 1200	Bandelier, LA 12119, Kiva 2, Hearth 1; Hubbell and Traylor 1982
	? 1282	AD 1225–1300 ?	Const in late 1100s to 1200	Bandelier, LA 12119, Room 10, Hearth 1; Hubbell and Traylor 1982
	? 1287	AD 1225–1300 ?	Const in late 1100s to 1200	Bandelier, LA 12119, Room 14, Hearth 4 (subfloor); Hubbell and Traylor 1982
	? 1398	AD 1225–1300 ?	Field 1100–1300	Gallina site 1, LA 14323, Room 4, Floor; Mackey ?
	? 1399	AD 1225–1300 ?	Field 1100–1300	Gallina, LA 12760, Pithouse hearth; Mackey ?
	? 1400	AD 1225–1300 ?	Field 1100–1300	Gallina, LA 14324, Pithouse hearth; Mackey ?
	? 1904	AD 950–1125 ?	Valdez Phase	Cerrita Ridge Site, Pithouse, Floor 2, Hearth; Woosley 1986; Boyer 1997
AD 1225–1300	? 24	AD 1300–1400	TR 1280 construction	LA 6462, Unit VI Kiva, F 45; Bussey 1968b
	? 25	AD 1300–1400	TR 1280 construction	LA 6462, Unit VI Kiva, F 45; Bussey 1968b
	536	AD 1300–1400 ?	1263r-1284vv; Santa Fe B/w	Pueblo Alamo, Room 3, hearth; Allen 1973; Robinson et al. 1973
	537	AD 1300–1400 ?	1263r-1284vv; Santa Fe B/w	Pueblo Alamo, Room 100, wall; Allen 1973; Robinson et al. 1973
	? 614	AD 1300–1400 ?	1215vv, 1241vv; Santa Fe B/w	Bandelier, LA 4997, Saltbush Pueblo, Kiva hearth (south,

Curve segment	Sample number	Multiple segments?	Independent dating implications	Comments
				younger)
	? 615	AD 1300–1400 ?	1215vv, 1241vv; Santa Fe B/w	Bandelier, LA 4997, Saltbush Pueblo, Kiva hearth (east, older)
	903		Field = 1200–1400; 1268vv in room fill	Nambe Falls, 29SF10, Room 2, Feature 123, hearth; Skinner et al. 1980
	904		Field = 1200–1400	Nambe Falls, 29SF10, Room 9, Feature 170, hearth; Skinner et al. 1980
	906		Field = 1200–1400	Nambe Falls, 29SF10, Room 8, burned west wall; Skinner et al. 1980
	944		Field = 1250–1350; 1269r from adjacent room	Nambe Falls, 29SF10, Room 32, Feature 191, hearth; Skinner et al. 1980
	1069		TR 1230–1240	LA 12063 (LG 231), Gallina unit house (LL-1), central hearth; Mackey and Holbrook 1978
	1070		TR 1244–1256	LA 12059 (LG 84), Gallina; Mackey and Holbrook 1978
	1072		TR 1238–1252	LA 12066 (LG 124N), Gallina unit house, central hearth; Mackey and Holbrook 1978
	1074		TR 1240–1247	LA 12054 (LG-77-U), Gallina unit house, circular hearth; Mackey and Holbrook 1978
	? 1075	AD 950–1125 ? AD 1125–1225 ?	Field 1000–1300	LA 12054 (LG77-P), Gallina pithouse, circular hearth; Mackey and Holbrook 1978
	? 1076	AD 950–1125 ? AD 1125–1225 ?	Field 1000–1300	LA 12056 (LG42), Gallina unit house, slab-lined hearth; Mackey and Holbrook 1978
	1077		TR1228–1260	LA 12062 (FS 28), Gallina unit house, hearth; Mackey and Holbrook 1978
	? 1113	AD 1125–1225 ?	Field = Pueblo III	Cochiti, LA 12522, Pithouse 1, central fire pit; Laumbach

Curve segment	Sample number	Multiple segments?	Independent dating implications	Comments
				et al. 1977
	? 1185	AD 1125–1225 ?	Const in late 1100s to 1200	Bandelier, LA 12119, Kiva 2, Hearth 1; Hubbell and Traylor 1982
	? 1282	AD 1125–1225 ?	Const in late 1100s to 1200	Bandelier, LA 12119, Room 10, Hearth 1; Hubbell and Traylor 1982
	? 1287	AD 1125–1225 ?	Const in late 1100s to 1200	Bandelier, LA 12119, Room 14, Hearth 4 (subfloor); Hubbell and Traylor 1982
	? 1398	AD 1125–1225 ?	Field 1100–1300	Gallina site 1, LA 14323, Room 4, Floor; Mackey ?
	? 1399	AD 1125–1225 ?	Field 1100–1300	Gallina, LA 12760, Pithouse hearth; Mackey ?
	? 1400	AD 1125–1225 ?	Field 1100–1300	Gallina, LA 14324, Pithouse hearth; Mackey ?
	1444	AD 1300–1400 ?	Field Pueblo III	Bandelier, LA 13086, Room 5, hearth R5C; Hunter-Anderson et al. 1979
	1584		1250–1300; may be slightly later	San Ysidro, LA 13197 (AS-8), Room W-1, Floor fire pit; Bice et al. 1998
	1585		1250–1300; may be slightly later	San Ysidro, LA 13197 (AS-8), Room W-1, Floor fire pit; Bice et al. 1998
	?1829	AD 1300–1400	Coalition aggregation period or later	Rowe Pueblo, LA 108, Room 11, Level 4A, Floor 1, F3H1, first story; Cordell ?
AD 1300-1400	24	AD 1225–1300 ?	TR 1280 construction	LA 6462, Unit VI Kiva, F 45; Bussey 1968b
	25	AD 1225–1300 ?	TR 1280 construction	LA 6462, Unit VI Kiva, F 45; Bussey 1968b
	? 26	AD 1400–1500 ?	Field = 1400	LA 6455, Kiva 54 or Room 52; Lange 1968b
	74		Field = 1300–1400; TR 1364	LA 70, Room 166, Level 4, firepit; Snow 1976
	75		Field = 1300–1400; TR 1364	LA 70, Room 166, Level 4, firepit; Snow 1976
	91		1239vv-1309+B	Pot Creek Pueblo, Unit 3, Room 2 (302); Crown 1991
	283	AD 1400–1500		
	? 536	AD 1225–	1263r–1284vv; Santa Fe	Pueblo Alamo, Room 3,

Curve segment	Sample number	Multiple segments?	Independent dating implications	Comments
		1300	B/w	hearth; J. Allen 1973; Robinson et al. 1973
	? 537	AD 1225–1300	1263r–1284vv; Santa Fe B/w	Pueblo Alamo, Room 100, wall; J. Allen 1973; Robinson et al. 1973
	545	AD 1400–1500 ?	Field = 14th century	LA 4955, Coronado State Monument, Site B, Kiva, Feature 21
	? 614	AD 1225–1300 ?	1215vv, 1241vv; Santa Fe B/w	Bandelier, LA 4997, Saltbush Pueblo, Kiva hearth (south, younger)
	? 615	AD 1225–1300 ?	1215vv, 1241vv; Santa Fe B/w	Bandelier, LA 4997, Saltbush Pueblo, Kiva hearth (east, older)
	705		Component 1, 1320s construction, as late as 1350s?	Arroyo Hondo, LA 12, 18-7, room wall; Creamer 1993
	936		Component I, 1310–1340	Arroyo Hondo, LA 12, K-15, hearth; Creamer 1993
	? 943	AD 1400–1500 ?	Provenience not cited in report; Component I or II	Arroyo Hondo, LA 12, N-3 hearth; Creamer 1993
	? 1444	AD 1225–1300	Field Pueblo III	Bandelier, LA 13086, Room 5, hearth R5C; Hunter-Anderson et al. 1979
	? 1740	AD 1400–1500 ?	Field = 1350–1450	Los Ranchos del Albuquerque, Chamisal 1, hearth
	1812	AD 1400–1500 ?	Glaze B occupation; probably just before 1400, but ...	LA 677, Pitroom 3, east hearth; Marshall 1982
	1813	AD 1400–1500 ?	Glaze B occupation; probably just before 1400, but ...	LA 677, Pitroom 3, south hearth; Marshall 1982
	1855	AD 1400–1500 ?	Glaze A and B, with little Glaze C	LA 25852, Pit room 2, fire pit; Hammack et al. 1983
AD 1400–1500	? 26	AD 1300–1400 ?	Field = 1400	LA 6455, Kiva 54 or Room 52; Lange 1968b
	283	AD 1300–1400 ?		
	? 545	AD 1300–1400	Field = 14th century	LA 4955, Coronado State Monument, Site B, Kiva, Feature 21

Curve segment	Sample number	Multiple segments?	Independent dating implications	Comments
	693		1381–1388 cutting dates; 1410+ general abandonment	Arroyo Hondo, LA 12, 15-6, wall and floor; Creamer 1993
	694		1381–1388 cutting dates; 1410+ general abandonment	Arroyo Hondo, LA 12, 15-6, hearth; Creamer 1993
	696		1381–1388 cutting dates; 1410+ general abandonment	Arroyo Hondo, LA 12, 16-36-5, hearth; Creamer 1993
	700		1381–1388 cutting dates; 1410+ general abandonment	Arroyo Hondo, LA 12, 16-34-4, hearth; Creamer 1993
	702		1381–1388 cutting dates; 1410+ general abandonment	Arroyo Hondo, LA 12, 11-5-5-1, hearth; Creamer 1993
	703		1381–1388 cutting dates; 1410+ general abandonment	Arroyo Hondo, LA 12, 11-8-3-4, hearth; Creamer 1993
	706		1381–1388 cutting dates; 1410+ general abandonment	Arroyo Hondo, LA 12, 11-9-6, wall; Creamer 1993
	? 943	AD 1300–1400 ?	Provenience not cited in report; Component I or II	Arroyo Hondo, LA 12, N-3 hearth; Creamer 1993
	1562		TR 1401+vv, 1412+vv	Bandelier, LA 16097, Room 1, Hearth 1; Traylor et al. 1990
	? 1740	AD 1300–1400 ?	Field = 1350-1450	Los Ranchos del Albuquerque, Chamisal 1, hearth
	? 1812	AD 1300–1400	Glaze B occupation; probably just before 1400, but ...	LA 677, Pitroom 3, east hearth; Marshall 1982
	? 1813	AD 1300–1400	Glaze B occupation; probably just before 1400, but ...	LA 677, Pitroom 3, south hearth; Marshall 1982
	1814		Glaze C occupation; just after 1400	LA 677, Kiva 2, Pit 6
	? 1855	AD 1300–1400	Glaze A and B, with little Glaze C	LA 25852, Pit room 2, fire pit; Hammack et al. 1983
AD 1500–1600				

Curve segment	Sample number	Multiple segments?	Independent dating implications	Comments
AD 1600–1900	92		ca. 1860	Ft. Burgwin, Hospital, Room 1; Woosley 1980
	93		ca. 1860	Ft. Burgwin, Hospital, Room 7; Woosley 1980
	123		Field = 1700–1750	LA 591, Las Majadas, Unit 1, Room 5, corner fireplace (Feature 6); Snow and Warren 1973
	124		Field = 1700–1750	LA 591, Las Majadas, Unit 1, Room 2, raised firebox (Feature 9); Snow and Warren 1973
	144		Field = 1620–1790	Pecos
	145		Field = 1620–1790	Pecos
	146		Field = 1620–1790	Pecos
	958		Field = 1620–	Pecos, Room 48, wall in SW corner
	960		Field = 1620–	Pecos, Room 28, NE corner, hearth
	961		Field = 1620–	Pecos, Room C-3, rectangular hearth

AD 400–600 and AD 600–800

Only a single result falls within each of these periods. Field assessment of the context was that the burn should date to the Basketmaker III period. The location of the result (11) agrees with that placement, probably shortly before AD 650.

AD 800–950

Five samples are potentially attributable to this period. Four (1854, 1857, 1858, and 1859) are from Early Developmental structures in the Jemez River Valley, and all four results are consistent with age assignments in the AD 825–875 period. The fifth sample (30) was collected from the Cochiti Reservoir area. Field expectation was for an age around AD 1000, and the result is consistent with that expectation.

AD 950–1125

Six samples are potentially attributable to this period. One (30), discussed above, falls at the early end of the period. Two samples from Valdez Phase structures (167, 1904) have relatively

imprecise results ($\acute{\alpha}_{95}$>2.0°) but may belong to this segment within the AD 1025–1125 portion of the curve. Sample 905 was collected from a Late Developmental structure at Nambe Falls and was expected to date within the AD 850–1125 period. The location of the result is consistent with the very end of that span. The remaining two results are samples from Gallina phase structures. Sample 1075 is unlikely to be from a context that dates before AD 1125. Sample 1076 has an imprecise result that could accommodate either a pre- or post-AD 1125 interpretation. However, a post-AD 1125 age is more likely.

AD 1125–1225

Thirteen samples are potentially attributable to this period. One (1183) from excavations at LA 12121 in Bandelier National Monument is exclusively and confidently dated to the last quarter of the 12th century. Three others from LA 12119 in Bandelier National Monument (1185, 1282, and 1287) are from a component with construction at the end of the 12th century and should date to the end of this period or the early decades of the next period. Two Valdez phase samples (167 and 1904) are ambiguously dated (see above). A sample from a fieldhouse within the Cochiti Reservoir pool (1113) is remarkably precise (α_{95}<1.0°), but its independent dating is weak within this period or perhaps the subsequent period. The result from Nambe Falls (905) either dates to the previous period or perhaps falls within the first decade or two of this period. Five samples are from Gallina structures, two of which may either date earlier or later than this period (1075 and 1076) and three of which may date to this period or to the AD 1225–1300 period (1398, 1399, and 1400).

AD 1225–1300

Twenty-eight of the DuBois samples are potentially attributable to this period. Two samples (24 and 25) from LA 6462 are associated with construction in the 1280s, and the results fall either at the very end of this period or the beginning of the next period. Pueblo Alamo is associated with construction dates spanning 1263–1284, and two hearths (536 and 537) have results that also fall either at the very end of this period or the early decades of the next. Saltbush Pueblo within Bandelier National Monument is ambiguously dated with non-cutting dates in the mid to early 13th century. The samples were taken from kiva hearths, one earlier (615) than the other (614). Four samples were measured from rooms in 29SF10 in the Nambe Falls area. Construction at the site as a whole appears to have been in the mid to late 13th century, but the abandonment date for the structures may fall within the early decades of the 14th century. Cochiti Reservoir excavations yielded sample 1113, which may date to this period or to the earlier period, while another sample (1444) could date to this period or the subsequent period. Samples from LA 12119 in Bandelier National Monument (1185, 1282, and 1287) either date to the early decades of this period or the final decades of the previous period. Two samples (1584 and 1585) from a room hearth at LA 13197 (AS-8) near San Ysidro are believed to date to the very late 13th century or perhaps into the first decade of the 14th century. A single sample from Rowe Pueblo (1829) may date to this period but probably dates to the 14th century. The remaining 10 samples are from Gallina sites. Five of these (1075, 1076, 1398, 1399, and 1400) are not associated with precise sources of independent dating and could date within this period or earlier periods. All of

the remaining results (samples 1069, 1070, 1072, 1074, and 1077) are from sites and components with tree-ring dates in the mid-13th century.

AD 1300–1400

Twenty results could potentially fall within this period. Two samples (24 and 25) from LA 6462, discussed above, are associated with construction in the 1280s and may date as late as the first decade of the 14th century. Another sample from the original Cochiti Reservoir excavations (26) was estimated to date to AD 1400 based on field observations, and it may date to this period or the subsequent period. Two samples from a fire pit in Room 166 at LA 70 (74 and 75) are associated with tree-ring dates in the 1360s and the results probably date to the late 14th century. One sample from Pot Creek Pueblo (91) should date late within the first quarter of the 14th century. A sample from an as yet unidentified site (283) was estimated to date to around 1400 based on field observations. Two samples from Pueblo Alamo (536 and 537) date the abandonment of rooms that were constructed in or after the 1280s, and they date to either the very end of the previous period or within the first decades of this period. Four samples were recovered from three sites in the Bernalillo area. A kiva sample from Coronado State Monument (545) was estimated in the field to have a 14th century age and could be relevant to either this period or the subsequent period. The other three samples are all associated with Glaze B occupations (1740, 1812, and 1813) either at the end of this period or within the first decades after AD 1400. Two samples from Saltbush Pueblo within Bandelier National Monument are associated with non-cutting dates as late as the mid-13th century (614 and 615). The results probably date to the preceding period, but they may extend into the early decades of this period. Two samples represent Component I at Arroyo Hondo (705 and 936) and therefore are well-dated to the mid-14th century, while a third sample from the site (943) was not assigned to either Component 1 or Component II and could date either to the mid-14th century or the early 15th century. LA 13086 within the Cochiti Reservoir pool was characterized as a Pueblo III component and could date to the 13th or early 14th century. Finally, a sample from a pit room at LA 25852 (1855) is associated with Glaze A, B, and small amounts of Glaze C pottery. It should be slightly later than samples 1812 and 1813, so it may fall within the last decades of this period or the first decades of the subsequent period.

AD 1400–1500

Seventeen results could be potentially relevant to this period. Samples 26, 283, 545, 943, 1740, 1812, 1813, and 1855 all have independent dating that either straddles the AD 1400 threshold or is ambiguous between this period and the previous period. Seven samples (693, 694, 696, 700, 702, 703, and 706) were collected from features and burned walls associated with Component II at Arroyo Hondo. Component II is well dated with initial construction in the 1380s and remodeling and additional construction as late as AD 1410. Abandonment and the burning documented by the samples should have occurred within the AD 1410s. LA 16097 is associated with non-cutting tree-ring dates in the first two decades of the 15th century, and sample 1562 should be dated at some point in the second decade of the 15th century or later. The final sample

attributed to this period is from LA 25852 (1814) and is associated with a Glaze C occupation that suggests a date within the middle third of the 15th century.

AD 1500–1600

No results within the DuBois database can be attributed to this time period at this time.

AD 1600–1900

Historic period sample results include a suite from Pecos Pueblo that are broadly assigned to the AD 1620–1790 period (144, 145, and 146). Another trio of samples from Pecos Pueblo is potentially contemporary, but the samples were not given an upper limiting age. Samples 123 and 124 are more narrowly dated to the AD 1700–1750 period based on their association with the site of Las Majadas, Unit 1. These compare with the much later (circa AD 1860) samples from Fort Burgwin (92 and 93).

Summary

There is a surprisingly rich body of comparative data for the northern Rio Grande region, especially when results from the DuBois dataset are combined with those of the Museum of New Mexico's ADL and the laboratory at Colorado State University. Although few data points originate from sites on the Pajarito Plateau itself, the complex culture history of the Coalition and Classic periods are well represented.

CONCLUSIONS

This review of archaeomagnetic dating is a work in progress. Unlike some other dating techniques, archaeomagnetic dating is accretional. The calibration curves must be compiled from the growing body of results from sample measurements. Although individual results are discrete and stable, the date range interpretations from those results are ephemeral, changing as the quality of the approximation of the true VGP curve changes. Despite a considerable amount of work by the three major practitioners of the technique over the past half-century, there is room for improvement in the performance of the current approximations of the VGP curve for the Southwest. Access to the Robert DuBois dataset is the single greatest step forward in this process, since the data have been only indirectly applied to the development of the two most commonly used dating curves in the Southwest. Improvements, both technical and theoretical, are expected over the next decade that will improve the reliability of this dating technique, but those improvements will require a thorough understanding of the strengths and limitations of the technique on the part of regional archaeologists.

CHAPTER 10
ARCHAEOLOGICAL OBSIDIAN AND SECONDARY DEPOSITIONAL EFFECTS IN THE JEMEZ MOUNTAINS AND THE SIERRA DE LOS VALLES, NORTHERN NEW MEXICO

M. Steven Shackley

INTRODUCTION

Distributed in archaeological contexts over as great a distance as Government Mountain in the San Francisco Volcanic Field in northern Arizona, the Quaternary sources in the Jemez Mountains, most associated with the collapse of the Valles Caldera, are distributed at least as far south as Chihuahua through secondary deposition in the Rio Grande, and east to the Oklahoma and Texas Panhandles through exchange. And like the sources in northern Arizona, the nodule sizes are up to 10 to 20 cm in diameter; El Rechuelos, Cerro Toledo Rhyolite, and Valle Grande (Valles Rhyolite derived from the Cerro del Medio dome complex) glass sources are as good a media for tool production as anywhere. While there has been an effort to collect and record primary source obsidian, the focus here has been to understand the secondary distribution of the Jemez Mountains sources. Until the recent land exchange of the Baca Ranch properties, the Valle Grande primary domes (i.e., Cerro del Medio) have been off limits to most research. The discussion of this source group here is based on collections by Dan Wolfman and others, facilitated by Los Alamos National Laboratory (LANL), the Museum of New Mexico, and recent sampling courtesy of the Valles Caldera National Preserve (VCNP; see Broxton et al. 1995; Shackley 2005a; Wolfman 1994).

Due to its proximity and relationship to the Rio Grande Rift System, potential uranium ore, geothermal possibilities, an active magma chamber, and a number of other geological issues, the Jemez Mountains and the Toledo and Valles Caldera particularly have been the subject of intensive structural and petrological study, particularly since the 1970s (Bailey et al. 1969; Gardner et al. 1986; Heiken et al. 1986; Ross and Smith 1955; Self et al. 1986; Smith et al. 1970; Figure 10.1 and 10.2). Half of the 1986 *Journal of Geophysical Research*, volume 91, was devoted to the then current research on the Jemez Mountains. More accessible for archaeologists, the geology of which is mainly derived from the above, is Baugh and Nelson's (1987) article on the relationship between northern New Mexico archaeological obsidian sources and procurement on the southern Plains, and Glascock et al.'s (1999) more intensive analysis of these sources, including the No Agua Peak source in the Taos Plateau Volcanic Field at the Colorado/New Mexico border.

This study is focused on the analysis of obsidian and rock samples submitted by LANL, and the report of the long-term secondary depositional study by this laboratory, in part funded by LANL. The secondary depositional study is geared toward an understanding of the probable patterns of prehistoric procurement of artifact-quality obsidian from sources in the Jemez Mountains.

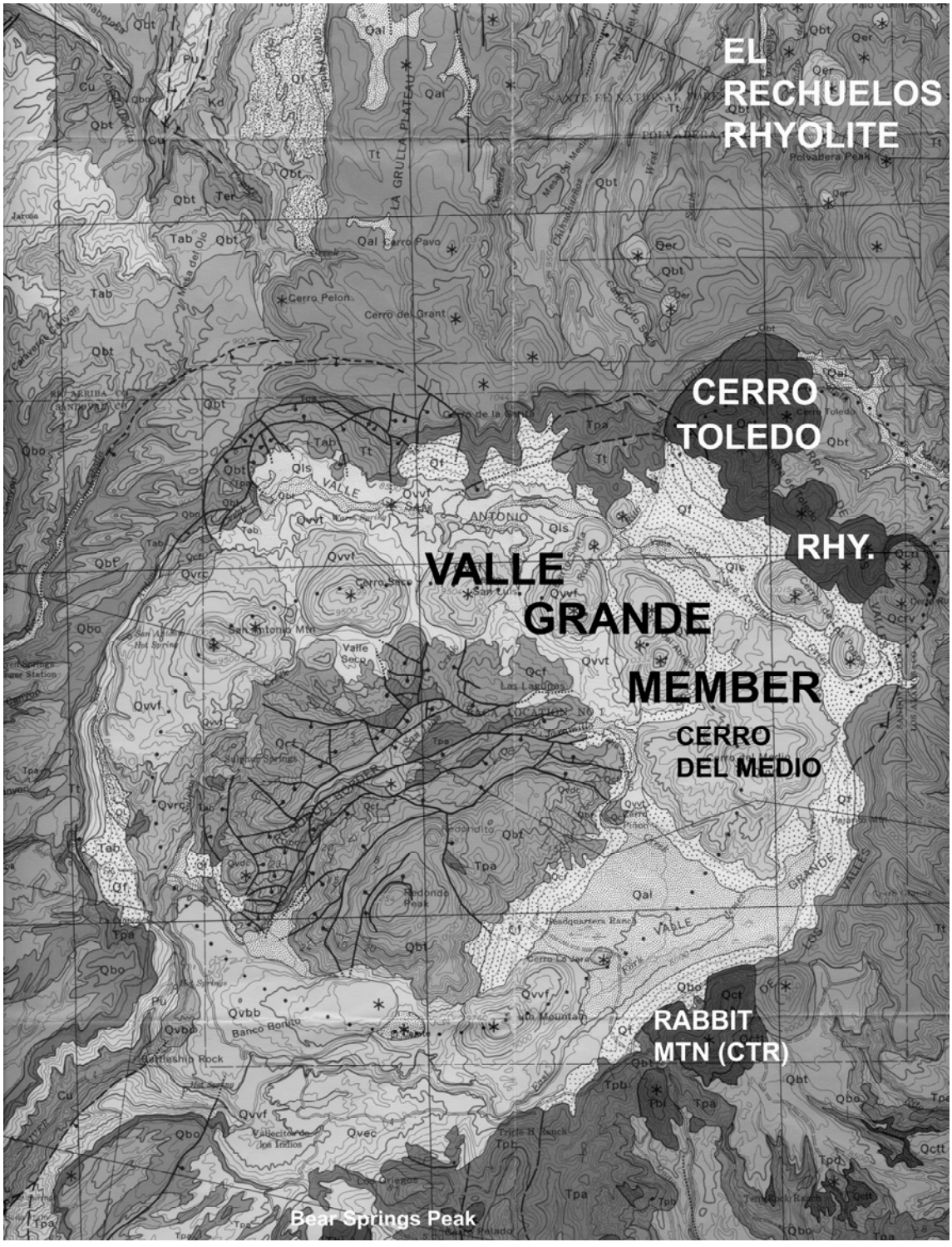

Figure 10.1. Topographical rendering of a portion of the Jemez Mountains, Valles Caldera, and relevant features (from Smith et al. 1970; formation explanations in Smith et al. 1970).

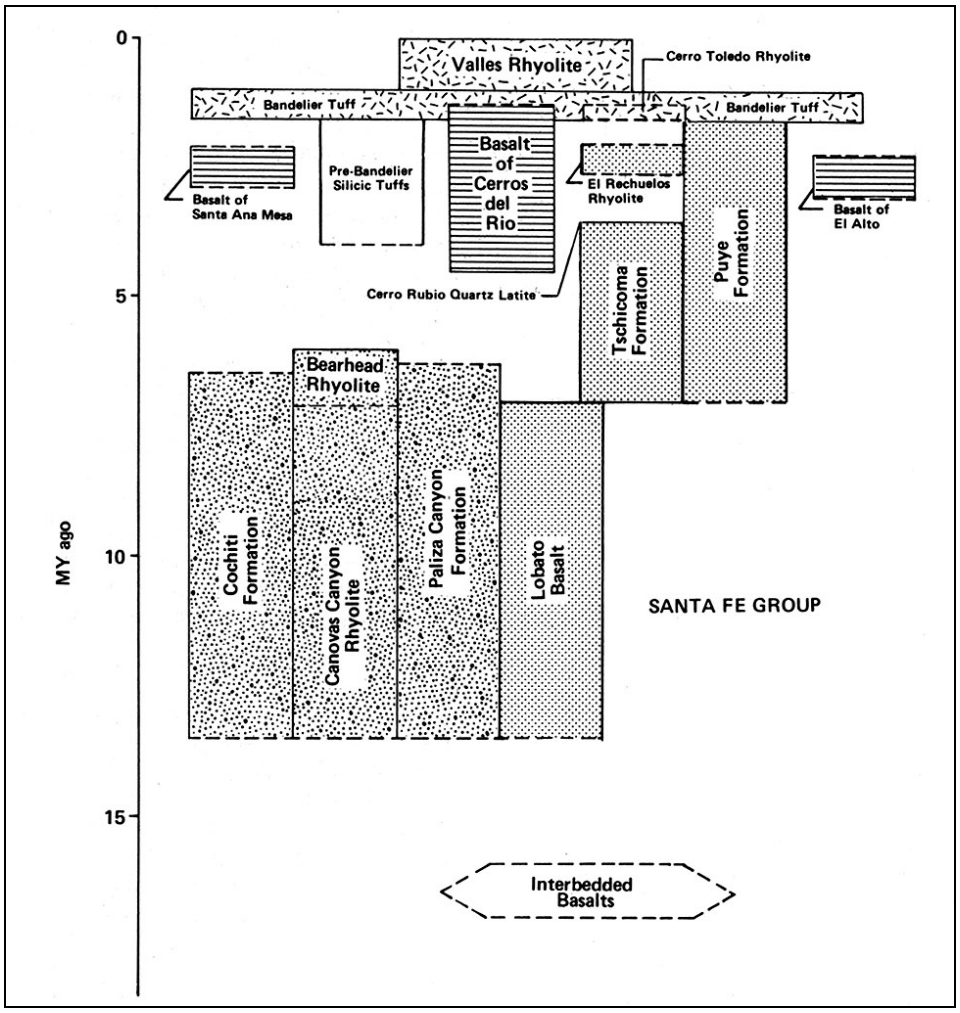

Figure 10.2. Generalized stratigraphic relations of the major volcanic and alluvial units in the Jemez Mountains (from Gardner et al. 1986). Note the near overlapping events at this scale for the Cerro Toledo and Valles Rhyolite members, and the position of Cerro Toledo Rhyolite at the upper termination of the Puye Formation.

BEDROCK AND ALLUVIAL DEPOSITION OF THE SIERRA DE LOS VALLES

Due to continuing tectonic stress along the Rio Grande, a lineament down into the mantle has produced a great amount of mafic volcanism during the last 13 million years (Self et al. 1986). Similar to the Mount Taylor field to the west, earlier eruptive events during the Tertiary more likely related to the complex interaction of the Basin and Range and Colorado Plateau provinces produced bimodal andesite-rhyolite fields, of which the Paliza Canyon (Keres Group), Canovas Canyon Rhyolite (Bear Springs Peak obsidian) and probably the Polvadera Group (El Rechuelos obsidian) is a part (Broxton et al. 1995; Shackley 1998a, 2005a; Smith et al. 1970). While both these appear to have produced artifact quality obsidian, the nodule sizes are relatively small due to hydration and devitrification over time (see Hughes and Smith 1993; Shackley 1995, 2005a). Later, during rifting along the lineament and other processes not well understood, first the

Toledo Caldera (ca. 1.45 Ma) and then the Valles Caldera (1.12 Ma) collapsed causing the eruptive events that were dominated by crustally derived silicic volcanism and dome formation (Self et al. 1986). The later eruptive sequence of the Valle Grande Member is significant for the prehistoric procurement of the obsidian as discussed below. The Cerro Toledo Rhyolite and Valle Grande Member obsidians are grouped within the Tewa Group due to their similar magmatic origins. The slight difference in trace element chemistry is probably due to evolution of the magma through time from the Cerro Toledo event to the Valle Grande events (see Hildreth 1981; Mahood and Stimac 1990; Shackley 1998a, 1998b). Given the relatively recent events in the Tewa Group, nodule size is large and hydration and devitrification minimal, yielding the best natural glass media for tool production in the Jemez Mountains.

Some of the potentially minor sources of archaeological obsidian from the Jemez Mountains area such as the glass from the Bland Canyon area appear to be better artifact-quality obsidian than previously reported. The exact sampling location for the Glascock et al. (1999) samples is apparently unknown (see also Wolfman 1994). The Bland Canyon data reported appear to be rare nodules from the Canovas Canyon Rhyolite, Bear Springs Peak eruptive events (ca. 8 to 9 mya), since obliterated by subsequent volcanism and thus making the nodules rare. In 2004, the Bear Springs Peak dome complex, part of the Canovas Canyon Rhyolite, was "discovered" and the elemental chemistry is identical to the "Bland Canyon Apache Tears" as reported by Glascock et al. (1999; see discussion below). This certainly suggests by this research that the eruptive history and trace element chemistry of artifact quality obsidian from the Jemez Mountains is somewhat more complex than originally described and warrants more intensive geoprospection, a major stimulus for the LANL project here.

SECONDARY DEPOSITION AND PREHISTORIC PROCUREMENT IN NORTHERN NEW MEXICO

Recent research investigating the secondary depositional regime from the Jemez Mountains (Sierra de los Valles), indicates that: 1) Valle Grande Member rhyolite and obsidian in the Jemez Mountains, the result of the most recent eruptive event that produced glass in the caldera, does not erode out of the caldera in nodules of any workable size; 2) During the Pleistocene, Cerro Toledo Rhyolite and glass, mainly the result of the Rabbit Mountain ash flow eruption deposited vast quantities of ash and quenched rhyolite through erosion in the Rio Grande basin as discussed above (Shackley 1998a, 2005a). While Cerro Toledo Rhyolite obsidian is found in secondary contexts in the Puye Formation along the northeastern margin of the caldera (Figures 10.3 and 10.4), the greatest quantity of obsidian found today in the Rio Grande alluvium most likely came from the Rabbit Mountain ash flow event (Gary Smith, personal communication 2005).

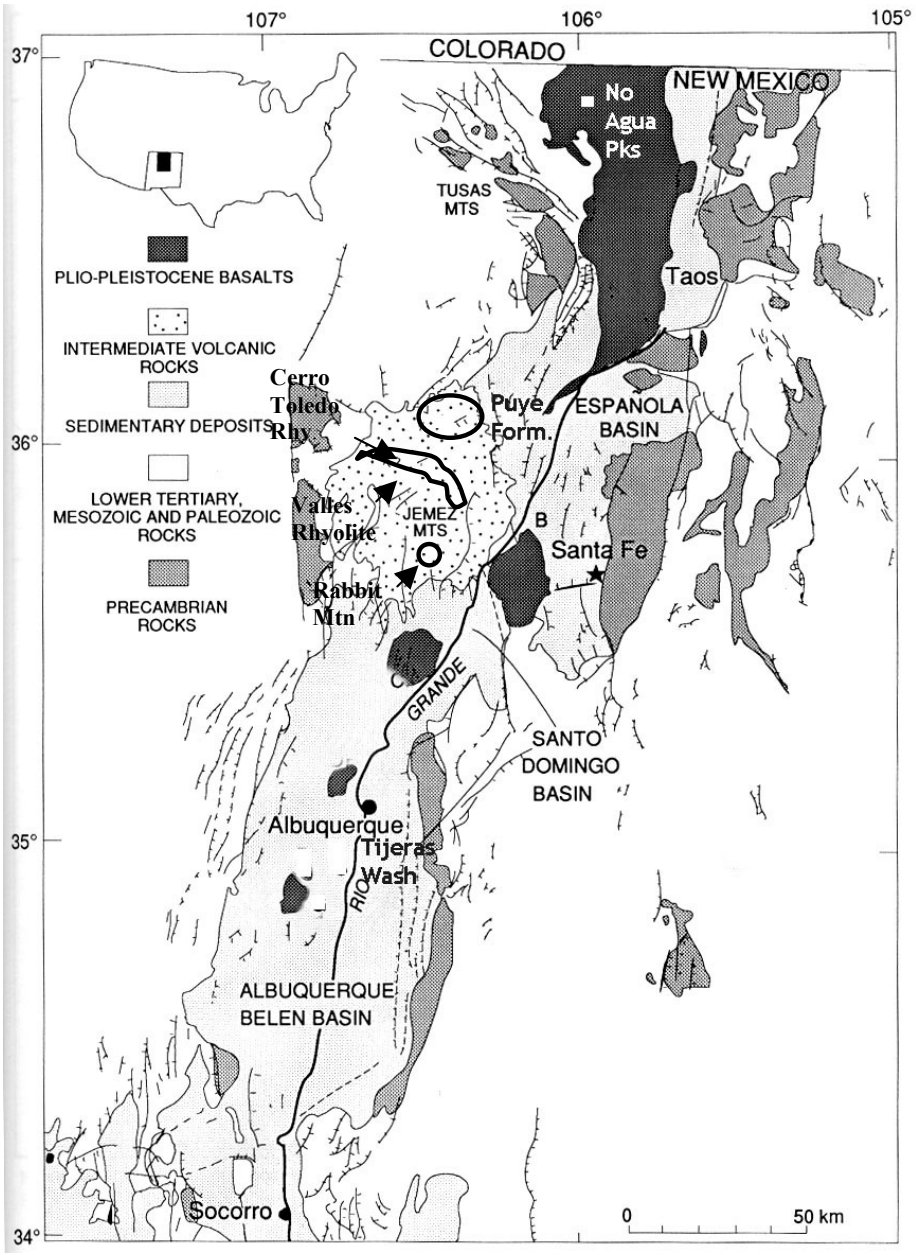

Figure 10.3. Generalized large-scale view of major obsidian source areas and relevant secondary depositional features in north-central New Mexico (adapted from Heiken et al. 1986).

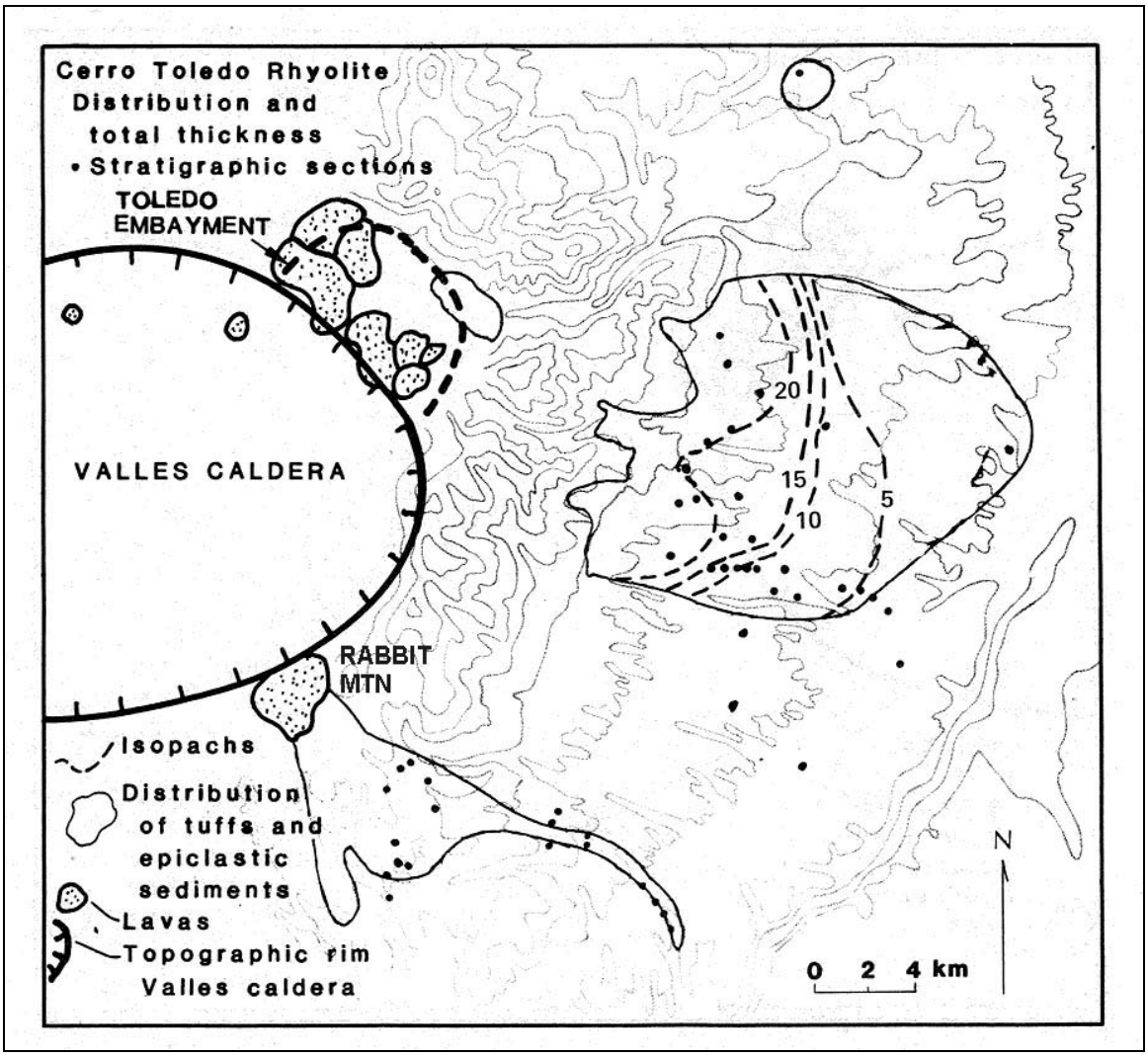

Figure 10.4. Distribution of tuffs and epiclastic sediments derived from Toledo Embayment and Rabbit Mountain eruptions (from Heiken et al. 1986).

There were six pyroclastic eruptive events associated with the Cerro Toledo Rhyolite:

> All tuff sequences from Toledo intracaldera activity are separated by epiclastic sedimentary rocks that represent periods of erosion and deposition in channels. All consist of rhyolitic tephra and most contain Plinian pumice falls and thin beds of very-fine-grained ash of phreatomagmatic origin. Most Toledo deposits are thickest in paleocanyons cut into lower Bandelier Tuff and older rocks [as with the Rabbit Mountain ash flow]. Some of the phreatomagmatic tephra flowed down canyons from the caldera as base surges (Heiken et al. 1986:1802).

Two major ash flows or ignimbrites are relevant here. One derived from the Toledo embayment on the northeast side of the caldera is a 20-km-wide band that trends to the northeast and is now highly eroded and interbedded in places with the earlier Puye Formation from around Guaje Mountain north to Santa Fe Forest Road 144. This area has eroded rapidly and obsidian from

this tuff is now an integral part of the Rio Grande alluvium north of Santa Fe. The other major ash flow is derived from the Rabbit Mountain eruption and is comprised of a southeast-trending 4-km-wide and 7-km-long "tuff blanket" interbedded with a rhyolite breccia 3 to 6 m thick that contains abundant obsidian (Heiken et al. 1986; see also Broxton et al. 1995). All of this is still eroding into the southeast trending canyons toward the Rio Grande. The surge deposits immediately south of Rabbit Mountain contain abundant obsidian chemically identical to the samples from the ridges farther south and in the Rio Grande alluvium. Heiken et al.'s ((1986:1810) neutron activation analysis of Rabbit Mountain lavas is very similar to those from this study (Table 10.1 here).

Table 10.1. Selected wavelength X-ray fluorescence spectroscopy (WXRF) oxide values (wt. %) for the three major archaeological obsidian source standards from the Jemez Mountains. Sample prefix "CDM" is from the Wolman (1994) sample collected from Cerro del Medio and designated as Valle Grande Rhyolite here. Samples analyzed whole after polishing to present a flat surface to beam as in Shackley (1998a, 2005a).

Sample Locality	Source Name	SiO_2	TiO_2	Al_2O_3	Fe_2O_3	MnO	MgO	CaO	Na_2O	K_2O	P_2O_3
081199-1-7	Cerro Toledo Rhyolite	74.44	0.09	10.74	1.07	0.06	0.00	0.19	4.06	3.93	0.02
CDM3-B	Valle Grande Rhyolite	75.07	0.10	11.56	1.19	0.05	0.20	0.43	4.10	4.75	0.04
080999-2-1	El Rechuelos Rhyolite	74.51	0.10	11.20	0.54	0.06	0.00	0.36	3.79	4.07	0.02

Both the Cerro Toledo Rhyolite glass and Mount Taylor glass is common in Quaternary alluvium of the Rio Grande as far south as Chihuahua and was frequently used as a toolstone source in prehistory (Church 2000; Shackley 1997). It is impossible to determine, however, in a finished artifact whether the raw material was procured from the primary or secondary sources, unless the artifact is very large (>5 to 10 cm), when it can be assumed that the artifact was procured from nearer the source.

COLLECTION LOCALITIES

The collection localities discussed here are not the result of a systematic survey to collect and record all the potential sources in the Jemez Mountains, but the result of an attempt to understand the secondary depositional regime of the sources flowing out from the Jemez Mountains into the surrounding stream systems, as noted above. The emphasis here was on understanding the secondary distribution of the major sources that appear in the archaeological record in the northern Southwest—El Rechuelos, Cerro Toledo Rhyolite, and Valle Grande. Additionally, the obsidian sample collection localities for those sources submitted by LANL are not described here specifically, but are plotted on Figure 10.5 and discussed in general below. The results of the analysis will be discussed below.

El Rechuelos

El Rechuelos is mistakenly called "Polvadera Peak" obsidian in the archaeological vernacular (see also Glascock et al. 1999). Polvadera Peak, a dacite or rhyodacite dome, did not produce artifact-quality obsidian. The obsidian artifacts that appear in the regional archaeological record are from El Rechuelos Rhyolite as properly noted by Baugh and Nelson (1987). Indeed, El Rechuelos obsidian is derived from a number of small domes north, west, and south of Polvadera Peak as noted by Baugh and Nelson (1987) and Wolfman (1994; see also Figure 10.5 here). Collections here were made at two to three small coalesced domes near the head of Cañada del Ojitos and as secondary deposits in Cañada del Ojitos (collection locality 080999 in Table 10.2). The center of the domes is located at UTM 13S 0371131/3993999 north of Polvadera Peak on the Polvadera Peak quadrangle. The three domes are approximately 50 meters in diameter each and exhibit an ashy lava with rhyolite and aphyric obsidian nodules up to 15 cm in diameter, but dominated by nodules between 1 and 5 cm. Core fragments and primary and secondary flakes are common in the area.

Small nodules under 10 to 15 mm are common in the alluvium throughout the area near Polvadera Peak. It is impossible to determine the precise origin of these nodules. Presumably they are remnants of various eruptive events associated with El Rechuelos Rhyolite. The samples analyzed, the results of which are presented in Table 10.2, are statistically identical to the data presented in Baugh and Nelson (1987) and Glascock et al. (1999).

El Rechuelos obsidian is generally very prominent in northern New Mexico archaeological collections. Although it is not distributed geologically over a large area, it is one of the finest raw materials for tool production in the Jemez Mountains. Its high quality as a toolstone probably explains its desirability in prehistory. Cerro Toledo Rhyolite and Valle Grande Rhyolite, while present in large nodule sizes, often have devitrified spherulites in the glass, so more careful selection had to be made in prehistory. In nearly 500 nodules collected from the El Rechuelos area, few of the nodules exhibited spherulites or phenocrysts in the fabric. Additionally, El Rechuelos glass is megascopically distinctive from the other two major sources in the Jemez Mountains. It is uniformly granular in character, apparently from ash in the matrix. Cerro Toledo and Valle Grande glass is generally not granular and more vitreous.

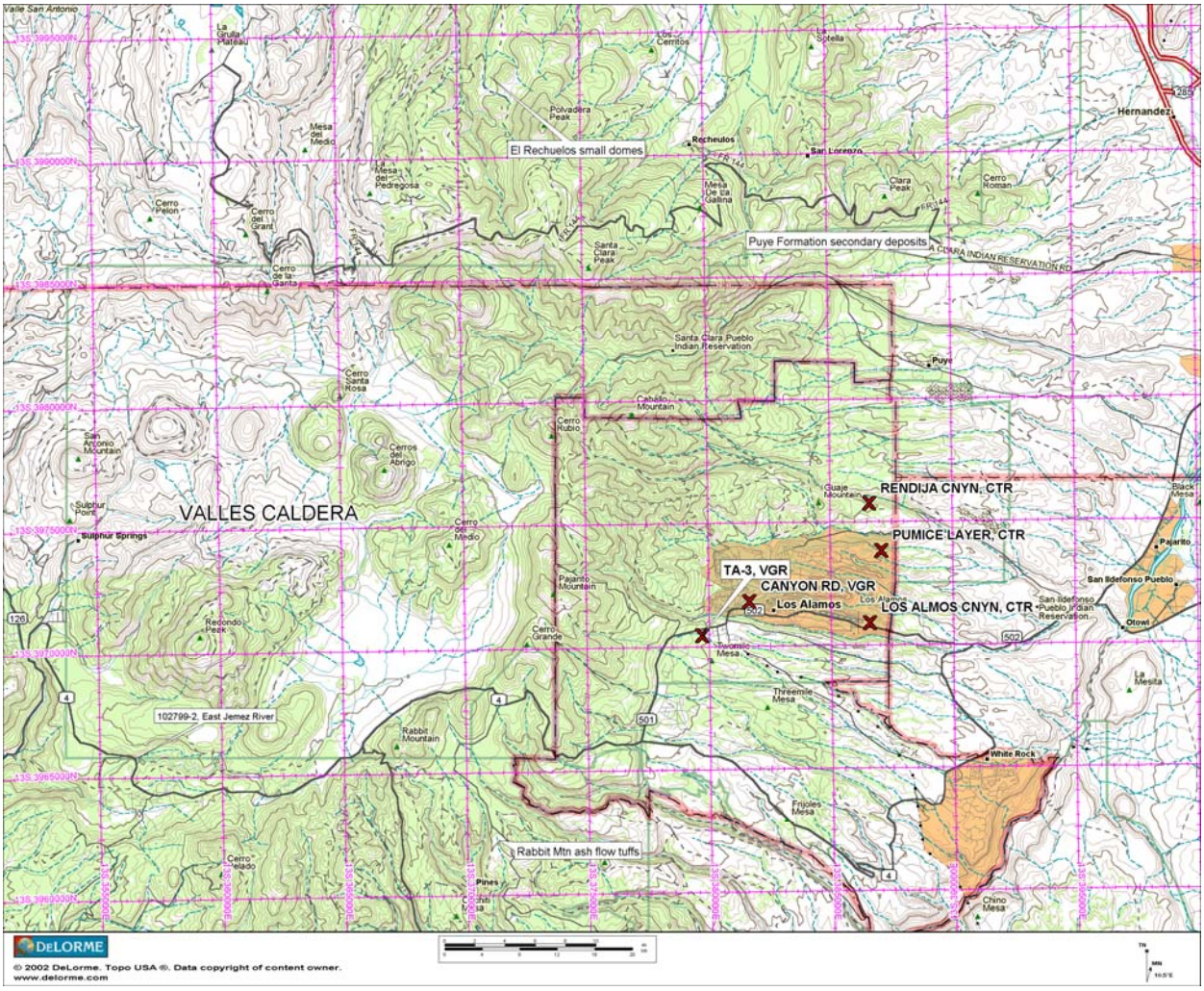

Figure 10.5. Obsidian collection localities in the Jemez Mountain region. Localities marked with an "X" are LANL marekanite collections as analyzed in the tables here. The others are collection localities by this lab as discussed here.

Table 10.2. Source standard elemental concentrations for El Rechuelos Rhyolite obsidian. Samples with "PP" prefix are those from the Wolfman collections as discussed in Wolfman (1994) and Glascock et al. (1999), and analyzed with energy-dispersive X-ray fluorescence spectroscopy (EDXRF) at Berkeley. Those with a "080999" prefix are from this study and locality discussed above and analyzed with WXRF at Berkeley (instrument settings as in Shackley 1998a, and http://www.swxrflab.net/ philipspw2400. htm).

SAMPLE	Ti	Mn	Fe	Rb	Sr	Y	Zr	Nb	Ba
PP-1[1]	543	451	6538	160	9	21	76	48	51
PP-2	560	434	7055	165	10	22	79	52	51
PP-3	526	430	6362	157	9	23	76	48	50
PP-1B	588	436	6504	149	4	25	68	49	n.m.
PP-2B	689	420	6922	156	2	23	75	45	n.m.

SAMPLE	Ti	Mn	Fe	Rb	Sr	Y	Zr	Nb	Ba
080999-2-1				151	11	23	79	46	16
080999-2-2				157	11	24	80	48	20
080999-2-3				154	11	24	81	47	21
080999-2-4				148	11	24	78	46	17
080999-1-1				147	10	23	78	45	16
080999-1-2				150	10	23	79	46	20
080999-1-3				146	10	23	77	45	15
080999-1-4				147	10	23	78	45	11
080999-1-5				146	10	22	77	45	17
080999-1-6				148	10	23	78	46	10

[1] Ti, Mn, and Fe not measured with WXRF; n.m. = no measurement.

Rabbit Mountain Ash Flow Tuffs and Cerro Toledo Rhyolite

Known in the vernacular as "Obsidian Ridge," this obsidian is derived from the Cerro Toledo Rhyolite/Rabbit Mountain eruptions, and following Baugh and Nelson (1987) and the geological literature are all classified as Cerro Toledo Rhyolite (Bailey et al. 1969; Gardner et al. 1986; Heiken et al. 1986; Self et al. 1986; Smith et al. 1970; Figures 10.1 and 10.5).

While Obsidian Ridge has received all the "press" as the source of obsidian from Cerro Toledo Rhyolite on the southern edge of the caldera, the density of nodules and nodule sizes on ridges to the west is greater by a factor of two or more. The tops of all these ridges, of course, are remnants of the Rabbit Mountain ash flow and base surge, and the depth of canyons like Cochiti Canyon is a result of the loosely compacted tephra that comprises this plateau. At Locality 081199-1 (UTM 13S 0371337/3962354), nodules on the ridge top are up to 200 per m^2 with over half that number of cores and flakes (Figures 10.6 and 10.7). This density of nodules and artifacts forms a discontinuous distribution all the way to Rabbit Mountain. The discontinuity is probably due to cooling dynamics and/or subsequent colluviation. Where high-density obsidian is exposed, prehistoric production and procurement are evident. At the base of Rabbit Mountain, the density is about 1/8 that of Locality 081199-1, and south of this locality the density falls off rapidly. At Locality 081199-1, nodules range from pea gravel to 16 cm in diameter (Figures 10.6 and 10.7 and Table 10.3). Flake sizes suggest that 10-cm-size nodules were typical in prehistory.

Figure 10.6. Locality 081199-1 south of Rabbit Mountain in the ash flow tuff. This locality has the highest density of artifact-quality glass of the Rabbit Mountain ash flow area. The apparent black soil is actually all geological and archaeological glass; one of the highest densities of geological and archaeological obsidian in the Southwest.

Figure 10.7. Mix of high-density geological obsidian and artifact cores and debitage (test knapping) at Locality 081199-1 south of Rabbit Mountain. Nodules ≈200/m^2, cores and debitage ≈100/m^2, some of the latter could be modern. Elemental concentrations for samples from this locality are shown in Table 10.3.

Cerro Toledo Rhyolite obsidian both from the northern domes and Rabbit Mountain varies from an excellent aphyric translucent brown glass to glass with large devitrified spherulites that make knapping impossible. This character of the fabric is probably why there is so much test knapping at the sources—a need to determine the quality of the nodules before transport. While spherulites in the fabric occur in all the Jemez Mountain obsidian, it seems to be most common in the Cerro Toledo glass and may explain why Valle Grande obsidian occurs in sites a considerable distance from the caldera even though it is not secondarily distributed outside the caldera in any quantity while Cerro Toledo obsidian is common throughout the Rio Grande alluvium. Indeed, in Folsom period contexts in the Albuquerque basin, Valle Grande obsidian was selected for tool production almost exclusively even though Cerro Toledo obsidian is available almost on-site in areas such as West Mesa (LeTourneau et al. 1996). So, while Cerro Toledo Rhyolite obsidian is and was numerically superior in the Rio Grande Basin, it wasn't necessarily the preferred raw material.

Table 10.3. Elemental concentrations for Cerro Toledo Rhyolite obsidian in the Jemez Mountains. All measurements in parts per million (ppm). Samples with numeric designations from Shackley's surveys. Those with alpha-numeric surveys from the Wolfman and LANL collections. Samples with Ti, Mn, and Fe concentrations analyzed by EDXRF. All others analyzed by WXRF. Instrumental conditions for both instruments discussed in Shackley (1998a).

SAMPLE	Ti	Mn	Fe	Rb	Sr	Y	Zr	Nb	Ba
BCC-1	429	600	10616	217	5	66	192	97	44
BCC-3	552	552	9986	215	5	66	187	97	49
BCC-4	583	547	10102	214	5	62	183	99	42
OR-1	543	550	10278	222	0	66	192	103	43
OR-2	432	425	8727	190	4	59	175	94	42
OR-3	531	534	9921	216	6	65	188	97	42
OR-4	457	577	10218	218	5	69	188	99	42
OR1B	491	536	9810	214	0	63	182	103	
OR2B	633	408	8242	179	1	58	162	92	
CCA-1	341	499	9446	197	4	60	174	90	39
CCA-2	338	516	9714	211	6	66	189	98	0
CCA-3	317	529	9759	208	0	60	184	97	41
081199-1-1				199	7	62	178	96	0
081199-1-2				198	7	61	177	94	1
081199-1-3				200	7	62	179	96	1
081199-1-4				207	6	63	187	99	1
081199-1-5				204	6	63	181	98	4
081199-1-6				204	7	63	184	99	9
081199-1-7				205	6	63	182	99	0
081199-1-8				217	7	67	193	105	15
080900-1				205	8	63	177	100	19
080900-2				204	7	62	175	99	3
080900-3				201	7	62	172	97	3

SAMPLE	Ti	Mn	Fe	Rb	Sr	Y	Zr	Nb	Ba
080900-A1				203	8	62	177	99	73
080900-A2				204	7	63	175	99	14
080900-A4				203	6	63	176	98	0
080900-A5				209	6	65	184	103	5
080900-A6				210	7	62	171	97	1

Valle Grande Rhyolite

While the primary domes like Cerro del Medio of Valle Grande Rhyolite (also called Valles Rhyolite and Cerro del Medio) were not originally visited for this study due to restrictions on entry to the caldera floor, surveys of the major stream systems radiating out from the caldera were examined for secondary deposits; San Antonio Creek and the East Jemez River, as well as the canyons eroding the outer edge of the caldera rim. In 2005 and 2006, the University of California, Berkeley, Archaeological Petrology Field School in collaboration with the VCNP began a more systematic collection of Cerro del Medio source standards from the dome complex, and collections along San Antonio Creek in the caldera proper. These data are included in Table 10.4.

In 1956, two geology graduate students from the University of New Mexico published the first paper on archaeological obsidian in the American Southwest, a refractive index analysis of Jemez Mountains obsidian (Boyer and Robinson 1956). In their examination of the Jemez Mountains sources, they noted that obsidian did not occur in the alluvium of San Antonio Creek where it crosses New Mexico State Highway 126, but did occur "in pieces as large as hen's eggs, but the material is not plentiful and must be searched for with care" in the East Jemez River alluvium where it crosses State Highway 4 (Boyer and Robinson 1956:336). A return to the latter locality, courtesy of Ana Steffen of VCNP (Locality 102799-2), exhibited about the same scenario as that recorded 43 years earlier. The alluvium exhibits nodules up to 40 mm in diameter at a density up to $5/m^2$, but generally much lower. Boyer and Robinson did find nodules up to 15.5 cm in diameter along the upper reaches of San Antonio Creek as shown in their plate reproduced here (Boyer and Robinson 1956:337; Figure 10.8).

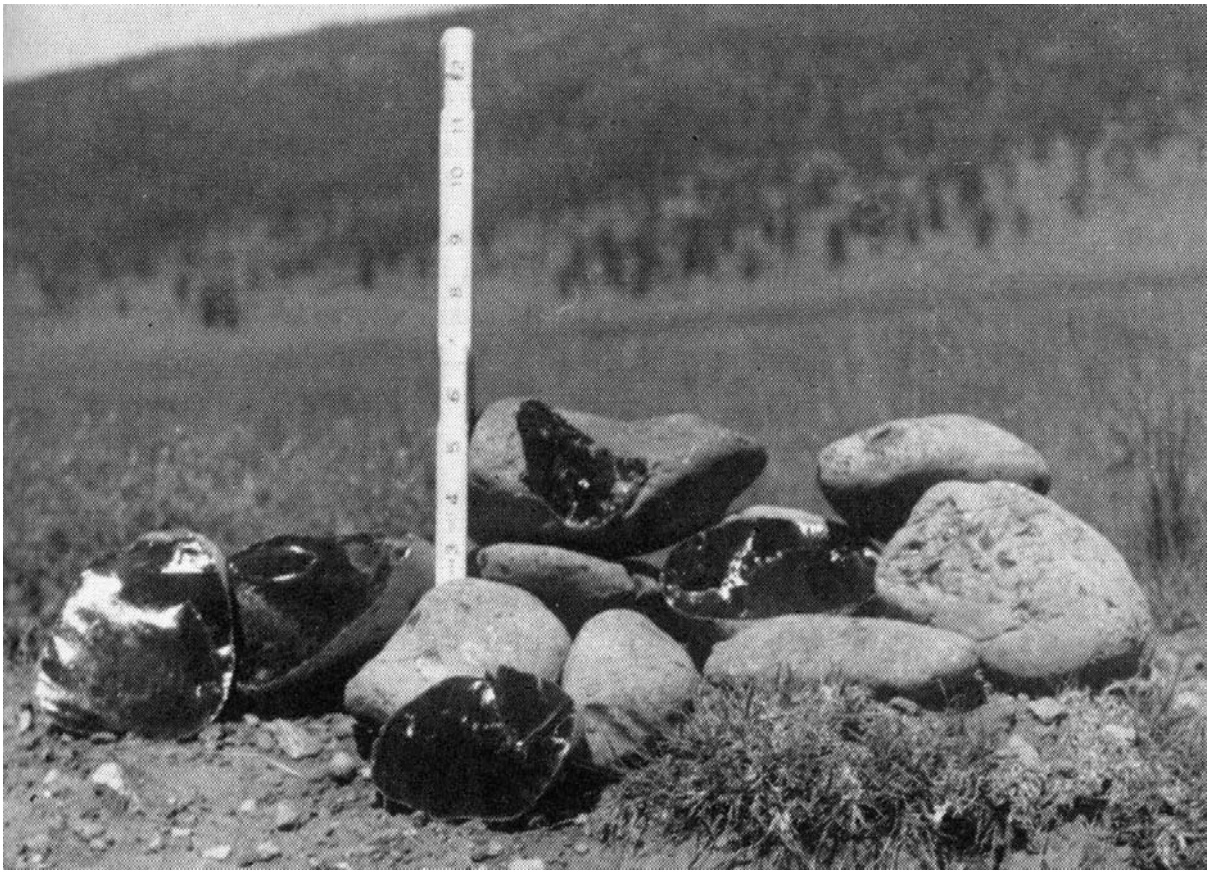

Figure 10.8. Valle Grande Rhyolite obsidian nodules photographed by Boyer and Robinson collected along San Antonio Creek in the caldera (1956:337).

My survey along San Antonio Creek from its junction with State Highway 126 for 10 miles upstream did not reveal any obsidian, as in the Boyer and Robinson study. Both Phil Letourneau and Ana Steffen discovered the same in similar surveys. It appears then that Valle Grande Rhyolite obsidian does not enter secondary contexts outside the caldera, at least in nodules of any size compared to Cerro Toledo Rhyolite. The 2005 and 2006 surveys along San Antonio Creek in the caldera indicate that by the time the secondary deposits reach the caldera rim, the nodule size is near pea gravel in diameter.

Valle Grande Rhyolite obsidian exhibits a fabric that seems to be a combination of El Rechuelos and Cerro Toledo. Some of the glass has that granular texture of El Rechuelos and some has devitrified spherulites similar to Cerro Toledo, and much of it is aphyric black glass. Flakes of Valle Grande obsidian can be indistinguishable from El Rechuelos or Cerro Toledo in hand sample. An elemental analysis of samples collected by Dan Wolfman from Cerro del Medio and the nodules in San Antonio Creek in this study are identical, indicating that Cerro Toledo glass does not enter the East Jemez River system (see Table 10.4).

In the Valle Grande Rhyolite obsidian so far analyzed from both Cerro del Medio proper and secondary deposits in the caldera, it is apparent that there is considerable variability in Rb (140 to 184 ppm; Table 10.4). Ana Steffen at the VCNP has noticed significant variability in ferric

versus ferrous iron (Steffen, 2005 personal communication). It would be worthwhile to sample the Cerro del Medio dome complex in a variety of areas in order to determine both the level of variability and the spatial distribution of that variability.

Table 10.4. Elemental concentrations for Valle Grande Rhyolite obsidian in the Jemez Mountains. All measurements in parts per million (ppm). Samples with numeric designations from Shackley's surveys. Those with alpha-numeric surveys from the Wolfman and LANL collections. Samples with Ti, Mn, and Fe concentrations analyzed by EDXRF. All others analyzed by WXRF. Instrumental conditions for both instruments discussed in Shackley (1998a).

SAMPLE	Ti	Mn	Fe	Rb	Sr	Y	Zr	Nb	Ba	La	Ce
102799-2-1				155	10	43	168	54	30		
102799-2-2				157	10	44	172	55	25		
102799-2-3				159	10	44	169	55	35		
102799-2-4				158	10	43	171	55	27		
102799-2-5				160	9	43	170	54	41		
102799-2-6				154	10	42	167	54	39		
102799-2-7				159	9	43	174	54	47		
102799-2-8				162	10	44	168	55	41		
102799-2-9				158	10	43	170	55	45		
102799-2-10				166	10	43	168	54	23		
102799-2-11				176	10	43	168	55	29		
102799-2-12				140	11	40	178	53	26		
102799-2-13				154	11	42	164	54	42		
102799-2-14				144	10	41	179	55	25		
102799-2-15				172	10	44	177	55	23		
CM-3-D	912	486	11600	184	5	47	181	52	30	38	76
CM-2-A	729	341	9030	158	5	40	173	52	26	34	67
CDMA-1				160	10	44	173	56	31		
CDM3B				159	10	44	174	56	39		
CDMV-1				158	10	44	173	55	32		
CDMA-2				158	10	43	174	55	34		
CDMA-3-B				156	10	43	172	54	35		
CDM 3-1				178	10	42	170	54	62		
CDM 3-2				158	10	44	174	55	38		
CDM 3-3				156	10	43	171	54	27		
CDM 1A				156	10	43	172	54	31		
CDM CM1				159	10	44	174	56	28		
CDM CM-3-E				161	11	43	172	54	55		

Canovas Canyon Rhyolite and Bear Springs Peak

The oldest (Tertiary: ca. 8 to 9 mya) obsidian source in the Jemez Mountains is the Bear Springs Peak dome complex, part of the Canovas Canyon Rhyolite domes and shallow intrusions (Tcc and Tcci) as reported by Kempter et al. (2003). Located at the far southern end of the Jemez Mountains, just south and adjacent to Jemez Pueblo Nation land, this Tertiary Period source exhibits only relatively small marekanites now, most smaller than 2 cm in diameter (see Figure 10.1). Although the nodule size was apparently small, Bear Springs Peak obsidian was used in prehistory, and was recovered in samples analyzed from Early Historic period contexts at Zuni Pueblo, probably a result of relationships between the Zuni and Jemez in the 17th century (Shackley 2005a). The data as analyzed by Craig Skinner and my lab, suggest that this may be the "Bland Canyon & Apache Tears" source as reported by Glascock et al. (1999:863), collected by Wolfman and reported by him in 1994 (Table 10.5).

Table 10.5. Elemental concentrations for Bear Springs Peak obsidian in the Jemez Mountains. All measurements in parts per million (ppm). Skinner and Shackley analyses combined.

Element	N	Minimum	Maximum	Mean	1 Std. Deviation
Ti	15	279	630	460	112
Mn	24	227	609	398	117
Fe	9	6245	7685	6593	431
Rb	24	106	128	116	5
Sr	24	36	54	43	4
Y	24	16	27	21	2
Zr	24	100	114	108	4
Nb	24	40	61	53	5
Ba	15	293	717	352	102

As with many of the Tertiary Period sources in the Southwest, Bear Springs Peak obsidian is present as marekanites in perlitic lava at the Bear Springs Peak dome proper and domes trending to the northeast toward and into Jemez Pueblo land. Nodules up to 5 cm occur as remnants in the perlite not unlike the environment at Sand Tanks (Shackley 2005a:20). The density of the nodules from pea gravel to 5 cm in the perlite lava is as much as 100/m^2, although most of the marekanites are under 2 cm. The glass itself is aphyric and nearly transparent in thin flakes similar to Cow Canyon and Superior obsidian, and some have noticeable dark black and nearly clear banding. It is an excellent media for tool production so that bipolar flakes are easily produced and pressure flaking is effective.

The marekanites have eroded into the stream systems to the south possibly as far as the Rio Grande, but marekanites bearing the chemistry have never been recorded in the southern Rio Grande alluvium as reported by Church (2000). Most likely the nodules are expended in the sediment load long before reaching the Rio Grande or have been covered by subsequent Quaternary sediments. It is safe to conclude that artifacts assigned to Bear Springs Peak would have to be originally procured at or near the Bear Springs dome complex. Probably the reason this source is not found in archaeological contexts more frequently is that it simply cannot

"compete" with the large nodule sources just to the north including Cerro Toledo Rhyolite, Valle Grande Rhyolite, and El Rechuelos obsidian. Finally, a new geology map for the Bear Springs Peak Quad is in draft form (Kempter et al. 2003).

MAGMATIC RELATIONSHIP BETWEEN THE GLASS SOURCES

The relatively short time period of eruptive events that produced artifact-quality obsidian in the Jemez Mountains from El Rechuelos to Valle Grande Rhyolite is reflected in the elemental chemistry as reported by a number of others discussed above (e.g., Baugh and Nelson 1987; Broxton et al. 1995; Gardner et al. 1986; Glascock et al. 1999). This relationship is readily evident in three-dimensional and biplots of the incompatible elemental composition of these sources as shown in Figures 10.9 and 10.10, the analysis of major and minor elements shown in Tables 10.2 through 10.4. Rubidium, zirconium, and yttrium are most sensitive in separating these sources. Indeed, a biplot of the elemental concentrations Zr versus Y can effectively separate all four Jemez Mountains sources, although it is NOT sufficient to eliminate the possibility that the analyzed artifacts could be from outside the Jemez Mountains group (Figures 10.9 and 10.10).

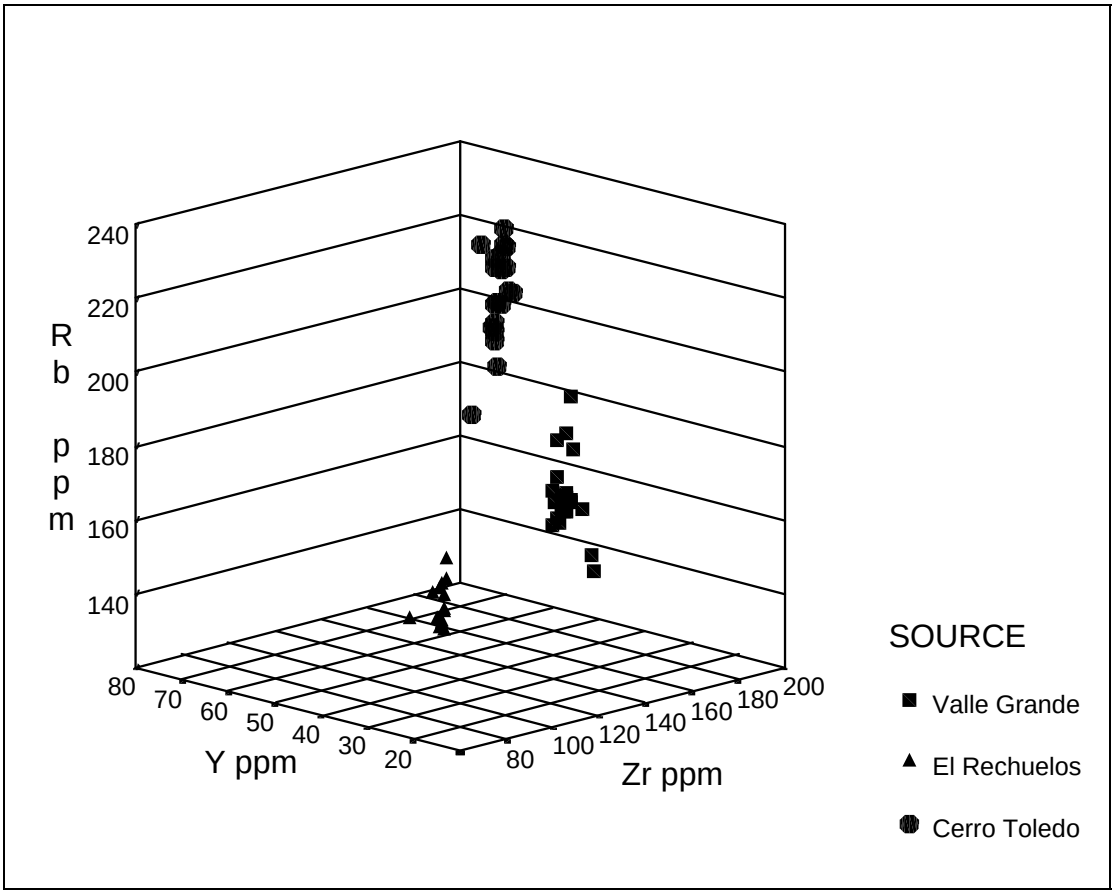

Figure 10.9. Rb, Y, Zr three-dimensional plot of Valle Grande, El Rechuelos, and Cerro Toledo Rhyolite obsidian source standards.

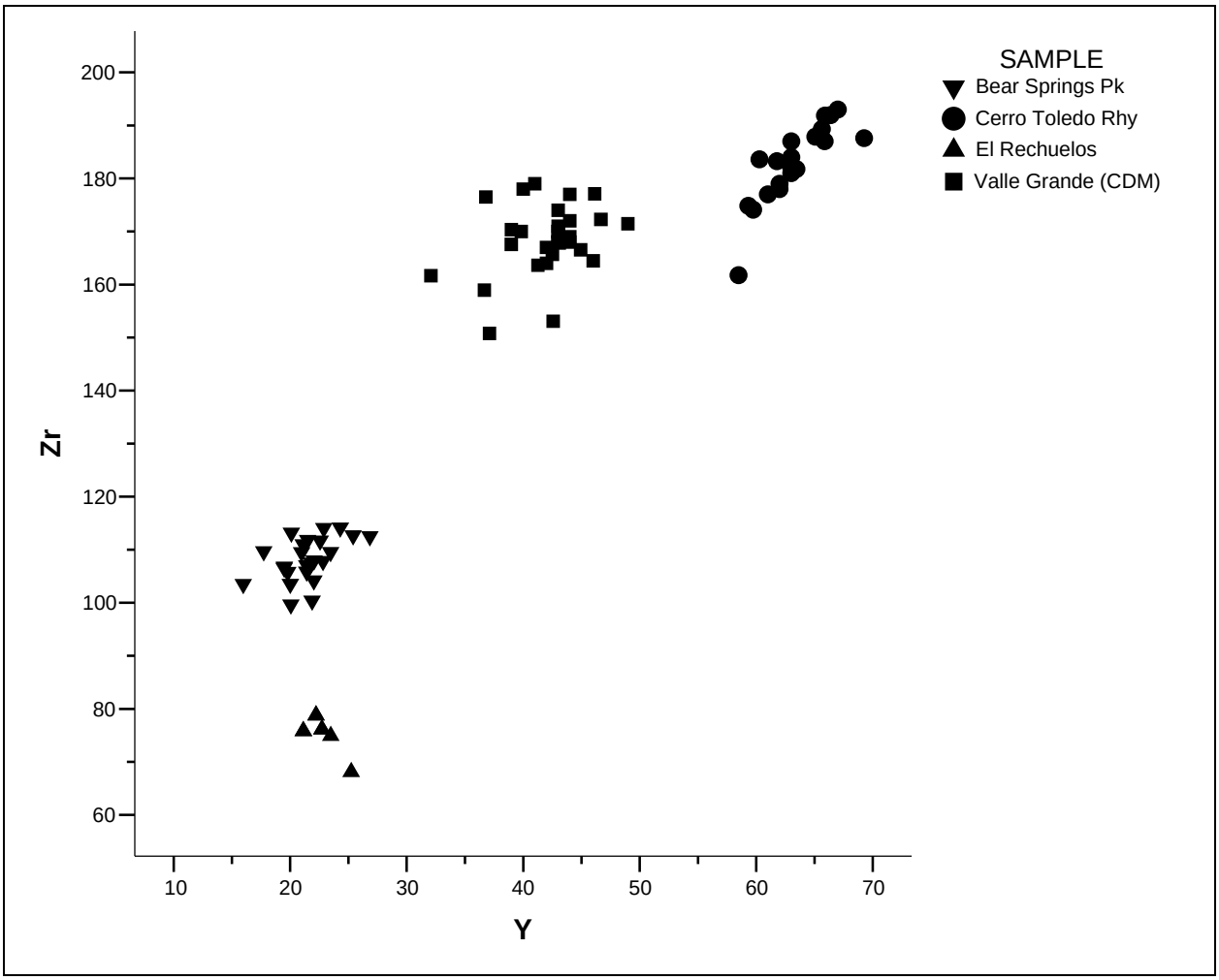

Figure 10.10. Zr versus Y biplot of the elemental concentrations for Valle Grande (Cerro del Medio), El Rechuelos, Cerro Toledo Rhyolite, and Bear Springs Peak obsidian source standards. High variability in Valle Grande and Cerro Toledo data are the result of the analysis of small secondary distribution nodules (see Davis et al. 1998).

THE LANL STUDY

A number of marekanite (obsidian) and ignimbrite or tephra samples were submitted for non-destructive WXRF analysis, in part to enlarge the secondary depositional study, and in part to determine the relationship between the marekanites and the ignimbrite or tuff that they are contained within (Table 10.6 and Figures 10.11 and 10.12). While this nondestructive study is certainly not as thorough as a more intensive analysis with prepared pellets and WXRF, the results are revealing. Most of these localities have been described by David Broxton in field notes from July 2002.

Table 10.6. WXRF nondestructive elemental analysis of obsidian and other rock samples from the LANL collection. Some samples submitted were too friable for nondestructive analysis.

Sample	Locality	Rb	Sr	Y	Zr	Nb	Ba	Source
Marekanites (obsidian)								
LCT-1-1	Los Alamos Cn	183	7	58	164	91	55	Cerro Toledo Rhy
LCT-1-2		168	6	54	149	83	63	Cerro Toledo Rhy
RC-4-1	Rendija Cn	202	6	61	169	97	4	Cerro Toledo Rhy
RC-4-2		199	5	62	170	98	4	Cerro Toledo Rhy
RC-4-3		203	7	63	173	99	13	Cerro Toledo Rhy
RC-4-4		205	6	64	178	102	8	Cerro Toledo Rhy
TA-3-1	TA-58	154	9	43	166	55	31	Valle Grande Rhy
TA-3-2		155	9	42	160	54	12	Valle Grande Rhy
PL-5-1	pumice near Rendija Cn	200	6	63	169	99	5	Cerro Toledo Rhy
PL-5-2		197	6	62	171	98	0	Cerro Toledo Rhy
PL-5-3		191	6	60	166	95	12	Cerro Toledo Rhy
BV07-02-16-1	Canyon Road	145	10	40	155	51	1	Valle Grande Rhy
BV07-02-16-2		149	9	43	161	53	26	Valle Grande Rhy
BV07-02-16-3		150	9	43	164	54	53	Valle Grande Rhy
Rock and Ignimbrite samples								
BV07-02-13-1	SR 502 road cut	16	479	27	132	16	516	
BVO7-02-10-1	Los Alamos Cn	153	25	52	200	67	37	
BVO7-02-11-1	Los Alamos Cn	125	28	43	202	55	40	
BVO7-02-14-1	SR 502 road cut	360	11	104	255	195	18	
BVO7-02-16-1	Canyon Road	145	48	50	161	49	835	
BVO7-02-17-1	Canyon Road	141	26	44	175	55	195	
BVO7-02-17-2	Canyon Road	146	29	46	173	55	639	
BVO7-02-18-1	Ski Hill Road	137	222	45	145	42	1493	
BVO7-02-18-2	Ski Hill Road	131	172	51	160	47	874	
BVO7-02-5-1	Los Alamos	311	27	108	284	160	92	
BVO7-02-8-1	Los Alamos	209	31	77	199	103	26	
RGM-1		145	102	24	215	8	769	standard
BHVO-1		10	405	27	177	20	134	standard

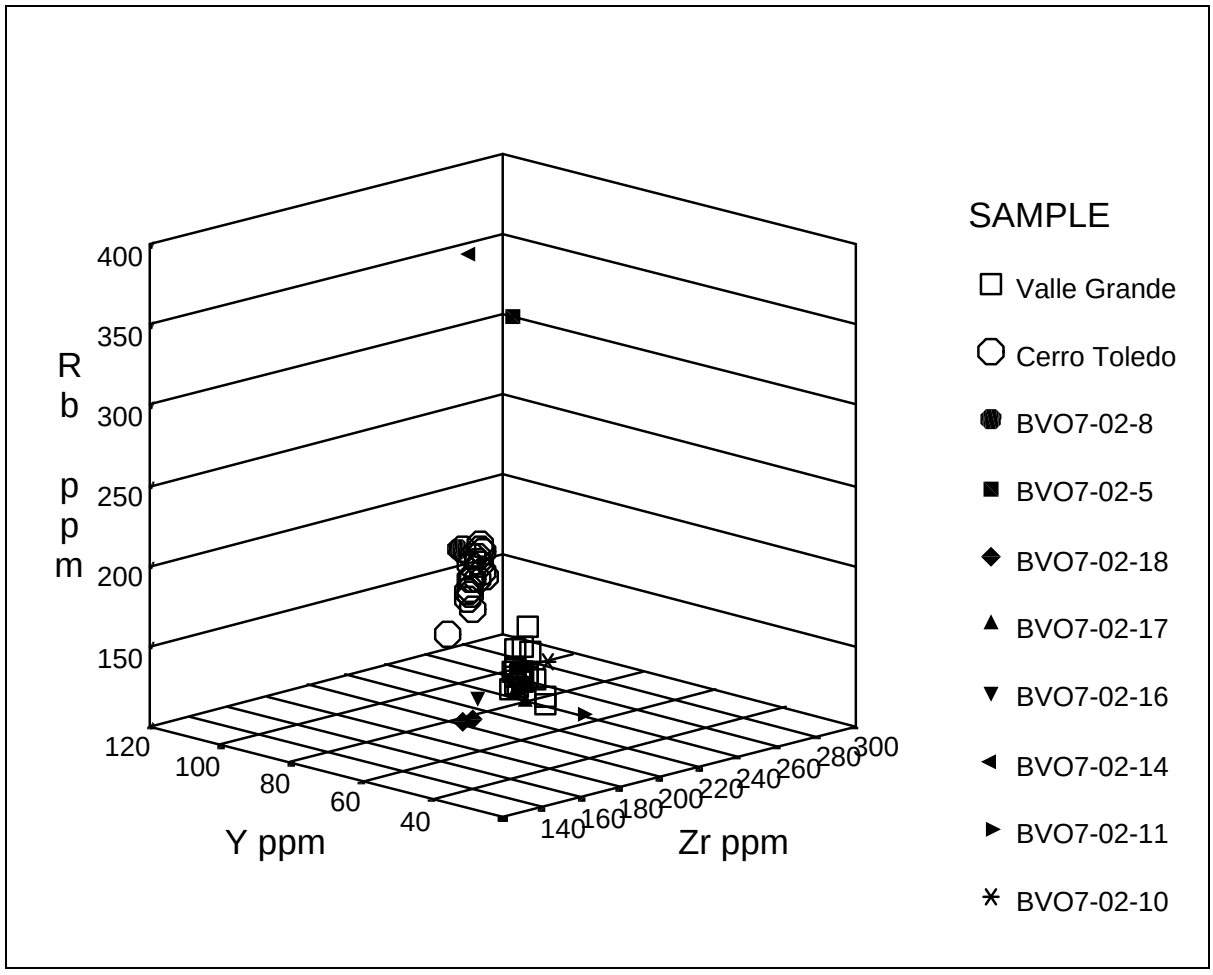

Figure 10.11. Rb, Y, Zr three-dimensional plot of Valle Grande Rhyolite and Cerro Toledo Rhyolite obsidian source standards and rock samples submitted by LANL. Samples from localities 5 and 14 are probably not rhyolite based on these elements analyzed.

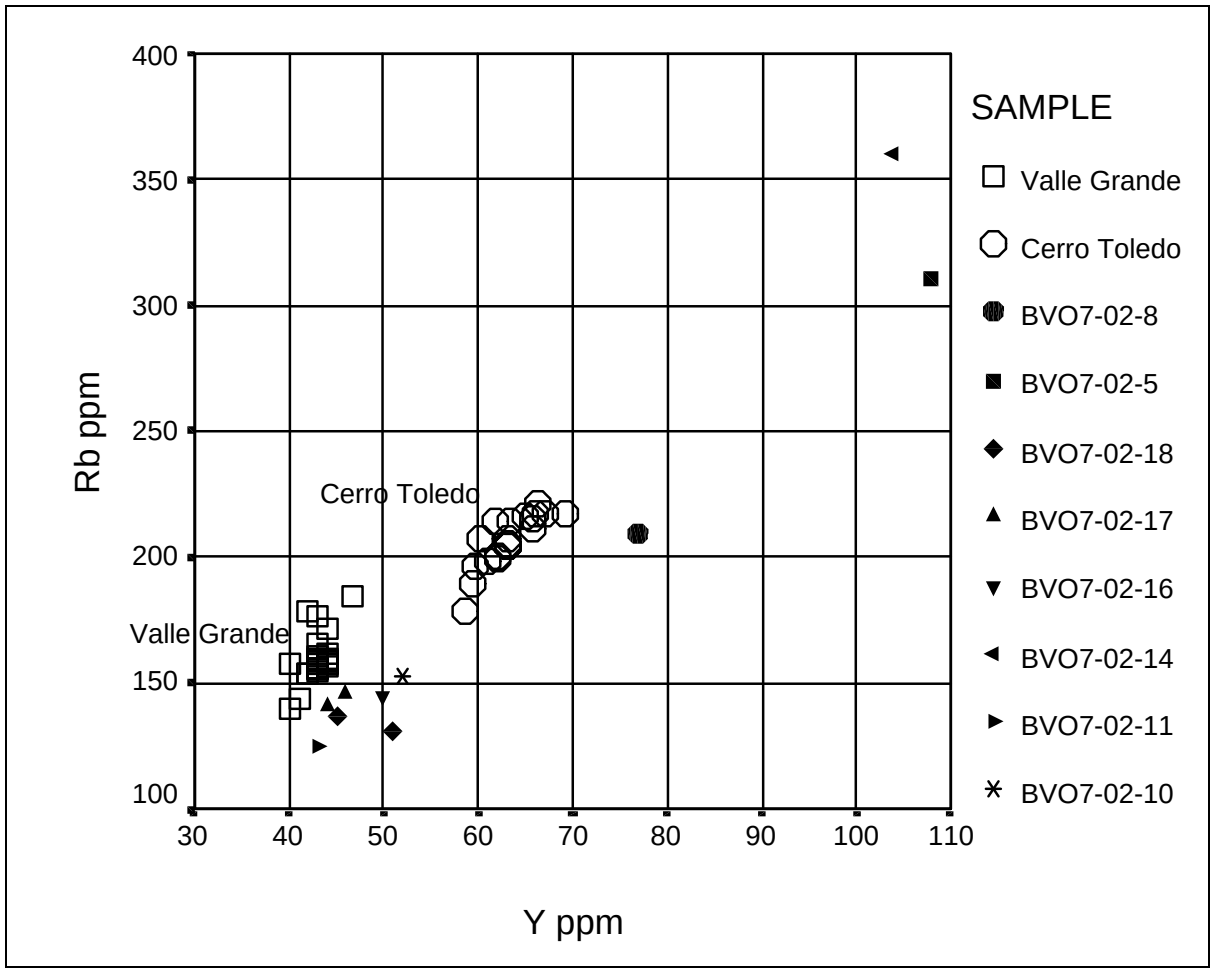

Figure 10.12. Rb, Y biplot of Valle Grande Rhyolite and Cerro Toledo Rhyolite obsidian source standards and rock samples submitted by LANL. Samples from localities 5 and 14 are probably not rhyolite based on these elements analyzed.

Obsidian Samples

Obsidian marekanite samples from five localities were submitted for analysis as shown in Table 10.6. While most of the samples were obsidian associated with the Cerro Toledo Rhyolite events and the Bandelier Tuff, a few of the samples appear to be post-Bandelier and exhibit an elemental composition consistent with Valle Grande Rhyolite obsidian (TA-3 and BV-07-02-16 localities; see Table 10.6, and Figures 10.11 and 10.12). While the sample is small here, it does appear that Valle Grande obsidian occurs in what Broxton designates as "post-Bandelier" sediments and these are in the western portion of LANL property closest to Cerro del Medio. Importantly, although this is the first example of Valle Grande obsidian *outside* the caldera rim, the nodule sizes are quite small, possibly representing small pieces of rhyolite lava quenched as pyroclastics during the eruption. I would stand by the conclusion that no archaeologically significant Valle Grande obsidian has eroded outside the caldera.

Rock Sample Analysis

Figures 10.10 and 10.11 exhibit the Rb, Y, and Zr plots of Cerro Toledo Rhyolite and Valle Grande Rhyolite obsidian source standard data and the submitted tephra samples, without the basalt or dacite lava included. Immediately apparent is that the vast majority of samples, based on these three elements, are most similar to Valle Grande, the post-Bandelier event, although none of the rock samples plot within the range of variability of the glass. This is typical of rhyolite versus obsidian, where post-emplacement weathering and other processes affect the crystalline lava more than glass (Shackley 1990; Zielinski et al. 1977). Additionally, concentration of Ba and Sr in feldspars, such as sanidine in rhyolites will often elevate the concentration of these elements relative to the obsidian produced by the same event in X-ray fluorescence analyses. This appears to be the case in this dataset in the obsidian recovered from locality BV-07-02-16 where the obsidian, consistent with Valle Grande glass, is relatively low in Ba and Sr, while the tephra sample is high in Ba and Sr (Table 10.6). I would, however, if given these samples as a blind test, suggest that they were somehow related to the Valle Grande Rhyolite.

Prehistoric Procurement and Secondary Deposition

The LANL study expands the range of the larger secondary depositional study. While some very small Valle Grande Rhyolite marekanites occur outside the caldera, their small size makes them insignificant as a raw material source. Cerro Toledo Rhyolite obsidian is a much more viable raw material source, apparently, in association with the Bandelier Tuff all around the perimeter of the caldera, including the LANL area and sediments further south and east. While it is impossible to determine whether obsidian artifacts recovered from sites in the LANL property were produced from primary or secondary sources, for Valle Grande at least, if the artifacts are larger than about 15 or 20 mm, the raw material probably came from the caldera floor near Cerro del Medio. With artifacts produced from Cerro Toledo Rhyolite obsidian, inferences about procurement are more difficult. Since large nodules (>30 mm) are common in sediments outside the caldera, these artifacts could be procured anywhere.

This study and the greater secondary depositional study reveal that an understanding of both primary and secondary sources of raw material are crucial in reconstructing procurement, exchange, and group interaction, and simple conjecture that obsidian is located somewhere in the Jemez Mountains yields but simple conclusions.

THE DACITE STUDY

More recently, a collaborative study between LANL, the Archaeological XRF Lab at Berkeley, and the Smithsonian Institution, has focused on the dacite used frequently for biface production in the Paleoindian and Archaic periods and for flake tools during the ceramic periods (Vierra et al. 2005; Shackley 2005b).

For a number of years we have noticed a very-fine-grained what appeared to be mafic or basalt raw material source in late Paleoindian contexts in northern New Mexico and southern Colorado. Indeed, a number of Cody, Plainview, and Folsom bifaces are produced from this material. Pegi Jodry and Brad Vierra have been working for a number of years with collectors and others, and determined that there were two possible very fine-grained volcanics that could be the sources for these raw materials—San Antonio Mountain in far northern New Mexico, in the Taos Plateau Volcanic Field, and Cerros del Rio, on the east side of Bandelier National Monument right above the river. After reconnaissance collections at the two probable sources, the short story is that the vast majority of "basalt" artifacts were indeed produced from one of these sources (Table 10.7).

However, these two "basalt" sources are not basalt at all. The San Antonio Mountain volcanics have been called basalt by archaeologists for years, despite Lipman and Mehnert's (1979) early analysis indicating a "rhyodacite." As you can see by the major compound rock classification, these rocks are firmly dacites (Figure 10.13). So, the two primary volcanic sources other than obsidian used by Late Paleoindian and Early Archaic knappers in the northern Rio Grande is a fine-grained dacite. Additionally, as originally reported by Newman and Nielsen (1987), a third dacite dome is located just east of Cerro Montoso, and this third source, called the Newman Dome here, takes care of that small group of dacite artifacts that are not produced from the other two "major" sources of dacite (Table 10.7). The elemental chemistry of these three sources is quite distinct (Figure 10.14). These analyses will form the database for future studies of volcanic rocks used in regional prehistory.

Table 10.7. Elemental concentrations for the three dacite sources in northern New Mexico. All measurements in parts per million. BHVO is a U.S. Geological Survey Hawaiite basalt source standard.

Source/Sample	Ti	Mn	Fe	Zn	Ga	Rb	Sr	Y	Zr	Nb
San Antonio Mountain										
061805-1-1	3610	742	36816	81	20	56	633	23	270	22
061805-1-2	3395	632	34262	80	17	55	591	21	246	16
061805-1-3	3683	548	34428	73	22	54	602	20	253	22
061805-2-1	3425	497	31906	77	20	52	515	22	201	27
061805-2-2	3665	633	35857	82	22	57	564	25	240	13
061805-2-3	3389	646	34805	79	21	57	602	22	247	28
061805-3-1	3561	609	35020	80	19	62	568	24	250	18
061805-3-2	3227	617	31823	75	24	61	569	24	256	10
061805-3-3	3521	651	32938	69	20	59	570	18	254	19
061805-4-1	3421	567	32598	79	20	56	532	22	233	30
061805-4-2	3300	550	33599	74	23	59	558	17	226	22
061805-4-3	3391	605	33415	71	20	52	546	23	230	17
061805-5-1	3581	716	35773	88	22	63	581	18	249	17
061805-5-2	3537	684	34228	78	24	59	591	26	255	24
061805-5-3	3143	586	32011	71	21	61	581	20	245	19
061805-6-1	4485	767	44577	98	23	69	653	19	269	20
061805-6-2	3264	674	35090	83	23	61	572	23	256	20
061805-6-3	3326	765	35273	81	18	57	573	23	244	18

Source/Sample	Ti	Mn	Fe	Zn	Ga	Rb	Sr	Y	Zr	Nb
061805-6-4	3393	631	34996	78	19	61	572	15	242	31
Cerro del Rio										
3	3356	2583	29734	80	19	47	814	6	197	19
1	2813	553	28290	76	20	41	771	15	193	23
2	3363	640	33390	71	24	40	822	14	207	20
4	3505	636	33790	89	18	49	826	16	200	12
5	3497	627	33069	70	21	44	839	11	202	28
9	3297	671	31776	71	19	49	806	15	208	19
7	3393	699	34613	71	22	47	878	19	213	21
8	3226	896	31766	71	19	39	813	15	198	32
6	3001	645	30915	73	19	39	818	16	180	19
10	3256	639	30699	74	19	42	814	13	206	25
Newman Dome										
1987 sample				62		50	214	15	82	8
Berkeley analysis				67		51	217	15	84	8
BHVO-2 (standard)	16071	1638	98090	70	23	10	382	19	162	17

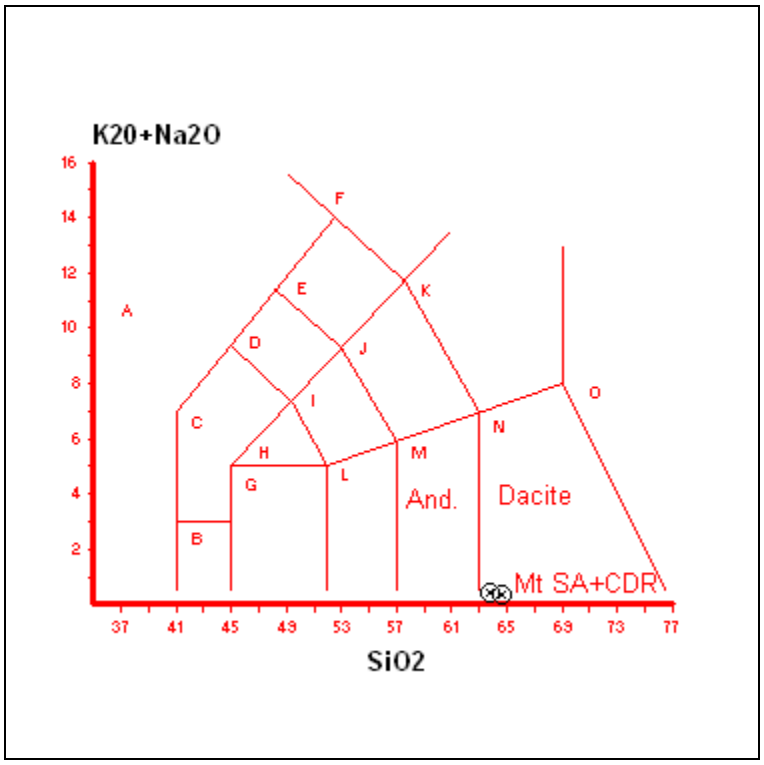

Figure 10.13. Cox et al. (1979) classification analysis of one San Antonio Mountain and Cerros del Rio sample.

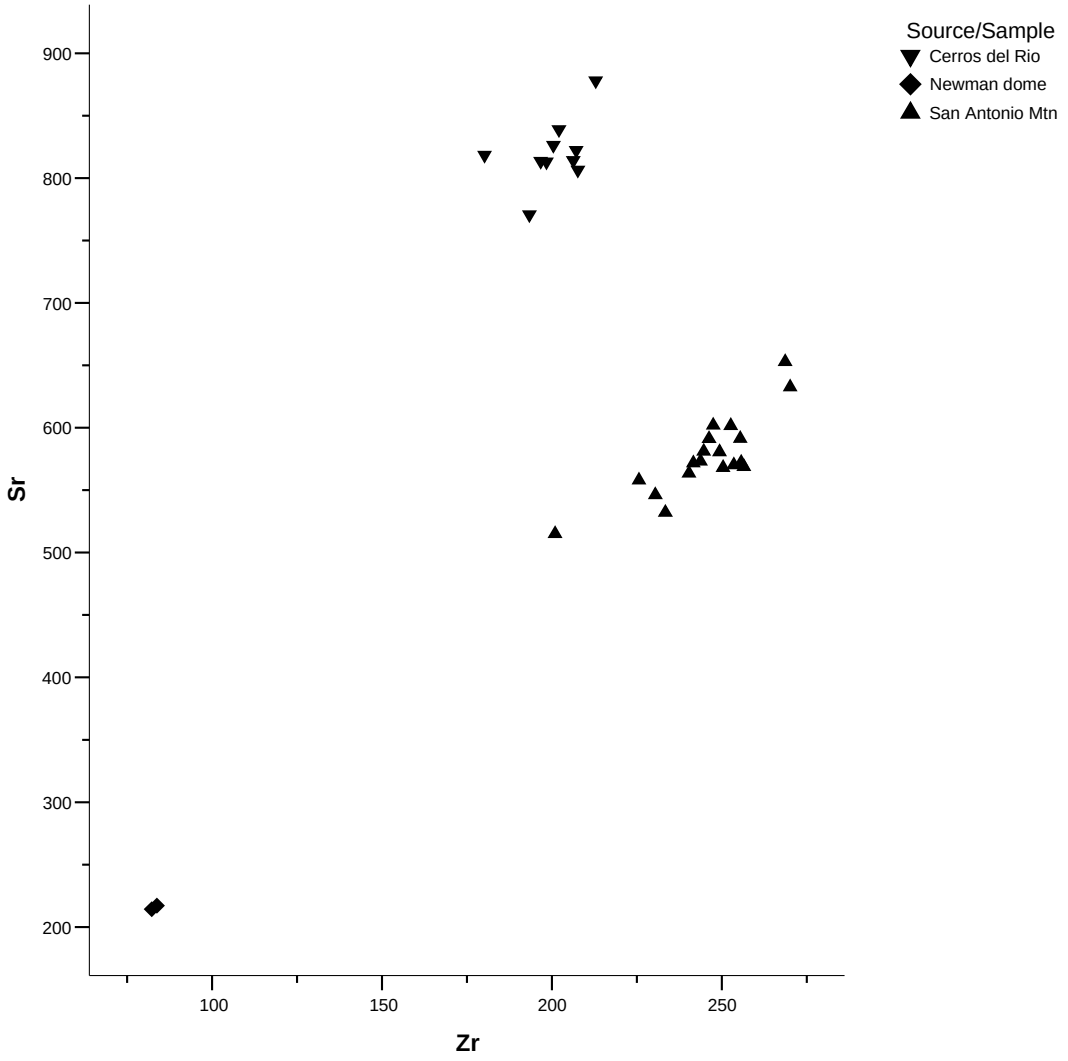

Figure 10.14. Sr versus Zr plot of the three dacite sources in northern New Mexico, from the data in Table 10.7.

CHAPTER 11
OBSIDIAN HYDRATION DATING BY INFRARED SPECTROSCOPY

Christopher M. Stevenson

INTRODUCTION

The obsidian hydration dating method provides an age estimate for natural glass artifacts based upon the penetration depth of diffused molecular water into the obsidian surface. A successful implementation of the dating method requires an estimation of the water diffusion coefficient and the precise measurement of the depth of diffusion. In this paper, the fundamental process behind water diffusion in obsidian is considered and it is demonstrated that infrared spectroscopic analysis of the glass matrix and hydrated layer has the potential to provide precise estimates of the critical variables. It is argued that the use of an IR approach will result in a more unified approach to the problem and result in a higher level of analytical precision.

The water diffusion process in obsidian has been poorly understood for many years and has lacked a good theoretical understanding. As a result, archaeometric studies evaluated the suitability of experimental designs to estimate diffusion coefficients through comparison with external chronological data (Stevenson 2000; Stevenson et al. 1998). Convergence in age estimates between obsidian samples and radiocarbon assays implied that the methods were appropriate even though a thorough explanation was lacking. However, investigations in the field of glass science have changed this situation. Hydrogen profiling of the hydrated layer has demonstrated that concentration-dependent diffusion is the dominant process (Anovitz et al. 1999) rather than the Fickian model previously proposed (Friedman and Long 1976). In addition, experimentation has shown that the *structural* water within the unaltered glass matrix in the form of hydroxyl and molecular water controls the forward advancement of the hydration layer (Stevenson et al. 1998; Tomozawa 1985) and the mobile species within the hydration layer is *molecular* water (Zhang and Behrens 2000) (Figure 11.1). Both of these key variables may be precisely estimated by infrared spectroscopy and have the potential to greatly improve the dating process. In this paper, the value of IR technology in measuring the structural water concentration and the extent of surface hydration is discussed.

PREVIOUS OBSIDIAN HYDRATION STUDIES IN NEW MEXICO

The obsidian hydration dating method has been extensively applied over the last 20 years in the New Mexico region with major projects occurring at Ft. Bliss in the Sonoran desert and within the Jemez Mountains (see Vierra and Harmon 2006 for a summary). Much of this earlier work was spurred by new developments in the method that included the use of high-temperature-derived hydration constants (Friedman and Long 1976; Michels 1983; Stevenson et al. 1989) for the estimation of archaeological rates at ambient conditions. A variety of experimental designs were used that included hydrothermal reaction at elevated pressure and vapor hydration at one atmosphere. Many of these initial experiments have been subsequently revised. However, the utility of the induced hydration approach has been demonstrated as a viable experimental

approach and one that continues today. In this paper, I continue to refine the induced hydration approach by the addition of infrared spectroscopy to the pool of analytical options.

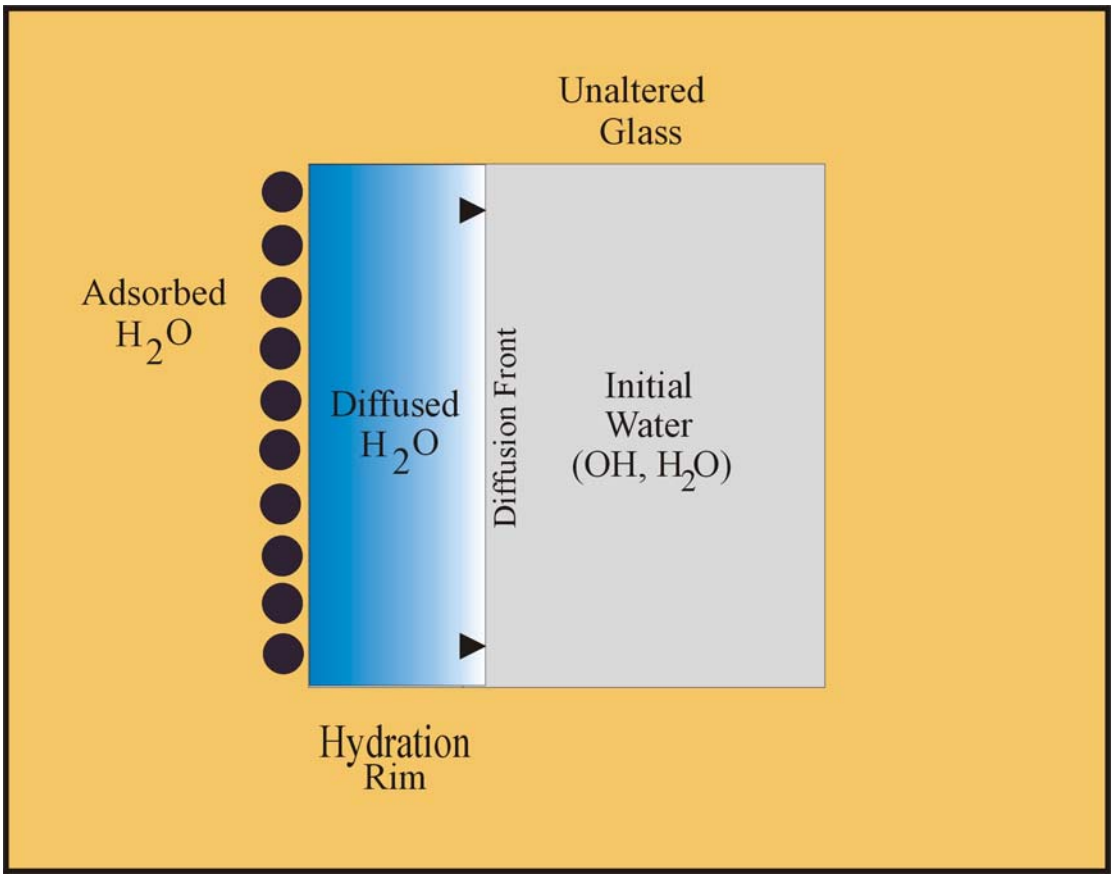

Figure 11.1. A schematic of the hydration layer showing the various forms of water on, and within, the glass.

This early laboratory work was accompanied by an effort to model the hydration history of sites and regions. Ground temperature and soil relative humidity were investigated as functions of elevation, aspect, depth below surface, and ground cover (Mundy 1993; Ridings 1991). The outcome of these studies revealed that precise estimates of these variables were highly complex, difficult to replicate, and inherently variable. For example, although a general relationship exists between altitude and declining temperature, there were always outliers that could not be explained by the modeling process. These same difficulties in developing temperature prediction equations have been encountered in regional studies conducted in New Zealand where the influence of micro-topographic differences and surface vegetation were recognized as having a profound influence (Jones et al. 1997). For the moment, it appears that high-resolution studies of soil temperature and relative humidity are required for each site under study.

Each of these avenues of investigation have raised questions and promoted the development of methodological improvements. Several recent reviews of the obsidian hydration dating method have tracked these events (Stevenson et al. 1998; Stevenson et al. 2000). These reviews stress two important points that will impact the use of obsidian hydration dating over the long term.

First, it is critical to understand the depositional context from which a datable artifact is recovered. How did that artifact cycle through the society, how was it discarded, and what cultural and natural processes result in its burial? Only then can the dated event (use/manufacture of the obsidian tool) be linked to the target event (Dean 1978), which may be the occupation of a pueblo room or the filling of a trash pit. If the depositional history of the artifact can be understood, then appropriate temperature and humidity values can be applied. Second, the direct measurement of glass structural water content is critical. Obsidian sources will exhibit a range in structural water concentration and even small differences can alter hydration rate estimates. It is no longer appropriate to infer that an obsidian source is uniform in structural water even though the trace element chemistry is highly uniform across the flow. Such uniformity must be demonstrated on a case-by-case basis. Only with this control over glass composition and context can the changes in approach to obsidian hydration dating discussed below be evaluated against other chronological indicators in the archaeological record.

Water Diffusion in Glass

The model of water diffusion in amorphous silicates developed by Doremus (1969) is the most appropriate descriptor of water diffusion in rhyolitic glass at low temperature because it accounts for the patterning in much of the experimental data (Doremus 1995). In a vapor environment, molecular water enters the glass network and reacts with the silicon-oxygen network to form SiOH groups:

$$\text{Si-O-Si} + H_2O = \text{SiOH} + \text{OHSi}$$

The molecular water is the mobile species while the newly formed OH groups are relatively fixed. It is assumed that OH group formation lags behind the movement of mobile water molecules and does not reach equilibrium.

It was also assumed in previous model development that the initial concentration of water in the glass is zero. However, obsidians may have structural water concentrations up to several weight percent. This will serve to exponentially increase the diffusion coefficient for ambient molecular water (D) as concentration increases (Stevenson et al. 1998; Zhang and Behrens 2000; Zhang et al. 1991). In the diffusion process this is believed to occur because the bonds of the Si-O-Si network are broken with the activation energy determined by the energy needed to break a single Si-O bond (Bruckner 1970; McMillan et al. 1994). The occurrence of greater amounts of SiOH in the network may weaken the neighboring Si-O-Si bonds, causing them to easily break and therefore lower the overall activation energy. It therefore becomes critical to determine the concentration of water within each sample to be dated.

It has been demonstrated that structural water is present within unhydrated obsidian as both molecular water (H_2O_m) and as hydroxyl (OH) (Newman et al. 1986; Silver and Stolper 1989; Stolper 1982). The sum of both species is referred to as the total water concentration (H_2O_t). Silver et al. (1990) demonstrated the relationship between the two species as a function of total water concentration. To develop obsidians of varying water content, obsidian from Mono Craters, California, was heated and quenched in a cold seal reactor at varying temperatures and cooling rates. Spectroscopic analysis revealed that at total water concentration of less than about 3 percent (weight percent) hydroxyl is the dominant species (Figure 11.2). As H_2O_t increases, the concentration of OH reaches a plateau at around 1 percent concentration. In contrast to this, molecular water is not detectable by infrared analysis when the total water is less than about 0.3 percent but then the concentration increases rapidly. The experimental data shows this trend to continue up to about 3 percent H_2O_m (Silver et al. 1990).

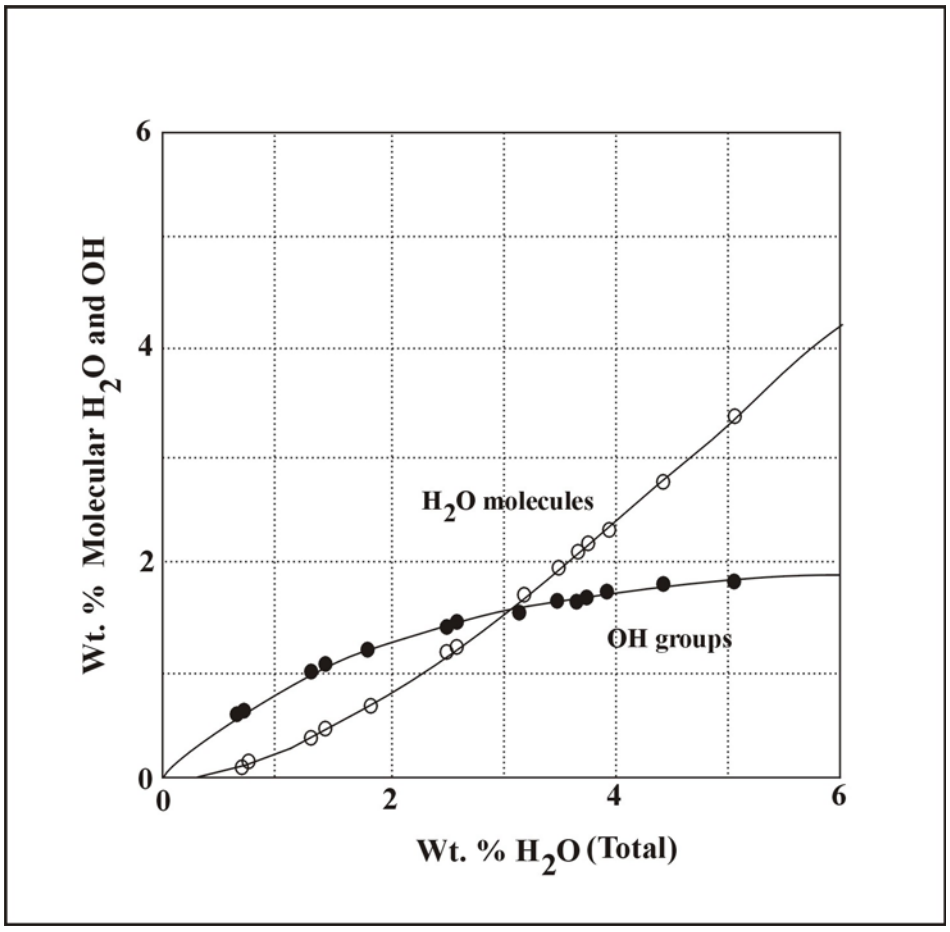

Figure 11.2. The proportional concentration between OH groups and H_2O molecules in obsidian (from Silver et al. 1990).

The diffusion of water in amorphous silicates is also strongly correlated with the concentration of water within the surface hydration layer (Drury et al. 1962; Lee et al. 1974; Nogami and Tomozawa 1984). This phenomenon is referred to as concentration-dependent diffusion. Within a narrow compositional range, the anhydrous component of the glass has little influence on the

mobility of water (Behrens and Nowak 1997). Under ambient temperatures (0 to 30° C), the diffusion coefficient does not follow the non-steady-state diffusion process and cannot be mathematically estimated with Fick's second law. Instead, as water enters the glass network the structure is depolymerized and allows additional water to enter the glass at a faster rate. This changing diffusion coefficient results in the formation of an S-shaped concentration-depth profile (Figure 11.3). However, experimental work shows that the leading edge of the diffusion profile advances into manufactured and natural glasses at the square root of time (Lanford et al. 1979; Stevenson et al. 1998; Tsong et al. 1980).

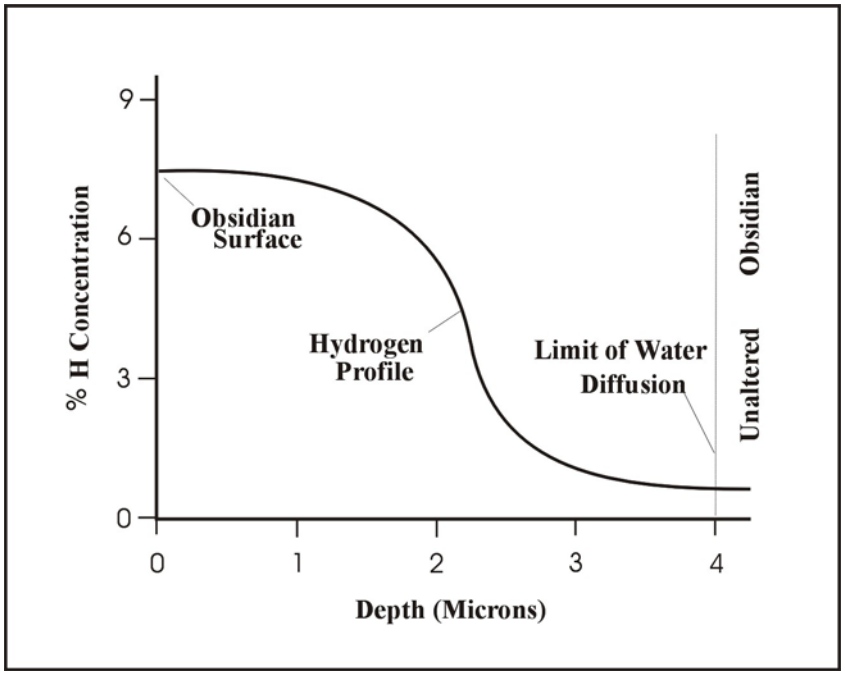

Figure 11.3. Concentration-dependent diffusion profile for obsidian.

The Hydration Dating Method

Based upon the discussion of water diffusion in obsidian, the implementation of the dating method will require two steps. The first step is to determine the depth of molecular water penetration into the glass from the surface. Conventional approaches have used optical microscopy because of the low cost. However, the uncertainty associated with each measurement is +/-0.25 um. This magnitude of error can lead to very generalized age estimates because of the wide standard deviations and defeats the objective of arriving at a precise chronological estimate. Secondary ion mass spectrometry (SIMS) has been used to significantly increase precision to +/-0.05 to 0.1 um, but the cost per sample is prohibitive for routine application. Infrared technology offers a compromise of high precision and lower cost. For example, the infrared photoacoustic (PAS) accessory (McClelland et al. 1993) has been used to successfully measure the absorbance of surface hydration layers and has been correlated with SIMS depth values to provide a highly precise depth calibration (Stevenson et al. 2000).

The second critical step is to determine the diffusion coefficients of H_2O_m at a specified ambient temperature as a function of the amount of glass structural water. Hydrothermal experimentation on obsidian and tektites with initial water concentrations between 0.01 percent and 0.4 percent have shown that the diffusion of molecular water (D) is exponentially related to initial concentration (Stevenson et al. 1998). The magnitude of D varies in response to OH at low structural water concentration and is further increased when structural H_2O_m is present. It is therefore critical to distinguish between OH and H_2O_m when assessing glass composition. Infrared transmission measurement on 0.5- to 2.0-mm-thick parallel-sided glass wafers have a precision of less than 2 percent (Newman et al. 1986) and is the conventional approach although determinations of H_2O_m have been successfully achieved by micro-reflectance Fourier transform infrared spectroscopy (FTIR) (G. Moore and McMillan 2000).

Infrared Spectroscopy

Infrared spectroscopy is a very useful technique for analyzing organic compounds, such as water, in the mid-infrared region (2.5 to 16 um; 5000 to 900 cm^{-1}). It is based on the principle that infrared radiation is absorbed by covalently bonded atoms, or molecules, and causes them to vibrate at the same frequency as the light source. A spectrum is created when a molecular vibration absorbs light at a specific frequency. This is very useful in the analysis of materials because there are several functional groups, or associations of atoms, that vibrate at the same frequency irrespective of the material in which they occur. One such association is hydrogen and oxygen; the focus of this study. A discussion of the properties of light, the types of vibrations and the determination of peak intensities and widths is covered in detail by B. Smith (1999) and the reader is referred to that paper for the fundamentals.

IR transmission spectroscopy has been extensively used to measure water in both manufactured and natural glasses (Bartholomew et al. 1980; Ihinger et al. 1999; Nowak and Behrens 1995; Scholze 1966; Wakabayashi and Tomozawa 1989). The concentration of water in obsidian has been the focus of extensive research because important clues exist about the eruptive history of volcanoes (Newman et al. 1988; Zhang and Behrens 2000). As a result, the number of water species in obsidian, their band locations, and absorption coefficients have been presented in detail (Newman et al. 1986; Zhang et al. 1997). In this paper, the focus was measuring the structural water (OH, H_2O_m) as well as the surface-diffused water (H_2O_m). An accurate determination will provide control over the critical parameters that control the hydration process.

Water Band Assignments

When the energy of the infrared light matches the vibrational energy level of a molecule it will be absorbed and excite the molecule causing the atoms to move. These complex vibrations can be partitioned into a set of *modes* (bending, stretching, contracting) that occur at specified frequencies within the infrared spectrum (Table 11.1). The total number of modes can be calculated. For a linear molecule such as hydroxyl (OH), the number of modes is estimated from the formula $3N-5$, where N is the number of atoms in the molecule. In the case of OH where only two atoms are present, the number of modes is equal to one. For a non-linear molecule such

as water, the formula is *3N-6* and the number of modes is equal to three for this three-atom molecule (B. Smith 1999).

Table 11.1. Water species, IR band location, and vibrational motion.

Band Location (cm^{-1})	Water Species	Vibration Motion
7100	OH	OH stretching, 1st overtone
	H_2O	OH stretching, 1st overtone
5200	H_2O	Combination OH stretching and HOH bending
4500	OH	Combination of Si-OH and Al-OH stretching
4000	OH	Uncertain
	H_2O	Uncertain
3570	OH	Fundamental stretching
	H_2O	Fundamental stretching
1630	H_2O	Fundamental bending

Figure 11.4 shows an infrared absorbance spectrum from 900 and 7100 cm^{-1} for an obsidian sample with the characteristic water peaks.

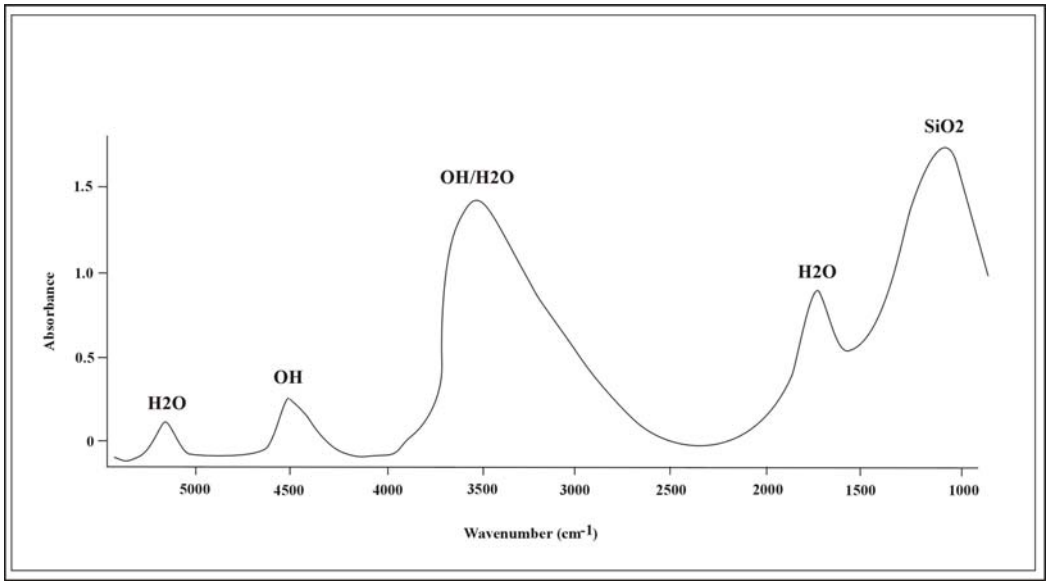

Figure 11.4. Water band locations in obsidian between 900 and 5200 cm^{-1}.

Six water bands are present within the wavenumber range (Newman et al. 1986). At 1630 cm^{-1}, there is a nearly symmetrical band that represents the fundamental bending mode of molecular water. The next band at 3570 cm^{-1} is a fundamental OH stretch for both hydroxyl and molecular water. It is a wide band whose asymmetry is generated by the numerous hydrogen bonds with other constituents of the glass. The small shoulder at 4000 cm^{-1} is a water band of uncertain assignment. It has been variously interpreted to represent hydrogen bonded to silanol groups,

molecular water and hydroxyl, and just molecular water. The band at 4500 cm^{-1} is a well-documented combination stretch of OH groups bonded as Si-OH and possibly OH-Al within the glass structure. The next at 5200 cm^{-1} is a band generated by basic OH stretching and HOH bending of molecular water. The last band at 7100 cm^{-1} is outside of the fundamental region and represents the first overtone of a fundamental OH stretch that occurs both in hydroxyl and molecular water (Newman et al. 1986).

The measurement uncertainty associated with all bands is less than 5 percent except for the band at 4000 cm^{-1}. At this wavenumber, background subtraction procedures are problematic and prevent highly repeatable measurements. The best precision can be obtained with the 3570 cm^{-1} water band where a 0.02 error in absorbance units translates into a 2 percent error at one unit of sample absorbance and a 4 percent error when the total absorbance is 0.5 units. This makes the 3570 cm^{-1} desirable for the measurement of very low amounts of structural water (<0.10%) in obsidian (Newman et al. 1986). Other less absorbing bands such as the molecular water bands at 1630 cm^{-1} and 5200 cm^{-1} , and the OH band at 4500 cm^{-1}, are more suitable for measuring greater water concentration levels (>0.10%) that compose the hydration layer.

Water Band Calibration

A quantitative determination of water concentration can be accomplished using Beer's law where weight percent concentration is related to absorbance intensity:

$$A = \varepsilon * l * c$$

where: A = absorbance, l = path length through the material expressed in microns or millimeters, c = the concentration in parts per million or weight percent, and ε is the molar absorptivity or a proportionality constant. This last value is an absolute measure of infrared absorbance at a specified wavenumber for a molecule. It is used to relate concentration to absorbance and must be empirically determined for each water band in the obsidian. To accomplish this, the intensity of infrared spectra is often compared with water concentrations determined by manometry.

The calibration of water bands in rhyolitic glass was initially attempted by Stolper (1982) and then quantified by Newman et al. (1986) for the concentration of total water between 0 and 2.5 percent. Ihinger et al. (1999) subsequently revised the molar absorptivity values based on refined manometry data but the molar absorptivities of Newman et al. (1986) were widely used for many years. A little more than 10 years later, Zhang et al. (1997) demonstrated that ε was not constant. They demonstrated that the ratio of the OH band at 4520 cm^{-1} to the H^2O band at 5230 cm^{-1} changed as a function of total water concentration, thus violating the fundamental assumption necessary for quantitative determinations. Zhang et al. (1997) developed new calibrations for these two water bands to compensate for changing values of ε that we will use in this analysis. This calibration can accurately calculate the concentration of total water up to 2.7 percent and is reported to be six times more reproducible than the previous calibration. The final equations for calculating the weight percent concentrations of H_2O_t, OH and H_2O_m are

$$H_2O_t = a_o A_{5230} + (b_o + b_1 A_{5230} + b_2 A_{4520}) A_{4520}$$

$H_2O_m = a_o A_{5230}/H_2O_t$

$OH = (b_o + b_1A_{5230} + b_2A_{4520}) A_{4520}/ H_2O_t$

where: $a_o = 0.04217 +/- 0.0013$ mm

$b_o = 0.04024 +/- 0.0023$ mm

$b_1 = -0.02011 +/- 0.0051$ mm^2

$b_2 = 0.0522 +/- 0.0051$ mm^2

Application of IR Spectroscopy to Obsidian Hydration Dating

The discussion of the obsidian hydration dating method demonstrated that molecular water from the environment enters the glass at a constant rate and forms an increasingly thick water rich surface layer over time. The rate of molecular water diffusion is dictated by the quantity of structural water present within the unaltered glass if temperature and other environmental parameters remain constant. IR spectroscopic analysis can obtain precise estimates of each water species (H_2O_m, OH) within the bulk matrix and on the surface of the glass. However, different IR sampling methods need to be used for bulk glass and the surface characterization.

Structural Water Measurement

Quantitative measurement of OH and H_2O_m in the unhydrated glass matrix may be obtained on transparent obsidians using the calibration constants discussed above. In this procedure, parallel-sided 1-mm-thick sections, approximately 1 cm^2 in area, are cut from an artifact or geological sample with a slow-speed wafering saw equipped with a diamond blade. Each side is polished to a 2-um finish using a variety of polishing grits to prevent scattering of the infrared beam. A mechanical polisher is commonly used so that the parallel sides are retained during the abrasion of the sample.

The prepared sample is placed on a sample mount within the spectrometer compartment and the infrared beam is passed through the sample (Figure 11.5). Absorption of the infrared light is converted into an infrared spectrum. The intensity of the water bands at 4500 cm^{-1} (OH) and 5200 cm^{-1} (H_2O) are determined by measurement of the peak heights using a flat background drawn at a tangent to the minima of each spectra. The measured absorbance values are then converted to water concentration values in units of weight percent.

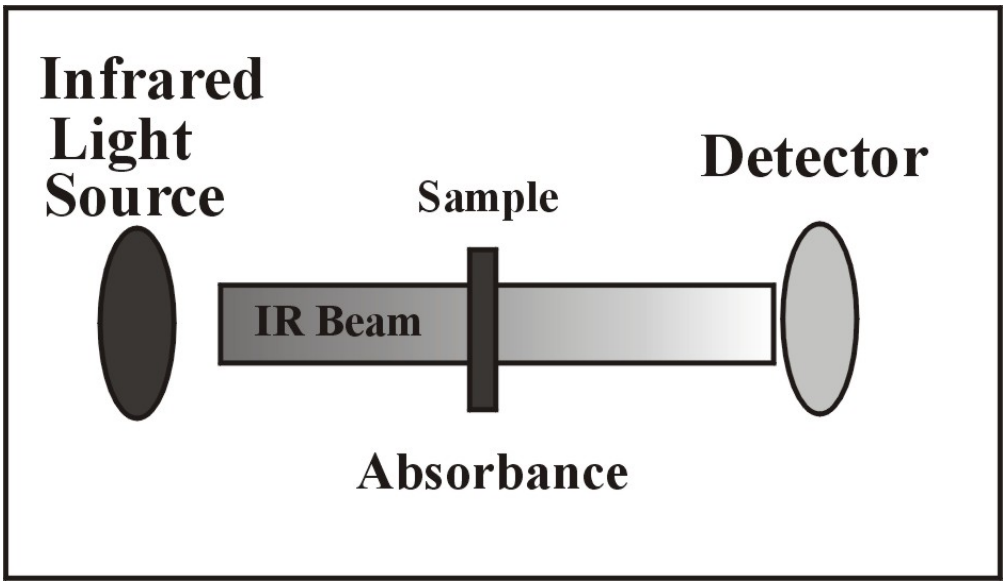

Figure 11.5. Infrared transmission measurement.

In order to obtain high-quality results, care must be taken to avoid imperfections and inclusions in the obsidian. Small voids or bubbles reduce the total quantity of glass exposed to the infrared beam and can lower water values. In contrast, concentrations of microlites may block the infrared beam and mimic a higher absorbance. This will inflate the final concentration. To avoid erroneous results it is necessary to avoid both voids and microlites by sampling regions of clear glass. To do this, a small aperture 3 to 6 mm in diameter is placed over the sample to allow only the preferred area to receive infrared light. The procedure will result in a representative value of water within the glass matrix. However, the use of a smaller sample area will result in a lower signal-to-noise ratio and a larger number of scans may be required to obtain satisfactory results. The analysis of opaque obsidians is not possible in transmission.

Our analysis of a variety of obsidians over the years has shown that total structural water content may vary significantly. Obsidians located within the American Southwest reflect this wide concentration range with total water values occurring between 0.10 percent and 1.58 percent. Table 11.2 lists the water concentration values for eight sources in Arizona and New Mexico. The Superior and Red Hill sources have been characterized with two to three separate samples and show that water concentrations may vary within a source. The remaining assays are on single samples. These data show the differences in structural water between obsidian sources but do not reflect the internal variation within each source. It is clear that if the infrared approach to obsidian hydration dating is to be correctly applied, each obsidian artifact represented within a lithic assemblage will need to be characterized to determine the concentration range of structural water. Some sources may have a restricted concentration range and may be represented by a single value with a low standard deviation. Other sources (e.g., Red Hill) may be highly variable. In this case, it may be required to assess the structural water content for each artifact to be dated. Only then can the correct rate constants be calculated.

Table 11.2. Structural water concentrations for some Southwestern obsidian sources.

Source	Location	Percent OH	Percent H_2O	Percent H_2O_t	A	E	Rate
Superior	Arizona	0.21–0.28	0	0.21–0.28	2.12/2.63	82703/81586	23.6/33.6
Antelope Wells	New Mexico	0.16	0	0.16	1.69	83760	16.5
Government Mtn.	New Mexico	0.18	0	0.18	1.87	83302	19.3
Gwynn Canyon	New Mexico	0.16	0	0.16	1.69	83760	16.5
Mule Creek	New Mexico	0.10	0	0.10	1.06	85585	8.2
Obsidian Ridge	New Mexico	0.24	0	0.24	2.35	82185	27.9
Polvadera Peak	New Mexico	0.24	0	0.24	2.35	82185	27.9
Red Hill	New Mexico	0.74–0.87	0.52–0.71	1.26–1.58	4.74/5.15	77811/77183	97.7/114.9

Hydration Layer Water Measurement

The optical measurement of the hydration layer at high magnification has been the standard for over 50 years. Determination of the inward limit of the diffusion front and thickness measurement relies on a change in the refractive index of the glass that is caused by the incorporation of molecular water into the matrix. The optical approach has produced much useful data but is fraught with many potential errors that can arise in sample preparation and focusing techniques (Jackson 1984; Stevenson et al. 1989). More importantly, a comparison of optically measured samples with layer hydrogen profiles conducted by SIMS revealed that optical measurements do not consistently occur at the diffusion front boundary (Anovitz et al. 1999). Infrared spectroscopy has the potential to overcome these problems by the elimination of sample preparation and through direct measurement of the diffusing species (H_2O_m).

The determination of the water concentration level within a hydration layer can be obtained with an infrared photoacoustic accessory (Figure 11.6). In this technique, a sample less than 10 mm in diameter is placed in a helium-filled chamber equipped with a high sensitivity microphone. The specimen absorbs the infrared radiation and undergoes an oscillatory heating and becomes a source of thermal waves. The waves within the bulk sample propagate to the surface and into the helium atmosphere. The photoacoustic signal is generated at the surface and is caused by the thermal expansion of the gas (McClelland et al. 1993). The magnitude of the signal varies in proportion to the concentration of the water species. The absorbance values are calculated from integrated peak areas. Each absorbance value represents an averaged measure for the entire surface of the sample exposed to the 5-mm-diameter infrared beam.

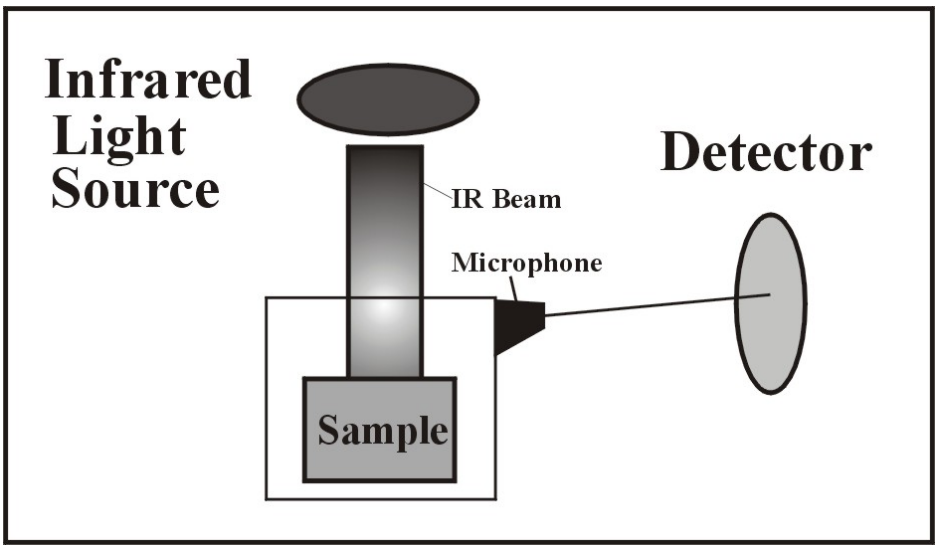

Figure 11.6. Infrared photoacoustic measurement.

No calibrations currently exist for the conversion of PAS band intensities to water concentration values. However, PAS absorbance intensities have been correlated with hydration layer depth measurements as determined by SIMS (Stevenson et al. 2000). Quantitative estimates of hydration layer thickness can be made up to a depth of 15 um (Figure 11.7).

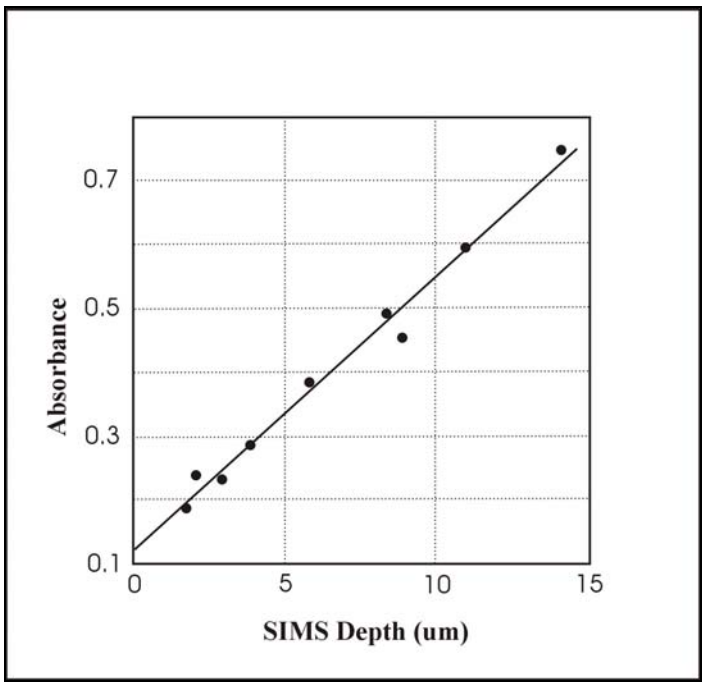

Figure 11.7. The relationship between infrared absorbance and depth of the hydration layer as determined by SIMS (after Stevenson et al. 2000).

The assumption behind this calibration is that water concentration, as reflected by absorption, will increase proportionally over time as diffusion proceeds. The linear relationship between IR absorption values and thickness supports this assumption.

Estimation of the Diffusion Coefficients

The diffusion coefficients for many types of obsidian have been empirically determined through hydrothermal experiments conducted at elevated temperatures. In the previous work of the author and others, glasses from different sources were hydrated in a vapour environment to determine the water diffusion coefficient at single temperature (160°C) and at multiple temperatures (150 to 180°C) to calculate the temperature dependence of diffusion or the activation energy. The coefficients were calculated from the optical thickness measurement of the induced hydration layers formed under known times of exposure to water vapour (Stevenson et al. 1998). These results provide the numerical constants for the Arrhenius equation so that a diffusion coefficient may be extrapolated to archaeological site conditions where temperatures are lower (10 to 30°C). The experimental coefficients were regressed with the glass structural water concentrations (Figure 11.8a, 11.8b) to develop prediction equations for the high-temperature-rate constants:

$$\text{Pre-exponential (A)} = 2.35 * (\ln(\text{percent OH})/\ln(10))^2$$

$$\text{Activation Energy (E)} = 76642 + (8943 * (\ln \text{percent OH}))$$

The infrared analysis of a sample of New Mexico obsidians (Table 11.2) has yielded water content values that range between 0.10 percent and 0.71 percent OH. Estimation of a diffusion coefficient for an ambient site temperature of 25°C is accomplished with the Arrhenius equation:

$$K = A \exp E/R*T$$

where: K = archaeological diffusion coefficient (um^2/1000 years)
A = preexponential (um^2/day at 160°C)
E = activation energy (Joules/mol)
R = universal gas constant
T = temperature (Kelvin)

This yields a diffusion coefficient that reflects the structural water concentration of the obsidian, a value may be used to convert measured hydration rim values to archaeological age estimates.

CONCLUSIONS

Water diffusion in glass is a complex problem. However, the fundamental components of the process are now beginning to be understood. It is clear that concentration-dependent diffusion accounts for the movement of molecular water into the glass structure. It is also established that the initial rate of molecular water diffusion is controlled by the quantity of structural water present within the glass matrix as a result of the incomplete removal of volatiles as the obsidian changes from a melt to a solid.

As a result of this understanding, it is possible to match the analytical methods to the problem at hand. Infrared spectroscopy is one method particularly suited to directly measuring the quantity of water in glass and the various species (OH, H_2O). Structural water can be quantitatively measured by simple infrared transmission and has replaced the difficult wet chemical methods. The amount of water in the hydration layer can be semi-quantitatively determined by infrared photoacoustic spectroscopy. An error estimate has not yet been determined for this application but we anticipate that it will approach that of other IR techniques and will only be several percent. This is preferable to the optical approach that involves extensive sample preparation and the estimation of the layer thickness under conditions of low resolution (+/-0.2 um).

The challenge for the immediate future requires that the calibration for the estimation of diffusion coefficients and activation energies from OH concentration be redone (Figure 11.8a and 11.8b). This calibration was developed by optical methods. Although there is a strong correlation between PAS signal intensity and SIMS depth, we anticipate that greater precision can be obtained if PAS is used to determine diffusion coefficients and activation energies on experimental samples. This is not a trivial experiment, but when completed it will tie all aspects of the obsidian hydration method to infrared spectroscopy.

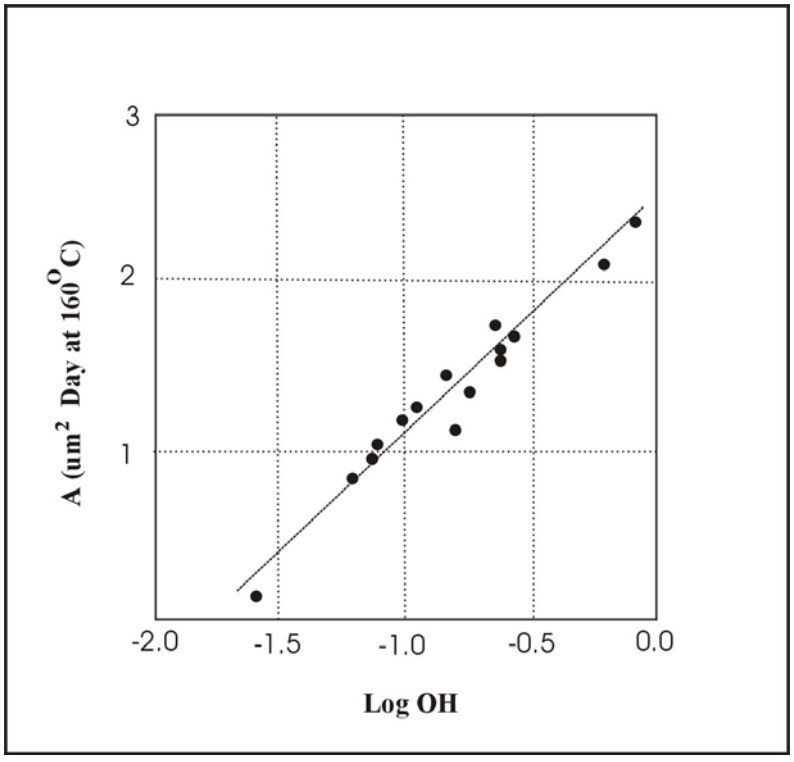

Figure 11.8a. The relationship between obsidian OH concentration and the pre-exponential.

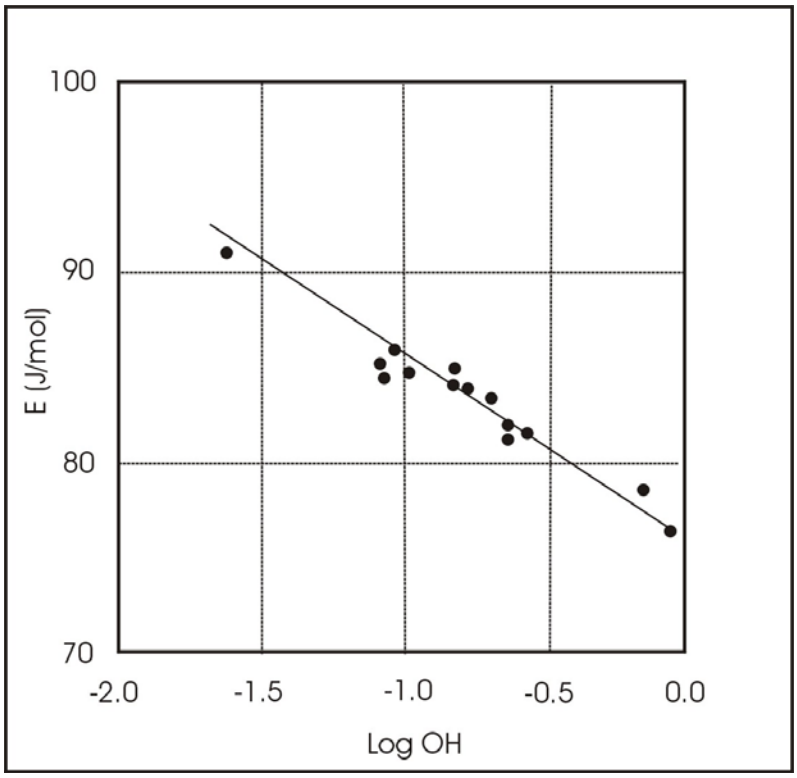

Figure 11.8b. The relationship between obsidian OH concentration and the activation energy.

CHAPTER 12
LUMINESCENCE DATING IN ARCHAEOLOGY

James Feathers

INTRODUCTION

Luminescence dating has long been treated with skepticism by American archaeologists (Feathers 2000). Although its popularity has been increasing lately, it remains under-utilized despite many recent advances in methodology and its potential for resolving chronological problems (Feathers 2003; Roberts 1997). Part of the reason for its under-utilization has been a lack of understanding of the rather arcane physics that underlie the method. This report is an attempt to increase this understanding.

Luminescence dating was developed in the 1960s and 1970s in the context of dating pottery and other ceramics. It has since been applied to dating burned lithics (Valladas 1992) and hearthstones as well as to dating buried sediments (Aitken 1985, 1998). In the case of pottery and burned lithics, the event dated is the last time the object was exposed to sufficient heat to reset the luminescence clock. For sediments the event dated is the last exposure to sufficient light. Often times these events are the ones that the archaeologist is interested in. Pottery is dated to when it was made or last used. Hearths can be dated to when the stones were heated, adobe when the bricks were made, and lithics either when they were heat-treated or accidentally burned during use. Sediments are dated to the time of their deposition. The convergence of the event of interest and the event that can be dated is the main strength of luminescence in archaeological applications (Feathers 2003). Unlike the case for radiocarbon, where dating artifacts often relies on association with organic matter, luminescence does not usually depend on making such connections.

The disadvantage of luminescence is the complicated underlying physics and the large number of variables that must be estimated to derive a date. This means that luminescence often has less precision than other dating methods, although methodological advances in the last few years (e.g., Murray and Wintle 2000) have improved considerably both precision and accuracy (Murray and Olley 2002). Error terms of less than 10 percent are commonplace. During some periods of time, such as the late prehistoric period (in the Americas), when radiocarbon has low resolution due to the flatness of the calibration curve, luminescence has been shown to outperform radiocarbon (e.g., Feathers 2005a; Lipo et al. 2005).

PHYSICAL BACKGROUND

Luminescence dating is rooted in what for most archaeologists is the unfamiliar world of solid state physics (Aitken 1985, 1998; Bøtter-Jensen et al. 2003). The phenomenon of luminescence is defined as light emitted from a substance after absorption of energy from an external source (Chen and McKeever 1997). What distinguishes luminescence from similar phenomena such as fluorescence is a time lag between the absorption of energy and the emission of light.

Luminescence can be used for dating for two reasons. First, the time lag, during which the substance remains in an excited or metastable state, may extend for millions of years, thereby providing a stable clock. Second, the metastable state can be removed in a matter of minutes or seconds by a stimulus, most commonly heat or light. When the stimulus is heat, the emitted light is called thermoluminescence (TL). When the stimulus is light, it is called optically stimulated luminescence (OSL). Such stimuli are, in effect, zeroing mechanisms and represent the events that are dated.

The external source of energy for dating applications is naturally occurring radioactivity in the sample and its immediate surroundings. Because such radioactivity is a continual process, the absorbed energy is built up through time, usually at a constant rate, until release by heat or light. This accumulated dose is called the paleodose, or equivalent dose (D_e). Dividing by the dose rate yields an age.

Luminescence is explained by reference to energy band theory (Figure 12.1) (Bøtter-Jensen et al. 2003, Chen and McKeever 1997; McKeever and Chen 1997). In complex crystalline solids with three-dimensional arrays of atoms, various energy levels of individual atoms overlap and form bands. In insulating materials, such as most constituents in ceramics or sediments, a gap is present between a lower band called the valence band, which corresponds to the ground state, and a higher band called the conduction band. In the valence band, electrons are closely tied to their parent atoms. The ionizing ability of natural radioactivity removes electrons from their parents and raises them across the gap to the conduction band where they can move about freely. In theory electrons cannot occupy energy levels within the gap, because of quantum rules, and if radioactivity (e.g., from ^{14}C) lacks the energy to raise electrons across the gap, no ionization occurs. When an electron is removed from an atom, the vacancy left behind in the valence band is called a hole. Electrons from an adjacent atom can fill the hole, creating a new hole in the adjoining atom. In this way holes can diffuse through the valence band in a similar way that electrons move through the conduction band. In ideal crystals, electrons that have been excited to the conduction band will return to the valence band and recombine with a hole once the energy from the external source is removed. But natural crystals contain defects in the form of substitutions, displaced atoms and lattice distortions. These can create localized charge deficiencies (balanced by an opposite charge deficiency elsewhere in the crystal). Electrons in the conduction band or holes diffusing through the valence band become attracted to these defects and can be "trapped." These traps occupy energy levels within the otherwise forbidden gap.

Once an electron or hole becomes trapped, a stimulus is required to remove them from the trap to the corresponding delocalized band. The amount of energy required to accomplish this is called the trap depth. Shallow traps require very little stimulus (heat or light) to empty and do so in a relatively short time under ambient conditions. Deep traps require high-energy stimulus to empty and can remain populated for very long periods of time. These latter traps are used for dating. When an electron or hole is released from a trap, it may recombine with opposite charge at another trap, called a recombination center, and both return to the ground state. The process of recombination is what results in the emission of light, or luminescence. Recombination centers have very high energy depth and release of charge from them is much more likely via recombination than from stimulus. Figure 12.1 illustrates the various transitions.

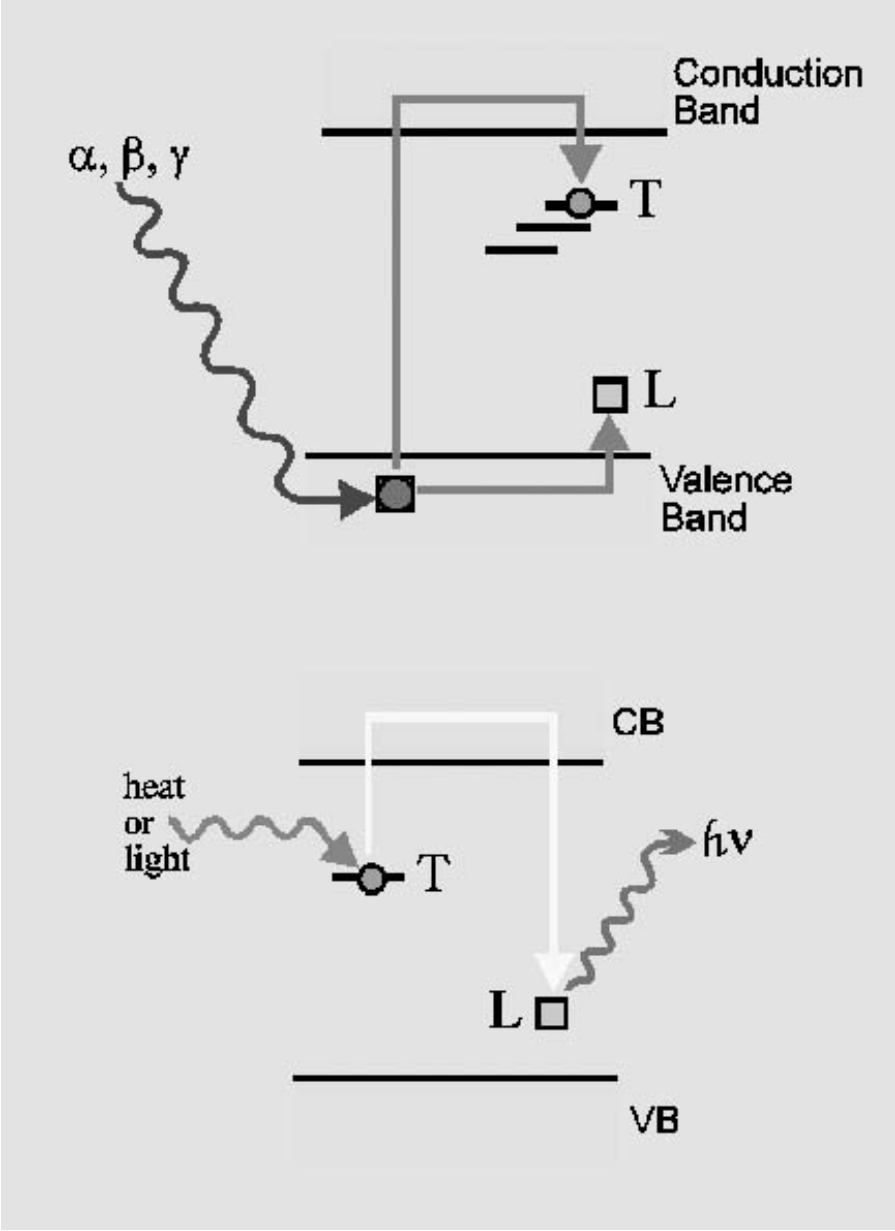

Figure 12.1. Energy level diagrams showing traps and various charge transitions. The ground state is represented by the valence band, while the conduction band is an excited state. Between the bands is a forbidden zone, which nevertheless contains energy levels associated with localized charge deficiencies caused by crystalline defects. T represents electron traps of various depths, while L represents a hole trap called a recombination or luminescence center. In the top diagram, ionizing radiation (alpha, beta or gamma radiation) lifts electrons to the conduction band where some of them are trapped at T. Electron vacancies or holes are trapped at L. In the bottom diagram heat or light provides a stimulus that releases the electron from the trap to the conduction band, where it then recombines with the hole at a recombination center resulting in the emission of photons (*h*υ). These diagrams were constructed by Dorothy Godfrey-Smith.

Figure 12.2 shows the full process involved. The horizontal axis is time and the vertical axis is the amount of absorbed energy in terms of the number of electrons and holes populating traps. Because luminescence is emitted when the traps are emptied, the luminescence signal intensity is proportional to the amount of trapped charge and can also be represented by the vertical axis. At some point in deep geological time, when the crystal is first formed, the traps are empty. With time, exposure to natural radioactivity ionizes atoms in the crystal and the traps begin to populate. Eventually, all the traps are filled and no additional radioactivity will increase the amount of trapped charge. This saturated level defines an upper limit to dating, which is around 100,000 years for quartz and perhaps a million years for feldspar. Then at some point in prehistoric time—when a pot was fired or when sediments associated with artifacts were exposed to light and deposited—the traps are emptied. After the pot is removed from heat or the sediments are buried, electron and hole traps begin to be repopulated and absorbed energy rebuilds. When the materials are transported to the lab and measured by heating (TL) or exposure to light (OSL), the resulting luminescence intensity is proportional to the amount of trapped charge accumulated since the last zeroing event. If the dose rate has been constant over this time, the luminescence intensity is proportional to time.

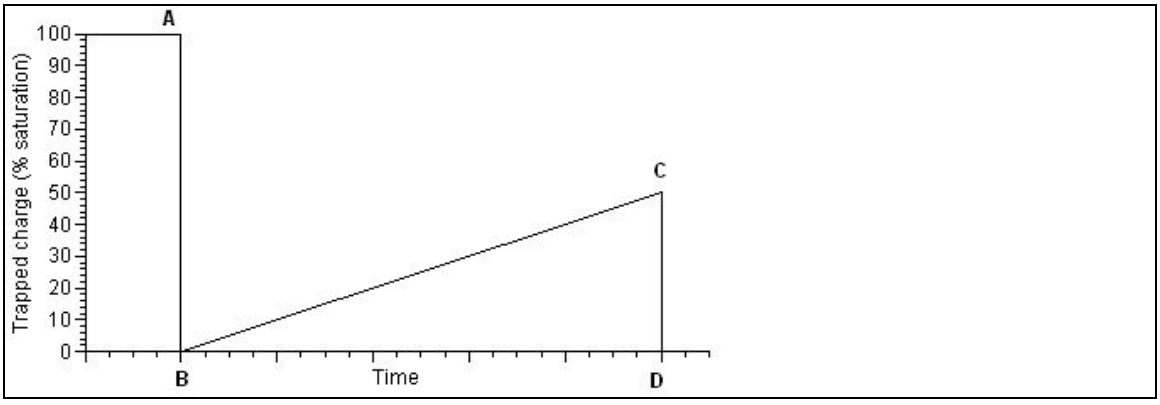

Figure 12.2. Schematic of the dating process. At some point in geological time (not shown) the traps are empty. Continual radioactivity results in filling of the traps until they are all filled to some saturation point (A). An event in prehistory, either exposure to heat or to light (B), empties the traps. As time goes on, the traps start filling again, until point C when the traps are emptied in the laboratory by applying heat (TL) or light (OSL), this time measuring the luminescence. The intensity of the signal is proportional to the amount of trapped charge, which if the dose rate is constant can be related to the time elapsed from B to D. (Figure from Feathers 2003).

RADIOACTIVITY

Can the dose rate be assumed constant through time? The principle contributors to the natural dose rate come from ^{40}K and the decay chains of ^{232}Th and ^{238}U. ^{232}Th and ^{238}U are parent radionuclides, the decay of which is the first of a series of decays through a number of daughter radionuclides until a stable isotope of lead is reached. The daughters have half lives much shorter than those of the parents, the consequence of which leads, in the absence of any other

geological process, to the activities of daughter and parents becoming the same. This condition where parent and daughters decay at the same rate is called secular equilibrium. The half lives of the two parents and of ^{40}K are very long, on the order of 10^9 years. Because the decay rates are so slow (but nevertheless measurable), radioactive composition changes only very slightly over archaeological time, meaning that the decay rate is virtually constant. The radioactivity measured today will almost be the same as what it would have been at the time of zeroing had it been measured then. Of course, radioactivity is not the only process affecting composition. Various geological processes, such as leaching, ion-exchange, or addition/removal of overburden, can alter the concentration of radionuclides within the effective range of the sample (about 30 cm). In many cases the effects of such processes are not significant and the constant dose rate assumption is safe. Changed concentrations can often be detected (and some times corrected) by the presence of systematic changes down a profile or by a condition of disequilibrium in the decay chains (where selective daughters or the parent have been added or removed) (Krbetschek et al. 1994). The possibility of changes in dose rate is something that always has to be taken into account in dating, but samples that cannot be dated because of it are not common (Olley et al. 1996). In addition to the major contributors to the dose rate, there are minor contributions from ^{87}Rb, ^{235}U (parent of another decay chain) and cosmic radiation. The latter can be significant for surface samples that have little internal radioactivity.

Another variable affecting radioactivity is the moisture content of the sample and its surroundings. Moisture absorbs radioactivity at a different rate than the sample, such that higher moisture contents mean a lower dose rate to the sample. Some estimate of past moisture content, which can change dramatically over time, is necessary, although large uncertainties in this estimation can be tolerated.

MEASUREMENTS

Two sets of measurements are required to produce a date. One is to measure the equivalent dose (D_e). This is done by calibrating the natural luminescence signal, measured on selected portions of the sample, against artificial radiation provided in the laboratory. The amount of radiation needed to produce a given amount of luminescence is called the sensitivity. The challenge is to make sure the natural signal and the calibrating signal are responding to the same sensitivity, and various procedures including a preheat to a temperature of about 200 to 260°C before each measurement are applied to accomplish this (Wintle and Murray 1998). The preheat is also designed to remove any unstable signal from shallow traps. The second set of measurements is to estimate the dose rate both of the sample and its immediate surroundings. These normally take place in the laboratory but field assessments of radioactivity are also employed—and recommended for complex environments.

The portion of the sample useful for dating is governed by both the composition and the effective ranges of various types of radioactivity. Terrestrial radioactivity consists of alpha, beta, and gamma radiation. Alpha particles are helium nuclei with high energies and short ranges, on the order of about 20 µm. Beta particles are electrons with medium ranges of up to 2 mm. Gamma particles are high-energy photons with ranges up to 30 cm in soil. ^{40}K is a beta and gamma emitter, while the various steps of the decay chains emit all three. Some minerals, such as

quartz, have little internal radioactivity, so that sand-sized quartz particles, for example, are affected just on their surfaces by alpha radiation. If a sample containing both coarse-grained quartz and fine grains were mixed together, the luminescence signal of the mixture could not readily be related to the dose rate because some of the luminescence is a function of just betas and gammas and some a function of betas, gammas, and alphas. One alternative is to measure luminescence on just coarse grains, usually either quartz or feldspars. Both produce luminescence signals that are responsive to dose and neither have internal sources of alpha irradiation. For quartz, the outer surfaces of the grains are removed by hydrofluoric acid, so that the luminescence is only a function of betas and gammas, easing analysis. Only a very weak etch can be applied to feldspars without dissolving the whole grain, but alpha radiation still only plays an insignificant role. Potassium-based feldspars do have internal beta radiation from ^{40}K. If the sample is fine-grained, like many ceramics, an option is to isolate polymineral fine grains, usually 1 to 8 or 4 to 11 μm. These are small enough to not attenuate alpha radiation, so the luminescence is a function of all three. Sample preparation then is a matter of isolating either coarse grains of quartz or feldspar or fine grains for measurement.

A further complication with alpha irradiation if fine grain measurements are being made is the lower efficiency of alpha particles in producing luminescence. Because alphas are so energetic and so short-ranged, they saturate all the traps in their immediate vicinity before they use up all their energy. The remaining energy goes to waste, in terms of luminescence, with the result that alphas are only about one-tenth as effective at producing luminescence as betas or gammas. This has to be taken into account when determining the dose rate. It is usually measured by comparing luminescence sensitivity determined by either alpha or beta irradiation. The ratio is called the b-value (Huntley et al. 1988).

The gamma radiation that affects the sample luminescence arises largely from outside the sample, because of its relatively long range. An estimation of the radioactivity of the immediate surroundings of the sample is therefore necessary. This can be measured in the field either by implanting radiation-sensitive dosimeters or by using portable gamma spectrometers. If the environment is relatively homogeneous, a representative sediment sample can also be collected and measured in the laboratory. This is what is normally done for ceramic dating. Figure 12.3 illustrates radioactive ranges and their effects on samples.

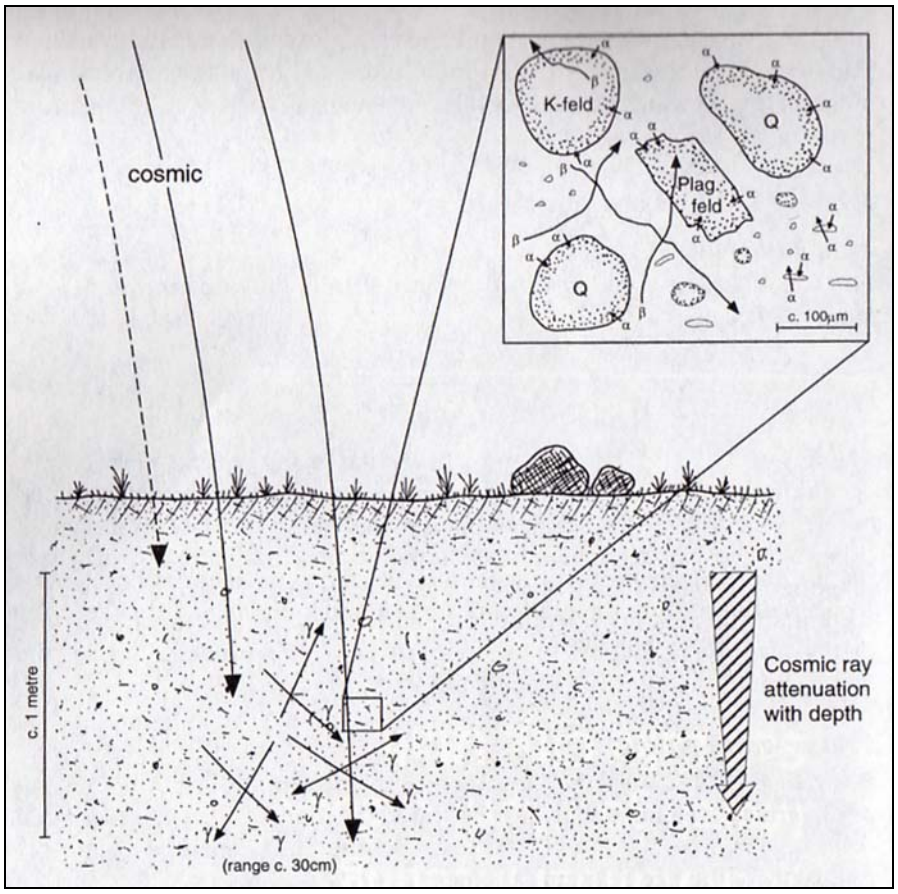

Figure 12.3. Ranges of different kinds of radiation are shown for typical sediment. The inset shows the penetration range of beta and alpha particles for different grain sizes. Dating is usually performed on either sand-sized grains of quartz or feldspar or on polymineral fine grains (4 to 11µm). (Figure by Stephen Stokes [Aitken 1998]).

Quartz and feldspar are both ubiquitous minerals, but they have their advantages and disadvantages. Feldspars have brighter luminescence signals and saturate at higher levels, making them useful for both very old and very young samples (Duller 1997). They are also the only mineral that responds significantly to infrared light stimulation (called IRSL), so that mineral separation is not necessary. But they suffer from a malady called anomalous fading. This is the loss of electrons through time under ambient conditions from traps that have sufficient depth that the electrons should not escape. It is explained by a concept in quantum theory called tunneling. If fading has occurred, the age will be underestimated, although various procedures have been proposed to circumvent fading or correct for its effects (Huntley and Lamothe 2000). Because it does not exhibit fading, quartz is often the preferred mineral for dating. But some quartz has low sensitivity and it saturates at relatively young ages (as young as ~ 50,000 years), so feldspars are commonly employed as an alternative. Polymineral fine grains may also suffer from anomalous fading, because feldspars often dominate the signal from them.

Calibration against artificial irradiation to determine D_e is accomplished through construction of a growth curve plotting irradiation against luminescence (Aitken 1985). Two general methods

are used. The first, called additive dose, involves applying increments of artificial dose to aliquots still containing the natural signal. D_e is determined by extrapolating the growth curve to the dose axis, a procedure that assumes the growth curve is the same shape in the extrapolated region as among the measured points. The assumption is often not valid (particularly for young samples) and the extrapolation is often with poor precision (common for old samples). The second, called regeneration, involves first reducing the natural signal to background on aliquots and then giving increments of dose to them. The growth curve is thus constructed from zero and D_e is determined by interpolating the natural signal into the growth curve. The problem with regeneration is possible sensitivity changes brought about in the process of reducing the natural signal to background. Sensitivity changes are caused by the redistribution of trapped charge that can alter preferred pathways of recombination. If the sensitivity changes, the regenerated growth curve may not have the same slope as the curve of which the natural signal is a part. In such cases, interpolation will produce an inaccurate D_e.

Traditionally, D_e has been measured using multi-aliquots. One set of aliquots is used to construct an additive dose curve and a second set (usually the ones from which the natural signal was measured on the first set) is used for regeneration. D_e is determined by an additive dose extrapolation corrected by an offset determined by the dose intercept of the regeneration curve (called supralinearity correction). Alternatively, the slope of the regeneration curve is adjusted by a multiplicative factor to match the sensitivity of the additive curve. The two curves are then shifted along the dose axis into coincidence by an amount equal to the D_e. This is called the slide method (Prescott et al. 1993) (Figure 12.4). The original authors of the slide method used the multiplicative factor just to test for sensitivity change and questioned whether it could be used to correct for it, but our laboratory has shown empirically, at least for TL on ceramics, that the slide method, even using the correction, produces the same answer as the method using supralinearity correction but often with better precision.

More recently, D_e from OSL has been determined using growth curves constructed on single aliquots. This has the obvious advantage of obviating the need to normalize among aliquots and has some other distinct benefits for sediment dating, which will be discussed later. The first attempt was using an additive dose technique (Duller 1995), but this did not overcome the extrapolation problems of additive dose and required some problematic corrections for successive measurements. A regeneration procedure became possible when a means to correct for sensitivity change was discovered. This was accomplished by administering a small test dose after each regeneration measurement (including the natural) (Murray and Wintle 2000). The OSL signal from the test dose has the same sensitivity as the regeneration measurement preceding it, allowing a way to normalize all measurements to the same sensitivity. This method is called single-aliquot regenerative dose (SAR) and is now the preferred method for measuring D_e with OSL (Table 12.1). A practical single-aliquot technique for TL has not been devised.

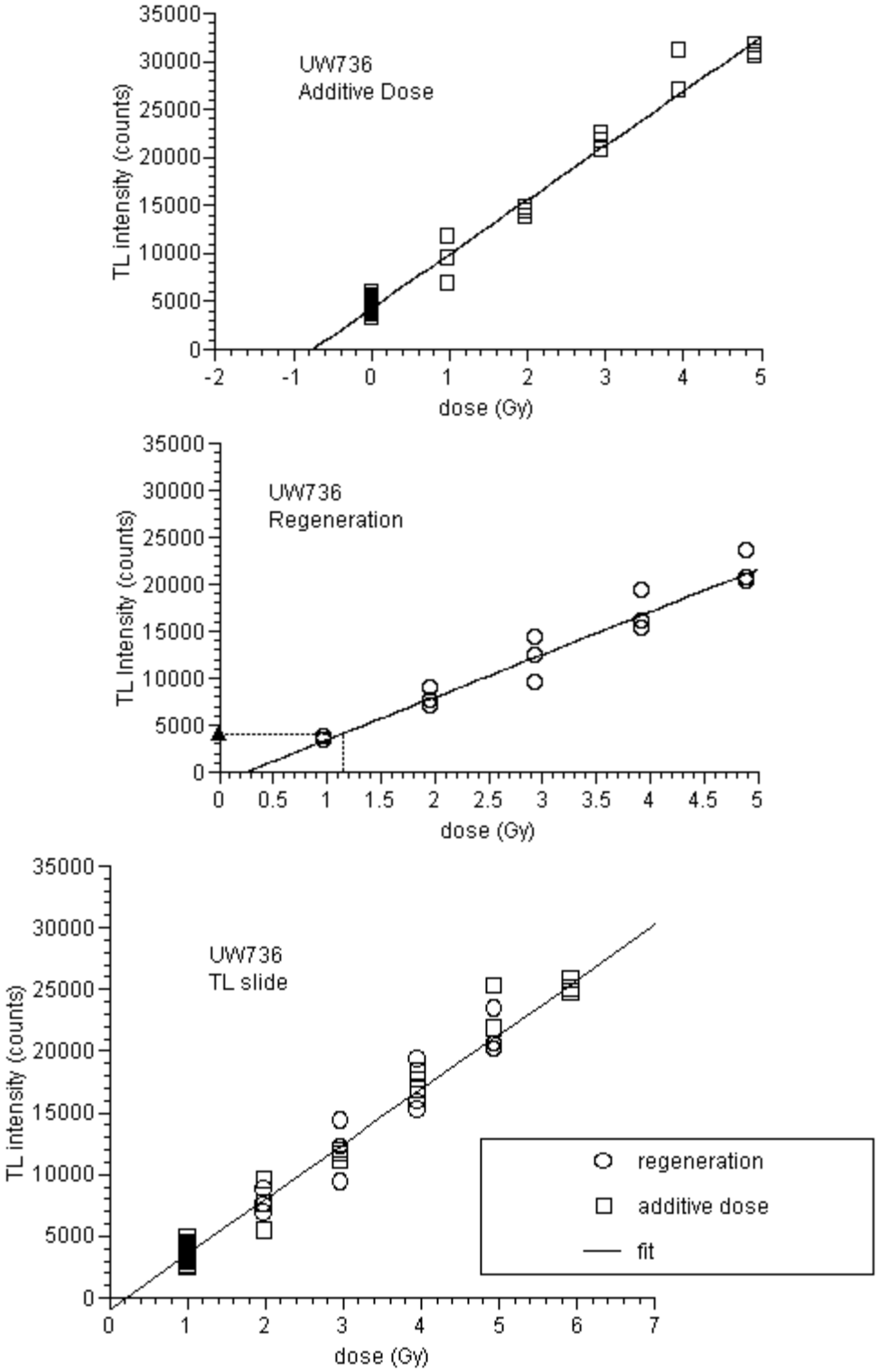

Figure 12.4. TL intensity. The top diagram shows an additive dose growth curve. The x-axis is artificial radiation dose administered in the laboratory (in Gy, the unit of absorbed dose). The points at zero dose represent the natural signal. Increments of dose are added to aliquots still containing the natural signal to construct the curve. Extrapolation from the

natural signals to the x-axis gives the amount of dose required to achieve the natural level. The middle diagram shows a regeneration growth curve, where increments of dose are administered to aliquots that have been zeroed. The natural signal is then interpolated into the curve as shown. The bottom diagram shows the additive dose and regeneration curves brought into coincidence by adjusting the regeneration points by a scale factor to make them parallel to the additive dose points and by shifting the points along the x-axis by an amount taken to be the equivalent dose. The sample is a prehistoric ceramic from New Mexico (Figure from Feathers 2003).

Table 12.1. Typical SAR sequence on single aliquot (Murray and Wintle 2000).

1. Dose (= 0 Gy if natural signal)
2. Preheat (e.g., 260°C for 10 seconds)
3. OSL (e.g., 60s at 125°C, stimulation using blue light, emission in UV), gives L_i
4. Fixed test dose (e.g., 5 Gy)
5. Cut heat (e.g., 160°C)
6. OSL (same as step 3), gives T_i
7. Repeat steps 1-6 for a range of regeneration doses bracketing the natural dose, a zero dose and a repeat (or recycle) point
8. Calculate L_i/T_i for natural and regeneration points and construct regeneration curve to determine D_E

DATING CERAMICS AND LITHICS

Dating ceramics are usually straightforward, because the heat necessary to make the ceramic is sufficient to reset fully the luminescence signal. This is not always the case with hearth stones or burned cherts. Sufficient heat from hearths does not always penetrate to the center of the rocks that form the hearth, requiring to sample near the surface or in the case of coarse-grained rocks using single-grain dating to isolate those grains most likely to have been heated sufficiently. Cherts were often heated in antiquity to improve flaking abilities, but often not high enough for luminescence dating (Dunnell et al. 1994). Cherts suitable for dating are often those that have been accidentally heated high enough, either by finding their way into a fire or by overheating during manufacture.

For either ceramics or lithics that have been heated sufficiently, luminescence provides a potential for dating that few other methods can match. For example, luminescence can be applied successfully to surface finds (Dunnell and Feathers 1994). This obviates the need for excavation to find datable material and thereby provides a cost-efficient way of dating for regional surveys. The ability of luminescence to date artifacts directly opens many opportunities (Feathers 2005a). It allows dating of small sites that lack diagnostics or other datable material. It allows the teasing apart of multiple occupations or otherwise mixed assemblages. By dating many artifacts from a single occupation, it allows estimations of occupation duration.

A drawback of luminescence dating of ceramics or lithics is lower precision than is obtainable from methods such as radiocarbon. In our laboratory, relative errors on ceramic or lithic dates

average about 10 percent. Lower precision is a consequence of the large number of variables that must be estimated to achieve a date and therefore the propagation of the errors from each. Inaccurate estimations of any one variable can also lead to systematic errors. These often stem from changes in dose rate through time, varying moisture contents (which affect the dose rate), and anomalous fading. Our laboratory is experimenting with using OSL and IRSL on fine grains for determining D_e. These have the advantage of allowing single aliquot methods that provide higher precision. We predict that relative errors of as low as 5 percent can be achieved. By measuring first with IRSL and then with OSL, called the double SAR method (Banerjee et al. 2001; Roberts and Wintle 2001), it may also be possible to circumvent fading on fine grains if the IRSL can largely remove the feldspar signal, so that the subsequent OSL stems largely from quartz. Work needs to be done to see how b-value differs among OSL, IRSL, and TL.

As already mentioned, luminescence for some periods can currently provide better resolution than radiocarbon because of the flatness of the radiocarbon calibration curve.

DATING SEDIMENTS

Because of its utility in geology, luminescence research has focused on sediment dating, rather than ceramics or lithics. Dating sediments is more difficult because of a stronger possibility that sunlight was not of sufficient intensity to reset the luminescence signal at the time of deposition and also because of the propensity of sediments to become mixed through turbation processes after deposition (Bateman et al. 2003). In either case, some grains will provide the correct age of deposition, while others will not.

The luminescence community has addressed this question in two ways. One is to base dating on the most bleachable components of the luminescence signal. OSL has gained popularity over TL because it involves traps that are much more readily emptied by sunlight (although a rapidly bleaching TL component can be isolated in quartz, the procedure is cumbersome.) Even within OSL, there are some components more bleachable than others and efforts have been made to detect partial bleaching by comparison of fast and slow components (Bailey et al. 2003; Singarayer and Bailey 2003). A popular method for this is the use of linear modulated OSL (LM-OSL), where the intensity of stimulating light is steadily increased during exposure (Bulur et al. 2000). The early part of the resulting curve is associated with the fast component, the latter part with slower components (Olley et al. 2004a; Yoshida et al. 2003).

Another way to assess partial bleaching or mixing from turbation is by dating single grains, or less desirably single aliquots with a small number of grains (Roberts et al. 1999). Most work has been done with quartz, but some with feldspar (Lamothe et al. 1994). To make this practical, special instrumentation has been developed that uses a finely tuned green light laser to stimulate single grains that have been isolated in grids on specially designed sample holders (Bøtter-Jensen et al. 2003). The resulting distribution of D_e values is not easy to interpret. Some of the variation is due to differences in precision (bright grains have higher precision than dull ones), differences in microdosimetry (at the scale of individual grains, dose rates will vary from grain to grain) and differences in luminescence properties (fading, thermal transfer) (Galbraith et al. 2005). The challenge is to separate out these kinds of variation (which are largely random) from

those caused by partial bleaching or turbation. Statistical models have been applied to determine an over-dispersion value that expresses the percentage of variation that cannot be accounted for by differential precision (Galbraith et al. 1999). For single grains, over-dispersion values of less than 10 to 15 percent are rare, and some have observed from independently dated samples that values less than about 20 percent represent single-aged samples (Olley et al. 2004a, 2004b). Geological evidence is often used to decide what portion of the distribution will likely represent the best age estimate. For example, for fluvial sediments, where partial bleaching is often a concern because of transport turbidity and the filtering effects of water on sunlight, the distributions are often positively skewed with a long tail of larger values (Jain et al. 2004; Wallinga 2002). In this case a "minimum age" is calculated to represent the best bleached grains. Minimum age models, which statistically isolate the lowest value grains that could form a single-age distribution, have also been applied to dating paleosols (Bush and Feathers 2003) and in sand dunes where there is evidence of deflation (Feathers et al. 2005).

Despite these problems, sediment dating has great potential in archaeology. Single-grain dating can be used to assess stratigraphic integrity (if sediments are mixed or not), which is very important for controversial issues such as pre-Clovis occupation. Evidence of mixing can also help with questions concerning site formation.

SAMPLE COLLECTION

Archaeologists collecting samples for luminescence dating only need to remember four guidelines. One is to avoid exposing the sample to radiation that will affect the luminescence signal: heat, light, X-rays. Ceramics are not usually a problem during the collecting process because the sherd surfaces can be exposed to light. In the laboratory, the outer surfaces are removed and only the internal portion is used for luminescence measurements. For the same reason, lithics are not usually a problem unless they are translucent. In the latter case they should be placed in an opaque container soon after collection. Unconsolidated sediments require more care to avoid light. A common practice is to collect the samples from cleared profiles or by coring using opaque cylinders. The ends of the cylinders will be exposed to light but they can be removed in the laboratory and the inner part used for dating. Airport X-rays are some times a problem and samples should be sent ground freight when possible.

The second guideline is to think about the radioactive environment. Because gamma radiation has a range of about 30 cm in sediment, anything within 30 cm of the sample will contribute to the dose rate of the sample. This is why for ceramics and lithics, it is customary to collect a sediment sample from adjacent to the sample. Assuming this sediment is representative of the radioactivity surrounding the sample, the gamma dose rate can be measured from it. Ideally one should choose sample locations where the radioactive environment is not too complex, so that this assumption holds. Samples from deposits that are homogeneous in composition will have the least ambiguity in determining the external dose rate. If complex environments cannot be avoided, consideration of how the external dose rate will be determined is necessary. Additional samples may need to be collected or on site dosimetry measurements may be advisable. In all cases, consultation with the luminescence specialist before collection is recommended. (Because the radioactivity of the sample itself also needs to be measured, it is important not to alter the

composition in any way. Adding glue or other substances to repair or label ceramics, for examples, should be avoided.

The third guideline is to select samples that have a high probability of having been zeroed at the time of interest. Again ceramics are usually not a problem, although specimens that are particularly soft, indicating very low firing temperatures, should be avoided. For lithics, choose samples that have clear evidence of heat damage. Sediments are more problematic and consultation with geologists about how they were deposited is advised. Aeolian deposits are usually well exposed to sunlight during deposition. Fluvial deposits can be problematic since water attenuates shorter wavelengths of light and high sediment load can further reduce light penetration. Colluvial sediments may also be problematic, depending on the mode of deposition. Even where bleaching is not complete, however, single-grain dating may allow isolation of those grains that were well-exposed.

The fourth guideline is the collection of sufficient sample. Ceramics should be at least 3 cm in diameter and 5 mm thick. In this case, bigger is better. Lithics should be somewhat larger to allow for difficulties in preparation. Samples for measuring radioactivity need only be about 100 g. Sediment samples for dating need to be about 400 g, depending on the grain-size distribution.

A final requirement is to provide the dating specialists with full provenience information on the sample, including latitude, longitude, altitude, depth of burial, stratigraphic relationships, sediment textures, and observations about moisture content. A profile map or photograph of sample contexts is useful.